Methods in Molecular Biology 1811

Springer Protocols

Giampaolo Zuccheri *Editor*

DNA Nanotechnology

Methods and Protocols

Second Edition

Humana Press

METHODS IN MOLECULAR BIOLOGY

Series Editor
John M. Walker
School of Life and Medical Sciences
University of Hertfordshire
Hatfield, Hertfordshire AL10 9AB, UK

For further volumes:
http://www.springer.com/series/7651

DNA Nanotechnology

Methods and Protocols

Second Edition

Edited by

Giampaolo Zuccheri

Department of Pharmacy and Biotechnology, University of Bologna, Bologna, Italy

Humana Press

Editor
Giampaolo Zuccheri
Department of Pharmacy and Biotechnology
University of Bologna
Bologna, Italy

ISSN 1064-3745 ISSN 1940-6029 (electronic)
Methods in Molecular Biology
ISBN 978-1-4939-8581-4 ISBN 978-1-4939-8582-1 (eBook)
https://doi.org/10.1007/978-1-4939-8582-1

Library of Congress Control Number: 2018944262

© Springer Science+Business Media, LLC, part of Springer Nature 2018, corrected publication 2018
This work is subject to copyright. All rights are reserved by the Publisher, whether the whole or part of the material is concerned, specifically the rights of translation, reprinting, reuse of illustrations, recitation, broadcasting, reproduction on microfilms or in any other physical way, and transmission or information storage and retrieval, electronic adaptation, computer software, or by similar or dissimilar methodology now known or hereafter developed.
The use of general descriptive names, registered names, trademarks, service marks, etc. in this publication does not imply, even in the absence of a specific statement, that such names are exempt from the relevant protective laws and regulations and therefore free for general use.
The publisher, the authors and the editors are safe to assume that the advice and information in this book are believed to be true and accurate at the date of publication. Neither the publisher nor the authors or the editors give a warranty, express or implied, with respect to the material contained herein or for any errors or omissions that may have been made. The publisher remains neutral with regard to jurisdictional claims in published maps and institutional affiliations.

Printed on acid-free paper

This Humana Press imprint is published by the registered company Springer Science+Business Media, LLC part of Springer Nature.
The registered company address is: 233 Spring Street, New York, NY 10013, U.S.A.

Preface

Both in research labs and in the world outside them, we are currently experiencing the mainstreaming of nanotechnology. After a few decades of discoveries and technological development of the new world at the bottom, now nanotechnology is at work in the industry as well as in many types of labs. Through mating with other sciences and technologies, it is helping to solve societal problems and to enable discoveries, often staying hidden under the hood of products and services.

The mainstreaming is evident at all levels, including the goals of governments and funding bodies. Nowadays funds are granted primarily for innovation in the industry and for the solution of grand societal challenges. Nanotech can contribute to both, but it must synergize and sometimes compete with other technologies in order to do so. Nanotechnology cannot work alone; rather it complements and enhances all other tools of science and technology. The growth of nanotechnology is continuing and it does so with the awareness that to spread and have an impact it must be shared. Methods developed in focused labs must be shared with others and with those that will put them to work in the field and make them part of complex procedures and collaborative efforts organized around the current and future needs of our society. A book of methods is one of the enabling tools of this process as it is an often-missing link between the technology developers and the users.

A few years have passed since the first edition of this book of methods on DNA nanotechnology. We have witnessed the further development of DNA nanotechnology to make ever more brilliantly conceived and realized nanostructures and to make them useful. More applications have come in the biosensing field. New uses and applications have arisen for DNA origami and many more researchers use them nowadays. This new edition contains new methods that enrich the library of the first edition to make a richer arsenal of methods for researchers and technologists expanding to DNA nanotechnology.

Several chapters of this new edition focus on these applicative uses of nanostructures, especially toward biosensing. A number of chapters focus on the use of DNA origami for arranging matter in the nanoscale or on their manipulation with the aid of other technologies, such as nanolithography. There are also chapters detailing the procedures for making nucleic acids nanostructures of different kinds, as these can implement the available set of building blocks for nanotechnology. A few chapters focus on methods to simulate complex nanostructures or on gathering insightful thermodynamic information from probing nanostructures.

This book has also been gifted with an introductory chapter written by Ned Seeman. The recognized father of the field of structural DNA nanotechnology traces some of its historical origins and charms us with a reminder that science and technology are still made by humans.

I trust this book will be able to give its little contribution to the uptake of DNA nanotechnology.

Bologna, Italy ***Giampaolo Zuccheri***

Contents

Preface . . . . . *v*
Contributors . . . . . *ix*

1 DNA Nanotechnology: From the Pub to Information-Based Chemistry 1
Nadrian C. Seeman

2 The Synthesis of Designer DNA 11
Rachel C. Little, Colette J. Whitfield, Eimer M. Tuite, and Andrew R. Pike

3 Synthesis of DNA-Based Nanowires 23
Alexander Kotlyar

4 Preparation of Anti-miR PNAs for Drug Development and Nanomedicine 49
Alex Manicardi, Roberto Gambari, Luisa de Cola, and Roberto Corradini

5 Loading of PNA and Other Molecular Payloads on Inorganic Nanostructures for Theranostics 65
Alessandro Bertucci, Simone Silvestrini, Roberto Corradini, and Luisa De Cola

6 Design and Characterization of pH-Triggered DNA Nanoswitches and Nanodevices Based on DNA Triplex Structures 79
Andrea Idili and Francesco Ricci

7 Characterizing Surface-Immobilized DNA Structures and Devices Using a Quartz Crystal Microbalance with Dissipation Monitoring (QCM-D) 101
Katherine E. Dunn, Martin A. Trefzer, Steven Johnson, and Andy M. Tyrrell

8 Hybridization Chain Reaction Design and Biosensor Implementation 115
Andrea Miti and Giampaolo Zuccheri

9 Ultrasensitive Detection of Metal Ions with DNA Nanostructure 137
Mingshu Xiao, Xiangmeng Qu, Li Li, and Hao Pei

10 Spatially Resolved Peptide-DNA Nanoassemblages for Biomarker Detection: A Synergy of DNA-Directed Immobilization and Nanografting 151
Abimbola Feyisara Adedeji, Elena Ambrosetti, Loredana Casalis, and Matteo Castronovo

11 LSPR Detection of Nucleic Acids on Nanoparticle Monolayers 163
Sophie Thamm, Andrea Csàki, and Wolfgang Fritzsche

12 DNA-Templated Silver Nanoclusters for DNA Methylation Detection 173
Hanie Ahmadzade Kermani, Morteza Hosseini, and Mehdi Dadmehr

13 Selection of Structure-Switching DNA Aptamers Binding Soluble Small Molecules and SPR Validation of Enrichment 183
Enrico Tenaglia, Fabio M. Spiga, and Carlotta Guiducci

14 Dielectrophoretic Stretching of DNA 199
Eva-Maria Laux, Frank F. Bier, and Ralph Hölzel

15 A Practical Guide to Molecular Dynamics Simulations of DNA Origami Systems 209
Jejoong Yoo, Chen-Yu Li, Scott Michael Slone, Christopher Maffeo, and Aleksei Aksimentiev

16 Single-Molecule Patterning via DNA Nanostructure Assembly: A Reusable Platform 231
Da Huang, Mark Freeley, and Matteo Palma

17 Directed Protein Adsorption Through DNA Origami Masks 253
Saminathan Ramakrishnan, Guido Grundmeier, and Adrian Keller

18 DNA Origami Structures Interfaced to Inorganic Nanodevices 263
Claudia Dalmastri, Weihua Han, Stefano Vespucci, Liqian Wang, and Piero Morales

19 Tuning Gold Nanoparticles Plasmonic Properties by DNA Nanotechnology 279
Valentina Masciotti, Denys Naumenko, Marco Lazzarino, and Luca Piantanida

20 DNA-Assisted Molecular Lithography 299
Boxuan Shen, Veikko Linko, and J. Jussi Toppari

21 Constructing Free Energy Landscapes of Nucleic Acid Hairpin Unfolding 315
Micah J. McCauley, Ioulia Rouzina, and Mark C. Williams

Erratum to: Selection of Structure-Switching DNA Aptamers Binding Soluble Small Molecules and SPR Validation of Enrichment E1

Index *333*

The original version of this book was revised. An erratum to this book can be found at https://doi.org/10.1007/978-1-4939-8582-1_22

Contributors

Abimbola Feyisara Adedeji • *Centro di Coordinamento Regionale per le Malattie Rare, Azienda Sanitaria Universitaria Integrata di Udine, Udine, Italy; School of Food Science and Nutrition, University of Leeds, Leeds, UK*

Hanie Ahmadzade Kermani • *Department of Life Science Engineering, Faculty of New Science and Technologies, University of Tehran, Tehran, Iran*

Aleksei Aksimentiev • *Department of Physics, University of Illinois, Urbana–Champaign, Urbana, IL, USA*

Elena Ambrosetti • *Department of Medical Biochemistry and Biophysics (MBB), Karolinska Institutet, Stockholm, Sweden; Nanoinnovation Lab—Elettra Sincrotrone Trieste, Trieste, Italy*

Alessandro Bertucci • *Institut de Science et d'Ingénierie Supramoléculaires (ISIS), Université de Strasbourg, Strasbourg, France*

Frank F. Bier • *IZI Branch Bioanalytics and Bioprocesses (IZI-BB), Fraunhofer Institute for Cell Therapy and Immunology, Potsdam-Golm, Germany; Institute of Biochemistry and Biology, University of Potsdam, Potsdam-Golm, Germany*

Loredana Casalis • *Nanoinnovation Lab—Elettra Sincrotrone Trieste, Trieste, Italy*

Matteo Castronovo • *School of Food Science and Nutrition, University of Leeds, Leeds, UK*

Luisa de Cola • *Institut de Science et d'Ingénierie Supramoléculaires (ISIS), Université de Strasbourg, Strasbourg, France*

Roberto Corradini • *Department of Chemistry, Life Sciences and Environmental Sustainability, University of Parma, Parma, Italy*

Andrea Csàki • *Leibniz Institute of Photonic Technologies, Jena, Germany*

Mehdi Dadmehr • *Department of Biotechnology, Payeme Noor University, Tehran, Iran*

Claudia Dalmastri • *ENEA, Centro Ricerche Casaccia, Rome, Italy*

Katherine E. Dunn • *Department of Electronic Engineering, University of York, HeslingtonYork, UK; Institute for Bioengineering, School of Engineering, University of Edinburgh, Edinburgh, Scotland, UK*

Mark Freeley • *School of Biological and Chemical Sciences, Queen Mary University of London, London, UK*

Wolfgang Fritzsche • *Leibniz Institute of Photonic Technologies, Jena, Germany*

Roberto Gambari • *Department of Life Sciences and Biotechnology, University of Ferrara, Ferrara, Italy*

Guido Grundmeier • *Technical and Macromolecular Chemistry, Paderborn University, Paderborn, Germany*

Carlotta Guiducci • *Institute of Bioengineering, Ecole Polytechnique Fédérale De Lausanne (EPFL), Lausanne, Vaud, Switzerland*

Weihua Han • *Centro NAST, Università di Tor Vergata, Rome, Italy; School of Physical Science and Technology, Lanzhou University, Lanzhou, China*

Ralph Hölzel • *IZI Branch Bioanalytics and Bioprocesses (IZI-BB), Fraunhofer Institute for Cell Therapy and Immunology, Potsdam-Golm, Germany; School of Physical Science and Technology, Lanzhou University, Lanzhou, China*

Morteza Hosseini • *Department of Life Science Engineering, Faculty of New Science and Technologies, University of Tehran, Tehran, Iran*

Da Huang • *School of Biological and Chemical Sciences, Queen Mary University of London, London, UK*
Andrea Idili • *Department of Chemistry, University of Rome Tor Vergata, Rome, Italy*
Steven Johnson • *Department of Electronic Engineering, University of York, York, UK*
Adrian Keller • *Technical and Macromolecular Chemistry, Paderborn University, Paderborn, Germany*
Alexander Kotlyar • *Department of Biochemistry & Molecular Biology, The George S. Wise Faculty of Life Sciences, Tel Aviv University, Ramat Aviv, Israel*
Eva-Maria Laux • *IZI Branch Bioanalytics and Bioprocesses (IZI-BB), Fraunhofer Institute for Cell Therapy and Immunology, Potsdam-Golm, Germany*
Marco Lazzarino • *IOM-CNR Laboratorio TASC, Trieste, Italy*
Chen-Yu Li • *Department of Physics, University of Illinois, Urbana–Champaign, Urbana, IL, USA*
Li Li • *Shanghai Key Laboratory of Green Chemistry and Chemical Processes, School of Chemistry and Molecular Engineering, East China Normal University, Shanghai, P. R. China*
Veikko Linko • *Biohybrid Materials, Department of Bioproducts and Biosystems, Aalto University, Aalto, Finland*
Rachel C. Little • *School of Chemistry, Newcastle University, Newcastle Upon Tyne, UK*
Christopher Maffeo • *Department of Physics, University of Illinois, Urbana–Champaign, Urbana, IL, USA*
Alex Manicardi • *Department of Chemistry, Life Sciences and Environmental Sustainability, University of Parma, Parma, Italy*
Valentina Masciotti • *Università Degli Studi di Trieste, Trieste, Italy; IOM-CNR Laboratorio TASC, Trieste, Italy*
Micah J. McCauley • *Department of Physics, Northeastern University, Boston, MA, USA*
Andrea Miti • *Department of Pharmacy and Biotechnology, University of Bologna, Bologna, Italy*
Piero Morales • *ENEA, Centro Ricerche Casaccia, Rome, Italy; Centro NAST, Università di Tor Vergata, Rome, Italy*
Denys Naumenko • *IOM-CNR Laboratorio TASC, Trieste, Italy*
Matteo Palma • *School of Biological and Chemical Sciences, Queen Mary University of London, London, UK*
Hao Pei • *Shanghai Key Laboratory of Green Chemistry and Chemical Processes, School of Chemistry and Molecular Engineering, East China Normal University, Shanghai, P. R. China*
Luca Piantanida • *IOM-CNR Laboratorio TASC, Trieste, Italy; Department of Physics, Durham University, Durham, UK*
Andrew R. Pike • *School of Chemistry, Newcastle University, Newcastle Upon Tyne, UK*
Xiangmeng Qu • *Shanghai Key Laboratory of Green Chemistry and Chemical Processes, School of Chemistry and Molecular Engineering, East China Normal University, Shanghai, P. R. China*
Saminathan Ramakrishnan • *Technical and Macromolecular Chemistry, Paderborn University, Paderborn, Germany*
Francesco Ricci • *Department of Chemistry, University of Rome Tor Vergata, Rome, Italy*
Ioulia Rouzina • *Department of Chemistry and Biochemistry, The Ohio State University, Columbus, OH, USA*
Nadrian C. Seeman • *Department of Chemistry, New York University, New York, NY, USA*

Boxuan Shen • *Department of Physics, Nanoscience Center, University of Jyväskylä, Jyväskylä, Finland; Biohybrid Materials, Department of Bioproducts and Biosystems, Aalto University, Aalto, Finland*

Simone Silvestrini • *Institut de Science et d'Ingénierie Supramoléculaires (ISIS) Université de Strasbourg, Strasbourg, France*

Scott Michael Slone • *Department of Physics, University of Illinois, Urbana–Champaign, Urbana, IL, USA*

Fabio M. Spiga • *Institute of Bioengineering, Ecole Polytechnique Fédérale De Lausanne (EPFL), Lausanne, Vaud, Switzerland*

Enrico Tenaglia • *Institute of Bioengineering, Ecole Polytechnique Fédérale De Lausanne (EPFL), Lausanne, Vaud, Switzerland*

Sophie Thamm • *Leibniz Institute of Photonic Technologies, Jena, Germany*

J. Jussi Toppari • *Department of Physics, Nanoscience Center, University of Jyväskylä, Jyväskylä, Finland*

Martin A. Trefzer • *Department of Electronic Engineering, University of York, York, UK*

Eimer M. Tuite • *School of Chemistry, Newcastle University, Newcastle Upon Tyne, UK*

Andy M. Tyrrell • *Department of Electronic Engineering, University of York, York, UK*

Stefano Vespucci • *Centro NAST, Università di Tor Vergata, Rome, Italy*

Liqian Wang • *Centro NAST, Università di Tor Vergata, Rome, Italy; Division of Physical Biology, Shanghai Institute of Applied Physics, Shanghai, China*

Colette J. Whitfield • *School of Chemistry, Newcastle University, Newcastle Upon Tyne, UK*

Mark C. Williams • *Department of Physics, Northeastern University, Boston, MA, USA*

Mingshu Xiao • *Shanghai Key Laboratory of Green Chemistry and Chemical Processes, School of Chemistry and Molecular Engineering, East China Normal University, Shanghai, P. R. China*

Jejoong Yoo • *Department of Physics, University of Illinois, Urbana–Champaign, Urbana, IL, USA*

Giampaolo Zuccheri • *Department of Pharmacy and Biotechnology, University of Bologna, Bologna, Italy*

Chapter 1

DNA Nanotechnology: From the Pub to Information-Based Chemistry

Nadrian C. Seeman

Abstract

The founding of structural DNA nanotechnology is described, birth pangs and all by the originator of the field. The excitement of the invention, the characters, and the roles are evident as a true celebration of scientific research.

Key words DNA Motifs, DNA Nanomechanical Devices, Self-Assembled DNA Crystals, Guests in DNA Crystals

Starting on August 23, 1977, I spent 4000 days on the biology faculty of SUNY/Albany. OK, really only 3983 days, but I round off. Just about every aspect of my life there was awful. I had had a very successful postdoctoral period as a biological crystallographer with Alex Rich at MIT, but then, when it came to finding a faculty position, this was the best I could do. On the depressing drive from Boston to Albany, injury was added to insult, when I pulled the transmission out of my car, and my arrival was delayed. I'd chosen the 50th anniversary of Sacco and Vanzetti's notoriously unjust execution as the most appropriate date to leave Boston, but did not get to Albany until the next day, owing to the breakdown.

SUNY/Albany had only recently (1963) started the transition from a teacher's college to a research university, and the previous teaching faculty was still about a quarter of the department. At my first faculty meeting, one of the teaching faculty stood up and stated that he could no longer support the presence of a Ph.D. program in the department because it had just hired a crystallographer (me). This guy was in charge of advisement, the assignment of undergraduates to faculty to "advise" them about courses and what to do about their failing attempts to enter the health professions. Since he disliked me because of my scientific bent, he always assigned me the

Giampaolo Zuccheri (ed.), *DNA Nanotechnology: Methods and Protocols*, Methods in Molecular Biology, vol. 1811,
https://doi.org/10.1007/978-1-4939-8582-1_1, © Springer Science+Business Media, LLC, part of Springer Nature 2018

least tractable advisees, often the ones with the largest senses of entitlement.

Fast-forward 1.5 years. During that time, I had recruited no graduate students from the pool of available candidates, largely mathophobic failed pre-meds who had joined the department as a holding pattern to figure out what to do with their lives, now that the health professions seemed closed to them. Without a graduate student labor force, I had been forced to depend on unreliable postdocs and undergraduates in a vain attempt to grow crystals. I had started a side-effort modeling the Holliday junction recombination intermediate, at the suggestion of Bruce Robinson, then a postdoc in the department. It was really closer to a scholastic than a scientific effort because naturally occurring Holliday junctions branch migrate, so any population is polydisperse: hence, there was no way at the time to test any hypotheses that might arise from our modeling. I took a plane trip with Greg Petsko to the American Crystallographic Association meeting in Honolulu, where he discussed an idea he had to trap oxygenation intermediates of hemoglobin. He planted a germ in my head that a reaction intermediate, such as the Holliday junction, could be trapped by cunning chemistry. Shortly after I came back from Hawaii, I realized that by trashing their symmetry, immobile Holliday junction intermediates could be obtained synthetically by using the right (synthetic) sequences; this realization turned the scholastic project into a scientific one. I was very excited and told everyone I saw. One of these people asked me if I could make a molecule with more than the four arms of a Holliday junction. I thought about it and realized that the sequence-symmetry rules, combined with inherent physical constraints, would enable the construction of junctions with up to eight arms.

Fast-forward another 16 months to the fall of 1980. The layout of my building put my office about 100 m from the men's room. One day I'm in there, in a stall, when the door opens and one of the undergraduates with a large sense of entitlement yells, "Is Ned Seeman in here?" I answered that I was and wanted to know what was going on. The student replied, "You're my Advisor!" To escape this type of harassment, I went to the campus pub to think about six-arm junctions.

The easiest way to draw any junction is as a planar starburst, looking like an intersection in a highway: Two roads intersecting with tetragonal symmetry form a four-arm Holliday junction (*see* Fig. 1). However, while having my first beer, I suddenly thought of Escher's woodcut, "Depth" (*see* Fig. 2). I recognized that the six-arm junction need not be thought of having coplanar helix axes, but could be three dimensional, like the fish in "Depth": Starting from the middle of the fish, there is a head, a tail, a top fin, a bottom fin, a left fin, and a right fin. However, something about "Depth" was far more important to me, a crystallographer

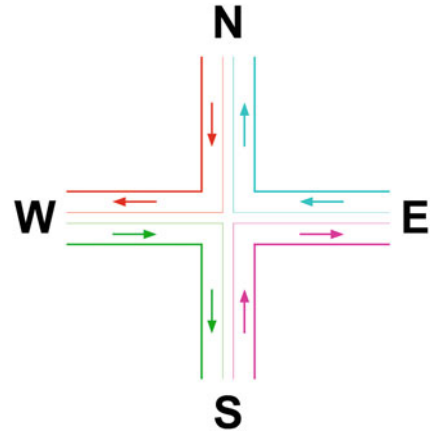

Fig. 1 *A Four-Way Intersection*. Four different roads, coming from the north, west, south, and east are shown, analogous to a 4-arm DNA-branched junction. The flow of traffic through the intersection is color coded, with the direction of traffic (in right-hand drive countries) indicated by arrows. Similar to DNA, each road has traffic going in two antiparallel directions

without crystals. The fish in it were organized just like the molecules in a molecular (or macromolecular) crystal, with periodicity relating parallel molecules front to back, left to right, and top to bottom. One difficulty with the crystallization experiment is that one has no idea which specific interactions to promote, hydrophobic, hydrophilic, salt bridges, or all at once in different directions. The key insight I had, the founding epiphany of DNA nanotechnology, was that one could use programmable "sticky ends" (*see* Fig. 3) to connect branched nucleic acid molecules into N-connected objects or lattices [1]. For example, a set of 83-arm junctions could be connected to form a molecule with the connectivity of a cube or a rhombohedron (*see* Fig. 4), such as Junghuei Chen and I reported in 1991 [2]. Of course, the goal was not merely to make nucleic acid crystalline constructs, but also to have them act as host lattices for macromolecular guests, a goal only partially realized today.

1991—Whoa!! That's a long way from 1980. Nothing happened quickly, at least for me. I was a crystallographer and had no clue how to obtain the oligonucleotides needed for DNA nanotechnology. I spent the summer of 1982 in Leiden, learning how to make oligonucleotides, and then it was three more years before we were really any good at it, i.e., it was 3 years until I was able to get a DNA synthesizer, and another year or so to get confident enough with it to make the 80-mer strands used in the construction of the cube. The paucity of graduate students in Albany was a severe handicap, one which I was unable to correct until I moved to the chemistry department at NYU in 1988. When we tried to publish the cube, we sent it to a journal where one reviewer said it

Fig. 2 *M.C. Escher's "Depth"*, Copyright 2017, The M.C. Escher Company-The Netherlands, All Rights Reserved. This image inspired the field of Structural DNA Nanotechnology. The fish are analogous to 6-arm junctions: Starting from their centers, they have a head, a tail, a top fin, a bottom fin, a right fin, and a left fin. In addition, they are organized like the molecules in a molecular crystal, demonstrating periodicity front to back, left to right, and top to bottom

represented the founding of a new field, and the other said, "Where's the biology?" There was none, and I could not convince the editor that biology was not necessary. When we sent it to *Nature*, one of the reviewers said about the revised version that he was convinced that we hadn't done what we claimed to have done, but could not say what was wrong. Fortunately, the editor there agreed with me.

Although the objects were never a key target, this publication was central in demonstrating that N-connected DNA species were not just a pipe dream. However, my goal was always self-assembled crystals. The first step in that process was to obtain a motif that was not floppy. It took a couple of passes to do that, but the double crossover (DX) motif was eventually shown by Xiaoping Yang, Xiaojian Li, and Jing Qi to be robust [3]. This enabled us, in

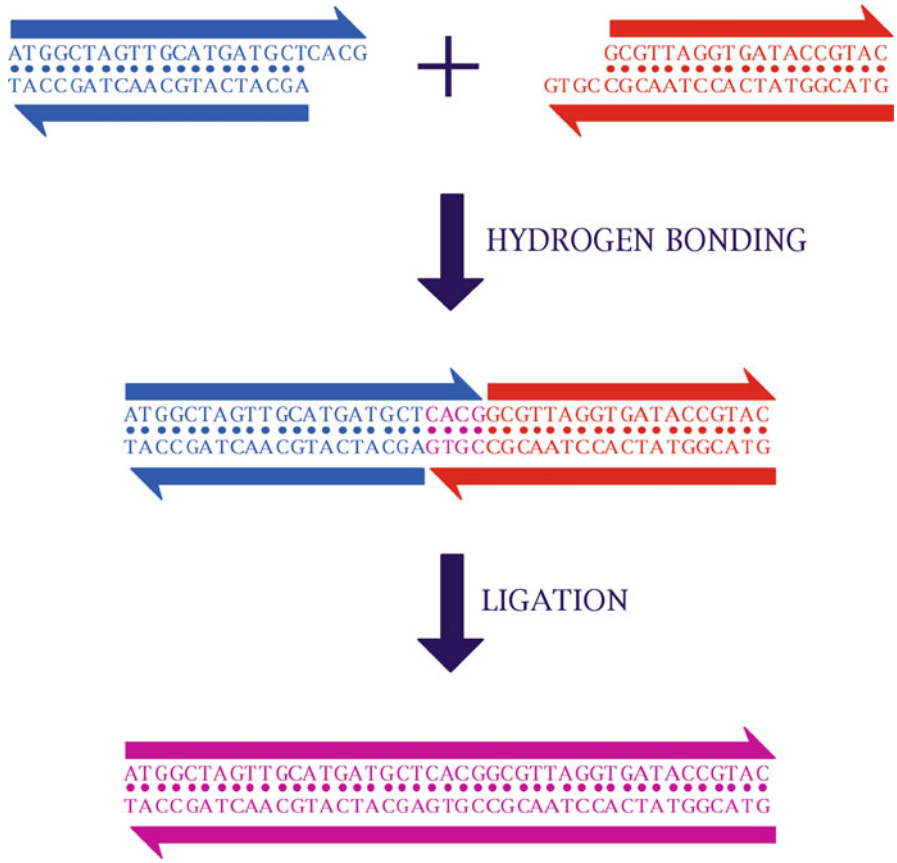

Fig. 3 *Sticky-Ended Cohesion*. Two unwound double helices are shown at the top. Their strands are slightly different lengths, creating overhangs that are called sticky ends. If the sticky ends are complementary and conditions are proper, the two molecules can cohere, as shown in the middle. It is possible to join the ends covalently by enzymatic (or sometimes nonenzymatic) ligation

collaboration with Erik Winfree, to self-assemble a 2D-patterned DNA lattice, which was reported in 1998 [4].

Of course the real goal was the self-assembly of 3D lattices. Virtually, all the motifs that we developed were characterized by parallel helix axes, and none of them proved to diffract at all. It was nearly another decade before my former student Chengde Mao developed the "tensegrity triangle" motif [5]. This motif contains three helices whose axes span 3-space. We don't completely understand why, but this robust motif self-assembled to yield crystals that diffract adequately for nucleic acids (*see* Fig. 5). It was not until 2009, 29 years after my afternoon in the Albany pub, that we published our first report of a self-assembled 3D crystal that diffracts well enough that its structure can be ascertained [6].

Another direction was initiated in 1999 when Chengde Mao was able to demonstrate a DNA nanomechanical device, one that changed shape as a consequence of the B ↔ Z transition [7]. This

Fig. 4 DNA Polyhedral Catenanes. A molecule with the connectivity of a cube or a rhombohedron

was a milestone, but not one of which I was overly fond, because I wanted to have a number of orthogonal devices in solution at once. About a year later, Bernie Yurke and his colleagues first demonstrated the toehold principle in a tweezers device that sometimes rearranged its strands during the transition [8]. In 2002, Hao Yan in our lab was able to make a robust toehold-based device that switched between the PX state and the JX_2 state, so that one end of it rotated a half-turn relative to the other [9]. Other devices included a clocked walker built by Bill Sherman [10], and an autonomous walker built by Tosan Omabegho [11]. An early example of combining a 2D lattice with a nanomechanical device was produced by Baoquan Ding, where the PX-JX_2 device was placed in a 2D array [12].

I was not trained as a chemist, but I quickly adopted the notion that purified material was probably better to use than unpurified material. A number of people were starting to get interested in what DNA nanotechnology could do, e.g., organize nanoparticles [13], but few of them came from chemistry or biochemistry, where purification was part of the mindset; consequently, physicists and computer scientists were not prominent among the practitioners. This changed completely with Paul Rothemund's development of DNA origami in 2006 [14]. He used typically an M13 single-stranded DNA of approximately 7250 nt of length to which he paired about 200–250 "staple" strands that folded it into any desired shape, starting with his iconic "smiley face." Key to the popularity of origami was the fact that strands that interacted only

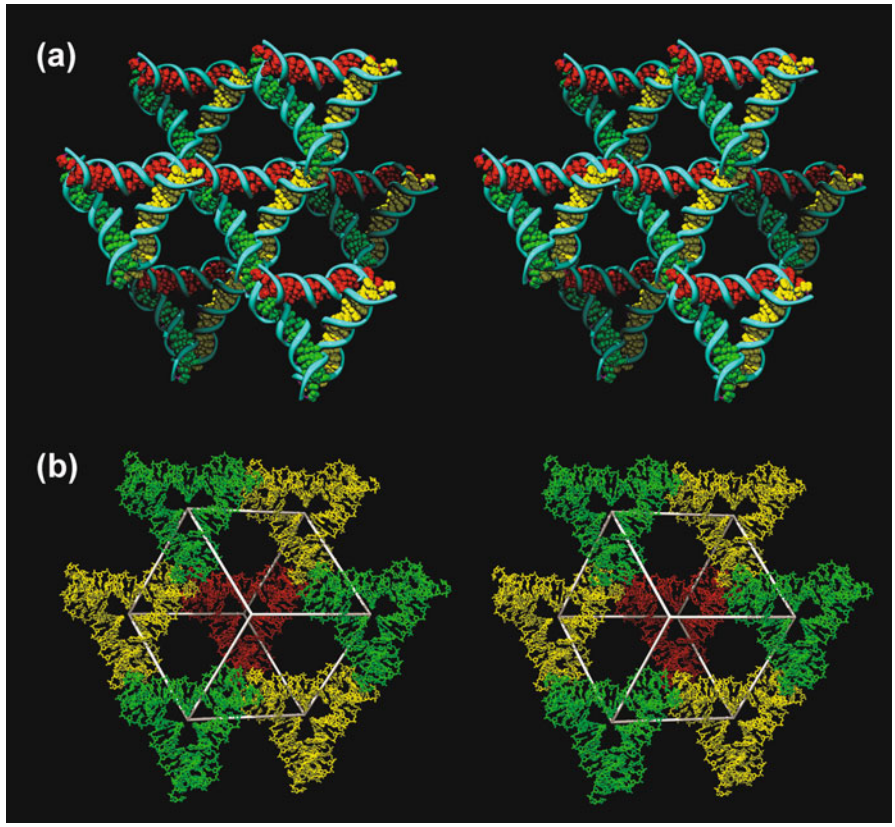

Fig. 5 *Stereographic Images of the Crystal Structure Built from Tensegrity Triangles.* (**a**) *The Surroundings of a Triangle*. Each triangle is joined to six other triangles by sticky-ended cohesion. The schematic shows that the three directions defined by the helix axes span 3-space. The red direction goes from rear to front, as does the green direction and the yellow direction. (**b**) *Eight Triangles Surround the Vertices of a Rhombohedron*. The red triangle sits on the rear vertex of a rhombohedron. It is connected to the three yellow triangles that flank vertices nearer to the viewer. The yellow triangles are connected to the green triangles that flank vertices nearer yet to the viewer. The front vertex has been left vacant for clarity, but would contain another red triangle

with the scaffold did *not* require purification. When we incorporated the PX-JX_2 device into a 2D array, it required 8 TX (three parallel helix axes) molecules in the crystalline repeat. The area covered by these eight molecules was about a third of a typical origami construct. Thus, origami was easier than the smaller constructs, and it avoided the costs of purification. It should be noted, however, that if a strand is interacting with anything other than the scaffold, purification is still required. William Shih and his students shortly thereafter moved origami into the third dimension [15]. Another popular method was invented by Peng Yin, the so-called bricks, in 2D [16] and 3D [17]. They are similar to origami in that a large number of strands are used, but their sequences and numbers are not constrained by the need for a scaffold.

In our lab, one of the first things we did with DNA origami was to use it as a surface on which to build a 3-step nanoscale assembly line [18]. When this project was performed by Hongzhou Gu and Jie Chao, it was clearly much simpler than using a 2D array, which would have required about 25 TX tiles. Of course, what about crystals of origami? We had a number of failures in 2D, until Wenyan Liu recognized that a better array would be available if the helix axes of the origami spanned 2-space; when that worked [19], we recognized that Chengde's tensegrity triangle motif also obeyed the same rule, that we call Wenyan Liu's rule: For N dimensions, use motifs whose helix axes span N-space.

Since the 1980s, the vision of DNA nanotechnology has included oriented guests, and the organization of nanoelectronic components. The first has been achieved roughly in 3D [20], and many workers are organizing nanoparticles and carbon nanotubes using DNA components. Recently, we have demonstrated that strands can be diffused in and out of crystals, indicating that machines can work in 3D [21]. It is impossible to acknowledge all of the work that has been done in the field, particularly with origami, involving logic and drug delivery. At my last count, there are well over 400 laboratories that have published in the area of DNA nanotechnology. The field has grown very rapidly during this century, and there are no indications that its growth is slowing down!

References

1. Seeman NC (1982) Nucleic acid junctions and lattices. J Theor Biol 99(2):237–247
2. Chen JH, Seeman NC (1991) The synthesis from DNA of a molecule with the connectivity of a cube. Nature 350(6319):631–633
3. Li XJ, Yang XP, Qi J, Seeman NC (1996) Antiparallel DNA double crossover molecules as components for nanoconstruction. J Am Chem Soc 118(26):6131–6140. https://doi.org/10.1021/Ja960162o
4. Winfree E, Liu FR, Wenzler LA, Seeman NC (1998) Design and self-assembly of two-dimensional DNA crystals. Nature 394:539–544. https://doi.org/10.1038/28998
5. Liu D, Wang MS, Deng ZX, Walulu R, Mao CD (2004) Tensegrity: construction of rigid DNA triangles with flexible four-arm DNA junctions. J Am Chem Soc 126 (8):2324–2325. https://doi.org/10.1021/ja031754r
6. Zheng JP, Birktoft JJ, Chen Y, Wang T, Sha RJ, Constantinou PE, Ginell SL, Mao CD, Seeman NC (2009) From molecular to macroscopic via the rational design of a self-assembled 3D DNA crystal. Nature 461(7260):74–77. https://doi.org/10.1038/nature08274
7. Mao CD, Sun WQ, Shen ZY, Seeman NC (1999) A nanomechanical device based on the B-Z transition of DNA. Nature 397:144–146
8. Yurke B, Turberfield AJ, Mills AP, Simmel FC, Neumann JL (2000) A DNA-fuelled molecular machine made of DNA. Nature 406:605–608
9. Yan H, Zhang XP, Shen ZY, Seeman NC (2002) A robust DNA mechanical device controlled by hybridization topology. Nature 415:62–65. https://doi.org/10.1038/415062a
10. Sherman WB, Seeman NC (2004) A precisely controlled DNA biped walking device. Nano Lett 4(9):1801–1801. https://doi.org/10.1021/nl048887a
11. Omabegho T, Sha R, Seeman NC (2009) A bipedal DNA Brownian motor with coordinated legs. Science 324:67–71. https://doi.org/10.1126/science.1170336
12. Ding B, Seeman NC (2006) Operation of a DNA robot arm inserted into a 2D DNA

crystalline substrate. Science 314:1583–1585. https://doi.org/10.1126/science.1131372

13. Zheng JW, Constantinou PE, Micheel C, Alivisatos AP, Kiehl RA, Seeman NC (2006) Two-dimensional nanoparticle arrays show the organizational power of robust DNA motifs. Nano Lett 6(7):1502–1504. https://doi.org/10.1021/nl060994c
14. Rothemund PWK (2006) Folding DNA to create nanoscale shapes and patterns. Nature 440:297–302
15. Douglas SM, Dietz H, Liedl T, Hogberg B, Graf F, Shih WM (2009) Self-assembly of DNA into nanoscale three-dimensional shapes. Nature 459:414–418. https://doi.org/10.1038/nature08165
16. Wei B, Dai MJ, Yin P (2012) Complex shapes self-assembled from single-stranded DNA tiles. Nature 485:623–626. https://doi.org/10.1038/nature11075
17. Ke YG, Ong LL, Shih WM, Yin P (2012) Three-dimensional structures self-assembled from DNA bricks. Science 338:1177–1183. https://doi.org/10.1126/science.1227268
18. Gu HZ, Chao J, Xiao SJ, Seeman NC (2010) A proximity-based programmable DNA nanoscale assembly line. Nature 465:202–205. https://doi.org/10.1038/nature09026
19. Liu WY, Zhong H, Wang RS, Seeman NC (2011) Crystalline two-dimensional DNA-origami arrays. Angew Chem Int Ed Engl 50 (1):264–267. https://doi.org/10.1002/anie.201005911
20. Zhao Y, Sha Y, Hao YD, Hernandez C, Birktoft JJ, Rusling DA, Chandrasekaran AR, Mao C, Seeman N DNA triplex binding examined in self-assembled DNA crystals. Paper presented at: FNANO, Snowbird, UTAH, U.S.A., 10–13 April, 2017
21. Hao YD, Kristiansen M, Sha RJ, Birktoft JJ, Hernandez C, Mao CD, Seeman NC (2017) A device that operates within a self-assembled 3D DNA crystal. Nat Chem 9(8):824–827. https://doi.org/10.1038/Nchem.2745

Chapter 2

The Synthesis of Designer DNA

Rachel C. Little, Colette J. Whitfield, Eimer M. Tuite, and Andrew R. Pike

Abstract

The synthesis of designer DNA requires an approach where the user can determine both the sequence and the number of nucleobases. The protocol outlined here describes an enzymatic method for the synthesis of long repeat-sequence DNA. The method utilizes a PCR-based approach; starting with short oligo-seeds, c.a. 20 bp, bearing a minimum of two repeating units of >8 bp sequences. During each heat-cool cycle, the oligo-seeds reanneal imperfectly leaving an overhang, which is then extended by the polymerase. The final length of the DNA is determined by the number of heat-cool cycles performed, reaching up to 20,000 bp after 20 cycles.

Key words DNA, Polymerase, Nanomaterials, PCR

1 Introduction

Short DNA oligonucleotides have been aggressively exploited by many research groups to construct a wide variety of nanostructures, including Holliday junctions, DNA tiles, and DNA origami [1–3]. Of these approaches, DNA origami also relies on a much longer DNA template strand (usually >7000 nt), which, as the technique suggests, is folded into the desired structure through complementary interactions with many short staple oligonucleotides. Short oligonucleotides are routinely produced by automated DNA synthesis but are limited in length (due to decreasing yield beyond 100-mers), restricted by sequence (multiple G bases are not easily incorporated), and can be expensive upon modification (tedious and costly synthesis of modified-phosphoramidites is required) [4, 5]. Therefore, having access to DNA of user-defined composition, which is longer than 100 bp would be an attractive and alternative route for the development of an even wider range of post-DNA origami nanoarchitectures.

This chapter describes an enzymatic methodology based on a PCR heat-cool cycle approach for the synthesis of designer DNA [6]. The protocol relies on the design of a starting oligo-seed of the

Giampaolo Zuccheri (ed.), *DNA Nanotechnology: Methods and Protocols*, Methods in Molecular Biology, vol. 1811, https://doi.org/10.1007/978-1-4939-8582-1_2, © Springer Science+Business Media, LLC, part of Springer Nature 2018

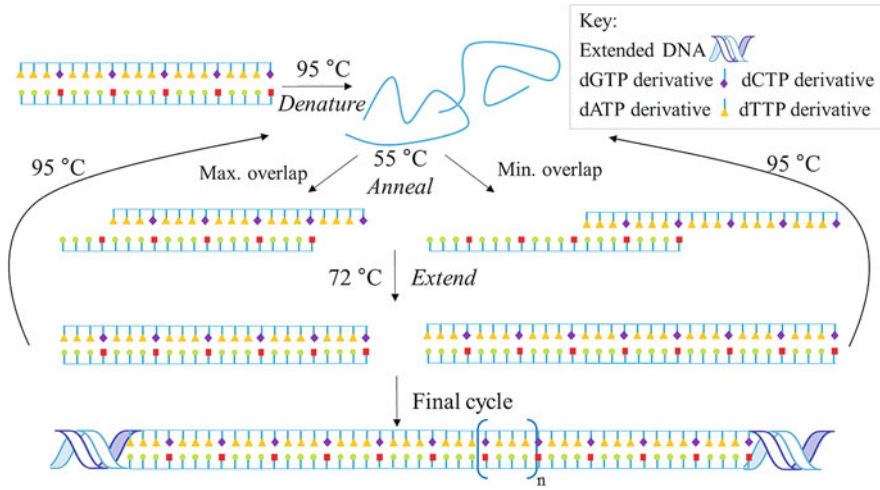

Scheme 1 DNA extension heat-cool cycles showing how a $[A_3G]_5/[T_3C]_5$ oligo-seed can be extended to give a range of products $[A_3G]_n/[T_3C]_n$, where n is any integer >5 determined by the number of cycles performed. Initially, DNA is heated to 95 °C to denature, then cooled to 55 °C to reanneal, followed by incubation at 72 °C to allow the DNA polymerase to extend the sticky ends

form; $[X]_2/[Y]_2$, where X and Y are any complementary sequences of over 8 bp. The synthesis of long DNA proceeds by a denaturation step at 95 °C followed by the incomplete annealing of the duplexes at 55 °C to form "sticky ends," an overhang of X on one end, and of Y on the opposite. During the final extension step at 72 °C, a polymerase of the general exonuclease minus variant adds one more X and Y sequence at the respective ends to yield the product; $[X]_3/[Y]_3$. This heat-cool cycle is repeated until the desired length of designer DNA is achieved, $[X]_n/[Y]_n$. Products over 20,000 bp can be routinely realized (*see* Scheme 1 for an overview of the method).

The $[X]_n/[Y]_n$ product will however contain a range of different lengths of DNA, as evidenced by long streaks in an electrophoretic gel (*see* Fig. 1). Narrow distribution bands can be extracted via a size recovery gel technique (*see* Fig. 2). The Lonza flash gel system™ is exploited to aid simple recovery of user-defined DNA lengths determined by a DNA ladder running adjacent to the extension product. The product is then visualized by AFM (*see* Fig. 3). In summary, the methodology described here can be utilized to synthesize designer DNA, of predetermined sequence and length.

2 Materials

All solutions should be prepared using ultrapure water (18.2 MΩ cm at 25 °C).

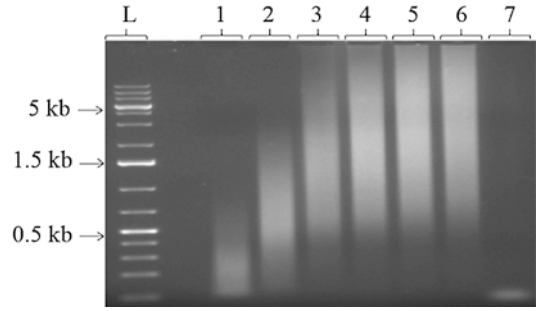

Fig. 1 Agarose gel of DNA extension products after 5, 10, 15, 20, 25, and 30 heat-cool cycles (lanes 1–6, respectively). Lane 7 contains the oligo-seeds and Lane L is a 75–20,000 bp DNA ladder

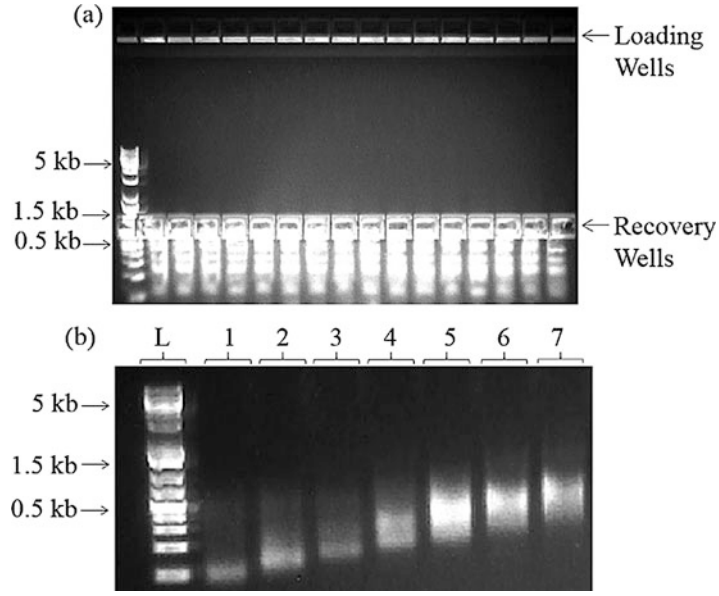

Fig. 2 (**a**) Lonza FlashGel size extraction of DNA of the desired length as the $[A_3GA_3G]_n/[T_3CT_3C]_n$ products move through a two-tiered recovery gel. The black gaps within the distribution of the DNA below the recovery wells shows where the DNA has been extracted. (**b**) Agarose gel of size recovered DNA products (lanes 1–7), showing narrower size distribution within each sample, Lanes 1–7, Lane L is a 75–20,000 bp DNA ladder

2.1 DNA Extension

1. Deoxyoligonucleotides (*see* **Note 1**) are purchased lyophilized (High Purity Salt Free) from Eurofins Genomics, Germany.
2. Deoxynucleotide triphosphates (dNTPs).
3. Exonuclease minus thermostable DNA polymerase (*see* **Note 2**).
4. DNA polymerase reaction buffer (*see* **Note 3**).
5. A thermocycler.

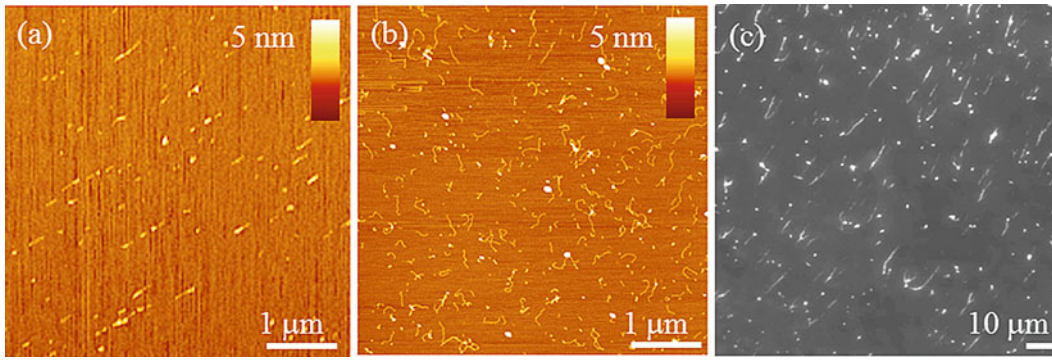

Fig. 3 AFM images of DNA extension products of 500 bp (with a contour length of about 170 nm) and 1500 bp (510 nm) in (**a**) and (**b**), respectively. (**c**) Fluorescence microscopic image of a 7000 bp (2400 nm) DNA extension product

6. 2 μL to 1 mL automatic pipettes.
7. Pipette tips.
8. 70% ethanol.
9. 1.5 mL micro-centrifuge tubes.
10. 0.2 mL PCR tubes.
11. Vortex mixer.

2.2 Purification and Characterization of Extended DNA

1. DNA purification kit such as the Qiagen QIAquick PCR purification kit.
2. Micro-centrifuge.
3. 1.5 mL micro-centrifuge tubes.
4. UV-Vis spectrophotometer.
5. Agarose.
6. DNA ladder (*see* **Note 4**).
7. 10× TBE buffer: Dissolve 121.1 g Tris base (tris(hydroxymethyl)aminomethane) (buffered to pH 8.3 with HCl), 61.8 g boric acid, and 7.4 g ethylenediaminetetraacetic acid (EDTA) in 1 L of distilled water.
8. 1× TBE buffer (running and gel buffer): Dilute 100 mL 10× TBE with 900 mL water to produce a 1× TBE solution.
9. DNA stain (*see* **Note 5**).
10. 6× DNA loading dye (*see* **Note 6**): 30% glycerol, 10 mM Tris–HCl, pH 7.6, 60 mM EDTA, 0.03% bromophenol blue (BPB), 0.03% xylene cyanol FF (XC) (*see* **Note 7**). First, prepare 100 mM Tris–HCl, pH 7.6 by the addition of 1.21 g Tris to 90 mL water and adjust to pH 7.6 by adding HCl dropwise and then making up to 100 mL with water. Prepare 1% weight to volume solutions of both BPB and XC by the addition of

0.01 g to 1 L water. Prepare 1 M EDTA by the addition of 2.92 g EDTA to 10 mL water. In a 30 mL tube, add 3 mL glycerol, 1 mL 100 mM Tris–HCl, pH 7.6, 300 µL of each 1% BPB and XC solution and 600 µL 1 M EDTA and make up to 10 mL with water.

11. Pipettes.
12. Pipette tips.
13. Gel cast.
14. Gel comb.
15. Electrophoresis power supply.
16. Trans-illuminator.
17. Two 100 mL liquid storage containers.
18. Four 1 L liquid storage containers.
19. A screw-cap 30 mL tube.
20. 1.5 mL micro-centrifuge tubes.

2.3 Size Recovery

1. Lonza FlashGel™ system.
2. Lonza FlashGel DNA Cassette, 1.2%, 16 + 1 well, double tier.
3. DNA ladder (*see* **Note 4**).
4. 6× DNA loading dye (*see* **Note 6**): 30% glycerol, 10 mM Tris–HCl, pH 7.6, 60 mM EDTA, 0.03% BPB, 0.03% XC (*see* **Note 7**): First prepare 100 mM Tris–HCl, pH 7.6 by the addition of 1.21 g Tris to 90 mL water and adjust to pH 7.6 by adding HCl dropwise and then make up to 100 mL with water. Prepare 1% weight to volume solutions of both BPB and XC by the addition of 0.01 g to 1 L water. Prepare 1 M EDTA by the addition of 2.92 g EDTA to 10 mL water. To a 30 mL screw-cap tube, add 3 mL glycerol, 1 mL 100 mM Tris–HCl, pH 7.6, 300 µL of each 1% BPB and XC solution, and 600 µL 1 M EDTA and make up to 10 mL with water.
5. Elution buffer: 10 mM Tris–HCl, pH 8.5.
6. 2 mL micro-centrifuge tubes.

2.4 Purification and Characterization of Isolated Designer DNA

1. Micro-centrifuge.
2. UV-Vis spectrophotometer.
3. Agarose (*see* **Note 8**).
4. DNA ladder (*see* **Note 4**).
5. 10× TBE buffer: Dissolve 121.1 g Tris base (buffered to pH 8.3 with HCl), 61.8 g boric acid, and 7.4 g EDTA in 1 L of distilled water.

2.4.1 Agarose Gel Electrophoresis

6. 1× TBE buffer (running and gel buffer): Dilute 100 mL 10× TBE with 900 mL water to produce a 1× TBE solution.
7. DNA stain (*see* **Note 5**).
8. 6× DNA loading dye (*see* **Note 6**): 30% glycerol, 10 mM Tris–HCl, pH 7.6, 60 mM EDTA, 0.03% BPB, 0.03% XC (*see* **Note 7**): first prepare 100 mM Tris–HCl, pH 7.6 by the addition of 1.21 g Tris to 90 mL water and adjust to pH 7.6 by adding HCl dropwise and then make up to 100 mL with water. Prepare 1% weight to volume solutions of both BPB and XC by the addition of 0.01 g to 1 L water. Prepare 1 M EDTA by the addition of 2.92 g EDTA to 10 mL water. To a 30 mL screw-cap tube, add 3 mL glycerol, 1 mL 100 mM Tris–HCl, pH 7.6, 300 μL of each 1% BPB and XC solution, and 600 μL 1 M EDTA and make up to 10 mL with water.
9. Gel cast.
10. Gel comb.
11. Electrophoresis power supply.
12. Trans-illuminator.
13. Two 100 mL liquid storage containers.
14. Four 1 L liquid storage containers.
15. A 30 mL screw-cap tube.
16. 1.5 mL micro-centrifuge tubes.

2.4.2 Atomic Force Microscopy (AFM) Sample Preparation

1. Mica.
2. 2 mM magnesium sulfate ($MgSO_4$): Dissolve 2.41 g of $MgSO_4$ in 10 mL of water.
3. Extended DNA sample.
4. Double-sided sticky tape.
5. A scanning probe microscopy mounting disc.
6. Scissors.
7. 1.5 mL micro-centrifuge tubes.
8. 0.5–10 μL automatic pipette.
9. Pipette tips.
10. Tweezers.
11. Nitrogen flow line.

3 Methods

3.1 DNA Extension

1. Clean all surfaces and pipettes with 70% ethanol solution.
2. Oligonucleotides were prepared by the addition of the required volume of water, (*see* **Note 9**) as stated by the supplier, to produce an end concentration of 100 μM.

3. In a 200 μL PCR tube (*see* **Note 10**), prepare a mix that is 0.5 μM deoxyoligonucleotides (*see* **Note 11**), 0.5 mM dNTPs (*see* **Note 12**), 1× DNA polymerase reaction buffer (*see* **Note 13**), and DNA polymerase (*see* **Note 14**) in a 20 μL (add water to volume). Reaction solutions are mixed by gentle pipetting.
4. Transfer the PCR tubes to the thermocycler.
5. Set the thermocycler to heat to 95 °C for 30 s, 55 °C for 30 s, and 72 °C for 30 s. Set the number of cycles to synthesize the desired length of DNA (*see* **Note 15**).
6. Perform the heat-cool cycles.
7. Store the samples at 4 °C until you are ready to purify them (*see* **Note 16**).

3.2 Purification and Characterization of Extended DNA

1. DNA purification can be performed using the DNA purification kit of choice and following the manufacturers protocol (*see* **Note 17**).
2. The concentration of DNA product is determined by reading the A_{260} on a UV-Vis spectrophotometer and multiplying by 50 ng/μL.
3. A 1% agarose gel is prepared by adding 1 g agarose per 100 mL of 1× TBE buffer and heating to dissolve (*see* **Note 18**). Allow the agarose to cool until hand hot and supplement with a DNA staining dye. Pour the gel into the cast with a comb (*see* **Note 19**) and allow to set for at least 30 min.
4. Add DNA loading dye to 20 μL of the extended DNA product and mix by gentle pipetting.
5. Load 20 μL of each sample into separate wells, ensuring there is space at either side for the DNA ladder.
6. Load 2–5 μL DNA ladder (*see* **Note 20**) into the wells at either side of the DNA samples (*see* **Note 21**).
7. Plug the electrodes into the electrophoresis power supply and set to 100 V (*see* **Note 22**).
8. Run the gel for 40–60 min and check how far it has run on a trans-illuminator (*see* **Note 23**). Run the gel until all the bands on the gel have separated.
9. Image the gel and note the maximum and minimum lengths produced to determine which lengths you would like to collect for the next part of the method.

3.3 Size Recovery

1. Prepare Lonza FlashGel Cassette (1.2%, 16 + 1 wells, double tier) by following the manufacturer's protocol.
2. Add 13.3 μL of 6× loading dye to 66.7 μL of approximately 50 ng/μL DNA sample to be recovered (*see* **Note 24**).
3. Load 2 μL of DNA ladder into the smallest of the wells.

4. Load 5 μL of the prepared DNA sample to the remaining wells.
5. Set the power supply to 200 V (*see* **Note 25**). Run the samples to just before the recovery wells. Stop the power supply and discard the waste from the wells. Fill the empty wells with 15 mL of elution buffer or water.
6. Restart the power supply and run the gel until the desired length of DNA is visible in the recovery wells (*see* **Note 26**). Stop the power supply and leave the gel to equilibrate for 1 min. Recover the solution from the wells into a 2 mL micro-centrifuge tube (*see* **Note 27**).
7. Refill each recovery well with 15 μL elution buffer or water.
8. Repeat **steps 7–9** until all the desired DNA lengths are recovered.

3.4 Purification and Characterization of Isolated Designer DNA

3.4.1 Purification and Agarose Gel Electrophoresis

1. DNA purification can be performed using the choice DNA purification kit and following the manufacturer's protocol (*see* **Note 28**).
2. The concentration of DNA product is determined by reading the A_{260} on a UV-Vis spectrophotometer and multiplying by 50 ng/μL.
3. A 1% agarose gel is prepared by adding 1 g agarose per 100 mL of 1× TBE buffer and heating to dissolve (*see* **Note 18**). Allow the agarose to cool until hand hot and supplement with a DNA staining dye. Pour the gel into the cast with a comb (*see* **Note 19**) and allow to set for at least 30 min (*see* **Note 29**).
4. Add DNA loading dye to 20 μL of the DNA product and mix by gentle pipetting.
5. Load 20 μL of each sample into separate wells ensuring there is space either side for the DNA ladder.
6. Load 2–5 μL DNA ladder (*see* **Note 20**) into the wells either side of the DNA samples (*see* **Note 21**).
7. Plug the electrodes into the power electrophoresis power supply and set to 100 V (*see* **Note 22**).
8. Run the gel for 40–60 min and check how far it has run on a trans-illuminator (*see* **Note 23**). Run the gel until all the bands on the gel have separated.
9. Image the gel.

3.4.2 AFM Sample Preparation

1. Dilute DNA samples to 5 ng/μL with water (*see* **Note 30**).
2. Add 2.5 μL diluted DNA sample to 2.5 μL of 2 mM $MgSO_4$.
3. Cut a 1 × 1 cm mica square.
4. Attach the mica to a mounting disc using double-sided sticky tape.

5. Remove a fresh layer of mica by placing single-sided sticky tape over the square and removing gently.
6. Tilt the disk at approximately 45° to the bench to provide a gradient for the DNA sample to descend.
7. Drop 5 μL of the 1 mM $MgSO_4$ DNA sample at the top of the mica surface.
8. Allow to incubate for 5 min.
9. Drop 5 μL of water at the same point on the mica surface.
10. Immediately pass a N_2 flow (*see* **Note 31**) in the same direction as the falling droplet until the droplet has passed over the mica surface.
11. Allow to dry under laminar flow for 1 h.
12. Analyze the sample by AFM.

4 Notes

1. Oligonucleotides require a repeating sequence to extend, *see* Scheme 1.
2. This method was optimized using a *Thermococcus gorganarius* DNA polymerase (Tgo-Pol) variant, Z3, which is exonuclease minus (exo^-), contains mutations in the fingers domain and is fused with Sso7d [7, 8]; however, commercial DNA polymerases that are exonuclease minus and thermostable are also compatible.
3. Tgo-Pol Z3 reaction buffer is prepared as a 10× stock solution (200 mM Tris–HCl, pH 8.8, 100 mM $(NH_4)_2SO_4$, 100 mM KCl, 1% Triton X-100, 1 mg/mL Bovine Serum Albumin (BSA), and 20 mM $MgSO_4$) and stored at 4 °C. If using a commercial DNA polymerase, use the corresponding reaction buffer.
4. Ladder requirements depend on the DNA length you aim to produce—commonly, 50–10,000 base pairs ladder is adequate.
5. Ethidium bromide is traditionally used; however, several alternatives are now available.
6. Commonly 5 or 6× concentration.
7. Store at 4 °C to extend the shelf life.
8. Agarose can be replaced with a Lonza FlashGel DNA Cassette, 1.2%, 12 + 1 well, single tier.
9. Volume required to result in 100 μM oligonucleotide concentration is commonly stated in the manufacturer's synthesis report.

10. Reaction master mix solutions can be made by multiplying each component by an equal ratio.
11. A 10× dilution in water is performed with each oligonucleotide before the final dilution into the reaction mixture. Oligonucleotide solutions are vortexed before dilutions are performed.
12. Prepare a 10 mM master mix by the addition of 100 μL each individual 100 mM dNTP stock to 600 μL water, vortex, aliquot to 10 lots of 100 μL and store at −20 °C.
13. If using Tgo-Pol Z3, reaction buffer consists of: 20 mM Tris–HCl, pH 8.8, 10 mM $(NH_4)_2SO_4$, 10 mM KCl, 0.1% Triton X-10, 1 mg/mL BSA, and 2 mM $MgSO_4$. If using a commercial DNA polymerase, use the corresponding provided reaction buffer.
14. 200 nM Tgo-Pol Z3 can be diluted to the required concentration using the reaction buffer. Commercial thermostable exo^- DNA polymerases can also be used following the manufacturer's protocol. Do not vortex DNA polymerase.
15. 5–30 cycles are optimal. An initial screen is required for each new repeating sequence to determine to optimum cycle number for the desired length.
16. Store at −20 °C if storage time is more than 16 h.
17. Samples should be eluted from the purification kit using 20 μL water if imaging by AFM, otherwise elute with the provided elution buffer.
18. Agarose is dissolved using a microwave. Swirl occasionally and stop heating when bubbling and all the agarose has dissolved.
19. Ensure the comb will produce enough wells for the number of samples plus two for the DNA ladder.
20. Vary the ladder volume depending on sample concentrations.
21. It is good practice to leave a free well between the ladder and the samples.
22. The voltage can be adjusted depending on the quality of the resolution and image required; 80 V usually produces well-defined gels but you can use up to 120 V if you require the results quickly for a subsequent step.
23. Ensure UV safety goggles are worn if the trans-illuminator is not in a sealed box. Handle the gel with care and wearing protective gloves.
24. The concentration of DNA can be 20–80 ng/μL to obtain an acceptable final yield. Concentrations lower than this will not recover enough DNA for use in future experiments.

25. The manufacturer's protocol states that the FlashGel Cassette should be run at 250 V. It has been found that slower running of the gel provides better conditions for recovery and increases the yield of the final size recovered product. Any voltage between 200 and 250 V may be used during this process.
26. Determination of extracted length is indicated by the ladder length. Ensure the ladder is continually referred to during extraction and note the extracted length against the fraction number.
27. The electrophoresis power supply can be started again for 10 s to allow for any residual DNA from the desired band to migrate into the wells. This should be done if the desired DNA length distribution has not been recovered or if the well does not look clear after initial recovery.
28. Samples should be eluted in 20 μL water from the column of the DNA purification system. Eluted DNA concentrations may be too low for UV-Vis detection. In case, concentrate the sample by evaporation and reevaluate in 10 μL. For long-term storage, elute samples in elution buffer.
29. If sample concentrations are low, i.e., less than 5 ng/μL use a Lonza FlashGel DNA Cassette single tier agarose gel to analyze the isolated designer DNA.
30. Higher concentrations may be required if using shorter DNA lengths.
31. Ensure that the nitrogen flow is gentle, i.e., just enough to move the droplet over the surface.

References

1. Holliday R (1964) A mechanism for gene conversion in fungi. Genet Res 5:282–304
2. Seeman NC (1999) DNA engineering and its application to nanotechnology. Trends Biotechnol 17:437–443. https://doi.org/10.1016/S0167-7799(99)01360-8
3. Rothemund PWK (2006) Folding DNA to create nanoscale shapes and patterns. Nature 440:297–302. https://doi.org/10.1038/nature04586
4. Weisbroda SH, Marx A (2008) Novel strategies for the site-specific covalent labelling of nucleic acids. Chem Commun 30:5675–5685. https://doi.org/10.1039/b809528k
5. Arthur M, Etheve-Quelquejeu M (2015) Covalent organic functionalization of nucleic acids. In: Charleux B, Coperet C, Lacote E (eds) Chemistry of organo-hybrids: synthesis and characterization of functional nano-objects. John Wiley & Sons, Hoboken, NJ
6. Whitfield CJ, Turley AT, Tuite EM, Connolly BA, Pike AR (2015) Enzymatic method for the synthesis of long DNA sequences with multiple repeat units. Angew Chem Int Ed 54:8971–8974. https://doi.org/10.1002/anie.201502971
7. Evans SJ, Fogg MJ, Mamone A et al (2000) Improving dideoxynucleotide–triphosphate utilisation by the hyper-thermophilic DNA polymerase from the achaeon *Pyrococcus furiosis*. Nucleic Acids Res 28:1059–1066
8. Jozwiakowski SK, Connolly BA (2011) A modified family-B archaeal DNA polymerase with reverse transcriptase activity. Chembiochem 12:35–37. https://doi.org/10.1002/cbic.201000640

Chapter 3

Synthesis of DNA-Based Nanowires

Alexander Kotlyar

Abstract

Here we describe novel enzymatic procedures for the production of long (from tens of nanometers to microns) double-stranded poly(dG)–poly(dC), triple-helical poly(dG)–poly(dG)–poly(dC), and quadruple-helical G4 DNA. All these molecules are uniform in size and possess improved mechanical and electrical properties with respect to a canonical random sequence double-stranded DNA. They can potentially be used as elements in nanoelectronic devices and circuits.

Key words DNA nanowires, Enzymatic synthesis, Klenow exo$^-$, Poly(dG)–poly(dC), G4-DNA, Triplex DNA

1 Introduction

The DNA molecule is an attractive candidate to wire electrons over long molecular distances. Charge migration along DNA molecules has been a subject of scientific interest for many years. It is currently accepted that a native, random sequence DNA is characterized by poor intrinsic conductivity. However, DNA molecules composed of repeating sequences exhibit better conductivity compared to random sequence ones [1–3]. Experimental demonstration of conducting behavior on short poly(dG)–poly(dC) DNA oligomers [1, 2] and the results of theoretical calculations show that poly(dG)–poly(dC), a homo-polymer consisting of poly(dC) and poly(dG) chains, exhibits better conductance than poly(dA)–poly(dT) [3]. This is mainly due to the fact that poly(dG)–poly(dC) provides better conditions for π overlap compared to poly(dA)–poly(dT) and to the lowest ionization potential of guanidine compared to other DNA bases [4]. The following guanine-rich DNA molecules: poly(dG)–poly(dC), poly(dG–dG)–poly(dC), and G4-DNA may therefore possess conductivity much higher than canonical random sequence DNA.

Poly(dG)–poly(dC) is a double-stranded deoxyribopolynucleotide polymer in which homopolymeric strands, poly(dC) and

Giampaolo Zuccheri (ed.), *DNA Nanotechnology: Methods and Protocols*, Methods in Molecular Biology, vol. 1811, https://doi.org/10.1007/978-1-4939-8582-1_3, © Springer Science+Business Media, LLC, part of Springer Nature 2018

poly(dG), are running in opposite directions. Commercial preparations poly(dG)–poly(dC) that were available in the past were used in electrical conductivity studies [5, 6]. We have demonstrated [7] that G-strand in the commercial preparations is composed of relatively short (500–1500 bases) poly(dG) fragments associated with the continuous C-strand. The presence of nicks in the G-strand strongly reduces the ability of the polymer to conduct current and limits its use in nanoelectronics. The molecules prepared by our technique [7] lack the above disadvantage. The enzymatic synthesis, conducted as described here, yields a double-stranded poly(dG)–poly (dC) composed of continuous dG- and dC-homopolymers of equal lengths. In addition, the synthesized poly(dG)–poly(dC) molecule can be functionalized by various groups attached to the 5′ ends of strands composing the DNA [7]. The functional group can be: single-stranded overhang sequences, fluorescent labels, thiol-groups, biotin moieties, and others. Thiols are known to interact specifically with gold nanoparticles and surfaces [8, 9]. The ability to attach SH-groups to the 5′ ends thus provides a tool for the selective binding of long poly(dG)–poly(dC) polymers to gold surfaces [10] and gold nanoelectrodes. This property is especially useful for application of the polymer in nanoelectronics.

Triple-stranded DNA molecules have been a subject of research for the past 55 years (for review, *see* [11–13]). Most of the triple-stranded structures studied so far were composed of tens of triads. We have reported [14] synthesis of long (thousands of bases) triple-stranded DNA, poly(dG–dG)–poly(dC), composed of continuous dG- and dC-homopolymers. The dG counterpart is twice longer than the poly(dC) one and is folded back on itself in a hairpin fashion. The contour length of these triplex structures can vary from tens to hundreds of nanometers. As in the case of poly (dG)–poly(dC) molecules, various functional groups, including fluorescent labels, thiols, and other functionalities, can be attached to the 5′ ends of DNA strands [14]. We have demonstrated that the triplex molecules are stiffer and more resistant to mechanical deformation, compared to random sequence DNA and poly(dG)–poly(dC) [14]. This, together with the ability to functionalize the triplex molecules is essential for their application in nanoelectronics.

It has been known for decades that G-rich DNA sequences containing runs of guanines (dG) can form G-quadruplex structures (for review, *see* [15–17]). These structures, commonly named G4-DNA, are composed of stacked planar tetrads. Each tetrad is composed of four guanine bases interacting with each other through Hoogsteen hydrogen bonding. The vast majority of studies in this field were focused on short (16–32 bases) self-folded G-rich sequences [18, 19]. In addition to intramolecular folding, G-rich oligonucleotides can assemble into long molecular fibers in

the presence of sodium and potassium ions [20, 21]. These fibers are very polymorphic, and are composed of short oligonucleotide fragments not covalently linked to each other [20, 21]. We have reported a method [22, 23] for synthesis of novel long (hundreds of nanometers) continuous G-based nanostructures, composed of hundreds of stacked tetrads. These nanostructures are uniform in size and contain no gaps. We have also demonstrated that the structures are characterized by higher stability, higher resistivity to heat [22, 23], higher charge polarizability [24], and electrical conductivity [25, 26] as compared to canonical double-stranded DNA. These properties make these structures very promising for nanoelectronic applications.

Enzymatic synthesis of the long, di-, tri- and tetra-stranded G-rich DNA-based nanostructures is described in detail below.

2 Materials

2.1 Synthesis of Poly (dG)–Poly(dC)

2.1.1 Preparation of $(dG)_{12}$–$(dC)_{12}$

1. 0.1 M LiOH solution: weigh 0.42 g of $LiOH{\cdot}H_2O$. Dissolve in 0.1 L of deionized/filtered water and filter through 0.22 μm Millipore Express PLUS membrane filter.
2. 0.1 M LiOH containing 10% acetonitrile: weigh 4.2 g of $LiOH{\cdot}H_2O$. Dissolve in 0.9 L of deionized/filtered water. Add 100 mL of acetonitrile (HPLC-S Gradient grade) and mix intensively.
3. Alkaline 1 M LiCl solution containing acetonitrile: weigh 42.4 g of LiCl. Dissolve in 0.9 L of 0.1 M LiOH and filter the solution through 0.22 μm Millipore Express PLUS membrane filter. Add 100 mL of acetonitrile (HPLC-S Gradient grade) and mix intensively.
4. 100% glacial acetic acid.
5. 1 M Tris–acetate (pH 7.8): weigh 121 g of Tris-base. Dissolve in 0.8 L of deionized water; adjust pH to 7.8 with glacial acetic acid; adjust the volume to 1 L with deionized/filtered water. Filter the solution through 0.22 μm Millipore Express PLUS membrane filter.
6. 2 mM Tris–acetate (pH 7.8): to 998 mL of deionized/filtered water add 2 mL of 1 M Tris–acetate (pH 7.8) and mix intensively.
7. 20 mM Tris–acetate (pH 7.8): to 980 mL of deionized/filtered water add 20 mL of 1 M Tris–acetate (pH 7.8) and mix intensively.
8. $(dG)_{12}$, an oligonucleotide composed of 12 G bases (*see* **Note 1**).
9. $(dC)_{12}$, an oligonucleotide composed of 12 C bases.

10. Dialysis tubing 10 mm (Sigma). Treat the tubing as follows: wash with running tap water for 3 h; treat with 0.3% (w/v) solution of sodium sulfide at 80 °C for 1 min; wash with tap water for 2–5 min at 60 °C; treat with 0.2% (v/v) solution of sulfuric acid for 10 min at room temperature; wash with tap water for 10–15 min. Store the tubing in 25% Ethanol at 4 °C. Rinse the tubing with running deionized water before use.
11. Ion-exchange DNA-NPR (4.6 × 75 mm, 2.5 μm), Tosoh (Japan).
12. Sephadex NAP-5 DNA-Grade column (GE Healthcare).
13. Agilent 1100 HPLC system with a photodiode array detector.
14. Eppendorf table centrifuge (model 5424).
15. Phenomenex HPLC column heater controller.
16. Laboratory Freeze Dryer Christ Alpha 1–4 (Osterode am Harz, Germany).

2.1.2 Synthesis of Poly (dG)–Poly(dC)

1. 5 M KOH solution: weigh 140 g of KOH. Dissolve in 0.5 L of deionized water.
2. 1 M potassium phosphate buffer (pH 7.5): weigh 136 g of KH_2PO_4. Dissolve in 0.7 L of deionized water; adjust pH to 7.5 with 5 M KOH; adjust the volume to 1 L with deionized water. Filter the solution through 0.22 μm Millipore Express PLUS membrane filter.
3. 1 M $MgCl_2$: weigh 20.3 g of $MgCl_2 \cdot 6H_2O$. Dissolve in 0.1 L of deionized water. Filter the solution through 0.22 μm Millipore Express PLUS membrane filter.
4. 1 M EDTA: weigh 29.2 g of EDTA (acid form). Dissolve in 0.1 L of deionized water. Filter the solution through 0.22 μm Millipore Express PLUS membrane filter.
5. 0.4 M DL-dithiothreitol (DTT): weigh 15.4 mg of DTT. Dissolve in 0.25 mL of deionized/filtered water. Store at −18 °C.
6. 100 mM dCTP: weigh 9.3 mg of dCTP. Dissolve in 0.2 mL of deionized/filtered water. Store at −18 °C.
7. 100 mM dGTP: weigh 10.1 mg of dGTP. Dissolve in 0.2 mL of deionized/filtered water. Store at −18 °C.
8. 10 μM $(dG)_{12}$–$(dC)_{12}$, a double-stranded DNA composed of 12 G and 12 C bases (*see* Subheading 3.1.4).
9. Klenow exo$^-$ (Klenow fragment of *E. coli* DNA polymerase I, lacking the 3' → 5′ exonuclease activity), 10 units/μL enzyme solution in glycerol (Epicentre, USA). Store the solution at −18 °C.
10. Dry bath incubator (MRC, Israel).

2.1.3 HPLC Purification of Poly(dG)–Poly(dC)

1. 1 M acetic acid solution: to 470 mL of deionized/filtered water add 30 mL of 100% acetic acid and mix intensively.
2. 20 mM Tris–acetate (pH 7.8): weigh 2.42 g of Tris-base. Dissolve in 0.8 L of deionized water; adjust pH to 8.0 with 1 M acetic acid; adjust the volume to 1 L with deionized/filtered water. Filter the solution through 0.22 μm Millipore Express PLUS membrane filter.
3. TSK-gel G-DNA-PW HPLC column (7.8 × 300 mm), (Tosoh, Japan).
4. Agilent 1100 HPLC system with a photodiode array detector.

2.2 Synthesis of Thiol-End-Labeled Poly(dG)–Poly(dC), SH-Poly(dG)–Poly(dC)-SH

2.2.1 Preparation of Thiol-End-Labeled $(dG)_{12}$–$(dC)_{12}$, SH-$(dG)_{12}$–$(dC)_{12}$–SH

1. 0.1 M LiOH solution: weigh 0.42 g of $LiOH{\cdot}H_2O$. Dissolve in 0.1 L of deionized/filtered water and filtered through 0.22 μm Millipore Express PLUS membrane filter.
2. 0.1 LiOH solution containing 10% acetonitrile: weigh 4.2 g of $LiOH{\cdot}H_2O$. Dissolve in 0.9 L of deionized/filtered water. Add 100 mL of acetonitrile (HPLC-S Gradient grade) and mix intensively.
3. 5 M HCl solution: to 215 mL of deionized/filtered water add 285 mL of 32% HCl and mix intensively.
4. Alkaline 1 M LiCl solution containing acetonitrile: weigh 42.4 g of LiCl. Dissolve in 0.9 L of 0.1 M LiOH and filter the solution through 0.22 μm Millipore Express PLUS membrane filter. Add 100 ml of acetonitrile (HPLC-S Gradient grade).
5. 1 M Tris–acetate (pH 7.8): weigh 121 g of Tris-base. Dissolve in 0.8 L of deionized water; adjust pH to 7.8 with glacial acetic acid; adjust the volume to 1 L with deionized/filtered water. Filter the solution through 0.22 μm Millipore Express PLUS membrane filter.
6. 2 mM Tris–acetate (pH 7.8): to 998 mL of deionized/filtered water add 2 mL of 1 M Tris–acetate (pH 7.8) and mix intensively.
7. 20 mM Tris–acetate (pH 7.8): to 980 mL of deionized/filtered water add 20 mL of 1 M Tris–acetate (pH 7.8) and mix intensively.
8. 0.4 M DL-Dithiothreitol (DTT): weigh 15.4 mg of DTT. Dissolve in 0.25 mL deionized/filtered water. Store at −18 °C.
9. SH-$(dG)_{12}$, an oligonucleotide composed of 12 G bases and functionalized with Thiol Modifier C6 S-S at 5′ end.
10. SH-$(dC)_{12}$, an oligonucleotide composed of 12 C bases and functionalized with Thiol Modifier C6 S-S at 5′ end.
11. Dialysis tubing 10 mm (Sigma). Treat the tubing as follows: wash with running tap water for 3 h; treat with 0.3% (w/v)

solution of sodium sulfide at 80 °C for 1 min; wash with tap water for 2–5 min at 60 °C; treat with 0.2% (v/v) solution of sulfuric acid for 10 min at room temperature; wash with tap water for 10–15 min. Store the tubing in 25% Ethanol at 4 °C. Rinse the tubing with running deionized water before use.

12. Ion-exchange DNA-NPR (4.6 × 75 mm, 2.5 μm), Tosoh (Japan).
13. Sephadex NAP-5 DNA-Grade prepacked column (GE Healthcare).
14. Agilent 1100 HPLC system with a photodiode array detector.
15. Phenomenex HPLC column heater controller.
16. Eppendorf table centrifuge (model 5424).
17. Laboratory Freeze Dryer Christ Alpha 1–4 (Osterode am Harz, Germany).

2.2.2 Synthesis of SH-Poly(dG)–Poly(dC)-SH

1. 5 M KOH solution: weigh 140 g of KOH. Dissolve in 0.5 L of deionized water.
2. 1 M potassium phosphate buffer (pH 7.5): weigh 136 g of KH_2PO_4. Dissolve in 0.7 L of deionized water; adjust pH to 7.5 with 5 M KOH; adjust the volume to 1 L with deionized water. Filter the solution through 0.22 μm Millipore Express PLUS membrane filter.
3. 1 M $MgCl_2$: weigh 20.3 g of $MgCl_2 \cdot 6H_2O$. Dissolve in 100 mL of deionized water. Filter the solution through 0.22 μm Millipore Express PLUS membrane filter.
4. 1 M EDTA: weigh 29.2 g of EDTA (acid form). Dissolve in 0.1 L of deionized water. Filter the solution through 0.22 μm Millipore Express PLUS membrane filter.
5. 0.4 M DL-dithiothreitol (DTT): weigh 15.4 mg of DTT. Dissolve in 0.25 mL of deionized/filtered water. Store at −18 °C.
6. 100 mM dCTP: weigh 9.3 mg of dCTP. Dissolve in 0.2 mL of deionized/filtered water. Store at −18 °C.
7. 100 mM dGTP: weigh 10.1 mg of dGTP. Dissolve in 0.2 mL of deionized/filtered water. Store at −18 °C.
8. 10 μM SH-$(dG)_{12}$–$(dC)_{12}$-SH, a double-stranded DNA composed of 12 G and 12 C bases and functionalized with SH groups (*see* Subheading 3.2.3).
9. Klenow exo$^-$ (Klenow fragment of *E. coli* DNA polymerase I, lacking the 3′ → 5′ exonuclease activity), 10 units/μL enzyme solution in glycerol from Epicentre (Chicago, USA). Store the solution at −18 °C.
10. Dry bath incubator (MRC, Israel).

2.2.3 HPLC Purification of Synthesized SH-Poly (dG)–Poly(dC)-SH

1. 100% Glacial acetic acid.
2. 1 M Tris–acetate (pH 7.8): weigh 121 g of Tris-base. Dissolve in 0.8 L of deionized water; adjust pH to 7.8 with glacial acetic acid; adjust the volume to 1 L with deionized/filtered water. Filter the solution through 0.22 μm Millipore Express PLUS membrane filter.
3. 2 mM Tris–acetate (pH 7.8): to 998 mL of deionized/filtered water add 2 mL of 1 M Tris–acetate (pH 7.8) and mix intensively.
4. 20 mM Tris–acetate (pH 7.8): to 980 mL of deionized water add 20 mL of 1 M Tris–acetate (pH 7.8) and mix intensively.
5. TSK-gel G-5000-PW HPLC column (7.8 × 300 mm) (Tosoh, Japan).
6. Agilent 1100 HPLC system with a photodiode array detector.

2.3 Synthesis of Poly (dG–dG)–Poly (dC) Triplex

2.3.1 Poly(dG–dG)–Poly (dC) Triplex Synthesis

1. 1 M KOH solution: weigh 56 g of KOH. Dissolve in 1 L of deionized water. Filter the solution through 0.22 μm Millipore Express PLUS membrane filter.
2. 1 M phosphate buffer (pH 7.5): weigh 136 g of KH_2PO_4. Dissolve in 0.7 L of deionized water; adjust pH to 7.5 with 5 M KOH; adjust the volume to 1 L with deionized water. Filter the solution through 0.22 μm Millipore Express PLUS membrane filter.
3. 1 M $MgCl_2$: weigh 20.3 g of $MgCl_2{\cdot}6H_2O$. Dissolve in 100 mL of deionized water. Filter the solution through 0.22 μm Millipore Express PLUS membrane filter.
4. 1 M EDTA: weigh 29.2 g of EDTA (acid form). Dissolve in 0.1 L of deionized water. Filter the solution through 0.22 μm Millipore Express PLUS membrane filter.
5. 0.4 M DL-dithiothreitol (DTT): weigh 15.4 mg of DTT. Dissolve in 0.25 mL of deionized/filtered water. Store at −18 °C.
6. 100 mM dGTP: weigh 10.1 mg of dGTP. Dissolve in 0.2 mL of deionized/filtered water. Store at −18 °C.
7. 1 mM (in base pairs) of 500–2000 base pairs poly(dG)–poly (dC) (*see* Subheading 3.1).
8. Klenow exo$^-$ (Klenow fragment of *E. coli* DNA polymerase I, lacking the 3′ → 5′ exonuclease activity), 10 units/μL enzyme solution in glycerol from Epicentre (Chicago, USA). Store the solution at −18 °C.
9. Dry bath incubator (MRC, Israel).

2.3.2 HPLC Purification of Synthesized Poly (dG–dG)–Poly(dC)

1. 1 M acetic acid solution: to 470 mL of deionized/filtered water add 30 mL of 100% glacial acetic acid and mix intensively.
2. 20 mM Tris–acetate (pH 7.8): weigh 2.42 g of Tris-base. Dissolve in 0.8 L of deionized water; adjust pH to 7.8 with glacial acetic acid; adjust the volume to 1 L with deionized/filtered water. Filter the solution through 0.22 μm Millipore Express PLUS membrane filter.
3. TSK-gel G-DNA-PW HPLC column (7.8 × 300 mm) (Tosoh, Japan).
4. Agilent 1100 HPLC system with a photodiode array detector.

2.4 Synthesis of G4 (Quadruple)-DNA

2.4.1 Purification of $(dC)_{20}$

1. 0.1 M NaOH solution: weigh 4 g of NaOH. Dissolve in 1 L of deionized water. Filter the solution through 0.22 μm Millipore Express PLUS membrane filter.
2. Glacial acetic acid 100%.
3. 1 M potassium phosphate buffer (pH 7.5): weigh 136 g of KH_2PO_4. Dissolve in 0.8 L of deionized water; adjust pH to 7.5 with 5 M KOH; adjust the volume to 1 L with deionized water. Filter the solution through 0.22 μm Millipore Express PLUS membrane filter.
4. 20 mM potassium phosphate buffer (pH 7.5) containing 10% acetonitrile: to 880 mL of deionized water add 20 mL of 1 M potassium phosphate buffer (pH 7.5) and filter the solution through 0.22 μm Millipore Express PLUS membrane filter. Add 100 mL of acetonitrile (HPLC-S Gradient grade) and mix intensively.
5. 0.5 M potassium phosphate buffer (pH 7.5) containing 10% acetonitrile; to 0.4 L of deionized water add 0.5 L of 1 M potassium phosphate buffer (pH 7.5) and filter the solution through 0.22 μm Millipore Express PLUS membrane filter. Add 100 mL of acetonitrile (HPLC-S Gradient grade) and mix intensively.
6. 1 M Tris–acetate (pH 7.8): weigh 121 g of Tris-base. Dissolve in 0.8 L of deionized water; adjust pH to 7.8 with glacial acetic acid; adjust the volume to 1 L with deionized/filtered water. Filter the solution through 0.22 μm Millipore Express PLUS membrane filter.
7. 2 mM Tris–acetate (pH 7.8): to 998 mL of deionized/filtered water add 2 mL of 1 M Tris–acetate (pH 7.8) and mix intensively.
8. $(dC)_{20}$, an oligonucleotide composed of 20 C bases.
9. Dialysis tubing 10 mm (Sigma). Treat the tubing as follows: wash with running tap water for 3 h; treat with 0.3% (w/v) solution of sodium sulfide at 80 °C for 1 min; wash with tap

water for 2–5 min at 60 °C; treat with 0.2% (v/v) solution of sulfuric acid for 10 min at room temperature; wash with tap water for 10–15 min. Store the tubing in 25% Ethanol at 4 °C. Rinse the tubing with running deionized water before use.

10. Ion-exchange PolyWax LP column (4.6 × 200 mm, 5 μm, 1000 Å) (Western Analytical Products).
11. Sephadex NAP-25 DNA-Grade prepacked column (15 × 50 mm) (GE Healthcare).
12. Ion-exchange HiTrap Q HP column (1 mL) (GE Healthcare).
13. Agilent 1100 HPLC system with a photodiode array detector.
14. Eppendorf table centrifuge (model 5424).
15. Laboratory Freeze Dryer Christ Alpha 1-4 (Osterode am Harz, Germany).

2.4.2 Synthesis of Poly (dG)–ɳ$(dC)_{20}$

1. 1 M KOH solution: weigh 56 g of KOH. Dissolve in 1 L of deionized water. Filter the solution through 0.22 μm Millipore Express PLUS membrane filter.
2. 1 M potassium phosphate buffer (pH 7.5): weigh 136 g of KH_2PO_4. Dissolve in 0.8 L of deionized water; adjust pH to 7.5 with 5 M KOH; adjust the volume to 1 L with deionized water. Filter the solution through 0.22 μm Millipore Express PLUS membrane filter.
3. 20 mM potassium phosphate buffer (pH 7.5): to 98 mL of deionized water add 2 mL of 1 M potassium phosphate buffer (pH 7.5). Filter the solution through 0.22 μm Millipore Express PLUS membrane filter.
4. 1 M $MgCl_2$: weigh 20.3 g of $MgCl_2{\cdot}6H_2O$. Dissolve in 100 mL of deionized water. Filter the solution through 0.22 μm Millipore Express PLUS membrane filter.
5. 1 M EDTA: weigh 29.2 g of EDTA (acid form). Dissolve in 0.1 L of deionized water. Filter the solution through 0.22 μm Millipore Express PLUS membrane filter.
6. 0.4 M DL-dithiothreitol (DTT): weigh 15.4 mg of DTT. Dissolve in 0.25 mL deionized/filtered water. Store at −18 °C.
7. 100 mM dGTP. Dissolve 10.1 mg of dGTP in 0.2 mL of deionized/filtered water. Store at −18 °C.
8. 10 μM $(dG)_{12}$–$(dC)_{12}$ (*see* Subheading 3.1.4).
9. HPLC purified $(dC)_{20}$ (*see* Subheading 3.4.1).
10. Klenow exo$^-$ (Klenow fragment of *E. coli* DNA polymerase I, lacking the 3′ → 5′ exonuclease activity), 10 units/μL enzyme solution in glycerol from (Epicentre, USA). Store the solution at −18 °C.
11. Dry bath incubator (MRC, Israel).

2.4.3 HPLC Purification of Synthesized Poly(dG)–N $(dC)_{20}$

1. 1 M acetic acid solution: to 470 mL of deionized/filtered water add 30 mL of 100% glacial acetic acid and mix intensively.
2. 20 mM Tris–acetate (pH 7.8): weigh 2.42 g of Tris-base. Dissolve in 0.8 L of deionized water; adjust pH to 7.8 with glacial acetic acid; adjust the volume to 1 L with deionized/filtered water. Filter the solution through 0.22 μm Millipore Express PLUS membrane filter.
3. TSK-gel DNA-G-DNA PW HPLC column (7.8 × 300 mm) (Tosoh, Japan).
4. Agilent 1100 HPLC system with a photodiode array detector.

2.4.4 Preparation of Poly (dG) Strands

1. 1 M NaOH solution: weigh 40 g of NaOH. Dissolve in 1 L of deionized water. Filter the solution through 0.22 μm Millipore Express PLUS membrane filter.
2. 0.1 M NaOH: to 900 mL of deionized/filtered water add 100 mL of 1 M NaOH and mix intensively.
3. TSK-gel DNA-G-DNA PW HPLC column (7.8 × 300 mm) (Tosoh, Japan).
4. Agilent 1100 HPLC system with a photodiode array detector.

2.4.5 Preparation of G4-DNA

1. 1 M acetic acid solution: to 470 mL of deionized/filtered water add 30 mL of 100% glacial acetic acid and mix intensively.
2. 2 mM Tris–acetate (pH 7.8): weigh 242 mg of Tris-base. Dissolve in 0.8 L of deionized water; adjust pH to 8.0 with glacial acetic acid; adjust the volume to 1 L with deionized/filtered water. Filter the solution through 0.22 μm Millipore Express PLUS membrane filter.
3. Sephadex NAP-25 DNA-Grade prepacked column (GE Healthcare).

3 Methods

3.1 Preparation of Poly(dG)–Poly (dC) (See Note 2)

Complete HPLC purification of $(dG)_{12}$ and $(dC)_{12}$ oligonucleotides comprising $(dG)_{12}$–$(dC)_{12}$ template-primer system is required for the synthesis of homogeneous poly(dG)–poly(dC) (*see* **Note 3**).

3.1.1 Preparation of $(dG)_{12}$–$(dC)_{12}$

3.1.2 HPLC Purification of $(dC)_{12}$

1. Transfer approximately 1 mg of a dry oligonucleotide powder to 1.5 mL plastic tube.
2. Add 1 mL of deionized/filtered water.
3. Shake the sample and vortex vigorously for 2 min; incubate at room temperature for 30 min and vortex again.

4. Centrifuge the sample for 2 min at 5000 × *g* at room temperature in order to get rid of insoluble compounds that could be present in the oligonucleotide preparation.
5. Transfer the entire supernatant to a new 1.5 mL plastic tube.
6. Connect an ion-exchange DNA-NPR column to the HPLC system and heat it to 60 °C using Phenomenex HPLC column heater controller.
7. Equilibrate the column with 20 mL of 0.1 M LiOH containing 10% acetonitrile at 60 °C and a flow rate of 0.5 mL/min.
8. Load 20–50 μL of the oligonucleotide sample at a flow rate of 0.5 mL/min. Do not overload the column. This can significantly reduce the separation efficiency.
9. Elute the oligonucleotide in 0.1 M LiOH and 10% acetonitrile with a linear LiCl gradient from 0 to 0.6 M for 35 min at 60 °C and a flow rate of 0.5 mL/min. Monitor the elution by measuring absorbance at 260 nm. A typical elution profile is shown in Fig. 1.
10. Collect the fraction containing $(dC)_{12}$ eluted between 18 and 18.5 min (corresponding peak is indicated by the arrows in Fig. 1). The total volume of the fraction should be approximately 0.3 mL.
11. Equilibrate a DNA-Grade NAP-5 column with 10 mL of 2 mM Tris–acetate (pH 7.8) at room temperature.

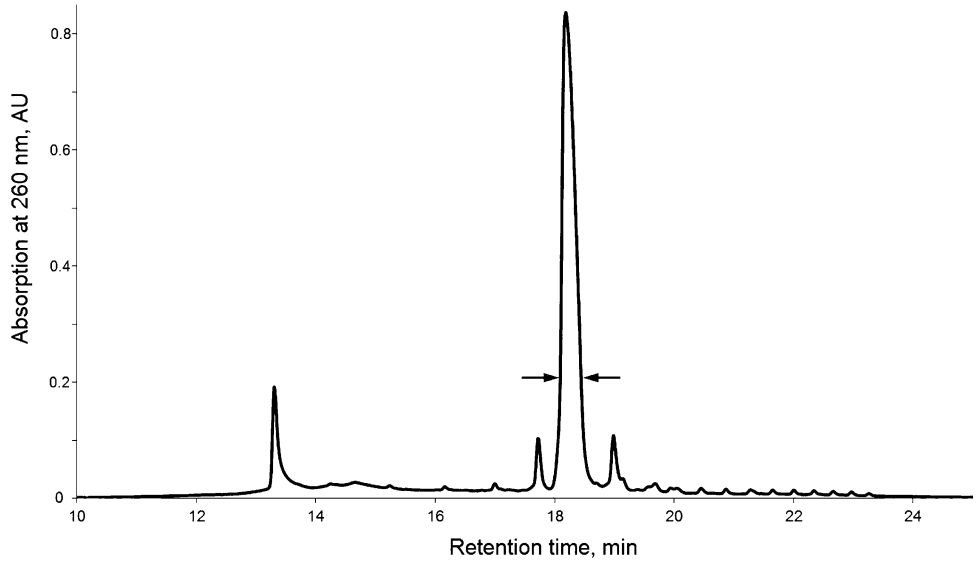

Fig. 1 Purification of $(dC)_{12}$ on a DNA-NPR column

12. Load 0.3 mL of the oligonucleotide sample obtained from the ion-exchange column (*see* **step 10**). Allow the sample to enter the column completely. Add 0.4 mL of Tris–acetate (pH 7.8). Allow the buffer to enter the column.
13. Place 1.5 mL Eppendorf plastic tube under the column; add 0.5 mL of 2 mM Tris–acetate (pH 7.8) and collect the eluate (*see* **Note 4**).
14. Freeze the sample in a dry ice/ethanol bath and lyophilize to dryness. It takes approximately 15 h to completely lyophilize the samples.
15. Store the dry sample at −18 °C.

3.1.3 HPLC Purification of $(dG)_{12}$ (See Note 3)

1. Transfer approximately 1 mg of a dry oligonucleotide powder to plastic 1.5 mL plastic tube.
2. Add l mL of 0.1 M LiOH.
3. Shake the sample and vortex vigorously for 2 min.
4. Centrifuge the sample for 2 min at 5000 × *g* at room temperature in order to get rid of insoluble compounds that could be present in the oligonucleotide preparation.
5. Transfer the entire supernatant to a new 1.5 mL plastic tube.
6. Connect a DNA-NPR column to the HPLC system and heat it to 60 °C using Phenomenex HPLC column heater controller.
7. Equilibrate the column with 0.1 M LiOH containing 10% acetonitrile at 60 °C and a flow rate of 0.5 mL/min.
8. Load 10–50 μL of the oligonucleotide sample at a flow rate of 0.5 mL/min.
9. Elute the oligonucleotide in 0.1 M LiOH containing 10% acetonitrile with a linear LiCl gradient from 0 to 0.6 M for 40 min at 60 °C and a flow rate of 0.5 mL/min. Monitor the elution by measuring absorbance at 260 nm. A typical elution profile is shown in Fig. 2.
10. Collect the fraction eluted between 35 and 35.5 min (corresponding peak is indicated by the arrows in Fig. 2). Total volume of the fraction should be approximately 0.3 mL.
11. Equilibrate a DNA-Grade NAP-5 column with 10 mL of 2 mM Tris–acetate (pH 7.8) at room temperature.
12. Load 0.4 mL of the oligonucleotide sample obtained from the ion-exchange column (*see* **step 10**). Allow the sample to enter the column completely. Add 0.4 mL of 2 mM Tris–acetate (pH 7.8) buffer. Allow the buffer to enter the column.
13. Place 1.5 mL plastic tube under the column; add 0.5 mL of 2 mM Tris-–acetate (pH 7.8) buffer and collect the eluate (*see* **Note 4**).

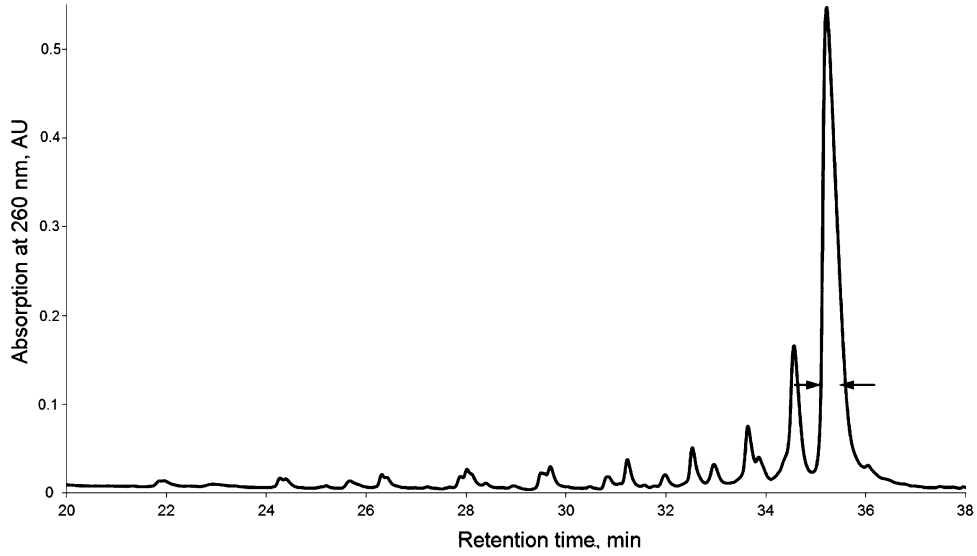

Fig. 2 Purification of $(dG)_{12}$ on a DNA-NPR column

14. Freeze the sample in a dry ice/ethanol bath and lyophilize to dryness. It takes approximately 15 h to completely lyophilize the sample.
15. Store the dry sample at −18 °C (*see* **Note 5**).

3.1.4 Annealing of Purified $(dC)_{12}$ and $(dG)_{12}$

1. Dissolve HPLC purified $(dC)_{12}$, obtained as described in Subheading 3.1.2, in 50–100 μL of 0.1 M LiOH.
2. Withdraw 10 μL from the sample and add to a quartz cuvette filled with 1 mL of 20 mM Tris–acetate (pH 7.8).
3. Measure absorption of the 100-fold diluted sample at 260 nm.
4. Calculate the concentration of the oligonucleotide using an extinction coefficient of 90 per mM per cm at 260 nm.
5. Dissolve HPLC purified $(dG)_{12}$, obtained as described in Subheading 3.1.3, in 50–100 μL of 0.1 M LiOH.
6. Withdraw 10 μL from the sample and add to a quartz cuvette filled with 1 mL of 20 mM Tris–acetate (pH 7.8).
7. Measure absorption of 100-fold diluted sample at 260 nm.
8. Calculate the concentration of the oligonucleotide using an extinction coefficient of 120 per mM per cm at 260 nm.
9. Mix proper volumes of $(dG)_{12}$ and $(dC)_{12}$ samples (*see* above) to obtain equal molar concentrations of the oligonucleotides. The final volume of the mixture should be approximately 100–200 μL and concentration of the oligonucleotides approximately 5–10 μM.

10. Transfer the mixture to a dialysis tubing and dialyze against 1 L of 20 mM Tris–acetate (pH 7.8) and 100 mM NaCl overnight at room temperature for 4–6 h.
11. Withdraw 10 μL from the dialyzed sample and add to a quartz cuvette filled with 0.9 mL of 20 mM Tris–acetate(pH 7.8).
12. Measure absorption of 100-fold diluted sample at 260 nm.
13. Calculate the concentration of the template-primer using an extinction coefficient of 177 per mM per cm at 260 nm.
14. Freeze the samples in a dry ice/ethanol bath and store −18 °C until use (*see* **Note 5**).

3.1.5 Enzymatic Synthesis of Poly(dG)–Poly (dC)

The method described here differs from the traditional PCR used for DNA synthesis. It is based on the unique property of DNA Polymerase (Klenow exo$^-$ fragment) to extend blunt-ended poly (dG)–poly(dC) molecules in the presence of dGTP and dCTP.

1. Prepare an assay for the DNA synthesis. Combine the following reagents in a 0.5 mL plastic tube for each reaction: 90 μL of deionized/filtered water, 6 μL of 1 M potassium phosphate buffer (pH 7.5), 0.3 μL of 1 M $MgCl_2$, 1 μL of 100 mM dCTP, 1 μL of 100 mM dGTP and 1.25 μL of 0.4 M DTT, for a total volume of 0.1 mL (you may scale up or down accordingly). Mix well by vortexing.
2. Add 0.3–0.5 μM $(dG)_{12}$–$(dC)_{12}$ template-primer. Mix well by vortexing.
3. Add 0.5 μL of Klenow exo^{--}, mix by vortexing and incubate the reaction at 37 °C in the air dry bath for 1 h. Incubation for an hour yields approximately 2000 base pair long poly (dG)–poly(dC) molecules (*see* Fig. 3). You may reduce or increase the amount of bases in the DNA by reducing or extending the incubation time respectively.
4. Add 2 μL of 1 M EDTA and vortex the sample to halt the reaction.

3.1.6 HPLC Purification of the Synthesized Poly (dG)–Poly(dC)

In order to separate the synthesized poly(dG)–poly(dC) from nucleotides, Klenow exo$^-$ and other components of the assay we recommend to use size-exclusion HPLC.

1. Connect the TSK-gel G-DNA-PW HPLC column to the HPLC system (*see* **Note 6**).
2. Equilibrate the column with 20 mM Tris–acetate (pH 7.8) at a flow rate of 0.5 mL/min at room temperature.
3. Load 100 μL of poly(dG)–poly(dC) sample, obtained as described above in Subheading 3.1.5, at a flow rate of 0.5 mL/min.

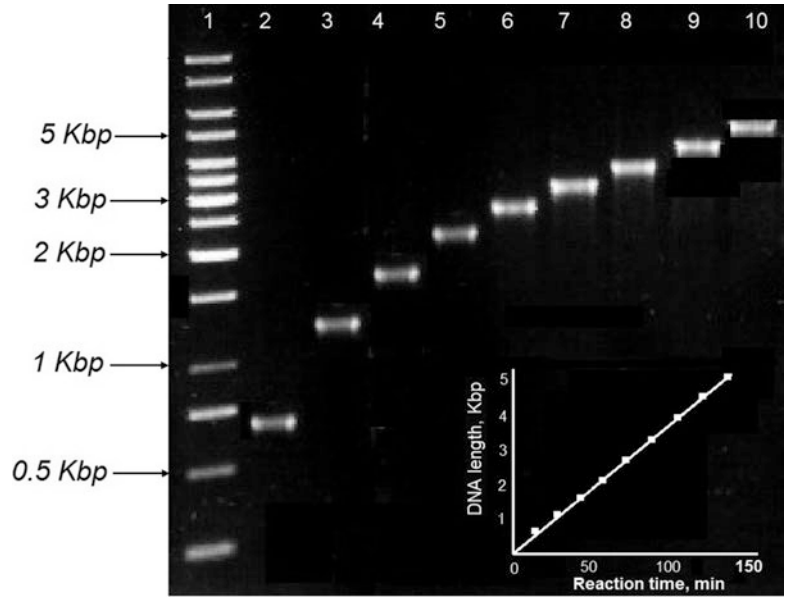

Fig. 3 Time course of poly(dG)–poly(dC) synthesis reaction. Polymerase extension assay was performed, in the presence of 0.2 μM $(dG)_{12}$–$(dC)_{12}$ and 20 μg/mL of Klenow exo$^-$; the incubation was set at 37 °C. Aliquots were withdrawn in 15 min for a total of 2 h 15 min. The reaction products were resolved on 1% agarose gel and stained with ethidium bromide. The marker bands of 1 kb DNA ladder (lane 1) are indicated to the left. Time-dependent products for 15, 30, 45, 60, 75, 90, 105, 120, and 135 min of the synthesis (lanes 2–10). The inset shows the dependence of the DNA length (in kb) on the reaction time

4. Elute the DNA in 20 mM Tris–acetate (pH 7.8) at a flow rate of 0.5 mL/min at room temperature. Monitor the elution by measuring absorbance at 260 nm.
5. Collect the fraction eluted just after the void volume. Total volume of the eluted fraction should be approximately 1 mL.
6. Withdraw 10 μL from the eluted fraction and add to a quartz cuvette filled with 1 mL of 20 mM Tris–acetate (pH 7.8).
7. Measure absorption of the sample at 260 nm.
8. Calculate the concentration of DNA in the sample using an extinction coefficient of 14.8 per mM per cm at 260 nm for the GC pair.
9. Transfer the solution into several 0.5 mL plastic tubes (0.1 mL per tube).
10. Freeze the DNA samples in a dry ice/ethanol bath and store −18 °C until use (*see* **Note 5**).

3.2 Preparation of SH-Poly(dG)–Poly (dC)-SH

The method enables to obtain homogeneous population of SH-poly(dG)–poly(dC)-SH characterized by high affinity to gold surfaces and electrodes.

3.2.1 HPLC Purification SH-$(dC)_{12}$ (See Note 3)

Complete HPLC purification of SH-$(dG)_{12}$ and SH-$(dC)_{12}$ oligonucleotides is required for synthesis of homogeneous SH-poly (dG)–poly(dC)-SH.

1. Transfer approximately 1 mg of a dry oligonucleotide powder to plastic 1.5 mL plastic tube.
2. Add l mL of deionized/filtered water.
3. Shake the sample and vortex vigorously for 2 min; incubate at room temperature for 30 min and vortex again.
4. Centrifuge the sample for 2 min at 5000 × *g* at room temperature in order to get rid of insoluble compounds that could be present in the oligonucleotide preparation.
5. Transfer the entire supernatant to a new 1.5 mL plastic tube.
6. Connect an ion-exchange DNA-NPR column to the HPLC system and heat it to 60 °C using Phenomenex HPLC column heater controller.
7. Equilibrate the column with 20 mL of 0.1 M LiOH containing 10% acetonitrile at 60 °C and a flow rate of 0.5 mL/min.
8. Load 10–50 μL of the oligonucleotide sample at a flow rate of 0.5 mL/min. Do not overload the column. This can significantly reduce the separation efficiency.
9. Elute the oligonucleotide in 0.1 M LiOH containing 10% acetonitrile with a linear LiCl gradient from 0 to 0.6 M for 35 min at 60 °C and a flow rate of 0.5 mL/min. Monitor the elution by measuring absorbance at 260 nm.
10. Collect the fraction corresponding to the highest absorption read at 260 nm (usually eluted between 18 and 20 min). Total volume of the fraction should be approximately 0.3 mL.
11. Equilibrate a DNA-Grade NAP-5 column with 10 mL of 2 mM Tris–acetate (pH 7.8) at room temperature.
12. Load 0.3 mL of the oligonucleotide sample obtained from the ion-exchange column (*see* **step 10**). Allow the sample to enter the column completely. Add 0. 4 mL of 2 mM Tris–acetate (pH 7.8). Allow the buffer to enter the column.
13. Place 1.5 mL plastic Eppendorf tube under the column; add 0.5 mL of Tris–acetate (pH 7.8) buffer and collect the eluate.
14. Freeze the sample in a dry ice/ethanol bath and lyophilize it to dryness. It takes approximately 15 h to completely lyophilize the sample.
15. Store the dry sample at −18 °C.

3.2.2 HPLC Purification of SH-$(dG)_{12}$ (See Note 3)

1. Transfer approximately 1 mg of a dry oligonucleotide powder to plastic 1.5 mL plastic tube.
2. Add l mL of 0.1 M LiOH.
3. Shake the sample and vortex vigorously for 2 min.
4. Centrifuge the sample for 2 min at 5000 × *g* at room temperature in order to get rid of insoluble compounds that could present in the oligonucleotide preparation.
5. Transfer the entire supernatant to a new 1.5 mL plastic tube.
6. Connect an ion-exchange DNA-NPR column to the HPLC system and heat it to 60 °C using Phenomenex HPLC column heater controller.
7. Equilibrate the column with 0.1 M LiOH containing 10% acetonitrile at 60 °C and a flow rate of 0.5 mL/min.
8. Load 10–50 μL of the oligonucleotide sample at a flow rate of 0.5 mL/min.
9. Elute the oligonucleotide in 0.1 M LiOH containing 10% acetonitrile with a linear LiCl gradient from 0 to 0.6 M for 40 min at 60 °C and a flow rate of 0.5 mL/min. Monitor the elution by measuring absorbance at 260 nm.
10. Collect the fraction corresponding to the highest absorption read at 260 nm (usually eluted between 35 and 37 min). Total volume of the fraction should be approximately 0.3 mL.
11. Equilibrate a DNA-Grade NAP-5 column with 10 mL of 2 mM Tris–acetate (pH 7.8) at room temperature.
12. Load 0.3 mL of the oligonucleotide sample obtained from the ion-exchange column (*see* **step 10**). Allow the sample to enter the column completely. Add 0.4 mL of 2 mM Tris–acetate (pH 7.8). Allow the buffer to enter the column.
13. Place 1.5 mL Eppendorf plastic tube under the column; add 0.5 mL of 2 mM Tris–acetate (pH 7.8) buffer and collect the eluate.
14. Freeze the sample in a dry ice/ethanol bath and lyophilize to dryness. It takes approximately 15 h to completely lyophilize the sample.
15. Store the dry sample at −18 °C (*see* **Note 5**).

3.2.3 Annealing of Purified SH-$(dC)_{12}$ and SH-$(dG)_{12}$

1. Dissolve HPLC purified SH-$(dC)_{12}$, obtained as described in Subheading 3.2.1, in 50–100 μL of 0.1 M LiOH.
2. Withdraw 10 μL from the sample and add to a quartz cuvette filled with 1 mL of 20 mM Tris–acetate (pH 7.8).
3. Measure absorption of 100-fold diluted sample at 260 nm.

4. Calculate the concentration of the oligonucleotide in the sample using an extinction coefficient of 90 per mM per cm at 260 nm.
5. Dissolve HPLC purified SH-$(dG)_{12}$, obtained as described in Subheading 3.2.2, in 50–100 μL of 0.1 M LiOH.
6. Withdraw 10 μL from the sample and add to a quartz cuvette filled with 1 mL of 20 mM Tris–acetate (pH 7.8).
7. Measure absorption of 100-fold diluted sample at 260 nm.
8. Calculate the concentration of the oligonucleotide in the sample using an extinction coefficient of 120 per mM per cm at 260 nm.
9. Mix proper volumes of SH-$(dG)_{12}$ and SH-$(dC)_{12}$ samples (*see* above) to obtain equal concentrations of the oligonucleotides. The final volume of the mixture should be approximately 100–200 μL and the concentration of each of the oligonucleotides approximately 10–30 μM.
10. Add 2.5 μL of 0.4 M DTT for each 100 μL of the mixture, and incubate at room temperature for 30 min.
11. Transfer the sample to a dialysis tubing and dialyze against 100 mL of 20 mM Tris–acetate (pH 7.8) buffer containing 100 mM NaCl and 2 mM DTT overnight at room temperature.
12. Withdraw 10 μL from the sample and add to a quartz cuvette filled with 1 mL of 20 mM Tris–acetate (pH 7.8).
13. Measure absorption of 100-times diluted sample at 260 nm.
14. Calculate the concentration of the template-primer using an extinction coefficient of 177 per mM per cm at 260 nm.
15. Freeze the samples in a dry ice/ethanol bath and store −18 °C until use (*see* **Note 5**).

3.2.4 Enzymatic Synthesis of SH-Poly (dG)–Poly(dC)-SH

1. Prepare an assay for the DNA synthesis. Combine the following reagents in a 0.5 mL plastic tube for each reaction: 90 μL of deionized water, 6 μL of 1 M potassium phosphate buffer (pH 7.5), 0.3 μL of 1 M $MgCl_2$, 1 μL of 100 mM dCTP, 1 μL of 100 mM dGTP and 1.5 μL of 0.4 M DTT, for a total volume of 0.1 mL (you may scale up or down accordingly). Mix well by vortexing.
2. Add 0.3–0.5 μM SH-$(dG)_{12}$–$(dC)_{12}$-SH template/primer. Mix well by vortexing.
3. Add 0.5 μL of Klenow exo^{--}, mix well by vortexing and incubate the reaction at 37 °C in the air dry bath for 1 h. Incubation for an hour yields approximately 500 base pair long poly(dG)–poly(dC) molecules. You may reduce or

increase the amount of bases in the DNA by reducing or extending the incubation time respectively (*see* **Note 7**).

4. Add 2 μL of 1 M EDTA and vortex the sample to halt the reaction.

3.2.5 HPLC Purification of the Synthesized SH-Poly (dG)–Poly(dC)-SH

1. Connect a TSK-gel G-DNA-PW HPLC column to the HPLC system.
2. Equilibrate the column with 20 mM Tris–acetate (pH 7.8) at a flow rate of 0.5 mL/min at room temperature.
3. Load 100 μL of SH-poly(dG)–poly(dC)-SH sample, synthesized as described in Subheading 3.2.4, at a flow rate of 0.5 mL/min.
4. Elute the DNA in 20 mM Tris–acetate (pH 7.8) at a flow rate of 0.5 mL/min at room temperature. Monitor the elution by measuring absorbance at 260 nm.
5. Collect the fraction eluted just after the void volume. Total volume of the collected fraction should be approximately 1 mL.
6. Withdraw 10 μL from the eluted fraction and add to a quartz cuvette filled with 0.9 mL of 20 mM Tris–acetate (pH 7.8).
7. Measure absorption of 100-fold diluted sample at 260 nm.
8. Calculate the concentration of DNA in the sample using an extinction coefficient of 14.8 per mM per cm at 260 nm for the GC pair.
9. Transfer the solution into several 0.5 mL plastic tubes (0.1 mL per tube).
10. Freeze the DNA samples in a dry ice/ethanol bath and store −18 °C until use (*see* **Notes 5** and **8**).

3.3 Preparation of Poly(dG–dG)–Poly (dC)

The method of poly(dG–dG)–poly(dC) synthesis described here is based on the extension of the G-strand in the double-stranded poly (dG)–poly(dC) DNA by the Klenow exo$^-$ fragment of DNA polymerase I in the presence of dGTP.

3.3.1 Enzymatic Synthesis of Poly (dG–dG)–Poly(dC)

1. Prepare an assay for the DNA synthesis. Combine the following reagents in a 0.5 mL plastic tube for each reaction: 77 μL of deionized water, 6 μL of 1 M potassium phosphate buffer (pH 7.5), 0.3 μL of 1 M $MgCl_2$, 0.5 μL of 100 mM dGTP and 1.5 μL of 0.4 M DTT, for a total volume of 0.1 mL (you may scale up or down accordingly). Mix well by vortexing.
2. Add 15 μL of 1 mM (in base pairs) of 500–2000 base pair long poly(dG)–poly(dC) solution. Mix well by vortexing.
3. Add 0.5 μL of Klenow exo$^-$, mix well by vortexing and incubate the reaction at 37 °C in the air dry bath for 4 h.
4. Add 2 μL of 1 M EDTA and vortex the sample to halt the reaction.

3.3.2 HPLC Purification of the Synthesized Poly (dG–dG)–Poly(dC)

1. Connect a TSK-gel G-DNA-PW HPLC column to the HPLC system.
2. Equilibrate the column with 20 mM Tris–acetate (pH 7.8) at a flow rate of 0.5 mL/min at room temperature.
3. Load 100 μL of poly(dG–dG)–poly(dC) sample, obtained as described in Subheading 3.3.1, at a flow rate of 0.5 mL/min.
4. Elute the triplex DNA in 20 mM Tris–acetate (pH 7.8) at a flow rate of 0.5 mL/min at room temperature. Monitor the elution by measuring absorbance at 260 nm.
5. Collect the fraction eluted just after the void volume. The total volume of the collected fraction should be approximately 1 mL.
6. Withdraw 10 μL from the DNA sample and add to a quartz cuvette filled with 0.9 mL of 20 mM Tris–acetate (pH 7.8) buffer.
7. Measure absorption of 100-fold diluted sample at 260 nm.
8. Calculate the concentration of DNA in the sample using an extinction coefficient of 20 per mM per cm at 260 nm for the GGC triad.
9. Transfer the solution into several 0.5 mL plastic tubes (0.1 mL per tube).
10. Freeze the DNA samples in a dry ice/ethanol bath and store −18 °C until use (*see* **Note 5**).

3.4 Preparation of G4 (Quadruple)-DNA

3.4.1 HPLC Purification of $(dC)_{20}$ (See Note 3)

1. Transfer approximately 1 mg of a dry oligonucleotide powder to plastic 1.5 mL plastic tube.
2. Add l mL of deionized/filtered water.
3. Shake the sample and vortex vigorously for 2 min; incubate at room temperature for 30 min and vortex again.
4. Centrifuge the sample for 2 min at 5000 × *g* at room temperature in order to get rid of insoluble compounds that could be present in the oligonucleotide preparation.
5. Transfer the entire supernatant to a new 1.5 mL plastic tube.
6. Connect an ion-exchange PolyWax LP column to the HPLC system.
7. Equilibrate the column with 20 mL of 20 mM potassium phosphate buffer (pH 7.5), 10% acetonitrile, at a flow rate of 0.7 mL/min at room temperature.
8. Load 150 μL of the oligonucleotide sample at a flow rate of 0.7 mL/min. Do not overload the column. This can significantly reduce the separation efficiency.
9. Elute the oligonucleotide with a linear gradient of potassium phosphate buffer (pH 7.5) from 0.02 to 0.5 M in 10% acetonitrile, for 60 min at a flow rate of 0.7 mL/min at room

temperature. Monitor the elution by measuring absorbance at 260 nm.

10. Collect the fraction corresponding to the highest absorption read at 260 nm (usually eluted between 30 and 40 min). Total volume of the fraction should be approximately 1 mL.
11. Equilibrate a Sephadex NAP-25 DNA-Grade column with 30 mL of 2 mM Tris–acetate (pH 7.8) at room temperature.
12. Load 1 mL of the oligonucleotide sample eluted from the ion-exchange column (*see* **step 10**). Allow the sample to enter the column completely. Add 1.7 mL of 2 mM Tris–acetate (pH 7.8). Allow the buffer to enter the column.
13. Place a 2 mL plastic tube under the column; add 2 mL of 2 mM Tris–acetate (pH 7.8) buffer and collect the eluate.
14. Transfer the solution into four 1.5 mL plastic tubes (0.5 mL per tube).
15. Freeze the sample in a dry ice/ethanol bath and lyophilize to dryness. It takes approximately 15 h to completely lyophilize the sample.
16. Store the dry sample at −18 °C.

3.4.2 Enzymatic Synthesis of Poly(dG)–n $(dC)_{20}$

Klenow exo$^-$ fragment of DNA Polymerase I is capable of producing double-stranded poly(dG)-n$(dC)_{20}$ composed of long continuous dG-strand and dC-oligonucleotides composed of 20 bases not covalently connected to each other in the presence dGTP and $(dC)_{20}$.

1. Dissolve HPLC purified $(dC)_{20}$, obtained as described in Subheading 3.4.1, in 200 μL of 20 mM potassium phosphate buffer (pH 7.5).
2. Withdraw 1 μL from the sample and add to a quartz cuvette filled with 1 mL of 20 mM potassium phosphate buffer (pH 7.5).
3. Measure absorption of 1000-fold diluted oligonucleotide at 260 nm.
4. Calculate the concentration of the oligonucleotide using an extinction coefficient of 144 per mM per cm at 260 nm.
5. Prepare an assay for the DNA synthesis. Combine the following reagents in a 0.5 mL plastic tube for each reaction: 78.5 μL of deionized water, 6 μL of 1 M potassium phosphate buffer (pH 7.5), 0.3 μL of 1 M $MgCl_2$, 1.5 μL of 100 mM dGTP and 1.5 μL of 0.4 M DTT, for a total volume of 0.1 mL (you may scale up or down accordingly). Mix well by vortexing.
6. Add 10 μL of 1 mM $(dC)_{20}$ to a final concentration of 100 μM.

7. Add 2 μL $(dG)_{12}$–$(dC)_{12}$ template/primer, prepared as shown in Subheading 3.1.4. Mix well by pipetting.
8. Add 0.5 μL of Klenow exo$^-$, mix well by vortexing and incubate the reaction at 37 °C in an air dry bath for 1 h. Two hour incubation yields poly(dG)–$n(dC)_{20}$ molecules composed of approximately 2000 base long G-stand. You may change the amount of bases in the strand accordingly by extending or reducing the incubation time.
9. Add 2 μL of 1 M EDTA and vortex the sample to halt the synthesis.

3.4.3 HPLC Purification of Synthesized Poly(dG)–n $(dC)_{20}$

1. Connect a TSK-gel DNA-G-DNA PW HPLC column to the HPLC system.
2. Equilibrate the column with 20 mM Tris–acetate (pH 7.8) at a flow rate of 0.5 mL/min at room temperature.
3. Load 100 μL of poly(dG)–$n(dC)_{20}$ sample, obtained as described in Subheading 3.4.2, at a flow rate of 0.5 mL/min.
4. Elute the DNA in 20 mM Tris–acetate (pH 7.8) at a flow rate of 0.5 mL/min at room temperature. Monitor the elution by measuring absorbance at 260 nm.
5. Collect the fraction eluted just after the void volume. Total volume of the eluted fraction should be approximately 1 mL.

3.4.4 Preparation of Poly(dG)

At pH higher than 12.5 the poly(dG) strand and the $(dC)_{20}$ fragments composing poly(dG)–$n(dC)_{20}$ dissociate from each other and elute separately from the HPLC column.

1. Connect a TSK-gel G-DNA-PW HPLC column to the HPLC system.
2. Equilibrate the column with 0.1 M NaOH solution at a flow rate of 0.5 mL/min at room temperature.
3. Transfer 100 μL of poly(dG)–$n(dC)_{20}$ solution, obtained as described in Subheading 3.4.3, to a 0.5 mL plastic tube.
4. Add 15 μL of 1 M NaOH and incubate for 10 min at room temperature.
5. Load the sample onto the column at a flow rate of 0.5 mL/min.
6. Elute the DNA in 0.1 M NaOH at a flow rate of 0.5 mL/min at room temperature. Monitor the elution by measuring absorbance at 260 nm.
7. Collect the fraction corresponding to the highest absorption read at 260 nm (usually eluted between 14 and 16 min). Total volume of the fraction should be approximately 1 mL.

3.4.5 Preparation of G4-DNA

Folding of the G-strand into intramolecular G4-DNA takes place upon pH reduction during passing of the alkaline strand solution through a Sephadex G-25 column equilibrated with a neutral buffer.

1. Equilibrate the NAP-5 DNA-Grade column with 10 mL of 2 mM Tris–acetate (pH 7.8) at room temperature.
2. Load 0.5 mL of the alkaline G-strand solution eluted from the TSK-gel G-DNA-PW HPLC column (*see* Subheading 3.4.4). Allow the sample to enter the column completely. Add 0.2 mL of 2 mM Tris–acetate (pH 7.8). Allow the buffer to enter the column.
3. Place 1.5 mL plastic tube under the column; add 0.7 mL of 2 mM Tris–acetate (pH 7.8) buffer and collect the eluate.
4. Measure absorption of the sample at 260 nm.
5. Calculate the concentration of the DNA (in tetrads) in the sample using an extinction coefficient of 36 per mM per cm at 260 nm.
6. The sample can be stored for 2–3 days at 4 °C. Longer storage is not recommended. Do not freeze the sample (*see* **Note 5**).

4 Notes

1. In our lab, oligonucleotides used throughout this method are commonly sourced from SBS Genetech (Beijing, China).
2. The protocol of poly(dG)–poly(dC) synthesis (described in Subheading 3.1) can be adapted for synthesis of poly (dA)–poly(dT), a double-stranded polymer composed of poly (dA) and poly(dT)-homopolymer strands.
3. Complete purification of oligonucleotides comprising template-primers from shorter and longer oligonucleotides, which are usually present in minor quantities in commercial preparations, is required. If primed by nonpurified template-primers, the synthesis yields polymer molecules with large length variability.
4. **Steps 8–13** can be repeated several times in order to obtain larger quantities of purified oligonucleotides for a large-scale synthesis of the poly(dG)–poly(dC).
5. The G-rich structures are unstable at low pH and undergo hydrolysis. We thus recommend storing the DNA samples at pH 7.5–8.5.
6. If the length of the synthesized poly(dG)–poly(dC) is shorter than 1 kbp, use TSK-gel G-5000-PW HPLC column (7.8 × 300 mm) (Tosoh, Japan) instead of TSK-gel G-DNA-PW HPLC column (7.8 × 300 mm) for the DNA purification.

7. Modifications (SH groups and others) placed at 5′-ends of the template-primer reduce the extension rate. Therefore, relatively large quantities of the enzyme should be added to obtain long modified poly(dG)–poly(dC) molecules.
8. Thiol groups can undergo spontaneous oxidation. We thus recommend to store SH-poly(dG)–poly(dC)-SH in the presence of 1 mM DTT. The DNA molecules can be separated from DTT by passing the sample through a NAP-5 or NAP-25 DNA-Grade column equilibrated with either 2 or 20 mM Tris–acetate (pH 7.8).

Acknowledgments

This work was supported by the Israel Science Foundation, 1589/14.

References

1. Porath D, Bezryadin A, de Vries S, Dekker C (2000) Direct measurement of electrical transport through DNA molecules. Nature 403:635–638. https://doi.org/10.1038/35001029
2. Hwang JSK, Kong J, Ahn DG, Lee S, Ahn DJS, Hwang W (2002) Electrical transport through 60 base pairs of poly(dG)-poly(dC) DNA molecules. Appl Phys Lett 81:1134–1136. https://doi.org/10.1063/1.1498862
3. Hennig D, Starikov EB, Archilla JFR, Palmero F (2004) Charge transport in poly(dG)-poly (dC) and poly(dA) poly(dT) DNA polymers. J Biol Phys 30:227–238
4. Yi J (2003) Conduction of DNA molecules: a charge-ladder model. Phys Rev B 68:193103. https://doi.org/10.1023/B:JOBP.0000046721.92623.a9
5. Lee H-Y, Tanaka H, Otsuka Y, Yoo K-H, Lee J-O, Kawai T (2002) Control of electrical conduction in DNA using oxygen hole doping. Appl Phys Lett 80:1670–1672. https://doi.org/10.1063/1.1456972
6. Yoo K-H, Ha DH, Lee J-O, Park JW, Kim J, Kim JJ, Lee H-Y, Kawai T, Choi H-Y (2001) Electrical conduction through poly(dA)–poly (dT) and poly(dG)–poly(dC)DNAmolecules. Phys Rev Lett 87:198102. https://doi.org/10.1103/PhysRevLett.87.198102
7. Kotlyar AB, Borovok N, Molotsky T, Fadeev L, Gozin M (2005) In vitro synthesis of uniform poly(dG)-poly(dC) by Klenow exo^{--} fragment of polymerase I. Nucleic Acids Res 33:525–535. https://doi.org/10.1093/nar/gki178
8. Nuzzo RG, Allara DL (1983) Adsorption of bifunctional organic disulfides on gold surfaces. J Am Chem Soc 105:4481–4483. https://doi.org/10.1021/ja00351a063
9. Sellers H, Ulman A, Shnidman Y, Eilerss JE (1993) Structure and binding of alkanethiolates on gold and silver surfaces: implications for self-assembled monolayers. J Am Chem Soc 115:9389–9401. https://doi.org/10.1021/ja00074a004
10. Hegner M, Wagner P, Semenza G (1993) Immobilizing DNA on gold via thiol modification for atomic force microscopy imaging in buffer solutions. FEBS Lett 336:452–456
11. Frank-Kamenetskii MD, Mirkin SM (1995) Triplex DNA structures. Annu Rev Biochem 64:65–95. https://doi.org/10.1146/annurev.bi.64.070195.000433
12. Sun JS, Garestier T, Helene C (1996) Oligonucleotide directed triple helix formation. Curr Opin Struct Biol 6:327–333
13. Radhakrishnan I, Patel DJ (1994) DNA triplexes: solution structures, hydration sites, energetics, interactions, and function. Biochemistry 33:11405–11416
14. Kotlyar AB, Borovok N, Molotsky T, Klinov D, Dwir B, Kapon E (2005) Synthesis of novel poly(dG)-poly(dG)-poly(dC) triplex structure by Klenow exo^{--} fragment of DNA polymerase I. Nucleic Acids Res 33:6515–6521. https://doi.org/10.1093/nar/gki963
15. Kerwin SM (2000) G-Quadruplex DNA as a target for drug design. Curr Pharm Des 6:441–478. https://doi.org/10.2174/1381612003400849

16. Davis JT (2004) G-quartets 40 years later: from 50-GMP to molecular biology and supramolecular chemistry. Angew Chem Int Ed 43:668–698. https://doi.org/10.1002/anie.200300589
17. Keniry MA (2001) Quadruplex structures in nucleic acids. Biopolymers 56:123–146. https://doi.org/10.1002/1097-0282(2000/2001)56:3<123::AID-BIP10010>3.0.CO;2-3
18. Parkinson GN, Lee MP, Neidle S (2002) Crystal structure of parallel quadruplexes from human telomeric DNA. Nature 417:876–880. https://doi.org/10.1038/nature755
19. Burge S, Parkinson GN, Hazel P, Todd AK, Neidle S (2006) Quadruplex DNA: sequence, topology and structure. Nucleic Acids Res 34:5402–5415. https://doi.org/10.1093/nar/gkl655
20. Sen D, Gilbert W (1992) Novel DNA superstructures formed by telomere-like oligomers. Biochemistry 31:65–70
21. Marsh TC, Vesenka J, Henderson E (1995) A new DNA nanostructure the G-wire imaged by scanning probe microscopy. Nucleic Acids Res 23:696–700
22. Kotlyar AB, Borovok N, Molotsky T, Cohen H, Shapir E, Porath D (2005) Long monomolecular guanine-based nanowires. Adv Mater 17:1901–1905. https://doi.org/10.1002/adma.200401997
23. Borovok N, Molotsky T, Ghabboun J, Porath D, Kotlyar A (2008) Efficient procedure of preparation and properties of long uniform G4-DNA nanowires. Anal Biochem 374:71–78. https://doi.org/10.1016/j.ab.2007.10.017
24. Cohen H, Sapir T, Borovok N, Molotsky T, Di Felice R, Kotlyar AB, Porath D (2007) Polarizability of G4-DNA observed by electrostatic force microscopy measurements. Nano Lett 7:981–986. https://doi.org/10.1021/nl070013b
25. Livshits GI, Stern A, Rotem D, Borovok N, Eidelshtein G, Migliore A, Penzo E, Wind SJ, Di Felice R, Skourtis SS, Cuevas JC, Gurevich L, Kotlyar AB, Porath D (2014) Long-range charge transport in single G4-DNA molecules. Nat Nanotechnol 9:1040–1046. https://doi.org/10.1038/nnano.2014.246
26. Livshits GI, Ghabboun J, Borovok N, Kotlyar AB, Porath D (2014) Comparative electrostatic force microscopy of tetra-and intramolecular G4-DNA. Adv Mater 26:4981–4985. https://doi.org/10.1002/adma.201401010

Chapter 4

Preparation of Anti-miR PNAs for Drug Development and Nanomedicine

Alex Manicardi, Roberto Gambari, Luisa de Cola, and Roberto Corradini

Abstract

Peptide Nucleic Acids (PNAs) are oligonucleotide mimics that can be used to block the biological action of microRNA, thus affecting gene expression post-transcriptionally. PNAs are obtained with solid-phase peptide synthesis, and can be easily conjugated to other peptides. Conjugation with R8-Peptide or modification of the PNA backbone (at C5 or C2 carbon) with arginine side chains allows efficient cellular uptake. The present protocol describes the synthesis of cationic PNAs that can be used alone as drugs or for efficient co-delivery in suitable inorganic nanocarriers.

Key words PNA, Backbone-modified PNA, Peptide carrier, Solid-phase synthesis, Drug delivery

1 Introduction

MicroRNAs (miRs) are short regulatory RNA oligonucleotides (21–24 nt long) that have been shown to play a very important role in post-transcriptional repression of gene expression. Targeting microRNAs is one of the possible strategies that can be put in place to regulate gene expression for therapeutic purposes, especially towards the development of new approaches for several pathologies, including cancer [1, 2]. Targeting miRs with oligonucleotides (anti-miR approach), unlike traditional antisense approach, allows to increase the production of proteins, through blocking the corresponding repressor miRs. This can be achieved in a very rational way by designing a sequence that is complementary to that of the miR (*see* **Note 1**), and using either oligonucleotides or modified oligonucleotides such as 2'-OMe-RNA, Locked Nucleic Acids (LNA), Phosphoramidate Morpholino Oligonucleotides (PMO) and Peptide Nucleic Acids (PNAs) to target it. PNAs (*see* Fig. 1a) are good candidates as possible drugs, since they are exceptionally stable in the biological environment. Their major limitation is their poor cellular uptake, which is dependent on cell lines and is not optimal for most of the possible target cells

Giampaolo Zuccheri (ed.), *DNA Nanotechnology: Methods and Protocols*, Methods in Molecular Biology, vol. 1811, https://doi.org/10.1007/978-1-4939-8582-1_4, © Springer Science+Business Media, LLC, part of Springer Nature 2018

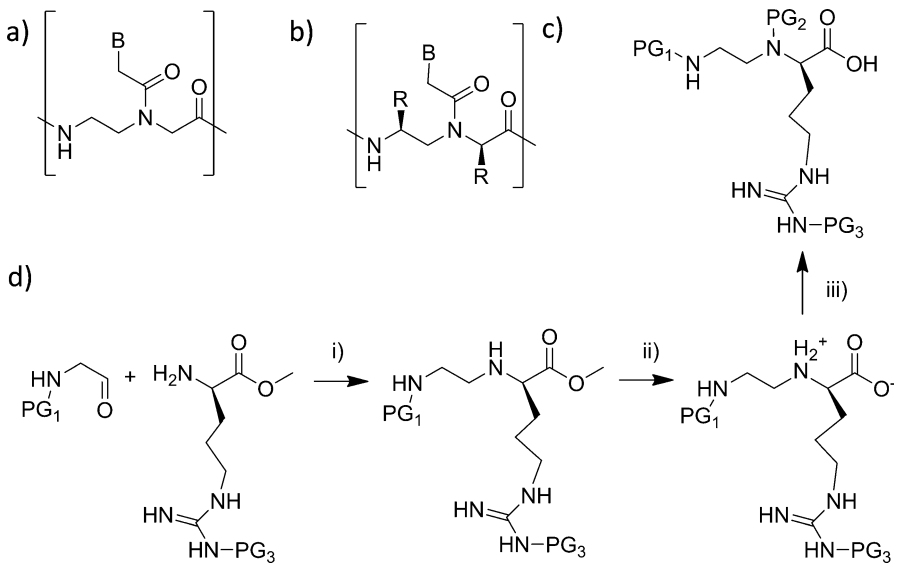

Fig. 1 (a) PNA; (b) backbone-modified PNA; (c) C2-modified PNA submonomer based on Arg side chain (PG_1 = Boc, PG_2 = Fmoc, PG_3 = Tosyl); (d) synthetic steps for obtaining the triply protected 2D-Arg submonomer: (i) Subheading 3.3, (ii) Subheading 3.4, (iii) Subheading 3.5

(*see* **Note 2**). However, since PNAs are obtained by solid-phase peptide synthesis methods, they can be easily modified with carrier peptides or small molecules. For example, conjugation with a tail of eight arginine residues (a carrier developed by P. Wender and collaborators [3]), allowed us to produce PNAs which were able to enter cells and inhibit miR210 [4], regulating cellular differentiation. The same strategy was used to target miR221, a tumor-associated miR, thus fostering the production of miR221-regulated tumor suppressors, such as $P27^{Kip1}$ [5]. This led to increased apoptosis in tumor cells [6].

An important aspect on PNAs research is the design and synthesis of modified structures, in particular backbone-modified PNAs bearing substituents either on C2 or on C5 carbon (*see* Fig. 1b). Using this approach, it is possible to incorporate the octaarginine structure in the PNA tract; in fact, arginine-modified PNAs showed a similar or superior uptake, but higher resistance to enzymatic degradation compared to the R_8-PNA analogs [7].

Various systems can be used to deliver PNAs to cells. For example, porous inorganic nanocarriers can accommodate PNAs in their cavities and allow co-delivery of PNA and other molecules, for theranostic applications [8, 9]. The methods for the co-loading of PNAs on such porous inorganic nanostructures are described in Chapter 5 of this volume. In this chapter, we describe the experimental procedures for PNA and cationic PNA synthesis.

2 Materials

Prepare all solutions using peptide synthesis (or higher) grade solvents stored over 3 Å molecular sieves in order to avoid the presence of water. Boc(Z)-protected PNA monomers can be obtained from ASM Research Chemicals (Germany); Fmoc (Bhoc)-protected PNA monomers can be obtained from Link Technologies (UK) or ASM Research Chemicals (Germany).

Solid-Phase Extraction (SPE) polypropylene (PP) empty tubes, equipped with a polyethylene frit (commercially available from several firms), are used as reactors for both manual and automatic synthesis. 6 mL tubes are used for 5 μmol scale or higher (up to 25 μmol scale), and 1 mL tubes are used for 1–2 μmol scale.

When performing manual synthesis, the reactors are equipped with a PTFE valve in order to control the suction during the filtration steps (removal of liquids from the reactor through vacuum apparatus).

2.1 Fmoc Synthesis—Automatic

Volumes should be calculated on the basis of the number of PNAs to be synthesized (*see* Subheading 3.1 below).

1. ChemMatrix-Rink amide resin.
2. 0.1 M Fmoc-protected monomers in *N,N*-dimethylformamide (DMF) or *N*-methyl-2-pyrrolidone (NMP) (*see* **Note 3**).
3. 0.47 M 2-(1H-benzotriazol-1-yl)-1,1,3,3-tetramethyluronium hexafluorophosphate (HBTU) in DMF (1.7827 g/10 mL).
4. 0.4 M diisopropylethylamine (DIPEA) in DMF/NMP (697 μL/10 mL).
5. Fmoc deprotection solution: 20% v/v piperidine in DMF.
6. Resin capping solution: solvent mix of DMF/Ac_2O 1:1 v/v (for resin loading).
7. Fmoc capping solution: solvent mix of DMF/Ac_2O/DIPEA with volume ratio of 89:5:6 (for other cycles).
8. Hydroxy-3,4-dihydro-4-oxo-1,2,3-benzotriazine (DhBtOH).
9. N,N′-diisopropylcarbodiimide.
10. Dichloromethane (DCM).

2.2 Boc Synthesis—Manual

1. 4-methylbenzhydrylamine (MBHA) resin.
2. 0.2 M Boc-protected monomers in DMF/NMP.
3. 0.2 M HBTU in DMF (7.58 mg/100 μL).
4. Boc deprotection solution: 5% v/v m-cresol in trifluoroacetic acid (TFA).
5. Boc capping solution: solvent mix of Ac_2O/pyridine/DMF with volume ratio of 1:25:25.
6. Piperidine wash: 10% piperidine v/v in DMF.

2.3 Synthesis of D-Arg(Tos) C2-Modified Backbone Methyl Ester

1. N-Boc-2-aminoacetaldehyde (e.g. from Sigma Aldrich).
2. Boc-D-Arg(Tos)-OH (e.g. from Sigma Aldrich purity >98%).
3. Sodium cyanoborohydride (synthesis grade).
4. 1 M thionyl chloride in methanol.
5. Methanol.
6. Acetic acid.
7. Ethyl acetate.

2.4 Synthesis of D-Arg(Tos) C2-Modified Backbone

1. Tetrahydrofuran (THF).
2. D-Arg(Tos) C2-modified backbone methyl ester as obtained from Subheading 3.3 below.
3. NaOH solution: 2.14 g NaOH (53.7 mmol) in 50 mL of water.
4. 1 M HCl solution in water.

2.5 Synthesis of Triply Protected D-Arg(Tos) C2-Modified Submonomer

1. 9-Fluorenylmethylchlorocarbonate (Fmoc-Cl).
2. D-Arg(Tos) C2-modified backbone as obtained from as of Subheading 3.4.
3. *N,O*-bis(trimenthylsilyl) acetamide (BSA).
4. *N,N*-diisopropyl-*N*-ethylamine (DIPEA).
5. Dichloromethane (DCM).

2.6 Synthesis of C2-PNA by Submonomer Strategy

1. 0.2 M Boc-protected submonomer as of Subheading 3.5.
2. 0.2 M HBTU in DMF (7.58 mg/100 μL).
3. Boc deprotection solution: 5% v/v m-cresol in trifluoroacetic acid (TFA).
4. Triply protected submonomer, obtained as described in Subheading 3.5 (0.25 M in NMP or DMF).
5. 0.22 M HBTU solution in DMF (8.338 mg/ 100 uL).
6. Carboxymethyl nucleobases CMB: thymine-1-yl acetic acid CMT, N^4-benzoxycarbonyl-N^1-carboxymethylcytosine CMC^z, N^6-benzylcarbonyl-N^9-carboxymethyladenine, CMA^z, commercially available at several sources, *see* **Note 4**).
7. Diisopropylcarbodiimide (DIC, reagent grade).
8. *N*-Ethyldiisopropylamine (DIPEA, >99% purity).

2.7 Cleavage of PNA from Resin and Purification

1. Cleavage solution for Fmoc synthesis: 10% v/v *m*-cresol in TFA.
2. Cleavage solution for Boc synthesis: TFA/trifluoromethylsulfonic acid (TFMSA)/*m*-cresol/thioanisole 6:2:1:1.
3. TFA.

4. Ethyl ether.
5. A centrifuge and centrifuge glass tubes.
6. HPLC-RP C18 column (e.g. 5 μm, 250 × 10 mm, Jupiter Phenomenex, 300 Å).
7. Eluent A for HPLC:water containing 0.1% TFA.
8. Eluent B for HPLC: acetonitrile containing 0.1% TFA.
9. An HPLC system with at least a UV-detector (260 nm needed).

3 Methods

3.1 Automatic Synthesis of PNAs and PNA-Peptide Conjugates with Fmoc Strategy

The protocol here described is applicable to Biotage Syro I equipped with inert gas option, but can be adapted to other automatic synthesizers.

1. Place 600 mg of ChemMatrix-RinkAmide® resin in a 12 mL reactor and allow it to swell for at least 30 min (*see* **Note 5**) in dichloromethane (DCM).
2. Mix a solution containing 0.12 mmol (for a loading of 0.2 mmol/g of resin) of the first Fmoc-protected amino acid or of the desired Fmoc-protected PNA monomer, together with 0.6 mmol (5 equivalents) of hydroxy-3,4-dihydro-4-oxo-1,2,3-benzotriazine (DhBtOH, 98.0 mg) and *N*,*N*′-diisopropylcarbodiimide (DIC, 92.9 μL) in 6 mL DMF/NMP. Allow the monomer to pre-activate for 10 min.
3. Remove DCM from the resin and wash five times with at least 6 mL of DMF.
4. Transfer the activated solution prepared at **step 2** into the reactor and shake vigorously with the orbital shaker in order to obtain a homogeneous suspension. Allow the coupling reaction to proceed for 5 h, under shaking, then filter the solution.
5. Add 6 mL of Resin Capping solution (Ac_2O/DMF 1:1 v/v). Let react for 15 min. Repeat this step twice (*see* **Note 6**).
6. Prepare a text file with the sequences to synthesize on the PC of the peptide synthesizer. Each sequence should be written from N-term to C-term, and listed in decreasing length order (*see* **Note 7**).
7. Calculate the volume of the different solutions required for the desired synthesis (*see* **Note 8**).
8. Introduce 25 mg of resin in the 2 mL reactor (for a 5 μmol synthesis scale). Place the reactor in the desired position of the reactor block.

9. Once all the reactors are placed in the block, wash them with 3 cycle of 1 mL DCM. All the resin beads should then be in the lower part of the reactor.
10. Load the monomer solutions in the amino acid (AA) rack and the other reagents as follow: bottle 1: Fmoc deprotection, bottle 2: DCM, bottle 3: DIPEA solution, bottle 4: HBTU solution, bottle 5: capping (*see* **Note 9**).
11. Purge every bottle and the AA rack with 0.5 bar of nitrogen for at least 5 min. Reduce the pressure to 0.2 bar. Set the shaking to 45 rpm (or adjust to similar conditions for custom instrument setting).
12. Program the automatic synthesis using the conditions described below at **steps 13–19**.
13. Swelling: 800 μL DCM, 20 min reaction (shake 15 s, break 2 min), 1 cycle, only for the first coupling cycle. (*see* **Note 10**)
14. DMF wash: 500 μL DMF, 20 s reaction (shake 10 s, break 2 min), 3 cycles.
15. Fmoc deprotection: 400 μL Fmoc deprotection solution, 8 min reaction (shake 10 s, break 2 min), 2 cycles (*see* **Note 11**).
16. Extensive wash: 500 μL DMF, 20 s reaction (shake 10 s, break 2 min), 3 cycles; 500 μL DCM, 20 s reaction (shake 10 s, break 2 min), 1 cycle; 500 μL DMF, 20 s reaction (shake 10 s, break 2 min), 3 cycles.
17. Coupling: 100 μL monomer solution, 20 μL HBTU solution, 50 μL DIPEA solution, 40 min reaction (shake 15 s, break 2 min), 2 cycles.
18. DMF wash: *see* **step 2**.
19. Capping: 400 μL Fmoc capping solution, 1 min reaction (shake 10 s, break 2 min), 2 cycles.
20. Perform an extensive wash.

3.2 Manual Synthesis of PNAs with Boc-Strategy

1. First monomer loading for Boc-synthesis. Repeat steps 1-5 of point 3.4 using the following conditions: resins 4-methylbenzhydrylamine (MBHA), Boc-protected amino acid or PNA monomer (0.2 mmol/g of resin), 1.1 equivalent of HBTU, and 3 equivalents of DIPEA, pre-activated for 2 min, coupling overnight; quenching of the remaining sites is performed with resin capping solution (15 min, twice).
2. Place 25 mg of resin in the 6 mL reactor (for a 5 μmol synthesis scale), and place the reactor on a suction apparatus (*see* **Note 12**).
3. Wash the resins with DCM; the resin beads should be in the lower part of the reactor.

4. Add 3 mL DCM to swell the resin for 30 min under orbital shaking (only for the first coupling cycle).
5. Wash with DCM: 3 mL DCM, three times.
6. Boc deprotection: add 1 mL Boc deprotection solution, 4 min reaction, 2 cycles.
7. Wash with 3 mL DCM, five times; then with 3 mL DMF, five times.
8. Coupling: mix 125 μL monomer solution, 120 μL HBTU solution, 8.72 μL DIPEA, and allow 2 min for pre-activation before transferring to the resin.
9. Transfer the activated monomer to the resin, and allow the coupling reaction to occur for 30 min, with orbital shaking.
10. Wash with 3 mL DMF, three times.
11. Capping: add 1 mL of the Boc capping solution, allow 1 min for the capping reaction, and repeat the reaction a second time.
12. DMF wash: repeat as in **step 10**.
13. Wash with 1 mL of piperidine solution, with 2 min shaking to remove the capping solution completely; repeat this operation a second time.
14. Wash with 3 mL of DMF for five times; then with 3 mL DCM for five times.

3.3 D-Arg(Tos) Backbone Methyl Ester Synthesis.

D-Arg(Tos)Backbone methyl ester synthesis is made according to the method originally reported in ref. [10].

1. D-Arg-(tosyl) methyl ester hydrochloride. Dissolve N-Boc-D-arginine$_{(tosyl)}$-OH (2 g, 4.67 mmol) in methanol (80 mL) with magnetic stirring. Cool the reaction mixture at 0 °C and add 5.8 mL of 1 M thionyl chloride in methanol (80 mmol) dropwise, then stir the solution for 6 h at room temperature.
2. Evaporate the methanol; add sufficient methanol to dissolve the residue (three times) and finally dry the compound. This yields D-Arg$_{(tosyl)}$ methyl ester hydrochloride (D-Arg$_{(Tos)}$-OMe HCl) in almost quantitative yield (*see* **Notes 13** and **14**).
3. Dissolve 764.9 mg of Boc-Gly-H (4.81 mmol) and 1.518 g of D-Arg$_{(Tos)}$-OMe HCl (4.01 mmol) in 30 mL of methanol and add 662 μL of DIPEA (4.01 mmol).
4. Stir the solution for 30 min at room temperature, then cool the reaction mixture to 0 °C with an ice bath and add 302.1 mg of $NaBH_3CN$ (4.81 mmol) (*see* **Note 15**) and 275 μL of acetic acid (4.81 mmol) to the stirred solution. The pH of the reaction should be between 4 and 5: if different, adjust the value accordingly.

5. Allow the reaction to stir for 30 min at 0 °C, then at room temperature for 2.5 h.
6. Monitor the reaction with TLC (ethyl acetate).
7. Evaporate the solvent and redissolve the residue in 200 mL of ethyl acetate; wash with saturated $NaHCO_3$ (200 mL, two times) and then with brine (200 mL).
8. Dry the organic layer over Na_2SO_4, filter, and evaporate the solvent to obtain the product as an oil.
9. Purify the product by flash chromatography using gradient elution from EtOAc to AcOEt/MeOH 9:1) the product should be under the form of a colorless foam. This preparation affords a yield around 60–70% (*see* **Note 16**).

3.4 D-Arg(Tos) Backbone Synthesis

D-Arg(Tos)Backbone synthesis is made according to the method originally reported in ref. [10].

1. Dissolve 2.60 g of the D-Arg backbone obtained as in Subheading 3.3 (5.37 mmol) in 50 mL of THF.
2. Add 50 mL of NaOH solution under stirring.
3. Stir the reaction mixture for 45 min (checked by TLC).
4. Evaporate the THF and then lower the pH of the solution to 7.1 with the HCl solution, to induce the precipitation of the zwitterion.
5. Cool the solution at 4 °C for 2 h, then filter over Buchner.
6. Dry under vacuum to obtain the product as a white solid. m.p.: 199.3 °C (dec) (*see* **Note 17**).

3.5 Synthesis of Triply Protected D-Arg Submonomer

D-Arg triply protected submonomer synthesis is made according to the method originally reported in ref. [10].

1. Disperse 2.42 g of the D-Arg backbone obtained as in Subheading 3.4 (5.00 mmol) in 170 mL of DCM, then add 3.7 mL of BSA (15 mmol) and 1.8 mL of DIPEA (11 mmol).
2. Stir the reaction mixture at room temperature for 30 min until the solution becomes nearly clear.
3. Cool to 0 °C and add 1.55 g of Fmoc-Cl (5.99 mmol).
4. Stir the mixture for 10 min at 0 °C, then for 2 h at room temperature (checked by TLC).
5. Quench the reaction by addition of 25 mL of methanol.
6. Evaporate the solvent.
7. Redissolve the residue in 150 mL of DCM.
8. Wash twice with 150 mL of saturated $KHSO_4$ and then with brine (150 mL).

9. Dry the organic layer over Na_2SO_4, filter and evaporate the DCM to obtain the crude as an oil.
10. Purify the product via column flash chromatography (DCM to DCM/MeOH 9:1) which is obtained as a pale yellow solid. m.p. 134.6 °C (dec.) (*see* **Note 18**).

3.6 Manual Synthesis of C-2 Modified PNAs with Boc-Strategy

Substitute **steps 8–9** (coupling) in Subheading 3.2 with the following steps:

1. Mix the submonomer obtained as of Subheading 3.5 (0.25 M in NMP or DMF) and the 0.22 M HBTU solution (in NMP or DMF). Add DIPEA (2 equiv. compared to the submonomer), and allow the pre-activation for 1 min.
2. Add the solution to the reactor containing the resin at the desired step for the introduction of C2-modified monomer (after deprotection) and allow to react under orbital shaking for at least 30 min at room temperature.
3. Filter off the coupling solution.
4. Wash with 3 mL of NMP or DMF for three times.
5. Repeat the coupling a second time with the same procedure described at **steps 1** and **2**.
6. Deprotect the Fmoc group with 1 mL of Fmoc deprotection solution; 8 minutes reaction, 2 cycles.
7. Mix the (Z-protected for A, C, for G *see* **Note 4**) 0.35 M carboxymethylnucleobase (CMB) solution in NMP with 0.3 M DhBtOH in NMP and 7 equiv. of DIC. Stir for 15 min.
8. Add the activated CMB solution to the resin, then let react for at least 1 h. Repeated couplings are necessary. At least a second coupling overnight is advisable for difficult sequences.
9. Wash thoroughly with NMP or DMF (*see* **Note 19**).

3.7 PNA Cleavage and Purification

1. For Fmoc synthesis, transfer the resin beads to a 1 mL PP reactor equipped with PE frit; for Boc synthesis transfer the resin beads to a 1 mL glass reactor equipped with sintered glass filter (*see* **Note 20**).
2. Use the cleavage solutions described in Subheading 2.7 (1 for Fmoc, 2 for Boc, according to the used strategy).
3. Cover the resin beads with the cleavage solution; for a 5 μmol scale, 400 μL are normally required.
4. Allow the reaction to stand for 1 h. In case of Fmoc synthesis and the presence of more than three arginine side chains, perform the reaction for 3 h in order to allow full Pbf removal.
5. Transfer the solution to a centrifuge tube and repeat the cleavage step (**steps 3** and **4**) on the resin for 1 h.

6. Transfer the second cocktail solution into the same centrifuge tube and wash the resin with TFA (400 μL, three times). Collect the TFA washings.
7. Add at least 10 volumes of ethyl ether and allow to stand at −20 °C for 2 h or at −78 °C for 5 min to induce the precipitation of the PNA.
8. Centrifuge the solution and resuspend the pellet in ether. The solution should be uniform. This step should be repeated at least twice.
9. Dry the crude PNA under vacuum and solubilize it in 1 mL milliQ water for the HPLC purification.
10. For PNA purification, use a RP-C18 column and a linear gradient from water +0.1% TFA to 50% acetonitrile +0.1% TFA in 30 minutes. PNA are normally eluted between minute 12 and 14 of the gradient, the presence of a polycationic structure normally decreases the retention time of the peak of about 0.5 min.

A typical HPLC-MS analysis of a purified PNA is reported in Fig. 2.

4 Notes

1. The design of anti-miR sequence can be full length or partial. PNAs partial sequences are usually designed by us by shifting the target sequence according to three criteria: (a) possible coverage of the "seed region" of target miRs (nucleotides 2–8), which can in principle increase the efficiency [11]; (b) minimal number and length of interferents (partially complementary sequences) as evaluated by a blast search in the nucleotide database (in the transcriptome); (c) chemical properties of PNA, including self-complementarity (the PairFold software from RNAsoft can be used for this purpose: http://www.rnasoft.ca/cgi-bin/RNAsoft/PairFold/pairfold.pl) and base distribution, which can affect synthesis and self-aggregation. Co-delivery of PNAs targeting different miRs can also be considered in order to reach higher biological effects. In this respect, it should be highlighted that different miRs (independently targeted by different PNAs) can coordinately target the 3′-UTR of a single target mRNA [2, 12].
2. Nonconjugated ("naked") PNA can show cellular uptake in certain cell lines, in particular neurons and astrocytes [13, 14].
3. DMF can be used instead of NMP for the preparation of monomers solution in order to reduce the synthesis costs, but a preliminary purge step (through nitrogen bubbling for at

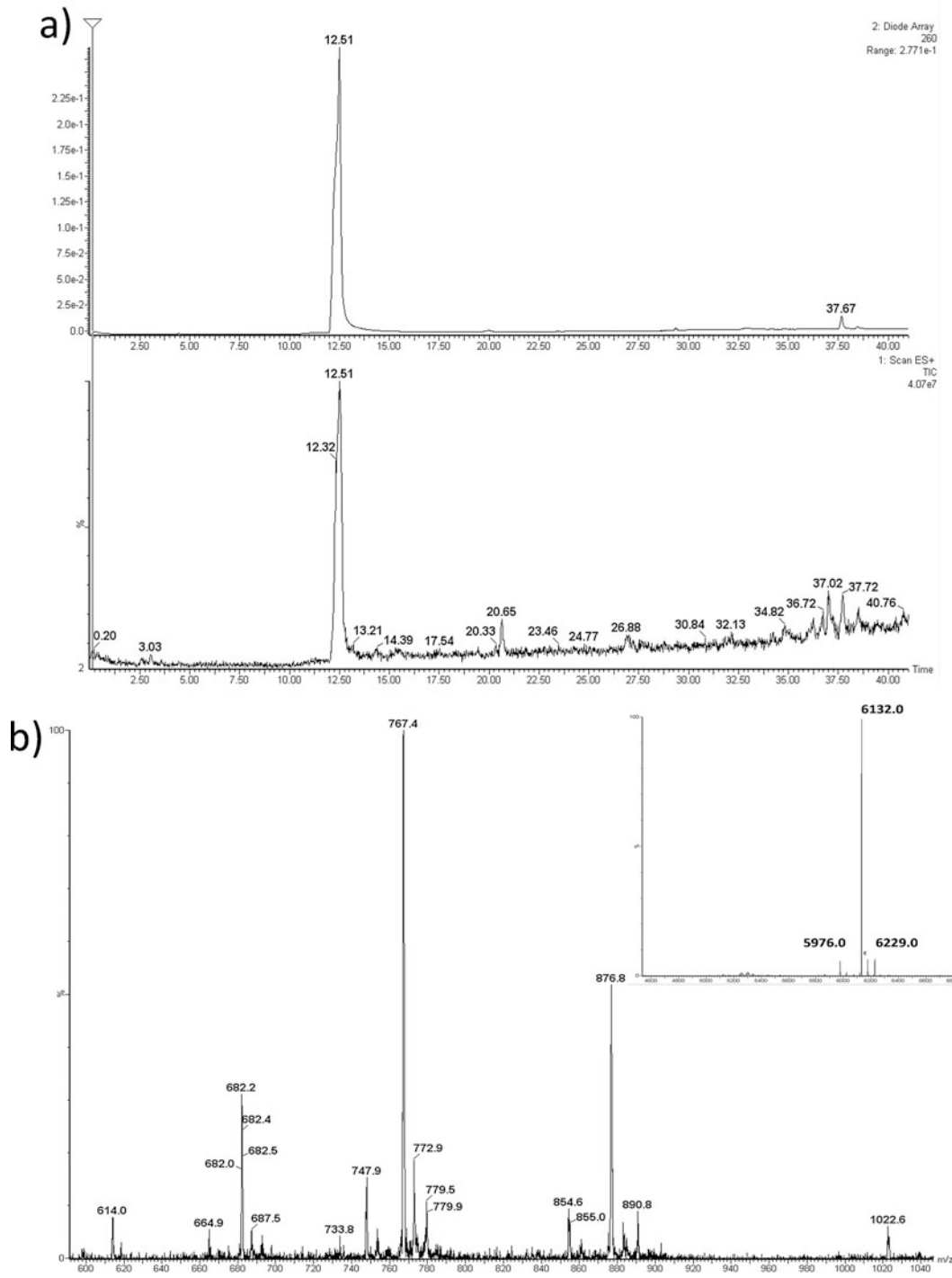

Fig. 2 HPLC-MS analysis of a typical PNA (anti-miR-221 with R_8 tail) after purification. (**a**) HPLC chromatogram (upper panel: UV_{260} trace, lower panel: MS trace); (**b**) ESI spectrum of the main peak (inset: reconstructed mass spectrum showing molecular weight). Data were obtained on a Micromass Quattro micro API (QqQ Detector) (from 100% H_2O to 50% CH_3CN in 30 min, 0.2% formic acid as modifier, flow: 1 mL/min)

least 20 min) is necessary in order to eliminate traces of dimethylamine possibly present that can affect the preservation of the monomer solution. The DMF solution of monomer can be stored for at least 1 month at −20 °C or for at least 1 week at 4 °C without affecting monomer stability.

4. N^2-Z-protected N^9-carboxymethylguanine is not presently commercially available; if guanine is needed, it can be synthesized using the procedures reported in ref. [15, 16]. N^2-Z-and O^6-Bn-protected N^9-carboxymethylguanine can be obtained using the procedures reported in ref. [17].
5. Depending on the starting resin, the swelling step requires vigorous stirring. However, using a 35–100 mesh resin should guarantee the correct loading and good PNA synthesis.
6. Resin loading by Fmoc-protected amino acids or PNA monomers can be evaluated monitoring the UV absorbance of the dibenzofulvene in 20% v/v piperidine in DMF using the formula $(A_{290}–A_{400})/(\mathrm{mg}_{\mathrm{resin}} \times 0.55 \times V_{\mathrm{solution}})$. Loading down to 0.15 mmol/g can be used with this protocol without variations. Where applicable, we recommend the use of a Fmoc-protected amino acid and this method, as this can ensure the possibility to effectively determine the resin loading using UV measurement.
7. This allows to reduce the arm movement, increasing machinery life. A software plugin does this minimization automatically, however we do not recommend to use it, especially when more than ten different sequences are synthesized, in order to avoid mistakes in reactor identity.
8. Due to DMF evaporation caused by the stream of nitrogen, it is often required to add at least 0.5 mL to AA solutions and 2 mL to DIPEA and HBTU solutions. For the other bottle, an excess of solution can be prepared. Solvent evaporation can be reduced by decreasing the flow of the inert gas and controlling that the solutions are kept under inert atmosphere for the whole synthesis. This additional volume should not be prepared if other peptide synthesizer, without inert gas, are used, however in those cases it is very important to reduce the vapor diffusion from deprotection solution, reducing the bottle opening using aluminum foil with a hole for the needle.
9. As an alternative, C5-modified monomers can be used in this synthesis. Monomers modified at 5′ with Arg (or Lys) side chains can be obtained using the protocols described in ref. [7], starting from commercially available Fmoc-L-$\mathrm{Arg}_{(\mathrm{Pbf})}$-OH (or Fmoc-L-$\mathrm{Lys}_{(\mathrm{Boc})}$-OH). L-stereochemistry is recommended since it allows better DNA/RNA binding. C2-Modified monomers with Arg (or Lys) side chain prepared in a similar manner should not be used, since in solid-phase protocols they are subjected to racemization [18].

10. If a NOVAPEG resin is used, reduce the DCM volume down to 500 μL and check if resin beads are attached to the upper part of the reactor when the swelling step is completed. If this is the case, reduction of the shaking speed should be applied.
11. This protocol is designed for a 2 equivalents/2 cycle approach, in case of difficult sequences (e.g. multiple guanine or adenine, sequence longer than 15mer) it is recommended to increase the number of equivalent to 3 by increasing all volumes. For cycles using higher equivalents, it is recommended to increase the monomer concentration to 0.2 M or higher. On doing that, remember that Fmoc-PNA-C(Bhoc)-OH have a solubility in the order of 0.25 M in DMF, so use of NMP is foreseen to avoid precipitation problems in this case.
12. This protocol is designed for a 5 equivalents/single cycle approach. When performing manual synthesis it is recommended to perform a Kaiser test to control the efficient coupling of the monomer. If the Kaiser test is positive, repeat the coupling cycle for a second time and increase the coupling time to 1 h for further cycles. It is well know that long guanine stretches are difficult to synthesize with this protocol: in that case, a 5 equivalent/2 cycles approach for that region of the probe can help in increasing the final yield.
13. Identity can be checked e.g. by ^{1}H NMR NMR (300 MHz, DMSO-d6): δ (ppm): 10.37 (sb, 3H), 8.64 (sb, 1H), 7.64 (apparent doublet, 2H), 7.38 (sb, 1H,), 7.29 (apparent doublet, 2H), 6.79 (sb, 1H), 4.0–3.9 (m, 1H), 3.71 (s, 3H), 3.1–3.0 (m, 2H), 2.34 (s, 3H), 1.8–1.7 (m, 2H), 1.5–1.4 (m, 2H). Full characterization can be found in ref. [20].
14. Alternatively, the same procedure can be performed using Boc-D-Lys$_{(2\text{-Cl-Z})}$-OH, using the same stoichiometric ratio.
15. Triacetoxy sodium borohydride can also be used to avoid the risk of hydrogen cyanide production during the work-up procedure; reaction yield will not be affected by this variation.
16. The product is then ready for the next step. Identity can be checked e.g. by ^{1}H NMR (300 MHz, DMSO-d6): $\delta = 7.64$ (d, 2H, J = 6 Hz), 7.29 (d, 2H, J = 6 Hz,), 7.03 (br s, 1H,), 6.72 (br s, 1H), 6.56 (br s, 1H), 3.61 (s, 3H), 3.34 (s, 1H), 2.86–3.23 (m, 6H), 2.35 (s, 3H), 1.61–1.26 (m, 13H). Full characterization can be found in ref. [10]. For Lysine, *see* characterization in ref. [19].
17. The product is then ready for the next step. Identity can be additionally checked e.g. by ^{1}H NMR (300 MHz, DMSO-d6): d = 7.97 (br s, 1H), 7.64 (d, 2H, J 5 9 Hz), 7.29 (d, 2H, J = 6 Hz), 6.98 (br s, 1H), 3.29–3.05 (m, 5H), 2.79–2.69 (m, 3H), 2.34 (s, 3H), 1.73–1.26 (m, 13H). Full characterization can be found in ref. [10]. For D-Lysine backbone, *see* characterization in ref. [19].

18. The product is then ready for the next step. Identity can be additionally checked e.g. by ^{1}H NMR (300 MHz, DMSO-d6): d = 7.92–7.82 (m, 2H), 7.70–7.59 (m, 4H), 7.18–7.45 (m, 6H), 4.16–4.33 (m, 3H), 3.38 (br s, 1H), 3.14–2.87 (m, 2H), 2.30 (s, 3H), 1.42–1.23 (m, 13H). Full characterization can be found in ref. [10]. For D-Lysine submonomer, *see* characterization in ref. [19].
19. This protocol is designed for a 7.5 equivalents cycle, but in most cases, a second coupling cycle (overnight) is advisable to increase the final yield of the desired product. Chloranil test can be used to evaluate the coupling efficiency on a secondary amine.
20. For Fmoc synthesis, the removal of the last Fmoc protective group should be performed before the transfer into the reactor, while this step can be omitted for Boc synthesis.

Acknowledgments

This work was partially supported by MIUR PRIN09 grant (20093N774P_001); R.G. and R.C. are supported by CIB, and by AIRC (IG 13575: peptide nucleic acids targeting oncomiR and tumor-suppressor miRNAs: cancer diagnosis and therapy).

References

1. Mishra S, Yadav T, Rani V (2016) Exploring miRNA based approaches in cancer diagnostics and therapeutics. Crit Rev Oncol Hemat 98:12–23
2. Gambari R, Fabbri E, Borgatti M, Lampronti I, Finotti A, Brognara E, Bianchi N, Manicardi A, Marchelli R, Corradini R (2011) Targeting microRNAs involved in human diseases: a novel approach for modification of gene expression and drug development. Biochem Pharmacol 82:1416–1429
3. Rothbard JB, Kreider E, Pattabiraman K, Pelkey ET, VanDeusen CL, Wright L, Wylie BL, Wender PA (2002) Arginine-rich molecular transporters for drugs: the role of backbone and side chain variations on cellular uptake. J Med Chem 45:3612–3618
4. Fabbri E, Manicardi A, Tedeschi T, Sforza S, Bianchi N, Brognara E, Finotti A, Breveglieri G, Borgatti M, Corradini R, Marchelli R, Gambari R (2011) Modulation of the biological activity of microRNA-210 with peptide nucleic acids (PNAs). ChemMedChem 6:2192–2202
5. Brognara E, Fabbri E, Aimi F, Manicardi A, Bianchi N, Finotti A, Breveglieri G, Borgatti M, Corradini R, Marchelli R, Gambari R (2012) Peptide nucleic acids targeting miR-221 modulate p27Kip1 expression in breast cancer MDA-MB-231 cells. Int J Oncol 41:2119–2127
6. Brognara E, Fabbri E, Bazzoli E, Montagner G, Ghimenton C, Eccher A, Cantù C, Manicardi A, Bianchi N, Finotti A, Breveglieri G, Borgatti M, Corradini R, Bezzerri V, Cabrini G, Gambari R (2014) Uptake by human glioma cell lines and biological effects of a peptide-nucleic acids targeting miR-221. J Neuro-Oncol 118:19–28
7. Manicardi A, Fabbri E, Tedeschi T, Sforza S, Bianchi N, Brognara E, Gambari R, Marchelli R, Corradini R (2012) Cellular uptakes, biostabilities and anti-miR-210 activities of chiral arginine-PNAs in Leukaemic K562 cells. Chembiochem 13:1327–1337
8. Bertucci A, Lülf H, Septiadi D, Manicardi A, Corradini R, De Cola L (2014) Intracellular delivery of peptide nucleic acid and organic molecules using zeolite-L nanocrystals. Adv Healthc Mater 3(11):1812–1817
9. Bertucci A, Prasetyanto EA, Septiadi D, Manicardi A, Brognara E, Gambari R, Corradini R, De Cola L (2015) Combined delivery of Temozolomide and anti-miR221

PNA using mesoporous silica nanoparticles induces apoptosis in resistant glioma cells. Small 11:5687–5695

10. Manicardi A, Calabretta A, Bencivenni M, Tedeschi T, Sforza S, Corradini R, Marchelli R (2014) Affinity and selectivity of C2- and C5-substituted "'chiral-box'" PNA in solution and on microarrays. Chirality 22:E161–E172
11. Torres AG, Fabani MM, Vigorito E, Williams D, Al-Obaidi N, Wojciechowski F, Hudson RHE, Seitz O, Gait MJ (2012) Chemical structure requirements and cellular targeting of microRNA-122 by peptide nucleic acids anti-miRs. Nucleic Acids Res 40:2152–2167
12. Brognara E, Fabbri E, Montagner G, Gasparello J, Manicardi A, Corradini R, Bianchi N, Finotti A, Breveglieri G, Borgatti M, Lampronti I, Milani R, Dechecchi MC, Cabrini G, Gambari R (2016) High levels of apoptosis are induced in human glioma cell lines by co-administration of peptide nucleic acids targeting miR-221 and miR-222. Int J Oncol 48:1029–1038
13. Tyler BM, McCormick DJ, Hoshall CV, Douglas CL, Jansen K, Lacy BW, Cusack B, Richelson E (1998) Specific gene blockade shows that peptide nucleic acids readily enter neuronal cells in vivo. FEBS Lett 421:280–284
14. Adlerz L, Soomets U, Holmlund L, Viirlaid S, Langel U, Iverfeldt K (2003) Down-regulation of amyloid precursor protein by peptide nucleic acid oligomer in cultured rat primary neurons and astrocytes. Neurosci Lett 336:55–59
15. Thomson SA, Josey JA, Cadilla R, Gaul MD, Fred Hassman C, Luzzio MJ, Pipe AJ, Reed KL, Ricca DJ, Wiethe RW, Noble SA (1995) Fmoc mediated synthesis of peptide nucleic acids. Tetrahedron 51:6179–6194
16. Heuer-Jungemann A, Howarth NM, Ja'Afaru SC, Rosair GM (2013) Development of a convenient route for the preparation of the N^2-Cbz-protected guaninyl synthon required for Boc-mediated PNA synthesis. Tetrahedron Lett 54:6275–6278
17. Thomson SA, Noble SA, Ricca DJ (1993) Peptide nucleic acids and their effect on genetic material. PCT Int Appl WO 9312129 A1 19930624 (Assignee: Glaxo Inc., USA)
18. Corradini R, Sforza S, Tedeschi T, Totsingan F, Manicardi A, Marchelli R (2011) Peptide nucleic acids with a structurally biased backbone. Updated review and emerging challenges. Curr Top Med Chem 11:1535–1554
19. Sforza S, Tedeschi T, Corradini R, Ciavardelli D, Dossena A, Marchelli R (2003) Fast, solid-phase synthesis of chiral peptide nucleic acids with a high optical purity by a submonomeric strategy. Eur J Org Chem 2003:1056–1063
20. Calabretta A, Tedeschi T, Di Cola G, Corradini R, Sforza S, Marchelli R (2009) Arginine-based PNA microarrays for APOE genotyping. Mol BioSyst 5:1323–1330

Chapter 5

Loading of PNA and Other Molecular Payloads on Inorganic Nanostructures for Theranostics

Alessandro Bertucci, Simone Silvestrini, Roberto Corradini, and Luisa De Cola

Abstract

Peptide Nucleic Acids (PNAs) are oligonucleotide mimics that can be used as drugs as they can interact with DNA and RNA targets in organisms. Loading PNAs into inorganic nanocarriers can improve their cellular uptake and co-delivering them together with drugs can improve the therapy efficacy by synergic effects. Furthermore, the functionalization of the carriers with labels allows theranostics, and the possibility to monitor the efficacy of the therapy in real time. The present protocol describes the synthesis of Zeolites-L nanocrystals and mesoporous silica nanoparticles and their loading with cationic PNAs and other smaller molecular weight payloads towards theranostics applications.

Key words PNA, Zeolites, Mesoporous silica nanoparticles, Nanomedicine, Drug delivery

1 Introduction

Nucleic acids, such as DNA, RNA, and PNA, are information-rich polymers that can be used to control the chemical behavior of cells. Their biotechnological use requires accurate delivery of these species into the cell itself, in order to deliver their chemical information necessary to carry out the specific tasks they code for. Such delivery aspects are central towards the development of new ways to formulate nucleic acids-based treatment for diverse diseases and conditions.

DNA transfection is at the base of gene therapy, the first protocols for use on humans dating back to the late eighties [1, 2]. The main role of a DNA delivery system is to avoid the denaturation of the double helix and to allow the payload to cross cell membranes.

RNA, and especially small interference RNA (siRNA), is being investigated for the treatment of cancer. siRNA are 20–23 base pairs oligonucleotides that can reversibly regulate gene expression, by matching posttranscriptionally with mRNA to block its functions.

Giampaolo Zuccheri (ed.), *DNA Nanotechnology: Methods and Protocols*, Methods in Molecular Biology, vol. 1811, https://doi.org/10.1007/978-1-4939-8582-1_5, © Springer Science+Business Media, LLC, part of Springer Nature 2018

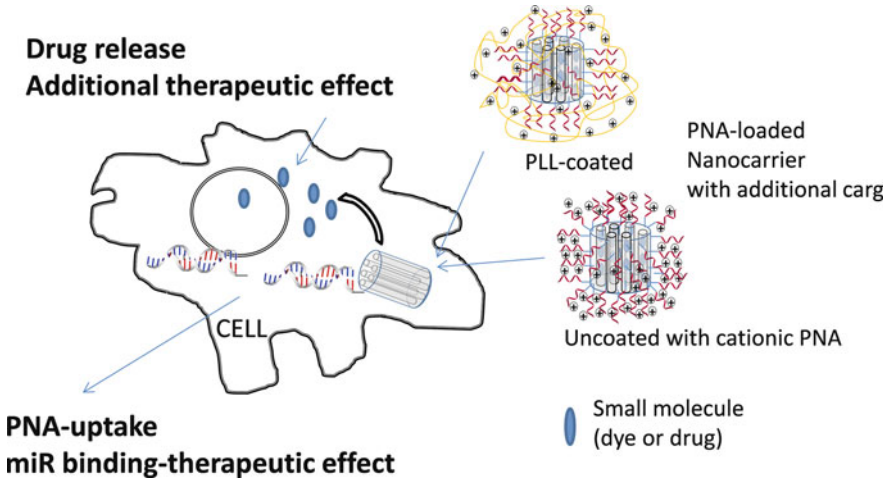

Fig. 1 Possible approaches for modified PNA and PNA-nanocarriers in anti-miR therapy

On its own, siRNA can trigger immune response, resulting unstable in the bloodstream. Moreover, like DNA, siRNA does not readily cross cell membranes [3]. PNAs (*see* Fig. 1a) are good candidates as possible drugs according to a number of possible therapeutic strategies exploiting them as oligonucleotide mimics for gene regulation and gene editing [4–6]. PNAs are exceptionally stable in the biological environment, but their major limitation is their poor cellular uptake, which is dependent on cell lines and is not optimal for most of the possible target cells. Several delivery systems can be used to introduce PNA into cells (*see* also Chapter 4 in this volume).

Porous inorganic nanocarriers have ideal physicochemical properties and can be used for the co-delivery of different types of molecules, using cavities to accommodate small molecules (e.g., drugs) and the outer surface as site for exposing recognition elements and functional macromolecules. For example, we could co-deliver a small molecule (4′,6-diamidine-2′-phenylindole dihydrochloride, DAPI) and DNA oligonucleotides using amino-modified zeolite-L nanocrystals coated with a biodegradable layer of poly-L-Lysine (PLL) [7]; after degradation of the PLL layer, both the DNA and DAPI were released. A similar strategy was used to deliver PNAs, which were covalently attached to the Zeolite-L nanocrystals surface, and small molecules such as DAPI or to visualize the containers using an insoluble dye, *N,N′-bis* (2,6-dimethylphenyl)perylene-3,4,9,10-tetracarbodiimide (DXP) entrapped in the zeolites channels [8]. In this case, the degradable PLL layer was found to be necessary to enhance the interaction with the cell surface and promote cellular uptake. The use of cationic PNAs conjugated to the zeolite-L surface allowed to obtain the delivery of PNA/small molecule loaded zeolite-L nanocrystals without the use of PLL coating [9].

Mesoporous silica nanoparticles (MSNPs) have also been considered as multifunctional delivery systems. MSNPs show excellent biocompatibility [10] and feature a large surface area thanks to a system of internal pores. The structure of these pores can be finely tuned by appropriate choice of the synthetic parameters [11, 12], along with the chemical composition of the surfaces of the particles. The latter has proven important not only to ensure the correct charge to facilitate the interaction with cell membranes but also to maximize the amount of the desired payload [13].

By using anti-miR221 PNA conjugated with octaarginine, it was possible to achieve the electrostatic adsorption of the PNA onto MSNPs loaded with the chemotherapeutic agent temozolomide. In this way, additive and synergistic effects of anti-miR and temozolomide could be observed [14]. Noteworthy, temozolomide-resistant cells were found to become more susceptible to the drug when anti-miR221 PNA was coadministered using these nanocarriers. Dual delivery of siRNA and DNA to induced pluripotent stem cells was also achieved by using fluorescent, positively charged MSNPs decorated with a large number of amino groups that acted as proton sponges to induce endosomal escape to the cytosol. This resulted in the differentiation of the stem cells into functional neurons [15].

In this Chapter, we describe the experimental procedures for the synthesis of Zeolites-L nanocrystals and mesoporous silica nanoparticles and their loading with cationic PNAs, such as those that can be prepared according to the methods in Chapter 4 of this volume (*see* Fig. 1). Further developments of these technologies are in progress; in particular, the persistence of the nanocarriers inside cells can be overcome using biodegradable nanomaterials such as breakable silica nanoparticles [16] or nanocapsules, as demonstrated in a proof-of-concept paper for the delivery of proteins [17].

2 Materials

2.1 Zeolite Nanocrystals

1. 15 g of Aerosil OX-50 (Evonik Resource Efficiency GmbH, Essen, Germany).
2. Solution A: add 4.84 g of KOH to 20.00 g of doubly distilled water. Then, add 1.56 g of $Al(OH)_3$. Reflux until clear.
3. Solution B: add 7.23 g of KOH to 21.68 g of doubly distilled water.
4. A T18 Ultra Turrax disperser (IKA) equipped with a S18N-19G dispersing tool, or analogue mixer.
5. One 100 mL hermetically sealable Teflon vessel.
6. A furnace equipped with rotating units (Memmert 200, Memmert GbmH).

2.2 Mesoporous Silica Nanoparticles (MSNP)

1. Tetraethylorthosilicate (TEOS) solution: 2.5 mL of TEOS in 3 mL of absolute ethanol.
2. Cetyl trimethylammonium bromide (CTAB).
3. 3 M solution of NaOH in water.
4. A centrifuge (radial centrifugal force of at least 30,000 × *g*).

2.3 Loading of PNAs and Small Molecules on Zeolite-L Nanocrystals

1. 0.3 mM DAPI (4′,6-diamidine-2′-phenylindole dihydrochloride, 98%) in ultrapure water.
2. 0.3 mM Oxazine 170 (5-(ethylimino)-10-Methyl-5H-benzo [a]phenoxazin-9-ethylamine monoperchlorate, 95%) in ultrapure water.
3. DXP (*N,N′-bis*(2,6-dimethylphenyl)perylene-3,4,9,10-tetracarbodiimide, 99%).
4. Zeolite nanocrystals preparations (as described in Subheading 3.1).
5. 30 μM PNA solution in 100 mM carbonate buffer (in H_2O): acetonitrile 9:1, pH = 9. PNA and PNA-peptide conjugates can be purchased from a commercial source (e.g. Panagene, NK) or synthesized as described in Chapter 4 of this Book. Cationic backbone-modified PNAs should be produced as described in Chapter 4 of this book.
6. 3-aminopropyl-triethoxysilane (APTES) for zeolites-L.
7. 0.1 M Succinic anhydride solution in dry DMSO.
8. 0.25 M Diisopropylcarbodiimide (DIC) in dry DMSO.
9. 0.25 M N-hydroxysuccinimide (NHS) solution in dry DMSO.
10. 100 mM solution of ethanolamine in 100 mM Tris buffer pH = 9.
11. 1% (w/v) Poly-L-Lysine hydrobromide solution in water.

2.4 Cellular Uptake Measurements

1. Culture medium for HeLa cells: 88% Dulbecco's Modified Eagle Medium (DMEM), 10% Fetal Bovine Serum, 1% Penicillin–Streptomycin, and 1% L-Glutamine 200 mM.
2. Supplies for cell culture (well plates, sterile pipettes, glass slides, etc.).
3. Phosphate Buffer Solution pH 7.4.
4. 25% Trypsin-EDTA solution, sterile-filtered.
5. 0.01 mg/mL working solutions of culture medium containing PNA-zeolites as prepared in Subheading 3.2.
6. 4% paraformaldehyde (PFA) solution.
7. Confocal microscope (e.g., Zeiss LSM 710 NLO Confocal Microscope).

2.5 Loading of PNAs and Small Molecules on MSNPs

1. MSNP preparations (as described in Subheading 3.2).
2. (3-aminopropyl)dimethylmethoxysilane (APDMES) for MSNP.
3. Temozolomide (CAS Number 85622–93-1, ≥ 98% purity) or other drug of interest.
4. 90 μM aqueous solution of cationic anti-miR PNA. PNA and PNA-peptide conjugates can be purchased from a commercial source (e.g. Panagene, NK) or synthesized as described in Chap. 4 of this volume. Cationic backbone-modified PNAs should be produced as described in Chapter 4 of this volume.

3 Methods

All aqueous solutions are prepared using doubly distilled water.

3.1 Preparation of Zeolite Nanocrystals

Zeolite nanocrystals (40–50 nm) synthesis is made according to the method previously reported [18].

1. Add 15 g of Aerosil OX-50 to 20.00 g of doubly distilled water and disperse it with the Ultra Turrax disperser (18,000 rpm) for 8 min. Keep for 1 h at room temperature and re-disperse for 8 min.
2. Add 40.06 g of the silica to Solution B.
3. Add solution A quickly to solution B and stir at room temperature until the dispersion becomes turbid.
4. Transfer the dispersion to a hermetically sealed, 100 mL Teflon vessel and carry out the crystallization at 170 °C for 6 h while rotating at 40 rpm in the furnace (*see* **Note 1**).
5. Cool the vessels to room temperature.
6. Washed the zeolites with double-distilled water until the supernatant shows a neutral pH.
7. Store at 4 °C for further use or for characterization (*see* **Note 2**).

3.2 Preparation of Mesoporous Silica Nanoparticles (MSNP)

MSNPs are prepared in a modified-Stöber process, which has been widely applied for the preparation of monodispersed silica nanoparticles between 50 and 2000 nm size, based on the ammonia-catalyzed hydrolysis of tetraethylorthosilicate (TEOS) in a water-alcohol mixture [14]. The presented protocol is for 100 nm MSNP.

1. Dissolve 0.5 g of cetyl trimethylammonium bromide (CTAB) in 240 mL of water together with 1.75 mL of 2 M aqueous NaOH (use a 500 mL round bottom flask with magnetic stir bar). Heat the solution to 80 °C and stir vigorously.
2. Add the TEOS solution to the CTAB-solution above. Stir overnight at 80 °C.

3. Collect the particles by centrifugation (30,000 × *g* for 20 min), discard the supernatant and wash them several times with water and ethanol (*see* **Notes 3** and **4**). This commonly results in a yield that exceed 80% (*see* **Note 5**).
4. Store at 4 °C for further use or for characterization (*see* **Note 6**).

3.3 Loading of Nanozeolites with Small Molecules and PNA

3.3.1 Loading of Cationic Fluorophore (DAPI or Oxazine 170) through Ion-Exchange

1. In a 50 mL round bottom flask, disperse zeolite-L nanocrystrals (150 mg) in 15 mL of a 0.3 mM aqueous solution of DAPI and stir overnight at 50 °C (or under reflux for oxazine 170).
2. Recover the final fluorescent material by centrifugation (30,000 × *g*, 30 min) and wash with water, checking the supernatant by fluorimetry until no emission from the dye is observed. In our experiments, dye loading could be quantified by thermogravimetric (TG)-analysis [7].

3.3.2 Loading of a Neutral Fluorophore (DXP) by Gas-Phase Insertion

1. Mix 100 mg of zeolite-L crystals with 0.5 mg DXP in a glass ampoule and dehydrate the mixture at 1.0×10^{-5} mbar for 6 h. Seal it afterwards.
2. Leave the mixture at 290 °C for 24 h to obtain the insertion of the dye.
3. Open the ampoule and then wash the zeolites with n-butanol until the supernatant does not show any fluorescence. In our experiments, the amount of inserted dye molecules for DXP was found to be 2.14 mg per 100 mg of zeolites by TG-analysis [7].

3.3.3 Surface Functionalization with Amines

1. Suspend 80 mg of zeolites by sonicating them in 10 mL of toluene or absolute ethanol for 30 min to yield a homogeneous dispersion. To this end, a benchtop ultrasound bath operating at 35 kHz typically suffices.
2. Add 50 μL of (3-Aminopropyl)trietoxysilane (APTES, 0.2 mmol) to this suspension together with a catalytic amount (2 μL) of trimethylamine and stir the mixture at room temperature overnight.
3. Collect the product by centrifugation and wash it three times with ethanol.

3.3.4 Carboxylic Acid Derivatization of Amino Groups

1. In a 25 mL round bottom flask, disperse 70 mg of the amino-modified zeolites in 10 mL of 0.1 M succinic anhydride solution in DMSO. Sonicate for 30 min and then stir overnight at room temperature.
2. Collect the particles by centrifugation for 20 min at 20,000 × *g* and wash three times with DMSO (*see* **Note 7**).

3.3.5 Electrostatic Binding of Cationic PNAs

1. Load 50 mg of carboxylic acid-functionalized nanoparticles in a 25 mL round bottom flask, together with 10 mL of a solution of DIC and NHS (both 0.25 M) in dry DMSO. Stir overnight at room temperature under nitrogen atmosphere.
2. Recover the modified particles as a solid pellet by centrifugation (20,000 × *g*, 20 min) and wash with DMSO.
3. Disperse 5 mg of the NHS-modified zeolites in 500 μL of a 30 μM PNA solution in 100 mM carbonate buffer (in H_2O): acetonitrile 9:1, pH = 9.
4. Stir the dispersion overnight at room temperature in a 5 mL vial.
5. Recover the PNA-loaded zeolites by centrifugation for 20 min at 20,000 × *g*, then wash three times with water. Quench the residual active ester groups by stirring overnight at room temperature with a 100 mM solution of ethanolamine in 100 mM Tris buffer, pH = 9.
6. Recover the final material by centrifugation and wash it three times with water (*see* **Note 8**).

In case of DNA or siRNA coating, it is possible to protect the oligonucleotides using an opposite charged degradable polymer such as Poly-L-lysine (vide infra).

3.3.6 Poly-L-Lysine Coating

1. Disperse 1 mg of e.g. DNA-zeolites in a 1% w/v solution of poly-L-lysine hydrobromide in water and stir at room temperature for 1 h.
2. Recover the final material by centrifugation (20,000 × *g*, 20 min) and wash with water.

The nanozeolites are now ready for their characterization and to be used for cell experiments (*see* next section and **Note 9**).

3.4 Cellular Uptake Measurements

1. Culture HeLa cells in 88% Dulbecco's Modified Eagle Medium (DMEM), 10% Fetal Bovine Serum, 1% Penicillin–Streptomycin, and 1% L-Glutamine 200 mM, at 37 °C and 5% of CO_2 conditioning for 48 h until 70–80% cell confluency is reached.
2. Wash the cells twice with Phosphate Buffer Solution pH 7.4 and treat them with trypsin for detachment.
3. Reseed approximately 50,000 cells on a glass cover slip inside a 6-well plate culture dish. Gently add 2 mL of fresh culture medium and let the cells grow overnight.
4. Gently add the working solutions of culture medium containing PNA-zeolites, 0.01 mg/mL, to the cells.
5. After 1, 4 and 24 h of incubation, remove the medium and wash the cells with PBS twice. Fix the cells with 4% paraformaldehyde (PFA) and stain the cell nuclei with DAPI.

6. Wash the cells three times with PBS. Remove the cover slip from the well and mount it onto the rectangular glass slide for microscopy analysis.

3.4.1 Confocal Microscopy of Treated Cells

Confocal micrographs can be obtained using a Zeiss LSM 710 confocal microscope system with 63× magnification, numerical aperture 1.3 of Zeiss LCI Plan-NEOFLUAR water immersion objective lens (Zeiss GmbH). All image processing can be performed using ZEN 2011 software.

1. Excite the specimens with lasers of wavelengths 405 nm, 488 nm and 594 nm, and collect the emitted light by lambda mode acquisition (in this mode, emission spectra are collected widely from 412 to 723 nm).
2. Raw data taken by the lambda mode acquisition can then be unmixed by utilizing the linear un-mixing tool of the software.

Alternatively, acquisition can be performed in the standard modality based on separate excitation/emission channels and final images achieved by overlapping the different acquisition windows.

Examples of uptake of anti-miR PNA-loaded uncoated zeolites are reported in Fig. 2. Uptake of coated PNA is reported in previous reports [17].

3.5 Incorporation of Drugs and Anti-miR PNA into MSNPs

3.5.1 Amine-Functionalization of MSNPs (NH_2-MSNPs)

1. In a 250 mL round bottom flask, add 150 μL of (3-aminopropyl)dimethylmethoxysilane (APDMES) to a dispersion of 400 mg of MSNPs in 100 mL ethanol, in the presence of a catalytic amount (2 μL) of triethylamine.
2. Stir the suspension overnight at room temperature.
3. Collect the particles by centrifugation at 30,000 × *g* for 20 min and wash them several times with ethanol (*see* **Note 10**).

3.5.2 Removal of CTAB from MSNPs Pores (Empty NH_2-MSNPs)

1. Shake the particles overnight in 50 mL of ethanol containing few drops of 37% aqueous HCl.
2. Collect the particles by centrifugation (20 min at 30,000 × *g*) and wash several times with ethanol and water (*see* **Note 11**).

3.5.3 Carboxylate-Functionalization of MSNPs (COOH-MSNPs)

1. Disperse 80 mg of empty NH_2-MSNPs in 10 mL of DMSO in a 25 mL round bottom flask.
2. Add 100 mg of succinic anhydride and stir the mixture overnight at room temperature.
3. Recover the material by centrifugation at 30,000 × *g* for 20 min and wash it three times with DMSO and twice with water.

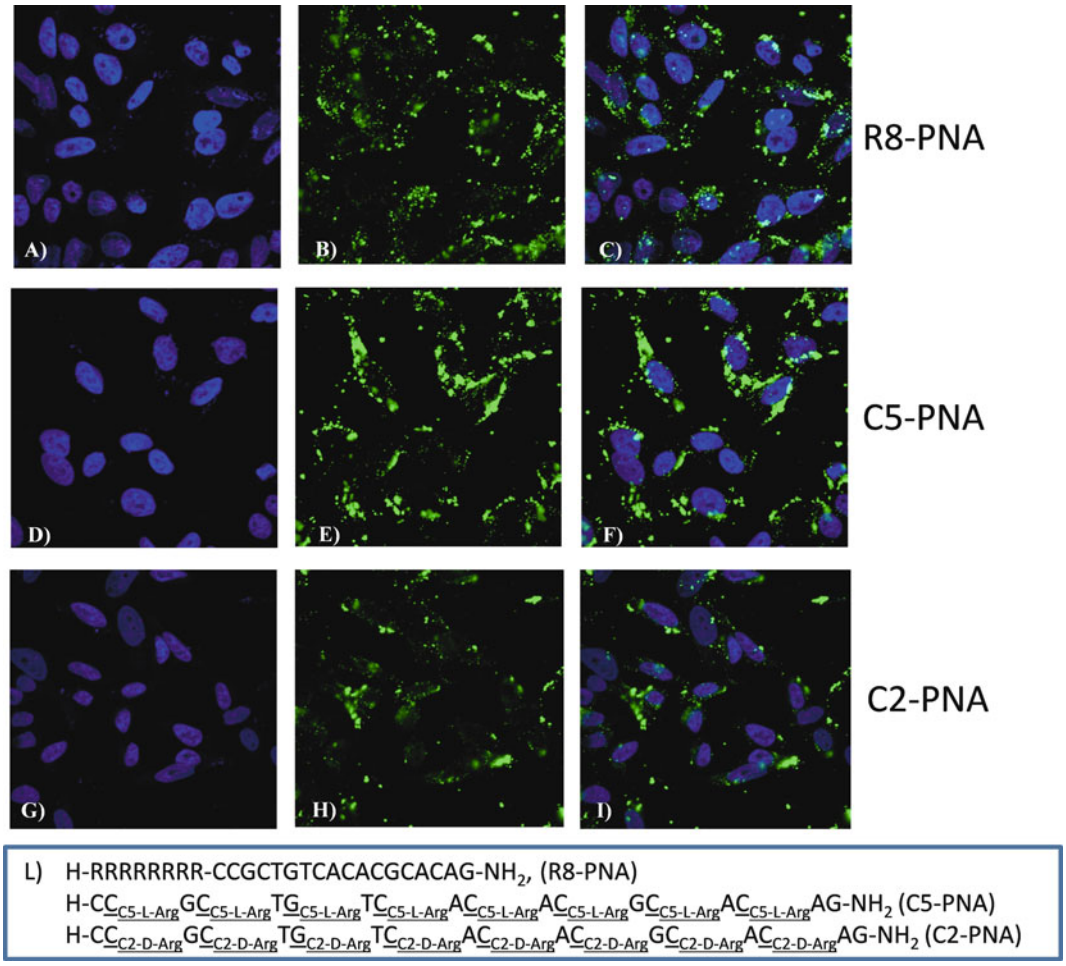

Fig. 2 Confocal micrographs of HeLa cells incubated with a 0.01 mg/mL dispersion of cationic PNA-zeolites for 4 h. (**a**, **d**, **g**) fluorescent image of cell nuclei stained with DAPI; (**b**, **e**, **h**) fluorescent image of DXP, showing the presence of the nanoparticles (**c**, **f**, **i**) overlay images; (**i**) sequences for anti-miR210 PNA used. Cellular uptake was found to depend on PNA structure (all have 8-arginine side chain and thus same charge), with C5-modified giving best results

3.5.4 Loading of Temozolomide (TMZ-MSNPs)

1. In a 25 mL round bottom flask, disperse 30 mg of COOH-MSNPs in 5 mL of methanol, and add 15 mg of temozolomide (TMZ) to the dispersion.
2. Sonicate the mixture at 35 kHz for at least 30 min to achieve a homogenous dispersion of the nanomaterial and then stir overnight at room temperature.
3. Evaporate the solvent at reduced pressure and wash the particles with methanol (once) and water (three times) to remove the drug adsorbed on the surfaces of the particles (*see* **Note 12**).

3.5.5 PNA-Functionalization of MSNPs (PNA-MSNPs)

1. In a 5 mL glass vial, disperse 10 mg of TMZ-MSNPs (presenting carboxylic groups on the surface) in 1 mL of a 90 μM aqueous solution of cationic anti-miR PNA.
2. Stir the mixture at room temperature for 4 h.
3. Collect the products by centrifugation (30,000 × *g*, 20 min) and wash it with water.

4 Notes

1. Make sure that Teflon vessels are tightly sealed, using mechanical help if possible. Any leakage of water vapor must be avoided, as this would negatively affect the formation of the crystals.
2. The characterization of the zeolite nanocrystals can be achieved by means of powder x-ray diffraction (XRD), zeta potential measurements, scanning electron microscopy (SEM) and transmission electron microscopy (TEM), and dynamic light scattering (DLS) [16, 17]. The zeta-potential measurement provides an immediate and fast indication of the presence of free Si-OH groups on the crystal surface, so that a net negative charge is displayed and the zeta potential of nonfunctionalized zeolite-L crystals is typically found between −25 and −35 mV.
3. Stirring must be as homogenous as possible, at a constant rate. It should also be checked that the stirring bar could homogenously spin as perfectly centered in the flask. Any variations or discontinuous actions will negatively affect the final shape and size of the particles.
4. Fluorescent MSNPs can be obtained in a one-pot synthesis following this alternative procedure. In a 500 mL round bottom flask, CTAB (0.5 g) is dissolved in water (240 mL) together with 1.75 mL of 2 M aqueous NaOH. The solution is then heated to 80 °C and stirred vigorously. Meanwhile, in a 10 mL round bottom flask, 2.5 mL of TEOS is dissolved in 3 mL of absolute ethanol, adding 50 μL of APTES and 0.1 mg of Cyanine 5-NHS ester dye (NHS-Cy5). This second solution is then added to the former CTAB flask and the final mixture is stirred overnight at 80 °C. The particles are finally recovered by centrifugation (30,000 × *g*, 20 min) and washed several times with water and ethanol.
5. Higher RCFs and/or longer centrifugation times are needed for smaller particles in order not to compromise the final yield.
6. The characterization of the synthesized MSNPs can be achieved by means of several techniques. Dynamic light scattering (DLS) can be immediately used to check the size distribution of the particles, while SEM and TEM can be employed

to further analyze particles size and shape. By means of HR-TEM, it is also possible to check the presence of the porous structure. The porosity and pore size can then be estimated by nitrogen adsorption (BET technique), as the amount of nitrogen adsorbed in the pores at varying pressures is correlated with pore volume, pore size, and the surface area of the nanomaterials. Additionally, small-angle X-ray scattering (SAXS) can be used for the characterization of MSNPs. SAXS is based on the elastic scattering of X-rays by a nanostructured sample, collecting the scattered light at very low angles (typically 0.1–10°). Measurements at this low angular range can provide information on ordered structural patterns, on the pore size and shape, and on the fractal dimension of the particles in this size range [18]. Based on the SAXS spectrum, one can analyze the porous structure of a nanoparticle by comparison with available fingerprinting patterns of specific geometries. This has been done, for instance, for 100 nm sized MSNPs, in order to check the presence of the typical 2D hexagonal lattice of channels.

7. Additional washing steps can be performed using toluene (or other volatile solvents) to remove all traces of DMSO and obtain dry particles for the following functionalization passages.
8. Confirmation of PNA attachment and quantification of PNA molecules present on the particles can be achieved using fluorescently labelled PNAs. Calculation can be made by difference using UV-Vis or fluorescence spectroscopy [16]. Alternatively, zeolites can be dissolved in hydrofluoric acid (HF) and the so-obtained solution analyzed using UV-Vis for quantification of the organic molecules attached (CAUTION! HF is a very aggressive and poisonous acid, it can cause deep tissue damages and systemic toxicity, and therefore proper protection and training for emergency handling must be carried out in advance).
9. Characterization can be performed with DLS and ζ-potential measurements (*see* Fig. 3).
10. During the whole functionalization procedure, MSNPs should never be dried out completely, as this would lead to aggregation and difficult re-dispersion. APDMES functionalization must be performed before the removal of the surfactant in the pores, as the latter prevents any unwanted reaction of the silane agents with the inner surface of the pores, which may lead to clogging of the pores.
11. Methods are reported in literature for CTAB removal, such as calcination or the milder Soxhlet extraction. *See* also the report by Croissant et al. [19].

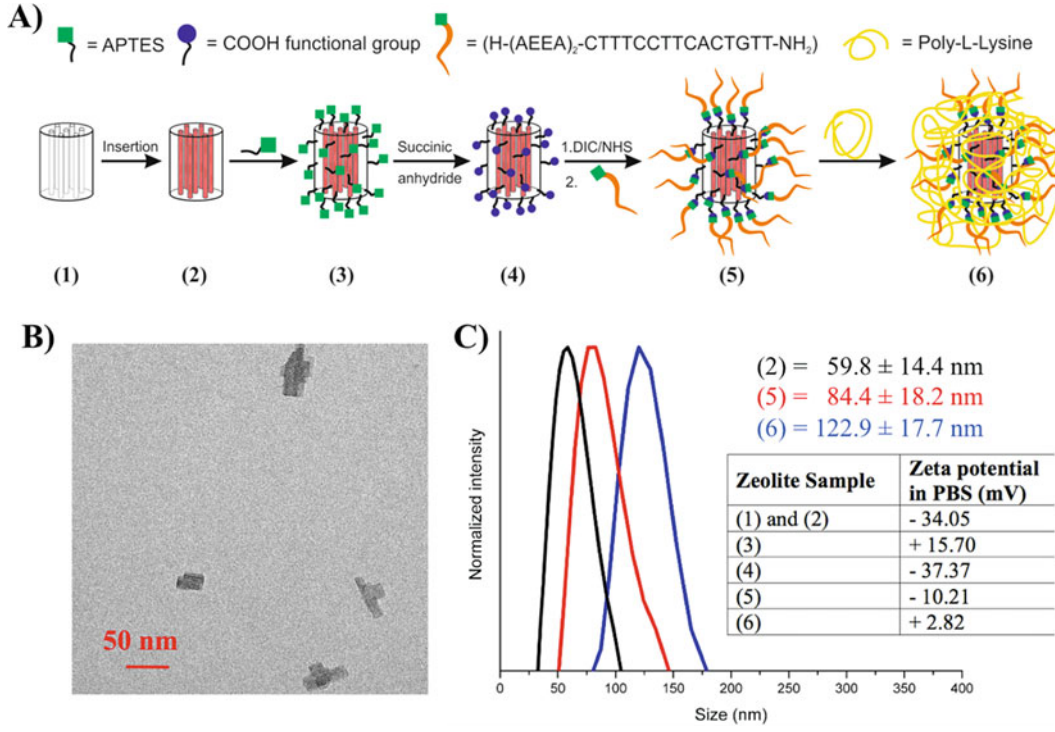

Zeolite Sample	Zeta potential in PBS (mV)
(1) and (2)	- 34.05
(3)	+ 15.70
(4)	- 37.37
(5)	- 10.21
(6)	+ 2.82

Fig. 3 (**a**) Schematic representation of the synthetic pathway for preparing PNA-zeolite-L nanoparticles; (**b**) TEM image of zeolite-L nanocrystals, (**c**) DLS measurement showing the size distribution of diverse functionalized particles; Table inset: Zeta-potential values obtained after each functionalization step (reprinted from ref. [9] with permission by Wiley-VCH)

12. This procedure, based on solvent evaporation followed by washing steps with solvent of different polarity, is known as impregnation. In this case, Temozolomide shows different solubility in methanol and water, so that a first rinsing with methanol can be used as first, strong purification step, followed by milder ones based on water. This is intended to selectively remove only the drug adsorbed on the particle surface and not the amount loaded into the pores.

Acknowledgments

This work was partially supported by MIUR PRIN09 grant (20093N774P_001), as well as by the French embassy in Italy and the French government through a MAEE grant for scientific cooperation between Italy and France (no. 778588G).

References

1. Baltimore D (1988) Gene therapy: intracellular immunization. Nature 335:395–396
2. Anderson WF (1992) Human gene therapy. Science 256:808–813
3. Kanasty R, Dorkin JR, Vegas A, Anderson D (2013) Delivery materials for siRNA therapeutics. Nat Mater 12:967–977
4. Nielsen P (2004) PNA technology. Mol Biotechnol 26:233–248
5. Babar IA, Cheng CJ, Booth CJ, Liang X, Weidhaas JB, Saltzman WM, Slack FJ (2012) Nanoparticle-based therapy in an in vivo microRNA-155 (miR-155)-dependent mouse model of lymphoma. Proc Natl Acad Sci U S A 109:E1695–E1704
6. Bahal R, Ali McNeer N, Quijano E, Liu Y, Sulkowski P, Turchick A, Lu Y-C, Bhunia DC, Manna A, Greiner DL, Brehm MA, Cheng CJ, López-Giráldez F, Ricciardi A, Beloor J, Krause DS, Kumar P, Gallagher PG, Braddock DT, Mark Saltzman W, Ly DH, Glazer PM (2016) In vivo correction of anaemia in β-thalassemic mice by γPNA-mediated gene editing with nanoparticle delivery. Nat Commun 7:13304
7. Lülf H, Bertucci A, Septiadi D, Corradini R, De Cola L (2014) Multifunctional inorganic nanocontainers for DNA and drug delivery into living cells. Chem Eur J 20:10900–10904
8. Bertucci A, Lülf H, Septiadi D, Manicardi A, Corradini R, De Cola L (2014) Intracellular delivery of peptide nucleic acid and organic molecules using zeolite-L nanocrystals. Adv Healthc Mater 1–6
9. Bertucci A (2015) Hybrid organic-inorganic interfaces for biomedical applications. Ph.D. thesis, University of Parma (Italy) and Strasbourg (France)
10. Zhang Q, Wang X, Li PZ, Nguyen KT, Wang XJ, Luo Z, Zhang H, Tan NS, Zhao Y (2014) Biocompatible, uniform, and redispersible mesoporous silica nanoparticles for cancer-targeted drug delivery in vivo. Adv Funct Mater 24:2450–2461
11. Firouzi A, Kumar D, Bull LM, Besier T, Sieger P, Huo Q, Walker SA, Zasadzinski JA, Glinka C, Nicol J, Margolese D, Stucky GD, Chmelka BF (1995) Cooperative organization of inorganic-surfactant and biomimetic assemblies. Science 267:1138–1143
12. Kruk M, Cao L (2007) Pore size tailoring in large-pore SBA-15 silica synthesized in the presence of hexane. Langmuir 23:7247–7254
13. Möller K, Müller K, Engelke H, Bräuchle C, Wagner E, Bein T (2016) Highly efficient siRNA delivery from core-shell mesoporous silica nanoparticles with multifunctional polymer caps. Nanoscale 8:4007–4019
14. Bertucci A, Prasetyanto EA, Septiadi D, Manicardi A, Brognara E, Gambari R, Corradini R, De Cola L (2015) Combined delivery of Temozolomide and anti-miR221 PNA using mesoporous silica nanoparticles induces apoptosis in resistant glioma cells. Small 11:5687–5695
15. Chang J-H, Tsai P-H, Chen W, Chiou S-H, Mou C-Y (2017) Dual delivery of siRNA and plasmid DNA using mesoporous silica nanoparticles to differentiate induced pluripotent stem cells into dopaminergic neurons. J Mater Chem B 5:3012–3023
16. Maggini L, Cabrera I, Ruiz-Carretero A, Prasetyanto EA, Robinet E, De Cola L (2016) Breakable mesoporous silica nanoparticles for targeted drug delivery. Nanoscale 8:7240–7247
17. Prasetyanto EA, Bertucci A, Septiadi D, Corradini R, Castro-Hartmann P, De Cola L (2016) Breakable hybrid organosilica nanocapsules for protein delivery. Angew Chem Int Ed 55:3323–3327
18. Ruiz AZ, Brühwiler D, Ban T, Calzaferri G (2005) Synthesis of zeolite L. tuning size and morphology. Monatsh Chem 136:77–89
19. Croissant J, Cattoën X, Man MWC, Gallud A, Raehm L, Trens P, Maynadier M, Durand JO (2014) Biodegradable ethylene-bis(propyl) disulfide-based periodic mesoporous organosilica nanorods and nanospheres for efficient in-vitro drug delivery. Adv Mater 26:6174–6180

Chapter 6

Design and Characterization of pH-Triggered DNA Nanoswitches and Nanodevices Based on DNA Triplex Structures

Andrea Idili and Francesco Ricci

Abstract

Triplex DNA is becoming a very useful domain to design pH-triggered DNA nanoswitches and nanodevices. The high versatility and programmability of triplex DNA interactions allows the integration of pH-controllable modules into DNA-based reactions and self-assembly processes. Here, we describe the procedure to characterize DNA-based triplex nanoswitches and more in general pH-triggered structure-switching mechanisms. Procedures to characterize pH-triggered DNA nanodevices will be useful for many applications in the field of biosensing, drug delivery systems and smart nanomaterials.

Key words DNA nanostructures, Nanoswitches, Triple helix, pH switching

1 Introduction

pH-regulated biomolecules play a key role in the modulation and tuning of a number of biological activities [1, 2], ranging from enzyme catalysis [3, 4] to protein folding [5], membrane function [6, 7], and apoptosis [8]. At the same time, pH represents an important and relevant physiological input both in healthy and pathological biological pathways [9]. For example, pH dysregulation is a hallmark of cancer, and many cancers are characterized by an inverted pH gradient between the inside and the outside of cells [9]. For these reasons, developing probes, switches, or nanomaterials that are able to respond to specific pH changes should prove useful for several applications including in vivo imaging, clinical diagnostics, and drug delivery [10–12].

By taking advantage of the high versatility and designability of DNA chemistry [13–21] several groups have recently developed pH-triggered DNA-based probes or nanodevices [22–33]. Such probes typically exploit DNA secondary structures that display pH dependence due to the presence of different pH-dependent DNA

Giampaolo Zuccheri (ed.), *DNA Nanotechnology: Methods and Protocols*, Methods in Molecular Biology, vol. 1811, https://doi.org/10.1007/978-1-4939-8582-1_6, © Springer Science+Business Media, LLC, part of Springer Nature 2018

motifs and modules. These include I-motif [24–26, 29, 32, 34], intermolecular triplex DNA [28, 31, 35–37], and, more recently, the A-motif [38, 39]. Despite the promising and advantageous characteristics of some of these DNA-based nanodevices, which include fast response times and sustained efficiency over several cycles, a drawback inevitably affects their performances: they all respond (with an exception [38]) over a fixed pH window that typically spans 0.2–1.8 pH units [29, 39–41]. These nanodevices, thus, cannot be adapted to provide a useful output outside these fixed pH windows.

In response to the above limitation, we have recently demonstrated programmable pH-triggered nanoswitches whose pH dependence can be finely tuned and edited over more than 5 units of pH [42, 43]. We have also demonstrated that the integration of such pH-dependent triplex forming domain into preexisting DNA-based reactions and self-assembly processes is a straightforward process that ultimately allows to control these processes at different pHs [44–46]. The present chapter aims to describe recent advances in the integration of triple helix structures within the broad area of DNA nanotechnology, in particular in the design and characterization of responsive DNA nanoswitches and nanodevices regulated and controlled by pH changes. More specifically, we describe here the experimental procedures and methodologies to characterize pH-triggered unimolecular triplex-based DNA nanoswitches [43].

Triplex structure formation requires a homopurinic–homopyrimidinic double-stranded Watson–Crick configuration, or duplex, and a single-stranded nucleotide sequence that acts as the third strand, also called TFO (triplex forming oligonucleotide) [47–49]. The third strand binds in the major groove of the duplex forming Hoogsteen or *reverse* Hoogsteen hydrogen bonds with the purines of the duplex (*see* Fig. 1). This also determines the orientation of the third strand with respect to the purines in the duplex. There are six different nucleotide triplets, also called motif, that allow the formation of two hydrogen bonds between the purines in the duplex and the nucleotides binding in the major groove [47–49]. Of note, triplex structure formation can involve a different number of DNA strands (*see* Fig. 1). This will affect not only its overall stability [50] but also its pH sensitivity and dependence on divalent cations [47–49, 51, 52].

We exploited the pH dependence of the Hoogsteen interactions in the parallel triplex structure to rationally design and engineer DNA-based nanoswitches that can respond to pH changes [28, 31, 36, 37, 43, 51]. More specifically, the CGC^+ parallel triplet requires the protonation of the N3 of cytosine in the third strand in order to form (average pK_a of protonated cytosines in triplex structure is ≈6.5) [52, 53] (*see* Fig. 1, right). In contrast, the TAT triplets are relatively stable at neutral pH and are only

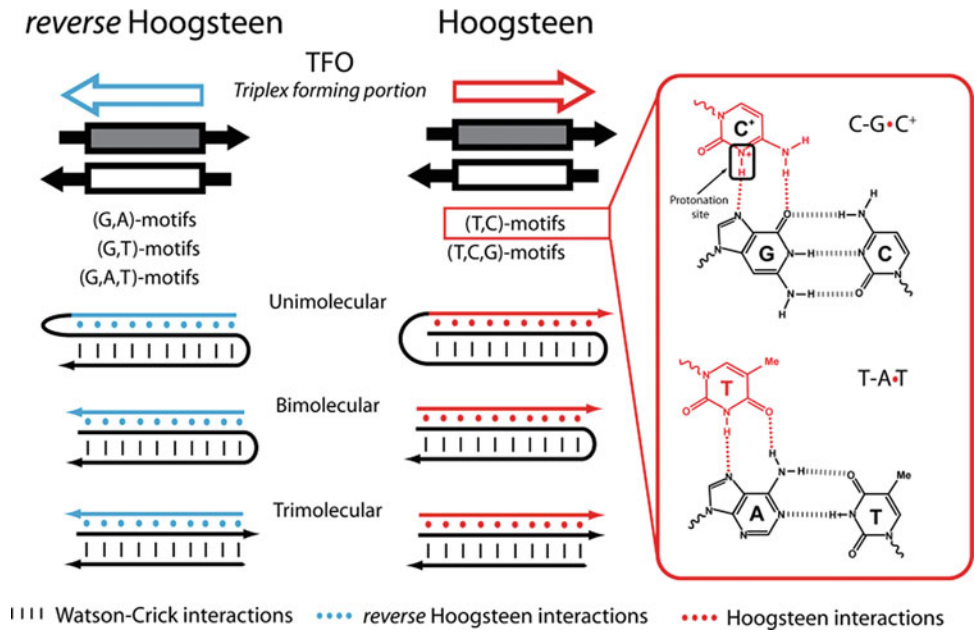

Fig. 1 Classification of triplex motifs. The third strand is parallel to the oligopurine strand in all Hoogsteen motifs (red), whereas it is antiparallel to the oligopurine strand in all reverse Hoogsteen motifs (blue). Among these different triplex motifs, parallel (T,C)-motif triplex presents a strong pH-dependence because it requires the protonation of the N3 of cytosine in the third strand to form CGC^+ triplets (right) and are only stable at acid pH (the average pK_a of protonated cytosines in triplex structures is 6.5) [53]. For this reason, triplex nanoswitches containing only CGC^+ triplets should unfold into an open duplex conformation at slightly acidic pHs. On the contrary, TAT are not sensitive to pH and the triplets should unfold at much higher pHs due to deprotonation of thymine (pK_a approximately 10) (right) [54]. Oligopyrimidine and oligopurine sequences are depicted as white and hatched boxes respectively, and the third strand oligonucleotide as a red or blue arrow. The 5′–3′ direction of each strand is shown by the sense of arrows

destabilized at pH above 10 due to the deprotonation of thymine (pK_a approximately 10) [54] (*see* Fig. 1, right). The switching strategy relies on a conformational change simply induced by the solution pH. A seminal work in this direction was reported by the group of Mao that designed a DNA nanoswitch containing three different strands [31]. At basic pH the three strands associate to form an open complex consisting of three 15-base-pair duplexes and a single-stranded region. At acidic pH (5.0) the single strand region can form Hoogsteen interactions with one of the duplex regions leading to a compact triplex structure (closed state). Such DNA nanoswitch can cycle reversibly between the closed and open state by changing the pH between 5.0 and 8.0. This work represents the first demonstration of a triplex-based DNA nanoswitch using protons as molecular input and as such should be considered as an important milestone to prove the possibility of using triplex DNA secondary structures as valuable tools in the field of DNA nanotechnology. Soon after this, the group of Zuccheri and Samorì

[28, 51] demonstrated the reversible formation/breakdown of a DNA triple-helix composed of two separate DNA strands labeled with a pair of optical reporters. The work highlights the high reversibility and fast kinetic of duplex/triplex transition thus suggesting their possible use in nanotechnology as artificial nanoswitches.

Recently, we reported a unimolecular triplex-based pH-dependent nanoswitch [43] composed of a DNA strand containing two self-complementary adjacent sections separated by a 5-base strand that form a 10-base intramolecular duplex DNA (Fig. 2). This duplex DNA is then able to form an intramolecular triplex structure with the other end of the DNA strand through Hoogsteen interactions. An interesting feature of such pH-nanoswitch, compared to other similar sensing devices based on other DNA secondary structures, is the fact that the pH sensitivity can be easily tuned and modulated by changing the relative content of CGC^+/TAT triplets (*see* Fig. 2). By doing so it was in fact possible to tune the pH

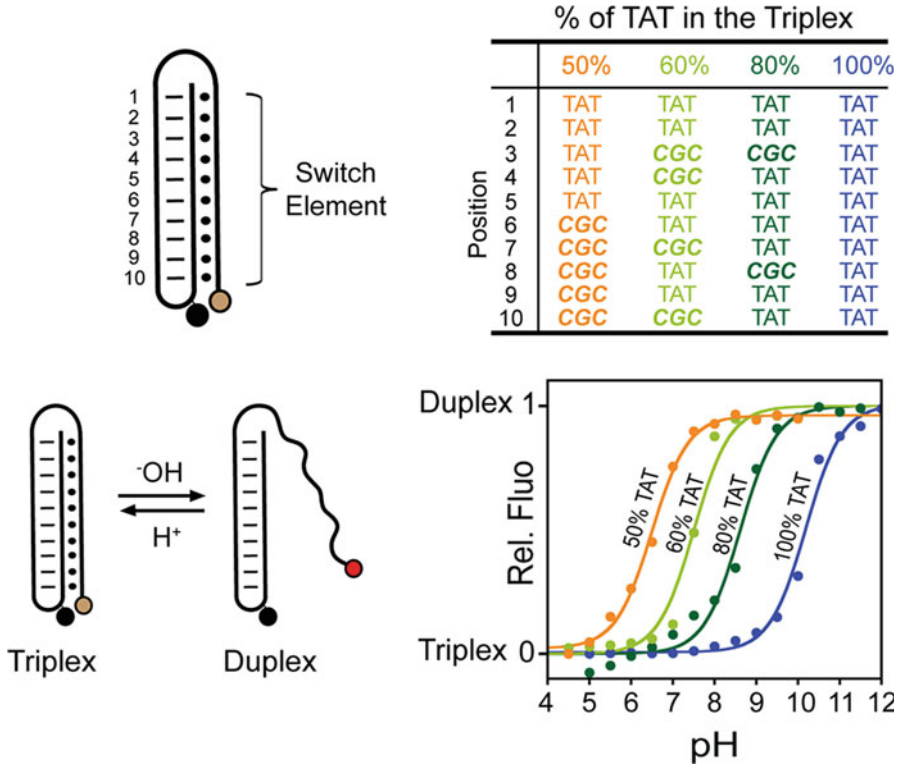

Fig. 2 Shown are the pH-titration curves (bottom, right) of the triplex nanoswitches (at 20 nM concentration) achieved in a universal buffer at 25 °C. Triplex-to-duplex transition is monitored through a pH-insensitive fluorophore (Alexa Fluor 680) inserted at the 5′-end and a quencher (Black-Hole Quencher 2, BHQ-2) internally located in the switch. The pH sensitivity of the triplex nanoswitches can be tuned by changing the CGC^+ *vs.* TAT content of the switch element, thus allowing to tune the pH window at which the triplex-to-duplex transition occurs (bottom, right). Reproduced from ref. [43] with permission from ACS

dependency of the nanoswitch over a window of more than 5 pH units (*see* Fig. 2).

For example, when the triplex structure contains only TAT triplets (100% TAT i.e., without any CGC^+ triplet), the triplex-to-duplex transition occurs at basic pHs (observed $pK_a = 10.2$) (*see* Fig. 2, blue curve). By gradually replacing TAT triplets with CGC^+ triplets, it is possible to precisely program the nanoswitch so that it opens at a specific lower pH. By replacing two TAT triplets with two CGC^+ triplets in the switch element's sequence, e.g., it is possible to reduce the observed pK_a of the nanoswitch from 10.2 to 8.6 (80% TAT, *see* Fig. 2, dark-green curve). The addition of four CGC^+ triplets in the sequence further moves the pK_a down to 7.5 (60% TAT, *see* Fig. 2, light green curve). Finally, a nanoswitch with an equal content of CGC^+ vs TAT triplets shows a complete opening at slightly acidic pHs ($pK_a = 6.5$) (50% TAT, *see* Fig. 2, orange curve). Note that triplex nanoswitches with higher CGC^+ percentage content in the sequence (i.e., 20% and 0% TAT) show the same pH dependence of the one containing an equal content of CGC^+ vs TAT (50% TAT) [43]. The modulated pH dependence at different TAT/CGC^+ contents might be explained by several factors. In the presence of low CGC^+ content (i.e., 80% TAT) the pK_a observed (8.6) is higher than that of the free cytosine (pK_a approximately 4.5) probably because of the predominant effect of the pH insensitive TAT triplets (pK_a approximately 10.2). On the other hand, as soon as 50% of the nanoswitch is composed of CGC^+ triplets (i.e., 50, 20, 0% TAT), its pK_a reaches a minimal value of approximately 6.5 [43]. This pK_a value remains, however, relatively higher than that of the free protonated cytosine likely due to both the stabilization provided by the formation of the Hoogsteen interactions (hydrogen bonds) and to the increase of base triplet stacking interactions in the nanoswitch [55, 56].

The possibility to design triplex-nanoswiches with tunable pH-dependence allows to cover an unprecedented wide range of pH over which the DNA-based nanoswitches are active. As it is the case for most DNA-based pH-triggered nanodevices, [29, 39, 40] each individual triplex nanoswitch shows a limited and fixed dynamic range (defined here as the pH range at which the switches display 10–90% of their maximum signal) which spans ~1.8 units of pH (*see*, e.g., 50% TAT, Fig. 3, left). This, in turn, corresponds to a change of $[H^+]$ concentration of 81-fold which represents the classic dynamic range window (the range of ligand concentration over which receptor occupancy shifts from 10% to 90%) inherent to single-site binding and Langmuir binding curves [57]. This fixed window can hinder the applicability of the triplex nanoswitches where changes over a wider range of pH require to be monitored with precision. To overcome this problem, it is possible to extend this dynamic range by combining two or more nanoswitches triggered over different pH windows [58]. For example, by combining

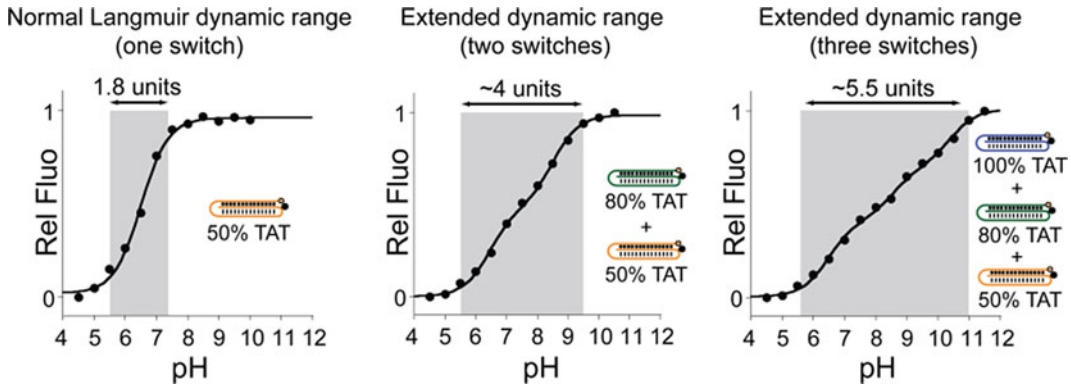

Fig. 3 By combining together two or more switches, it is possible to create a pH-sensor displaying extended dynamic ranges. Left: A single switch shows a typical fixed dynamic range of approximately 1.8 units of pH (here the 50% TAT is only an example, *see* Fig. 2). Center: By combining in the same solution two switches (i.e., 50% TAT and 80% TAT), each triggered over pH windows that are two orders of magnitude apart (*see* Fig. 2), it is possible to extend the useful dynamic range to about 4 units of pH. Right: It is possible to further extend the useful pH dynamic range (about 5.5 units of pH) by using together in the same solution three different nanoswitches (50%, 80%, and 100% TAT). Shown are the pH-titration curves obtained using a universal buffer and a total concentration of triplex nanoswitches of 20 nM (*see* Subheadings 2 and 3). Reproduced from ref. [43] with permission from ACS

the 50% TAT and 80% TAT nanoswitches it is possible to build a pH sensor with a dynamic range that spans ~4.0 units of pH (from 5.5 to 9.5) (*see* Fig. 3, center). Similarly, by combining three nanoswitches (50%, 80%, and 100% TAT), it is possible to build a pH sensor displaying a dynamic range of ~5.5 units of pH (from 5.5 to 11.0) (*see* Fig. 3, right).

The triplex nanoswitches are reversible, show a fast response time (<200 ms) and only respond over a specific pH window. To demonstrate this, three nanoswitches that are triggered over three well-separated pH windows (20%, 60%, and 100% TAT, *see* Fig. 4) [43] have been selected and tested with a series of cyclic pH-jump experiments (*see* Fig. 4). In the first experiment, for example, the pH of the three solutions containing the nanoswitches (each solution containing a different nanoswitch) was cycled from pH 5.0 to 7.0 and back to pH 5.0 for five times (*see* Fig. 4, top). Only the 20% TAT switch was triggered over this pH window, while the other two nanoswitches (60% and 100% TAT) did not give any significant signal change. In the other two series of experiments (*see* Fig. 4, center and bottom), different pH jumps have been selected to trigger only one nanoswitch. In all three experiments, it is possible to observe a high reversibility of the nanoswitches' signal and a minimal cross-activation coming from the other two switches. As expected, the fluorescence change observed was consistent with the opening/closing of a single nanoswitch thus further demonstrating both the reversibility and specificity of the triplex nanoswitches.

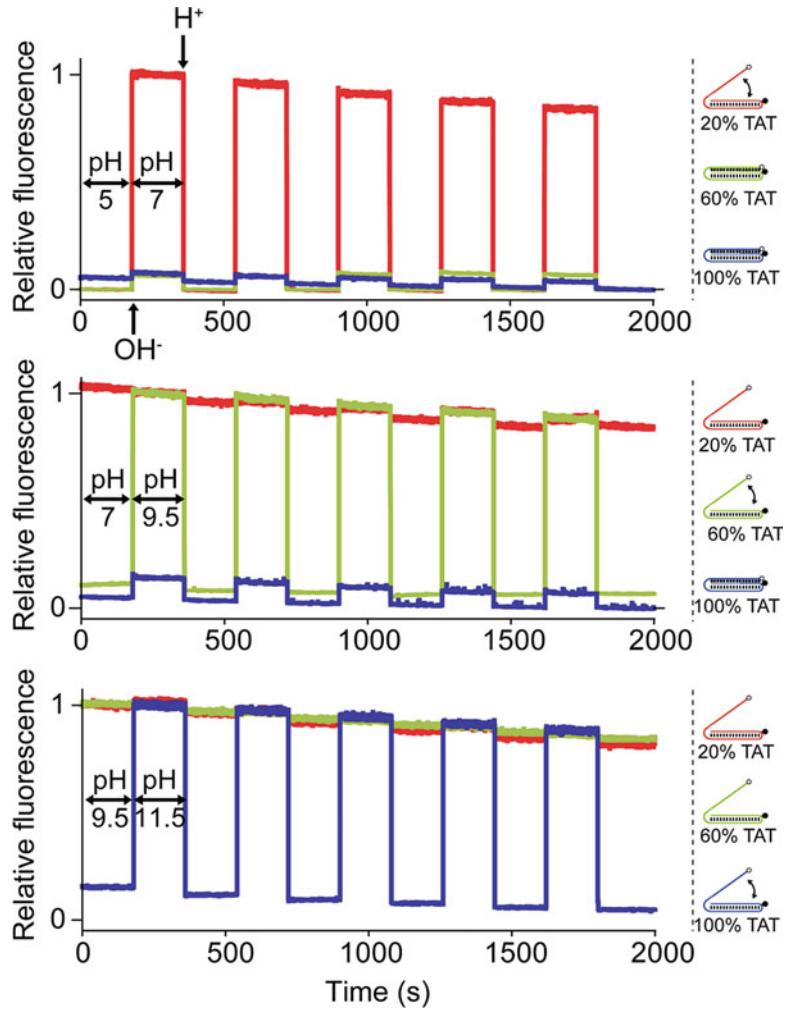

Fig. 4 Triplex pH nanoswitches show high reversibility and no cross-activation. This is demonstrated by cyclically changing the pH of three solutions each containing a single nanoswitch (20%, 60%, and 100% TAT). Top: Cycling the pH from 5.0 to 7.0 (and vice versa) only activates the most unstable switch (20% TAT, red line), while no significant signal is observed for the switches with higher TAT content (60% TAT, 100% TAT). Center: A pH change from 7.0 to 9.5 leads to opening/closing of only the 60% TAT nanoswitch (green line). Within this pH window, the 100% TAT switch (blue line) remains closed, while the 20% TAT switch is already completely open. Bottom: When the pH solution is cycled between 9.5 and 11.5, it is possible to observe the opening/closing transition of the 100% TAT (blue line), while the other two nanoswitches are already completely open within this pH range. Each solution contains only one nanoswitch (20 nM), and the pH of the solution was cyclically changed by adding small aliquots of 3 M NaOH or HCl. In this experiment we selected the 20% TAT switch over the 50% TAT switch [43], because the former displays a slightly steeper dose-response curve which better prevents cross-activation. Reproduced from ref. [43] with permission from ACS

The pH-triggered structure-switching mechanism of the triplex nanoswitches can be used to design and engineer DNA reactions based on toehold strand displacement [44]. In general in the toehold strand displacement reaction (*see* Fig. 5a), one (or more) DNA strand(s) hybridized with a template strand, which includes an exposed sticky-end called "toehold" domain, is displaced by an input strand (IS) that is complementary to the toehold domain and partially (or fully) complementary to the template strand (S), through a branch migration process [59, 60]. Recently, we have proposed two strategies in which the pH sensitivity of the triplex DNA was employed to achieve pH-control over the displacement reaction [44]. In the first strategy (*see* Fig. 5b), a clamp-like [61], triplex-forming DNA prevents strand displacement at acidic pH (*see* Fig. 5b, Panel I), while at basic pH the strand-displacement reaction can proceed with optimal kinetic (Fig. 5b, Panel II). In the second strategy (*see* Fig. 5c), in contrast, the input strand contains a pH-dependent clamp-like triplex forming portion that only under acid/neutral conditions can bind the duplex target and starts the strand displacement process (*see* Fig. 5c, Panels I and II). So, both strategies rely on the use of pH-dependent triplex forming clamp-like nanoswitches. In the first strategy, triplex formation is utilized to lock the strand and inhibit strand displacement. In the second strategy, in contrast, clamp-like triplex formation triggers strand displacement. Recently, toehold-exchange DNA strand displacement has been used to assemble dynamic and static DNA-based nanostructures, the possibility to activate/inhibit such process through a simple change of the solution's pH can be used to introduce additional control over the formation and functionality of DNA structures [62].

Apart from toehold strand-displacement reaction, other processes are often used in the field of DNA-nanotechnology. For example, the hybridization chain reaction (HCR) [63], a process through which two metastable DNA hairpins react with each other to form concatemer-like nanowires in the presence of a triggering single strand, has been used to achieve a spatiotemporal control of the self-assembly process of nucleic acid based nanostructures. HCR allows controlling the catalytic self-assembly of superior structures by using a DNA strand as trigger [64–66]. Recently, the functional units (hairpins) of HCR have been rationally reengineered to contain triplex-forming pH-dependent domains [46]. This allows to control the catalytic process using pH. In one strategy, one of the two hairpins was designed with a pH-dependent triplex-forming tail that can be opened only under basic conditions. The triplex structure thus acts as a molecular trap sequestering the toehold domain and preventing initiator binding and the start of polymerization. In a second strategy, the initiator contains a triplex-forming portion that allows to trigger the HCR process only at acidic pHs.

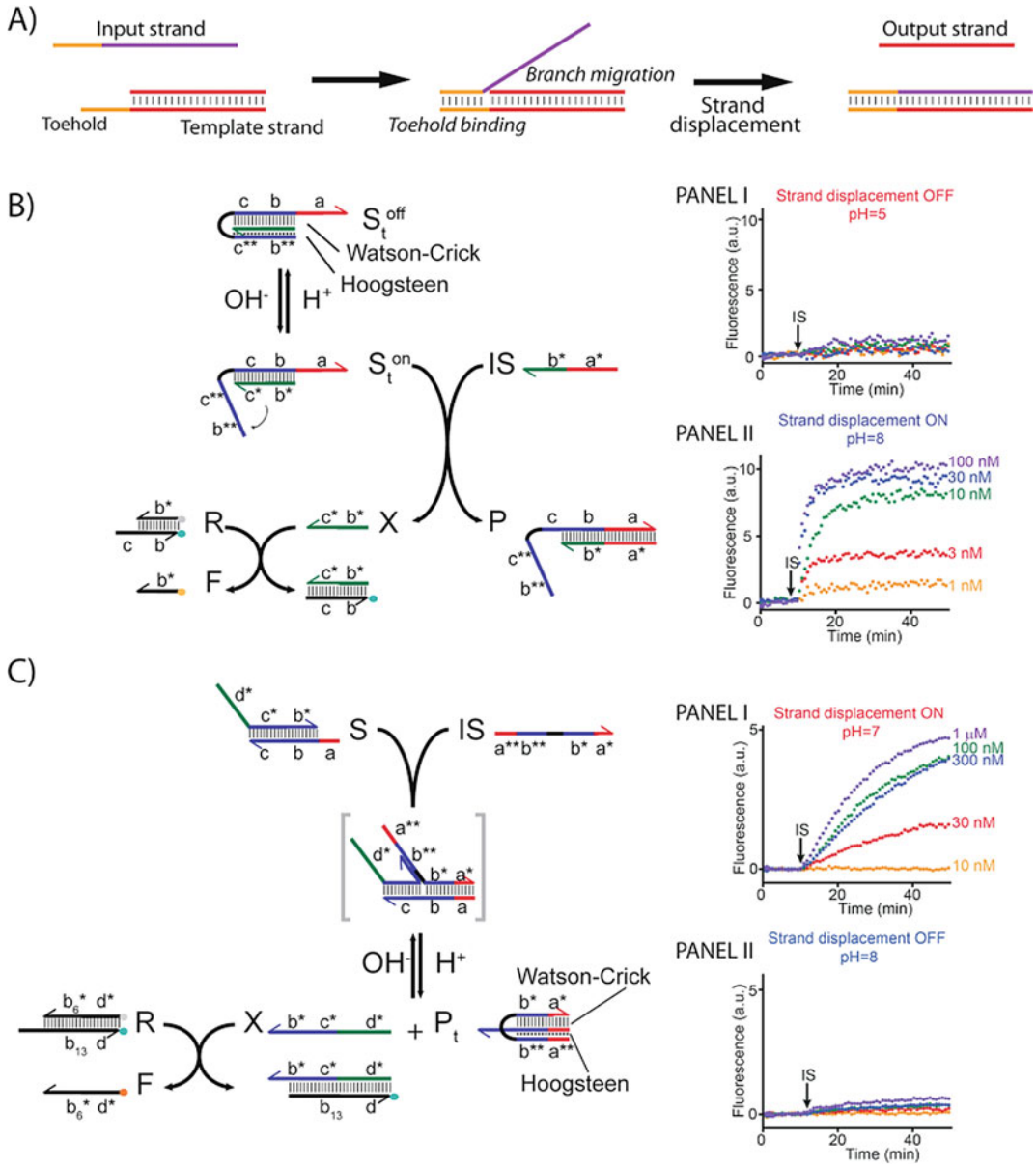

Fig. 5 pH-controlled DNA reactions. (**a**) Mechanism of a toehold-based strand-displacement reaction. (**b**) The pH-controlled toehold-based DNA strand displacement strategy activated only at basic pH. At acid pH, the additional Hoogsteen interactions in the clamp-like triplex domain, integrated in the template strand, provide an increased stabilization to the template complex that prevents branch migration upon input strand (IS) addition (Panel I). On the contrary, at basic pH Hoogsteen interactions are destabilized leading to an active complex template characterized by a simple duplex conformation. Then the exposed toehold domain can hybridize with the input strand and through a branch migration process displace the output strand (Panel II). (**c**) In the second strategy the toehold-based DNA strand displacement process is activated at acidic/ neutral pHs. The input strand is designed to comprise a triplex-domain DNA sequence that can bind through a clamp-like mechanism a strand in the template complex. At acidic/ neutral pHs, triplex formation through Hoogsteen interactions provides an additional energetic contribution that allows strand displacement to occur. On the contrary, under basic conditions, the input strand can only form Watson–Crick interactions and, due to the content and length of the toehold domain and invading portion, the branch migration process is unfavored. Reproduced from ref. [44] with permission from ACS

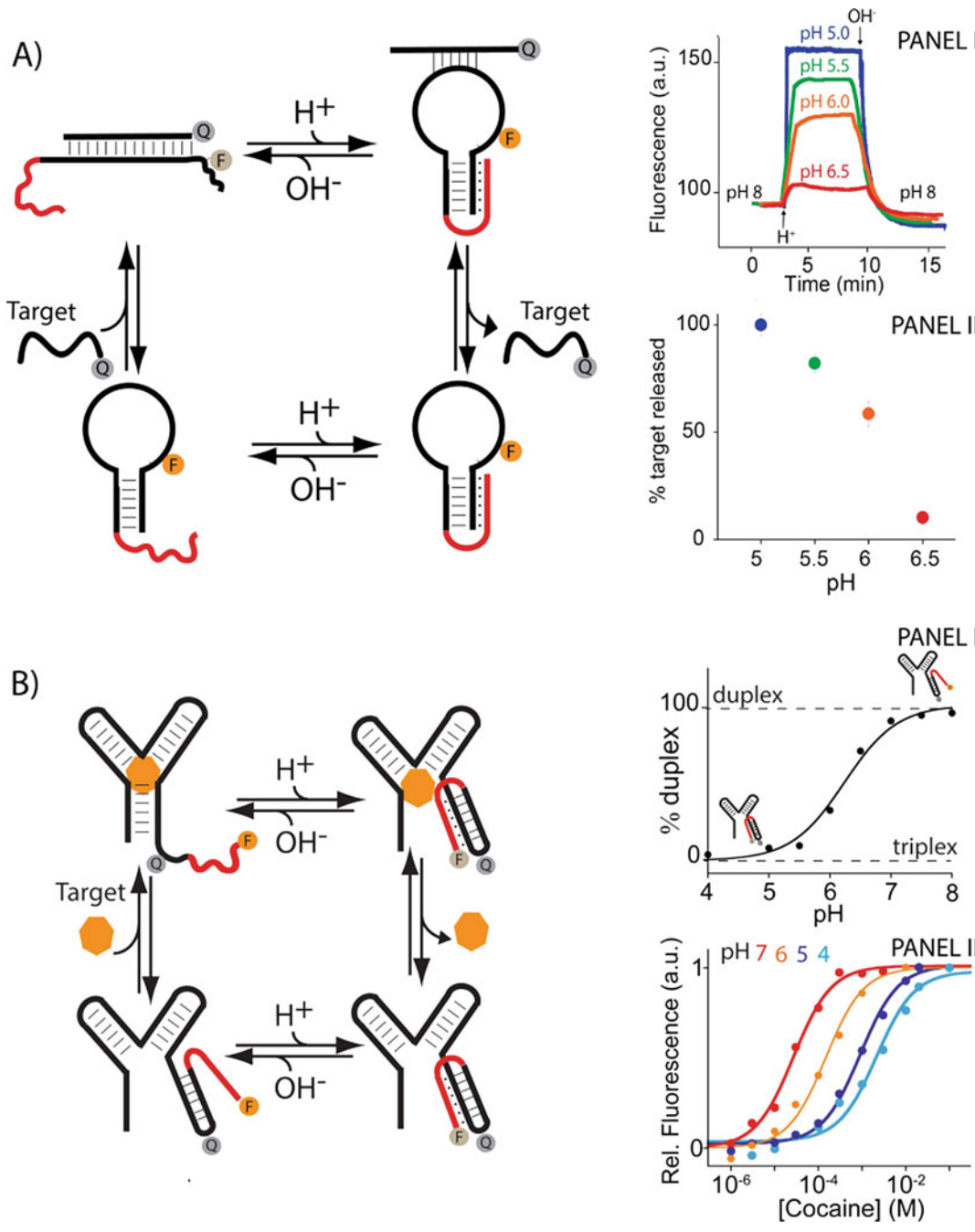

Fig. 6 pH-controlled DNA nanodevices. pH-triggered nanodevices have been reengineered by introducing in their original sequence a triplex forming pH-dependent domain so that their binding affinity for their targets can be modulated with pH. (**a**) The classic stem-loop molecular beacon has been reengineered by designing a pH-dependent triplex-forming stem (red). While at acid pH this triplex stem is highly stable, it completely unfolds to a simple duplex stem at pH higher than 7.5. The additional interactions of the triplex structure makes the stem (and thus the nonbinding state) more stable and difficult to be opened by the target, observing a poorer affinity for the target at acid pH. Therefore, the DNA-based nanodevice, through pH changes, can

pH-triggered triplex domain formation has been also used as allosteric module to design DNA-based nanodevices in order to modulate and control their activities by pH [45, 67]. Specifically, we have demonstrated that such pH-responsive nanodevices can be used to load or release a specific target via simple pH changes (*see* Fig. 6). In a first demonstration of this approach, the classic stem-loop molecular beacon was reengineered to design a pH-dependent triplex-forming stem (*see* Fig. 6a). This triplex stem is highly stable at acidic pHs and completely unfolds to a simple duplex stem at pHs higher than 7.5. Because the additional Hoogsteen interactions in the stem makes it more stable, it is possible to observe a poorer affinity for the specific DNA target at acidic pHs. So, the affinity of this triplex molecular beacon can be modulated by pH. This receptor can thus act as a DNA-based nanoswitch that, through pH changes, can reversibly load and release its target in a controlled fashion (*see* Fig. 6a, Panel I and II). By gradually decreasing the pH of the solution from pH 8.0 to 6.5, 6.0, 5.5, and 5.0, for example, it is possible to observe a reversible and gradual loading and release of the target from the pH-dependent molecular beacon. A similar approach was also adopted for a more complex DNA-based aptamer. More specifically, the cocaine-binding aptamer [68], which is thought to fold into a three-way junction upon target binding, was reengineered by adding a unimolecular triplex-DNA forming tail (*see* Fig. 6b). This tail can form a pH-dependent triplex that inhibits folding of the aptamer and thus affects its affinity (*see* Fig. 6b, panel I). The affinity of this engineered cocaine-binding aptamer can be thus modulated with pH (*see* Fig. 6b, panel II). This allows using this aptamer as a nanodevice that can load/release its cargo by changing the solution pH. This strategy thus consists in rationally inserting a pH-sensitive triplex-DNA domain that affects its affinity for the target in a pH-dependent fashion (*see* Fig. 6b). For this reason, the strategy appears quite versatile and can be adapted to potentially any nucleic acid receptor without sequence-specific limitations.

Fig. 6 (continued) reversibly load and release its target in a controlled fashion. By gradually decreasing the pH of the solution from pH 8.0 to 6.5, 6.0, 5.5, and 5.0, it is possible to observe a reversible and gradual loading and release of the target from the nanodevice (Panel I). Shown are also the percentages of target released calculated from the increase in fluorescence signal (Panel II). (**b**) The classic cocaine-binding aptamer [68] has been reengineered by introducing at its 3′-end a unimolecular triplex-DNA forming tail that, when folded, inhibits folding of the aptamer and thus its ability to bind its target. The pH-triggered triplex-to-duplex transition of this tail was demonstrated by fluorescence measurements at different pHs. At increasing pHs the triplex-structure unfolds thus increasing the relative fluorescence signal (Panel I). Because triplex formation stabilizes an alternative nonactive conformation of the aptamer, it is possible to modulate the affinity of this engineered cocaine-binding aptamer by changing the pH of the solution (Panel II). Reproduced from ref. [45] with permission from ACS

The use of triplex-forming domains as functional units to control devices and reactions in DNA-based nanotechnology represents a straightforward way to add novel functions into DNA nanodevices. The examples shown above, for example, demonstrate that it is quite easy to exploit the formation of the triplex structures to rational design novel pH-triggered nanoswitches, or to insert pH-dependent triplex DNA domains into preexisting DNA-based reactions and self-assembly processes. The high-specificity of triplex-forming sequences allows employing different pH-dependent nanodevices or sequences in the same solution. These can be used to build or control more complex structures based on, for example, several branched reactions. Finally, because the pH window at which such triplex DNA structures is sensitive can be tuned by simply changing the CGC^+ content, different DNA reactions could in principle be triggered or controlled at different pH threshold levels [42].

2 Materials

All chemicals were of analytical grade. Prepare all buffer solutions at room temperature (unless indicated otherwise) using ultrapure water (resistivity >18 MΩ cm at 25 °C). All buffers should be stored in at 5 °C.

2.1 Oligonucleotides

1. The unimolecular triplex oligonucleotides labeled with a fluorophore/quencher couple (i.e. Alexa Fluor 680/Black Hole Quencher 2), and purified by HPLC by IBA GmBH (Göttingen, Germany) (*see* **Note 1**).
2. Oligo storage buffer 1: 10 mM Tris, 0.2 mM EDTA at pH 7.9.
3. Oligo storage buffer 2: 10 mM phosphate buffer, 50 mM NaCl, 4 mM MgCl at pH 7.4.

2.2 pH Titration Curve by Fluorescence Measurement

1. 0.1 M Hydrochloric acid solution: add about 200 mL of ultrapure water in a 500 mL graduated cylinder and add 4.1 mL of HCl 33% (w/w) (about 12.1 M). Make up to 500 mL with ultrapure water (*see* **Note 2**).
2. 1 M Sodium hydroxide solution: add about 300 mL of ultrapure water in a 500 mL polypropylene beaker, add 20 g of sodium hydroxide (*see* **Note 2**), and pour the solution into a 500 mL polypropylene flask. Make up to 500 mL with ultrapure water.
3. Universal Buffer stock solution [69] (*see* **Note 3**): add about 100 mL of ultrapure water to a 500 mL graduated cylinder. Weigh the following salts: 8.9 g (0.05 mol) of sodium phosphate dibasic dihydrate ($Na_2HPO_4{\cdot}2H_2O$), 7.00 g (0.0333 mol) of citric acid monohydrate ($C_6H_8O_7{\cdot}1H_2O$)

Table 1
Volume (in mL) of 0.1 M HCl to use to set the pH of the universal buffer working solution[a]

pH	4	5	6	7	8	9	10	11
X.0	25.8	23.1	20.1	16.8	14.4	12.2	9.3	7.5
X.5	24.4	21.7	18.4	15.4	13.6	10.7	8.5	5.4

[a]Choose the volume for the desired pH value: column for pH unit value, row for decimal value (e.g., 18.4 mL for pH = 6.5)

and 3.54 g (0.057 mol) of boric acid (H_3BO_3) and transfer to the cylinder. Add 121.5 mL of 1 M sodium hydroxide and make up to 500 mL with ultrapure water.

4. Universal buffer (citrate/phosphate/borate buffer) working solutions at different pHs [69] (*see* **Note 3**): in a 50 mL volumetric cylinder add the specific amount of 0.1 M hydrochloric acid described in Tables 1 to 10 mL of the buffer stock solution to obtain the pH value desired, and make up to 50 mL with ultrapure water.
5. Varian Cary Eclipse Fluorometer (Agilent Technologies, USA) or analogous, fluorescence quartz cuvette, and temperature controller.

2.3 Extending Dynamic Range of the Triplex pH-Triggered Nanoswitch

1. A set of two or more triplex pH-triggered nanoswitches containing a different content of TAT/CGC^+ and therefore displaying a different pH-dependence (or pK_a values) (*see* **Note 4**).
2. Varian Cary Eclipse Fluorometer (Agilent Technologies, USA) or analogous, fluorescence quartz cuvette, and temperature controller.

2.4 Cyclic pH-Triggered Folding and Unfolding Experiments by Kinetic Fluorescence Measurement

1. Universal buffer (citrate/phosphate/borate buffer) at the desired pH values.
2. 3 M NaOH: add about 300 mL of ultrapure water in a 500 mL polypropylene beaker, add 60 g of sodium hydroxide (*see* **Note 2**), and pour the solution into a 500 mL polypropylene flask. Make up to 500 mL with ultrapure water.
3. 3 M HCl: add about 200 mL of ultrapure water in a 500 mL graduated cylinder and add 123.3 mL of HCl 33% (w/w) (about 12.1 M). Make up to 500 mL with ultrapure water (*see* **Note 2**).
4. Varian Cary Eclipse Fluorometer (Agilent Technologies, USA) or analogous, fluorescence quartz cuvette with magnetic stirrer and temperature controller.

2.5 Kinetic Characterization by Stopped Flow Measurements

1. Universal buffer (citrate/phosphate/borate buffer) at the desired pH values.
2. NaOH solutions at different concentrations (0.005, 0.0075, 0.01, 0.015, 0.02, 0.025 M) (*see* **Note 5**).
3. HCl solutions at different concentrations (0.005, 0.0075, 0.01, 0.015, 0.02, 0.025 M) (*see* **Note 5**).
4. SX20 Stopped-Flow Spectrometer (Applied Photophysics, USA) and temperature controller or analogous.

3 Methods

3.1 Oligonucleotides

1. Dissolve the oligonucleotide nanoswitches in oligo storage buffer 1 at the concentration of 100 μM. Aliquot and store at −30 °C.
2. Dilute one aliquot of the specific nanoswitch to 1 μM in oligo storage buffer 2 (oligo stock solution).
3. Heat the oligo stock solution to 95 °C for 5 min and cool to reach room temperature in 2 h.
4. Determine the concentration of the triplex nanoswitch using the oligo stock solution by measuring the absorbance at 260 nm using a UV-VIS spectrophotometer and a 100 μL quartz cuvette with 1 cm path length.

3.2 pH Titration Curve by Fluorescence Measurement

1. Use the universal buffer at the desired pH value.
2. Dilute the oligo stock solution of the relative triplex nanoswitch to 20 nM in the universal buffer at the desired pH value.
3. Obtain fluorescence measurements using a Cary Eclipse Fluorimeter (Agilent Technologies, USA) or analogous equipment with excitation at 679 (±5) nm and acquisition between 690 and 712 nm and with the temperature controller set up at a temperature of 25 °C.
4. Build a pH-titration curve plotting the fluorescence value at 701 nm (corresponding to the maximum emission of the fluorophore Alexa Fluor 688) in function of the relative pH values (*see* Fig. 2 and **Note 6**).
5. Obtain an estimation of the pK_a for the triplex nanoswitch from the analysis of the pH-titration curve (*see* **Note 7**).

3.3 Extending the Dynamic Range of the Triplex pH-Triggered Nanoswitch

1. Mix two or more nanoswitches oligonucleotides to reach a total nanoswitch concentration of 20 nM. Choose unimolecular triplex nanoswitches that respond in different pH windows, as needed (*see* **Note 4**).
2. Calculate the optimal mixture of triplex nanoswitches in terms of their relative concentrations by simulations as follows: a)

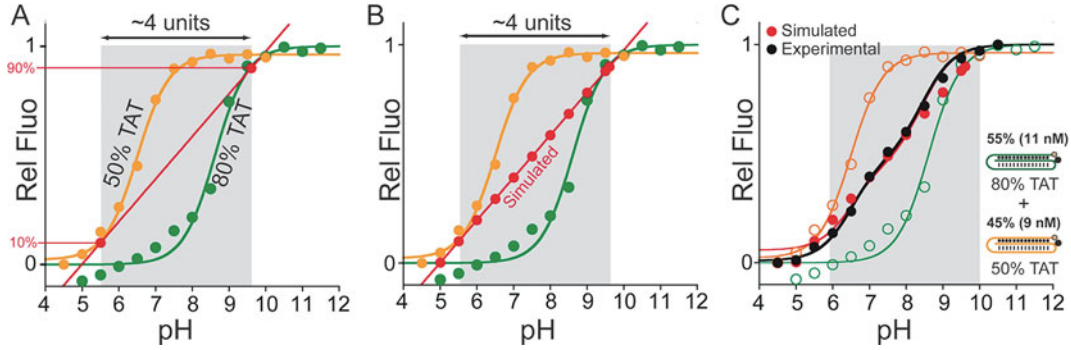

Fig. 7 Simulations to extend the dynamic range of the triplex nanoswitch. (**a**) To build the linear range of interest it is necessary to choose two specific points along the normalized pH-titration curves of the selected triplex nanoswitches, in this case 50% and 80% TAT. The first point will correspond to 10% of the maximum signal for the 50% TAT (orange) and the second to 90% of the maximum signal for the 80% TAT (green) in order to achieve an extending dynamic range of about 4 pH units; (**b**) By fitting these two points with a linear equation, it is possible to predict a set of points along the line and these will represent the real data that will be obtained during the experiment; (**c**) Using the equation in **step 4** of Subheading 3.3 to fit the simulated points along the line will allow to estimate the value for the concentration coefficients for each nanoswitch. From these coefficients, it is possible to calculate the relative concentrations for each nanoswitch to use in the experiment. Shown are the pH-titration curves obtained experimentally using a universal buffer (citrate/phosphate/borate buffer) and a total concentration of triplex nanoswitches of 20 nM

Select two nanoswitches that show a difference of about 100-fold or less in pH-sensitivity (i.e. 50% and 80% TAT); b) Build the linear range of interest by choosing two specific points along the normalized pH-titration curves of the selected triplex nanoswitches in order to achieve an extended dynamic range of about 4 pH units (*see* **Fig. 2**); c) These two selected points will correspond to the first and the last points of the simulated extended linear range (*see* Fig. 7a). Specifically, the first point will correspond to 10% of the maximum signal for the 50% TAT and the second to 90% of the maximum signal for the 80% TAT (*see* Fig. 7a).

3. Fit these two points with a linear equation to determine the slope and the y-intercept of the line. Using these estimated values calculate a set of points along the line (see Fig. 7b) to simulate the linear range that will be obtained during the experiment.
4. Use the following equation to estimate the relative concentration for each triplex nanoswitches (i.e. 50% and 80% TAT) in order to experimentally obtain the simulated extended dynamic range:

$$F = F_0 + X^{50\%\mathrm{TAT}} \cdot \left(\frac{[H^+] \cdot \left(F_{\mathrm{duplex}} - F_{\mathrm{triplex}}\right)^{50\%\mathrm{TAT}}}{[H^+] \cdot K_{\mathrm{a}}^{50\%\mathrm{TAT}}} \right) + X^{80\%\mathrm{TAT}} \cdot \left(\frac{[H^+] \cdot \left(F_{\mathrm{duplex}} - F_{\mathrm{triplex}}\right)^{80\%\mathrm{TAT}}}{[H^+] \cdot K_{\mathrm{a}}^{80\%\mathrm{TAT}}} \right) + (\ldots\ldots)$$

where $(F_{\mathrm{triplex}} - F_{\mathrm{duplex}})$ represents the amplitude of the fluorescence signal provided by each of the nanoswitches in the duplex and triplex states, $[H^+]$ represents the total concentration of hydrogen ions, $K_{\mathrm{a}}^{\%\mathrm{TAT}}$ is the observed acid constant for the nanoswitch, and $X^{\%\mathrm{TAT}}$ is the concentration coefficient for each nanoswitch [58]. Using this equation to fit the simulated points along the line allows to estimate the value for the concentration coefficients for each nanoswitch (*see* Fig. 7c). The first three parameters ($(F_{\mathrm{triplex}} - F_{\mathrm{duplex}})$, $[H^+]$ and $K_{\mathrm{a}}^{\%\mathrm{TAT}}$) can be easily obtained from the pH titration curve of each triplex nanoswitch. The concentration coefficient represents the fraction for the specific nanoswitch with respect to the total nanoswitch concentration.

5. Using the concentration obtained through the simulation, prepare the solutions of the selected triplex nanoswitches in the universal buffer (citrate/phosphate/borate buffer) at the desired pH values.
6. Build a pH-titration curve by taking the fluorescence value at 701 nm (corresponding to the maximum emission of the fluorophore Alexa Fluor 688) in function of the relative pH values (*see* Fig. 7c).

3.4 Cyclic pH-Triggered Folding and Unfolding Experiments by Kinetic Fluorescence Measurement

1. Dilute the oligo stock solution of the triplex nanoswitch to 20 nM in universal buffer titrated at a pH value where the triplex probe is completely folded.
2. Monitor the fluorescence signal of the folded state of the triplex nanoswitch until a constant value is reached.
3. Cyclically add the specific amounts of 3 M NaOH or HCl solution to the solution of nanoswitch in the fluorimeter cuvette to induce a shift in the state of folding (*see* **Notes 8** and **9**).
4. Obtain real-time fluorescence measurements using a Cary Eclipse Fluorimeter (Agilent Technologies, USA) or analogous with excitation at 679 (±5) nm and acquisition at 701 nm, with the temperature controller set at a temperature of 25 °C and the magnetic stirrer set on (*see* **Note 10**).

3.5 Kinetic Characterization by Stopped Flow Measurements

1. Dilute the stock solution of the triplex nanoswitch to 100 nM in universal buffer at a pH value where the triplex nanoswitch is completely folded (or unfolded), depending on the specific unfolding or folding reaction that will be characterized.
2. Set the SX20 Stopped-Flow Spectrometer (Applied Photophysics, USA, or analogous instrument) to work at 25 °C.
3. Set-up the unfolding (or folding) reactions of the triplex probe in the stopped-flow equipment so that it mixes the 100 nM triplex nanoswich with the required concentrations of NaOH or HCl in a 1:1 volume ratio (*see* **Note 11**).
4. Initiate the folding (or unfolding) experiment and monitor the reaction as a function of time by following the fluorescence of Alexa Fluor 680 (excitation at 679 nm ± 10 nm and emission monitored above 692 nm using a high pass filter). Repeating the measurement at least ten times.
5. Determine the folding/unfolding rate constants by using the best fit to a classic single exponential function and using a kinetic trace that is the average of ten measurements (*see* Fig. 8).

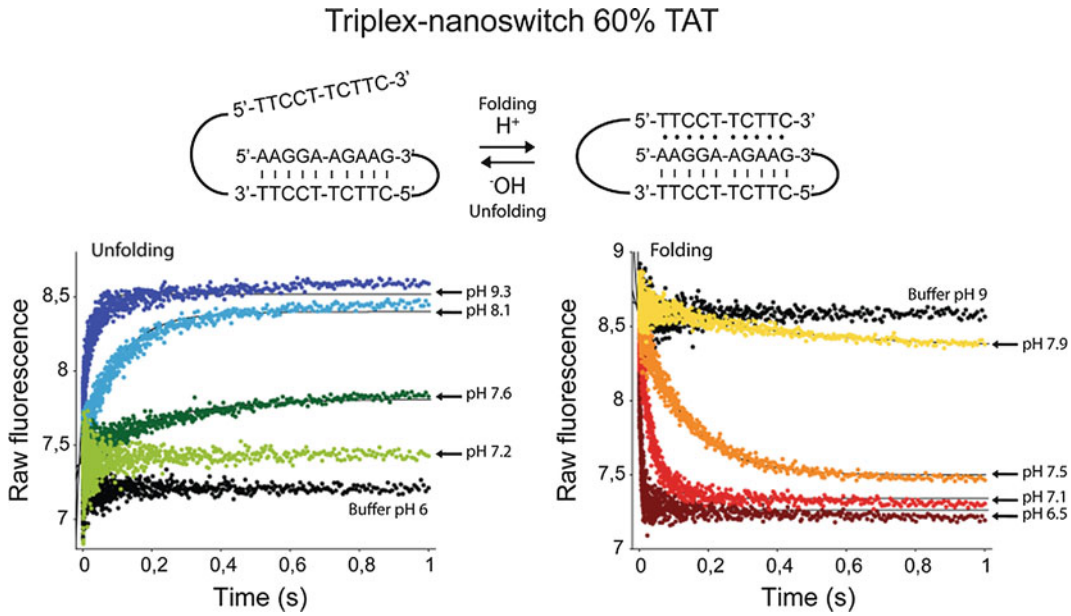

Fig. 8 The 60% TAT nanoswitch responds to pH variation within milliseconds. For the unfolding experiments (left) the nanoswitch was first equilibrated at pH 6.0 in the universal buffer (citrate/phosphate/borate buffer) (condition at which the switch is completely folded). The pH was then rapidly changed to the values indicated in the figure using a 1:1 mixing experiment with NaOH (0.005, 0.0075, 0.01, 0.015 M). For the folding experiment (right), the nanoswitch was first equilibrated at pH 8.0 in the universal buffer (citrate/phosphate/borate buffer) (condition at which the nanoswitch is completely unfolded). The pH was then rapidly changed to the values indicated in the figure using a 1:1 mixing experiment with HCl (0.005, 0.0075, 0.01, 0.015 M). Each kinetic trace shown is an average of ten measurements. Reproduced from ref. [43] with permission from ACS

4 Notes

1. Note that during the design of the unimolecular triplex probe the following criteria should be taken into account: (a) the pH-dependence of the nanoswitch is directly correlated to the relative content of CGC^+/TAT triplets present in the triplex structure (*see* Fig. 2) [43]; (b) The fluorophore and quencher have to be specifically located on the DNA structure in order to monitor the pH-triggered triplex to duplex transition (*see* Fig. 2); (c) The fluorophore chosen has to be insensitive to pH over a wide pH window. For example, Alexa Fluor dyes remain highly fluorescent over a broad pH range and are available in several distinct fluorescent colors, ranging from blue to red to near-infrared [70].
2. Dissolution of HCl or NaOH is exothermic, and the resulting heat may cause heat burns.
3. Universal buffer (citrate/phosphate/borate buffer) allows to cover a wide pH range between pH 2.0 and 12.0, and the variation in ionic strength with pH is not significant [69].
4. Triplex nanoswitches show a limited and fixed pH dynamic range (defined here as the pH range at which the switches display 10–90% of their maximum signal) which spans approximately 1.8 units of pH. To extend this fixed pH window it is needed to combine triplex nanoswitches with different pH-sensitivity in the same solution. More specifically, nanoswitches differing by 100-fold in pH-sensitivity produce a wide highly linear pH dynamic range [58].
5. To prepare NaOH and HCl solutions at varying concentrations use 3 M stock solution through serial dilutions.
6. Using a control triplex nanoswitch which is labeled with only the fluorophore allows to characterize its fluorescence emission in function of the pH at the specific experimental conditions (*see* Fig. 9). This allows to avoid pH-induced changes of the fluorescence signal.
7. The pH titration curves can be fitted using the following equation:

$$F = F_{\text{triplex}} + \left(\frac{[H^+] \cdot (F_{\text{duplex}} - F_{\text{triplex}})}{[H^+] \cdot K_a^{\text{obs}}} \right)$$

Where F_{triplex} and F_{duplex} represent the fluorescence intensities of the probe in the triplex state (closed) and duplex state (open), respectively and where $[H^+]$ represents the total concentration of hydrogen ions and K_a^{obs} is the observed acid constant for the nanoswitch.

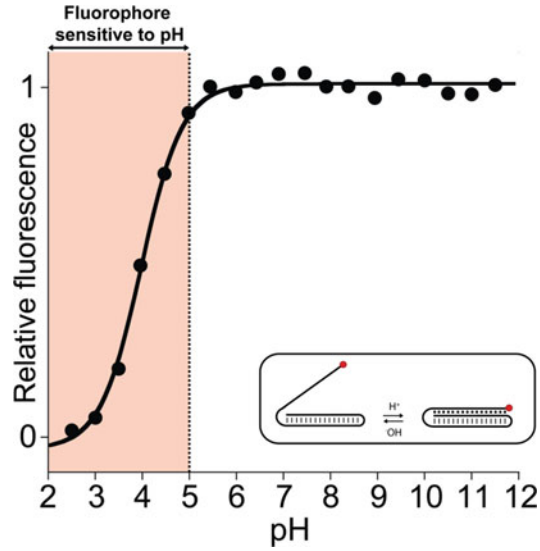

Fig. 9 To confirm that the fluorophore used (AlexaFluor 680) is insensitive to pH in the range covered by the triplex pH-triggered nanoswitches, a control probe that contains only the fluorophore (at the 3′ end) can be used [70]. Naturally, the fluorophore is positioned at the same location in all the other nanoswitches. pH titration curve of control nanoswitch demonstrate as the fluorescence intensity of the Alexa Fluor 680 remains constant between pH 5 and pH 12, the pH range at which the triplex nanoswitches perform best. Reproduced from ref. [43] with permission from ACS

8. To precisely program the pH jump in a reversible way, it is recommended to simulate the pH changes using a pH-meter (equipped with a microelectrode) and a tube with the same universal buffer solution and volume used in the kinetic fluorescence experiment. Through the pH-meter, observe the relative pH value to find the right amount of NaOH or HCl to achieve the desired pH jump.
9. Note that to obtain a rapid mixing of the solutions, it is highly recommended to use a magnetic stirrer in the cuvette and to pipet the solution up and down after each addition of the NaOH or HCl solutions.
10. After several pH jumps, it is possible to observe a small drift of fluorescence signal over time due to photobleaching of the fluorophore (i.e., Alexa Fluor 680) for the specific experimental conditions used (*see* Fig. 10). To avoid this, it is sufficient to change the acquisition time and bandwidth (*see* the caption of Fig. 10 for details).
11. Using a pH-meter (equipped with a microelectrode) and the same solutions used during the experiment, it is possible to simulate the 1:1 stopped flow mixing experiment to find out the pH reached after the addition of the NaOH/HCl solutions (*see* Fig. 9).

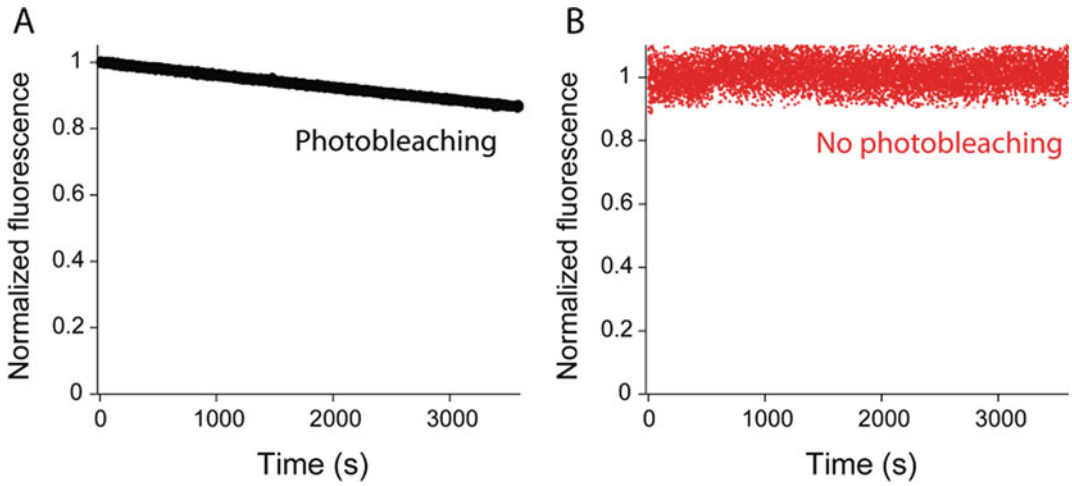

Fig. 10 The fluorophore Alexa Fluor 680 is subject to photobleaching due to the specific experimental conditions used. Left: by continuously measuring the pH nanoswitches and using an excitation bandwidth (5 nm) and an acquisition time of 0.2 s it is possible to observe a drift of the signal fluorescence of about 15% after about 30 min. Right: the same continuous measurement using a smaller excitation bandwidth (0.2 nm) and an acquisition time of 0.4 s showed no drift of signal after 30 min. The experiments shown in this figure were performed using the reference switch used in Fig. 7 in a buffered solution (citrate/phosphate/borate buffer) at pH 7.0. Reproduced from ref. [43] with permission from ACS

References

1. Lukin JA, Ho C (2004) The structure-function relationship of hemoglobin in solution at atomic resolution. Chem Rev 104:1219–1230
2. McLachlan GD, Cahill SM, Girvin ME, Almo SC (2007) Acid-induced equilibrium folding intermediate of human platelet profiling. Biochemistry 46:6931–6943
3. Nishi T, Forgac M (2002) The vacuolar (H^+)-ATPases – nature's most versatile proton pumps. Nat Rev Mol Cell Biol 3:94–103
4. Slepkov ER, Rainey JK, Sykes BD, Fliegel L (2007) Structural and functional analysis of the Na^+/H^+ exchanger. Biochem J 401:623–633
5. Matsuyama S, Llopis J, Deveraux QL, Tsien RY, Reed JC (2000) Changes in intramitochondrial and cytosolic pH: early events that modulate caspase activation during apoptosis. Nat Cell Biol 2:318–325
6. Paroutis P, Touret N, Grinstein S (2004) The pH of the secretory pathway: measurement, determinants, and regulation. Physiology 19:207–215
7. Busa WB, Nuccitelli R (1984) Metabolic regulation via intracellular pH. Am J Phys 246: R409–R438
8. Tews I, Findeisen F, Sinning I, Schultz A, Schultz JE, Linder JU (2005) The structure of a pH-sensing mycobacterial adenylyl cyclase holoenzyme. Science 308:1020–1023
9. Webb BA, Chimenti M, Jacobson MP, Barber DL (2011) Dysregulated pH: a perfect storm for cancer progression. Nat Rev Cancer 11:671–677
10. Zhou K, Liu H, Zhang S, Huang X, Wang Y, Huang G, Sumer BD, Gao J (2012) Multicolored pH-tunable and activatable fluorescence nanoplatform responsive to physiologic pH stimuli. J Am Chem Soc 134:7803–7811
11. Gallagher FA, Kettunen MI, Day SE, Hu D-E, Ardenkjær-Larsen JH, Zandt RI, Jensen PR, Karlsson M, Golman K, Lerche MH, Brindle KM (2008) Magnetic resonance imaging of pH in vivo using hyperpolarized ^{13}C-labelled bicarbonate. Nature 453:940–943
12. Saha S, Prakash V, Halder S, Chakraborty K, Krishnan Y (2015) A pH-independent DNA nanodevice for quantifying chloride transport in organelles of living cells. Nat Nanotechnol 10:645–651
13. Bath J, Turberfield AJ (2007) DNA nanomachines. Nat Nanotechnol 2:275–284
14. Seeman NC (2010) Nanomaterials based on DNA. Annu Rev Biochem 79:65–87
15. Dittmer WU, Reuter A, Simmel FC (2004) A DNA-based machine that can cyclically bind

and release thrombin. Angew Chem Int Ed 43:3550–3553
16. Douglas SM, Bachelet I, Church GM (2012) A logic-gated nanorobot for targeted transport of molecular payloads. Science 335:831–834
17. Zhou C, Yang Z, Liu D (2012) Reversible regulation of protein binding affinity by a DNA machine. J Am Chem Soc 134:1416–1418
18. Thomas JM, Yu H-Z, Sen D (2012) A mechano-electronic DNA switch. J Am Chem Soc 134:13738–13748
19. Gareau D, Desrosiers A, Vallée-Bélisle A (2016) Programmable quantitative DNA nanothermometers. Nano Lett 16:3976–3981
20. Ranallo S, Rossetti M, Plaxco KW, Vallée-Bélisle A, Ricci F (2015) A modular, DNA-based beacon for single-step fluorescence detection of antibodies and other proteins. Angew Chem Int Ed 54:13214–13218
21. Andersen ES, Dong M, Nielsen MM, Jahn K, Subramani R, Mamdouh W, Golas MM, Sander B, Stark H, Oliveira CLP, Pedersen JS, Birkedal V, Besenbacher F, Gothelf KV, Kjems J (2009) Self-assembly of a nanoscale DNA box with a controllable lid. Nature 459:73–76
22. Shimron S, Magen N, Elbaz J, Willner I (2011) pH-programmable DNAzyme nanostructures. Chem Commun 47:8787–8789
23. Wang Z-G, Elbaz J, Willner I (2011) DNA machines: bipedal walker and stepper. Nano Lett 11:304–309
24. Li T, Famulok M (2013) I-motif-programmed functionalization of DNA nanocircles. J Am Chem Soc 135:1593–1599
25. Liu D, Balasubramanian S (2003) A proton-fuelled DNA Nanomachine. Angew Chem Int Ed 42:5734–5736
26. Liu D, Bruckbauer A, Abell C, Balasubramanian S, Kang D-J, Klenerman D, Zhou D (2006) A reversible pH-driven DNA nanoswitch array. J Am Chem Soc 128:2067–2071
27. Zhou J, Amrane S, Korkut DN, Bourdoncle A, He H-Z, Ma D-L, Mergny J-L (2013) Combination of i-motif and G-quadruplex structures within the same strand: formation and application. Angew Chem Int Ed 52:7742–7746
28. Brucale M, Zuccheri G, Samorì B (2005) The dynamic properties of an intramolecular transition from DNA duplex to cytosine-thymine motif triplex. Org Biomol Chem 3:575–577
29. Modi S, Swetha MG, Goswami D, Gupta GD, Mayor S, Krishnan Y (2009) A DNA nanomachine maps spatiotemporal pH changes in living cells. Nat Nanotechnol 4:325–330
30. Chen L, Di J, Cao C, Zhao Y, Ma Y, Luo J, Wen Y, Song W, Song Y, Jiang L (2011) A pH-driven DNA nanoswitch for responsive controlled release. Chem Commun 47:2850–2852
31. Chen Y, Lee S-H, Mao C (2004) A DNA nanomachine based on a duplex-triplex transition. Angew Chem Int Ed 43:5335–5338
32. Wang W, Yang Y, Cheng E, Zhao M, Meng H, Liu D, Zhou D (2009) A pH-driven, reconfigurable DNA nanotriangle. Chem Commun (7):824–826
33. Liedl T, Simmel FC (2005) Switching the conformation of a DNA molecule with a chemical oscillator. Nano Lett 5:1894–1898
34. Liu H, Xu Y, Li F, Yang Y, Wang W, Song Y, Liu D (2007) Light-driven conformational switch of i-motif DNA. Angew Chem Int Ed 46:2515–2517
35. Han X, Zhou Z, Yang F, Deng Z (2008) Catch and release: DNA tweezers that can capture, hold, and release an object under control. J Am Chem Soc 130:14414–14415
36. Yang M, Zhang X, Liu H, Kang H, Zhu Z, Yang W, Tan W (2015) Stable DNA nanomachine based on duplex-triplex transition for ratiometric imaging instantaneous pH changes in living cells. Anal Chem 87:5854–5859
37. Li X-M, Song J, Cheng T, Fu P-Y (2013) A duplex-triplex nucleic acid nanomachine that probes pH changes inside living cells during apoptosis. Anal Bioanal Chem 405:5993–5999
38. Saha S, Chakraborty K, Krishnan Y (2012) Tunable, colorimetric DNA-based pH sensors mediated by A-motif formation. Chem Commun 48:2513–2515
39. Chakraborty S, Sharma S, Maiti PK, Krishnan Y (2009) The poly dA helix: a new structural motif for high performance DNA-based molecular switches. Nucleic Acids Res 37:2810–2817
40. Ohmichi T, Kawamoto Y, Wu P, Miyoshi D, Karimata H, Sugimoto N (2005) DNA-based biosensor for monitoring pH in vitro and in living cells. Biochemistry 44:7125–7130
41. Nesterova IV, Nesterov EE (2014) Rational design of highly responsive pH sensors based on DNA i-motif. J Am Chem Soc 136:8843–8846
42. Hu Y, Cecconello A, Idili A, Ricci F, Willner I (2017) Triplex DNA nanostructures: from basic properties to applications. Angew Chem Int Ed. https://doi.org/10.1002/ange.201701868
43. Idili A, Vallée-Bélisle A, Ricci F (2014) Programmable pH-triggered DNA nanoswitches. J Am Chem Soc 136:5836–5839

44. Amodio A, Zhao B, Porchetta A, Idili A, Castronovo M, Fan C, Ricci F (2014) Rational design of pH-controlled DNA strand displacement. J Am Chem Soc 136:16469–16472
45. Porchetta A, Idili A, Vallée-Bélisle A, Ricci F (2015) General strategy to introduce pH-induced allostery in DNA-based receptors to achieve controlled release of ligands. Nano Lett 15:4467–4471
46. Idili A, Porchetta A, Amodio A, Vallée-Bélisle A, Ricci F (2015) Controlling hybridization chain reactions with pH. Nano Lett 15:5539–5544
47. Vasquez KM, Glazer PM (2002) Triplex-forming oligonucleotides: principles and applications. Q Rev Biophys 35:89–107
48. Frank-Kamenetskii MD, Mirkin SM (1995) Triplex DNA structures. Annu Rev Biochem 64:65–95
49. Radhakrishnan I (1994) DNA triplexes: solution structures, hydration sites, energetics, interactions, and function. Biochemistry 33:11405–11416
50. Lee H-T, Arciniegas S, Marky LA (2008) Unfolding thermodynamics of DNA pyrimidine triplexes with different molecularities. J Phys Chem B 112:4833–4840
51. Kolaric B, Sliwa M, Brucale M, Vallée RAL, Zuccheri G, Samori B, Hofkens J, De Schryver FC (2007) Single molecule fluorescence spectroscopy of pH sensitive oligonucleotide switches. Photochem Photobiol Sci 6:614–618
52. Sugimoto N, Wu P, Hara H, Kawamoto Y (2001) pH and cation effects on the properties of parallel pyrimidine motif DNA triplexes. Biochemistry 40:9396–9405
53. Leitner D, Schröder W, Weisz K (2000) Influence of sequence-dependent cytosine protonation and methylation on DNA triplex stability. Biochemistry 39:5886–5892
54. Saenger W (1984) Principles of nucleic acid structure. Springer, New York
55. Soto AM, Loo J, Marky LA (2002) Energetic contributions for the formation of TAT/TAT, TAT/CGC+, and CGC−/CGC+ base triplet stacks. J Am Chem Soc 124:14355–14363
56. Asensio JL, Lane AN, Dhesi J, Bergqvist S, Brown T (1998) The contribution of cytosine protonation to the stability of parallel DNA triple helices. J Mol Biol 275:811–822
57. Ferrell JE Jr (1996) Tripping the switch fantastic: how a protein kinase cascade can convert graded inputs into switch-like outputs. Trends Biochem Sci 21:460–466
58. Vallée-Bélisle A, Ricci F, Plaxco KW (2012) Engineering biosensors with extended, narrowed, or arbitrarily edited dynamic range. J Am Chem Soc 134:2876–2879
59. Seelig G, Soloveichik D, Zhang DY, Winfree E (2006) Enzyme-free nucleic acid logic circuits. Science 314:1585–1588
60. Zhang DY, Seelig G (2011) Dynamic DNA nanotechnology using strand-displacement reactions. Nat Chem 3:103–113
61. Idili A, Plaxco KW, Vallée-Bélisle A, Ricci F (2013) Thermodynamic basis for engineering high-affinity, high-specificity binding-induced DNA clamp Nanoswitches. ACS Nano 7:10863–10869
62. Amodio A, Adedeji AF, Castronovo M, Franco E, Ricci F (2016) pH-controlled assembly of DNA tiles. J Am Chem Soc 138:12735–12738
63. Dirks RM, Pierce NA (2004) Triggered amplification by hybridization chain reaction. Proc Natl Acad Sci U S A 101:15275–15278
64. Yin P, Choi HMT, Calvert CR, Pierce NA (2008) Programming biomolecular self-assembly pathways. Nature 451:318–322
65. Sadowski JP, Calvert CR, Zhang DY, Pierce NA, Yin P (2014) Developmental self-assembly of a DNA tetrahedron. ACS Nano 8:3251–3259
66. Nie Z, Wang P, Tian C, Mao C (2014) Synchronization of two assembly processes to build responsive DNA nanostructures. Angew Chem Int Ed 53:8402–8405
67. Del Grosso E, Idili A, Porchetta A, Ricci F (2016) A modular clamp-like mechanism to regulate the activity of nucleic-acid target-responsive nanoswitches with external activators. Nanoscale 8:18057–18061
68. Stojanovic MN, de Prada P, Landry DW (2001) Aptamer-based folding fluorescent sensor for cocaine. J Am Chem Soc 123:4928–4931
69. Östling S, Virtama PA (1946) Modified preparation of the universal buffer described by Teorell and Stenhagen. Acta Phys Scand 11:289–293
70. Panchuk-Voloshina N, Haugland RP, Bishop-Stewart J, Bhalgat MK, Millard PJ, Mao F, Leung WY, Haugland RP (1999) Alexa dyes, a series of new fluorescent dyes that yield exceptionally bright, photostable conjugates. J Histochem Cytochem 47:1179–1188

Chapter 7

Characterizing Surface-Immobilized DNA Structures and Devices Using a Quartz Crystal Microbalance with Dissipation Monitoring (QCM-D)

Katherine E. Dunn, Martin A. Trefzer, Steven Johnson, and Andy M. Tyrrell

Abstract

A quartz crystal microbalance with dissipation monitoring can be used to study the mass and structure of surface-immobilized layers of molecules, in real time. Here we describe the use of the technique to study DNA structures and devices.

Key words QCM-D, Surface-immobilization, DNA nanostructures, DNA molecular machines

1 Introduction

DNA machines on surfaces are receiving increasing attention due to their potential for incorporation into new types of DNA computers. For example, surface immobilization can permit spatial localization of molecular circuits, leading to higher speed, sharper switching, greater modularity, and increased parallelization [1]. Surface-immobilized DNA devices may also play a significant role in hybrid bioelectronic systems, in which biomolecular machinery is fully integrated with conventional electronic circuitry [2]. Such technology could exhibit the advantages of biomolecular computation (low power dissipation, inherently parallel processing, biocompatibility), while harnessing the capability of silicon circuits to overcome some of the shortcomings, such as slow operation.

However, immobilization of molecules on a surface can affect their behavior. On surfaces, DNA strands hybridize more slowly [3], changes are observed in the transition threshold for peptide restructuring [4], and the operation of restriction enzymes can be inhibited [5]. Consequently, if surface-immobilized DNA structures and devices are to be exploited in any applications, it is necessary to study their properties in situ on the surface.

Giampaolo Zuccheri (ed.), *DNA Nanotechnology: Methods and Protocols*, Methods in Molecular Biology, vol. 1811,
https://doi.org/10.1007/978-1-4939-8582-1_7, © Springer Science+Business Media, LLC, part of Springer Nature 2018

A quartz crystal microbalance with dissipation monitoring (QCM-D) [6] allows both the mass and viscoelastic properties of surface-immobilized DNA structures and devices to be observed in real time [7–9]. The technique involves the use of a sensor consisting of a piezoelectric quartz disc with a gold electrode on either side (Fig. 1a, b). A voltage is applied across the electrodes, causing the sensor to oscillate. The resulting acoustic wave propagates through any molecules immobilized on the sensor surface and into the solution above it. The crystal oscillation frequency, f, is related to the mass of the sensor and the mass deposited on its surface. To measure the viscoelastic properties of a surface-immobilized molecular layer, the quality factor (Q) of the quartz resonator is measured. This is achieved by switching off the drive voltage, and extracting a time constant, τ, for the decay of the amplitude. The dissipation, D, is then $1/Q$, where $Q = \pi f \tau$.

For rigid layers, an observed frequency change is directly proportional to the mass change, in accordance with the Sauerbrey

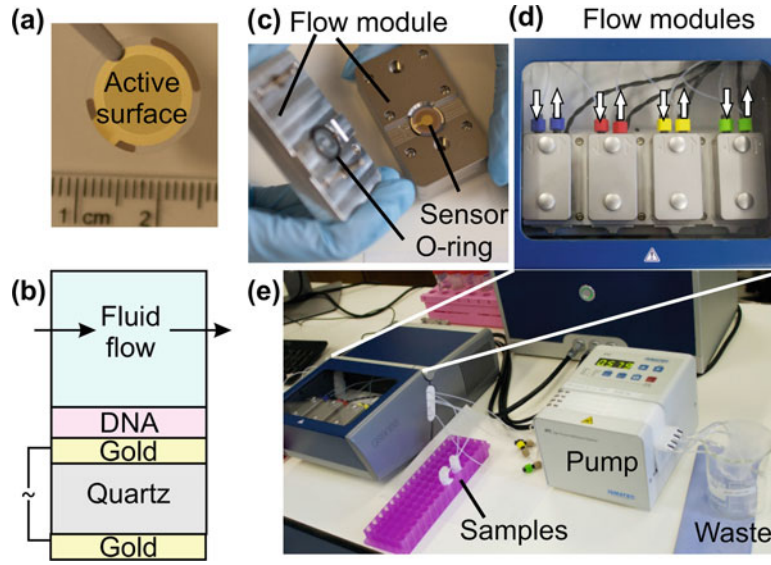

Fig. 1 Quartz Crystal Microbalance with Dissipation Monitoring. (**a**) QCM-D sensor, which consists of a piezoelectric quartz disc with gold electrodes on either side. This image shows the active side of a Biolin QSX-301 sensor, which has a diameter of 14 mm and a thickness 0.3 mm. (**b**) Schematic of the operating principle of QCM-D. An AC voltage is applied across the gold electrodes, causing the sensor to oscillate. The resulting acoustic wave propagates into the solution above the sensor. The fluid flow is driven by a peristaltic pump. (**c**) Installation of a sensor in a flow module, showing the reverse side. (**d**) Four flow modules set up in the Q-sense apparatus, with tubing connected. White arrows show the direction of flow, which is also indicated by the markings on the flow modules themselves. (**e**) Overall setup, showing samples, flow modules, the main apparatus, the pump and a waste beaker

equation [7]. This relation is often not valid for biomolecular layers, which may be highly viscoelastic. In this case, the properties of the surface-immobilized molecules can be evaluated (for a particular point or segment of the experiment) by calculation of the acoustic ratio $\Delta D/\Delta f$ [8, 9] or (for an entire experiment) by examination of plots of ΔD against Δf [10]. For dynamic processes, frequency and/or dissipation data may be plotted as a function of time and fitted to yield estimates of rates [10]. Comparison of the magnitude of frequency or dissipation changes in different experiments may also provide useful insight.

The sensor is placed in a flow module (Fig. 1c), and solutions can be introduced using tubing and a pump. The system we use (Fig. 1d, e) contains four flow modules, which means that we can run four independent experiments in parallel. We have used this system to study a range of DNA nanostructures and devices, exploring how surface immobilization affects the dynamics of toehold-mediated strand displacement on surfaces [10], the switching of DNA logic gates [11], and the operation of a new rotary DNA nanomotor [12]. Here we explain in detail the technique that we use and demonstrate that we can reliably achieve reproducible results. We will describe the procedure for immobilizing a thiol-modified DNA molecule on a gold surface and observing hybridization or toehold-mediated strand displacement. We use the term "capture strand" to refer to a single-stranded thiol-modified DNA oligonucleotide, and the term "capture complex" to refer to a partially double stranded DNA molecule that contains a capture strand hybridized to one or more other DNA strands (as shown in Fig. 2a, c). The "target" is the molecule that interacts with the capture strand/complex.

Variants on this method have also been used in our laboratory to study antibody mimetics [13] and proteins involved in biomineralization [14]. The apparatus can also be used to make electrochemical and QCM-D measurements simultaneously, and this facility has been used in our laboratory to study the surface modification chemistry that was to be used in a new biosensor that could make both photonic and electrochemical measurements [15].

2 Materials

All solutions should be prepared using ultrapure water (e.g.: MilliQ, 18.2 MΩ cm at 25 °C).

1. Ethanol, analytical grade, 100%.
2. Hamilton syringe.
3. Solution of Hellmanex® III (approx. 2%): dispense approximately 1 L of water into a suitable bottle, and add approximately 20 mL of Hellmanex III 100% concentrate (*see* **Note 1**).

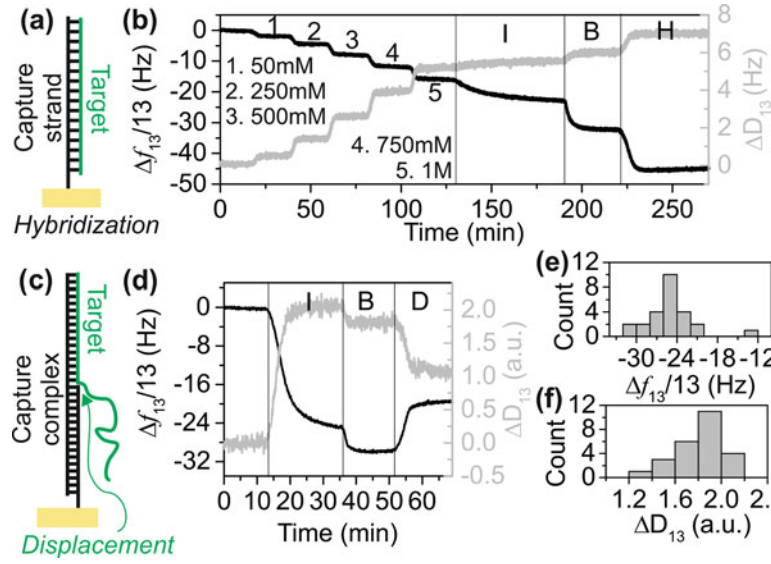

Fig. 2 Representative QCM-D experiments. (**a**) The DNA strands used to study hybridization. The black strand is a "capture strand" that is immobilized on the gold surface via a thiol modification at the 3′ end (sequence: ACACGCATACACC-CAT). The green strand is the "target strand" (sequence: ATGGGTGTATGCGTGT, the reverse complement of the capture strand). (**b**) QCM-D data for a hybridization experiment; part of this data was used in ref. [2]. The first section shows the effect of salt concentration on the frequency and dissipation baselines. When the measurement was started, ultrapure (MilliQ) water was being flowed through the system. Five solutions of 1× TE containing the indicated concentration of NaCl were then used, before immobilization (phase marked "I") of a 300 nM solution of capture strand (part (**a**), black strand) in 1 M NaCl/1× TE. The phase marked "B" corresponds to backfilling with 1 mM MCH in 1 M NaCl/1× TE, and the final phase ("H") shows the hybridization of the immobilized capture strand with a target strand (part (**a**), green) at 300 nM in 1 M NaCl/1× TE. (**c**) The molecules used in the study of toehold-mediated DNA strand displacement [10]. (**d**) Immobilization ("I") of preformed capture complex (part (**c**), black) at 300 nM, backfilling ("B") with 1 mM MCH, displacement ("D") with target strand (part (**c**), green) at 900 nM. The running buffer was 1 M NaCl/1× TE throughout. Data was used in ref. [10]. (**e**, **f**) Measured frequency and dissipation shifts for immobilization of capture complex shown in (**c**) (black structure) in repeated experiments

4. 1× TE: 10 mM Tris–HCl pH 8.0, 1 mM EDTA. Prepare 100 mL of 1× TE, e.g.: by dilution of a purchased stock solution of 100× TE (*see* **Note 2**).
5. 2 M NaCl/1× TE: Use 50 mL of the 1× TE stock to dissolve 5.844 g of NaCl, yielding 2 M NaCl/1× TE.
6. 1× running buffer: use equal volumes of the 2 M NaCl/1× TE and 1× TE solutions to prepare 20 mL of 1 M NaCl/1× TE. Mix by vortexing.

7. Capture strand/capture complex: upon receipt, resuspend the DNA oligonucleotides in 1× TE to form stock solutions of thiol-modified capture strand and other components (*see* **Note 3**). For a QCM-D experiment with N sensors, use stock solutions of DNA, and the previously prepared stocks of 1× TE and 2 M NaCl/1× TE to prepare N 800 μL aliquots of capture strand/complex at 300 nM (*see* **Note 4**) in 1× running buffer.
8. Backfilling agent, 6-mercapto-1-hexanol (MCH, *see* **Note 5**): use a Hamilton syringe to add approximately 1.4 μL of mercaptohexanol (assuming 97% purity; density is 0.981 g/mL and molecular weight is 134.24 g/mol) to 10 mL of running buffer. Rinse the Hamilton syringe with ethanol after use.
9. Target DNA: upon receipt, resuspend DNA in 1× TE. For the QCM-D experiment, prepare a working solution of target strand/complex (T) at the desired concentration in 1× running buffer (*see* **Note 6**). Mix by vortexing.
10. Lint-free wipes.
11. Compressed nitrogen stream (*see* **Note 7**).
12. Ultrasonic bath.
13. UV-ozone cleaner.
14. QCM-D apparatus: we use a Biolin Scientific Q-sense E4 machine (now known as a Q-sense Analyser).
15. QCM-D sensors (*see* **Note 8**): we normally use gold-coated AT-cut quartz sensors, fundamental frequency 4.95 MHz ± 50 kHz, from Biolin Scientific (reference number QSX-301).
16. Parafilm.
17. Tweezers (steel, with broad rounded tips that will not damage the sensor).

3 Method

3.1 Cleaning the Sensors

1. Clean the tweezers (*see* **Note 9**).
2. Use the tweezers to place the required number of sensors (*see* **Note 10**) in a UV-ozone reactor, with the active surface (larger of the two gold electrodes) facing upwards. Clean for 10 min (*see* **Note 11**).
3. Remove the sensors from the UV-ozone reactor and immerse in a 2% solution of Hellmanex III, in a small jar or beaker. Place the jar/beaker in an ultrasonic bath, and sonicate for 10 min (*see* **Note 12**).
4. Remove the sensors from the jar/beaker and place in a second jar/beaker, which in this case should contain water. Do not allow the sensors to dry because smears may appear on the

surface. Place the new jar/beaker in the ultrasonic bath, and sonicate for 10 min.

5. Repeat **step 4** with a jar containing fresh water (*see* **Note 13**).
6. Dry the sensors gently with nitrogen gas (*see* **Note 14**).
7. Repeat **step 2**, but this time clean the sensors for 30 min.
8. Soak the sensors in 100% ethanol for 30 min (*see* **Note 15**).
9. Dry the sensors gently with nitrogen gas (*see* **Note 16**).

3.2 Performing the QCM-D Experiment

The following operations should be verified against the manufacturer's instructions for the QCM instrumentation in use. The following applies to the instrument we employ [16].

1. Open the flow module. Check the O-rings (*see* **Note 17**).
2. Install each sensor in a flow module, ensuring it is correctly seated, the right way up and in the correct orientation (*see* Fig. 1c). Tighten the screws holding the flow module together (*see* **Note 18**), install the flow module in the machine and secure using the latch.
3. Connect the tubing (*see* **Note 19**).
4. Close the lid of the Q-sense and switch it on.
5. Open the QCM software (Qsoft). Activate the temperature control and set the temperature to 16 °C (*see* **Note 20**). Wait a few minutes until the system equilibrates.
6. Start running ultrapure water through the system at a flow rate of 100 μL/min. When the full length of tubing has been filled (water is emerging into the waste beaker), set up the measurement. Find the frequencies for all sensors that are in use, and look at all overtones (*see* **Note 21**). We usually check the values of frequency, dissipation and amplitude for the first three. Typical values for dissipation and amplitude are given in Table 1 for the first three overtones for the type of sensors we normally use.

Table 1
Typical values of dissipation and amplitude for first three overtones, for QSX301 sensors in ultrapure water or running buffer (note that the range of initial values of *D* is larger than the shift ΔD induced by a change in buffer). The fundamental frequency of the sensors is 4.95 MHz ± 50 kHz

Overtone	D ($\times 10^{-6}$, a.u.)	Amplitude (a.u.)
1	380–420	18–20
3	180–210	13–15
5	150–160	9–11

Values are approximate

7. Start the measurement. Continue running water through the system for approximately 1 h (*see* **Note 22**). It is very important to ensure that the quantity of liquid in the input tube is sufficient for the entire duration of the step. If it is not sufficient, the pump must be stopped before the tubes run dry to avoid creating bubbles in the system. This applies at all stages of the experiment (*see* **Note 23**).
8. Turn the pump off. Switch inlet tubes to a stock of 1× running buffer.
9. Switch the pump on again. When the running buffer reaches the sensor surface, the frequency and dissipation will change significantly.
10. After the running buffer reaches the sensor surface and a flat signal has been established, switch the pump off. Change the pump rate to 20 μL/min and restart (*see* **Note 24**).
11. Set up a new measurement in the software. Find all overtone frequencies again. Set appropriate sampling by moving the signal-to-noise slider to the desired position. If the process to be examined is unlikely to be either particularly fast or particularly slow, leave the slider in the default central position. The sampling rate is usually not critical and in our experience the central setting is appropriate for most experiments.
12. Start the measurement. Allow the system to record for a few minutes to establish the baselines (*see* **Note 25**). While waiting, cut several pieces of Parafilm (approx. 5 cm × 5 cm) and remove its backing paper.
13. Stop the pump. Switch from running buffer to capture strand/complex samples in Eppendorfs (*see* **Note 26**). Ensure that the tubing reaches the bottom of the Eppendorf, close the lid as far as possible without crushing the tubing, and wrap Parafilm around the Eppendorf and the tubing to secure the setup and create a seal.
14. Restart the pump. It will take some time for the sample to reach the sensor: 10–20 min, depending on the length of the tubing.
15. Monitor the frequency and dissipation until a plateau is achieved (*see* **Note 27**).
16. Stop the pump and switch to the backfilling agent MCH in Eppendorfs. Avoid breathing the vapours and switch the sample as quickly as possible (*see* **Note 28**).
17. Repeat **steps 14** and **15**.
18. Now stop the pump again and switch to the target sample in Eppendorfs. Repeat **steps 14** and **15** (*see* **Note 29**).

19. When the experiment is complete, stop the measurement.
20. Stop the pump. Switch to 2% Hellmanex, restart the pump and run this through the system at the maximum flow rate for several minutes.
21. Stop the pump, switch to water, restart pump and run water through the system for several minutes (*see* **Note 30**).
22. Allow the tubes to empty fully and then stop the pump. Switch the Q-sense and pump off.
23. Dismantle the system. Dry the sensors by placing them carefully on a lint-free wipe and then inverting them. Do not use air flow because this could blow chemicals from the experiment around the lab.
24. Save the data (*see* **Note 31**).
25. Empty ultrasonic bath (*see* **Note 32**), turn off nitrogen stream at regulator if appropriate and dispose of waste in appropriate manner, in accordance with local regulations.

4 Notes

1. Hellmanex III is a concentrated alkaline detergent [17]. In dilute form, it is usually used to clean quartz or glass optical components for applications such as spectrophotometry. It causes skin irritation, serious eye irritation and may cause respiratory irritation. It may be corrosive to metals but we have not experienced any difficulties using the 2% solution with gold or steel. When handling the concentrate, avoid breathing in any vapours and wear safety glasses, nitrile gloves, and laboratory coats. For dilution, Hellmanex concentrate should be added to water rather than the other way around. If water is added to Hellmanex, a lot of bubbles appear and it is difficult to ensure that the correct volume of water is added. The accuracy of the final concentration of Hellmanex is not critical, and we use the level mark on a 1 L bottle rather than employing a measuring cylinder. We store the 1 L stock at room temperature for shared use.
2. We find it convenient to use 50 mL centrifuge tubes to prepare all buffers. The frequency and dissipation measured by the QCM-D system are extremely sensitive to buffer composition, because the concentration of salts and other components in the buffer affects the viscosity and density of the solution, modifying the frequency of the acoustic waves and, as a consequence, also affecting the dissipation. This means that extraordinary care must be taken to ensure that the buffer composition does not change throughout the experiment. Figure 2b shows the effect of flowing through TE buffer with an

increasing concentration of salt. Increasing NaCl concentration from 0 to 1 M causes the Δf baseline to change by approximately 16 Hz, whereas the immobilization of a DNA monolayer only causes a shift of approximately 7 Hz. The salt concentration also affects the dissipation values.

3. We obtain the capture strand oligonucleotides with the incorporated thiol modification, and we request HPLC purification. The thiol modification can be placed at either the 5′ or the 3′ end of the strand, and it is usually supplied in oxidized (disulphide) form, with short alkane chains on either side of the disulphide bond. It is not necessary to reduce this before use. Upon receipt of the DNA we resuspend it in 1× TE, usually to a final concentration of 100 μM, and then store it at −20 °C. Repeated freeze-thaw cycles should be avoided and, for some applications, it may therefore be necessary to prepare aliquots.
4. We have found that a concentration of 300 nM allows formation of a sufficiently dense monolayer within a reasonable timeframe (20–30 min), without using an excessive quantity of DNA. During the experiment, our system will use 20 μL of the sample every minute, which means that it is advisable to prepare around 800 μL for each sensor to be used.
5. MCH (full name 6-Mercapto-1-hexanol) has a stench. It causes skin irritation, serious eye irritation and may cause respiratory irritation. We keep the stock (97%) solution in a dessicator at room temperature and handle it in a fume hood, with eye protection, nitrile gloves, and laboratory coats. We dispose of all MCH waste via a chemical waste disposal route, including any material used to wipe the Hamilton syringe. The dilute 1 mM working solutions also have a smell, and we keep these in sealed containers as much as possible. When it is necessary to open these containers outside the fume hood to insert the QCM-D inlet tube, we avoid breathing the vapours and ensure that they are opened for the shortest possible time before being sealed firmly with Parafilm. The stock solution of MCH is rather viscous and it is necessary to dispense it using a Hamilton syringe. We find that Hamilton syringes that are left unused for some time may seize up, and it is sometimes necessary to free the plunger by twisting before the syringe can be used. The user should take great care not to bend the plunger or stab him/herself with the needle. Sometimes bubbles form in the extracted liquid, and we find that these can be eliminated by repeatedly emptying and refilling the syringe slowly, while keeping the tip of the needle under the surface of the liquid. The syringe barrel should be inspected before use and cleaned if necessary as recommended by the manufacturer. The exact concentration of MCH is not critical.

6. We find that standard desalting purification is adequate for unmodified DNA strands. The volume of target prepared depends on the experiment, and if hybridization/displacement is expected to take a long time, a larger volume will be required. We have found that the concentration range 300 nM to 3 μM is suitable.
7. We believe that compressed air would be an acceptable alternative.
8. Sensors can be obtained with a range of coatings. Colleagues in our lab have also used sensors coated with SiO_2, using the same cleaning protocol as for the gold-coated variety [15]. Alternative immobilization chemistries are thus possible.
9. We designate a pair of tweezers for use only with QCM-D sensors. As a minimum, before use, the tweezers should be squirted with ethanol and dried with a lint-free tissue or compressed nitrogen. For a more thorough cleaning, the tweezer tips should be dipped in Hellmanex, thoroughly swirled in water, dipped in ethanol, wiped with lint-free tissue and dried with nitrogen if required. Tweezers should be cleaned briefly with ethanol at each stage of the cleaning protocol that does not involve immersion of the tweezer tips in a cleaning solution.
10. It is usually helpful to clean at least one extra sensor. For inexperienced users, handling the sensors may be tricky, and it is common to drop a sensor during the cleaning process. If a sensor falls face-down on the lab bench it can become contaminated, and ideally should not be used. Sensors should be handled with great care, being held at the edges; the tweezer tips should not touch the active area of the sensor. It is possible for a sensor to break if dropped or subjected to a cleaving force, and if this occurs the pieces should be disposed of in a sharps bin. We find that sensors can be reused many times, but large scratches on the surface or chips on the sensor edge may impede performance.
11. UV-ozone cleaners are a relatively common piece of equipment, and are sometimes used to clean atomic force microscopy probes. UV light and ozone are both hazardous, and the manufacturer's safety precautions should be followed at all times. In particular, the chamber should not be opened until 5 min after the cleaning process has finished, to avoid releasing ozone in the lab.
12. For safety reasons, the ultrasonic bath should always be switched off before samples are added or removed. The sensors should be placed in a holder to ensure that they do not touch each other. If a holder is not available, sensors may be placed unprotected in a jar or beaker, but the number of sensors in

each vessel should be cut down to reduce the risk of scratches and other damage. The active area should be exposed to the cleaning fluid.

13. We wash sensors twice in water to ensure that *all* traces of the Hellmanex detergent are removed.
14. When drying the sensors, try to avoid evaporation of the solvent on the surface. Use the air flow to push droplets off the edge of the sensor, and wick them away using a lint-free tissue.
15. In some of our experiments, we have found that sensors soaked in ethanol for periods greater than 30 min appeared to exhibit reduced capacity for DNA immobilization. We are not sure if this is significant or merely coincidental, and we do not have an explanation for the postulated phenomenon. As a precaution, we recommend strictly limiting the ethanol soak time to 30 min.
16. Sensor cleaning typically takes around 2½ h. If the planned QCM-D experiment is expected to take a long time, it may be necessary to clean the sensors the day before. In this case, we prefer to store the sensors immersed in water in a clean jar with a lid. Alternatively, we store them dry in a container covered with a lid or Parafilm and then use a brief cleaning step in the morning, comprising a 10 min UV-ozone clean and a dunk in ethanol, followed by standard drying with nitrogen.
17. In the system we use, there are two O-rings, one on each side of the module. They should be intact, undamaged and correctly seated in the appropriate groove. Sometimes they stick together, such that there are two O-rings on one side and no ring on the other. This must be rectified before installation of the sensor.
18. VERY IMPORTANT: if the screws are not tight, the seal may not be good. We have also found that the module can get stuck in its mounting if the screws are loose. If this happens, a lot of force is needed to release the latch that holds the module in place and there is a risk of damage to the instrument.
19. The fluid runs from the sample tube into the flow module, following the arrow on the top of the flow module, through the peristaltic pump and into a waste beaker. Ensure that the waste beaker is in place before activating the pump to avoid spillage. We recommend covering the beaker with Parafilm, which helps to secure the tubing. As can be seen in Fig. 1e, the mounts for the tubes clip into the peristaltic pump. The clips are released by squeezing the tabs, and this can cause the end of the tube to kick upwards, potentially flicking the user with liquid. Take care not to allow fingers or long hair to be caught in the workings of the pump, which may be exposed if

less than four of the flow modules are in use. Arrange the input and output tubes so that they will not be squished when the lid is closed. Never run liquid through a flow module that does not contain a sensor. We find it helpful to color-match the ferrules on the inlet and outlet tubing.

20. It is advisable to use a temperature below ambient, such that the solubility of environmental gases is higher inside the machine than outside, reducing the chance of bubble formation in the system. The value selected depends on the laboratory environment.
21. If the system fails to find one of the resonances, it is possible to change the frequency sweep parameters and search for that resonance separately. If no resonances are found for a particular flow module, this suggests that the sensor may be damaged or incorrectly placed. Remove the inlet tube for that sensor from the water supply, run the pump to clear the tube, open the flow module and check the sensor.
22. We have found that the frequency and dissipation baselines often take some time to stabilize. It may be possible to dispense with this step or shorten it. Continuous measurement during the water flush step helps to identify whether the sensors are recording stable values. Occasionally, one sensor will continue to display drift while the others stabilize. Under these circumstances, we do not use the drifting sensor and continue the experiment with the stable ones.
23. When a bubble forms in the system, the frequency and dissipation exhibit sudden, large jumps. In some cases, the original values will be restored when the liquid returns, but on other occasions, the baseline will be different afterwards. Bubble formation should generally be avoided. If the user observes a bubble at the very start of the tubing, it may be possible to eliminate this by running the pump in reverse or trimming the tubing with scissors.
24. The flow rate can significantly affect the processes to be studied and must be kept constant throughout the experiment. During sample changing the pump should be left off for the minimum length of time.
25. If your experiment calls for the use of more than one running buffer, you should begin the measurement by establishing the baseline for each buffer. It may be appropriate to intersperse the buffers with water rinse steps. For running buffer and samples, we recommend using one sample container for each flow module.
26. It is best to arrange the samples such that there are two on each side of the machine. Do not use centrifuge (Falcon/Corning) tubes for DNA samples because DNA may adhere to the sides

of the tubes, lowering the effective concentration of sample that reaches the sensors. Sometimes the signals jump slightly when the pump is stopped, and may not return to the original values when the pump is restarted. In this case, it may be necessary to discard the dataset.

27. The values obtained for the first overtone are rarely reliable. Immobilization of a DNA capture strand or capture complex typically takes 15–30 min (phase marked "I" in Fig. 2b, d). The overtone-normalized frequency shift for immobilization of a capture complex containing 16 base pairs and 16 unpaired nucleotides is typically 20–30 Hz (Fig. 2e), and the corresponding dissipation shift is on average 1.8×10^{-6} a.u. (Fig. 2f, "$\times 10^{-6}$" scale factor omitted). An increase in surface-immobilized mass leads to a decrease in frequency and vice versa. Dissipation shifts tend to be associated with changes in viscoelastic properties, but in a viscoelastic monolayer dissipation and frequency changes tend to be coupled [10].
28. The purpose of backfilling is to improve the quality of the surface-assembled DNA monolayer, blocking gaps and inhibiting nonspecific surface adsorption. Backfilling typically occurs within 5–15 min (Fig. 2b, d, phase marked "B"). The shape of the traces (kinetics, size of frequency/dissipation shifts) can vary, depending on the quality of the monolayer formed in the immobilization step.
29. Hybridization (phase marked "H" in Fig. 2b) leads to a decrease in frequency and increase in dissipation. Toehold-mediated strand displacement (phase marked "D" in Fig. 2d) usually leads to an increase in frequency as mass is lost from the surface, but the trace does not necessarily follow a monotonic function [10]. Extraction of reaction rates may be more complicated than for the corresponding experiments in solution, due to phenomena such as intermolecular interactions.
30. It is necessary to clean the system briefly after each experiment. At intervals, the flow modules need to be cleaned more thoroughly, and should be dismantled for cleaning according to the manufacturer's instructions. We have found that it can be quite difficult to separate the two halves of the flow module, and they should be separated in such a way that they will not have far to fall if dropped. A thorough clean should be instigated if the quality of data obtained has begun to deteriorate, or abnormal drift is detected.
31. Note that some software will automatically normalize the data, dividing through by the overtone number.
32. If the ultrasonic bath is not emptied, it soon becomes cloudy and unpleasant.

Acknowledgments

We are grateful to EPSRC for funding through Platform Grant EP/K040820/1 and the University of York for an Institutional Equipment Grant, which funded the purchase of the QCM-D apparatus.

References

1. Chandran H, Gopalkrishnan N, Phillips A, Reif J (2011) Localized hybridization circuits. In: Cardelli L, Shih W (eds) DNA computing and molecular programming, DNA 2011, Pasadena. LNCS, vol 6937. Springer, Berlin, pp 64–83. https://doi.org/10.1007/978-3-642-23638-9_8
2. Dunn KE, Morgan TL, Trefzer MA, Johnson SD, Tyrrell AM (2015) Surface-immobilized DNA molecular machines for information processing. In: Lones M, Tyrrell A, Smith S, Fogel G (eds) Information processing in cells and tissues, IPCAT 2015, San Diego. LNCS 9303. Springer, pp 3–12. https://doi.org/10.1007/978-3-318-23108-2_1
3. Peterson AW, Heaton RJ, Georgiadis RM (2001) The effect of surface probe density on DNA hybridization. Nucleic Acids Res 29:5163–5168. https://doi.org/10.1093/nar/29.24.5163
4. White SJ, Johnson SD, Sellick MA, Bronowska A, Stockley PG, Wälti C (2015) The influence of two-dimensional organization on peptide conformation. Angew Chem Int Ed Engl 54:974–978. https://doi.org/10.1002/anie.201408971
5. Castronovo M, Lucesoli A, Parisse P, Kurnikova A, Malhotra A, Grassi M et al (2011) Two-dimensional enzyme diffusion in laterally confined DNA monolayers. Nat Commun 2:297. https://doi.org/10.1038/ncomms1296
6. Dixon MC (2008) Quartz crystal microbalance with dissipation monitoring: enabling real-time characterization of biological materials and their interactions. J Biomol Tech 19:151–158
7. Okahata Y, Matsunobu Y, Ijiro K, Mukae M, Murakami A, Makino K (1992) Hybridization of nucleic acids immobilised on a quartz crystal microbalance. J Am Chem Soc 114:8299–8300. https://doi.org/10.1021/ja00047a056
8. Papadakis G, Tsortos A, Gizeli E (2010) Acoustic characterization of nanoswitch structures: application to the DNA Holliday junction. Nano Lett 10:5093–5097. https://doi.org/10.1021/nl103491v
9. Papadakis G, Tsortos A, Bender F, Ferapontova EE, Gizeli E (2012) Direct detection of DNA conformation in hybridization processes. Anal Chem 84:1854–1861. https://doi.org/10.1021/ac202515p
10. Dunn KE, Trefzer MA, Johnson S, Tyrrell AM (2016) Investigating the dynamics of surface-immobilized DNA nanomachines. Sci Rep 6:29581. https://doi.org/10.1038/srep29581
11. Dunn KE, Trefzer MA, Johnson S, Tyrrell AM (2016) Assessing the potential of surface-immobilized molecular logic machines for integration with solid state technology. BioSystems 146:3–9. https://doi.org/10.1016/j.biosystems.2016.05.006
12. Dunn KE, Leake MC, Wollman AJM, Trefzer MA, Johnson S, Tyrrell AM (2017) An experimental study of the putative mechanism of a synthetic autonomous rotary DNA nanomotor. R Soc Open Sci 4:160767. https://doi.org/10.1098/rsos.160767
13. Koutsoumpeli E, Tiede C, Murray J, Tang A, Bon RS, Tomlinson DC, Johnson S (2017) Antibody mimetics for the detection of small organic compounds using a quartz crystal microbalance. Anal Chem 89:3051–3058. https://doi.org/10.1021/acs.analchem/6b04790
14. Chang EP, Roncal-Herrero T, Morgan T, Dunn KE, Rao A, Kunitake JAMR et al (2016) Synergistic biomineralization phenomena created by a combinatorial nacre protein model system. Biochemistry 55:2401–2410. https://doi.org/10.1021/acs.biochem.6b00163
15. Juan-Colás J, Parkin A, Dunn KE, Scullion MG, Krauss TF, Johnson SD (2016) The electrophotonic silicon biosensor. Nat Commun 7:12769. https://doi.org/10.1038/ncomms12769
16. Biolin Scientific (2014) Q-Sense E4 operating manual
17. Hellma Analytics (2017) Hellmanex® III: the special cleaning concentrate from Hellma. http://www.hellma-analytics.com/text/197/en/hellmanex%C2%AE-iii.html. Accessed 24 Mar 2017

Chapter 8

Hybridization Chain Reaction Design and Biosensor Implementation

Andrea Miti and Giampaolo Zuccheri

Abstract

DNA biosensors could overcome some of the common drawbacks of lab-based techniques for nucleic acids detection for diagnostics purposes. One of the main impediments for such applications of DNA biosensors is their lack of sensitivity: this can prevent their full exploitation in the diagnostic analytical field. DNA nanotechnology could enhance DNA biosensors and let them perform at the required high sensitivity. Well-designed, programmable self-assembly reactions can be triggered by a specific nucleic acid target. The Hybridization Chain Reaction (HCR) is a self-assembly strategy in which the target nucleic acid sequence triggers the formation of long nicked double-stranded DNA nanostructures. This can be performed in solution or on a surface, and the process can be coupled to different signal transduction schemes. We here describe the methods to design and test HCR reactions for the detection of different nucleic acid targets in solution and the procedures to exploit this strategy on surfaces with an electrochemical biosensing platform.

Key words Hybridization chain reaction, Self-assembly, Biosensors

1 Introduction

Until the 80s, DNA has been always considered mainly as the molecule for data storage in lifeforms, with a poor repertoire of structures or applications in different contexts. In the past decades, starting with the pioneering work of Nadrian Seeman [1, 2], this polymer has been involved in quite different kinds of studies and consequent applications, suggesting a new way to think about DNA. DNA nanotechnology exploits the powerful features of nucleic acids, such as programmable base-pairing properties, a well-known structure and the great stability and flexibility towards radically different goals compared to their role in organisms. DNA may be nowadays considered a self-assembling building block for objects in the nanoscale, or more interestingly, it can be considered a versatile object, able to generate dynamic and automatic switchable devices thanks to metastable conditions in a dynamic

Giampaolo Zuccheri (ed.), *DNA Nanotechnology: Methods and Protocols*, Methods in Molecular Biology, vol. 1811,
https://doi.org/10.1007/978-1-4939-8582-1_8, © Springer Science+Business Media, LLC, part of Springer Nature 2018

disequilibrium [3]. An example of this kind of dynamic process is the toehold-mediated strand displacement (TMSD), in which alternative metastable secondary structures of nucleic acid species have an important role. The TMSD is an isothermal reaction involving nucleic acids in which one strand displaces a second strand in the interaction with a third one that is in some grade complementary to both. The thermodynamic stability determines the favorite interaction. In this way, DNA nanostructures can be also kinetically controlled by properly defining the involved sequences [4]. The Hybridization Chain Reaction (HCR), invented by Dirks and Pierce in 2004 [5], is a simple yet powerful implementation of this kind of tunable process. This reaction consists of the isothermal assembly of stable DNA monomers in bigger structures at the addition of a specific initiator. The monomers in the original reaction design have hairpin-like secondary structures, composed of a long stem (18 nt), a short loop and a short corresponding overhanging toehold (both 6 nt). The easiest way to design this kind of reaction involves just two species of hairpins in equal molar concentrations. The two species stably coexist in solution, thanks to their metastability, without any interaction in the experiment timescale. The equilibrium of the system is altered by the initiator with a proper sequence: this triggers a cascade reaction of subsequent hybridizations, or more precisely, a cascade of toehold-mediated strand displacements, leading to the formation of a long nicked double-stranded DNA. In absence of the initiator, the folded secondary structure of the monomers prevents the triggering of the reaction, since the toehold is closed within. The initiator activates the first hairpin, leading to the exposure of the short loop sequence, suitable for the binding to and opening of a second hairpin. The second hairpin, once incorporated, restarts the cycle with another copy of the first hairpin, and so on (*see* Fig. 1).

DNA biosensors could play an important role in the detection and quantification of nucleic acids targets and to this purpose, they can potentially replace some lab-based techniques such as qPCR and Next Generation Sequencing in applications where cost, easiness to use, size of the device and portability could become an issue. One of the main drawbacks of DNA biosensors is their lack of sensitivity in the detection of targets. An effective strategy to overcome this issue may be offered by DNA nanotechnology through the implementation of self-assembly reactions triggered by the recognition of the target, hence the interest to use HCR as detection method for the biosensing of nucleic acids targets (DNA or RNA). HCR is based on an enzyme-free isothermal process. It is very simple in principle and it could be very sensitive and specific. The product is quantitatively and qualitatively related to the amount of the specific target and, finally, HCR can be combined with various strategies of signal transduction. Therefore, the design and characterization of a highly specific and effective hybridization

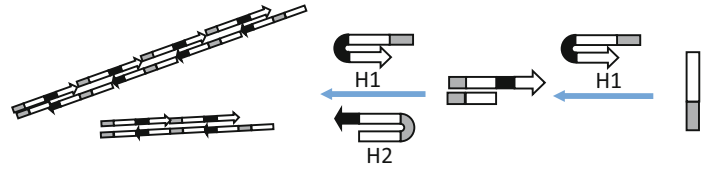

Fig. 1 Scheme of HCR in solution for the detection of microRNA

chain reaction would facilitate the application of biosensors. Recently, our group described the adaptation of HCR on surface for the plasmonic and electrochemical detection of pathogen DNA in samples [6]. Many publications show different strategies using HCR for diagnostic purposes thanks to its simplicity and suitability [7–10].

A general setup of a HCR-based detection method involves:

1. Election of the initiator, its sequence, depending on the goal and on the adopted strategy.
2. Selection of the convenient thermodynamic and structural features of the monomers to ensure the proper thermodynamic stability and kinetic properties of the system in the desired conditions. Ang and Yung proposed possible guidelines to design stable HCR monomers in order to get a highly effective HCR in solution [11]. The use of dedicated computer tools employing physical thermodynamic models is very useful.
3. Experimental analysis of the DNA oligonucleotides in the reaction conditions is needed. Electrophoresis gel analysis helps to investigate the efficiency of the formation of the intermediate complex and the final nanostructures. AFM could also be useful to study the general morphology of the products.
4. Once the reaction is well characterized and its efficiency is proved, the implementation on a biosensing platform is the next step, involving the choice of a strategy and methods for signal transduction coupled to the hybridization chain reaction amplification.

Here we describe methods for each step of the above-proposed pipeline. We have been able to design hybridization chain reactions specific for different targets such as short sequences, such as microRNA sequences, and sequences of pathogen DNA.

2 Materials

All solutions should be prepared in ultrapure water (resistivity >18 MΩcm at 25 °C, such as from a MilliQ apparatus from Millipore).

2.1 HCR in Solution and Reaction Mixtures

1. Single-stranded sequences of oligonucleotides, hairpins, and target DNA at 100 μM concentration in water. These are commonly stored at −20 °C. Aliquots are allowed to fully thaw before use and stored as working aliquots at 4 °C.
2. HCR buffer: 0.5 M NaCl, 50 mM Na_2HPO_4, pH 6.8.
3. A PCR thermal cycler (such as the Thermo Scientific Sprint PCR) to perform thermal treatment of the samples.

2.2 Nondenaturing PAGE for HCR Products Characterization

1. 40% Acrylamide solution (Acrylamide/bis-acrylamide 37.5:1), of a purity suitable for electrophoresis.
2. 10% Ammonium persulfate (APS) in water: prepare fresh before use.
3. N,N,N,N′-tetramethyl-ethylenediamine (TEMED).
4. 5× TBE buffer: 445 mM Tris–boric acid, pH 8.0, 10 mM ethylenediaminetetraacetic acid tetrasodium salt (EDTA-Na_4).
5. Loading Buffer: prepare 0.2% w/v solution of bromophenol blue (BB) and xylene cyanol FF (XC) in 50% v/v glycerol solution in 1× TBE.
6. SYBR Gold nucleic acid gel stain solution, 10,000× stock solution in DMSO (Invitrogen). Prepare 1× solution in 1× TBE buffer before use.
7. DNA ladder: pUC19 DNA/MspI (Hpa II) (store at 4 °C).
8. An apparatus for vertical PAGE electrophoresis (we use the PROTEAN II xi cell large format electrophoresis chamber and the Mini PROTEAN II, depending on the desired size of the gel, from Bio-Rad).
9. Electrophoresis power supply (such as the Powerpac 300, from Bio-Rad).
10. A gel documentation system (such as the Gel Doc 1000, from Bio-Rad).
11. Gel loading pipette tips appropriate for the thickness and length of the well in the PAGE gel.

2.3 AFM Characterization of HCR Products

1. AFM deposition buffer: 10 mM HEPES, 10 mM NaCl, 5 mM MgCl, pH 7.5.
2. 1× TE: 10 mM Tris-HCl, 1 mM EDTA, pH 8.0.
3. Centrifugal filter units, MWCO 100 kDa (like Amicon Ultra-0.5 mL centrifugal filters).
4. Freshly cleaved muscovite mica (EMS).
5. Atomic Force Microscope (such as a Multimode system, from Bruker) with proper cantilevers with probes to image in air sample, preferably in an intermittent contact mode (the technique name can vary for the AFM model in use).

2.4 Biosensor Surface Preparation and Characterization

1. TCEP solution: 300 μM Tris(2-carboxyethyl) phosphinehydrochloride (TCEP).
2. 1 mM solution of 6-mercapto-1-hexanol (MCH) in ultrapure water, freshly prepared.
3. 100 μM thiolated oligonucleotide probes (Eurofins MWG or Sigma-Genosys).
4. 99.99% pure gold wire (Electron Microscopy Sciences).
5. Muscovite mica discs or squares (to be cleaved just before use).
6. High-vacuum evaporator with a resistively heated specimen stage (from Edwards or other).
7. Round glass cover slides (12 mm in diameter).
8. EpoTek 377 (Epoxy Technology Inc., Billerica, MA, U.S.A.).
9. PBS buffer: 10 mM NaCl, 197 μM KCl, 291 μM Na_2HPO_4, 131 μM KH_2PO_4.
10. A plasma Cleaner, (Femto, Diener Plasma surface technology).

2.5 HCR Detection on Surface and Electrochemical Characterization

1. Oligonucleotide sequences were purchased from Eurofins MWG and Sigma-Genosys.
2. Costumer made 3-electrodes electrochemical cell, consisting of a single chamber that covers the gold electrodes.
3. KCl 0.1 M solution in ultra-pure water.
4. PBS buffer, 10 mM NaCl, 197 μM KCl, 291 μM Na_2HPO_4, 131 μM KH_2PO_4.
5. Hairpin oligonucleotides buffer 0.5 M NaCl, Na_2HPO_4 50 mM, pH 6.8.
6. Electrochemical workstation (μAutolab, Metrohm Autolab B.V., Utrecht, The Netherlands).

3 Methods

3.1 Design of DNA Sequences

We describe the general procedures adopted to design couples of hairpins specific for a selected target sequence of interest in diagnostics, such as microRNA and sequences for the detection of pathogens. First, special attention is required to elect the target sequence, taking into account the length and base composition of the candidate sequences. Bibliographic research, bioinformatics analysis or database mining are useful to this purpose (*see* **Note 1**). A proper set of oligonucleotide probes and hairpins can be consequently designed to detect the target sequence and consequently to perform HCR amplification. NUPACK represents a powerful instrument for the design of self-assembly reactions such as HCR. It is a software focused on the design and analysis of nucleic acids secondary structure in systems involving different

interacting strands [12] (http://www.nupack.org—as visited in July 2017). NUPACK includes two main tools: (1) the Design tool allows to design sequences for more strands at the same time, intended to adopt a specific secondary structure and to interact to form specific complexes [13–16]. (2) The Analysis tool can be used to perform the thermodynamic analysis of a theoretical dilute solution of interacting nucleic acid strands and gather information about the system in the elected conditions. It calculates the partition function and the minimum free energy secondary structure for possible complexes of an arbitrary number of interacting nucleic acids strands. Moreover, it shows the equilibrium concentration of the species in a diluted solution [17–19]. Other strategies may be adopted using different tools (*see* **Note 2**).

3.1.1 Generation of Candidate Sequences

The following procedures allow designing probes and hairpins using NUPACK. The software needs all the following information to generate candidate sequences. Parameters not mentioned here are used at their default settings. Below, the scripts used in NUPACK web application to generate candidate sequences for a specific target are presented and each step listed.

1. Specify the theoretical experimental conditions as follow:

   temperature = 25.0
   material = dna
   sodium = 0.5
   trials = 3 (number of designs).

2. Describe the target structures of hairpin-like monomers in DU + notation (*see* **Note 3**). Keep the toehold and the loop at 6 nt length. Input the elected length of the stem, as a function of the target sequences, in this case 16–17 nt stem. Specify the structure of the expected complexes in the same way.

   #
   # target structures
   #
   structure hp1 = U6D17(U6)
   structure hp2 = D17U6U6
   structure miR-17 = U23
   structure miR-17-hp1 = D23(U23+)
   structure miR-17-hp1-hp2 = D23(D23(+U23)+)

3. Input the sequence domains using IUPAC nucleic acid notation. The target sequence is sectioned into two domains, one corresponding to the 3′ portion complementary to the first hairpin 5′ toehold (domain b), and the other complementary to the adjacent stem portion of the hairpin (domain a). Leave the loop region (domain c) as a random sequence for NUPACK to generate (*see* **Note 4**). The sequences of the

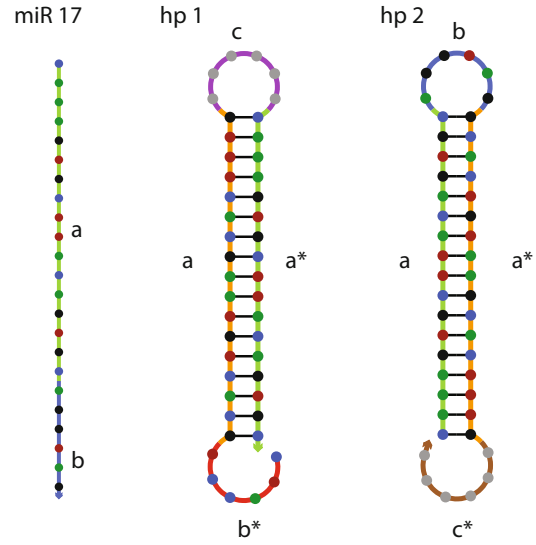

Fig. 2 Images from NUPACK design tool (www.nupack.org). Structures and domains depicted for monomers specific for miR17 detection

hairpins can be divided in four domains, where two of them are complementary, to form the stem.

```
#
# sequence domains
#
domain a = CAAAGTGCTTACAGTGC
domain b = AGGTAG
domain c = NNNNNN
```

4. Describe the sequences of the species defined in the structure section as a function of the previously defined domains. In Fig. 2, the target structures and corresponding domains are depicted. In this notation, "a*" is the sequence complementary to "a."

```
#
# strands (optional, used for threading sequence information
# and for displaying results)
#
hp1.seq = b* a* c a
hp2.seq = a b a* c*
miR-17.seq = a b
miR-17-hp1.seq = b* a* c a a b
miR-17-hp1-hp2.seq = b* a* c a a b a* c* a b
```

5. Insert the pattern of bases to avoid as shown (use IUPAC nucleic acid notation).

```
#
# prevent sequence patterns
```

Fig. 3 NUPACK results with candidate sequences (www.nupack.org) for HCR specific for miR17. The "Normalized Ensemble Defect" quantifies how much the generated sequence missed the inserted instructions: it is the average percent of nucleotides incorrectly paired at the equilibrium compared to the specified constrains and structures. Stop conditions for this parameter can be set in the design instructions

#
prevent = AAAA, CCCC, GGGG, UUUU, KKKKKK, MMMMMM, RRRRRR, SSSSSS, WWWWWW, YYYYYY

6. Check the design preview.
7. Run the Design and check the results (*see* Fig. 3).

3.1.2 Check of the Candidate Sequences

Probe, target and hairpins candidates should be then checked using the NUPACK analysis tool, testing for probe-target and hairpin-target binding in the theoretical reaction conditions and checking the predicted concentration of each species and complex at the equilibrium, as is shown in Fig. 4 (*see* **Note 5**).

1. Select DNA as starting material.
2. Select 25 °C as reaction condition temperature.
3. Set 3 as number of interacting strand to test the theoretical behavior of the two hairpins in solution in presence of the target or select 2 in absence of the target. The number of complex size can be changed as preferred to investigate complexes involving a variable number of species. Set 5, to investigate also complexes involving more monomers.
4. In advanced options, choose NaCl concentration 0.5 M and 0.0 M for Mg.
5. Input the sequences in the corresponding field. Input the target sequence and the sequences of hairpin-like monomers as shown in individual fields, specifying their unique names.
6. Set the concentrations of all species according to the elected reaction conditions. We set to 0.5 μM or below.
7. Keep all the other settings as default and run the analysis to obtain the results in the specified conditions.

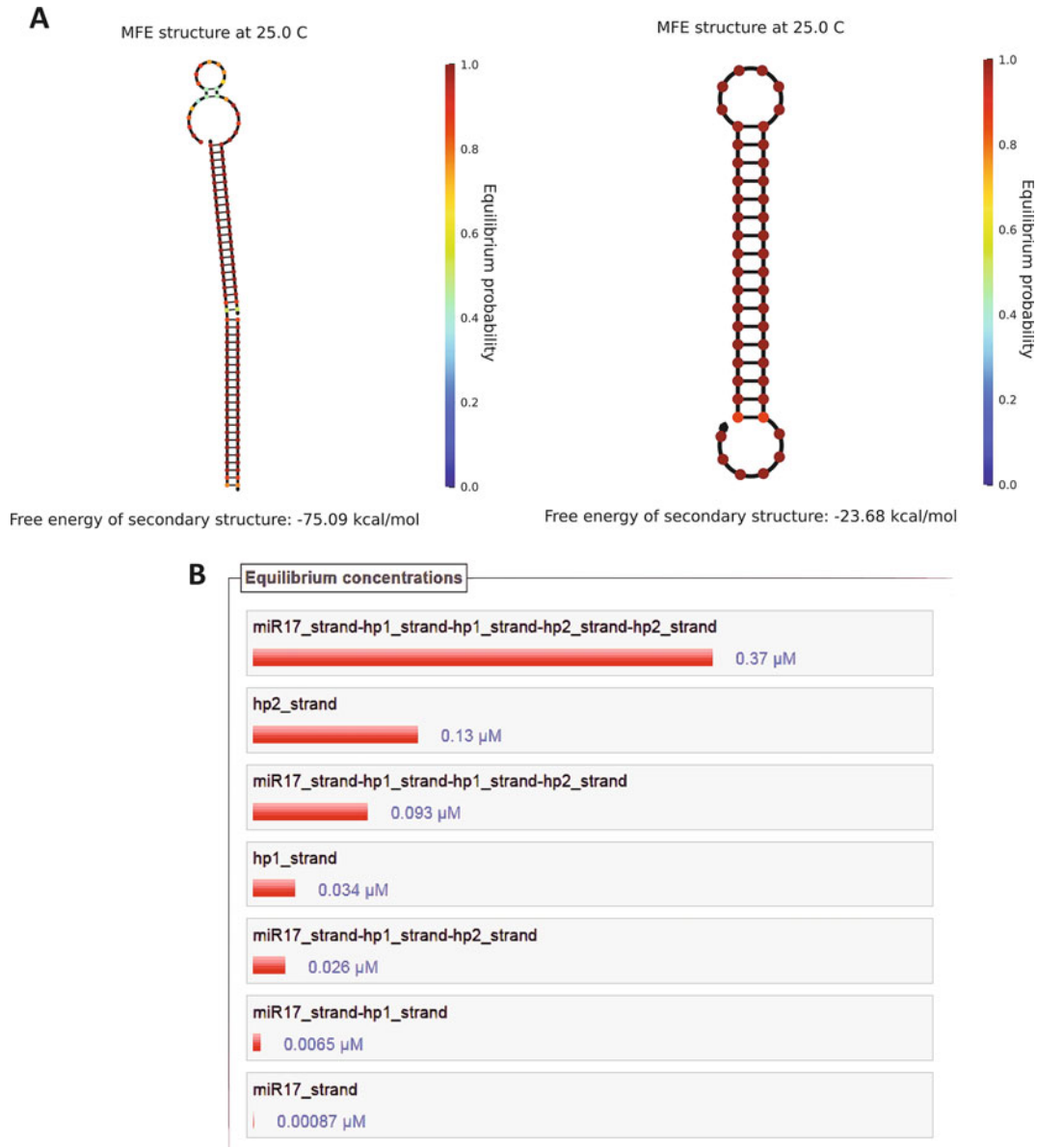

Fig. 4 NUPACK analysis: (**a**) Minimum free energy structures calculated by the analysis tool for hp1-hp2-miR17 complex (left) and hp1 (right), specific for miR17. (**b**) Concentration of the complex and different species at the equilibrium in the specified conditions

3.2 HCR Reaction in Solution

The samples are usually diluted in the HCR buffer. It is important to disrupt any possible alternative secondary structure in the nucleic acid species through a thermal treatment of the samples before setting up the reaction mixtures. During this step, each species should find the most energetically favored secondary structure. All species (hairpins and target) can be mixed in stoichiometric amounts by adding a volume of target solution to the hairpins

mixture and left to react spontaneously at room temperature. Different ratios of target to hairpins can be used in modeling the detection of lower concentrations of target.

1. Dilute the stock solution of oligonucleotides (target and hairpins) to 3 μM inHCR buffer in PCR tubes.
2. Do a thermal treatment with the PCR thermal cycler: 95 °C for 5 min, then cool down to 20 °C in 1 h (0.02 °C/s) (*see* **Note 6**).
3. Prepare the hairpin mixture by mixing 10 μL of each hairpin species in a 0.5 mL Eppendorf tube.
4. Prepare several dilutions of the target oligonucleotide making serial dilutions: for example from 3 μM to 0.003 μM.
5. Add 10 μL of target solution to the hairpin mixture (for a total reaching volume of 30 μL).
6. Keep the reaction at room temperature for at least for 1 h (*see* **Note 7**) and immediately characterize the reaction products (*see* **Note 8**).

3.3 Characterization of the HCR Product

3.3.1 Nondenaturing PAGE for Characterization of HCR Products in Solution

In this context, gel electrophoresis is the most convenient analysis method for the characterization of DNA nanostructures in solution. We use nondenaturing PAGE for the characterization of HCR products. The triggering of the reaction should lead to an amount of products easily distinguishable with gel electrophoresis, as they will form higher molecular weight bands (*see* **Note 8**). PAGE allows to check the stoichiometry and the success of the self-assembly reaction in the elected conditions. WARNING: acrylamide is neurotoxic. Avoid using acrylamide powder for preparing solutions. Use all precautions, gloves, goggles and protective garment to prevent skin contact with the acrylamide solution during the procedures. Use precast gels if available.

1. Set up the gel as specified by the PAGE apparatus manufacturer.
2. Under the chemical hood, prepare the needed amount of 10% acrylamide in a flask of volume equal to at least three times the required solution. For 50 mL: add 10 mL of 5× TBE solution to 20 mL of ultrapure water, then add 12.5 mL of 40% acrylamide solution and bring to 50 mL with ultrapure water (*see* **Note 10**). Stir the solution until homogeneous.
3. Add 250 μL of 10% APS and 25 μL of TEMED to the acrylamide solution, mix well by swirling the flask, then cast the gel according to the manufacturer's instructions or the preferred procedure (*see* **Note 11**).
4. Use a plastic Pasteur pipette to quickly but gently pour the acrylamide solution between the two glass plates and insert the comb. Avoid trapping air bubbles in the wells and in the body of the gel during this step. Make sure that no leakages occur

before gel polymerization. Leave at room temperature for at least 1–2 h for completing the polymerization and for best reproducibility (*see* **Note 12**).

5. When the gel is completely polymerized, use it immediately or store it at 4 °C in a sealed package (such a Ziploc bag or analogous) avoiding drying (do not keep for longer than 2–3 days).
6. Set up the polymerized gel in the electrophoresis cell. Add 1× TBE buffer (running buffer) to fill the chambers of the electrophoretic device, making sure that there are no leakages.
7. Prepare the samples for PAGE analysis: add 3 μL of nondenaturing loading buffer to 3 μL of HCR reaction mixture (*see* **Note 13**) and 7 μL of ultrapure water. Centrifuge the samples briefly before loading (*see* **Note 14**).
8. Remove the comb. Carefully rinse the wells using a syringe with a fine needle to squirt running buffer inside each of the wells to remove nonpolymerized acrylamide efficiently (*see* **Note 15**).
9. When the wells are clean, carefully load the samples using a pipette and gel loading pipette tips appropriate for the wells thickness and length. Load the reference DNA ladder as the last sample or separated from the samples by an empty lane to avoid marker contaminations (in case, load the empty lanes with 1× loading buffer).
10. Turn on the thermostat and circulating water, setting the temperature to 25 °C. Secure the lid of the gel box and connect the electrodes to a DC power supply (Powerpac 300 or similar) making sure the polarity is correct. Run the gel at 5 V/cm for 30 min or till the samples enter into the gel, than at constant voltage 10 V/cm for 3–4 h depending on the size of the investigated DNA complexes, temperature, and gel density (*see* **Note 16**).
11. Disassemble the electrophoresis box and stain the gel in 1× SYBR Gold solution in 1× TBE for 5 min (*see* **Note 17**). Keep it in the dark during the staining.
12. Acquire the gel image in fluorescence using an electrophoresis documentation system (like the Gel doc, Biorad). *See* Fig. 5 for example.

3.3.2 AFM Characterization of HCR Products

Characterization through AFM can provide information about the size and the shape of the HCR products, in order to get more information about the growth of the nanostructures, their morphology and length. The samples need to be diluted and cleaned-up before AFM imaging. Starting from the experimental conditions previously described, samples are diluted 1:100. After a wash step through centrifugal ultrafiltration, the HCR product is collected in the buffer for the deposition on mica for AFM imaging.

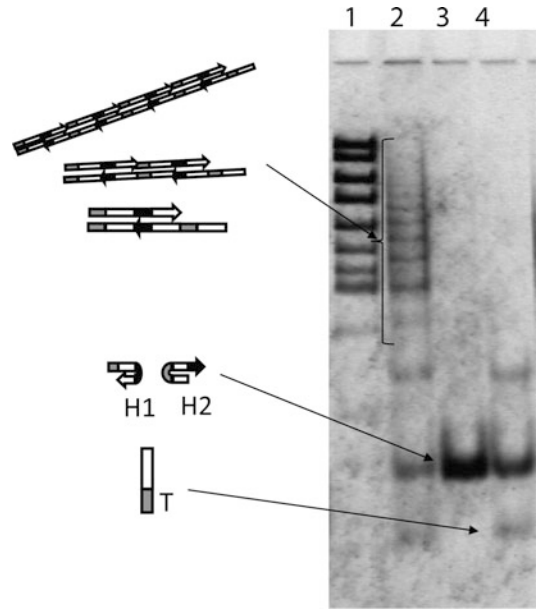

Fig. 5 Characterization of HCR specific for miR21 sequence. Molecular weight marker in Lane1. As also shown by the schemes on the side, the reaction of specific target with hairpins is in lane 2, the HCR monomers in absence of the target is in lane 3, while lane 4 shows the mix of the first hairpin with the miRNA sequence

1. Collect 5 μL of HCR reaction mixture and dilute it by adding 495 μL of 1× TE buffer.
2. Load the solution in the centrifugal filter device (100 kDa MWCO).
3. Centrifuge for 8 min at 11,200 × *g*.
4. Discard the filtrate and add 200 μL of AFM imaging buffer to the same filter unit and centrifuge for 5 min at 11,200 × *g*.
5. Collect the samples by inverting the filter unit and placing it in over a new tube. Centrifuge for 3 min at 100 × *g* to transfer the HCR product to the new tube.
6. Layer 10 μL of the filtered HCR product onto a freshly cleaved mica disc glued on a steel disk. Leave to adsorb for 5 min (*see* **Note 18**).
7. Wash with about 1 mL of ultrapure water added dropwise and dry with a gentle stream of nitrogen.
8. Load the disk on the AFM and scan the adsorbed sample according to the method in use (we currently prefer ScanAsyst mode in air for routine checking, available on Bruker AFM systems). *See* Fig. 6 for example AFM images of the HCR product.

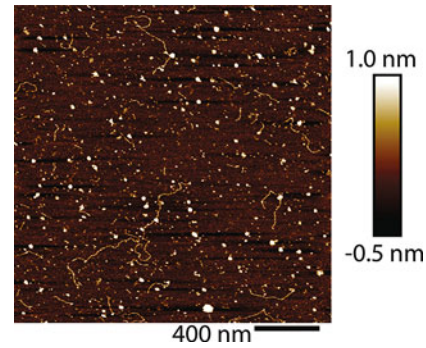

Fig. 6 Example AFM image of the HCR products. The average length of the products here has been measured as 200 nm, while structures up to 1 μm long are visible

3.4 Biosensor Surface Preparation and Derivatization for Electrochemical Measurements

Template-stripped gold disks are used to build the sensors. They are prepared according to the procedure outlined below (analogous to that described in Chapter 10 of this book), adapted from [20].

1. In a high-vacuum evaporator, deposit a 200 nm layer of ultra-pure gold (Electron Microscopy Sciences, 99.99% purity) onto muscovite mica which had been previously conditioned at about 300 °C overnight in the vacuum (10^{-6} Torr or less). We use resistive heating of a gold wire in an Edwards high-vacuum evaporator with a resistively heated temperature-controlled specimen stage.
2. After cooling, glue round glass cover slides (12 mm in diameter) on the evaporated gold with EpoTek 377 epoxy resin. Use about 10 μL each disc taking care of not trapping air bubbles. Cure the glue at 150 °C for 2 h.
3. Just before use, separate the glass cover slide with the ultra-flat gold layer from the mica by gently prying them apart by hand or with the help of a pair of tweezers. Make sure no mica flakes are left on gold (testing conductivity with a multi-meter could prove helpful).
4. Deprotect the thiolated oligos by adding concentrated oligonucleotide stock solution to achieve a 10 μM oligo solution in an about 300 μM solution of TCEP. Incubate for 1 h at 37 °C before use (oligo solution with TCEP can be stored at 4 °C for further use).
5. Dilute the 10 μM deprotected thiolated oligo stock to 2 μM in PBS buffer just before use.
6. Layer 10 μL of 2 μM deprotected thiolated oligonucleotide solution in PBS buffer on the surface of a freshly exposed template-stripped gold electrode disk and leave overnight at

room temperature (taking precautions for preventing the evaporation of the solution, such as incubating in a sealed humid chamber).

7. Wash the gold disc thoroughly but quickly with ultrapure water.
8. Passivate the gold surface by layering 20 μL of 1 mM 6-mercapto-1-hexanol (MCH) solution. Leave for 30 min at room temperature taking precautions for preventing the evaporation of the solution.
9. Wash quickly with ultrapure water. Preferably, install in the biosensor while still wet and use, or, alternatively, store at 4 °C in a small amount of PBS buffer or in a dry state (the reproducibility of results might depend on the storage conditions).

3.5 Electrochemical Capacitive Detection of HCR on Surface

HCR can be used in a simple electrochemical label-free detection system. We employed an HCR reaction on the surface for making a capacitive biosensor employing a "sandwich" format: the target DNA is specifically recognized by a probe immobilized on the gold surface. Later, the hairpins mixture is added to allow the amplification through HCR (*see* Fig. 7) anchored to the bound target DNA. The HCR product formed on surface leads to a change in capacitance on the interface. Measurements can be carried out using a custom-built three-electrode electrochemical cell. This can be simply designed to host an integrated reference electrode and a platinum wire auxiliary electrode in proximity of the working electrode. A cast polydimethylsiloxane (PDMS) cell is a good choice and it can achieve an efficient seal for fluidic control and minimize the volumes of the needed solutions. The gold surface functionalized with the thiolated probe represents the

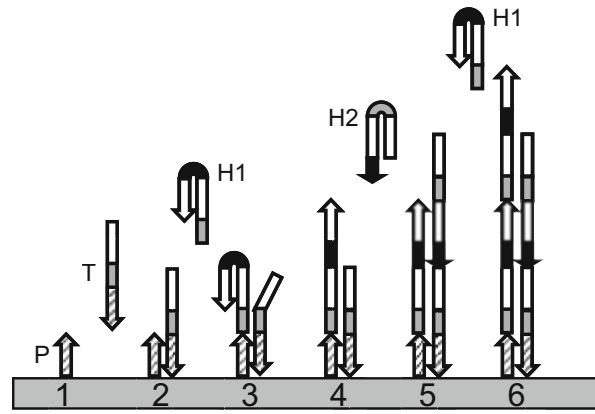

Fig. 7 Scheme of HCR on surface for electrochemical biosensor detection. Figure republished from ref. [6] with permission from Elsevier

working electrode. The cell is connected to an electrochemical workstation (in our case a μAutolab III, Metrohm Autolab B.V., The Netherlands).

3.5.1 Electrochemical Cell Assembly and Capacitive Measurements

The operations are merely sketched here, as they will depend on the electrochemical cell in use.

Capacitive measures can be performed by applying the method described by Berggren and coworkers [21, 22]. A gold surface with a SAM of alkanethiols is close to the ideal condition of an electrode without charge transfer across the electrode-solution interface when a potential is applied. This is an Ideal Polarizable Electrode (IPE) and it could be described as an equivalent RC circuit, involving a capacitance and a resistance in series (*see* Fig. 8).

The applied potential leads to a non-Faradaic current at the interface between surface and solution. This current decrease over time follows a known relation that can be used to calculate the values of resistance and capacitance of the interface. To calculate the capacitance, data are fitted with the RC model. The method needs a fast potentiostat and a relatively low concentration of electrolyte,

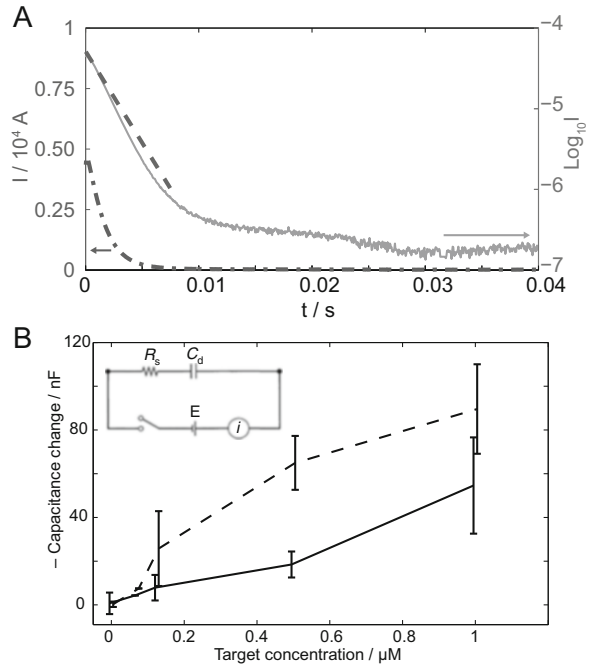

Fig. 8 (**a**) Current decay over time after the application of a 50 mV potential (solid line on the Log scale, dash-dot line on the linear scale). Fitting to RC model of the first points of the current decay Log10(I): the regression line is showed (dashed line). (**b**) Calibration curves of a capacitive DNA sensor before HCR amplification (points connected by the solid line) and after HCR amplification (points connected with dashed line); in the inset, the RC circuit used for the analysis of potentiostatic step experiments. Panel B modified from ref. [6] with permission from Elsevier

and requires the detection of the initial part of the current decay curve. Change in capacitance occurs after target hybridization and hybridization chain reaction and it is possible to evaluate these changes over time and target concentration. The measurements are performed acquiring the current decay in absence of the target, until a stable capacitance is reached. After the treatment with target and hairpins, the measurement is repeated and the capacitance variation upon the hybridization event can be calculated.

1. Open the cell and load the functionalized gold disc.
2. Close the cell making sure all electrodes are in place and connected to their respective wires for the electrochemical workstation. Avoid touching the surface of the gold disc.
3. Inject buffer in the cell to check for any leakage. Reassemble the cell if necessary. Avoid trapping air bubbles in the cell and make sure all electrodes are immersed in the measurement solution.
4. Connect the system to the potentiostat.
5. The system is now ready to measure.
6. Equilibrate the gold surface in the electrochemical cell in the PBS buffer.
7. Substitute the buffer solution with a new volume of the same PBS buffer, to perform the measurements.
8. Apply series of potential steps of +50 mV and −50 mV to the working electrode with respect to the open circuit potential. Measure the resulting current decay in the transient after the step. Use a sampling rate of at least 20 kHz until stable capacity is reached.
9. Inject 100 μL of target solution at the test concentration (and hybridization buffer). Wait for 30 min (or for the time defined in the desired protocol variation).
10. Substitute the cell (hybridization) buffer with PBS buffer.
11. Measure the current decay over time while applying potential steps, as described above, until stable capacitance is reached.
12. Wash with PBS buffer.
13. Add 100 μL of mixture of hairpins at 2 μM each in HCR buffer. Wait 30 min or the reaction time of choice.
14. Substitute the HCR buffer with PBS buffer.
15. Measure the current decay over time while applying potential steps, as described above, until stable capacitance is reached.

3.5.2 Data Analysis

The system can be described as an equivalent RC circuit involving a capacitance and a resistance placed in series (*see* Fig. 8). Current decreases over the time (t) through a relation described by the following equation:

$$i = \frac{E}{\mathrm{Rs}} \times \exp\left(-\frac{t}{\mathrm{RsCd}}\right) \quad (1)$$

where Rs is the resistance, Cd the system capacitance, E the applied potential step, i(t) the current as a function of time t after the step. Equation 1 can be used to calculate the values of resistance and capacitance of the interface. Equation 1 can be linearized as:

$$\log(i) = \log\left(\frac{E}{\mathrm{Rs}}\right) - \frac{t}{2.303\mathrm{RsCd}} \quad (2)$$

From the value of intercept, it is possible to determine Rs, while the capacitance (Cd) value can be obtained from the slope of the linear regression. This linear relation is valid only for the first points of the sampled current decay over time. To calculate the capacitance, perform the analysis on the first points of the current signal, and then fit with the RC model.

1. Collect the current decay data over time (*see* Fig. 8).
2. Calculate the Log_{10} of the current values.
3. Discard the first few points and select the following 10–15 points to calculate the linear regression to obtain the best trend-line fitting the data (R^2 should be >0.99). Calculate Rs value from the intercept and Cd from the slope of Eq. 2.
4. Plot the capacitance after addition of target DNA and HCR (*see* Fig. 8).

4 Notes

1. The DNA sequences of probes and hairpins were designed directly based on the selected targets, such as genes from pathogenic microorganisms (e.g. *Cryptosporidium parvum*) viruses and microRNA. Promising targets could be found through bibliographic searches and database mining. For example, specific circulating microRNAs of diagnostic interest have been found in various database, such as miRBase (www.mirbase.org—visited in July 2017) and miRandola (www.mirandola.iit.cnr.it—visited in July 2017). NCBI's BLAST (https://blast.ncbi.nlm.nih.gov/Blast.cgi—visited in July 2017) was used to look for similarities between different microRNAs in order to identify competitors in the hybridization chain reaction. For pathogenous DNA detection, some regions of selected genes known to be specific for a strain of interest were chosen. We considered advantageous, especially for long sequences, to screen the entire sequence of an elected gene for candidate regions with good potential binding and low interfering secondary structure and dimerization with a custom-

made script (written in MATLAB) using RNAcofold ver.1.80 [23, 24]. Moreover, the NUPACK analysis tool and the RNAfold webserver (http://rna.tbi.univie.ac.at/cgi-bin/RNAWebSuite/RNAfold.cgi—visited in July 2017) were used to individually check the candidate sequences for self-complementarities and predicted secondary structures interfering with the target recognition. The candidate sequences with the lowest interfering secondary structure and dimerization were finally elected.

2. Other software packages are available for sequence design. We have previously also used NANEV to generate self-assembling sequences. NANEV is a software utility for the generation of random sequences starting from information about the complementarity and the composition of each strand [25]. It employs evolutionary methods and combines different design paradigms: (a) A negative design paradigm that is the sequence symmetry minimization (SSM) to eliminate as much as possible undesired interaction between the specified strands. (b) A positive design paradigm, such as the energy minimization aiming to keep at the maximum the specific desired interactions. The software permits to define subsequences involved in the assembly and combine them to generate the final strands. The entire set of interacting DNA strands is described as formed by complementary subsequences. Although NUPACK includes the same models, NANEV can be simpler to use.
3. The specified target structures must not be connected. In DU+ notation, Dx represents a duplex of length x, while Ux defines an unpaired region of length x. Each structure is described in 5′–3′ direction and each duplex is followed immediately by the substructure delimited by the duplex, enclosed in brackets. More parentheses are used if more elements are included in the substructure. The character "+" is used to break strands. (www.nupack.org, Zadeh, Ph.D. thesis, California Institute of Technology, 2011).
4. The easiest way to design couples of hairpins is to insert domains of the target sequence in the sequence of the hairpin-like monomers. This would be the main constrain of the system, since an entire portion of the hairpin has to hybridize with the target to trigger the reaction. This fact would affect the thermodynamics and the kinetics of the system, from target recognition to the self-assembly of the hairpins. If HCR reaction is designed to be triggered by a randomly generated sequence, such constrictions are avoided. Setting no specific domains in the NUPACK design scripts, thus describing strands just as composed of random bases (N), NUPACK randomly generates all the species involved, initiator included and better self-assembling sequences are obtained. In this ideal

(and idealized) case, this approach would help preventing self-complementarities and undesired secondary structures and a better hybridization chain reaction can be reached.

5. The results of the NUPACK thermodynamic analysis are very useful to prevent important undesired secondary structures and interactions between strands during the design, but the real behavior of the strands in the experimental observations may be different. Check the sequences as well as you can in these steps to avoid undesired interactions. Moreover, alternative uncommon interactions and structures are often not taken into account by NUPACK models. Therefore it is better to check the strands to look for sequence features that could lead to behaviors not predicted by the models, for example, peculiar bases patterns such as C or G repeats could lead to alternative structures of nucleic acids.
6. The sample can be left cooling for 1 h at room temperature after 5 min at 95 °C, according to the original HCR protocol [5].
7. Different reaction times have been tested and they might depend on the sequences. In most cases, in our hands, an incubation time of 1 h is enough to enable the characterization of the nanostructures.
8. After the fast formation of the products, the reaction keeps going slowly thanks to hairpins remaining in solution. This aspect should be considered when a later characterization is required. When later characterization is required, the HCR products can be stored at 4 °C. AFM images obtained from the HCR products after 3 days of storage at 4 °C showed assembled nanostructures completely analogous to the freshly prepared ones.
9. HCR products may also run as a smear in gel electrophoresis, probably due to background reaction noise that could be avoided, for example, by reducing the hairpin concentrations. The size of the HCR product depends on the stoichiometry of the reaction between hairpins and target. If the initiator is very diluted, the HCR product can reach a higher molecular weight, so that the molecular weight difference should be clearly visible in the electrophoretic gel.
10. For small format gel (ten wells) using miniProtean electrophoresis cell (Biorad), add 2.5 mL Acrylamide stock solution to 2 mL TBE 5× solution, then make 10 mL with ultrapure water.
11. For miniProtean electrophoresis cell, add 62.5 μL of APS 1% and 6.25 μL of TEMED to the entire 10 mL prepared solution (*see* **Note 9**), mix vigorously and cast the gel.

12. The time for polymerization could change with the room temperature. Sometimes less than 1 h is enough, but it could take longer. Be careful that all the gel is polymerized before proceeding with the electrophoresis.
13. It is convenient not to overload the wells. If comparison between lanes is needed, it is always better to load same amounts of DNA species in each wells, to be able to know the reagents consumption after the reaction.
14. For miniProten gel, a smaller volume is required: add 1 μL of loading buffer to 3 μL of HCR sample and 1 μL of ultrapure water.
15. Samples are prepared for loading when the gel is well polymerized, cast and set up in the buffer tank. When it is sure that the buffer chambers do not leak and the samples are ready, remove the comb, clean the wells, and load the samples immediately.
16. Usually, we run 15-wells large format gel at 25 °C, to maintain the room temperature condition during the analysis and to avoid overheating during the run. If room temperature is higher in the lab, it is convenient to run the gel at lower temperature to preserve the resolution and gel integrity. The running time depends on the running temperature, acrylamide percentage and buffer composition. Changing running buffer would need a revision of these conditions and of the running time. Small format gel (ten wells) in miniProtean II cell were usually run setting the voltage at up to 80 V.
17. Time of staining in SYBR Gold could vary. Each aliquot of SYBR Gold solution may be used a few times by adjusting the staining time and storing the solution at 4 °C between uses. For a fresh solution of SYBR Gold in 1× TBE, 5 min of staining is usually enough.
18. Since mica is negatively charged, multivalent cations would help shielding the negative charges of both DNA and surface, improving the adsorption. A magnesium or nickel solution can be used to treat mica for a few minutes before the DNA adsorption or, alternatively, DNA can be diluted in a buffer containing magnesium.

References

1. Seeman NC (2007) An overview of structural DNA nanotechnology. Mol Biotechnol 37 (3):246–257. https://doi.org/10.1007/s12033-007-0059-4
2. Seeman NC (2010) Structural DNA nanotechnology: growing along with Nano letters. Nano Lett 10(6):1971–1978. https://doi.org/10.1021/nl101262u
3. Zhang DY, Seelig G (2011) Dynamic DNA nanotechnology using strand-displacement reactions. Nat Chem 3(2):103–113. https://doi.org/10.1038/nchem.957
4. Srinivas N, Ouldridge TE, Sulc P, Schaeffer JM, Yurke B, Louis AA, Doye JPK, Winfree E (2013) On the biophysics and kinetics of toehold-mediated DNA strand displacement.

Nucleic Acids Res 41(22):10641–10658. https://doi.org/10.1093/nar/gkt801

5. Dirks RM, Pierce NA (2004) Triggered amplification by hybridization chain reaction. Proc Natl Acad Sci U S A 101(43):15275–15278
6. Spiga FM, Bonyar A, Ring B, Onofri M, Vinelli A, Santha H, Guiducci C, Zuccheri G (2014) Hybridization chain reaction performed on a metal surface as a means of signal amplification in SPR and electrochemical biosensors. Biosens Bioelectron 54:102–108. https://doi.org/10.1016/j.bios.2013.10.036
7. Chen Y, Xu J, Su J, Xiang Y, Yuan R, Chai YQ (2012) In situ hybridization chain reaction amplification for universal and highly sensitive Electrochemiluminescent detection of DNA. Anal Chem 84(18):7750–7755. https://doi.org/10.1021/ac3012285
8. Cai S, Cao ZJ, Lau CW, Lu JZ (2014) Label-free technology for the amplified detection of microRNA based on the allosteric hairpin DNA switch and hybridization chain reaction. Analyst 139(22):6022–6027. https://doi.org/10.1039/c4an01178c
9. Chen QG, Guo QQ, Chen Y, Pang J, Fu FF, Guo LQ (2015) An enzyme-free and label-free fluorescent biosensor for small molecules by G-quadruplex based hybridization chain reaction. Talanta 138:15–19. https://doi.org/10.1016/j.talanta.2015.02.002
10. Zhu Q, Chai YQ, Zhuo Y, Yuan R (2015) Ultrasensitive simultaneous detection of four biomarkers based on hybridization chain reaction and biotin-streptavidin signal amplification strategy. Biosens Bioelectron 68:42–48. https://doi.org/10.1016/j.bios.2014.12.023
11. Ang YS, Yung LYL (2016) Rational design of hybridization chain reaction monomers for robust signal amplification. Chem Commun 52(22):4219–4222. https://doi.org/10.1039/c5cc08907g
12. Zadeh JN, Steenberg CD, Bois JS, Wolfe BR, Pierce MB, Khan AR, Dirks RM, Pierce NA (2011) NUPACK: analysis and design of nucleic acid systems. J Comput Chem 32(1):170–173. https://doi.org/10.1002/jcc.21596
13. Dirks RM, Lin M, Winfree E, Pierce NA (2004) Paradigms for computational nucleic acid design. Nucleic Acids Res 32(4):1392–1403. https://doi.org/10.1093/nar/gkh291
14. Wolfe BR, Porubsky NJ, Zadeh JN, Dirks RM, Pierce NA (2017) Constrained multistate sequence design for nucleic acid reaction pathway engineering constrained multistate sequence design for nucleic acid reaction pathway engineering. J Am Chem Soc 139(8):3134–3144. https://doi.org/10.1021/jacs.6b12693
15. Zadeh JN, Wolfe BR, Pierce NA (2011) Nucleic acid sequence design via efficient ensemble defect optimization. J Comput Chem 32(3):439–452. https://doi.org/10.1002/jcc.21633
16. Wolfe BR, Pierce NA (2015) Sequence design for a test tube of interacting nucleic acid strands. ACS Synth Biol 4(10):1086–1100. https://doi.org/10.1021/sb5002196
17. Dirks RM, Pierce NA (2003) A partition function algorithm for nucleic acid secondary structure including pseudoknots. J Comput Chem 24(13):1664–1677. https://doi.org/10.1002/jcc.10296
18. Dirks RM, Pierce NA (2004) An algorithm for computing nucleic acid base-pairing probabilities including pseudoknots. J Comput Chem 25(10):1295–1304. https://doi.org/10.1002/jcc.20057
19. Dirks RM, Bois JS, Schaeffer JM, Winfree E, Pierce NA (2007) Thermodynamic analysis of interacting nucleic acid strands. SIAM Rev 49(1):65–88. https://doi.org/10.1137/060651100
20. Hegner M, Wagner P, Semenza G (1993) Ultralarge atomically flat template-stripped au surfaces for scanning probe microscopy. Surf Sci 291:39–46
21. Berggren C, Bjarnason B, Johansson G (1998) An immunological interleukin-6 capacitive biosensor using perturbation with a potentiostatic step. Biosens Bioelectron 13(10):1061–1068. https://doi.org/10.1016/s0956-5663(98)00058-x
22. Berggren C, Stalhandske P, Brundell J, Johansson G (1999) A feasibility study of a capacitive biosensor for direct detection of DNA hybridization. Electroanalysis 11(3):156–160. https://doi.org/10.1002/(sici)1521-4109(199903)11:3<156::aid-elan156>3.0.co;2-o
23. Bernhart SH, Tafer H, Muckstein U, Flamm C, Stadler PF, Hofacker IL (2006) Partition function and base pairing probabilities of RNA heterodimers. Algorithms Mol Biol 1:10. https://doi.org/10.1186/1748-7188-1-3
24. Hofacker IL, Fontana W, Stadler PF, Bonhoeffer LS, Tacker M, Schuster P (1994) Fast folding and comparison of RNA secondary structures. Monatsh Chem 125(2):167–188. https://doi.org/10.1007/Bf00818163
25. Goodman RP (2005) NANEV: a program employing evolutionary methods for the design of nucleic acid nanostructures. Biotechniques 38(4):548–550

Chapter 9

Ultrasensitive Detection of Metal Ions with DNA Nanostructure

Mingshu Xiao, Xiangmeng Qu, Li Li, and Hao Pei

Abstract

In spite of its greatly scientific and technological importance, developing rapid, low cost and sensitive microarray sensors for onsite monitoring heavy metal contamination remains challenging. Here we develop a DNA nanostructured microarray (DNM) with a tubular three-dimensional sensing surface and an ordered nanotopography for rapid and sensitive multiplex detection of heavy metal ions. In our design, DNA tetrahedral-structured probes (TSPs) are used to engineer the sensing interface with spatially resolved and density-tunable sensing spots, improving the micro-confined molecular recognition. Meanwhile, a bubble-mediated shuttle reaction inside the DNM-functionalized microchannel improves the target-capturing efficiency. Thus, the sensitive and selective detection of multiple heavy metal ions (i.e., Hg^{2+}, Ag^{+}, and Pb^{2+}) with this novel DNM biosensor can be achieved within 5 min. Moreover, the detection limit is down to 10, 10, and 20 nM for Hg^{2+}, Ag^{+}, and Pb^{2+}, respectively. Therefore, the DNM biosensor capable of simultaneously detecting multiple heavy metal ions with sensitivity and selectivity shows great potential to be point-of-test devices.

Key words DNA nanostructures, Multiplex detection, Metal ions detection, Ultrasensitive detection, Microchannel

1 Introduction

The rapid and sensitive detection and monitoring of environmental toxins, including heavy metals is of great significance for the health of humans and the ecosystem [1–3]. Often, a contamination event results from multiple toxic ingredients and thus a multiplex detection strategy need to be adopted for the readout of all relevant chemicals [4–6]. The construction of advanced sensing interfaces and fluorescence imaging devices has enabled the use of high-throughput microarray-based platforms [7, 8]. Nevertheless, rationally building a fast, sensitive, and easy-to-use microarray sensor remains a challenge [9, 10], and engineering a heterogeneous sensing interface promoting the faster kinetics and advantageous thermodynamics for probe-target interactions is desired [11, 12].

Giampaolo Zuccheri (ed.), *DNA Nanotechnology: Methods and Protocols*, Methods in Molecular Biology, vol. 1811, https://doi.org/10.1007/978-1-4939-8582-1_9, © Springer Science+Business Media, LLC, part of Springer Nature 2018

Sensor performance depends on the affinity between molecular targets and the surface-tethered probes [13] and by the interfacial properties including the orientation, ordering, and density of probes, as well as the diffusion rate of the target of interest to the probes [14]. The reduction of the sensors to the nanoscale can increase the mass transport rate and thus the detection sensitivity [15, 16]. However, a trade-off must be found, as too small a nanosensing area exposes a small number of molecular probes thus reducing the probability of collision and binding between the surface probes and the soluble analytes. Molecules can typically diffuse by 10–100 μm in solution [17], while binding events require nanometer proximity between binding partners: a trans-scale design of sensor integrating nanoscopic features onto macroscopic surfaces is a prerequisite. Probe-target recognition can be greatly improved once the dynamic targets are closely confined to the static surface-tethered nanoprobes arranged in the macroscale. Considering the radial-diffusion feature of analytes at the microscale or nanoscale interface, we assume that rolling up a traditional two-dimensional (2D) flat planar sensing surface into a three-dimensional (3D) tubular sensing surface in the inside face of a microfluidic channel is expected to improve the sensor performance [18].

Self-assembled DNA nanostructures have been used to a great advantage in engineering molecular recognition events and programmable sensing-interfaces [19–21]. Using these, we designed a spatially resolved 3D tubular DNA-nanostructured microarray (DNM) for the rapid and sensitive multiplex detection of heavy-metal ions (*see* Fig. 1). The microarray is organized inside a microchannel. To construct the DNM, target-specific DNA tetrahedral-structured probes (TSPs) (sequences of TSPs listed in Table 1, and sequences of TSPs probes and Reporter DNA listed in Table 2) were rapidly self-assembled and incorporated into a droplet array [22, 23]. This is then moved to the designated locations for immobilization and sensor engineering [24]. The DNM were evenly spaced along the microchannel, achieving probe surfaces with highly ordered probe orientations, controlled density and circular arrangement. This setup endowed the micro-confined microarray sensor with improved sensitivity and selectivity.

The method describes the preparation of the microchannel DNM biosensor with tetrahedral DNA nanostructures and its use with a low-cost bubble-based *shuttle reaction strategy*. This uses air bubbles to separate multiple reagent *plugs* (in segmented-flow microfluidics, discrete liquid droplets are encapsulated or spaced by a carrier fluid: these droplets are termed "plugs"). This bubble-mediated strategy avoided the designation and fabrication of complex microchannels as well as complex user procedures. With the method herein described, this DNM biosensor can detect multiple heavy metal ions (i.e., Hg^{2+}, Ag^{+}, and Pb^{2+}) within 5 min. The

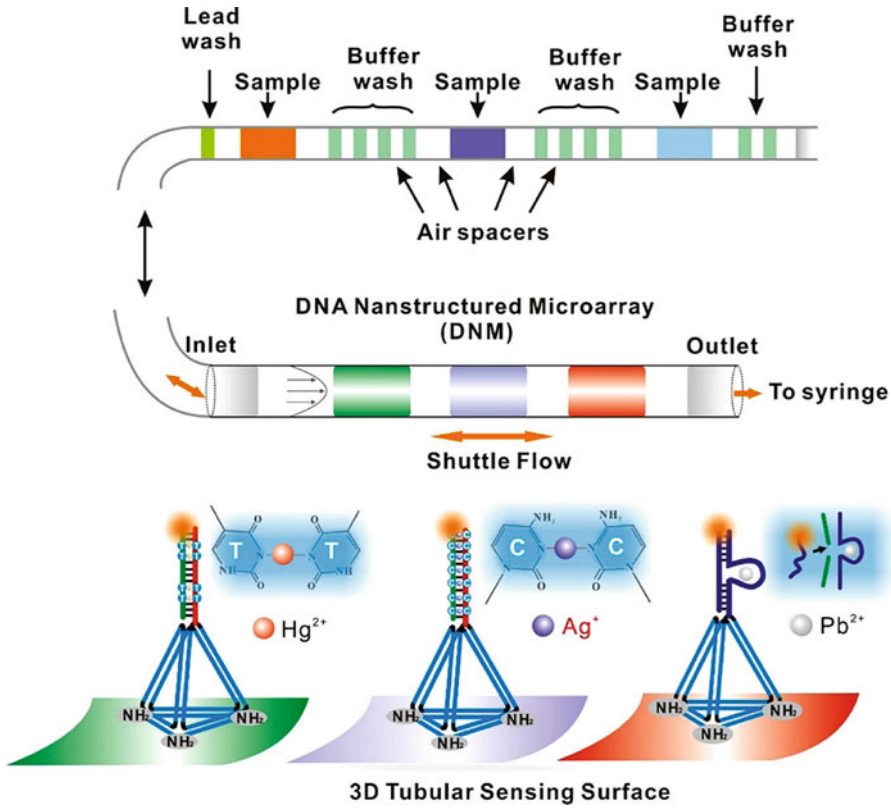

Fig. 1 Construction of 3D tubular DNM sensor inside microchannels for the detection of Hg^{2+}, Ag^{+}, and Pb^{2+} based on bubble-mediated shuttle reaction (reproduced from ref. [18] with permission from ACS)

Table 1
Sequences of TSPs

Oligo	Sequence (5′–3′)
TSP-A	Probe-ACATTCCTAAGTCTGAAACATTACAGCTTGCTACACGAGAAGAGCCGCC ATAGTA
TSP-B	NH_2-C_6-TATCACCAGGCAGTTGACAGTGTAGCAGCTGTAATAGATGCGAGGGT CCAATAC
TSP –C	NH_2-C_6-TCAACTGCCTGGTGATAAAACGACACTACGTGGGAATCTACTATGGC GGCTCTTC
TSP –D	NH_2-C_6-TTCAGACTTAGGAATGTGCTTCCCACGTAGTGTCGTTTGTATTGGA CCCTCGCAT

corresponding detection limit is down to 10, 10, and 20 nM for Hg^{2+}, Ag^{+}, and Pb^{2+}, respectively (*see* Figs. 2 and 3). In conclusion, this sensitive and selective DNM sensor has great potential developed as point-of-care test devices.

Table 2
Sequences of TSPs probes and reporter DNA

Description	Oligo DNA	Sequence (5′–3′)
Mercury ion assay	TSP-A1 (mercury ion specific sequence)	TTCGTTCCTGTTTGCGAAAAAAAAAAACATTCCTAAGTCTG AAACATTACAGCTTGCTACACGAGAAGAGCCGCCATAGTA
	Reporter sequence	CGCATTCAGGTTCGTA-Cy3
Silver ion assay	TSP-A2 (silver ion specific sequence)	CACACACACACACACACACACAAAAAAAAAAAACATTCCTAAG TCTGAAACATTACAGCTTGCTACACGAGAAGAGCCGCCAT AGTA
	Reporter sequence	CTCTCTCTCTCTCTCTCTCTC-Cy3
Pb ion assay	TSP-A3 (Pb ion specific sequence)	CATCTCTTCTCCGAGCCGGTCGAAATAGTGAGTCAGACATA TTTTTTTTTTACATTCCTAAGTCTGAAACATTACAGCTTG CTACACGAGAAGAGCCGCCATAGTA
	Substrate strand reporter sequence	TATGTCTGACTCACTTArAGGAAGAGATGTATGTCTGACTC ACTTAGGAAGAGATG-Cy3

2 Materials

Prepare all solutions using ultrapure water with a sensitivity of 18 MΩ cm at 25 °C and analytical grade reagents. Prepare and store all reagents at room temperature (unless indicated otherwise). Diligently follow all waste disposal regulations when disposing of waste materials.

2.1 DNA TSPs Probe

1. TE buffer (10 mM Tris, 1 mM EDTA, pH 8.0): dissolve 1.211 g of Tris and 0.372 g of Na_2EDTA in about 900 mL of ultrapure water (*see* **Note 1**). Mix and adjust the pH with HCl (*see* **Note 2**). Make up to 1 L with water. Store at 4 °C.
2. TM buffer (20 mM Tris, 50 mM $MgCl_2$, pH 8.0): dissolve 2.422 g of Tris and 2.975 g of $MgCl_2$ in about 900 mL of ultrapure water. Mix and adjust the pH with HCl (*see* **Note 2**). Make up to 1 L with water. Store at 4 °C.
3. Stock solutions of each DNA oligonucleotide at 100 μM in TE buffer (*see* **Note 3**).
4. 10× TAE buffer (400 mM Tris, 200 mM acetic acid, 20 mM EDTA): weigh 48.456 g of Tris and 7.444 g of Na_2EDTA, add 11.32 mL of concentrated acetic acid (*see* **Note 4**) and prepare a 1 L solution. Store at 4 °C.
5. PAGE running buffer (40 mM Tris, 2 mM EDTA, 20 mM acetic acid): weigh 4.846 g Tris and 0.744 g Na_2EDTA, add 1.132 mL acetic acid (*see* **Note 4**) and prepare a 1 L solution. Store at 4 °C. Alternatively, dilute from 10× TAE buffer with ultrapure water.

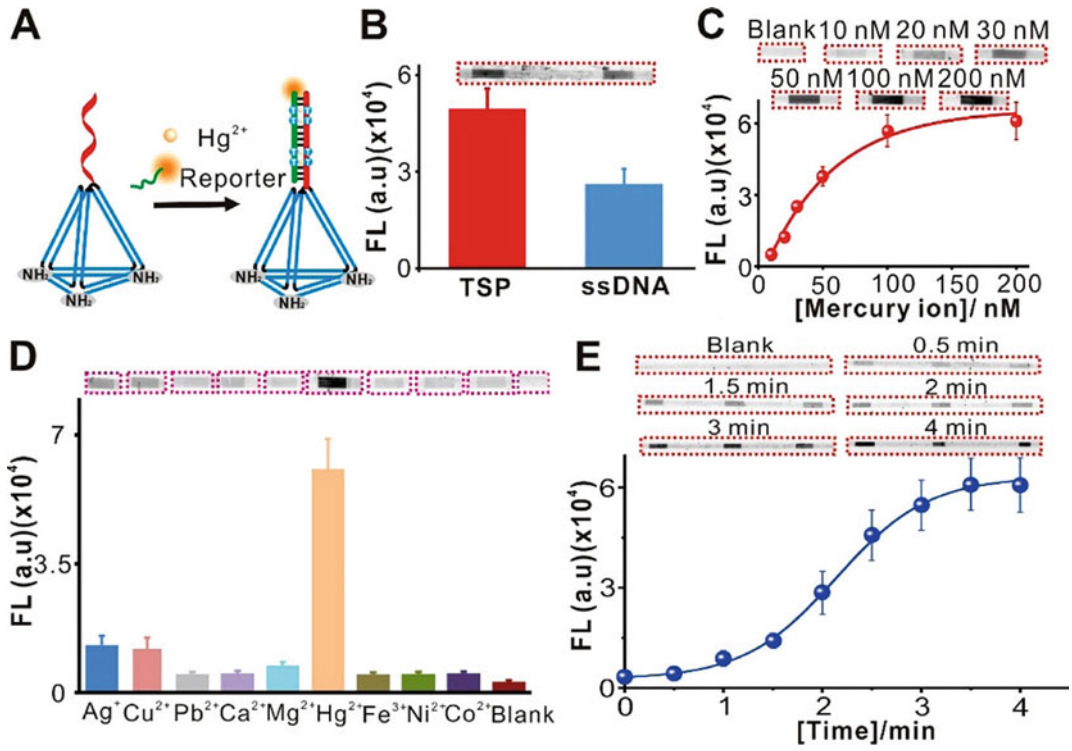

Fig. 2 Three-dimensional tubular DNM sensor for the Hg ion assay. (**a**) The presence of Hg ions is transduced to fluorescence signals through the formation of T-Hg^{2+}-T configuration. (**b**) Comparison of TSP- and ssDNA probe-based sensor performance (with 100 nM Hg^{2+}). The inset displays the corresponding fluorescent images. (**c**) Fluorescence intensities and corresponding fluorescent images (shown as inset) of DNM-sensing spots in the presence of Hg^{2+} at 10, 20, 30, 50, 100, or 200 nM. (**d**) Selectivity of DNM-based Hg^{2+} sensor over different metal ions. (**e**) Fluorescence intensity vs. shuttle hybridization time (with 200 nM Hg^{2+}). The inset displays the fluorescent images of three different DNM-sensing spots inside microchannels at corresponding hybridization times. (reproduced from ref. [18] with permission from ACS)

6. 30% acrylamide/Bis solution (29.2:0.8, acrylamide:bis): Add 29.2 g of acrylamide monomer and 0.8 g of bis-acrylamide (cross-linker) to about 40 mL of ultrapure water. Add a spatula of AG 501-X8 (D) mixed-resin beads (Bio-Rad) and stir for 30 min. Make up to 100 mL with water and filter through a 0.45 μm Corning filter (*see* **Note 5**). Store at 4 °C in a bottle wrapped with aluminum foil (*see* **Note 6**).
7. 10% Ammonium persulfate solution in water (*see* **Note 7**).
8. *N*,*N*,*N*′,*N*′-Tetramethyl-ethylenediamine. Store at 4 °C (*see* **Note 8**).
9. 6× gel loading solution for nondenaturing electrophoresis (Sangon Biotech, Shanghai or equivalent).
10. GelRed gel staining solution (formulate according to the manufacturer's instructions).

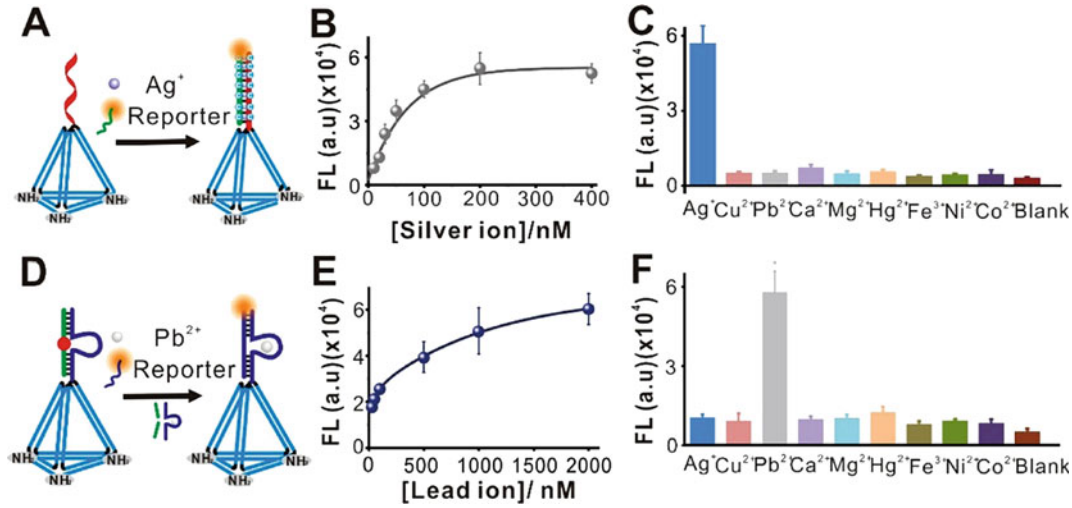

Fig. 3 Three-dimensional tubular DNM sensor for the silver and Pb ion assay. (**a**) The presence of silver ions was transduced to fluorescence signals through the formation of C-Ag^+-C configuration. (**b**) Fluorescence spectra of the DNM-based Ag^+ sensor upon addition of Ag^+ (10, 20, 30, 50, 100, 200, or 400 nM). (**c**) Selectivity of the DNM-based Ag^+ sensor over different metal ions. (**d**) The detection scheme for Pb ions. (**e**) Fluorescence intensities in the presence of Pb^{2+} (20, 50, 100, 500, 1000, or 2000 nM). (**f**) Selectivity of the DNM-based Pb^{2+} sensor to different metal ions. (reproduced from ref. [18] with permission from ACS)

11. DNA molecular weight size markers: 20 bp DNA ladder.
12. Dialysis tubing.

2.2 DNM Functionalized Microchannel

1. 10% NaOH: Weigh 10 g sodium hydroxide and bring to 100 mL with ultrapure water (*see* **Note 9**).
2. Capillary: Glass capillary with inner diameters of 200 μm.
3. Piranha solution (30:70 v/v sulfuric acid to 30% hydrogen peroxide): Add 70 mL 30% hydrogen peroxide to a 200 mL glass beaker. Make up to 100 mL with sulfuric acid (*see* **Note 10**). WARNING: piranha solution reacts violently with organic materials and should be handled with extreme caution. Wear safety goggles, appropriate gloves, and acid resistant apron over a lab coat. Always handle piranha solution under a fume hood. Prepare only as much as is needed; do NOT store any piranha solution or hold it in closed containers.
4. Mixture of ethanol/H_2O/3-Aminopropyltriethoxysilane (APTES) (95:3:2 by volume): Add 95 mL ethanol to a 100 mL graduated cylinder. Add 3 mL ultrapure water to the cylinder. Make up to 100 mL with APTES (*see* **Note 11**). Store at 4 °C.
5. 10× PBS buffer (100 mM phosphate buffer, pH 7.4): dissolve 11.51 g of Na_2HPO_4 and 2.28 g of NaH_2PO_4 in about of 900 mL of ultrapure water. Bring to 1 L with ultrapure water. Store at 4 °C.

6. 1× PBS buffer (10 mM phosphate buffer, pH 7.4). dissolve 1.151 g of Na_2HPO_4 and 0.228 g NaH_2PO_4 in about of 900 mL of ultrapure water. Bring to 1 L with ultrapure water. Store at 4 °C.
7. 5% glutaraldehyde: add 20 mL 25% glutaraldehyde to 80 mL of 10× PBS buffer (*see* **Note 12**). Store at 4 °C.
8. Aldehyde blocking solution (2.5 mg/mL $NaBH_4$ in PBS buffer with 25% (v/v) ethanol, pH 7.4): add 25 mL of ethanol to a 100 mL graduated cylinder. Add 0.25 g of $NaBH_4$ and 1× PBS buffer to 100 mL. Store at 4 °C (*see* **Note 13**).
9. Pentanol.
10. A slotted vial auto sample device: make slotted vials by cutting slots at the bottom of PCR tubes. Insert one side of the aldehyde modified capillary into the vial slot. Connect other side to the syringe pump.

2.3 Metal Ion Detection

1. A syringe pump (LSP02-1B; LongerPump).
2. 10 μL aliquots of various concentrations of metal ions to be tested.
3. 5 μL aliquots of 1.5 μM Cy3-labeled reporter oligos (*see* **Note 14**).
4. Washing buffer (20 mM Tris–HCl, pH 7.0): Add 24.227 g of Tris–HCl to about 900 mL of ultrapure water. Mix and adjust pH with HCl (*see* **Note 2**). Make up to 1 L with ultrapure water. Store at 4 °C.
5. A confocal laser fluorescence microscope (Typhoon 9210) and ImageQuant software (GE Healthcare) or equivalent.

3 Methods

Carry out all procedures at room temperature unless otherwise specified.

3.1 Synthesis and Purification of DNA TSPs

1. Mix 1 μL of each of the four oligonucleotides stock solutions (TSP-A*n* for the specific ion, TSP-B, TSP-C and TSP-D, *see* Tables 1 and 2) with 96 μL of TM buffer (10 μM conc. of each oligo).
2. Heat the resulting mixture to 95 °C for 10 min and cool to 4 °C in 30 s using a Peltier model PTC-200 thermal cycler or analogous [25].
3. Mix 600 μL 10× TAE buffer, 2 mL acrylamide mixture, and 4 mL ultrapure water in a 20 mL centrifuge tube. Degas with helium for 10 min.

4. Add 60 μL of 10% ammonium persulfate solution to the acrylamide mix. Mix well.
5. Add 6 μL of TEMED, mix and immediately cast a gel within a 7.25 cm × 10 cm × 1.5 mm gel cassette. Allow space for stacking gel and gently overlay with isobutanol or water (*see* **Note 15**). Insert a 10-well gel comb immediately without introducing air bubbles. Allow the gel to polymerize for 30 min.
6. Take out the gel from the casting frame and clamp it in the gel apparatus. Fill the gel chambers with 1× TAE buffer. Remove the comb carefully (*see* **Note 16**).
7. Prepare the samples for the gel by mixing 5 μL of the DNA samples with 1 μL 6 × loading buffer.
8. Rinse the loading tip a few times with ultrapure water (*see* **Note 17**). Insert the loading tip to a few mm from the well bottom. Deliver the samples into the well. Repeat for all samples. Rinse the tip with ultrapure water after loading for a few times.
9. Attach the power supply to the electrophoresis apparatus (*see* **Note 18**) and run at 80 V for 1 h (*see* **Note 19**).
10. Following electrophoresis, switch off the power supply and take out the gel plates, remove the gel. Place the gel in the staining solution for 30 min. Stain the gel until the bands are properly seen. Determine the approximate molecular weight of the TSP bands by comparing them with the available DNA markers.
11. Cut out the TSP bands and obtain the gel slice. Place the gel slice in a small bag of dialysis tubing (*see* **Note 20**). Add a minimal volume of 1× TAE buffer just enough to surround the gel slice. Seal the bag (*see* **Note 21**). Fill the horizontal mini-gel apparatus with 1× TAE buffer. Place the dialysis bag in the apparatus, on the gel platform. Place the dialysis bag close to the negative electrode (*see* **Note 22**).
12. Apply 80 V to the apparatus, and allow the DNA to elute at this potential for 1 h. Recover the bag. Open carefully and recover the buffer with a pipette. Rinse the bag and gel slice once with 200 μL of 1× TAE buffer (*see* **Note 23**).
13. Measure the concentration of the recovered TSPs and, in case, set to 50 μM with the method of choice.

3.2 Fabrication of DNM Functionalized Microchannel

By this method, we commonly obtain DNM-functionalized capillaries with $3.72 \pm 0.27 \times 10^{12}$ TSPs/cm^2 [14].

1. Clean the capillary with 10% NaOH solution for 10 min.
2. Wash the capillary with ultrapure water and clean using piranha solution for 1 h at 80 °C.

3. Dry the capillary with nitrogen gas, and then treat the capillary with the ethanol/H_2O/3-Aminopropyltriethoxysilane (APTES) mix for 1 h.
4. Rinse the capillary successively with ethanol and ultrapure water.
5. Heat the capillary to 120 °C for 1 h.
6. Immerse the capillary in 5% glutaraldehyde overnight. Store at 4 °C, if needed.
7. Dry the aldehyde modified capillary under a flow of nitrogen gas.
8. Prepare a 50 μM solution of the TSPs in TM buffer. Generate a droplet array of amino-derivatized TSPs or amino-functionalized ssDNA droplet array using the slotted-vial auto sample device (using pentanol as the carrier). Incubate the capillary with the droplet array overnight at room temperature.
9. Rinse the capillary with TM buffer.
10. Reduce the functionalized capillary with the aldehyde blocking solution at room temperature. Store at 4 °C for further use.

3.3 Metal Ion Detection with DNM Functionalized Microchannel

1. Prepare a sample plugs array made by the desired amounts of aqueous solution plugs, an air bubble plug and a washing buffer plug (*see* Fig. 1b). Each aqueous solution plug is made by adding 10 μL of solution of the desired metal ion at the test concentration to 5 μL of Cy3-labeled reporter oligo solution (*see* Table 2).
2. Connect the DNM-functionalized capillary with the sample plug array via the inlet. Connect the DNM-functionalized capillary with a syringe pump via the outlet.
3. Drive the sample plug array from the inlet to the capillary with a flow rate of 5 μL/min. Move the sample plugs array successively through the DNM-sensing interface. Pause the syringe pump when the sample plugs array approaches the outlet of the capillary.
4. Flow the sample plugs array backward through the DNM-sensing interface with a flow rate of 5 μL/min. Repeat the process for multiple times.
5. Rinse the capillary passing the washing buffer plug over the DNM-sensing interface with a flow rate of 5 μL/min.
6. Utilize a confocal laser fluorescence microscope to evaluate the efficiency of the DNM sensor for the metal ion. Record the fluorescence signal at an excitation wavelength of 532 nm and an emission wavelength of 580 nm. Use a resolution of 10 μm.
7. Analyze the fluorescence image with ImageQuant software.

4 Notes

1. Warming up the water (to about 37 °C) helps in the dissolution of Tris. It is important to adjust the pH of the solution after equilibration at room temperature.
2. Concentrated HCl (12 N) can be used at first to narrow the gap from the starting pH to the required pH. From then on it would be better to use a series of HCl (e.g., 6 and 1 N) with lower ionic strengths to avoid a sudden drop in pH below the required pH.
3. Centrifuge with 12,000 × *g* for 60 s before dissolving the DNA to avoid loss.
4. Operate in a fume hood and wear a mask and appropriate personnel protection equipment when using the concentrated acetic acid to avoid acid contacting with eyes and skin.
5. Wear a mask when weighing acrylamide. To avoid exposing acrylamide to coworkers, cover the weigh boat containing the weighed acrylamide with another weigh boat when transporting it to the fume hood. Transfer the weighed acrylamide to the cylinder inside the fume hood and mix on a stirrer placed inside the hood. Unpolymerized acrylamide is a neurotoxin and care should be exercised to avoid skin contact. Mixed resin AG 501-X8 (D) (anion- and cation-exchange resin) is used when acrylamide solution is made, since it removes charged ions (e.g., free radicals) and allows longer storage. Some investigators store the prepared acrylamide along with this resin in the refrigerator. However, we filter them out before storage. The used mixed resin should be disposed as hazardous waste. Manufacturer's warning states that this resin is explosive when mixed with oxidizing substances. The resin contains a dye that changes from blue-green to gold when the exchange capacity is exhausted.
6. The acrylamide solution can be stored at 4 °C for 1 month. Acrylamide hydrolyzes to acrylic acid and ammonia. The acrylamide mixture, buffer, and water can be prepared in large batches, frozen in aliquots, and used indefinitely. Remove the required amount, bring to room temperature, and add the other ingredients for casting our own gels.
7. We find that it is best to prepare this fresh each time.
8. We find that storing at 4 °C reduces its pungent smell.
9. Wear gloves and place a small beaker on the scale before weighing NaOH. Take out a certain amount of NaOH and quickly weigh the NaOH to avoid moisture. Add ultrapure water rapidly and stir gently with glass rod to avoid skin contact.

10. Wear a mask and use a glass rod for drainage when adding the sulfuric acid into 30% hydrogen peroxide. Do not change the order of addition. Stir gently in place for half hour before further use.
11. Wear a mask before using APTES to avoid breathing APTES. It would be better to operate in the fume hood.
12. Operate in a fume hood and wear a mask (besides appropriate gloves and other personal protective equipment) when using glutaraldehyde to avoid breathing vapors.
13. We find that it is best to prepare this fresh each time.
14. Wrap the Cy3-labeled reporter with aluminum foil to avoid light decomposition.
15. Seal the gel cassette with 1% agarose. Overlay the resolving gel with water for gels having acrylamide concentration lower than 8% and use isobutanol for gels of 10%. This overlay prevents contact with atmospheric oxygen in addition to helping to level the resolving gel solution.
16. Remove the comb carefully to avoid breaking the well.
17. Rinse the loading tip a few times with ultrapure water. Make sure that all the water in the loading tip is poured out before loading the samples.
18. Attach the power supply by putting the lid. Make sure that the connection is in correct way, ie., black to black and red to red. Make sure the migration in the right direction.
19. Centrifuging the samples prior to the run helps remove insoluble debris. Add a drop of 0.1% bromophenol blue to the upper chamber buffer and form a much stronger dye front during the electrophoretic run. Do not allow the dye front to go out of the gel.
20. The bag may be knotted to form the ends. Use dialysis clip for handling the bag easier and more convenient.
21. Seal the bag. Take care to exclude all air bubbles to avoid the separation effect.
22. Weigh the bag down with glass slides to prevent the dialysis clip from floating. Do not use metal as a weight, for it distorts the electric field. Tap the bag to the gel platform to keep it from floating if floating.
23. Rinse the bag and gel slice once with 200 μL of 1× TAE buffer. Add sodium acetate and ethanol if desired. Pellet the TSPs and wash one time with 70% ethanol.

Acknowledgments

This work was supported by the National Natural Science Foundation of China (21505045, 21675167, 21373260, 21305034, 31571014), Shanghai Pujiang Program (15PJ1401800, 16PJ1402700), China Postdoctoral Science Foundation (2015 M581565), introduction of major R&D projects of Fujian province (No. 2014I2005), Natural Science Foundation of Fujian Province of China (2015 J01064), Academy of Finland (297580), and Jane and Aatos Erkko Foundation (4704010).

References

1. Vasyukov D, Anahory Y, Embon L, Halbertal D, Cuppens J, Neeman L, Finkler A, Segev Y, Myasoedov Y, Rappaport ML, Huber ME, Zeldov E (2013) A scanning superconducting quantum interference device with single electron spin sensitivity. Nat Nanotechnol 8(9):639–644. https://doi.org/10.1038/nnano.2013.169
2. Tian Y, Wang Y, Xu Y, Liu Y, Li D, Fan C (2015) A highly sensitive chemiluminescence sensor for detecting mercury (II) ions: a combination of exonuclease III-aided signal amplification and graphene oxide-assisted background reduction. Science China Chem 58(3):514–518. https://doi.org/10.1007/s11426-014-5258-9
3. Miao P, Tang YG, Wang L (2017) DNA modified Fe_3O_4@au magnetic nanoparticles as selective probes for simultaneous detection of heavy metal ions. ACS Appl Mater Inter 9(4):3940–3947. https://doi.org/10.1021/acsami.6b14247
4. Chin CD, Laksanasopin T, Cheung YK, Steinmiller D, Linder V, Parsa H, Wang J, Moore H, Rouse R, Umviligihozo G (2011) Microfluidics-based diagnostics of infectious diseases in the developing world. Nat Med 17(8):1015–1019. https://doi.org/10.1038/nm.2408
5. Yang F, Zuo X, Li Z, Deng W, Shi J, Zhang G, Huang Q, Song S, Fan C (2014) A bubble-mediated intelligent microscale electrochemical device for single-step quantitative bioassays. Adv Mater 26(27):4671–4676. https://doi.org/10.1002/adma.201400451
6. Das J, Cederquist KB, Zaragoza AA, Lee PE, Sargent EH, Kelley SO (2012) An ultrasensitive universal detector based on neutralizer displacement. Nat Chem 4(8):642–648. https://doi.org/10.1038/nchem.1367
7. Yu X, Labaer J (2015) High-throughput identification of proteins with AMPylation using self-assembled human protein (NAPPA) microarrays. Nat Protoc 10(5):756–767. https://doi.org/10.1038/nprot.2015.044
8. Dong XC, Hong Y, Wu M, Chen G, Dai Z, Zhang YZ, Chen G (2016) 3D printed microfluidic device with microporous Mn_2O_3 modified screen printed electrode for real-time determination of heavy metal ions. ACS Appl Mater Inter 8(48):32940–32947. https://doi.org/10.1021/acsami.6b10464
9. Hu L, Harleytrochimczyk A, Cheng S, Hao H, Chi WS, Carraro C, Shi T, Tang Z, Maboudian R (2016) Nanowire-assembled hierarchical $ZnCo_2O_4$ microstructure integrated with low power microheater for highly sensitive formaldehyde detection. ACS Appl Mater Inter 8(46):31764–31771. https://doi.org/10.1021/acsami.6b11054
10. Lei Z, Gao J, Liu X, Liu D, Wang Z (2016) Poly(glycidyl methacrylate-co-2-hydroxyethyl methacrylate) brushes as peptide/protein microarray substrate for improving protein binding and functionality. ACS Appl Mater Inter 8(16):10174–10182. https://doi.org/10.1021/acsami.6b01156
11. Squires TM, Messinger RJ, Manalis SR (2008) Making it stick: convection, reaction and diffusion in surface-based biosensors. Nat Biotechnol 26(4):417–426. https://doi.org/10.1038/nbt1388
12. Pei H, Li F, Wan Y, Wei M, Liu H, Su Y, Chen N, Huang Q, Fan C (2012) Designed diblock oligonucleotide for the synthesis of spatially isolated and highly hybridizable functionalization of DNA-gold nanoparticle nanoconjugates. J Am Chem Soc 134(29):11876–11879. https://doi.org/10.1021/ja304118z
13. Pei H, Li J, Lv M, Wang J, Gao J, Lu J, Li Y, Huang Q, Hu J, Fan C (2012) A graphene-based sensor array for high-precision and adaptive target identification with ensemble aptamers.

J Am Chem Soc 134(33):13843–13849. https://doi.org/10.1021/ja305814u

14. Lin M, Wang J, Zhou G, Wang J, Wu N, Lu J, Gao J, Chen X, Shi J, Zuo X (2015) Programmable engineering of a biosensing interface with tetrahedral DNA nanostructures for ultrasensitive DNA detection. Angew Chem Int Ed 54(7):2151–2155. https://doi.org/10.1002/anie.201410720
15. Zhang L, Fang M (2010) Nanomaterials in pollution trace detection and environmental improvement. Nano Today 5(2):128–142. https://doi.org/10.1016/j.nantod.2010.03.002
16. Farimani AB, Dibaeinia P, Aluru NR (2017) DNA origami-graphene hybrid nanopore for DNA detection. ACS Appl Mater Inter 9(1):92–100. https://doi.org/10.1021/acsami.6b11001
17. Kelley SO, Mirkin CA, Walt DR, Ismagilov RF, Toner M, Sargent EH (2014) Advancing the speed, sensitivity and accuracy of biomolecular detection using multi-length-scale engineering. Nat Nanotechnol 9(12):969–980. https://doi.org/10.1038/Nnano.2014.261
18. Qu X, Fan Y, Hong C, Jiang L, Zhang H, Zhang G, Li L, Wang L, Song S, Yang T (2017) Bubble-mediated ultrasensitive multiplex detection of metal ions in three-dimensional DNA nanostructure-encoded microchannels. ACS Appl Mater Inter 9(19):16026–16034. https://doi.org/10.1021/acsami.7b03645
19. Pei H, Zuo X, Pan D, Shi J, Huang Q, Fan C (2013) Scaffolded biosensors with designed DNA nanostructures. NPG Asia Mater 5(5):e51. https://doi.org/10.1038/am.2013.22
20. Chao J, Zhang Y, Zhu D, Liu B, Cui C, Su S, Fan C, Wang L (2016) Hetero-assembly of gold nanoparticles on a DNA origami template. Science China Chem 59(6):730–734. https://doi.org/10.1007/s11426-016-5596-x
21. Yao G, Li J, Chao J, Pei H, Liu H, Zhao Y, Shi J, Huang Q, Wang L, Huang W (2015) Gold-nanoparticle-mediated jigsaw-puzzle-like assembly of supersized plasmonic DNA origami. Angew Chem Int Ed 54(10):2966–2969. https://doi.org/10.1002/anie.201410895
22. Du WB, Fang Q, Fang ZL (2006) Microfluidic sequential injection analysis in a short capillary. Anal Chem 78(18):6404–6410. https://doi.org/10.1021/ac060714d
23. Du WB, Fang Q, Qiaohong He A, Fang ZL (2005) High-throughput nanoliter sample introduction microfluidic chip-based flow injection analysis system with gravity-driven flows. Anal Chem 77(5):1330–1337. https://doi.org/10.1021/ac048675y
24. Qu XM, Wang YQ, Shi Z, Fu GC, Zeng X, Li X, Chen H (2012) Probe droplet arrays generated in the capillary for microarray analysis. Biosens Bioelectron 38(1):342–347. https://doi.org/10.1016/j.bios.2012.06.022
25. Li ZH, Zhao B, Wang DF, Wen YL, Liu G, Dong HQ, Song SP, Fan CH (2014) DNA nanostructure-based universal microarray platform for high-efficiency multiplex bioanalysis in biofluids. ACS Appl Mater Inter 6(20):17944–17953. https://doi.org/10.1021/am5047735

Chapter 10

Spatially Resolved Peptide-DNA Nanoassemblages for Biomarker Detection: A Synergy of DNA-Directed Immobilization and Nanografting

Abimbola Feyisara Adedeji, Elena Ambrosetti, Loredana Casalis, and Matteo Castronovo

Abstract

Peptide microarrays are becoming a promising alternative to protein microarrays due to the challenges associated with protein immobilization and purification. Here, we put forward a novel experimental-based approach that combines DNA-directed immobilization, nanografting, and atomic force height measurements to immobilize computationally designed cyclic peptide on an ultra-flat gold substrate. This procedure yields peptide-DNA nanoarrays, which can bind to the solvent-exposed site on the Beta-2-microglobulin (β2m).

Key words DNA-directed immobilization (DDI), Atomic force microscope (AFM), Nanografting, Cyclic peptide, Beta-2-microglobulin (β2m)

1 Introduction

Developing high-throughput screening platforms with proteins as bio-sensing elements is of great importance in experimental biology, biophysics, development of new drugs and the point-of-care diagnostics for profiling proteins that are progressive signatures of disease, such as cancer, cardiovascular disease, and so on [1–4]. However, the advances in protein microarrays have been slower due to the challenges associated with protein immobilization. These challenges are: random conformation and orientation after immobilization step [5, 6], difficulty in modifying the protein for proper immobilization on the surface without influencing its bioactivity and native state [4, 6], and short shelf life of the arrays due to protein denaturation [6]. Here, we show how to combine DNA-directed immobilization and atomic force nanolithography approach termed Nanografting to immobilize the peptide-terminated DNA molecules, to form spatially confined nanoarrays on

Giampaolo Zuccheri (ed.), *DNA Nanotechnology: Methods and Protocols*, Methods in Molecular Biology, vol. 1811, https://doi.org/10.1007/978-1-4939-8582-1_10, © Springer Science+Business Media, LLC, part of Springer Nature 2018

gold surface. These then serve to detect Beta-2-microglobulin (β2m), an overexpressed biomarker associated with ovarian cancer [7, 8]. Quantitatively, we could detect solvent-exposed site on Beta-2-microglobulin at a 100 μM concentration (*see* Fig. 2) and we could also determine the affinity of peptide-DNA nanoassemblages towards β2m (*see* [9]).

2 Materials

Prepare all the buffer solutions in ultra-pure water (milliQ-H_2O), of resistivity 18.2 MΩcm at 25 °C and filter before use with sterile syringe filter of 0.22 μm pore size. Also, purchase only HPLC purified grade DNA, peptide, and Beta-2-microglobulin (β2m) from their respective companies. Store all the stock solutions at room temperature, except where stated otherwise.

2.1 Stock Solutions

1. 5 M NaCl: dissolve 87.66 g of NaCl in 500 mL of ultrapure water.
2. 1 M Tris–HCl: dissolve 60.57 g of Tris base in about 300 mL of water, titrate to pH 8.5 with 37% HCl and bring to 500 mL with ultrapure water.
3. 0.5 M EDTA: add 208.1 g of Ethylenediaminetetraacetic acid disodium salt dihydrate (EDTA-Na_2) into 800 mL of ultrapure water. Adjust the pH to 8.0 with 37% HCl. Bring to 1 L with ultrapure water.
4. 1 M Sodium phosphate buffer: dissolve 138.0 g of monobasic sodium phosphate ($NaH_2PO_4 \cdot H_2O$) in 800 mL of ultrapure water and then adjust the pH to 7.0 with concentrated NaOH and bring to 1 L. Store it at room temperature.

2.2 Synthetic Oligonucleotides

1. Thiolated oligo stock solution (SH-$(CH_2)_6$–5′-CTTCACG ATTGCCACTTTCCAC-3′): 100 μM concentration in ultrapure water (*see* **Note 1**). Store at −20 °C in 10 μL aliquots (*see* **Note 2**).
2. Amino-modified oligo stock solution complementary to the thiolated oligo (NH_2-$(CH_2)_6$–5′-GTGGAAAGTGGCAATC GTGAAG-3′): 100 μM concentration in ultrapure water (*see* **Note 1**). Store at −20 °C in 10 μL aliquots (*see* **Note 2**).

2.3 Gold Chips

1. Sheets of clear ruby muscovite (Mica muscovite Corp., New York, USA) of the desired size that fit the beam evaporator stage.
2. TOEG-6 stock solution (268.8 μM in ethanol): Add 1.5 μL of TOEG-6 (Top oligo-ethylene glycol-terminated alkylthiols

(TOEG-6: HS-$(CH_2)_{11}$-$(OCH_2CH_2)_6$-OH, ProChimia Surfaces Sp. z o.o., Poland.) to 10 mL of absolute ethanol (*see* **Note 3**).

3. Absolute ethanol (Sigma Aldrich, Italy).
4. p-doped silicon wafers (p-doped silicon wafers from any vendor can be used, as no specific purity is required).
5. Photoresist adhesive (SU8–100 negative tone photoresists, MicroChem, USA).
6. Stanley-199 blades.
7. Electron beam evaporator with gold target.
8. A dicer for silicon wafers.
9. An oven for incubation up to 150 °C.

2.4 Nanografting and AFM Height Measurements

1. Nanografting and imaging buffer: 10 mM Tris, 1 mM EDTA, 1 M NaCl at pH 7.2, prepared with the above-described stock solutions. Adjust the pH with HCl.
2. 1 μM thiol-modified single-stranded (ss) DNA (22 base pair long) in nanografting and imaging buffer.
3. NSC 18/no Al silicon nitride cantilever tip with spring constant 2.8 N/m (MikroMasch, Bulgaria).
4. CSC 38/no Al silicon nitride cantilever tip with spring constant 0.03 N/m (MikroMasch, Bulgaria) for imaging peptide arrays before and after protein recognition.
5. Ultra-flat gold substrates passivated with top-oligo ethylene glycol monolayer (as of Subheading 3.1).

2.5 Solulink Oligos-Protein Conjugation Kit

1. Solulink Protein-oligo conjugation kit (TriLink Biotechnologies).
2. Stock solution of a cyclic peptide at 2 mg/mL in 1× Solulink Modification buffer (available as 10× in the kit). For β2m, use a peptide of sequence CYFTKTDRRFQC (purchased with 95% from ProteoGenix SAS, Schiltigheim, France).
3. Spin columns (7 kDa 0.5 mL Zeba Columns—Thermofisher Scientific).

2.6 Hybridization with Peptide-Terminated DNA Molecules

1. Hybridization buffer: 10 mM Tris, 1 mM EDTA, 1 M NaCl at pH 7.2, preparared with the above described stock solutions. Adjust the pH with HCl (note: this is the same as nanografting buffer).
2. 100 nM solution of peptide-DNA hybrids in hybridization buffer.
3. Oven for incubation at 37 °C.

2.7 Binding Assays

1. Binding buffer: 25 mM sodium phosphate, 50 mM NaCl, at pH 7.0.
2. Target protein stock solution: 1 mM Beta-2-microglobulin (β2m) in binding buffer.

3 Methods

Perform all AFM experiments in the contact mode of atomic force microscopy, i.e. the nanografting of thiol-modified ssDNA molecules and the topographic imaging of peptide-terminated DNA nanoassemblages before and after β2m recognition.

3.1 Preparation and Curing of Gold Chips

Gold is deposited on freshly cleaved mica using an electron beam evaporator operating at room temperature and at a pressure of 10^{-6} mbar. Subsequently, the gold layer is transferred to p-doped silicon. (*See* also Chapter 8 of this volume for an alternative similar method to obtain gold chips.)

1. Deposit 20 nm of gold on the muscovite mica sheet at 0.01 nm/s.
2. Increase the rate of evaporation to 0.1 nm/s till a film of 100 nm thickness is obtained. Store the gold-mica slice in a plastic case at room temperature.
3. Use a Stanley-199 blade to cut gold-on-mica slice into 5×5 mm^2 chips.
4. Cut silicon wafers to 4×4 mm^2 chips with a silicon dicer and ensure you do not touch or scratch the polished section of the silicon wafer.
5. Apply photoresist adhesive on the highly reflective gold face of the gold-mica slices and attach the polished section of the silicon on the adhesive. Press the silicon onto the adhesive (*see* **Note 4**).
6. With tweezers, place all the silicon-gold-mica sandwiches onto a glass slide and move the glass slide into oven for curing process. Cure at 130 °C for 24 h.
7. After the curing, turn off the oven and allow it to cool slowly to room temperature.
8. Transfer the sandwiches into a dry Petri dish and store in a cool and clean area.

3.2 Preparation of Top-Oligo-Ethylene Glycol Self-Assembled Monolayer (TOEG-6SAM) on Ultra-Flat Gold Substrate

1. Submerge the ultra-flat gold chip in the 100 μM TOEG-6 solution and incubate for 6 h at room temperature (alternatively, this step can be carried out at 4 °C).
2. Prepare five 1.5 mL microcentrifuge tubes for serial rinsing: put 100% ethanol in the first two tubes and nanografting buffer in the third, fourth and fifth tube.

3. Using pointed-tweezers, transfer the TOEG-6-passivated gold chip to the first rinsing tube and leave it there for 5 min (*see* **Note 5**).
4. Transfer the chip sequentially to the other four rinsing tubes, leaving it 5 min in each of them (*see* **Note 6**).
5. At the end of rinsing step, use clean tweezers to remove the gold chip from the last rinsing tube and place it on a clean sheet of parafilm with the gold side facing up and the silicon base on the paraffin sheet.
6. Add a drop of nanografting buffer on the gold chip.
7. Mount the TOEG-6-functionalized gold chip in the AFM liquid cell and ensure that it stays submerged in nanografting buffer. This operation will differ depending on the AFM instrumentation in use (*see* **Note 7**).

3.3 Conjugation of Cyclic Peptide with Amine-Modified Single-Stranded Oligonucleotides

Use the Solulink superior bioconjugation kit. This includes a peptide modification step (with the kit HyNic) and an oligo modification step (with S-4FB). The modified parts are then coupled.

1. Peptide modification with HyNic: in a 1.5 mL microcentrifuge tube, add 10 mol equivalents of HyNic (as available in the Solulink kit) to the desired volume of 2.0 mg/mL cyclic peptide in Modification buffer.
2. Briefly mix the solution using a vortex set a the minimum speed.
3. Allow to react for 90 min at room temperature.
4. Desalt the HyNic-modified peptide into conjugation buffer using a spin column (*see* Subheading 2.5).
5. DNA modification with S-4FB: Exchange the amino-modified single-stranded DNA (22 bp, complementary to the thiol-modified DNA) into ultrapure water using a spin column (*see* Subheading 2.5).
6. Measure the concentration of DNA by reading the absorbance at 260 nm and adjusting the concentration to 1.9 mM (corresponding to 0.5 OD/μL; make sure the reaction volume is >10 μL).
7. Add 20 mole equivalents of S-4FB to the oligonucleotide solution. Allow the reaction to proceed for 2 h at room temperature.
8. Exchange the 4FB-modified DNA to conjugation buffer with a spin column (*see* Subheading 2.5).
9. Cyclic peptide-DNA conjugation: add equimolar amounts of S-4FB-modified DNA and HyNic-modified peptide in 1× TurboLink Catalyst Buffer (using the 10× provided with the

Solulink kit). Vortex the reaction solution gently and allow the reaction to proceed overnight at 4 °C.

10. Exchange the reaction buffer with PBS buffer with a spin column (*see* Subheading 2.5).
11. Measure the concentration of the peptide-oligo hybrid by spectrophotometric quantification at 354 nm. The yield of DNA-protein conjugation is quantifiable by UV spectrophotometry since the bis-arylhydrazone group formed in the DNA-protein anchoring points adsorbs at a specific wavelength (354 nm—ε = 29,000). In this way, calculating the ratio between the determined concentration of bis-arylhydrazone groups and the relative concentration of protein, it is possible to simply obtain a quite accurate estimation of the number of conjugated DNA sequences per protein.
12. Store at −20 °C.

3.4 Generation of Spatially Resolved Thiol-Modified Single Stranded DNA Probes on SAM Passivated Gold Substrate

1. Add fresh DNA-free nanografting buffer in the AFM liquid cell with the TOEG-6-functionalized gold inside.
2. Remove the AFM cantilever holder and rinse it with isopropanol and then with ultrapure water. Then blow dry with nitrogen. (This procedure might differ for different AFMs, *see* **Note 8**.)
3. Mount a new NSC 18/no Al cantilever in the cantilever holder and in the AFM microscope.
4. Select a new cantilever from the box of NSC 18/no Al and mount it in the cantilever holder.
5. Gently rinse again the holder with the mounted cantilever with ultrapure water and blow dry with a gentle stream of nitrogen.
6. Mount the cantilever holder in the AFM head.
7. Launch the AFM workspace software and position the laser spot on the back of the cantilever.
8. Perform a fast scan on the gold surface in AC mode at a very high amplitude set point to examine the surface and to select a clean section for the nanografting process.
9. Use the *SV-align* software or analogous (*see* **Note 9**) to save the tip-surface reference area for the subsequent nanografting step.
10. Withdraw from the surface, raise the AFM head, remove the cantilever holder and then repeat the wash **step 2** above.
11. Remove the nanografting buffer from the sample situated within the AFM liquid cell and layer 100 μL of 1 μM solution of thiol-modified oligonucleotide onto the gold substrate.
12. Pipette 2 μL of the 1 μM solution of thiol-modified oligonucleotide on the mounted cantilever in the holder.
13. Re-align the laser spot on the back of the cantilever.

14. Reposition the AFM on the previously imaged portion of the gold surface (the operation will depend on the availability of auxiliary software/hardware).
15. Record a fast scan image of the surface at high amplitude setpoint in AC mode.
16. Switch AFM imaging to contact mode and engage at high force (high setpoint).
17. Select square area 1 × 1 μm and apply about 120 nN of force (high force) and perform a full scan (*see* Fig. 1b). The application of high force within the selected area will results into tip-induced substitution immobilization, in which the TOEG-6 molecules within the selected section is replaced with the thiol-modified DNA molecules from the surrounding 1 μM DNA solution.
18. Repeat **step 16** and create a 3 × 3 matrix of ssDNA nanoarrays within the TOEG-6 passivated gold substrate.
19. Return the AFM to AC mode and record a fast imaging of the 20 × 20 μm nanografted domain at a very low force (high amplitude setpoint).
20. Save the position of the nanografted section (such as using *SV align*, similar utilities of manual procedures).
21. Retract from the surface and remove the cantilever holder from the AFM.
22. Rinse the cantilever holder gently (with the mounted cantilever) and blow dry with nitrogen.
23. Remove the cantilever and return it back into its box.
24. Remove the leftover solution of thiol-modified DNA from the gold surface and rinse it with DNA-free nanografting buffer.

3.5 Hybridization of Cyclic Peptide-Terminated DNA Molecules with the Immobilized DNA on the Surface

1. Add 100 μL of 100 nM of cyclic-peptide-oligonucleotide conjugate solution in hybridization buffer (same as nanografting buffer) onto the sample, and transfer the chip in a Petri dish. Cover the dish, place it in an oven at 37 °C and incubate for 1 h.
2. Remove the peptide-oligo solution from the chip surface.
3. Rinse the chip with DNA-free nanografting buffer, leaving the chip surface wet with DNA-free nanografting buffer.

3.6 Imaging the Nanografted Domain after the Hybridization Step

1. Introduce the gold chip with the hybridized peptide-oligo conjugate in the AFM liquid cell.
2. Mount the AFM back to the original position to image the surface.

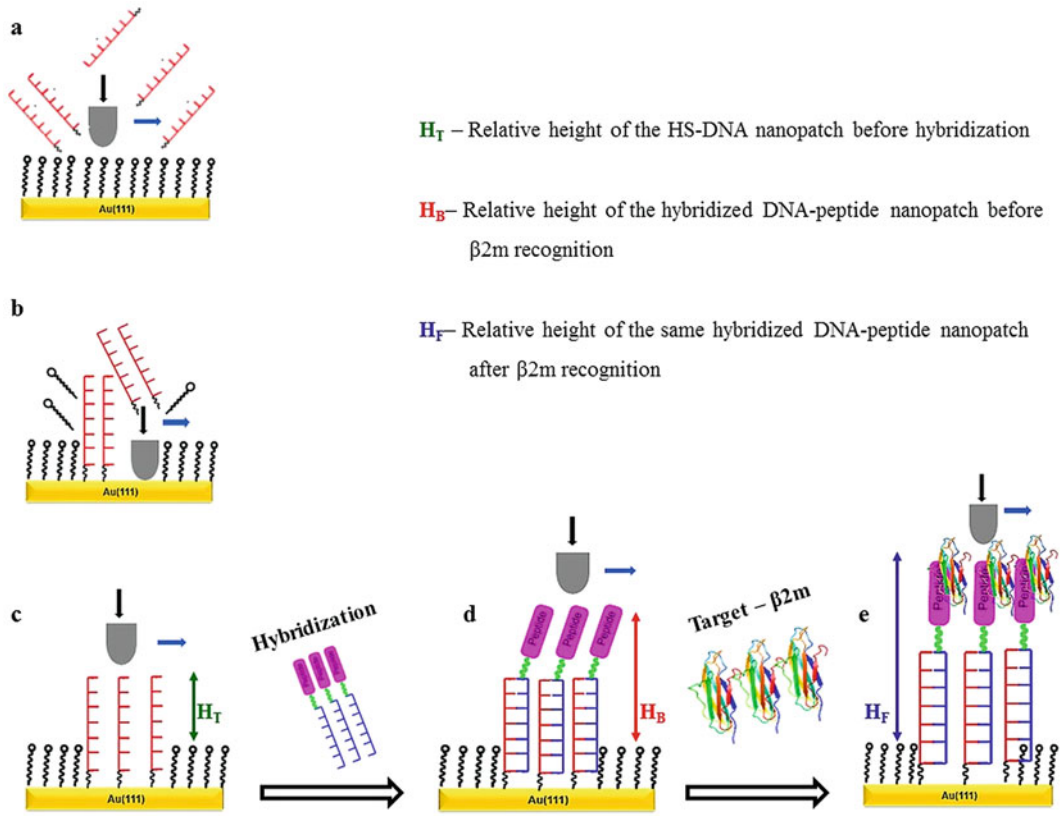

Fig. 1 AFM-based approach for immobilization of cyclic peptide and detection of β2m-cyclic peptide interactions on surfaces. The schematics represent the step-by-step procedures of the AFM nanolithography approach termed Nanografting; (**a**) Scan of the AFM tip at a low nominal load (about 0.2 nN) over a given section of a monolayer of protein-repellent ethylene glycol-terminated alkyl thiol on an ultra-flat gold surface embedded in the 1 μM solution of thiol-modified ssDNA molecules, followed by the removal of the alkyl thiols from the pre-selected section of the ultra-flat gold substrate at high nominal force (about 120 nN) and grafting of C6-thiol-modified single-stranded (ss)DNA in place of the previous alkyl thiol on the surface as shown in (**b**). This yields laterally confined ssDNA molecules with respect to neighboring monolayer of protein-repellent alkyl thiol as represented in (**c**). Subsequently, the complementary cyclic-peptide conjugates were immobilized onto (**c**) by means of DNA-directed immobilization (DDI) through sequence-specific base pairing, and resulted into laterally confined peptide-DNA assemblage as shown in (**d**). After the successful generation of (**d**), the peptide-DNA assemblage is ready to be used for protein recognition (**e**), in our case β2-microglobulin (β2m)

3. Mount a new CSC 38/no al cantilever in the AFM cantilever holder. This has a lower spring constant if compared to that used in Subheading 3.2.
4. Rinse the new cantilever using the usual cleaning procedure (*see* Subheading 3.4).
5. Add 2 μL of DNA-free nanografting buffer on the cantilever.

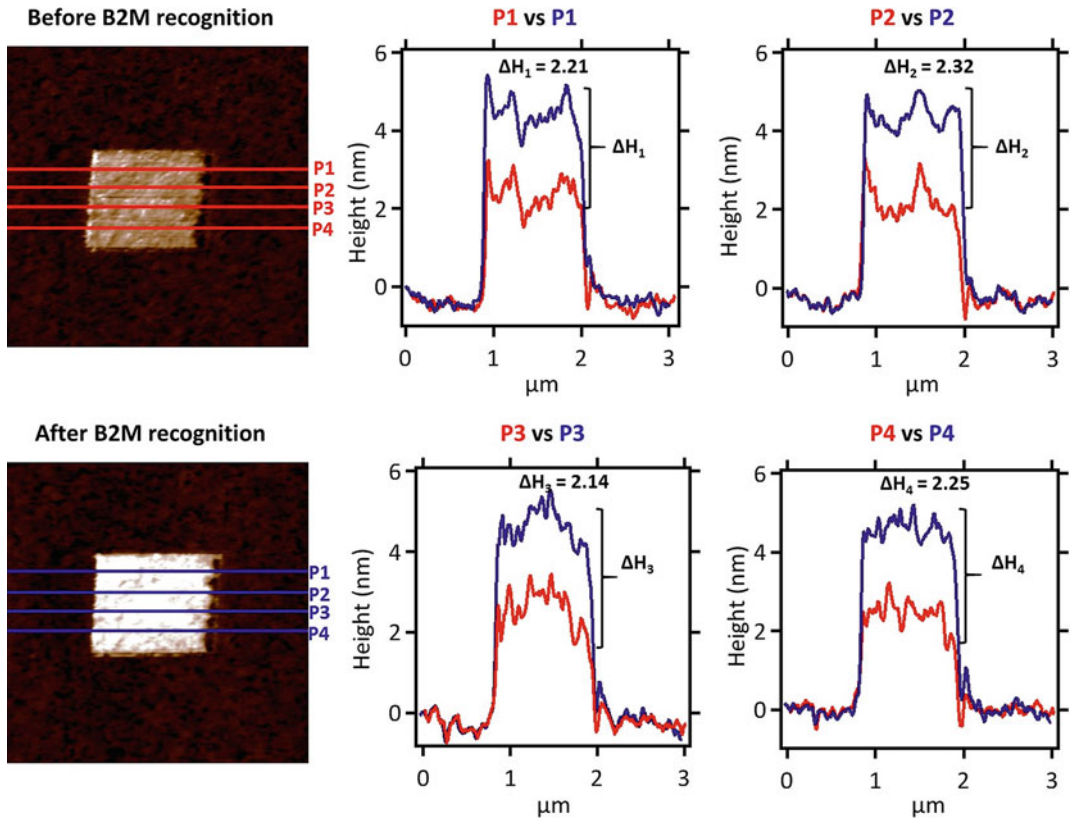

Fig. 2 An example of the height measurement procedure employed in determining the average height difference across the topographic AFM micrograph of peptide-DNA assemblage before and after β2m recognition (100 μM concentration)

6. Install the cantilever holder back into its place, and reposition the AFM head back on the same imaging area as used before (*see* Subheading 3.4).
7. Scan the nanografted domain. A higher contrast image should be obtained with confined cyclic-peptide nanoassemblages surrounded by the TOEG-6 SAM on the gold surface.
8. Zoom in to each of the nanoassemblage, and record a topographic height image with scan size 3 × 3 μm of each nanoassemblage (*see* Fig. 2).
9. Save the tip-sample position for subsequent imaging (Subheading 3.8).

3.7 Binding Assays of β2m and Peptide-DNA Nanoassemblages

1. Remove the AFM head, rinse the cantilever holder gently and blow dry.
2. Remove the nanografting buffer from the gold chip sample, rinse with fresh DNA-free nanografting buffer.

3. Rinse the gold chip twice with binding buffer. Keep 100 μL of binding buffer on the sample for 10 min (*see* **Note 10**).
4. At the end of equilibration, remove the binding buffer, then add the desired concentration of β2m protein in binding buffer (for example 100 μM, obtained from the target protein stock solution) on the gold chip and incubate for 1 h at 25 °C.
5. Remove the β2m solution from the sample. Rinse twice with β2m-free binding buffer.
6. Equilibrate the gold chip with imaging buffer for 10 min at room temperature.

3.8 Imaging the Nanografted Domain after the Protein Binding Assay

1. Mount the AFM system and reposition the scan on the portion of the gold surface with the nanoassemblages (with the help of alignment references, or other).
2. Image the experimental area and obtain height topographic images after the binding assay, as described in Subheading 3.6.
3. Disengage the AFM from the surface.
4. Rinse the cantilever holder using isopropanol, ultrapure water, and then blow dry gently. Thereafter, return the cantilever into CSC 38/no AL box.
5. Rinse the sample with fresh nanografting buffer. Store the sample sealed in a Petri dish at 4 °C.

3.9 Detection of B2m-Peptide Binding by AFM Height Measurements

1. Open the topographic image of the nanoassemblage before binding assay and after the binding assay on the AFM image processing software.
2. Flatten the two images using second order flattening and take 4–5 height profiles across the two images (*see* Fig. 2).
3. Collate the height points in each profile with respect to before and after binding assay (red and blue profile) and use the statistics function in the AFM analysis software to subtract the height profile before the binding assay from that after the binding assay. Average the final wave. This gives you ΔH for that profile (such as ΔH_1 for P1 vs. P1, *see* Fig. 2).
4. Calculate the mean of the all ΔHs. This corresponds to the binding signal. It can show the successful recognition of β2m in solution by the peptide-DNA nanoassemblages on the surface.

4 Notes

1. Briefly spin the microtubes containing oligonucleotides received from the commercial provider with a benchtop centrifuge to collect all the solution at the top and bottom. Vortex

mix the prepared 100 μM stocks for 30 min at room temperature before use or storage.

2. It is advisable to check the concentration of the oligonucleotides with an absorbance spectrometer (reading at 260 nm) in order to confirm proper resuspension and the manufacturer's specifications.
3. The volume suggested for making 268.8 μM concentration of top-oligo ethylene glycol is based on the values of relative density, moles, and mass provided by the manufacturer. It is advisable to check the data sheet of the vendor from which you purchase the top-ethylene glycol-6 before preparing the TOEG-6 solution.
4. Do not over-press silicon on the gold interface, a few strikes of tweezers on the nonpolished section of the silicon is sufficient.
5. We commonly flick the tube gently with a finger during the rinsing, to facilitate the suspension of nonadsorbed molecules.
6. At the end of each rinsing step, rinse the pointed tweezers first with isopropanol, then with ultrapure H_2O and then blow them dry with compressed air or nitrogen.
7. If your AFM can scan a specimen attached on a glass slide, you can create home-made liquid cell by cutting a small square shape at the center of parafilm sheet and then attach it on the clean glass slide. To aid the adhesion of the parafilm on glass, use wafer tweezers to stretch the parafilm. Ensure that the square opening (liquid gate) is firmly adhered to the glass, to avoid the loss of buffer during experiment.
8. Do not to pour isopropanol and ultrapure water directly on the cantilever, let the direction of the pouring be 45° to the plane of the cantilever holder and blow-dry gently with nitrogen.
9. A utility program of the AFM operating software, such as *SV-align*, can help to keep record of experimental section on the surface, so as to ease the subsequent experiment, that depends on monitoring the changes on the previous experimental section on the surface. If such software is not available, then crop the video panel of the prior experimental section and then use your eyes to match the image with the live image.
10. This step is essential for the equilibration of the macroenvironment.

References

1. Sutandy FXR, Qian J, Chen C-S, Zhu H (2013) Overview of protein microarrays. Curr Protoc Protein Sci Chapter 27:Unit 27.1. https://doi.org/10.1002/0471140864.ps2701s72
2. Kodadek T (2001) Protein microarrays: prospects and problems. Chem Biol 8:105–115. https://doi.org/10.1016/S1074-5521(00)90067-X

3. Ramachandran N, Srivastava S, Labaer J (2008) Applications of protein microarrays for biomarker discovery. Proteomics Clin Appl 2:1444–1459. https://doi.org/10.1002/prca.200800032
4. Camarero JA (2008) Recent developments in the site-specific immobilization of proteins onto solid supports. Biopolym Pept Sci Sect 90:450–458. https://doi.org/10.1002/bip.20803
5. Talapatra A, Rouse R, Hardiman G (2002) Protein microarrays: challenges and promises. Pharmacogenomics 3:527–536. https://doi.org/10.1517/14622416.3.4.527
6. Wikipedia page on protein microarrays. https://en.wikipedia.org/wiki/Protein_microarray. Accessed 1 Jun 2017
7. Fung ET (2010) A recipe for proteomics diagnostic test development: the OVA1 test, from biomarker discovery to FDA clearance. Clin Chem 56:327–329. https://doi.org/10.1373/clinchem.2009.140855
8. Sun W, Gui L, Zuo X, Zhang L, Zhou D, Duan X, Ren W, Xu G (2016) Human epithelial-type ovarian tumour marker beta-2-microglobulin is regulated by the TGF-β signaling pathway. J Transl Med 14:75. https://doi.org/10.1186/s12967-016-0832-x
9. Soler MA, Rodriguez A, Russo A, Adedeji AF, Dongmo Foumthuim CJ, Cantarutti C, Ambrosetti E, Casalis L, Corazza A, Scoles G, Marasco D, Laio A, Fortuna S (2017) Computational design of cyclic peptides for the customized oriented immobilization of globular proteins. Phys Chem Chem Phys 19:2740. https://doi.org/10.1039/c6cp07807a

Chapter 11

LSPR Detection of Nucleic Acids on Nanoparticle Monolayers

Sophie Thamm, Andrea Csàki, and Wolfgang Fritzsche

Abstract

Noble metal nanoparticles are well known for their unique optical properties. Density oscillations of the nanoparticle conduction electrons are induced at a specific frequency by an external incident light beam. This phenomenon is known under the term localized surface plasmon resonance (LSPR). The spectral position of the resonance band is determined by shape, size, and material of the nanoparticle and influenced by changes of the local refractive index of the surrounding medium. The latter gives the opportunity to use noble metal nanoparticles as label-free bioanalytical sensors. Biomolecules can be bound directly on the nanoparticle surface, which leads to a change of the local refractive index, and a shift of the peak maximum is detected by absorbance spectroscopy. This method is used for bioanalytical diagnostics. Here, a DNA sensing protocol for real-time measurements in situ using this system will be presented. A dense layer of noble metal nanoparticles is immobilized on a glass substrate and implemented in a microfluidic chamber, where the spectroscopic measurements are conducted.

Key words Nanoparticles, Localized surface plasmon resonance, DNA, Detection, Bioanalytical diagnostic

1 Introduction

Detection of biomolecular binding, of the adsorption of thin biofilms or of conformational changes of macromolecules is of high interest in various branches of biology, medicine and pharmacy. One possible detection method is based on the optical spectroscopy of metallic nanostructures exhibiting localized surface plasmon resonances. It represents a label-free approach, with rather high sensitivity in comparison to other label-free techniques [1]. The occurring resonance band is sensitive to changes of the surrounding medium, which gives the opportunity to utilize them as label-free bioanalytical sensors. Biomolecules binding on the nanoparticle surface lead to a change of the local refractive index, which results in a shift of the peak wavelength [2, 3]. Due to the strong confinement of the electromagnetic field around the nanoparticles surface,

Giampaolo Zuccheri (ed.), *DNA Nanotechnology: Methods and Protocols*, Methods in Molecular Biology, vol. 1811, https://doi.org/10.1007/978-1-4939-8582-1_11, © Springer Science+Business Media, LLC, part of Springer Nature 2018

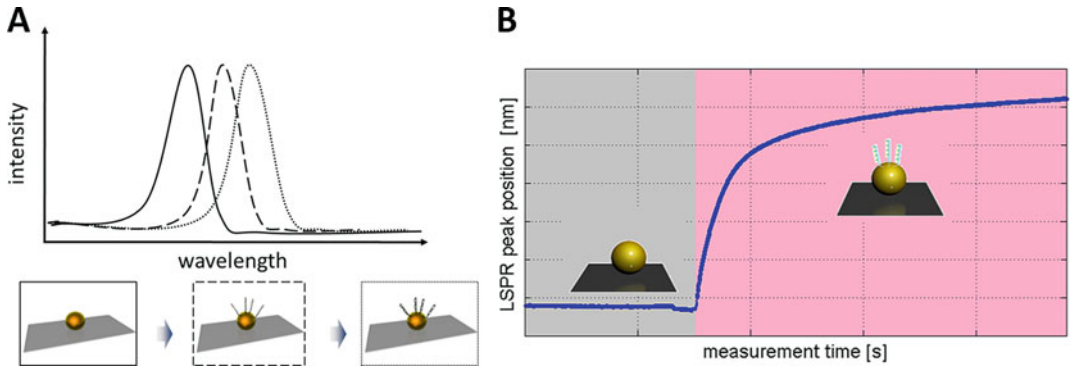

Fig. 1 (**a**) Principle of LSPR DNA biosensing. Naked particles (left) are modified with single-stranded DNA (capture or receptor) of a specific DNA sequence complementary to the target (analyte) DNA (center). When the target DNA is present, it will bind on these capture-DNA-modified particles (right). The respective spectra are shown; capture DNA leads to a red-shift, the additional binding of the target DNA to another shift. (**b**) Real-time detection of the resonance wavelength shift caused by binding of the capture DNA on the particle surface

high surface sensitivities for small biomolecules can be achieved. The detection of such small biomolecules, here DNA, is based on a specific biomolecule–biomolecule interaction. The adsorption of thiolated oligonucleotides (around 20–25 nt), named capture DNA, on spherical gold nanoparticles leads to a first, and the following hybridization with the complementary target DNA to a second shift in the LSPR wavelength (*see* Fig. 1). In biosensing, the first step results in a biosensor (a sensor functionalized with a molecule that binds specifically to the target molecules, acting as receptor or capture). The second step represents the biosensing, the detection of the analyte molecule.

The measurement setup, named ensLSPR (ensemble of nanoparticles), consisting of a microfluidic pump, a tungsten light source, a spectrometer, two optical fibers and a microfluidic chamber is shown in Fig. 2. Both the biofunctionalization of the gold nanoparticles with capture DNA and the binding of the target DNA are performed under fluid flow conditions. The extinction spectra of the nanoparticle layers are measured continuously, which leads to a real-time tracing of the maximum peak position change. This allows the characterization of the different steps of the sensor preparation, as well as the subsequent sensing, and therefore it additionally yields kinetic information.

The online detection is controlled by a custom-built LabView program (LabView 8.6). A spectrum is recorded continuously (every 2 s). In order to minimize the noise of position of the LSPR peak, the centroid of the LSPR peak is calculated as described in ref. [4].

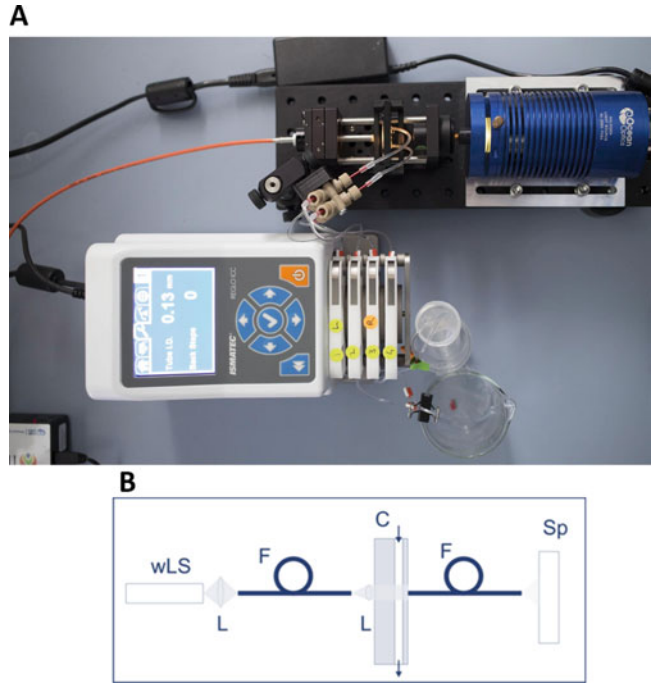

Fig. 2 (**a**) EnsLSPR setup (**b**) Scheme of the measurement setup, *wLS* white light source, *L* lens, *F* fiber, *C* flow chamber, *Sp* spectrometer

2 Materials

All solutions should be prepared using ultrapure water (e.g., MilliQ, >18 MΩ cm at 25 °C).

2.1 Cleaning of Glass Slides

1. Glass slides.
2. Alkaline remover (rinsing agent like Palmolive, Fit).
3. Acetone, Rotisol (Carl Roth, Germany), ethanol, and ultrapure water.

2.2 Silanization

1. 1% (3-aminopropyl)triethoxysilane (APTES) in 1 mM acetic acid. This must be prepared between 10 and 15 min before its use, to achieve a controlled partial hydrolysis of APTES.

2.3 Immobilization of Gold Nanoparticles

1. APTES-coated glass slides.
2. Gold nanoparticles (BBI Solutions, Cardiff, UK): 80 nm in diameter, 1.10×10^{10} particles/ml ($OD_{525} = 1.0$) (*see* **Note 1**).

2.4 DNA Detection

1. 26-nt oligonucleotide as capture DNA with the sequence of 5′-TCAAAGTAAAAGTCCTGGTTCGCCAT-3′, thiol C6 at 5′ (biomers.net, Germany) (*see* **Note 2**).
2. 26-nt oligonucleotide as target DNA with the sequence of 5′-ATGGCGAACCAGGACTTTTACTTTGA-3′ from *biomers.net GmbH* (biomers.net, Germany).
3. CB buffer (adsorption buffer): 0.5 M trisodium citrate-dihydrate, pH 3.0 by HCl [5] (*see* **Note 1**).
4. Running buffer (5× SSC): 0.75 M NaCl, 75 mM trisodium citrate, pH 7.0 with HCl (*see* **Note 1**).
5. 1 mM 6-mercapto-1-hexanol (MCH) in ultrapure water (*see* **Note 3**) [6, 7].
6. 0.1 M NaOH [8] (*see* **Note 3**).

2.5 Equipment

1. Centrifuge (UniCen 15DR by *Herolab GmbH*, Wiesloch, Germany).
2. Oxygen plasma etcher (200G Plasma System by *TePla GmbH*, Wettenberg, Germany).
3. Halogen light source (HL-2000 by *Ocean Optics*, Dunedin, USA) with a filter <400 nm.
4. Spectrometer (Cypher II by *B&W Tek Inc.*, Newark, USA).
5. Pump (Ismatec Reglo ICC by *Cole-Parmer GmbH*, Wertheim, Germany).
6. Two optical large-core fibers.
7. ensLSPR fluidic cell (custom made). Microfluidic tubings should be kept as short as possible to avoid extensive diffusion of analyte solutions.

3 Methods

The first objective is a thorough cleaning of the glass slides. To increase the affinity of the gold nanoparticles to the glass surface, the glass slides are functionalized with amine groups. Therefore, a wet chemical silanization is used [9, 10]. The third step is the immobilization of the gold nanoparticles. After this procedure, the sensor is finished and ready for the measurement—the detection of DNA—based on LSPR.

3.1 Cleaning of Glass Slides

1. Clean the glass slides with rinsing agent and further with acetone, Rotisol, ethanol and ultrapure water in ultrasonic bath for 10 min each.
2. Dry the slides with a flow of nitrogen gas.
3. Etch the slides by oxygen plasma for 60 min, 380 W and 1.6 mbar. This procedure removes organic adsorbates and thereby activates the glass slides for the silanization.

3.2 Silanization

In order to increase the affinity of the gold nanoparticles to the glass surface the glass slides are functionalized with aminosilane.

1. Treat the cleaned slides with 1% APTES in 1 mM acetic acid for 10 min.
2. Wash the slides with ultrapure water.
3. In case of immediate use, treat the slides for 2 min in an ultrasonic bath with ultrapure water and dry under a nitrogen flow.
4. For storage, dry the slides with nitrogen and store under argon (for subsequent use, execute **step 3** above).

3.3 Immobilization of Gold Nanoparticles

1. Centrifuge 2 ml of 80 nm gold nanoparticles for 8 min at 3220 × *g*.
2. Discard the supernatant (in our case 1900 μL for 20-fold concentration).
3. Resuspend the nanoparticles in ultrapure water. (At this step, they should be at about 20-fold concentration with respect to the commercial preparation.).
4. Incubate a 20 μL drop of the 20-fold concentrated gold nanoparticle solution for 60 min on the APTES coated glass slide. The drop should be carefully laid (and confined) in the area where the nanoparticle film is desired to form (*see* **Note 4**).
5. Gently wash the slides with ultrapure water and gently dry them with nitrogen. *See* Fig. 3 for atomic force microscopy (AFM) images of the rather dense nanoparticle layer and the corresponding spectra.

3.4 DNA Detection

The peristaltic pump is used at a flow rate of 20 μL/min throughout the procedure.

1. Activate and clean the chip by oxygen plasma etching for 10 s at 1.6 mbar and 380 W.
2. Assemble the measurement system with the activated slide in the fluidic chamber.
3. Pump CB buffer (adsorption buffer) into the chamber (*see* **Note 5**).

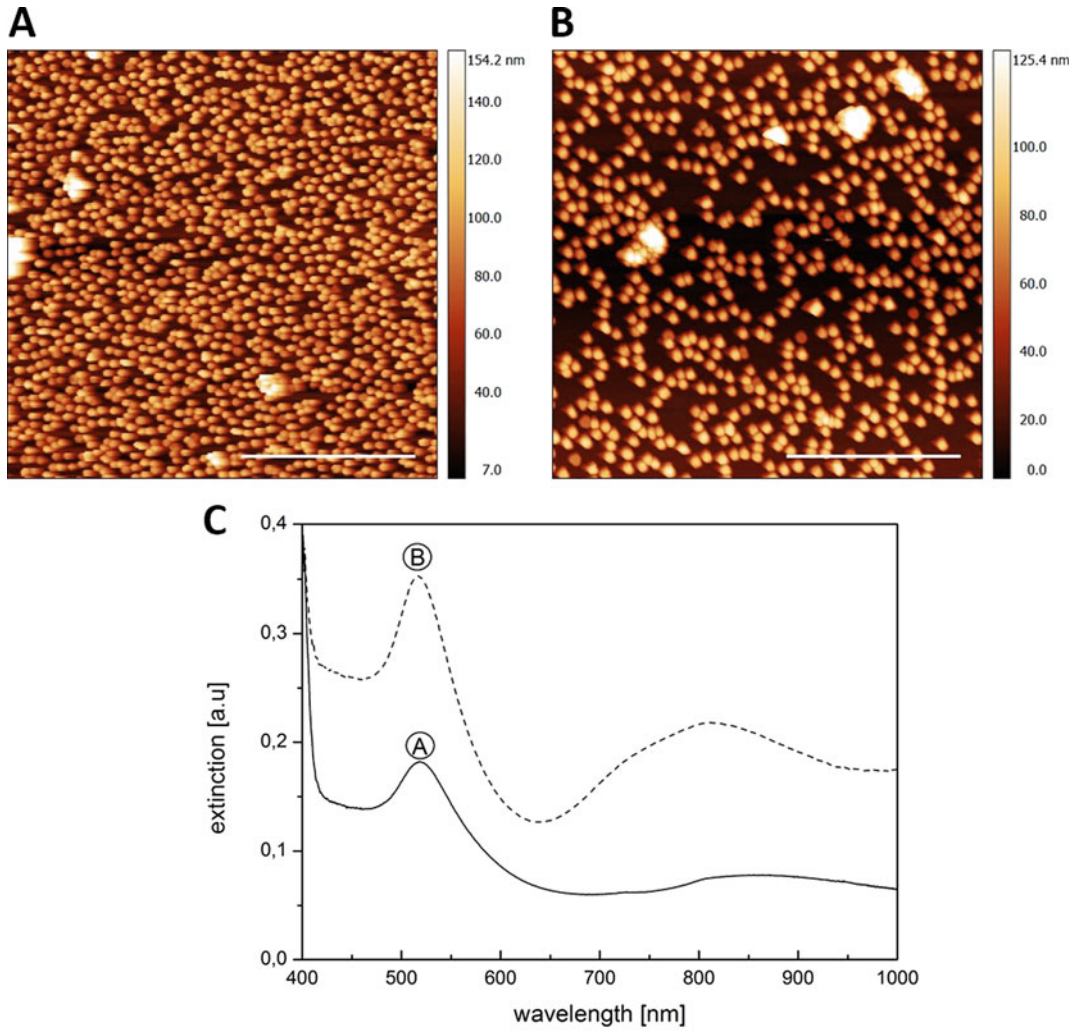

Fig. 3 Atomic force microscopy (scale bar 2 μm) of the sensor substrates with immobilized 80 nm gold nanoparticles for different incubation time (**a**: 10 min incubation, **b**: 60 min incubation) and the corresponding spectra (**c**)

4. Inject 1 μM thiolated capture DNA in CB buffer for at least 5 min. The adsorption of thiolated DNA commonly causes a wavelength shift of a few nm (typically 2–3 nm; 2.44 nm in the shown measurement) in the adsorption spectrum.
5. Change the CB buffer with running buffer (5× SSC) (*see* **Note 5**).
6. Inject 1 mM MCH in ultrapure water into the chamber until the signal is stable, 5 min should be enough. The MCH coadsorbs with the thiolated capture DNA on the gold nanoparticle surface in order to improve the hybridization yield. The particle surface is thereby covered and so passivated against nonspecific adsorption of DNA (i.e., along the strands) (*see* **Note 6**).

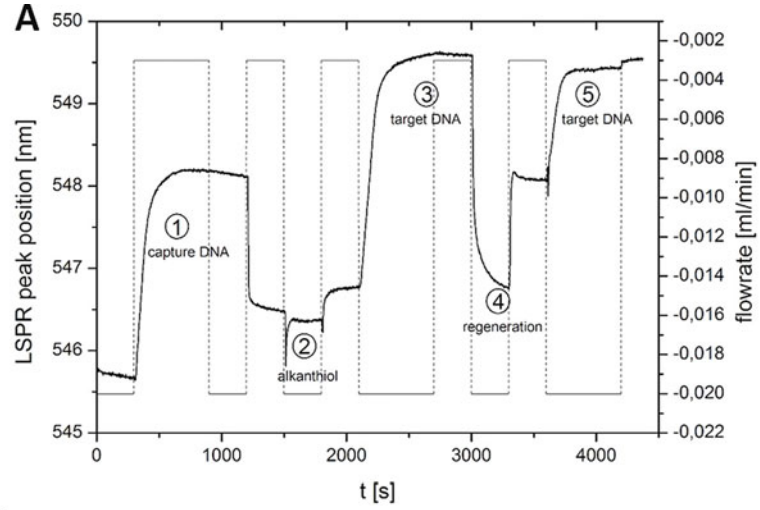

B

20161209_Au80nm_Candida
80nm Au-NP (20fold, 1h incubation)
5xSSC, 1mM MCH, 0.1M NaOH
rinsing with H_2O
peristaltic pump ISMATEC
24.1°C

time [s]	[min]	[h]	flowrate [µl/min]	peak pos. [nm]	shift [nm]
0	0	0.0 CB ph3	20	545.71	
300	5	0.1 1 µM Candida_spp in CB ph3	20	548.15	2.44
900	15	0.3 CB ph3	20		
1200	20	0.3 5xSSC	20		
1500	25	0.4 MCH	20		
1800	30	0.5 5xSSC	20	546.71	
2100	35	0.6 1 µM c_Candida in 5xSSC	20	549.60	2.89
2700	45	0.8 5xSSC	20		
3000	50	0.8 NaOH	20		
3300	55	0.9 5xSSC	20	548.03	
3900	65	1.1 1 µM c_Candida in 5xSSC	20	549.41	1.38
4500	75	1.3 5xSSC	20		

Fig. 4 EnsLSPR sensing measurement. (**a**) (1) adsorption of capture DNA $\Delta\lambda = 2.44$ nm, (2) coadsorption with MCH, (3) hybridization with target DNA $\Delta\lambda = 2.89$ nm, (4) regeneration with NaOH, (5) 2nd hybridization with the target DNA $\Delta\lambda = 1.38$ nm. (**b**) Description of the corresponding protocol and results, as from the instrument software

7. Inject 1 µM complementary target DNA in running buffer (5× SSC) until the signal reaches a plateau, at least 15 min. Binding of covalent DNA should lead to a wavelength shift of a few nanometers (typically 2–3 nm; 2.89 nm in the shown measurement) in the adsorption spectrum (*see* **Note 6**).
8. Regenerate the sensor by flowing 0.1 M NaOH. This destroys the hydrogen bonds between the bases, and thereby removes the target DNA specifically. A new binding experiment is now possible. A complete measurement procedure is shown in Fig. 4.

4 Notes

1. Every buffer and the gold nanoparticle solution should be filtered (with a 0.22 μm pore filter).
2. The thiol group of the capture DNA has to be intact. It is important that the DNA forms no hairpins. In the first case the adsorption and in the second case the hybridization will be seriously hampered or even fail.
3. The MCH and NaOH solutions need to be prepared fresh. Their state is crucial for the success of the method.
4. A 20-fold concentration of the gold nanoparticle stock solution is recommended. The resulting spectra show a high intensity that leads to optimal measurements. Nevertheless, it is possible to measure with a lower concentration of nanoparticles. That applies to the incubation time too. An incubation time of 60 min is recommended. The spectrum shows a lower intensity for lower incubation times, and the monolayer of the gold nanoparticles is not as dense as after a 60 min incubation.
5. Dilution and running buffer should be the same, otherwise the refractive index of the solution will change and so impede the measurement.
6. The necessary volumes of the solutions depend on chamber-thickness, tube diameter and flow rates.

Acknowledgments

We thankfully acknowledge Jacqueline Jatschka for further measurements as well as Andrè Dathe and Ondrej Stranik for the data recording script and the setup. The funding of ExoDiagnos (EU Era-NET-AiFZIM KF2206925CR4) and TRACE (EU Era-NET-KIT 02WU1348A) is gratefully acknowledged.

References

1. Kreibig U, Vollmer M (1995) Optical properties of metal clusters, Series in materials science, vol 25. Springer, Berlin
2. Schneider T, Jahr N, Jatschka J, Csaki A, Stranik O, Fritzsche W (2013) Localized surface plasmon resonance (LSPR) study of DNA hybridization at single nanoparticle transducers. J Nanopart Res 15(4):1–10. https://doi.org/10.1007/s11051-013-1531-7
3. Jatschka J, Dathe A, Csáki A, Fritzsche W, Stranik O (2016) Propagating and localized surface plasmon resonance sensing—a critical comparison based on measurements and theory. Sens Bio-Sensing Res 7:62–70. https://doi.org/10.1016/j.sbsr.2016.01.003
4. Dahlin AB, Tegenfeldt JO, Höök F (2006) Improving the instrumental resolution of sensors based on localized surface Plasmon resonance. Anal Chem 78(13):4416–4423. https://doi.org/10.1021/ac0601967
5. Zhang X, Servos MR, Liu J (2012) Instantaneous and quantitative functionalization of gold nanoparticles with thiolated DNA using a pH-assisted and surfactant-free route. J Am Chem Soc 134(17):7266–7269. https://doi.org/10.1021/ja3014055

6. Herne TM, Tarlov MJ (1997) Characterisation of DNA probes immobilized on gold surfaces. J Am Chem Soc 119:8916–8920
7. Levitcky R, Herne TM, Tarlov MJ, Satija SK (1998) Using self-assembly to control the structure of DNA monolayers on gold: a neutron reflectivity study. J Am Chem Soc 120:9787–9792
8. Dupont-Filliard A, Billon M, Livache T, Guillerez S (2004) Biotin/avidin system for the generation of fully renewable DNA sensor based on biotinylated polypyrrole film. Anal Chim Acta 515(2):271–277. https://doi.org/10.1016/j.aca.2004.03.072
9. Fang Y, Hoh JH (1998) Surface-directed DNA condensation in the absence of soluble multivalent cations. Nucleic Acids Res 26(2):588–593
10. Csáki A, Jahn F, Latka I, Henkel T, Malsch D, Schneider T, Schröder K, Schuster K, Schwuchow A, Spittel R, Zopf D, Fritzsche W (2010) Nanoparticle layer deposition for plasmonic tuning of microstructured optical fibers. Small 6(22):2584–2589. https://doi.org/10.1002/smll.201001071

Chapter 12

DNA-Templated Silver Nanoclusters for DNA Methylation Detection

Hanie Ahmadzade Kermani, Morteza Hosseini, and Mehdi Dadmehr

Abstract

DNA methylation entails the covalent addition of a methyl group to C-5 position of cytosine by a family of DNA methyltransferase enzymes and has a significant role in gene regulation. Epigenetic changes such as DNA methylation of CpG islands located in the promoter region of some tumor suppressor genes are very common in human diseases such as cancer. Detection of aberrant methylation pattern could serve as an excellent diagnostic approach. It is key to develop methods for the direct and simple detection of methylated DNA or of methyltransferase activity without using antibodies, chemical modification, labeling and enzymatic treatments. In this study, we employ DNA-templated silver nanoclusters for detection of DNA methylation. This method entails use of cytosine rich DNA sequence as an effective template. By monitoring changes in fluorescence intensity, DNA methylation and DNA methyltransferase activity is detected. Upon DNA methylation, the fluorescence intensity of DNA templated Ag/NCs is decreased in a linear range when the concentration of methylated DNA is increased.

Key words Silver nanoclusters, DNA methylation, Fluorescence, Biosensors

1 Introduction

Nanoclusters (NCs) have recently been developed by combining the virtues of materials chemistry and nanotechnology. Metal nanoclusters are particles composed of a small number of atoms that possess a size comparable to the Fermi wavelength of an electron and have distinguished properties due to their quantum confinement [1–4]. The interaction of these novel agents with light results in electron transition between their discrete energy levels and enable them to show strong luminescence, long term photo stability and high emission rates due to the specific characteristics of their synthesizer scaffold [5]. These optically active nanomaterials are used to construct the optical biosensors. Among metal nanoclusters, fluorescent silver nanoclusters (Ag NCs) are promising candidates in biological applications [6–9] due to their simple synthesis and good biocompatibility. There are different

Giampaolo Zuccheri (ed.), *DNA Nanotechnology: Methods and Protocols*, Methods in Molecular Biology, vol. 1811,
https://doi.org/10.1007/978-1-4939-8582-1_12, © Springer Science+Business Media, LLC, part of Springer Nature 2018

kinds of scaffolds which are employed to synthesize AgNCs, such as DNA [6–13], thiols [14–16], polymers [17, 18] peptides and proteins [19–21]. Ag NCs are regarded as an element class that could be located within cytosine rich DNA strands in aqueous solution, have drawn much attention in the field of bioassay [22, 23]. The fluorescence emission based on Ag NC fluorophores stabilized by oligonucleotide contains a wide range between visible and near infrared range, which is tunable by different oligonucleotide sequences [9, 24]. The properties of these nanomaterials introduced them as promising candidate sensors for many analysts [25]. The combination of DNA–AgNCs and the specific G-rich sequence and also using extra C and G in the loops within the double stranded DNA exhibit bright fluorescence for DNA detection, single nucleotide polymorphism, and enzyme activity [6, 25–28]. Since the silver nanoclusters synthesis is highly dependent on specificity of the DNA sequences. In this study, we present a protocol to synthesize silver nanoclusters for the direct detection of DNA methylation and DNA methyltransferase activity assay. A specific site in the CpG islands of a tumor suppressor gene promoter was selected as our DNA scaffold for the synthesis of silver nanoclusters (*see* **Note 1**). We observed that a double stranded DNA with an inserted C6 loop in our probe can be used as a convenient scaffold for Ag NCs synthesis. Ag NCs formed by unmethylated DNA exhibited red color under UV light and intense fluorescence while it did not exhibit such properties with methylated DNA (*see* Fig. 1). This would help us to distinguish between unmethylated and methylated targets [29]. Also we performed an experiment using DNA methyltransferase, MSssI to methylate the fluorescent unmethylated DNA. Enzymatic methylation of unmethylated DNA with bright fluorescence leads turning off the intense emission of nanoclusters [30]. A downward trend in fluorescence signal was seen upon increasing the DNA methyltransferase enzyme concentration to Ag NCs (*see* Fig. 2).

2 Materials

All solutions are prepared with ultrapure water (resistivity >18 MΩcm at 25 °C, such as from a MilliQ apparatus by Millipore).

1. TE buffer: 10 mM Tris–HCl, 1 mM EDTA, pH 7.5 (make from stocks or 1 M Tris pH 7.5 and 0.5 M EDTA pH 7.5).
2. 10× hybridization buffer: 500 mM NaCl, 10 mM Tris–HCl, 1 mM EDTA, pH 8.0.
3. Phosphate buffer: 20 mM Sodium phosphate, 1 mM magnesium acetate, pH 7.0.

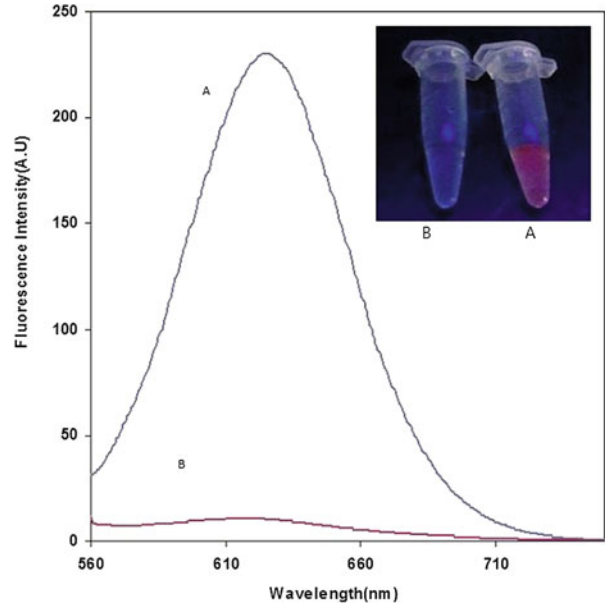

Fig. 1 Fluorescence spectra of unmethylated (A) and methylated (B) DNA Ag NCs. The inset shows photograph of synthesized Ag NCs under UV irradiation

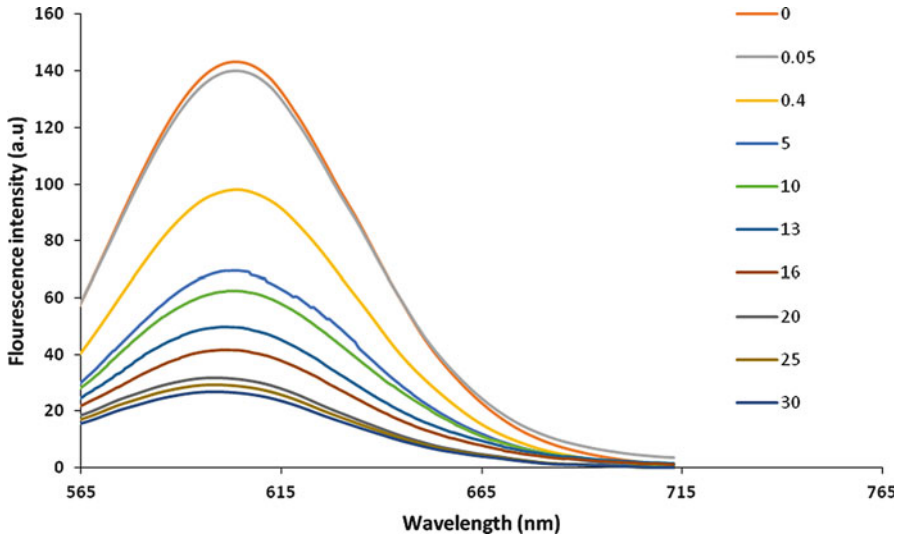

Fig. 2 Emission spectrum of DNA AgNCs probe with different concentrations of M.SssI. The concentrations of M.SssI are 0, 0.4, 5, 10, 13, 16, and 20 U/mL

Table 1
Sequences of the used oligonucleotides

Name	Sequence (5′–3′)
Probe	**TCCGCTTCCCGCCCCCCACCCGCACTCCGC**
Unmethylated target	**GCGGAGTGCGGGTCGGGAAGCGGA**
Methylated DNA	**GC(CH3)GGAGTGC(CH3)GGGTC(CH3)GGGAAGC(CH3)GGA**
Partially methylated DNA	**GC(CH3)GGAGTGCGGGTCGGGAAGCGGA**
Partially methylated DNA	**GC(CH3)GGAGTGC(CH3)GGGTCGGGAAGCGGA**

4. Methylated, unmethylated, and partially methylated DNA sequences (*see* Table 1).
5. M.SssI CpG Methyltrasferase enzyme and 10× reaction buffer: 10 mM potassium phosphate (pH 7), 400 mM KCl, 1 mM DTT, 1 mM EDTA, 0.2 mg/ml BSA, and 50% (v/v) glycerol (Thermo scientific).
6. 50× SAM solution (S-adenosylmethionine) (Thermo Scientific).
7. Silver nitrate stock solution: 5 mL of 0.1 M $AgNO_3$.
8. Silver nitrate working solution (1.5 mM): add 15 μL of silver nitrate stock solution to 985 μL of ultrapure water.
9. Sodium borohydride stock solution: 5 mL of 0.1 M $NaBH_4$.
10. Perkin Elmer LS-45 fluorescence spectrometer (Buckinghamshire, UK) or analogous.
11. Specord 250 spectrophotometer (Analytic Jena, Germany) or analogous.
12. Transmission electron microscope (TEM) (Zeiss, EM10C, 80 kV, Germany).

3 Methods

3.1 DNA/Ag NCs Synthesis by Unmethylated and Methylated DNAs

As cytosine loops (C-loop) have a reliable efficiency for the synthesis of silver nanoclusters, the sense strand (detection probe) was designed with six extra cytosine bases inserted inside the sequence to form a C-loop. The detection probe is hybridized with the complementary antisense target. The C-loop can bind the Ag ions through its cytosine bases and localize them inside the loop. In a typical DNA-AgNCs synthesis protocol, after the hybridization and reduction process, the formed silver nanoclusters emit intense fluorescence.

1. Prepare a 100 μM Oligonucleotide stock solution in TE buffer pH 7.5 by resuspending the commercial lyophilized oligonucleotide.

2. Mix 7.5 μL of the 100 μM probe DNA with 7.5 μL of 100 μM unmethylated or fully methylated or partially methylated targets to 30 μL of 2× hybridization buffer (diluted from 10×), to prepare different reaction mix aliquots.
3. Denature the DNA mix at 95 °C for 15 min.
4. Cool slowly to room temperature and incubate at 37 °C for 1 h to complete the annealing process and form DNA duplexes.
5. Add 73 μL of phosphate buffer to the mix.
6. Add 6 μL of silver nitrate working solution to provide Ag^+ in a molar ratio of 6:1 with respect to to total oligonucleotide DNA. Stir for 5 min and incubate for 15 min at room temperature.
7. Reduce the bound Ag^+ with $NaBH_4$ ($Ag/NaBH_4$/DNA = 6:6:1, molar ratio). Immediately before its use, dilute 15 μL of sodium borohydride solution with 985 μL of ultrapure water (1.5 mM working conc.).
8. Add 6 μL of the 1.5 mM $NaBH_4$ to the DNA duplexes/$AgNO_3$ solution. Store for 12 h at room temperature and in the dark (*see* **Notes 2–4**). The formed DNA/Ag NCs are used without any further purification.

3.2 Characterization of DNA/Ag NCs

A full characterization procedure usually entails spectroscopic characterization of the nanocluster properties (UV-Vis spectroscopy, fluorescence spectroscopy) and morphological characterization by TEM.

1. For UV-Vis spectroscopy, the analysis should focus on peaks in the 400 and 550 nm regions. NC grown on unmethylated DNA shows both absorption peaks at around 400 and 550 nm (*see* Fig. 3) which are attributed to the electronic transitions of small silver nanoclusters. The peak at 550 nm was the distinct absorption peak of DNA/Ag NCs [24, 31, 32] and is attributed to the pink color and intense fluorescence of unmethylated DNA/Ag NCs. On the other hand, the UV–vis absorption spectrum of methylated DNA/Ag NCs shows no peaks at 550 nm.
2. Fluorescence spectra of the solutions are measured upon excitation at 530 nm. A strong fluorescence emission intensity was observed at 620 nm for unmethylated DNA/Ag NCs. This fluorescence is stable for several days. On the other hand, a very weak fluorescence is commonly observed for methylated DNA/Ag NCs (*see* Fig. 1).
3. TEM imaging can be performed by adsorbing the NC on formvar-coated copper grids (mesh 300 or similar). TEM micrographs shows silver nanoclusters with an average diameter between 1 and 2 nm form both on methylated and unmethylated DNA scaffolds (*see* Fig. 4a, b).

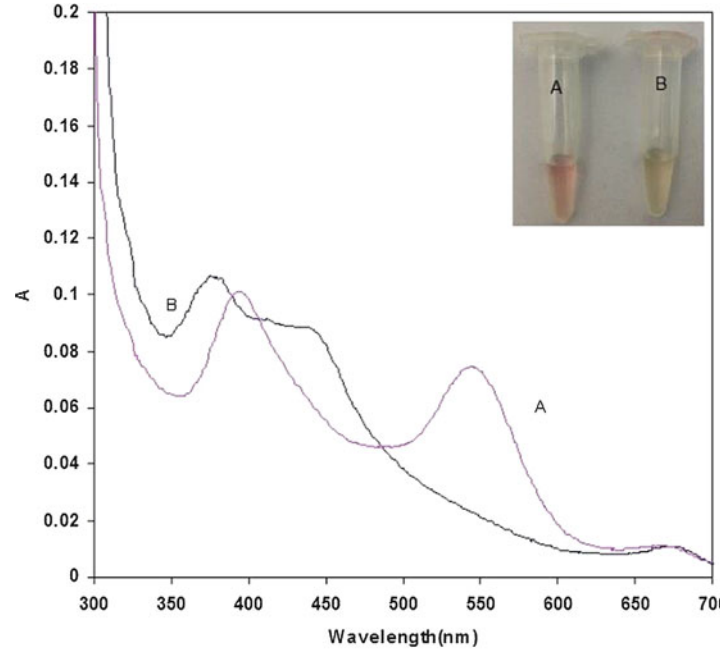

Fig. 3 UV-Vis spectra of unmethylated (A) and methylated (B) DNA/Ag NCs. The inset shows photograph of synthesized Ag NCs under visible light

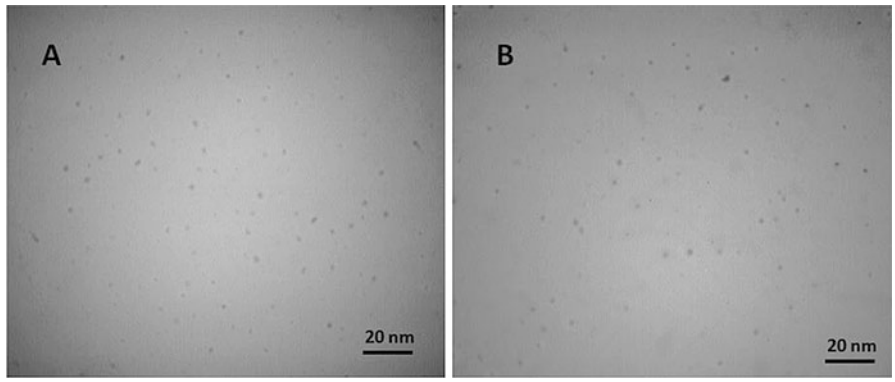

Fig. 4 TEM images of synthesized Ag NCs by unmethylated (**a**) and methylated (**b**) DNA and size distribution histogram of Ag NCs of unmethylated (**c**) and methylated (**d**) DNA

3.3 Detection of DNA Methylation

A decreased fluorescence is witnessed for NC prepared on partially methylated sequences, if compared to unmethylated DNA, or as a result of enzymatic methylation of oligonucleotides when NC have been prepared before methylation. The presence of even one methylated cytosine causes a considerable quenching on the intensity of fluorescence of nanoclusters (*see* Fig. 5).

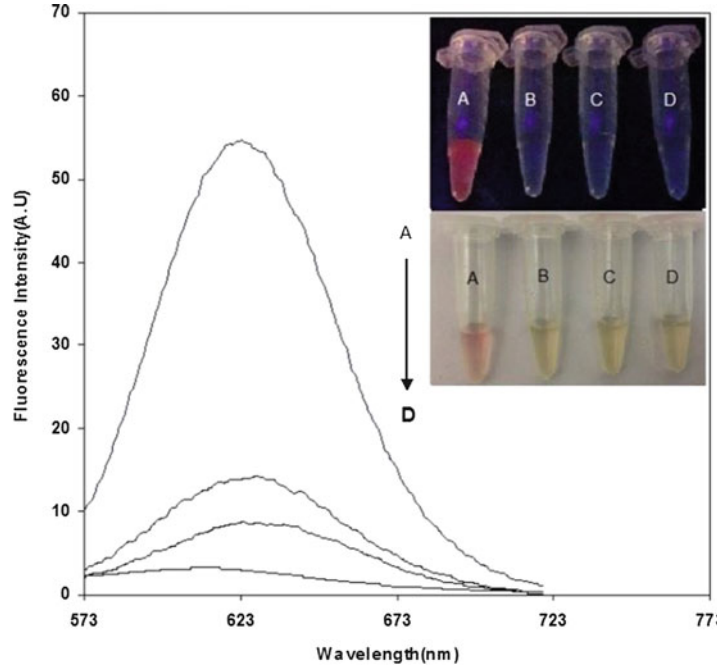

Fig. 5 Fluorescence spectra of DNA/AgNCs with different methylation ratios, The insets show color changes of DNA/Ag NCs under UV irradiation and visible light From left to right Ag NCs with unmethylated target (A), One methylated cytosine target (B), Two methylated cytosine target (C), Fully methylated target (D) respectively

3.3.1 Assay for DNA Methyltransferase Activity

1. Prepare two aliquots of Ag-NC. Incubate one aliquot at 37 °C for 15 min as a reference specimen (*see* **Note 4**).
2. Add the desired concentration of M.SssI DNA methyltransferase enzyme and SAM to the other aliquot of Ag-NCs, after incubating them in the same condition (at 37 °C for 15 min) (*see* **Notes 5–7**).
3. Characterize both specimens with fluorescence spectroscopy (*see* Subheading 3.2). Figure 3 shows the fluorescence emission of the DNA/Ag NCs which were treated with different concentrations of M.SssI MTase. The intensity of the fluorescence peak decreases upon increasing the concentration of M.SssI in the range of 0.4–20 U/mL. Fluorescence quenching correlates with the amount of methylated cytosines and so with the methyltransferase activity.

3.3.2 M.SssI DNA Methyltransferase Inhibition Assay

The inhibition of M.SssI DNA methyltransferase can be investigated using Gentamicin (0–1 μM) by incubating DNA/Ag NCs with M.SssI MTase and SAM together with different concentrations of Gentamicin (*see* Fig. 6). The activity of M.SssI MTase

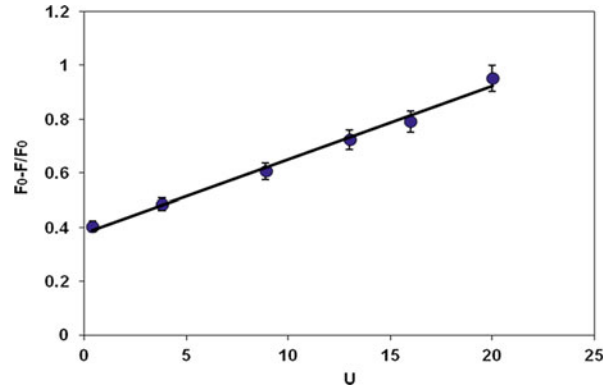

Fig. 6 Inhibitory effect of Gentamicin on the activity of M.SssI. The concentration of M.SssI is 4 U/mL. (F_0 is fluorescence intensity of AgNCs incubated with 4 U/mL M.SssI and F is the fluorescence intensity of AgNCs incubated with 4 U/mL M.SssI with different concentrations of Gentamicin: 0, 0.3, 0.6, 0.8, and 1 μM)

decreased with the increase of inhibitor concentration while the concentration of M.SssI was kept at 4 U/mL. An IC50 value of 0.5 μM was recorded (*see* **Note 8**).

4 Notes

1. A specific site in the CpG islands of adenomatous polyposis coli (APC) tumor suppressor gene promoter was selected as our DNA scaffold for the synthesis of silver nanoclusters.
2. Sodium borohydride solution should be freshly prepared.
3. Sodium borohydride solution should be added to the mixture with repetitive pipetting and vigorous shaking for 5 min.
4. At the initial stage, the solutions are pale yellow under visible light which have been resulted from surface plasmon resonance produced by silver nanoparticles [33].
5. M.SssI methyltransferase (C-5 cytosine-specific DNA methylase) (C5 MTase) is an enzyme that specifically methylates the C5 carbon of cytosines in DNA to produce C5-methylcytosine.
6. The enzyme completes modification of all CpGs in 15 min at 37 °C.
7. The role of S-adenosylmethionine (SAM) as a cofactor is the donation of methyl group.
8. IC_{50} is defined as the concentration of inhibitor which is required to reduce the enzyme activity by 50%.

Acknowledgements

The authors thank the research Council of University of Tehran (Grant 28645/01/02) for financial support of this work.

References

1. Diez I, Pusa M, Kulama S, Jiang H, Walter A, Goldman S, Muller A, Ikkala O, Ras R (2009) Color tunability and electrochemiluminescence of silver nanoclusters. Angew Chem 48 (12):2122–2125
2. Shen Z, Duan H, Frey H (2007) Water soluble flourescent Ag nanoclusters obtained from multiarm star poli (acrylic acid) as molecular hydrogel templates. Adv Mater 19(3):349–352
3. Vosch T, Antoku Y, Hsiang CI, Gonzalez JI, Dickson RM (2007) Strongly emissive individual DNA-encapsulated Ag nanoclusters as single molecule fluorophores. Adv Mater 104 (31):12616–12621
4. Zhang J, Xu S, Kumacheva E (2005) Photogeneration of flourescent silver nanoclusters in polymer microgels. Adv Mater 17 (19):2336–2340
5. Zhang L, Wang E (2014) Metal nanoclusters: new flourescent probes for sensors and bioimaging. NanoToday 9:132–157
6. Gwinn EG, O'Neill P, Guerrero AJ, Bouwmeester D, Fygenson DK (2008) Sequence-dependent fluorescence of DNA-hosted silver nanoclusters. Adv Mater 20:279–283
7. Sengupta B, Ritchie CM, Buckman JG, Johnsen KR, Goodwin PM, Petty JP (2008) Base-directed formation of fluorescent silver clusters. J Phys Chem 112:18776–18782
8. Shah P, Rorvig-Lund A, Chaabane SB, Thulstrup PW, Kjaergaard HG, Fron E, Hofkens J, Yang SW, Vosch T (2012) Design aspects of bright red emissive silver nanoclusters/DNA probes for micro DNA detection. ACS Nano 6:8803–8814
9. Richards CI, Choi S, Hsiang JC, Antoku Y, Vosch T, Bongiorno A, Tzeng YL, Dickson RM (2008) Olignucleotide-stabilized Ag nanocluster fluorophores. J Am Chem Soc 130:5038–5039
10. Sharma J, Yeh HC, Yoo H, Werner JH, Martinez JS (2010) A complementary palette of fluorescent silver nanoclusters. Chem Commun 46:3280–3282
11. O'Neill PR, Velazquez LR, Dunn DG, Gwinn EG, Fygenson DK (2009) Hairpins with poly-C loops stabilize four types of fluorescent Ag_n: DNA. J Phys Chem C 113:4229–4233
12. Zhou ZX, Du Y, Zhang LB, Dong SJ (2012) A label-free, G-quadruplex DNAzyme-based fluorescent probe for signal-amplified DNA detection and turn-on assay of endonuclease. Biosens Bioelectron 34:100–105
13. Ma K, Shao Y, Cui QH, Wu F, Xu SJ, Liu GY (2012) Base-stacking-determined fluorescence emission of DNA abasic site-templated silver nanoclusters. Langmuir 28:15313–15322
14. Cathcart N, Mistry P, Makra C, Pietrobon B, Coombs N, Niaraki MJ, Kitaev V (2009) Chiral thiol-stabilized silver nanoclusters with well-resolved optical transitions synthesized by a facile etching procedure in aqueous solutions. Langmuir 25:5840–5846
15. Ganguly M, Pal A, Negishi Y, Pal T (2013) Synthesis of highly fluorescent silver clusters on gold(I) surface. Langmuir 29:2033–2043
16. Cliffel DE, Zamborini FP, Gross SM, Murray RW (2000) Mercaptoammonium-monolayer-protected, water-soluble gold, silver, and palladium clusters. Langmuir 16:9699–9702
17. Yanagihara N, Uchida K, Wakabayashi M, Uetake Y, Hara T (1999) Effect of radical initiators on the size and formation of silver nanoclusters in poly(methyl methacrylate). Langmuir 15:3038–3041
18. Qu F, Li NB, Luo HQ (2013) Highly sensitive fluorescent and colorimetric pH sensor based on Polyethylenimine-capped silver nanoclusters. Langmuir 29:1199–1205
19. Zhou TY, Huang YH, Li WB, Cai ZM, Luo F, Yang CL, Chen X (2012) Facile synthesis of red-emitting lysozyme-stabilized Ag nanoclusters. Nanoscale 4:5312–5315
20. Guevel XL, Hotzer B, Jung G, Hollemeyer K, Trouillet V, Schneider M (2011) Formation of fluorescent metal (au, Ag) nanoclusters capped in bovine serum albumin followed by fluorescent and spectroscopy. J Phys Chem C 115:10955–10963
21. Mathew A, Sajanlal PR, Pradeep TA (2011) Fifteen atom silver cluster confined in bovine serum albumin. J Mater Chem 21:11205–11212

22. Liu YQ, Zhang M, Yin BC, Ye BC (2012) Attomolar ultrasensitive MicroRNA detection by DNA-scaffolded silver-nanocluster probe based on isothermal amplification. Anal Chem 84:5165–5169
23. Li J, Zhong X, Zhang H, Le XC, Zhu J (2012) Binding-induced fluorescence turn-on assay using aptamer-functionalized silver nanocluster DNA probes. Anal Chem 84:5170–5174
24. Petty JT, Zheng J, Hud NV, Dickson RM (2004) DNA-templated Ag nanocluster formation. J Am Chem Soc 126:5207–5212
25. Han B, Wang E (2012) DNA-templated fluorescent silver nanoclusters. Anal Bioanal Chem 402:129–138
26. Zhang K, Wang K, Xie M, Zhu X, Xu L, Yang R (2014) DNAtemplated silver nanoclusters based label-free fluorescent molecular beacon for the detection of adenosine deaminase. Biosens Bioelectron 52:124–128
27. Zhua S, Zhaob X, Zhanga W, Liua Z, Qia W, Anjuma S (2013) Fluorescence detection of glutathione reductase activity based on deoxyribonucleic acid-templated silver nanoclusters. Anal Chim Acta 786:111–115
28. Qian Y, Zhang Y, Lu L, Cai Y (2014) A label-free DNA-templated silver nanocluster probe for fluorescence on-off detection of endonuclease activity and inhibition. Biosens Bioelectron 51:408–412. https://doi.org/10.1016/j.bios.2013.07.060
29. Dadmehr M, Hosseini M, Hosseinkhani S, Ganjali MR, Sheikhnejad R (2014) Label free colorimetric and fluorimetric direct detection of methylated DNA based on silver nanoclusters for cancer early diagnosis. Biosens Bioelectron 73:108–111
30. Ahmadzade Kemani H, Hosseini M, Dadmehr M, Ganjali MR (2016) Rapid restriction enzyme free detection of DNA methyltransferase activity based on DNA templated silver nanoclustes. Anal Bioanal Chem 408:4311–4318
31. Vlasta Bonačić-Koutecký V, Pittner J, Boiron M (1999) An accurate relativistic effective core potential for excited states of Ag atom: an application for studying the absorption spectra of Ag_n and Ag_n^+ clusters. J Chem Phys 110:3876–3886
32. Marchetti AP, Muenter AA, Baetzold RC, McCleary RT (1998) Formation and spectroscopic manifestation of silver clusters on silver bromide surfaces. J Phys Chem B 102:5287–5297
33. Mulfinger L, Solomon SD, Bahadory M, Jeyarajasingam AV, Rutkowsky SA, Boritz C (2007) Synthesis and study of silver nanoparticles. J Chem Educ 84:322–325

Chapter 13

Selection of Structure-Switching DNA Aptamers Binding Soluble Small Molecules and SPR Validation of Enrichment

Enrico Tenaglia, Fabio M. Spiga, and Carlotta Guiducci

Abstract

Capture-SELEX is an effective molecular strategy enabling the discovery of structure-switching aptamers, which might find useful application in molecular detection or separation. We here provide a protocol to perform capture-SELEX for DNA aptamers binding soluble small molecules, which includes a straightforward functional validation by SPR. The SELEX strategy here described is adaptable to any water-soluble molecular target and might foster the development of DNA aptamers binding therapeutic small molecules, at the great advantage of clinical bioanalytics.

Key words Structure-switching aptamers, Capture SELEX, Small molecule aptamers, Surface plasmon resonance

1 Introduction

Nucleic acid aptamers, from Latin "*aptus,*" *adapted* and Greek "μέρο" (*méros*), *form*, are single-stranded oligonucleotides that can bind nonnucleotidic targets with affinities that compete with the ones of antibodies. Aptamers can be obtained through an in vitro selection process denominated SELEX (systematic evolution of ligands by exponential enrichment) [1]. This consists of an iterative procedure involving the exposure of a pool of oligonucleotides to candidate targets, the partition of bound molecules and their exponential amplification by means of PCR. Due to their molecular features, aptamers are particularly suited for bioanalytical applications [2], particularly so in the case of small molecular targets. Despite their versatility, the number of validated aptamers targeting small molecules is limited [3]. A major constraint to their discovery, in the case of classical SELEX approaches, is the necessity to immobilize the target on a surface, a process that implies

The original version of this chapter was revised. An erratum to this chapter can be found at https://doi.org/10.1007/978-1-4939-8582-1_22

Giampaolo Zuccheri (ed.), *DNA Nanotechnology: Methods and Protocols*, Methods in Molecular Biology, vol. 1811, https://doi.org/10.1007/978-1-4939-8582-1_13, © Springer Science+Business Media, LLC, part of Springer Nature 2018

modifying the native molecule and that can be technically challenging and costly (mostly for the availability of limited surface immobilization chemistries). The application of SELEX to conjugated targets can lead, moreover, to aptamers that do not bind the native version of the molecule of interest, but rather its conjugated form, hampering their use for the direct detection of free molecular species in solution. Capture SELEX [4] has been developed to circumvent these limitations and it has been successfully implemented on RNA/DNA backbones to produce aptamers against small molecular targets, encompassing a diverse range of applications [5–7]. Common to these protocols is the use of structure switching aptamers [8] that change conformation upon binding to ligands, and which are partitioned and amplified after the interaction with their target in its native, soluble form.

In general, aptamer candidates are retrieved from late (SPR validated) iterations of the SELEX, based on the principle that the evidence of binding corroborates the existence of enriched ssDNA sequences recognizing the target of interest.

The ultimate purpose of the aptamer discovery pipeline is the retrieval of functional aptamer sequences that bind the target of choice. This can be effectively done also by next-generation sequencing, but the description of this process goes beyond the scopes of this protocol, since the preparation of the material for sequencing and the analytical strategy of resulting data are customizable and need to be adjusted to the technology employed.

In this chapter, we present an integrated solution to select and characterize the binding properties of DNA aptamers binding small molecules. The SELEX approach we describe is a variant of capture-SELEX for DNA aptamers composed of a central variable region of 60 nucleotides enclosed within two constant regions at the 5′ and the 3′ (*see* Fig. 1a). As reported in Fig. 1b, the DNA aptamers are designed to be anchored on streptavidin-coated beads through an adaptor oligo. According to the idea of capture-SELEX, the exposure of DNA oligos to their target in solution produces an energetically-favored conformational change. This leads to their detachment from the magnetic beads and their liberation in the bulk solution. The protocol described here includes a semiquantitative PCR procedure to monitor sequence enrichment along the SELEX and a straightforward SPR pipeline to verify the binding efficacy of selected aptamer pools, which only requires the immobilization of DNA sequences on bare gold surfaces, without the need for fluorescent labeling or indirect signal amplifications.

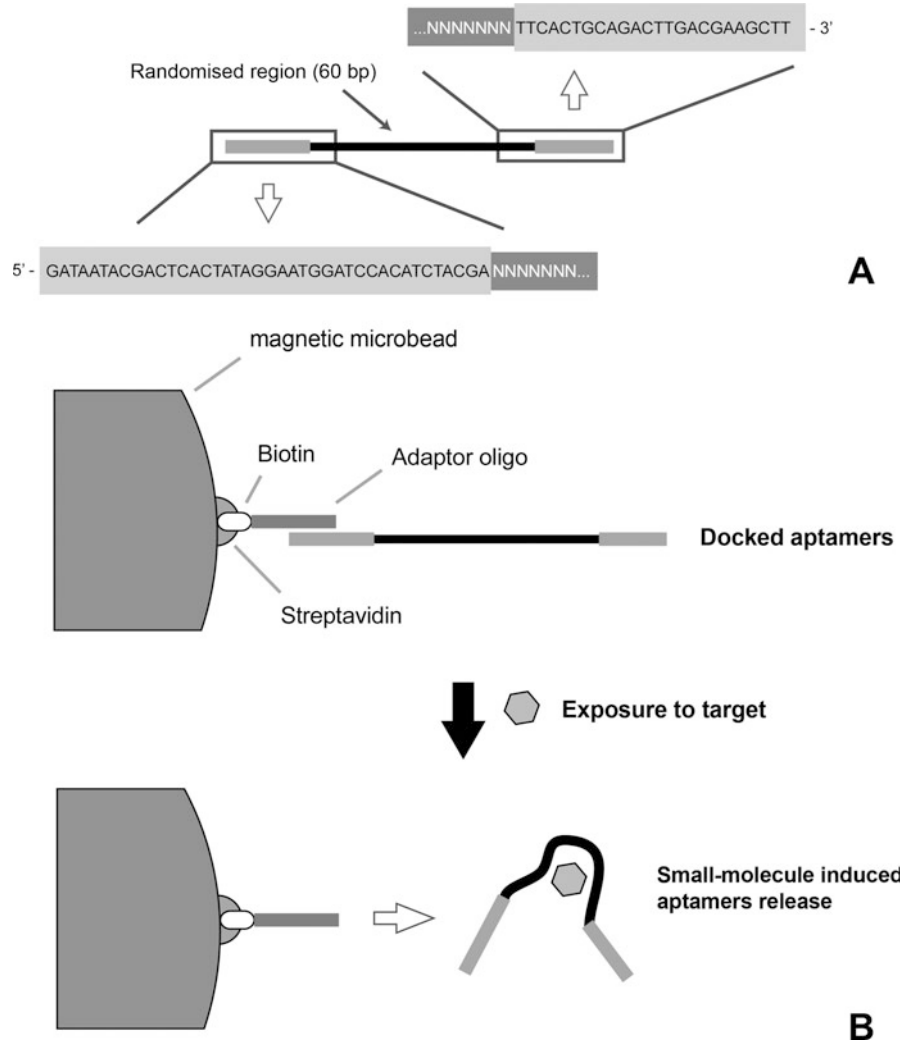

Fig. 1 Molecular structure of the ssDNA aptamers and diagram of the molecular strategy for the capture-SELEX protocol. (**a**) The structure of the ssDNA aptamers employed for this protocol is reported. The constant regions at the 5′ and 3′ are indicated in light grey, while the central randomized domain is indicated in black. (**b**) ssDNA sequences undergoing selection are hybridized to biotinylated adaptor oligos, which conjugate to streptavidin-coated magnetic beads ("docked aptamers"). The binding of ssDNAs to molecular targets induces a conformational change that produces the detachment of aptamers from the bead–oligo complexes and their release in solution

2 Materials

All solutions should be made with ultrapure water (18 MΩ cm at 25 °C) and should be filtered before use.

2.1 SELEX and PCR

1. 100 μM stock solutions of HPLC-purified oligonucleotides in 1× TE buffer pH 8.0 (for library generation and PCR amplifications, example sequences are reported in Table 1).

Table 1
Sequences for aptamer starting library and library amplification primers

Starting library	5'-GGAATGGATCCACATCTACGA-$(N)_{60}$-TTCACTGCAGACTTGACGAA-3′
Amplification primer FWD	5′- GATAATACGACTCACTATAGGAATGGATCCACATCTACGA-3′
Amplification primer REV (5′-phosphorylated)	5′-phospho-AAGCTTCGTCAAGTCTGCAGTGAA-3′
Amplification primer FWD (5′-thiolated)	5′-C_6Thio-GATAATACGACTCACTATAGGAATGGATCCACATCTACGA-3′
Adaptor oligo	5′-TGGATCCATTCCATGCATCGATCGATC-3′-biotin

2. Taq polymerase, 5 U/μL.
3. Deoxynucleotide mix (dNTPs): 10 mM in each dNTP, in ultrapure water.
4. λ-exonuclease 10 U/μL with vendor-provided 10× λ-exonuclease reaction buffer (Thermo Fisher Scientific).
5. Magnesium chloride: 100 mM solution in water.
6. ChargeSwitch® PCR cleanup kit (Thermo Fisher Scientific).
7. M-280 streptavidin-coated magnetic Dynabeads® (Thermo Fisher Scientific).
8. Bind & Wash buffer (BW) 1×: 5 mM Tris–HCl (pH 7.5), 0.5 mM EDTA, 1 M NaCl.
9. BB buffer 1×: 50 mM Tris pH 7.4, 500 mM NaCl.
10. PCR mix: 2 mM $MgCl_2$, 0.2 mM dNTPs, 1 μM each primer (including a phosphorylated reverse primer) (*see* Table 1), 0.0125 U/μL Taq polymerase.

2.2 Electrophoresis Verification of PCR Amplicons

1. TBE 10×: (Tris–Borate–EDTA, pH 8.3): mix 108 g Tris base, 55 g boric acid, 40 mL of 0.5 M EDTA (pH 8.0). Adjust final volume to 1 L with ultrapure water.
2. Gel-Red DNA dye (stock solution is 10.000×) (Biotium).
3. Acrylamide gel mix: 3.3 mL of 30% acrylamide–bisacrylamide 29:1, 1 mL of 10× TBE, 4.2 g of urea, 10 μL of TEMED (*N*, *N*, *N*′,*N*′-tetramethylethylenediamine), ultrapure water to 10 mL. Slightly warm up the solution in a microwave oven to facilitate the dissolution of urea, if needed. Filter the solution using a 0.22 μm syringe filter.
4. 10% solution of ammonium persulfate.
5. 2× Denaturing gel loading buffer (appropriately dilute the commercial solution with ultrapure water).

2.3 Surface Plasmon Resonance Chip Functionalization

1. 1× TE: 10 mM Tris–HCl pH 7.4, 1 mM EDTA.
2. 6-mercaptohexanol: 1 mM 6-mercaptohexanol in 1× TE.
3. TCEP (tris(2-carboxyethyl)phosphine hydrochloride), powder.
4. 10× phosphate buffer saline (PBS): 1.37 M NaCl, 120 mM phosphate, 27 mM KCl.
5. Sensor chip Au (bare gold surface) (Biacore, GE Healthcare).

3 Methods

3.1 Aptamer Library Preparation: PCR Amplification and Gel Electrophoresis Verification

The starting pool of aptamers undergoing SELEX is generated from a chemically synthetized library of oligonucleotides containing a central randomized region of 60 nucleotides enclosed between two adaptor regions that are used for PCR amplification and for the hybridization of aptamers to magnetic microbeads (*see* Fig. 1a). An aliquot of the randomized ssDNA starting library is amplified by PCR to generate the first SELEX pool. The outcome of the PCR can then be verified by performing a denaturing gel electrophoresis on 10% polyacrylamide using a 10 μL aliquot of the product.

1. Add about 2 nmol of the ssDNA starting randomized library to 4 mL of PCR mix.
2. Perform a PCR with the following cycling conditions: 2 min at 95 °C, 30 s at 95 °C and 30 s at 72 °C repeated for 25 times, finally 5 min at 72 °C (*see* **Note 1**).
3. Prepare the acrylamide gel mix in a Falcon tube, leaving the 10% ammonium persulfate solution aside. Use the entire 10 mL or scale up if necessary as a function of the gel system in use.
4. Add 25 μL of the 10% APS solution.
5. Mix thoroughly by inverting the Falcon tube, and quickly pour the gel solution in the casting chamber, then insert the comb. Once polymerized, clean the gel wells with running buffer (1× TBE) using a needle and syringe.
6. Set the constant running voltage at 250 V and prerun the gel for 30–40 min.
7. Add 10 μL of the PCR product to 10 μL of 2× denaturing loading buffer.
8. Heat up to 80 °C for 3 min on a thermoblock, then place the samples on ice. Load on the gel after the prerun is complete.
9. Run the gel at 25 V/cm for 50 min.
10. After the run, immerse the gel in a 1× Gel-Red solution on a rocking platform for 30 min and then observe at an UV transilluminator to evaluate the outcome of the PCR.

3.2 DNA Purification and λ-Exonuclease dsDNA–ssDNA Conversion

The PCR product can be purified using the ChargeSwitch PCR purification kit, according to the instruction of the manufacturer. The dsDNA-to-ssDNA conversion is performed by digestion with λ-exonuclease, which selectively processes phosphorylated strands in the 5′–3′ direction. After purification, this ssDNA product can be used to load the magnetic microbeads for the SELEX.

1. Perform the purification of the PCR product with 300 μL of ChargeSwitch magnetic beads slurry according to the manufacturer's protocol.
2. Quantify the obtained purified dsDNA by UV spectrophotometry (*see* **Note 2**).
3. Dissolve 100 μg of dsDNA in 4.5 mL of 1× λ-exonuclease reaction buffer.
4. Add 15–21 μL of λ-exonuclease to the mix (*see* **Note 3**). Incubate at 37 °C for 4 h.
5. Deactivate the λ-exonuclease by incubating at 80 °C for 10 min.
6. Purify the obtained ssDNA with the ChargeSwitch kit, using 300 μL of bead slurry.
7. Quantify the concentration of the purified ssDNA using a spectrophotometer (*see* **Note 4**).

3.3 Hybridization of the ssDNA with the Biotinylated Oligo and Loading on Streptavidin-Coated Microbeads

In order to be exposed to the target small molecule of choice, the library of candidate DNA aptamers obtained after PCR amplification are hybridized with a 3′-biotinylated adaptor oligo (*see* Fig. 1b). The incubation of streptavidin-coated magnetic microbeads with the ssDNA aptamers hybridized to adaptor oligos generates the bead–aptamer complex that is then exposed to the target molecule.

1. Add 24 μg of purified ssDNA to 4.8 μg of biotinylated adaptor oligo (*see* Table 1) and bring the volume to 8 mL with BW buffer. Mix by vortexing. Split in eight aliquots of 1 mL each.
2. Incubate the aliquots in a thermoblock at 95 °C for 10 min, then at 60 °C for 5 min and then slowly cool to 4 °C (with a temperature ramp of 0.05 °C/s).
3. Pool the aliquots and add 360 μL of M280 Dynabeads previously equilibrated in BW buffer.
4. Incubate overnight on a rotation wheel at 4 °C.
5. Remove the magnetic beads loaded with the library from the suspension using the suitable magnet (*see* **Note 5**) and save for later use.
6. Quantitate the free DNA left in the bead-free solution by measuring the UV adsorption with a spectrophotometer.

Calculate the amount of DNA loaded on the beads and estimate the efficiency (*see* **Note 6**).

7. Wash the microbeads with the bound aptamers library with 5.4 mL of 1× BB buffer at 4 °C (15 times the used microbeads volume). Separate the beads again using the provided magnet (*see* **Note 7**).
8. Repeat **step 7**.
9. Resuspend the microbeads slurry in 4 mL of 1× BB buffer.

3.4 Selection Step: Exposure of the Bead–DNA Complexes to the Target Small Molecule

The small molecule exposure (aptamer elution) is the step where the aptamers binding the target are released in solution and are eventually retrieved from the bead–DNA complexes that are removed by a magnet (*see* **Note 8**).

During the selection step, a control procedure to monitor the progressive enrichment of DNA should always be established by retaining an aliquot of the prewashed beads for a small-scale control experiment (*see* Fig. 2 and **Note 9**).

1. Take two 25 μL aliquots of the magnetic bead–aptamer conjugate (*see* Fig. 2).
2. Bring the volume of the first aliquot to 300 μL with 1× BB buffer (*see* **Note 10**).
3. Bring the volume of the second aliquot to 300 μL with 1× BB buffer containing the same concentration of the target molecule used for the iterative SELEX.

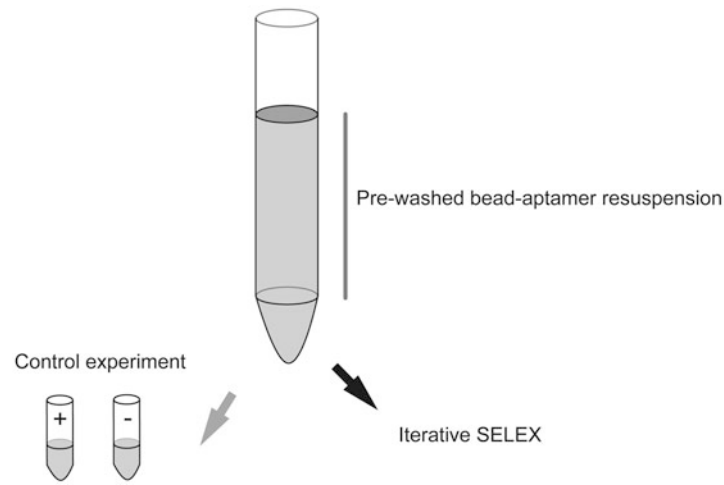

Fig. 2 Partition of the complexed ssDNA–streptavidin beads for the iterative SELEX and control experiments. A sample aliquot of the prewashed ssDNA–-magnetic bead complex can be employed to establish a semiquantitative PCR based control experiment to assess the progressive enrichment of DNA molecules against the specific target

4. Incubate both tubes in rotation at 4 °C for 1 h and store at 4 °C for further use.
5. Resuspend the remaining and main amount of the bead slurry in 4 mL of 1× BB buffer containing the desired concentration of target molecule for the selection. Incubate in rotation at 4 °C for 1 h (*see* **Note 11**).
6. After the incubations, separate the magnetic microbeads and recover the supernatants from the major selection mix (**step 5**, above) and from both the control aliquots the major selection (**step 4**, above).
7. Purify the DNA using the ChargeSwitch kit, as done before. Use 100 μL of purification beads for the major SELEX eluate (from **step 5**) and 15 μL for each of the control aliquots.
8. Store approximately 30% of the DNA purified from the major SELEX eluate and 50% of each of the control aliquots at 4 °C (*see* **Note 12**).
9. Save the main part (70%) of the purified SELEX eluate for the subsequent SELEX cycle (*see* Subheading 3.6). Use the remaining 50% of the two control aliquots for the semiquantitative PCR to assess step-specific enrichment (*see* Subheading 3.5).

3.5 Semiquantitative PCR for the Progressive Verification of Enrichment

The semiquantitative PCR procedure is performed on the aliquots of the ssDNA purified from the control experiments in order to monitor the progressive SELEX enrichment.

The PCR reaction is divided in amplification aliquots, which are extracted from the thermocycler after a different number of amplification cycles (*see* Fig. 3a). A relative estimate of the amount of DNA recovered from each control sample can be inferred from electrophoretic analysis of the PCR specimens at different cycle numbers. The effectiveness of the SELEX can be estimated from the enrichment in amplicon in the positive control (beads-aptamers eluted with the target molecule). This can be compared to the amplicon from the negative control (beads-aptamers eluted with the BB buffer only). *See* an example in Fig. 3b (black arrows).

1. Set up two series of semiquantitative PCR adding 50% of the two eluted SELEX controls (positive and negative) to 385 μL of PCR mix.
2. Split each reaction mix in eight different PCR tubes. Run two series of PCR amplifications with the following program: 2 min at 95 °C, followed by 25 cycles of 30 s at 95 °C, finally 30 s at 72 °C.
3. Withdraw tubes for both the positive and the negative control PCRs at the desired amplification cycles, and store them on ice to interrupt the polymerase reaction.

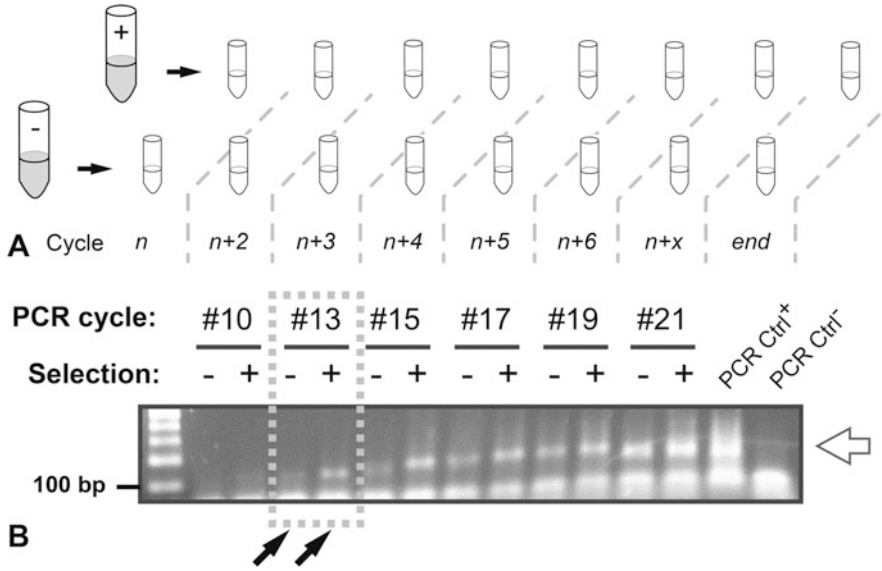

Fig. 3 Semiquantitative PCR to assess the effective enrichment of ssDNA undergoing selection. (**a**) Diagram of the semiquantitative PCR strategy to assess the enrichment of ssDNA in the control experiment. (**b**) Example of a semiquantitative evaluation of ssDNA enrichment for a SELEX performed to obtain aptamers against tobramycin [7]

4. Load samples on an electrophoretic gel and assess the cycle at which enrichment in the positive control elution is evident if compared to the negative one (*see* Fig. 3b).

3.6 PCR Amplification of the Eluted SELEX ssDNA and Closing of a SELEX Iteration

The SELEX cycle ends with the amplification of the ssDNA eluted from the bead–aptamer complexes after the exposure to the small molecule of interest (*see* Fig. 4). Such amplified "enriched library" is then processed analogously to the starting library in a new SELEX cycle (repeat the protocol from Subheading 3.2). The process can be continued until satisfactory binding is obtained, e.g., as evaluated from SPR characterization (*see* Subheading 3.7 below).

1. Add 70% of the ssDNA eluted and purified from the SELEX cycle (*see* Subheading 3.4, **step 9**) to 4 mL of PCR mix.
2. Perform a PCR with the following cycling conditions: 2 min at 95 °C, 30 s at 95 °C and 30 s at 72 °C repeated for 25 times, finally 5 min at 72 °C (*see* **Note 1**).
3. Verify the success and quality of the PCR by using gel electrophoresis (as in Subheading 3.1, **step 3** and following).
4. Purify and process the new dsDNA as in Subheading 3.2 and following, in order to perform an additional SELEX cycle.

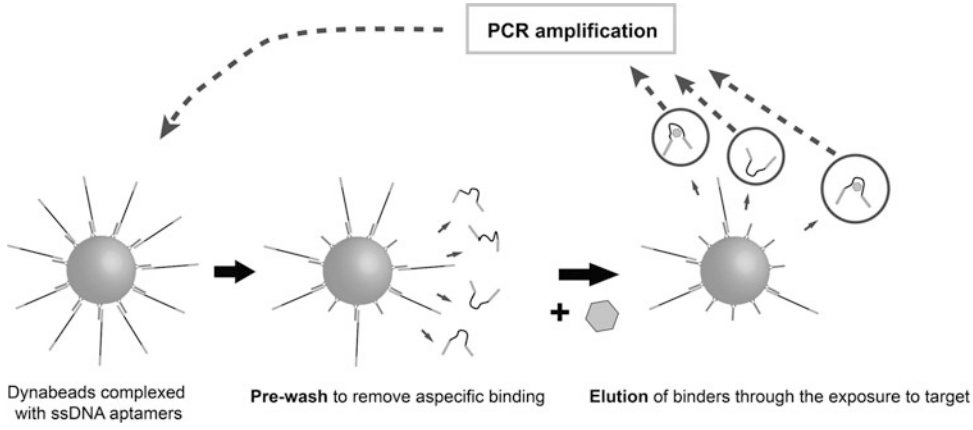
PCR amplification
Dynabeads complexed with ssDNA aptamers
Pre-wash to remove aspecific binding
Elution of binders through the exposure to target

Fig. 4 Summarizing diagram of the capture-SELEX approach. The process consists in the iteration of bead–DNA complex formation, prewash (i.e., background noise reduction) and elution of ssDNA binding to targets. The number of iterations to follow will be dictated by the outcome of the control SPR experiments to verify target binding

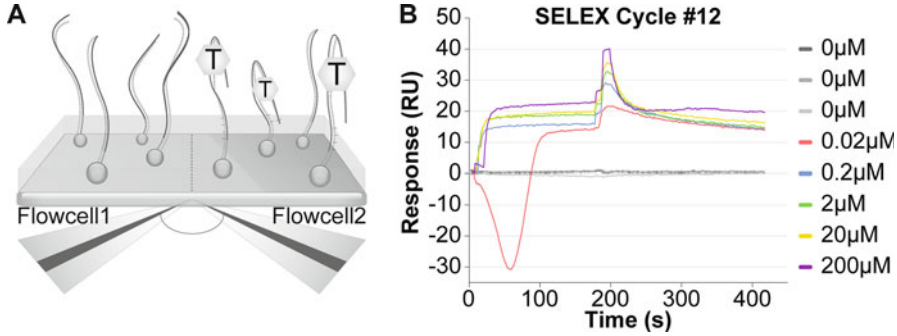

Fig. 5 Au chip functionalization and SPR experiment to verify binding. (**a**) Experimental (flow cell 2) and reference cell (flow cell 1) of a Biacore Au sensor chip functionalized, respectively, with thiolated sequences amplified from SELEX iteration pools and reference sequences from the early step of the SELEX. Aptamer sequences from the SELEX iterations should bind the molecular target of choice. (**b**). SPR binding curves obtained testing different concentrations of tobramycin on a gold chip functionalized with DNA from the 12th iteration of a SELEX for tobramycin aptamers [7]. Figure modified from [7] with permission from ACS

3.7 Evaluation of Aptamer Selection—SPR Assessment of Binding

The evaluation of the functionality of ssDNAs undergoing selection is key to corroborate the effectiveness of the SELEX and to make an educated decision on whether to progress with the iterations. This protocol includes a procedure to verify the progressive enrichment of functional sequences by surface plasmon resonance (SPR) binding experiments. This makes use of a thiolated version of the SELEX libraries at the desired cycle and of a reference pool of sequences derived from the early step of the SELEX (or from the initial library) (*see* Fig. 5a). ssDNA libraries are anchored on an SPR chip through a 5′-thiol. The libraries are exposed to solutions with different concentrations of the target molecule, in order to infer preliminary kinetic properties of the interaction (*see* Fig. 5b).

3.7.1 Thio-PCR from SELEX Pools: Amplification, dsDNA Purification, and λ-Exonuclease Digestion

1. Add about 3 ng of the purified ssDNA from the SELEX cycle to 300 μL of PCR mix containing a 5′-thiolated version of the forward primer, together with the 5′-phophorilated reverse primer.
2. Perform a PCR amplification as described in Subheading 3.1, **step 2**: 2 min at 95 °C, 30 s at 95 °C and 30 s at 72 °C repeated for 25 times, finally 5 min at 72 °C.
3. Perform λ-exonuclease digestion as described in Subheading 3.2, **step 3** and following. Adjust the amount of λ-exonuclease according to the amount of purified dsDNA.
4. Perform the purification of the ssDNA using the ChargeSwitch kit employing a 30 μL aliquot of purification beads (*see* **Note 13**).

3.7.2 Functionalization of the Gold Surface of the SPR Chip

The bare gold surface of the SPR chips is functionalized with DNA through the terminal thiol at the 5′ end of the aptamer sequences obtained after the thio-PCR. This part of the protocol and the following are proposed as examples as they strongly depend on the available SPR instrumentation.

1. To deprotect the thiolated ssDNA, add TCEP to a final concentration of 1 mM in a volume of 45 μL. Incubate for 15 min. at room temperature. Stop the reaction by adding 5 μL of 10× PBS.
2. Denature the oligos at 95–99 °C for 10 min. on a thermoblock, and then quickly cool on ice for 2–3 min.
3. Prepare a 50 μL solution of 0.6 μM (deprotected) thiolated ssDNA from the SELEX cycle to be tested (from its thio-PCR, as described above).
4. Prepare a 50 μL solution of 0.6 μM (deprotected) thiolated ssDNA from an early cycle of SELEX, or the initial library (from its thio-PCR as described) in 1× TE to be used as reference.
5. Functionalize the experimental cell and the reference cell of the SPR chip with the test library and the reference library, respectively (*see* **Notes 14–16**).
6. Following functionalization, wash the SPR chip surface with 1× TE.
7. Passivate the chip surface with a 1 mM solution of 6-mercaptohexanol in 1× TE for 30 min at room temperature.
8. Extensively wash the chip with 1× TE.

3.7.3 SPR Verification of DNA–Target Binding and Data Analysis

The differential approach of the SPR allows for deducing the incremental affinity shown by selected DNA along the SELEX process, proving the effectiveness of the SELEX undertaken. The

process follows the principles of any empirical SPR binding experiment, and it should be performed according to the best-practice procedures for the available SPR instrumentation. Different concentrations of the target of interest should be exposed to the chip surfaces. Binding profiles are observed in order to derive the kinetic properties of the interaction under examination. The SPR raw data can be adjusted and analyzed with Scrubber 2.0 (Biologics, Australia) using double referencing and bulk correction.

The maximal response (R_{Max}) obtained at the SPR is used as a measure of the progress in the selection of binding aptamers (as the oligonucleotide surface density is kept virtually constant).

4 Notes

1. It is recommended to avoid extending the amplification beyond 25 cycles because of the possible appearance of amplicons of aberrant sizes.
2. The amount of total DNA recovered after the PCR and the purification protocol above should exceed 100 μg.
3. It is advisable to confirm this amount of enzyme with the instructions provided by the vendor, as unit description could change amongst vendors.
4. It would be recommended at this stage to perform a gel electrophoresis of the purified ssDNA, to verify the presence of a band corresponding to the expected size of the DNA aptamers (~120 bp).
5. This operation should be done according to the bead manufacturers' instructions, as they can be updated over time.
6. In our experience, we commonly expect an average bead loading of around 45–50%.
7. This step is critical for the success of the SELEX protocol. The exposure of the bead–aptamer complexes to the sole buffer of selection (devoid of the small molecule of interest) is a procedure that reduces the diversity of the initial library. It removes from the complex those sequences that might be loosely bound to the magnetic beads, as well as those aptamers switching their conformation after exposure to the selection buffer environment alone. The selection buffer should ideally replicate the condition of detection where aptamers obtained through the SELEX will be employed. By performing a SELEX in these conditions, one might favor the selection of sequences that are effectively operating in the detection environment (e.g., a complex matrix like diluted/prefiltered serum). Notably, a counterselection step can be added at this stage to help discovering aptamers discriminating modified forms of a given

molecule (e.g., a certain drug from its primary metabolites). To attain that, the prewashing steps should be performed with a solution additionally containing the countertarget(s).

8. The elution step should be adjusted to the target molecule by taking into account its solubility, its stability in solution and, importantly, the expected "working concentration range" for the aptamers discovered through the SELEX (i.e., aptamers to employ in clinical biosensors should ideally be selected at clinically relevant drug concentrations). The SELEX iterations can be customized to refine target affinities by incrementing, progressively, the selection stringency (i.e., by a progressive reduction of the concentration of the target molecule in the exposure step).
9. Though this step is not strictly necessary to validate the SELEX process, it might be indicative of possible issue with the protocol being implemented, like nonideal selection stringency leading to the loss of potential binding sequences throughout the iterations.
10. This step uses prewashing solution: BB buffer in the described case. Consider also setting up a control for counterselection, if this is included in the protocol.
11. This step is to elute the ssDNA aptamers candidates that bind the target and are released from the beads. The incubation temperature is chosen to limit the spontaneous melting of partially hybridized ssDNA-adaptor sequences, reducing the background release of sequences with poor affinity to the target.
12. 30% of the iterative SELEX eluate can be used, if necessary, to repeat SELEX steps or to produce thiolated libraries for the SPR validation of binding.
13. The purified samples should be analyzed by gel electrophoresis.
14. The bare gold surface of the SPR chip should be treated with plasma prior to functionalization, in order to increase its hydrophilicity. To do so, expose the bare chip to O_2 plasma (0.6 mbar, 50 W) for 1 min.
15. The concentration of thiolated ssDNA suggested here can be considered as a starting point and it should be adjusted in the optimization for the library in use (*see* **Note 17**).
16. Our protocol includes an overnight (16 h) functionalization of the bare gold chip using a Biacore external functionalization unit connected to a syringe pump. The procedure can be adapted to the available equipment. The constant exchange of the solution in contact with the gold chip surface favors a uniform local concentration of DNA aptamers at the gold surface–liquid interface throughout the process.

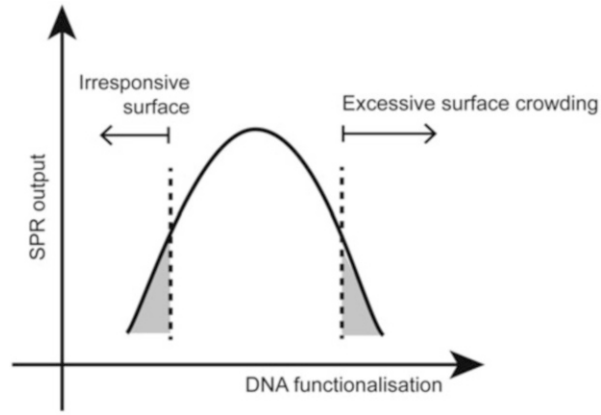

Fig. 6 Dependency of the SPR signal output on the SPR chip functionalization. The range of surface functionalization providing acceptable SPR signals is between two undesired regions of insensitive low-density surface and too high-density surface, where crowding might impede binding and conformational changes (*see* **Note 17**)

17. The conditions of binding tested at the SPR should ideally replicate the selection procedure, for what concerns chosen buffers, ionic strength, pH and temperature. These parameters affect the tertiary conformation of aptamers and they might influence the outcome of binding experiments. A critical point of the SPR based approach is the reduced size of small molecules. Such reduced mass results in small SPR signals, which have to be maximized by empirically optimizing the surface density of aptamers on the chip surface. This is obtained by titrating the concentrations of thiolated ssDNA used for the functionalization of the gold surface. It encompasses a concentration range that is limited, at one extreme, by excessive surface crowding (impeding the conformational change of aptamers upon binding and hence reducing their ability to bind the target) and at the other by low oligo concentrations that might produce a passive surface that barely produces signals (*see* Fig. 6).

References

1. Tuerk C, Gold L (1990) Systematic evolution of ligands by exponential enrichment: RNA ligands to bacteriophage T4 DNA polymerase. Science 249:505–510. https://doi.org/10.1126/science.2200121
2. Sefah K, Phillips JA, Xiong X, Meng L, Simaeys DV, Chen H, Martin J, Tan W (2009) Nucleic acid aptamers for biosensors and bio-analytical applications. Analyst 134:1765–1775. https://doi.org/10.1039/B905609M
3. McKeague M, McConnell EM, Cruz-Toledo J, Bernard ED, Pach A, Mastronardi E, Zhang X, Beking M, Francis T, Giamberardino A, Cabecinha A, Ruscito A, Aranda-Rodriguez R, Dumontier M, DeRosa MC (2015) Analysis of in vitro aptamer selection parameters. J Mol Evol 81:150–161. https://doi.org/10.1007/s00239-015-9708-6
4. Stoltenburg R, Nikolaus N, Strehlitz B (2012) Capture-SELEX: selection of DNA Aptamers for

aminoglycoside antibiotics. J Anal Meth Chem 2012:e415697. https://doi.org/10.1155/2012/415697

5. He J, Liu Y, Fan M, Liu X (2011) Isolation and identification of the DNA aptamer target to acetamiprid. J Agric Food Chem 59:1582–1586. https://doi.org/10.1021/jf104189g
6. Reinemann C, Freiin von Fritsch U, Rudolph S, Strehlitz B (2016) Generation and characterization of quinolone-specific DNA aptamers suitable for water monitoring. Biosens Bioelectron 77:1039–1047. https://doi.org/10.1016/j.bios.2015.10.069
7. Spiga FM, Maietta P, Guiducci C (2015) More DNA–aptamers for small drugs: a capture–SELEX coupled with surface Plasmon resonance and high-throughput sequencing. ACS Comb Sci. https://doi.org/10.1021/acscombsci.5b00023
8. Nutiu R, Li Y (2003) Structure-switching signaling aptamers. J Am Chem Soc 125:4771–4778. https://doi.org/10.1021/ja028962o

Chapter 14

Dielectrophoretic Stretching of DNA

Eva-Maria Laux, Frank F. Bier, and Ralph Hölzel

Abstract

The spatial control of DNA and of self-assembled DNA constructs is a prerequisite for the preparation of DNA-based nanostructures and microstructures and a useful tool for studies on single DNA molecules. Here we describe a protocol for the accumulation of dissolved λ-DNA molecules between planar microelectrodes by the action of inhomogeneous radiofrequency electric fields. The resulting AC electrokinetic forces stretch the DNA molecules and align them parallel to the electric field. The electrode preparation from off-the-shelf electronic components is explained, and a detailed description of the electronic setup is given. The experimental procedure is controlled in real-time by fluorescence microscopy.

Key words Alignment, Dielectrophoresis, DNA, Electrokinetics, Interdigitated electrodes, Stretching

1 Introduction

For the construction of well-defined structures in nanometer dimensions, the self-assembling properties of DNA are exploited in a multitude of approaches [1–4]. Still, there remains a gap between the nanoworld and the macroscopic world. This gap can be bridged by the combination of well defined, easily synthesized, micrometer-long DNA strands like that of λ-DNA with planar microelectrode systems that are produced by standard photolithography. This is accomplished by the application of radiofrequency electric fields between planar, interdigitated electrodes (IDE) [5, 6]. Since the electrodes are only about 100 nm thick, they produce a strongly inhomogeneous field close to their edges. This electric field gradient attracts any polarizable matter toward the electrode edges. This so-called dielectrophoretic effect depends on the electrical properties of the DNA and its surrounding medium as well as on field parameters like voltage and frequency [7, 8]. Depending on the frequency applied, this also leads to stretching forces that disentangle and elongate the macromolecule, and align the molecules parallel to the electric field

Giampaolo Zuccheri (ed.), *DNA Nanotechnology: Methods and Protocols*, Methods in Molecular Biology, vol. 1811, https://doi.org/10.1007/978-1-4939-8582-1_14, © Springer Science+Business Media, LLC, part of Springer Nature 2018

[9–11]. Such elongation and alignment allows, e.g., to measure the conductivity of single or a few DNA strands [12] or to dissect DNA at spatially defined sites [13]. Although photolithography is a standard method in electronic manufacturing, it is not readily accessible for laboratories in the biosciences. Therefore, we have developed a simple method to prepare interdigitated microelectrodes from off-the-shelf commercially available components [14–17]. With these electrodes, linear λ-DNA is accumulated in the electrode gaps, where the DNA strands are aligned and stretched parallel to the electric field.

2 Materials

2.1 Electronic Devices

1. A standard laboratory function generator that covers the frequency range from around 100 Hz to at least 1 MHz, preferably 10 MHz or even higher. The output voltage level should reach at least 10 V_{pp} (i.e., 5 V_p or 3 V_{RMS}) (*see* **Note 1**).
2. An amplifier that covers the frequency range of 100 Hz to at least 1 MHz, preferably higher frequencies. Its output should reach at least 30 V_{pp}, better 50–70 V_{pp} (*see* **Note 2**).
3. A simple single-pole single-throw toggle switch mounted in a flat plastic box with two BNC female connectors (*see* **Note 3**).
4. Seven coaxial cables with BNC male connectors.
5. BNC tees.
6. A twin-wired cable.
7. A demodulator probe (*see* **Note 4**).
8. A polyester capacitor 3.3 μF (*see* **Note 5**).
9. Two digital multimeters (*see* **Note 6**).
10. A frequency counter (*see* **Note 7**).
11. An oscilloscope, with bandwidth of at least 10 MHz (*see* **Note 8**).

2.2 Microscopy

1. Fluorescence microscope with FITC filter set or equivalent. It should also allow brightfield reflected light observation.
2. Cooled CCD camera.
3. Personal computer with suitable control software for image acquisition.

2.3 Electrode Preparation

1. SAW components (Epcos, X6964 M, 43.75 MHz) with overall 17 electrodes of 1.5 mm length and 22 μm width, the electrode gaps are also 22 μm wide.
2. Female and corresponding male 2-pin headers.
3. Thermal laminating film.

4. Wires.
5. Electrically conducting silver paint.
6. Microscope glass slides.
7. Microscope coverslips (18 mm × 18 mm) (*see* **Note 9**).
8. Cutter, puncher, tweezers.
9. Soldering iron, solder.
10. Two-component adhesive (epoxy based).

2.4 DNA Staining

Ultrapure water with a conductivity <1 μS/cm must be used for all dilutions.

1. 0.3 μg/μL linear, λ bacteriophage ds-DNA (Fermentas) in 10 mM Tris–HCl buffer, pH = 7.6, 1 mM EDTA (*see* **Note 10**). Make 50 μL aliquots and store at −20 °C.
2. DNA working solution: dilute one 50 μL aliquot of λ ds-DNA in a ratio of 1:200 with ultrapure water.
3. PicoGreen (Quant-iT™ PicoGreen® dsDNA Reagent and Kits from Molecular Probes, dissolved in DMSO) (*see* **Note 11**). Make aliquots of 50 μL each and store at 2–6 °C. Dilute an aliquot in a ratio 1:200 with water for working concentration.

3 Methods

3.1 Setting Up Electronics

1. Connect the generator output with the input of a wideband power amplifier by a coaxial cable (typically with BNC connectors).
2. Connect the amplifier output with a polyester 3.3 μF capacitor to a switch (*see* **Note 5**).
3. Cut one side of a coaxial cable with male BNC connectors to about 50 cm length. Remove the insulation of the free end and solder it to a flexible and thin twin-wired cable of about 20 cm length (*see* **Note 12**). Solder the free end to a two-conductor male header.
4. Place a BNC tee between the capacitor and the switch. Use this branch, further BNC tees and coaxial cables to connect additional instrumentation for signal control at position 1 in Fig. 1.
5. Connect the DC voltage input of a digital multimeter to a demodulator probe that is plugged into the female side of one of those BNC tees.
6. Connect a second multimeter to position 1 (*see* Fig. 1) via a BNC tee and a coaxial cable. Set the multimeter range to AC voltage (*see* **Note 13**).

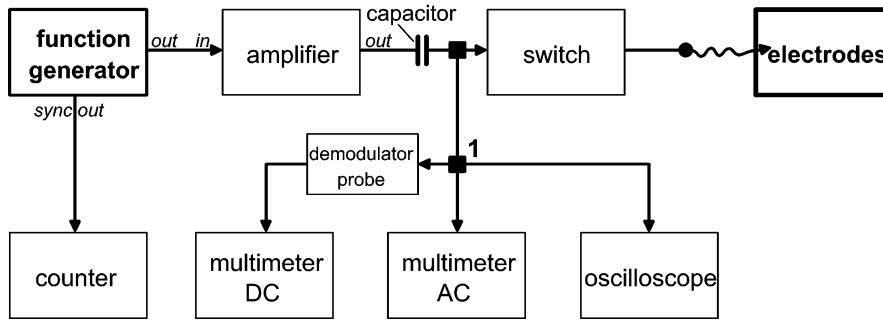

Fig. 1 Electronic setup for dielectrophoresis experiments

7. Connect the input of an oscilloscope to position 1 to control signal shape, amplitude, frequency and possible DC offset.
8. Connect a counter to the function generator sync out port for frequency control (*see* **Note 14**).
9. Set the signal shape of the frequency generator to a sine wave.

3.2 Preparation of Electrode Chips from SAW Resonators

SAW (surface acoustic wave) resonators consist of interdigitated electrode (IDE) fingers, made from aluminum, which are deposited photolithographically on for example quartz substrates (*see* **Note 15**).

1. The actual electrode chip of the SAW element X6964 M is contained in a plastic case of 2 mm thickness. The chip itself is 2 mm wide and 11 mm long. It is fixed to a somewhat larger copper support. To remove the case, open it carefully by milling. Mill just at the edges of the horizontally placed case about 1 mm deep leaving intact a central rectangle of about the size of the chip. The central open volume containing the chip should become accessible. Take care to keep the chip's surface free from any particles.
2. Use forceps to remove the central lid with gentle force.
3. Remove the chip together with its copper support with the help of tweezers. Try to leave the thin wires that are bonded to the chip intact.

3.3 Preparation of the Electrode Assembly for Dielectrophoresis Experiments

1. Solder two thin wires, e.g., copper wires, with lengths of approximately 3 cm to a female header.
2. Glue the header onto a microscope glass slide near the edge of the slide (*see* **Note 16**) using two-component epoxy adhesive.
3. Place the chip including the copper support onto the glass slide and mount it with epoxy adhesive. Take care not to place any adhesive on the chip surface. At the same time, it is useful to place some epoxy beside the chip close to the ends of the thin bonding wires.

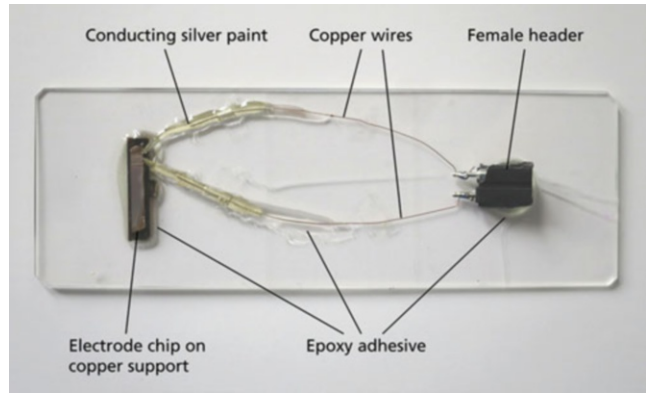

Fig. 2 Electrode chip prepared for dielectrophoresis experiments

4. There are two electrode areas. Connect the smaller one (which covers about a tenth of the whole surface) to the 3 cm copper wires (*see* **step 1** above) with electrically conducting silver paint. If the bond wires are lost, draw thin lines of silver paint directly to each end of the IDEs (*see* **Note 17**).
5. Prepare the sample chamber by cutting or punching a hole into a piece of laminating film that will serve as a spacer. The hole is intended to leave the electrodes free while covering the rest of the electrode chip, and its size and shape should be customized to match the electrode array size (typically with a diameter of around 3 mm; *see* **Note 18**).
6. Place the laminating film onto the electrode chip with the hole leaving the electrode array free, and heat the chip on a hot plate to 85 °C. As soon as the laminating film becomes transparent, it can be pressed against the chip surface using a clean microscope slide to attach it to the chip (*see* **Note 19**).
7. After letting the chip cool to room temperature, it is ready to be used for dielectrophoresis experiments (*see* Fig. 2).

3.4 Stretching of DNA

1. Place the microscope slide with the electrode chip under a fluorescence microscope, chose a magnification that allows observation of ideally the whole electrode array (*see* **Note 20**). Set the focus on the electrode chip using brightfield reflected light.
2. Mix 1 μL of DNA working solution with 1 μL of PicoGreen working solution by pipetting the solutions directly into the sample chamber of the electrode chip (SAW electrode chip prepared for dielectrophoresis according to Subheading 3.2.). Actual volumes depend on the size of the opening in the laminating film and on its thickness.
3. Seal the sample chamber by placing a coverslip on top to prevent sample evaporation.

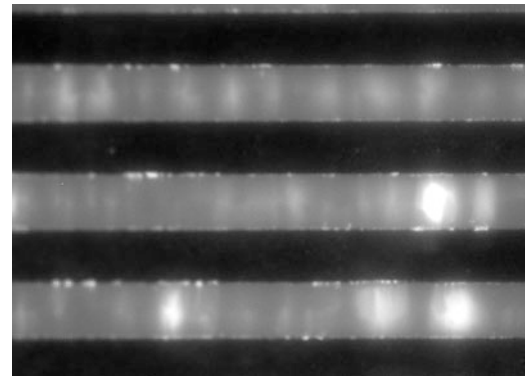

Fig. 3 Fluorescence micrograph of DNA strands, stained with Pico Green, aligned and stretched between interdigitated electrodes (electrodes appear dark). Electric field parameters: 1 MHz, 25 V_{pp}. Imaging conditions: 40× objective, 500 ms exposure time

4. Connect the twin-wired cable electric setup (*see* Subheading 3.1) to the female headers on the microscope slide. Take care to have the switch in its off position.
5. Reset the focus on the electrode chip using brightfield reflected light, then switch to fluorescence mode using appropriate filters (*see* **Note 21**).
6. Apply approx. 25 V_{pp} at 1 MHz by setting the switch on (*see* **Note 22**).
7. Monitor for increase of fluorescence in the electrode gaps because of bundles of stretched and aligned DNA strands (*see* Fig. 3). The amount of DNA between the electrode gaps increases with time and saturates when most of the sample volume has been cleared from the DNA. At the same time bleaching of the fluorophores decelerates the fluorescence increase until it prevails, finally (usually after some minutes) leading to fluorescence fading away. Often the DNA bundles move parallel to the electrodes. Depending on the frequency, some of the DNA is collected at the electrode edges in a compact shape.
8. Disconnect the headers.
9. Remove the coverslip.
10. Rinse the electrode chip with water to remove the DNA (*see* **Note 23**) and dry the electrode chip in a stream of nitrogen.
11. The electrode chips are reusable and can be stored at room temperature in air.

4 Notes

1. Some function generators deliver peak-to-peak voltages up to 30 V_{pp}. In this case, the power amplifier can be omitted. Typical manufacturers are for example Keysight, PeakTech, Rohde&Schwarz, Tektronix, Toellner, TTi, or Wavetek. We use Wavetek Model 193. An instrument equipped with separate control dials each for frequency and voltage is more convenient than modern devices with push buttons or only a single dial.
2. Typical manufacturers for amplifiers are Keysight, Krohn-Hite, or Toellner. We use Toellner TOE 7606.
3. The switch serves to decouple the electrodes from the signal source during adjustments of voltage and frequency.
4. The demodulator probe rectifies the AC signal and delivers a DC voltage that amounts to nearly the AC voltage peak value. This accuracy is sufficient for the present purpose at frequencies above 30 kHz. We use Testec TT-DE 112.
5. The capacitor keeps away any residual DC voltage from the electrodes that could lead to bubble formation at the electrodes due to electrolysis. Electrolytic aluminum or tantalum capacitors are not suitable due to their high leakage currents. Capacitance values of around 1 μF are sufficient at frequencies above 3 kHz. The capacitor voltage rating should amount to at least the maximal used peak voltage.
6. Most multimeters are suitable (Fluke, Keithley, Keysight, PeakTech, UniT, and many others). Bench multimeters with built-in display light and mains supply are helpful, especially in the dark in the course of fluorescence observation. We use Mastech M9803R, Uni-Trend UT803 and Keithley 2110.
7. Typical manufacturers of counters are, among others, BK Precision, Keysight, Rigol, Rohde&Schwarz, and Textronix. We use Voltcraft 7202.
8. Nearly any type of oscilloscope is suitable (e.g., Keysight, Tektronix, Rohde&Schwarz, Voltcraft). We use Hameg HM 307. If an oscilloscope with on-screen display of the actual signal amplitude is available, neither the multimeters nor the demodulator probe are needed.
9. We find it useful to cut or break the coverslips carefully into smaller pieces to avoid a tilt of the coverslip when lying on the narrow electrode substrate. Precise cutting can be accomplished by scratching with a diamond knife and subsequent breaking along the scratch.

10. Alternative DNA samples can be used as long as they are double-stranded and their contour length is of the same length or shorter than the electrode gap.
11. Alternative stains for double-stranded DNA can be used if matching filter sets are available at the fluorescence microscope.
12. The flexible cable avoids any impact of accidental movement of the switch or the cable.
13. An illuminated bench multimeter is helpful. Most low-cost multimeters only work up to around 1 kHz, some to 10 kHz. More expensive ones up to more than 100 kHz. This extra multimeter is needed because the demodulator probe is working with sufficient accuracy only at frequencies down to 30 kHz.
14. In a minimized setup, just a function generator and the electrodes are sufficient. However, counter, multimeters and oscilloscope are highly recommended, since they allow sufficient control over experimental parameters.
15. Whilst the present protocol describes the use of SAW elements with 22 μm electrodes in a plastic case, other commercially available types are also suitable. The resonator R2633 from Siemens/Matsushita has been used in ref. [14]. It consists of a quartz substrate of 4 mm length, 1 mm width and 0.5 mm height with two pairs of interdigitated electrodes sealed in a cylindrical metal can. Each electrode consists of 35 fingers of 800 μm length and 2.3 μm width, leaving an interelectrode gap of 1.7 μm. The similar resonator PARS 433.92 from Kyocera contains a quartz substrate of about 3 mm length and 0.7 mm width placed on a ceramic support in a rectangular metal case [15, 16]. The electrodes are composed of 628 fingers with 150 μm length and 1.4 μm width each, separated by 1.1 μm gaps. The design of the SAW resonator R820 from Epcos is similar. A quartz substrate of $2.3 \times 0.9 \times 0.5$ mm^3 carries a pair of interdigitated electrodes composed of 170 fingers each. They are 215 μm long and 1.95 μm wide, separated by 1.4 μm wide gaps [17]. Removing the case can be accomplished as follows: First, the metal case is thinned with a dental drill while avoiding actually opening it. Then the lid is removed by gentle force using fine pliers or tweezers. By this means the electrodes are kept free from contaminations. A fittingly cut flat silicon rubber and a coverslip prevent evaporation of the sample solution. There are also various other SAW components available. However, their internal structure often is more complicated than just simple IDEs. Therefore they are suitable for dielectrophoretic manipulation only in very special cases. Take care to check whether the adhesive used by the manufacturer

for mounting the chip is itself fluorescent. Alternative commercial sources for interdigitated microelectrodes are MicruX Technologies (Spain) and Laser Micromachining (UK).

16. Arrange it in such a way that the male header at the end of the twin-wired cable (*see* **step 3** of Subheading 3.1) can be easily plugged in. The xy-stage clamp of the microscope may interfere with this header. Turning the microscope objective revolver may be impeded by the header and twin-wire.
17. An extra thin brush helps to paint thin connections more precisely.
18. The thickness of heat laminating film usually amounts to 80 μm. However, there are other thicknesses available up to at least 250 μm. This allows the sample volume to be adjusted by proper choice of spacer thickness and size of the opening.
19. Be careful not to shift the laminating film laterally when pressing it to the chip surface.
20. Depending on the dimensions of the IDE array, a microscope objective with 4× or 10× magnification is suited.
21. PicoGreen has its absorption maximum at 502 nm and its emission maximum at 523 nm when bound to nucleic acids and can be monitored using filter sets recommended for FITC.
22. Start with the voltage turned down to a minimum and slowly increase the voltage.
23. Permanent immobilization of DNA can be achieved with the use of smaller electrode structures, which are also accessible from commercially available SAW resonators, usually down to electrode and gap widths of approximately 1 μm, respectively. Electric field parameters have to be optimized for each electrode system individually. However, frequencies in the range of 0.1–1 MHz are recommended for DNA stretching. Start with a low voltage and increase it slowly until DNA stretching is observed. Usually, lower voltages are needed when using electrodes with narrower gap widths. If the voltage is further increased, DNA can be immobilized permanently on the electrodes, which means that the DNA is not removed by rinsing.

Acknowledgments

The authors thank Katrin Nicklas for help with electrode preparations. Financial support by The Brandenburg Ministry of Sciences, Research and Cultural Affairs (MWFK) within the framework StaF and by the European Regional Development Fund (ERDF) is gratefully acknowledged. We also thank the German Research Foundation (DFG) for funding in the program Essence (SPP 1857 HO1298/4-1).

References

1. Carbone A, Seeman NC (2002) Circuits and programmable self-assembling DNA structures. Proc Natl Acad Sci U S A 99:12577–12582. https://doi.org/10.1073/pnas.202418299
2. Rothemund PWK (2006) Folding DNA to create nanoscale shapes and patterns. Nature 440:297–302. https://doi.org/10.1038/nature04586
3. Niemeyer CM (2007) Functional devices from DNA and proteins. Nano Today 2:42–52. https://doi.org/10.1016/S1748-0132(07)70058-0
4. Bier FF, Hölzel R (2008) Nucleic acid based nanostructures—recent advancements and the impact of NUCAN. AIP Conf Proc 1062:3–12. https://doi.org/10.1063/1.3012301
5. Washizu M, Kurosawa O (1990) Electrostatic manipulation of DNA in microfabricated structures. IEEE Trans Ind Appl 26:1165–1172
6. Tuukkanen S, Kuzyk A, Toppari JJ, Häkkinen H, Hytönen VP, Niskanen E, Rinkiö M, Törmä P (2007) Trapping of 27 bp–8 kbp DNA and immobilization of thiol-modified DNA using dielectrophoresis. Nanotechnology 18:295204. https://doi.org/10.1088/0957-4484/18/29/295204
7. Pohl H (1978) Dielectrophoresis. Cambridge University Press, Cambridge
8. Pethig R (2010) Dielectrophoresis: status of the theory, technology, and applications. Biomicrofluidics 4:022811. https://doi.org/10.1063/1.3456626
9. Hölzel R, Gajovic-Eichelmann N, Bier FF (2003) Oriented and vectorial immobilization of linear M13 dsDNA between interdigitated electrodes—towards single molecule DNA nanostructures. Biosens Bioelectron 18:555–564. https://doi.org/10.1016/S0956-5663(03)00024-1
10. Kumemura M, Collard D, Yamahata C, Sakaki N, Hashiguchi G, Fujita H (2007) Single DNA molecule isolation and trapping in a microfluidic device. ChemPhysChem 8:1875–1880. https://doi.org/10.1002/cphc.200700268
11. Hyun C, Kaur H, McNabb DS, Li J (2015) Dielectrophoretic stretching of DNA tethered to a fiber tip. Nanotechnology 26:125501. https://doi.org/10.1088/0957-4484/26/12/125501
12. Tuukkanen S, Kuzyk A, Toppari JJ, Hytönen VP, Ihalainen T, Törmä P (2005) Dielectrophoresis of nanoscale double-stranded DNA and humidity effects on its electrical conductivity. Appl Phys Lett 87:183102. https://doi.org/10.1063/1.2117626
13. Yamamoto T, Kurosawa O, Kabata H, Shimamoto M, Washizu M (2000) Molecular surgery of DNA based on electrostatic micromanipulation. IEEE Trans Ind Appl 36:1010–1017. https://doi.org/10.1109/IAS.1998.729860
14. Henning A, Henkel J, Bier FF, Hölzel R (2008) Label-free electrical quantification of the dielectrophoretic response of DNA. BMC Biophys 1:4. https://doi.org/10.1186/1757-5036-1-4
15. Henning A, Bier FF, Hölzel R (2010) Dielectrophoresis of DNA: quantification by impedance measurements. Biomicrofluidics 4:022803. https://doi.org/10.1063/1.3430550
16. Li S, Yuan Q, Morshed BI, Ke C, Wu J, Jiang H (2013) Dielectrophoretic responses of DNA and fluorophore in physiological solution by impedimetric characterization. Biosens Bioelectron 41:649–655. https://doi.org/10.1016/j.bios.2012.09.036
17. Stanke S, Bier FF, Hölzel R (2011) Fluid streaming above interdigitated electrodes in dielectrophoresis experiments. Electrophoresis 32:2448–2245. https://doi.org/10.1002/elps.201100096

Chapter 15

A Practical Guide to Molecular Dynamics Simulations of DNA Origami Systems

Jejoong Yoo, Chen-Yu Li, Scott Michael Slone, Christopher Maffeo, and Aleksei Aksimentiev

Abstract

The DNA origami method exploits the self-assembly property of nucleic acids to build diverse nanoscale systems. The all-atom molecular dynamics (MD) method has emerged as a powerful computational tool for atomic-resolution characterization of the in situ structure and physical properties of DNA origami objects. This chapter provides step-by-step instructions for building atomic-scale models of DNA origami systems, using the MD method to simulate the models, and performing basic analyses of the resulting MD trajectories.

Key words Molecular dynamics, DNA nanotechnology, DNA origami, Bionanotechnology, Computer simulations

1 Introduction

The DNA origami method utilizes the strong specificity of complementary DNA molecules to enable low-cost fabrication of custom three-dimensional nanoscale objects [1, 2]. In the DNA origami method, distant parts of a long DNA strand are brought into close spatial proximity by association with a collection of short (~20–60 bp) synthetic DNA strands [3, 4]. The resulting structures appear to be made of many approximately parallel DNA duplexes connected by a network of four-arm Holliday junctions. Although the method was first described only 10 years ago, practical DNA origami devices have already been demonstrated [5–10], which includes systems for performing nanoscopic measurements [11–13], focusing electromagnetic fields below the diffraction limit [14, 15], and enhancing enzymatic catalysis [16, 17].

Electronic supplementary material: The online version of this chapter (https://doi.org/10.1007/978-1-4939-8582-1_15) contains supplementary material, which is available to authorized users.

Giampaolo Zuccheri (ed.), *DNA Nanotechnology: Methods and Protocols*, Methods in Molecular Biology, vol. 1811, https://doi.org/10.1007/978-1-4939-8582-1_15, © Springer Science+Business Media, LLC, part of Springer Nature 2018

The rise of the DNA origami method may in part be attributed to the method's abstract representation of complex self-assembled objects. Several interactive software packages, including Tiamat [18], Nanoengineer-1, and caDNAno [19], allow the user to intuitively draw the parallel helices in desired locations while automated algorithms perform the more tedious tasks, such as sequence assignment for the short synthetic "staple" strands. Of these software packages, caDNAno has emerged as the most widely used, due in part to its easy-to-use interface, its ability to automatically generate staple strands, and its ability to scale to large structures.

The DNA origami design software packages model origami objects as collections of idealized, rigid rods, each rod representing a DNA duplex. However, recent high-resolution cryo-electron microscopy reconstruction of a DNA origami object revealed considerable deviations from the idealized design [20]. The time and cost associated with experimental characterization of DNA origami structure make structure prediction through computational approaches an attractive alternative.

Simulations of DNA origami objects have been performed using models that provide different levels of detail including both coarse-grained [21–25] and atomistic models [26–31]. In general, coarse-grained descriptions trade accuracy for lower computational costs. Since atomic features are often important at the nanometer scale, the focus of this chapter is on atomistic simulations. In particular we describe the use of all-atom molecular dynamics (MD) simulations, wherein the motion of every atom in the system is described according to classical mechanics. Our group has used this method previously to characterize and predict the structural, mechanical, chemical, and transport properties of DNA origami objects [26–31].

In this chapter, we describe the protocol for all-atom MD simulations of DNA origami using the NAMD [32] package starting from a caDNAno design. As an example, we use a caDNAno design file of a six-helix cylindrical structure (**hextube.json**), which is provided along with this document. We will convert the caDNAno file to an all-atom structure file in the PDB format, submerge the structure in $MgCl_2$ solution, and perform MD simulations of the solvated structure.

All files necessary to perform modeling tasks described in this chapter can be found at **http://bionano.physics.illinois.edu/sites/default/files/origamitutorial.tar.gz**, (Supplementary Material 1). It is recommended that you follow this chapter's instructions on a Linux workstation. If you are a Windows user, we recommend you install Cygwin to obtain a Unix-like shell. For commands typed into the Cygwin shell, you will need to change all the file path separators "/" into "\". Please contact the Aksimentiev Group for any questions about this chapter.

All URLs, file and directory names and commands that will be manually entered are marked in **bold**. When typing the commands, please enter them verbatim, unless directed otherwise. Note that we will type commands in two different terminals. One is the UNIX/LINUX terminal that runs a shell process (BASH, CSH, TCSH, etc.). "SHELL> **COMMAND**" indicates that **COMMAND** should be typed in the shell terminal. The other is the VMD Tk console terminal; in the VMD menu, select Extensions and Tk Console. "TKCON> **COMMAND**" indicates that **COMMAND** should be typed in the VMD Tk console.

2 Materials

2.1 Software

1. **caDNAno.** Download caDNAno 2 from **http://cadnano.org**. caDNAno is one of the most popular computer-aided origami design programs. caDNAno enables rapid design of DNA origami objects, runs on Windows and Mac platforms, and can be run as a plugin of Autodesk Maya or as a standalone program. For more information on caDNAno, please refer to the caDNAno manual.
2. **ENRG MD web server.** Access it at **http://bionano.physics.illinois.edu/origami-structure**. The ENRG MD web server converts caDNAno output files to an appropriate format for visualization and simulation. As the tool is available entirely online, it requires no installation. It can convert DNA origami structures using the square or honeycomb lattices, and can use the default m13mp18 template or a custom user-provided sequence for the DNA scaffold.
3. **VMD.** Download VMD from **http://www.ks.uiuc.edu/Research/vmd**. VMD is a program for visualization and analysis of atomic biomolecular structures [33]. VMD supports all major computer platforms and provides a programming interface based on the Tcl scripting language. Tcl scripts will be used throughout this chapter for both building and analyzing DNA origami objects. VMD runs on any system, but benefits greatly from the latest graphics hardware that supports CUDA. For more information on VMD, please refer to the VMD User Guide [34] and the VMD Tutorial [35]. After installation, VMD is run either by typing **vmd** in the terminal (Linux systems) or by clicking the icon (Windows and Mac systems).
4. **NAMD.** Download NAMD [32] from **www.ks.uiuc.edu/Research/namd**. NAMD is a highly scalable molecular dynamics code that supports CUDA-based acceleration. NAMD can be used on any machine (from laptop to supercomputers) running Linux/UNIX, Mac OS X, or Windows operating systems. However, for DNA origami systems, it is

highly recommended to perform simulations using multiple compute nodes on parallel clusters or supercomputers. For more information on NAMD, please refer to the NAMD User Guide [36] and NAMD Tutorial [37].

5. **Perl.** Download Perl from **https://www.perl.org/get.html.** Perl is a general-purpose scripting language available across all major platforms. It is used in this chapter to generate magnesium hexahydrate restraints and to convert an atomic model of a DNA origami object into a sparser "chickenwire" model for the purpose of visualization.

2.2 Required Files

1. **origamiTutorial package.** All files used in this chapter (scripts and other support files) are available in an archive on the publisher website or at **http://bionano.physics.illinois.edu/sites/default/files/origamitutorial.tar.gz**. Extracting the archive in a working directory on your filesystem will create the **origamiTutorial** directory containing four subdirectories. Each subdirectory contains files required by one section in this chapter. The subdirectories extracted from **origamitutorial.tar.gz** are labeled **step1**, **step2**, **step3**, and **step4**, corresponding to Subheadings 3.1, 3.2, 3.3, and 3.4 of this chapter.
2. **CHARMM force field with corrections for ion–DNA interactions.** Download the topology and parameter files of the CHARMM force field from **http://mackerell.umaryland.edu/charmm_ff.shtml**. Select the c36 version. Download the CHARMM stream file for water and ions with corrections for ion–DNA interactions from **http://bionano.physics.illinois.edu/CUFIX**. The CHARMM topology file for nucleic acids, **top_all36_na.rtf**, the CHARMM parameter file for nucleic acids, **par_all36_na.prm**, and the stream file for water and ions **toppar_water_ions_cufix.str** are used in this tutorial. These three files are also included in the **origamitutorial.tar.gz** package.

3 Methods

Here we describe our protocols for preparing models of DNA origami systems and simulating these models using the MD method. If you wish to design a DNA origami system, go to Subheading 3.1. The three following sections (Subheadings 3.2, 3.3, and 3.4) cover construction, simulation, and analysis of atomistic models of a DNA origami system, respectively. In Subheading 3.2, we describe methods for converting an abstract design of a DNA origami system obtained in Subheading 3.1 to an atomistic model suitable for MD simulations. In Subheading 3.3, we explain

the strategy for equilibrating the atomistic DNA origami structure in an electrolyte solution. In Subheading 3.4, we introduce a few general analysis methods that are useful for monitoring the equilibration process.

3.1 Designing a DNA Origami Object Using caDNAno

Our first task is to build a DNA origami object using the caDNAno program and the ENRG MD web server. An MD simulation requires two separate files, a PDB file and a PSF file, to define a system. The PDB file contains coordinates of all atoms in the system. The PSF file is complementary to the PDB file and contains chemical information about the system including masses and charges of the atoms as well as chemical bond information. Here we construct a hexagonal tube structure that consists of six DNA helices. The scripts used in this section are located in the **step1** subdirectory.

1. **Open caDNAno.** First open caDNAno by double-clicking its icon on a Mac or Windows computer.
2. **Start a new session.** Click "New" and choose a honeycomb type. Fig. 1 shows an example session of caDNAno.
3. **Choose six helices in a hexagonal arrangement**, as shown in Fig. 1.
4. **Draw the DNA paths to** produce the hexagonal tube structure.

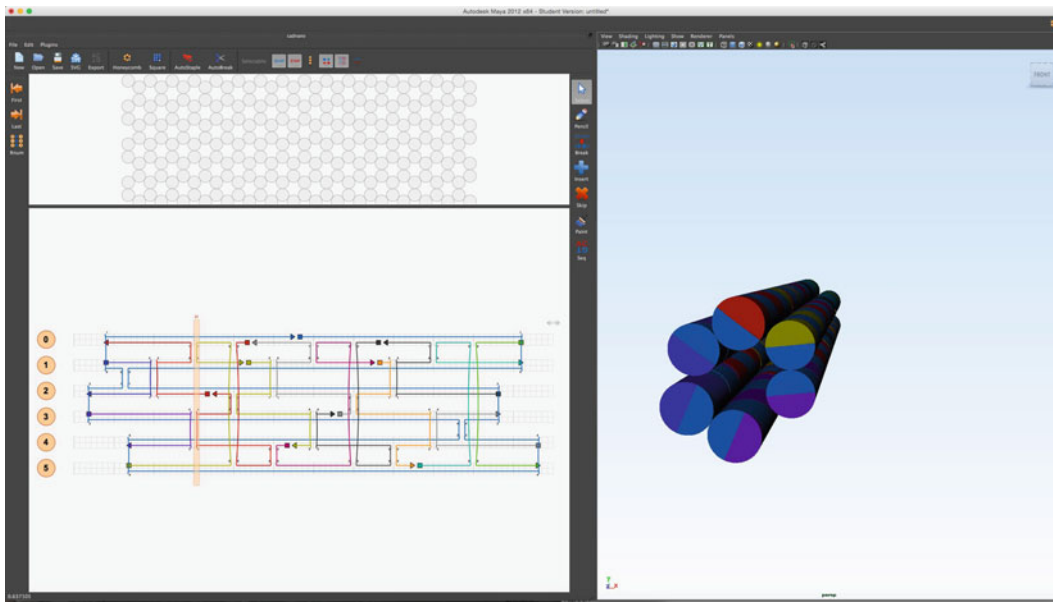

Fig. 1 A screenshot of a caDNAno session showing the design of our DNA origami example: hextube

5. **Save the design.** Click "Save". The resulting file is **hextube.json**, which can be found in the **step1** folder. One can follow the remaining steps using any custom-design file instead of **hextube.json**.

3.2 Building an Optimized Atomistic Structure

Next, we convert the **hextube.json** file to a structure file in the PDB format using the server, **http://bionano.physics.illinois.edu/origami-structure**, as shown in Fig. 2.

As shown in Fig. 2, we named our project "**hextube**" and uploaded the **hextube.json** file. We set the origami lattice type to honeycomb. For the scaffold, one can select the default m13mp18 sequence or choose to upload a custom DNA sequence.

1. **Open a web browser.** Any web browser will work.
2. **Open the ENRG MD web site.** With any web browser, navigate to **http://bionano.physics.illinois.edu/origami-structure**. An example of the ENRG MD web server session is shown in Fig. 2.
3. **Name the session.** Type in the job title **hextube**.
4. **Upload the json file.** Click "Choose file" and select **hextube.json**.

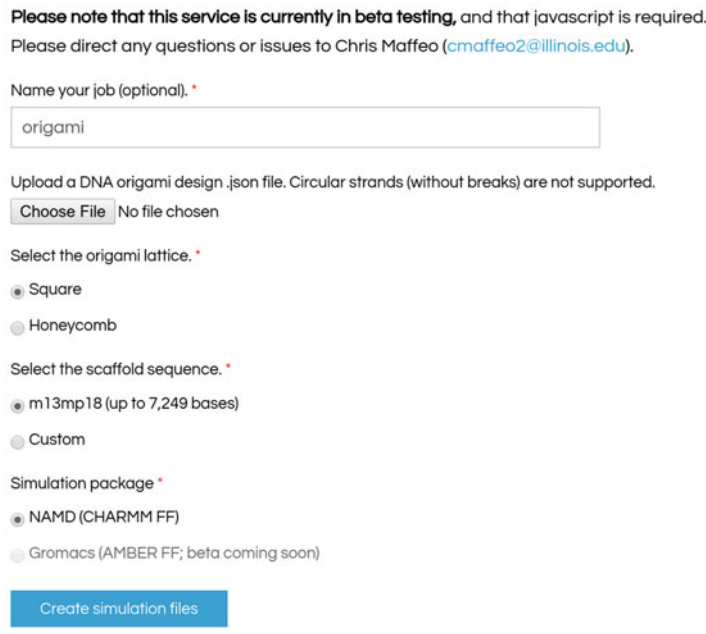
Please note that this service is currently in beta testing, and that javascript is required.
Please direct any questions or issues to Chris Maffeo (cmaffeo2@illinois.edu).
Name your job (optional). *
origami
Upload a DNA origami design .json file. Circular strands (without breaks) are not supported.
Choose File
No file chosen
Select the origami lattice. *
Square
Honeycomb
Select the scaffold sequence. *
m13mp18 (up to 7,249 bases)
Custom
Simulation package *
NAMD (CHARMM FF)
Gromacs (AMBER FF; beta coming soon)
Create simulation files

Fig. 2 Using the ENRG MD web server to convert a caDNAno design file to a PDB-formatted atomic structure. Make sure your selections match exactly what is shown

5. **Select the origami lattice type.** The hexagonal tube structure is designed based on the honeycomb lattice, so choose "Honeycomb".
6. **Select the scaffold sequence.** Choose the default M13 vector sequence.
7. **Create simulation files.** Clicking "Create simulation files" will initiate the conversion process, which will generate a download link upon completion.
8. **Download the simulation files.** Download the simulation files by clicking the download link. The file name of the downloaded archive will be **hextube.tar.gz**. Please put the hextube.tar.gz file in the **origamiTutorial** folder and extract it. The extracted **hextube** directory will contain the following files:
   - hextube.psf: The CHARMM format PSF file.
   - hextube.pdb: The PDB format file of the all-atom structure.
   - hextube.namd: The NAMD input file for the structure optimization simulations.
   - hextube.exb: Extrabonds restraints for structure optimization.
   - charmm36.nbfix: CHARMM36 force field files.

   Other files: In addition, the archive includes files that aid in creating a "chickenwire" representation, an output directory and a README file.

If a custom JSON file was created in Subheading 3.1, one can remove the **step2** directory and change **hextube** directory to **step2**. Otherwise, one can use the existing **step2** directory, which includes all files from **hextube.tar.gz**.

9. **Check the downloaded file.** One can see the three-dimensional structure of the DNA origami object by loading the PSF and PDB files to the VMD program. In VMD Main window, click "File" and "New Molecule", navigate to **hextube.psf** file in **step2** directory using the "Browse" button, and click "Load" button. After loading the PSF file, a molecule with "ID 0" will appear in "VMD Main" window. Click the newly created line in "VMD Main" window, click "File" and "Load Data Into Molecule", navigate to **hextube.pdb** file, and click "Load" button. Alternatively, a new molecule can be loaded to VMD by typing the following command to the VMD Tk console: "TKCON> **mol load psf hextube.psf pdb hextube.pdb**". Then, a molecular structure will appear in the "VMD OpenGL Display" window. For example, Fig. 3 (top) shows the structure of hextube.pdb obtained using the web server. The structure in Fig. 3 (top) is unrealistic because the DNA helices are parallel to one another and the bonds in the Holliday junctions are abnormally stretched, Fig. 4a.

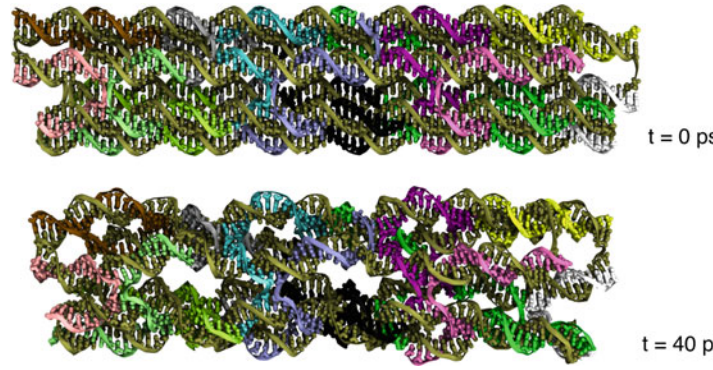

Fig. 3 The hexagonal tube structure before (top) and after (bottom) structure optimization. A 40 ps ENRG MD simulation performed in vacuum with the extrabonds restraints is sufficient to produce the expected chickenwire arrangement of the DNA helices. The molecular graphics images were obtained using VMD's, Drawing Methods "Licorice" for the "not backbone and noh" selection and "NewCartoon" for the "backbone" selection; the Coloring Method was set to "SegName"

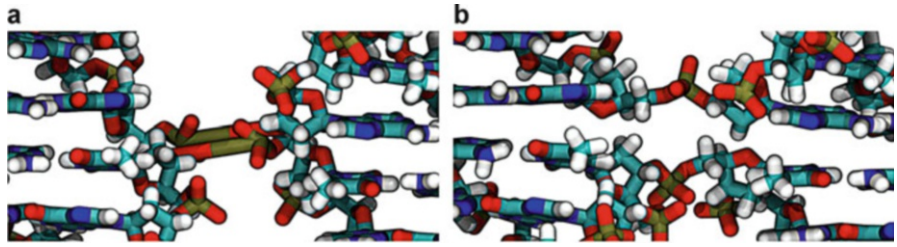

Fig. 4 Holliday junction conformations before (**a**) and after (**b**) the optimization using the NAMD. The molecular graphics images were obtained using VMD's Drawing Method "Licorice" and Coloring Method "Name"

As described in our previous study [31], a more realistic structure can be obtained by performing an ENRG MD simulation of the structure in vacuum using the network of elastic restraints (**hextube.exb**) provided by the web server, and as described below. See the NAMD manual for a detailed description of the extrabonds command (e.g., http://www.ks.uiuc.edu/Research/namd/2.7/ug/node26.html).

10. **Prepare a NAMD run**. The initial optimization of the structure can be performed by running an MD simulation using the NAMD input file, **hextube.namd**, provided by the web server. Please navigate to the **step2** directory and modify the restart frequency ("restartfreq") and number of simulation steps ("run") as such:

    restartfreq 4800

    run 21,600

11. **Note the use of extrabonds**. Extrabonds serve two different purposes: to imitate the DNA–DNA repulsion observed in explicit solvent simulations and to enforce stability of the DNA helices. The extrabonds are specified in the NAMD input file as follows:

    extraBonds on

    extraBondsFile hextube.exb

12. **Run NAMD**. Perform the MD simulation by typing the following into a terminal:

    SHELL> **namd2 hextube.namd > hextube.log &**

13. **Monitor the NAMD run.** The MD run will write output files into the **output** directory. In practice, the required simulation time depends on the size of the DNA origami object. For a relatively small system such as the hexagonal tube object, 40 ps seems long enough to get a realistic conformation, Fig. 3 (bottom). For a ~7500 bp object, 2 ns was sufficient to achieve a fully relaxed structure [31].

14. **Save the optimized structure to PDB.** Before we proceed, we need to save the last frame of the trajectory as a PDB file for the tasks described in the next section:

    SHELL> **vmd -dispdev text -e ../step3/save_pdb.tcl -args hextube.psf output/hextube-1.coor hextube_min.pdb**

Note that the above command should be entered as a single line. An example of this output (**hextube_min.pdb**) has been placed in the **step2** directory, along with the initial PSF and PDB files.

3.3 MD Simulations of DNA Origami in Explicit $MgCl_2$ Solution

As each nucleotide of DNA carries the charge of an electron, a DNA origami object has a high charge density. In experiment, DNA origami objects are usually stabilized by divalent cations, typically Mg^{2+}. In this section, we describe a protocol for simulating a DNA origami structure in an explicit electrolyte solution. All files necessary for the simulations are included in the **step3** folder. Navigate to the **step3** folder before proceeding to the following steps.

1. **Insert Mg^{2+}**. In this step, we neutralize a DNA origami object by inserting the appropriate number of Mg^{2+} ions. Previously, we have shown that the standard parameterization of Mg^{2+} ions is not suitable for simulations of dense DNA systems [38]. We have also shown that modeling a Mg^{2+} ion as a magnesium hexahydrate complex ($MGHH^{2+}$) brings simulated

DNA–DNA forces in agreement with experiment [38–40]. Hence, all our DNA origami simulations employ a $MGHH^{2+}$ model of Mg^{2+} ions [26]. Because $MGHH^{2+}$ molecules diffuse slowly, it is beneficial to place them initially in proximity to the DNA origami structure. The following custom script will place $MGHH^{2+}$ molecules close to the DNA origami. In the terminal, execute:

SHELL> **vmd -dispdev text -e add_mgh_ver2_3.tcl -args ../step2/hextube.psf ../step2/hextube_min.pdb hextube_MGHH 516**

The first two arguments **step2/hextube.psf** and **step2/hextube_min.pdb** are the PSF and PBD files from the last frame of the structure optimization simulation. The third argument "hextube_MGHH" is the prefix for the output PSF and PDB files. The last argument "516" is the number of $MGHH^{2+}$ molecules to be added, which can be adjusted depending on the size of the final simulation box and the desired concentration of Mg^{2+}. The resulting system should look like the one shown in Fig. 5a.

2. **Solvate the system**. In experiment, DNA origami objects self-assemble in aqueous solutions. In order to simulate a DNA origami object under experimental conditions, we need to surround the object with solution. We use the **solIon.tcl** script to add water to the system. The script also adds Cl^- ions to make the entire system electrically neutral. In the terminal, run the following command:

   SHELL> **vmd -dispdev text -e solIon.tcl.**

   which will produce the final solvated hexagonal tube system (**hextube_MGHH_WI.psf** and **hextube_MGHH_WI.pdb**). Note that the number of monovalent ions can be adjusted by modifying **solIon.tcl**. Figure 5b shows an image of the solvated structure.

3. **Create extrabonds for $MGHH^{2+}$**. The six water molecules in an $MGHH^{2+}$ complex are strongly coordinated through direct contact interactions with the Mg^{2+} ion. However, the structure of $MGHH^{2+}$ can be easily broken during an MD simulation of a DNA origami object because of the large electrostatic forces between DNA and Mg^{2+}. To prevent undesired dissociation of the $MGHH^{2+}$ complexes, we add harmonic restraints between the magnesium atom and the oxygen atoms of the water in each $MGHH^{2+}$ using the extrabonds function of NAMD. Running the **mghh_extrabonds.pl** script in the terminal will generate extrabonds definitions for NAMD.

   SHELL> **perl mghh_extrabonds.pl hextube_MGHH_WI.pdb > mghh_extrabonds**

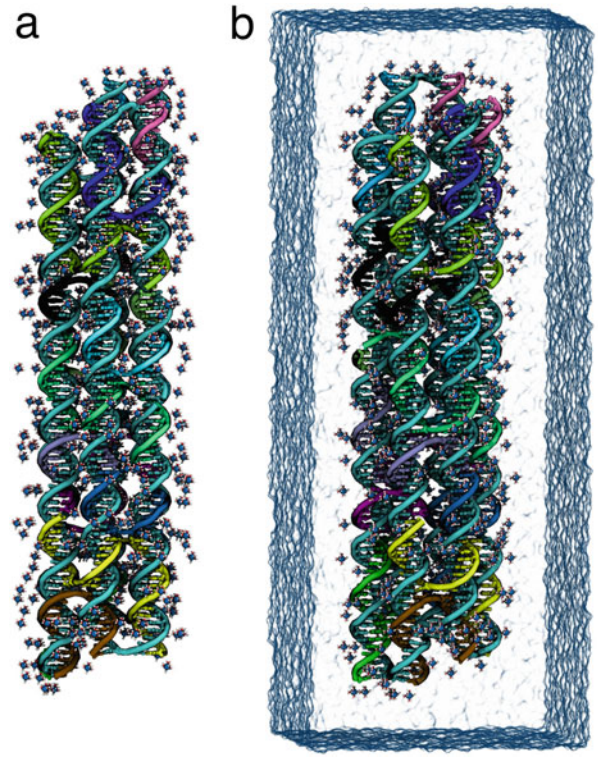

Fig. 5 Hexagonal tube structure including $MGHH^{2+}$ (**a**) and the solvation box (**b**). The molecular graphics images were obtained using VMD's Drawing Method "New Cartoon" with "Aspect Ratio" 1.0 and "Thickness" 1.5 for the selection "backbone" and Drawing Method "Licorice" with "Bond Radius" 0.8 for the selection "nucleic and not backbone and noh." Coloring Method for DNA was "SegName." The transparent water box was drawn using Drawing Method "MSMS" with "Probe Radius" 5.5 and Material "GlassBubble" for the selection "name OH2"

Alternatively, you can use the Tcl version of the same script:

SHELL> **tclsh mghh_extrabonds.tcl hextube_MGHH_WI.pdb > mghh_extrabonds**

To use the extrabonds restraints in an NAMD simulation, the following lines need to be added to the NAMD configuration script:

extraBonds on

extraBondsFile ./mghh_extrabonds

These lines are already included in all NAMD scripts used in this tutorial. If you plan to use extrabonds restraints in a future simulation, remember to include the files in your version of the

NAMD configuration script. All PSF, PDB, and extrabonds files produced in this chapter are in the **step3** directory.

4. **Equilibrate the solvated structure using NAMD**. Equilibrating a DNA origami structure is not a trivial task. Two main forces could break the local structure of a DNA origami object. One of them is the electrostatic repulsion between the phosphates of the DNA strands. The other is the torsion at the crossovers. To avoid breaking base pairs while relaxing the global structure, we simulate a DNA origami object with an elastic network model (ENM) of harmonic restraints that reinforce base pairing and base stacking. We gradually reduce the strength of the spring constants before running a fully unrestrained equilibration simulation. The following protocol will simulate the hexagonal tube with ENM restraints using a force constant $k = 0.5, 0.1, 0.01$, and 0 (kcal/mol/Å^2) for 4.8 ns for each value of k. Although this protocol works for most small-to-medium DNA origami structures, one may need to modify the protocol, in particular the duration of a free equilibration simulation ($k = 0$), to achieve a proper relaxation of a DNA origami structure. The following command run in a terminal window will generate ENM extrabonds files with the three force constants:

   SHELL> **sh mk_extra.sh**

   For the $k = 0$ simulation, we simply turn off the ENM constraints.
   Then, run the simulations one after another:

   SHELL> **namd2 equil_min.namd > equil_min.log**

   SHELL> **namd2 equil_k0.5.namd > equil_k0.5.log**

   SHELL> **namd2 equil_k0.1.namd > equil_k0.1.log**

   SHELL> **namd2 equil_k0.01.namd > equil_k0.01.log**

   SHELL> **namd2 equil_k0.namd > equil_k0.log**

   Note that each run except the first run is a continuation from the previous run using the restart files; for example, **equil_k0.1.namd** input file uses three restart files created by **equil_k0.5.namd**, **equil_k0.5.restart.coor**, **equil_k0.5.restart.vel**, and **equil_k0.5.restart.xsc**. Each run generates a trajectory file (DCD) and box size file (XST). Example DCD and XST output files can be found in the **step4** directory for the readers who want to proceed without actually running the simulations. Keep in mind these are significantly compressed versions of what you will produce. Your simulations will be 50 times longer if you do not modify the NAMD scripts. If

your simulations in the **step3** directory are successful, copy newly generated DCD and XST files to the **step4** directory:

SHELL> **cp *.dcd *.xst ../step4**

It is strongly recommended to monitor your simulations by reading the simulation logs (*see* **Note 1**). If your simulation does not run or it ends sooner than expected, the simulation log might specify the reason; *see* **Notes 2–4** for an explanation of different error types.

3.4 Analysis of the MD Trajectories

In this section, we will analyze the resulting simulation trajectories using the provided scripts. Specifically, we will first determine the change of the simulation box size during the simulation. Then we will calculate the Root Mean Square Deviation (RMSD) of the hexagonal tube with respect to its initial coordinates and count the number of broken base pairs to monitor structural integrity. Next, to check for charge neutrality, we will measure the total charge surrounding the hexagonal tube. Finally, we will convert the atomistic representation of the hexagonal tube into a "chicken-wire" representation to visualize the global conformation more efficiently. Please note that there are other ways to assess whether a simulation has reached equilibrium [26, 27, 41].

The script files for the analysis are included in **step4** folder. Please make sure you are in the **step4** folder before proceeding.

1. **Size of the simulation box.** In the previous section, we used the "solvate" plugin of VMD to add water to the simulation system, which usually underestimates the number of water molecules needed to fill the simulation box containing a DNA origami object. As a result, the simulation box shrinks when the system is simulated under 1 atm of pressure. Thus, the change of the simulation box size can be used to monitor the process of equilibration. The following command will extract the box size information from the **equil_kN.xst** file ($N = 0.5$, 0.1, 0.01 and 0) and print the box size along the x, y, and z axes in the **equil_kN_X.dat**, **equil_kN_Y.dat** and **equil_kN_Z.dat** files:

   SHELL> **sh grepBoxTrace.sh.**

   In the output file, the first column is the simulation time in nanoseconds, and the second column is the length of the object in Angstroms. You can use the plotting software of your choice (e.g., xmgrace) to visualize the data. The result should look similar to that shown in Fig. 6. The simulation box should shrink in the first 300 ps. After that, the box size should become stable.

2. **RMSD**. In this step, we will measure RMSD, which characterizes the amount by which a given selection of atoms deviates from its initial coordinates. The script **measureRMSD.sh** will

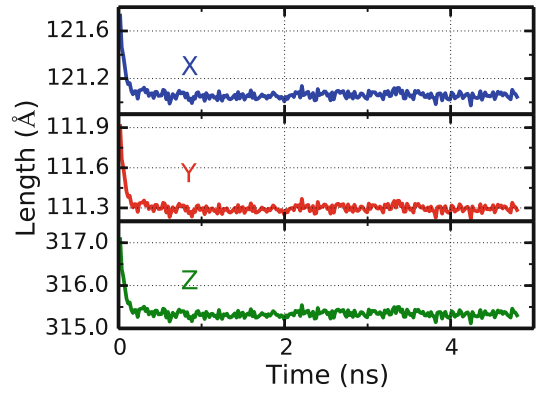

Fig. 6 The size of the simulation box versus the simulation time

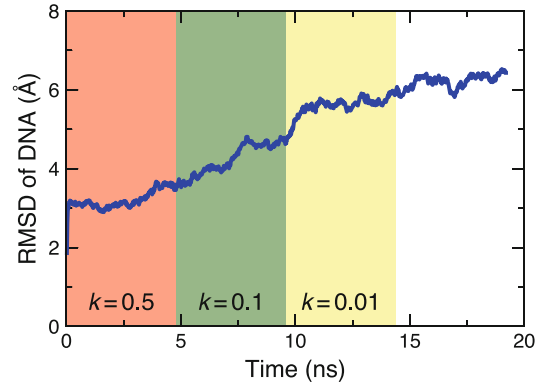

Fig. 7 The RMSD of the hexagonal tube DNA origami from its idealized design

take all the trajectories, measure the RMSD of each frame relative to the initial structure in **hextube_MGHH_WI.pdb**, and write the data to **sim_RMSD.dat**.

SHELL> **sh measureRMSD.sh**

In the output file (**sim_RMSD.dat**), the first column is the simulation time in nanoseconds, and the second column is the RMSD in Angstroms. If you plot the first column as the *x*-axis and the second column as the *y*-axis, the graph should look like the one in Fig. 7. The hexagonal tube is a relatively simple DNA origami structure. After the first 15 ns, the RMSD reached a nearly constant value.

3. **Counting the number of broken base pairs**. Computing RMSD is a method for monitoring the integrity of the simulated structure. Counting the number of broken base

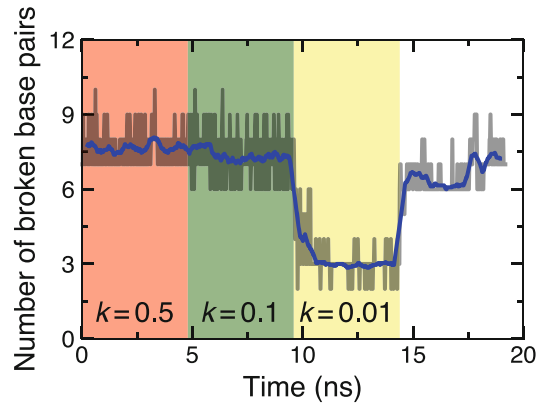

Fig. 8 The number of broken base pairs in the hexagonal tube DNA origami structure

pairs is another effective method specific to DNA origami structures. The script, **countBrokenBps.tcl** achieves this by computing the number of intact base pairs for each frame of an MD trajectory and subtracting that number from the number of base pairs in the idealized structure. In the script, a base pair is considered intact if the H1 or N1 atom of a purine is within 3 Å of the N3 or H3 atom of a pyrimidine, and the angle formed by the N1–H1–N3 or N1–H3–N3 atoms is greater than 140 degrees. These atoms participate in the central Watson–Crick hydrogen bond. Type the following command in the terminal to count the number of broken base pairs in the DNA origami and save the output to **sim_BrokenBps.dat**.

SHELL> **sh countBrokenBps.sh**

In the output file (**sim_BrokenBps.dat**), the first column is the simulation time in nanoseconds, and the second column is the number of broken base pairs. A plot can be found in Fig. 8: the gray trace is the raw data. The blue trace is the running average obtained using a 0.5 ns window.

4. **Total charge**. To neutralize the DNA origami charge, we added $MGHH^{2+}$ molecules. When the system reaches equilibrium, the ionic atmosphere around the DNA origami object should also reach equilibrium. To characterize equilibration of the ion atmosphere, we measure the total charge of all atoms residing within 2 nm of the DNA origami structure as a function of the simulation time. Because we did not invoke the "wrapAll" option in the NAMD configuration file, atoms could wander from one periodic image of the system to the other and hence we need to wrap the trajectories first. The following command will call **AlignWrap.tcl** to place all atoms of the

MD trajectories into the same periodic image of the system and save the output.

SHELL> **sh AlignWrap.sh**

In VMD, you can load the DCD file before wrapping and after wrapping to compare the difference. Now, the wrapped DCD files are ready for analysis. Type the following command in the terminal to measure the charge of the DNA origami and its environment and save the output to **sim_Charge.dat**.

SHELL> **sh measureCharge.sh**

In the output file (**sim_Charge.dat)**, the first column is the simulation time in nanoseconds, and the second column is the charge due to all atoms within 2 nm of the DNA atoms in the units of the elementary charge, the charge of a proton. If you plot the first column as the *x*-axis and the second column as the *y*-axis, the graph should look like the one in Fig. 9. The gray trace is the raw data. The blue trace is the running average obtained using a 0.5 ns window.

5. **Chickenwire representation**. DNA origami objects are complex macromolecules that consist of hundreds to thousands of nucleotides distributed over multiple DNA strands. The atomic representations commonly used to visualize the outcome of an MD simulation are sometimes too detailed, which can make it difficult to appreciate the global conformation of a DNA origami object. An alternative approach is to use the chickenwire representation [20], which can complement the atomic-level representations of the structures. In the chickenwire representation, a base pair is represented by a single point placed at its center of mass, and such points are connected if the two base pairs are stacked in a helix or linked by a crossover. Fig. 10 illustrates the outcome of each modeling procedure

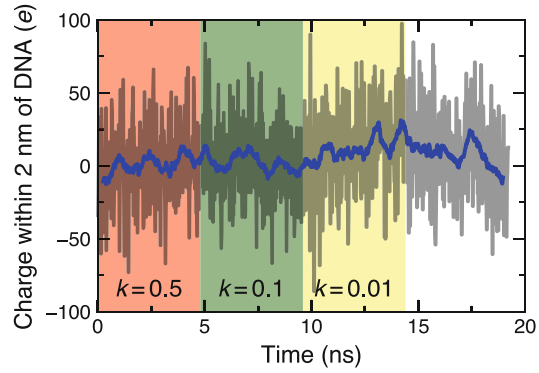

Fig. 9 The total charge of the DNA origami object and the surrounding electrolyte

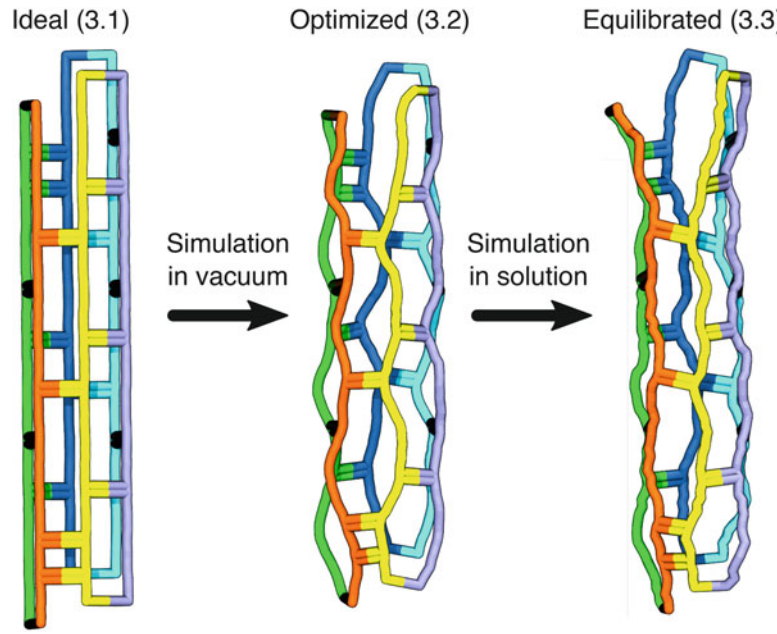

Fig. 10 Transformation of the hexagonal tube structure from its ideal design to an equilibrated conformation. Each of the three structures represents the outcome of the modeling tasks described in Subheadings 3.1, 3.2, and 3.3, respectively. To draw the chickenwire structures, Coloring Method "SegName" and Drawing Method "Licorice" with Bond Radius 2.5 were used

described in Subheadings 3.1, 3.2, and 3.3 using the chickenwire representation.

Here, as an example, we will convert the last snapshot of the equilibration simulation into the chickenwire representation. First, you will need to save the last frame of your equilibration simulation in the PDB format. The script **writePDB.tcl** will do this automatically, by loading **equil_k0.dcd** and saving the last frame as a PDB file:

SHELL> **vmd -dispdev text -e writePDB.tcl**

Note that conversion to a chickenwire representation applies only to atoms of DNA, which are selected in the script using:

[atomselect top nucleic]

Once the atomic PDB file **equil_k0.pdb** is written, one can convert it to a PDB file for chickenwire using the Perl script pdb2chickenwire.pl:

SHELL> **pdb2chickenwire.pl --ndx=../step2/chickenwire.for.make_ndx equil_k0.pdb > chickenwire.pdb**

Essentially, **pdb2chickenwire.pl** computes the center of mass of each base pair and writes the center of mass coordinates using a PDB file format. To compute the center of mass, the Perl script needs to know which two bases form a base pair. The list of base pairs is given in **chickenwire.for.make_ndx**, which is included in the archive from the ENRG MD server (*see* Subheading 3.2).

The PDB file produced by the Perl script contains position information required to draw a chickenwire representation but does not contain the connectivity information (base stacking and crossovers). For visualization using VMD, one needs to use the PSF file (**chickenwire.psf**) from the ENRG MD web server archive (*see* Subheading 3.2) that contains the necessary connectivity information. One can load the chickenwire PDB file into VMD using the following command in the VMD Tk console:

TKCON> **mol load psf ../step2/chickenwire.psf pdb chickenwire.pdb**

4 Notes

1. In the first few steps of equilibration, the system can be unstable. You should check the properties such as the total energy, temperature, and pressure, among others, to make sure there are no abnormal fluctuations. It is also recommended that you read your simulation logfile, which usually has the suffix .log. This file contains information on the above properties, as well as any warnings NAMD might have about your simulation. If your simulation ends unexpectedly, the logfile will also record the exact cause. The causes can vary from simply not finding one of your simulation input files, to a critical error in the simulation causing it to become unstable. Below are several possible errors you might encounter.
2. Some errors, including Rattle errors and "atoms moving too fast" occur when the atoms in your system are subject to unusually large forces, although they can occasionally occur otherwise. The logfile will identify atoms that are usually very close to the problem area, for example:

   ERROR: Constraint failure in RATTLE algorithm for atom 235!

   ERROR: Constraint failure; simulation has become unstable.

   These errors can occur when the system has not gone through enough steps of energy minimization. If the error occurs right

after minimization, ensure that the total energy in the system has stopped decreasing by the end of minimization, otherwise consider minimizing for longer (note, however, that the 4800 steps used in this guide is usually many times longer than necessary). If the problem persists, look closely at the initial structure using VMD, particularly around the affected atoms (for the example above, the selection text "same residue as pbwithin 8 of serial 235" would be useful). It is possible that some atoms may be placed in a configuration that minimization is unable to resolve. For example, problems usually arise when atoms are placed such that a bond pierces an aromatic ring or when two macromolecules are strongly overlapping. Remember to check for clashes with periodic images. If you encounter a problem like this you may need to rebuild the system. If the problem area is small, you may be able to remove the problem by selecting and moving atoms using the **moveby** command.

3. Equilibration in NPT allows the box size to fluctuate. This can cause errors if the box size shrinks or expands excessively along any of the system dimensions. This error is usually of the form below.

   FATAL ERROR: Periodic cell has become too small for original patch grid! Possible solutions are to restart from a recent checkpoint, increase margin, or disable useFlexibleCell for liquid simulations.

   First, make sure that the dimensions of the system in the configuration file match the physical dimensions of the system. Usually this error only occurs when the option **useFlexibleCell** is turned on. If this option is on, restarting the simulation from a recent checkpoint will likely resolve the issue. It might be necessary to disable flexible cells and to run the simulation in the NVT (constant volume) ensemble. The NVT ensemble is also recommended if you are running a simulation that includes externally applied forces or electric fields. Running these types of simulations in NPT guarantees this error will eventually occur.

4. It is possible that there can be insufficient water molecules in a simulation system, which will result in vacuum bubbles during equilibration. There are several solutions for this. You can resolvate after equilibration, placing additional water molecules inside the bubbles. You can also run your simulation in NPT with the DNA position fixed, allowing the box size to fluctuate until it reaches a value appropriate for the amount of water molecules in the system. As the latter solution does not involve the placement of additional water molecules, it is the better approach of the two.

Sometimes, the bubbles are large enough that their removal would cause an abrupt change in the box size, resulting in unstable MD simulations. In this case, increasing **langevinPistonPeriod** and **langevinPistonDecay** by a factor of 10 can be helpful. By changing these options, the box size is less responsive to the internal pressure, making the MD simulation more stable. After the box size becomes stable, those parameter values should be reverted to their original values.

References

1. Seeman NC (2007) An overview of structural DNA nanotechnology. Mol Biotechnol 37:246–257. https://doi.org/10.1007/s12033-007-0059-4
2. Pinheiro AV, Han D, Shih WM, Yan H (2011) Challenges and opportunities for structural DNA nanotechnology. Nat Nanotechnol 6:763–772. https://doi.org/10.1038/nnano.2011.187
3. Rothemund PWK (2006) Folding DNA to create nanoscale shapes and patterns. Nature 440:297–302. https://doi.org/10.1038/nature04586
4. Douglas SM, Dietz H, Liedl T et al (2009) Self-assembly of DNA into nanoscale three-dimensional shapes. Nature 459:414–418. https://doi.org/10.1038/nature08016
5. Dietz H, Douglas SM, Shih WM (2009) Folding DNA into twisted and curved nanoscale shapes. Science 325:725–730. https://doi.org/10.1126/science.1174251
6. Han D, Pal S, Nangreave J et al (2011) DNA origami with complex curvatures in three-dimensional space. Science 332:342–346. https://doi.org/10.1126/science.1202998
7. Zadegan RM, Jepsen MDE, Thomsen KE et al (2012) Construction of a 4 zeptoliters switchable 3D DNA box origami. ACS Nano 6:10050–10053. https://doi.org/10.1021/nn303767b
8. Andersen ES, Dong M, Nielsen MM et al (2009) Self-assembly of a nanoscale DNA box with a controllable lid. Nature 459:73–76. https://doi.org/10.1038/nature07971
9. Liedl T, Högberg B, Tytell J et al (2010) Self-assembly of three-dimensional prestressed tensegrity structures from DNA. Nat Nanotechnol 5:520–524. https://doi.org/10.1038/nnano.2010.107
10. Langecker M, Arnaut V, Martin TG et al (2012) Synthetic lipid membrane channels formed by designed DNA nanostructures. Science 338:932–936. https://doi.org/10.1126/science.1225624
11. Liu S, Su W, Li Z, Ding X (2015) Electrochemical detection of lung cancer specific microRNAs using 3D DNA origami nanostructures. Biosens Bioelectron 71:57–61. https://doi.org/10.1016/j.bios.2015.04.006
12. Nickels PC, Wünsch B, Holzmeister P et al (2016) Molecular force spectroscopy with a DNA origami-based nanoscopic force clamp. Science 354:305–307. https://doi.org/10.1126/science.aah5974
13. Schmied JJ, Forthmann C, Pibiri E, Lalkens B (2013) Supporting information for DNA origami nanopillars as standards for three-dimensional superresolution microscopy. Nano Lett 13:781–785. https://doi.org/10.1021/nl304492y
14. Thacker VV, Herrmann LO, Sigle DO et al (2014) DNA origami based assembly of gold nanoparticle dimers for surface-enhanced Raman scattering. Nat Commun 13(5):3448. https://doi.org/10.1038/ncomms4448
15. Kuzyk A, Yang Y, Duan X et al (2016) A light-driven three-dimensional plasmonic nanosystem that translates molecular motion into reversible chiroptical function. Nat Commun 7:10591. https://doi.org/10.1038/ncomms10591
16. Linko V, Eerikäinen M, Kostiainen MA (2015) A modular DNA origami-based enzyme cascade nanoreactor. Chem Commun 51:5351–5354. https://doi.org/10.1039/C4CC08472A
17. Liu M, Fu J, Hejesen C et al (2013) A DNA tweezer-actuated enzyme nanoreactor. Nat Commun 4:2127. https://doi.org/10.1038/ncomms3127
18. Williams S, Lund K, Lin C et al (2009) Tiamat: a three-dimensional editing tool for complex DNA structures. In: Goel A, Simmel FC, Sos'ik P (eds) DNA 2008: DNA Computing, pp 90–101. Springer, Berlin, Heidelberg. https://doi.org/10.1007/978-3-642-03076-5_8

19. Douglas SM, Marblestone AH, Teerapittayanon S et al (2009) Rapid prototyping of 3D DNA-origami shapes with caDNAno. Nucleic Acids Res 37:5001–5006. https://doi.org/10.1093/nar/gkp436
20. Bai X-c, Martin TG, Scheres SHW, Dietz H (2012) Cryo-EM structure of a 3D DNA-origami object. Proc Natl Acad Sci U S A 109:20012–20017. https://doi.org/10.1073/pnas.1215713109
21. Kim DN, Kilchherr F, Dietz H, Bathe M (2012) Quantitative prediction of 3D solution shape and flexibility of nucleic acid nanostructures. Nucleic Acids Res 40:2862–2868. https://doi.org/10.1093/nar/gkr1173
22. Pan K, Kim D-N, Zhang F et al (2014) Lattice-free prediction of three-dimensional structure of programmed DNA assemblies. Nat Commun 5:5578. https://doi.org/10.1038/ncomms6578
23. Sedeh RS, Pan K, Adendorff MR et al (2016) Computing nonequilibrium conformational dynamics of structured nucleic acid assemblies. J Chem Theory Comput 12:261–273. https://doi.org/10.1021/acs.jctc.5b00965
24. Doye JPK, Ouldridge TE, Louis AA et al (2013) Coarse-graining DNA for simulations of DNA nanotechnology. Phys Chem Chem Phys 15:20395. https://doi.org/10.1039/c3cp53545b
25. Snodin BEK, Romano F, Rovigatti L et al (2016) Direct simulation of the self-assembly of a small DNA origami. ACS Nano 10:1724–1737. https://doi.org/10.1021/acsnano.5b05865
26. Yoo J, Aksimentiev A (2013) In situ structure and dynamics of DNA origami determined through molecular dynamics simulations. Proc Natl Acad Sci U S A 110:20099–20104. https://doi.org/10.1073/pnas.1316521110
27. Li C-Y, Hemmig EA, Kong J et al (2015) Ionic conductivity, structural deformation, and programmable anisotropy of dna origami in electric field. ACS Nano 9:1420–1433. https://doi.org/10.1021/nn505825z
28. Slone SM, Li C-Y, Yoo J, Aksimentiev A (2016) Molecular mechanics of DNA bricks: in situ structure, mechanical properties and ionic conductivity. New J Phys 18:55012. https://doi.org/10.1088/1367-2630/18/5/055012
29. Göpfrich K, Li C-Y, Mames I et al (2016) Ion channels made from a single membrane-spanning dna duplex. Nano Lett 16:4665–4669. https://doi.org/10.1021/acs.nanolett.6b02039
30. Göpfrich K, Li CY, Ricci M et al (2016) Large-conductance transmembrane porin made from DNA origami. ACS Nano 10:8207–8214. https://doi.org/10.1021/acsnano.6b03759
31. Maffeo C, Yoo J, Aksimentiev A (2016) De novo reconstruction of DNA origami structures through atomistic molecular dynamics simulation. Nucleic Acids Res 44:3013–3019. https://doi.org/10.1093/nar/gkw155
32. Phillips JC, Braun R, Wang W et al (2005) Scalable molecular dynamics with NAMD. J Comput Chem 26:1781–1802. https://doi.org/10.1002/jcc.20289
33. Humphrey W, Dalke A, Schulten K (1996) VMD: visual molecular dynamics. J Mol Graph 14:33–38. https://doi.org/10.1016/0263-7855(96)00018-5
34. VMD user guide. http://www.ks.uiuc.edu/Research/vmd/current/ug/ug.html
35. VMD tutorial. http://www.ks.uiuc.edu/Training/Tutorials/vmd/tutorialhtml/index.html
36. NAMD user guide. http://www.ks.uiuc.edu/Research/namd/current/ug/
37. NAMD tutorial. http://www.ks.uiuc.edu/Training/Tutorials/namd/namd-tutorial-unix-html/index.html
38. Yoo J, Aksimentiev A (2012) Improved parametrization of Li^+, Na^+, K^+, and Mg^{2+} ions for all-atom molecular dynamics simulations of nucleic acid systems. J Phys Chem Lett 3:45–50. https://doi.org/10.1021/jz201501a
39. Yoo J, Aksimentiev A (2012) Competitive binding of cations to duplex DNA revealed through molecular dynamics simulations. J Phys Chem B 116:12946–12954. https://doi.org/10.1021/jp306598y
40. Yoo J, Aksimentiev A (2016) The structure and intermolecular forces of DNA condensates. Nucleic Acids Res 44:2036–2046. https://doi.org/10.1093/nar/gkw081
41. Yoo J, Aksimentiev A (2015) Molecular dynamics of membrane-spanning DNA channels: conductance mechanism, electro-osmotic transport, and mechanical gating. J Phys Chem Lett 6:4680–4687. https://doi.org/10.1021/acs.jpclett.5b01964

Chapter 16

Single-Molecule Patterning via DNA Nanostructure Assembly: A Reusable Platform

Da Huang, Mark Freeley, and Matteo Palma

Abstract

Here we describe a facile strategy of general applicability for controlling the immobilization of individual nanomoieties on nanopatterned surfaces with single-molecule control. We combine the ability of DNA nanostructures as programmable platforms, with a one-step Focused Ion Beam nanopatterning, to demonstrate the controlled immobilization of DNA origami functionalized with individual quantum dots (QDs) at predesigned positions on glass coverslips and silicon substrates. Remarkably, the platform developed is reusable after a simple cleaning process, and can be designed to display different geometrical arrangements.

Key words DNA origami, Nanopatterning, Nanotechnology, FIB, AFM, Fluorescence microscopy

1 Introduction

The controlled organization of individual molecules and nanostructures with nanoscale accuracy is of great importance in the investigation of single-molecule events in biological and chemical assays, as well as for the fabrication of the next generation optoelectronic devices [1–4]. A key requirement for such applications is the controlled organization of single molecules and nanomoieties from solution to surfaces. In this regard, the precise patterning of individual molecules into hierarchical structures has attracted substantial research interest in recent years. Lithographic nanopatterning has been employed in the formation of biomolecular arrays, of oligonucleotides and proteins [5–10], as well as for the controlled organization of nanoparticles [11–15]. Additionally, DNA has commonly been used as a single-molecule scaffold [16–18]. Also for the assembly of nanoparticles and nanocrystals into organized hierarchical structures [19–26].

In this chapter, we present a method of general applicability for the controlled assembly of individual functional nanomoieties in ordered arrays. As a proof of concept, we describe the placement of

Giampaolo Zuccheri (ed.), *DNA Nanotechnology: Methods and Protocols*, Methods in Molecular Biology, vol. 1811, https://doi.org/10.1007/978-1-4939-8582-1_16, © Springer Science+Business Media, LLC, part of Springer Nature 2018

single QDs within a nanopatterned substrate [27]. Our strategy combines the programming ability of DNA as a scaffolding material [28–32], with a one-step lithographic process.

First, the nanopatterning process is described as using Focused Ion Beam (FIB) to produce patterned substrates for subsequent DNA controlled immobilization. This one-step ion-beam procedure creates nanoaperture arrays on glass coverslips or silicon substrates coated with gold. The strategy avoids the use of resist polymers, and further allows the substrate to be reusable after a simple cleaning procedure. The shape, size, and geometrical arrangement of the nanoapertures can be easily tailored to meet different requirements.

The apertures in the patterned substrate provide functional spaces in which DNA nanostructures can be covalently tethered [33]. The DNA origami is designed with amine anchoring groups, which react with carboxyl-terminated silanes on the surface of the substrates. DNA nanostructures are designed to exhibit one, two, or three QDs, conjugated via biotin–streptavidin interactions. The arrays are then characterized by atomic force microscopy (AFM) and fluorescence microscopy.

2 Materials

2.1 FIB Nanopattern Fabrication

In our Laboratory, we have employed a Thermal Evaporator for metal deposition, and FEI™ Quanta™ 3D FEG Scanning Electron Microscope (SEM) and Focused Ion Beam (FIB) system for FIB nanopatterning.

1. Glass coverslips, Ø 13 mm, No. 0 (Thermo Fisher).
2. Silicon substrates (InterQuest), cut into 10 mm × 10 mm square slides.
3. Piranha solution: in a clean and dry glass container, slowly add 30% H_2O_2 to concentrated H_2SO_4 (3:1 v/v conc. H_2SO_4:30% H_2O_2). Expect the solution to become extremely hot up to a boil (risk of splashing!). Batches of over 100 ml require cooling in an ice bath when mixed. *WARNING*: piranha solution reacts violently with organic materials and should be handled with extreme caution. Wear safety goggles, appropriate gloves, and acid resistant apron over a lab coat. Always handle piranha solution under a fume hood. Prepare only as much as is needed; do NOT store any piranha solution or hold it in closed container.
4. 100% ethanol.
5. Deionized (DI) Millipore water (resistivity of 18 MΩ cm).
6. Teflon mini-rack (Invitrogen).

7. Gold (Au), 1.0 mm wire, 99.999% purity.
8. Chromium (Cr), grit, 99.95% coating quality.
9. Diamond tipped pen.
10. PELCO Tabs™, Carbon Conductive Tabs, 12 mm OD (Ted Pella).
11. 3M™ Copper Conductive Tape, Single Adhesive Surface (Ted Pella).
12. Standard SEM Pin Stub Mount, Ø 12.7 mm × 8 mm pin height (Ted Pella).
13. Tick tweezers, stainless steel.

2.2 Preparation of Origami and Functionalization of Nanopatterned Surfaces

1. 50× Tris–Acetate-EDTA buffer (TAE): 2 M Tris–Acetate, 0.05 M EDTA, pH 8.0. Store at room temperature.
2. TAEMg buffer: 1× TAE buffer, 12.5 mM $MgCl_2$.
3. TM buffer: 5 mM Tris buffer (pH 8.2 with HCl), 30 mM $MgCl_2$.
4. TMC buffer: TM buffer with 0.6 mM carboxyethylsilanetriol.
5. MOPSM buffer: MOPS buffer (10 mM; pH 8.1), 30 mM $MgCl_2$.
6. Activating solution: 50 mM EDC (1-ethyl-3-(3-dimethylaminopropyl)-carbodiimide, 100 mM sulfo-NHS (*N*-hydroxysulfosuccinimide) in MOPSM buffer.
7. M13mp18 single-stranded DNA, 1.0 μg/μL. Store at −20 °C.
8. Oligonucleotides: 220 staple strands (include modified strands), *see* Tables 1 and 2 for the list of unmodified and modified sequences, store at −20 °C.
9. Qdot® 605 Streptavidin Conjugate (Thermo Fisher), store at 4 °C, do not allow to freeze.
10. Amicon® Ultra-0.5 ml Centrifugal Filters, 100 kDa MWCO (Millipore).
11. Dialysis membrane (25 nm pore size).
12. Muscovite mica sheets (Agar Scientific), freshly cleaved immediately before use.
13. PBS (phosphate buffered saline): 2.7 mM potassium chloride, 0.14 M sodium chloride, 1.5 mM potassium phosphate, and 8 mM sodium phosphate, pH 7.4.
14. Parafilm.
15. 6-well plates.
16. Benchtop ultrasonic cleaner.
17. A plasma cleaner (Harrick PDG-32G-2 or analogous).

Table 1
List of modified staple strands (DNA origami strands)

Oligo name	Sequence
Biotin-t5s8g	ACAAGAAAGCAAGCAAATCAGATAACAGCCATATTATTTATT-Biotin
Biotin-t5s18g	CCAAGCGCAGGCGCATAGGCTGGCAGAACTGGCTCATTATTT-Biotin
Biotin-t5s28g	TTAATGAAGTTTGATGGTGGTTCCGAGGTGCCGTAAAGCATT-Biotin
Amino-t1s2i	CCTTTTTTCATTTAACAATTTCATAGGATTAGTT-Amino
Amino-t1s12i	AGGGATAGCTCAGAGCCACCACCCCATGTCAATT-Amino
Amino-t1s22i	CGCGTCTGATAGGAACGCCATCAACTTTTACATT-Amino
Amino-t2s3g	TTTGATGATTAAGAGGCTGAGACTTGCTCAGTACCAGGCGTT-Amino
Amino-t2s13g	ACAGTCAAAGAGAATCGATGAACGACCCCGGTTGATAATCTT-Amino
Amino-ti2s13g	AGACGTTACCATGTACCGTAACACCCCTCAGAACCGCCACTT-Amino
Amino-t2s23g	AGAGTCAAAAATCAATATATGTGATGAAACAAACATCAAGTT-Amino
Amino-ti2s23g	TGGCAATTTTTAACGTCAGATGAAAACAATAACGGATTCGTT-Amino
Amino-tj2s23g	GTAACCGTCTTTCATCAACATTAAAATTTTTGTTAAATCATT-Amino
Amino-t4s3g	TTTAACGGTTCGGAACCTATTATTAGGGTTGATATAAGTATT-Amino
Amino-t4s13g	ACATAGCGCTGTAAATCGTCGCTATTCATTTCAATTACCTTT-Amino
Amino-ti4s13g	AGCGTAACTACAAACTACAACGCCTATCACCGTACTCAGGTT-Amino
Amino-t4s23g	CGTTCTAGTCAGGTCATTGCCTGACAGGAAGATTGTATAATT-Amino
Amino-ti4s23g	GATTATACACAGAAATAAAGAAATACCAAGTTACAAAATCTT-Amino
Amino-tj4s23g	GGATAGGTACCCGTCGGATTCTCCTAAACGTTAATATTTTTT-Amino

2.3 Atomic Force Microscopy

In our laboratory, Atomic Force Microscopy (AFM, Bruker Dimension Icon) was performed using the ScanAsyst™ mode.

1. Compressed air.
2. ScanAsyst-Air probes (silicon tip on Nitride lever, f0: 70 kHz, k: 0.4 N/m) (Bruker, USA).

2.4 Fluorescence Microscopy

Confocal laser scanning microscopy (CLSM) was performed on an inverted microscopy, Leica TCS SP5 equipped with an HCX PL APO lambda blue 63×/1.4 oil objective lens.

1. Microscope Slides, 1.2–1.5 mm thick.
2. Fingernail polish.

Table 2
List of unmodified staple strands (DNA origami strands)

Oligo name	Sequence
t1ls18h	AATACTGCGGAATCGTAGGGGGTAATAGTAAAATGTTTAGACT
t1ls28h	TCTTTGATTAGTAATAGTCTGTCCATCACGCAAATTAACCGTT
t1ls8h	CAGAAGGAAACCGAGGTTTTTAAGAAAAGTAAGCAGATAGCCG
t1s12i	TCATATGTGTAATCGTAAAACTAGTCATTTTC
t1s14i	GTGAGAAAATGTGTAGGTAAAGATACAACTTT
t1s16i	GGCATCAAATTTGGGGCGCGAGCTAGTTAAAG
t1s18i	TTCGAGCTAAGACTTCAAATATCGGGAACGAG
t1s22i	TCGGGAGATATACAGTAACAGTACAAATAATT
t1s24i	CCTGATTAAAGGAGCGGAATTATCTCGGCCTC
t1s26i	GCAAATCACCTCAATCAATATCTGCAGGTCGA
t1s28i	CGACCAGTACATTGGCAGATTCACCTGATTGC
t1s2i	CGGGGTTTCCTCAAGAGAAGGATTTTGAATTA
t1s4i	AGCGTCATGTCTCTGAATTTACCGACTACCTT
t1s6i	TTCATAATCCCCTTATTAGCGTTTTTCTTACC
t1s8i	ATGGTTTATGTCACAATCAATAGATATTAAAC
t2s11g	AGAAAAGCCCCAAAAAGAGTCTGGAGCAAACAATCACCAT
t2s13g	ACAGTCAAAGAGAATCGATGAACGACCCCGGTTGATAATC
t2s15f	ATAGTAGTATGCAATGCCTGAGTAGGCCGGAG
t2s17f	AACCAGACGTTTAGCTATATTTTCTTCTACTA
t2s1g	GATAAGTGCCGTCGAGCTGAAACATGAAAGTATACAGGAG
t2s21g	CCTGATTGCTTTGAATTGCGTAGATTTTCAGGCATCAATA
t2s25f	AAGGAATTACAAAGAAACCACCAGTCAGATGA
t2s27f	GGACATTCACCTCAAATATCAAACACAGTTGA
t2s5f	CCGGAACCCAGAATGGAAAGCGCAACATGGCT
t2s7f	AAAGACAACATTTTCGGTCATAGCCAAAATCA
t3s10g	GTCAGAGGGTAATTGATGGCAACATATAAAAGCGATTGAG
t3s14e	CAATATGACCCTCATATATTTTAAAGCATTAA
t3s16e	CATCCAATAAATGGTCAATAACCTCGGAAGCA
t3s18g	AACTCCAAGATTGCATCAAAAAGATAATGCAGATACATAA
t3s20g	CGCCAAAAGGAATTACAGTCAGAAGCAAAGCGCAGGTCAG
t3s24e	TAATCCTGATTATCATTTTGCGGAGAGGAAGG

(continued)

Table 2
(continued)

Oligo name	Sequence
t3s26e	TTATCTAAAGCATCACCTTGCTGATGGCCAAC
t3s28g	AGAGATAGTTTGACGCTCAATCGTACGTGCTTTCCTCGTT
t3s30g	AGAATCAGAGCGGGAGATGGAAATACCTACATAACCCTTC
t3s4e	TGTACTGGAAATCCTCATTAAAGCAGAGCCAC
t3s6e	CACCGGAAAGCGCGTTTTCATCGGAAGGGCGA
t3s8g	CATTCAACAAACGCAAAGACACCAGAACACCCTGAACAAA
t4s11g	GCAAATATTTAAATTGAGATCTACAAAGGCTACTGATAAA
t4s15f	CAGGCAAGATAAAAATTTTTAGAATATTCAAC
t4s17f	GATTAGAGATTAGATACATTTCGCAAATCATA
t4s1g	TAGCCCGGAATAGGTGAATGCCCCCTGCCTATGGTCAGTG
t4s21g	GCGCAGAGGCGAATTAATTATTTGCACGTAAATTCTGAAT
t4s25f	TAGGAGCATAAAAGTTTGAGTAACATTGTTTG
t4s27f	TGACCTGACAAATGAAAAATCTAAAATATCTT
t4s5f	CTCAGAGCATATTCACAAACAAATTAATAAGT
t4s7f	GGAGGGAATTTAGCGTCAGACTGTCCGCCTCC
t5s10g	GATAACCCACAAGAATGTTAGCAAACGTAGAAAATTATTC
t5s14e	TTAATGCCTTATTTCAACGCAAGGGCAAAGAA
t5s16e	TTAGCAAATAGATTTAGTTTGACCAGTACCTT
t5s18g	TAATTGCTTTACCCTGACTATTATGAGGCATAGTAAGAGC
t5s20g	AACACTATCATAACCCATCAAAAATCAGGTCTCCTTTTGA
t5s24e	AATGGAAGCGAACGTTATTAATTTCTAACAAC
t5s26e	TAATAGATCGCTGAGAGCCAGCAGAAGCGTAA
t5s28g	GAATACGTAACAGGAAAAACGCTCCTAAACAGGAGGCCGA
t5s30g	TTAAAGGGATTTTAGATACCGCCAGCCATTGCGGCACAGA
t5s4e	CCTTGAGTCAGACGATTGGCCTTGCGCCACCC
t5s6e	TCAGAACCCAGAATCAAGTTTGCCGGTAAATA
t5s8g	TTGACGGAAATACATACATAAAGGGCGCTAATATCAGAGA
t6s15g	ATAAAGCCTTTGCGGGAGAAGCCTGGAGAGGGTAG
t6s17f	TAAGAGGTCAATTCTGCGAACGAGATTAAGCA
t6s25g	TCAATAGATATTAAATCCTTTGCCGGTTAGAACCT
t6s27f	CAATATTTGCCTGCAACAGTGCCATAGAGCCG

(continued)

Table 2
(continued)

Oligo name	Sequence
t6s5g	CAGAGCCAGGAGGTTGAGGCAGGTAACAGTGCCCG
t6s7f	ATTAAAGGCCGTAATCAGTAGCGAGCCACCCT
t7s10g	ATAAGAGCAAGAAACATGGCATGATTAAGACTCCGACTTG
t7s14e	ATGACCCTGTAATACTTCAGAGCA
t7s16e	TAAAGCTATATAACAGTTGATTCCCATTTTTG
t7s18g	CGGATGGCACGAGAATGACCATAATCGTTTACCAGACGAC
t7s20g	GATAAAAACCAAAATATTAAACAGTTCAGAAATTAGAGCT
t7s24e	ACAATTCGACAACTCGTAATACAT
t7s26e	TTGAGGATGGTCAGTATTAACACCTTGAATGG
t7s28g	CTATTAGTATATCCAGAACAATATCAGGAACGGTACGCCA
t7s30g	GAATCCTGAGAAGTGTATCGGCCTTGCTGGTACTTTAATG
t7s4e	GCCGCCAGCATTGACACCACCCTC
t7s6e	AGAGCCGCACCATCGATAGCAGCATGAATTAT
t7s8g	CACCGTCACCTTATTACGCAGTATTGAGTTAAGCCCAATA
t8s17g	TAATTGCTTGGAAGTTTCATTCCAAATCGGTTGTA
t8s27g	CGCGAACTAAAACAGAGGTGAGGCTTAGAAGTATT
t8s7g	AGCCATTTAAACGTCACCAATGAACACCAGAACCA
t9s10h	TATCTTACCGAAGCCCAAACGCAATAATAACGAAAATCACCAG
t9s16e	ACTAAAGTACGGTGTCGAATATAA
t9s18g	TGCTGTAGATCCCCCTCAAATGCTGCGAGAGGCTTTTGCA
t9s20h	AAAGAAGTTTTGCCAGCATAAATATTCATTGACTCAACATGTT
t9s26e	ACCACCAGCAGAAGATGATAGCCC
t9s28g	TAAAACATTAGAAGAACTCAAACTTTTTATAATCAGTGAG
t9s30h	GCCACCGAGTAAAAGAACATCACTTGCCTGAGCGCCATTAAAA
t9s6e	CCATTAGCAAGGCCGGGGGAATTA
t9s8g	GAGCCAGCGAATACCCAAAAGAACATGAAATAGCAATAGC
t10s17h	ACCAACCTAAAAAATCAACGTAACAAATAAATTGGGCTTGAGA
t10s27h	AACTCACATTATTGAGTGTTGTTCCAGAAACCGTCTATCAGGG
t10s7h	ACGACAATAAATCCCGACTTGCGGGAGATCCTGAATCTTACCA
t12s19h	CCTGACGAGAAACACCAGAACGAGTAGGCTGCTCATTCAGTGA
t12s29h	ACGTGGACTCCAACGTCAAAGGGCGAATTTGGAACAAGAGTCC

(continued)

Table 2
(continued)

Oligo name	Sequence
t12s9h	TGCTATTTTGCACCCAGCTACAATTTTGTTTTGAAGCCTTAAA
t1s10e	AGAGAATAACATAAAAACAGGGAAGCGCATTA
t1s10g	AGAGAATAACATAAAAACAGGGAAGCGCATTA
t1s14e	ATTTTCTGTCAGCGGAGTGAGAATACCGATAT
t1s14i	CAACAGTTTATGGGATTTTGCTAATCAAAAGG
t1s16e	ATTCGGTCTGCGGGATCGTCACCCGAAATCCG
t1s16i	GCCGCTTTGCTGAGGCTTGCAGGGGAAAAGGT
t1s18g	CGACCTGCGGTCAATCATAAGGGAACGGAACAACATTATT
t1s18i	GCGCAGACTCCATGTTACTTAGCCCGTTTTAA
t1s20e	ACAGGTAGAAAGATTCATCAGTTGAGATTTAG
t1s20g	AGAGAATAACATAAAAACAGGGAAGCGCATTA
t1s24e	CAGTTTGACGCACTCCAGCCAGCTAAACGACG
t1s24i	AGGAAGATGGGGACGACGACAGTAATCATATT
t1s26e	GCCAGTGCGATCCCCGGGTACCGAGTTTTTCT
t1s26i	CTCTAGAGCAAGCTTGCATGCCTGGTCAGTTG
t1s28g	TTTCACCAGCCTGGCCCTGAGAGAAAGCCGGCGAACGTGG
t1s28i	CCTTCACCGTGAGACGGGCAACAGCAGTCACA
t1s30g	AGAGAATAACATAAAAACAGGGAAGCGCATTA
t1s30e	CGAGAAAGGAAGGGAAGCGTACTATGGTTGCT
t1s4e	TTATCAAACCGGCTTAGGTTGGGTAAGCCTGT
t1s4i	TTTAACCTATCATAGGTCTGAGAGTTCCAGTA
t1s6e	TTAGTATCGCCAACGCTCAACAGTCGGCTGTC
t1s6i	AGTATAAAATATGCGTTATACAAAGCCATCTT
t1s8g	TTTCCTTAGCACTCATCGAGAACAATAGCAGCCTTTACAG
t1s8i	CAAGTACCTCATTCCAAGAACGGGAAATTCAT
t2s11g	CCTCAGAACCGCCACCCAAGCCCAATAGGAACGTAAATGA
t2s15f	CACGCATAAGAAAGGAACAACTAAGTCTTTCC
t2s17f	ATTGTGTCTCAGCAGCGAAAGACACCATCGCC
t2s1g	AAAACAAAATTAATTAAATGGAAACAGTACATTAGTGAAT
t2s21g	GCTCATTTTTTAACCAGCCTTCCTGTAGCCAGGCATCTGC
t2s23g	GTAACCGTCTTTCATCAACATTAAAATTTTTGTTAAATCA

(continued)

Table 2
(continued)

Oligo name	Sequence
t2s25f	ACGTTGTATTCCGGCACCGCTTCTGGCGCATC
t2s27f	CCAGGGTGGCTCGAATTCGTAATCCAGTCACG
t2s5f	ACTAGAAATATATAACTATATGTACGCTGAGA
t2s7f	TCAATAATAGGGCTTAATTGAGAATCATAATT
t3s10g	AACGTCAAAAATGAAAAGCAAGCCGTTTTTATGAAACCAA
t3s14e	GTTTTGTCAGGAATTGCGAATAATCCGACAAT
t3s16e	GACAACAAGCATCGGAACGAGGGTGAGATTTG
t3s18g	TATCATCGTTGAAAGAGGACAGATGGAAGAAAAATCTACG
t3s20g	TTAATAAAACGAACTAACCGAACTGACCAACTCCTGATAA
t3s24e	TGTAGATGGGTGCCGGAAACCAGGAACGCCAG
t3s26e	GGTTTTCCATGGTCATAGCTGTTTGAGAGGCG
t3s28g	GTTTGCGTCACGCTGGTTTGCCCCAAGGGAGCCCCCGATT
t3s30g	TAGAGCTTGACGGGGAGTTGCAGCAAGCGGTCATTGGGCG
t3s4e	GATTAAGAAATGCTGATGCAAATCAGAATAAA
t3s6e	CACCGGAATCGCCATATTTAACAAAATTTACG
t3s8g	AGCATGTATTTCATCGTAGGAATCAAACGATTTTTTGTTT
t4s11g	AGGTTTAGTACCGCCATGAGTTTCGTCACCAGGATCTAAA
t4s15f	TAGTTGCGAATTTTTTCACGTTGATCATAGTT
t4s17f	GTACAACGAGCAACGGCTACAGAGGATACCGA
t4s1g	GAGCAAAAGAAGATGAGTGAATAACCTTGCTTATAGCTTA
t4s21g	GTTAAAATTCGCATTAATGTGAGCGAGTAACACACGTTGG
t4s25f	AGTTGGGTCAAAGCGCCATTCGCCCCGTAATG
t4s27f	CGCGCGGGCCTGTGTGAAATTGTTGGCGATTA
t4s3g	ACATAGCGCTGTAAATCGTCGCTATTCATTTCAATTACCT
t4s5f	GTTAAATACAATCGCAAGACAAAGCCTTGAAA
t4s7f	CCCATCCTCGCCAACATGTAATTTAATAAGGC
t5s10g	TCCCAATCCAAATAAGATTACCGCGCCCAATAAATAATAT
t5s16e	AACAGCTTGCTTTGAGGACTAAAGCGATTATA
t5s20g	ACCAGTCAGGACGTTGGAACGGTGTACAGACCGAAACAAA
t5s26e	TGCTGCAAATCCGCTCACAATTCCCAGCTGCA
t5s30g	CTAAATCGGAACCCTAAGCAGGCGAAAATCCTTCGGCCAA

(continued)

Table 2
(continued)

Oligo name	Sequence
t5s6e	GTGTGATAAGGCAGAGGCATTTTCAGTCCTGA
t6s13f	ACAGACAGCCCAAATCTCCAAAAAAAAATTTCTTA
t6s15c	CGAGGTGAGGCTCCAAAAGGAGCC
t6s17f	ACCCCCAGACTTTTTCATGAGGAACTTGCTTT
t6s23f	CGGCGGATTGAATTCAGGCTGCGCAACGGGGGATG
t6s25c	TGGCGAAATGTTGGGAAGGGCGAT
t6s27f	TGTCGTGCACACAACATACGAGCCACGCCAGC
t6s3f	TCCCTTAGAATAACGCGAGAAAACTTTTACCGACC
t6s5c	GTTTGAAATTCAAATATATTTTAG
t6s7f	AATAGATAGAGCCAGTAATAAGAGATTTAATG
t7s10g	GCCAGTTACAAAATAATAGAAGGCTTATCCGGTTATCAAC
t7s18g	AAAACACTTAATCTTGACAAGAACTTAATCATTGTGAATT
t7s20g	ACCTTATGCGATTTTATGACCTTCATCAAGAGCATCTTTG
t7s28g	TTCCAGTCCTTATAAATCAAAAGAGAACCATCACCCAAAT
t7s30g	CAAGTTTTTTGGGGTCGAAATCGGCAAAATCCGGGAAACC
t7s8g	GCGCCTGTTATTCTAAGAACGCGATTCCAGAGCCTAATTT
t8s15f	CGGTTTATCAGGTTTCCATTAAACGGGAATACACT
t8s17c	GGCAAAAGTAAAATACGTAATGCC
t8s25f	TCTTCGCTATTGGAAGCATAAAGTGTATGCCCGCT
t8s27c	GCGCTCACAAGCCTGGGGTGCCTA
t8s5f	TTCTGACCTAAAATATAAAGTACCGACTGCAGAAC
t8s7c	TCAGCTAAAAAAGGTAAAGTAATT
t9s10g	ACGCTAACGAGCGTCTGGCGTTTTAGCGAACCCAACATGT
t9s20g	TGGTTTAATTTCAACTCGGATATTCATTACCCACGAAAGA
t9s30g	CGATGGCCCACTACGTATAGCCCGAGATAGGGATTGCGTT
tsrem1	GCGCTTAATGCGCCGCTACAGGGC
t5s2et6s23c3T	TTAATTAATTTTTTACCATATCAAA
t7s4et8s25c2T	TTAATTTCATCTTAGACTTTACAA
t9s6et10s27c1T	CTGTCCAGACGTATACCGAACGA
t11s8et12s29c0T	TCAAGATTAGTGTAGCAATACT
t5s12et6s3c3T	TGTAGCATTCCTTTTATAAACAGTT

(continued)

Table 2
(continued)

Oligo name	Sequence
t7s14et8s5c2T	TTTAATTGTATTTCCACCAGAGCC
t9s16et10s7c1T	ACTACGAAGGCTTAGCACCATTA
t11s18et12s9c0T	ATAAGGCTTGCAACAAAGTTAC
t5s22et6s13c-T	GTGGGAACAAATTTCTATTTTTGAG
t7s24et8s15c2T	CGGTGCGGGCCTTCCAAAAACATT
t9s26et10s17c1T	ATGAGTGAGCTTTTAAATATGCA
t11s28et12s19c0T	ACTATTAAAGAGGATAGCGTCC

3 Methods

3.1 FIB Nanopattern Fabrication

3.1.1 Preparation and Cleaning

It is important to carry out proper cleaning procedures before moving to the surface patterning and chemical functionalization. Any contamination, even nanoscopic, not removed prior to patterning will result in defects on the final sample surface (*see* **Note 1**).

1. Place new glass coverslips or silicon substrates on the Teflon mini-rack and immerse the rack in piranha solution; let soak for 5 min (*see* **Note 2**).
2. Take the slides out of the piranha solution and immerse in DI water for 2 min.
3. Sonicate the slides in ethanol for 15 min.
4. Sonicate the slides in DI water for 15 min.
5. Blow dry with a stream of inert gas (Ar or N2) (*see* **Note 3**).
6. Place the slides in the plasma cleaner under high power for 5 min (*see* **Note 4**). It is now possible to proceed to metal deposition.

3.1.2 Metal Deposition

Cleanliness is of paramount importance here. All work should be performed avoiding any contaminants. Using high purity metal sources is crucial for the metal coating layer quality.

1. Preheat a hot plate to 180 °C and place the precleaned slides on a hot plate for 5 min to remove any adsorbed water.
2. Place the slides on the Thermal Evaporator holder with the cleaned sides facing down (*see* **Note 5**).
3. Evaporate a 1 nm adhesion layer of Cr. This is necessary for the Au to adhere to the glass/silicon surfaces.

4. Next, deposit a 3 nm thick layer of Au on top of the Cr layer (*see* **Note 6**).
5. Anneal the metal-coated coverslips on a hot plate at 300 °C for 1 h (*see* **Note 7**).

3.1.3 Ion-Beam Pattern Writing

A focused ion-beam writing technique uses a focused beam of ions to scan and pattern the sample surface. A very high electric field applied onto a liquid metal ion source (LMIS) generates ions, which are focused by electrostatic lenses. The ions hit the specimen surface and fabricate the surface as designed. We use FIB to fabricate nanoapertures arrays on the metal-coated substrates. The nanoarray we designed is 7 μm by 7 μm and consists of sixty-four 200 nm by 200 nm nanoapertures spaced 1 μm apart. This ensures that each individual aperture is optically resolvable and discrete, once functionalized and imaged via fluorescence microscopy (*see* **Note 8**). Figure 1a shows the FIB patterning process.

1. Use a diamond pen to scratch a visible mark on the sample slide; this will help track the location of the patterned area (*see* **Note 9**).
2. Attach the metal-coated slides (*see* Subheading 3.1.2) onto the specimen stub mount using a carbon conductive tab. Attach copper conductive tape over the slide surfaces and mount. Place the sample into the FIB system chamber and evacuate to working vacuum pressure (*see* **Note 10**).
3. Focus the sample in the electron beam channel and tilt the sample stage 52° to face the ion beam column. Focus again in the ion beam channel. Move the working area to the position of the marked area (*see* **Note 11**).
4. Import the preloaded patterns and start milling the surface, following the pattern by ion beam. Ion beam mill the surface under a 30 kV/50 pA condition. Set various milling depth parameters for covering all the different thickness of metal layer. Wait until the milling program is finished, then check the patterned surface under the electron beam channel (*see* **Note 12**).
5. Vent the vacuum and take the patterned slides out of the sample chamber. Carefully remove the slide from specimen stub mount and remove the carbon tab and the copper tape (*see* **Note 13**).

3.2 Preparation of DNA Origami and Functionalization of Nanopatterned Surfaces

A standard amide coupling is carried out to covalently immobilize DNA origami on the patterned area. Briefly, the DNA origami solution is cast on the patterned substrate in the presence of Mg^{2+} (to induce initial physisorption). A solution of carboxyethylsilane is then cast on the surface to form carboxylic terminating monolayers in the patterned nanoapertures and amide coupled to the amino

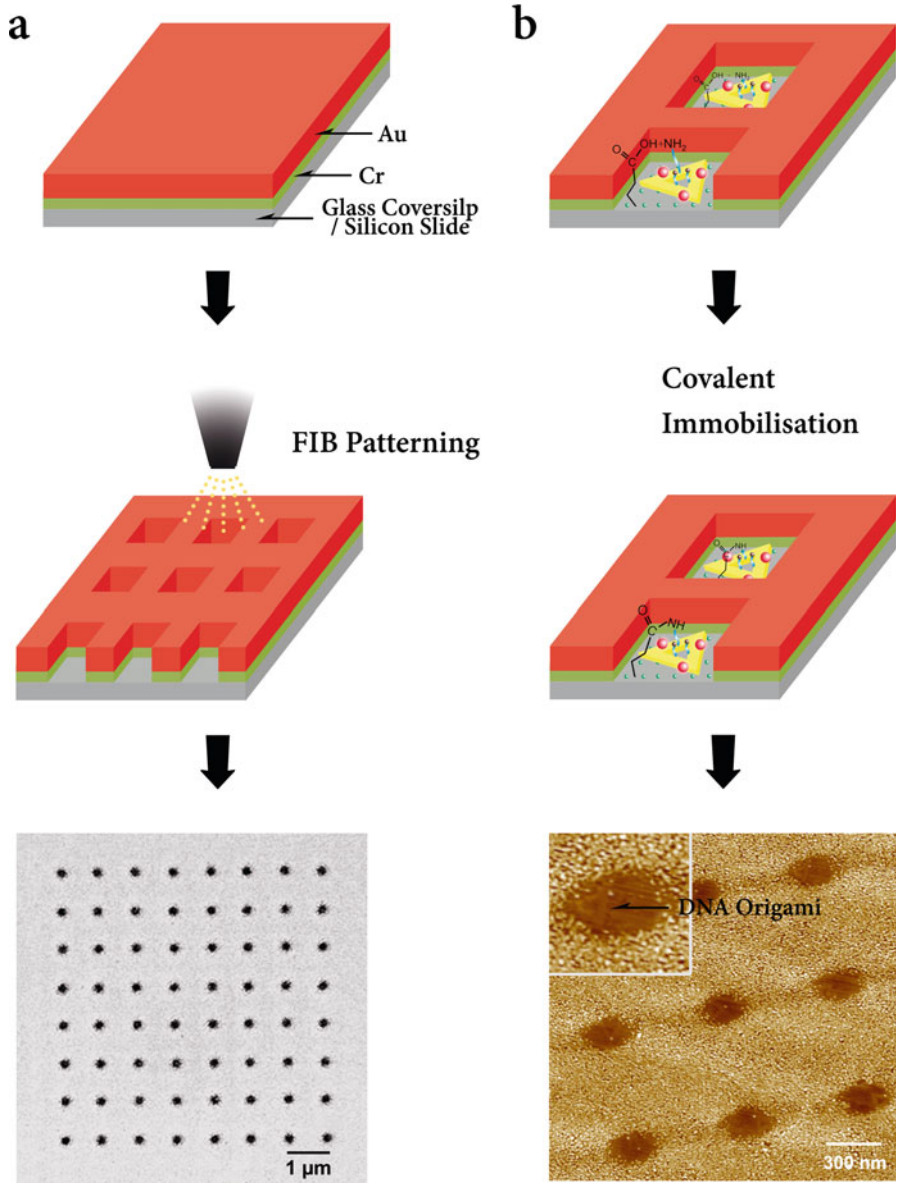

Fig. 1 Scheme of the FIB nanofabrication and DNA origami covalent immobilization. (**a**) FIB surface patterning scheme; (**b**) covalent immobilization scheme

anchors on DNA origami via the activating agents (NHS and EDC). Physisorbed DNA origami is washed away, while the covalently bound structures remain on the surface within the patterned apertures.

The DNA origami was designed with 15 amino anchors and 1, 2, or 3 sticky ends, binding to the QDs, so that the QD derivatization can be modulated (*see* Tables 1 and 2 for the DNA sequences).

3.2.1 Preparation of DNA Origami and Derivatization with QD

1. Combine 10 nM M13mp18 scaffold and 100 nM staple strands (*see* **Note 14**) in 100 μl of TAEMg buffer.
2. Heat the solution to 90 °C and cool it to room temperature at a rate of 0.2 °C per minute in a PCR thermocycler.
3. Purify the DNA origami from unincorporated staples with a Millipore Amicon Ultra 100 kDa spin column in a benchtop microcentrifuge by spinning at 15,000 × *g* for 2 min. Repeat the wash three times refilling the spin column with TAEMg buffer. Collect the retentate according to the manufacturer's instructions.
4. Adjust the concentration of the origami to 20 nM. Store at −20 °C if needed.
5. To functionalize the QDs, biotin-modified DNA complementary to the origami sticky ends was attached to streptavidin-functionalized QDs by combining at a 5:1 ratio (oligonucleotides–QD) and cooling down from 37 °C slowly for over 2 h.
6. Remove the excess free oligonucleotides by dialysis against TAEMg (with a 25 nm pore cellulose membrane).
7. Adjust the QD-DNA solution to 20 nM in TAEMg.
8. Combine 3 μl of 20 nM DNA origami solution and 3, 6, or 9 μl (for 1 QD, 2 QD, or 3 QD structures respectively) of 20 nM QD-DNA solution and make up to 60 μl with TAEMg. Heat this solution to 47 °C and cool slowly to room temperature in a PCR thermocycler to hybridize the QDs to the DNA origami. Store at 4 °C if needed.

3.2.2 Functionalization of Nanopatterned Surfaces with DNA Origami

1. Place the patterned substrates on a microscope slide with the pattern facing up. Place the microscope slide inside the chamber of an O_2/plasma cleaner for 5 min at high power to clean the substrates. Remove the cleaned substrates and place in a 6-well plate.
2. Dilute the QD-derivatized DNA origami to 1 nM in TM buffer and cast a 60 μl drop on the patterned substrate.
3. Roll up and wet a small piece of Kimwipes with DI water, then place it in the well with the substrate. Stretch Parafilm over the open 6-well plate and place the lid on top. Then place the 6-well plate on a shaker for 90 minutes at room temperature.
4. After incubation, wash the still wet substrates with the TM buffer by pipetting 60 μl of the buffer up and down several times, taking care not to touch the surface with the tip. Repeat the washing approach eight times.
5. Wash the substrate eight times with 60 μl of TMC buffer using the same method as in **step 4** above. Replace the Parafilm and place the 6-well plate on the shaker for 2 min.

6. Remove the 6-well plate from the shaker and wash the substrates with 60 µl of MOPSM buffer for six times, using the same washing method as **step 4** above.
7. Add 60 µl of activating solution to the substrate. (This will double the volume on the surface while halving the concentration of EDC and sulfo-NHS.) Mix the solution by pipetting several times up and down. Cover the 6-well plate again with Parafilm and place on the shaker for 10 min.
8. Remove the 6-well plate from the shaker and remove 60 µl of the liquid from the surface with a pipette and discard it. Wash the substrates for eight times with the MOPSM buffer, followed by eight washes with 100 µl PBS with 125 mM Na^+.
9. Wash the substrates with several ml of DI water from a wash bottle.
10. Blow the specimens dry with a gentle stream of nitrogen gas for AFM imaging or keep it dry for confocal imaging.

3.3 Atomic Force Microscopy

Atomic force microscopy (AFM) is used to investigate the surface geometry of nanofabricated apertures and the controlled placement of DNA origami. AFM can achieve a resolution down to the nanometer scale to reveal functionalized DNA origami structures and their immobilization in the patterned area. We obtain a close to complete immobilization of a single triangular DNA origami per aperture (with a 90% yield), rather than multiple (3%), or none (7%).

1. Blow the slide (with or without immobilized DNA origami) dry with a stream of inert gas (Ar or N2) and place the slide on the sample stage.
2. Use ScanAsyst-Air mode (Bruker, USA) with a ScanAsyst-Air probe to scan the slide surface. Focus on the pattern area around the diamond pen mark (*see* **Note 15**).
3. Zoom in to reveal the detailed structure of the nanoapertures and of the immobilized DNA origami (*see* Fig. 2).

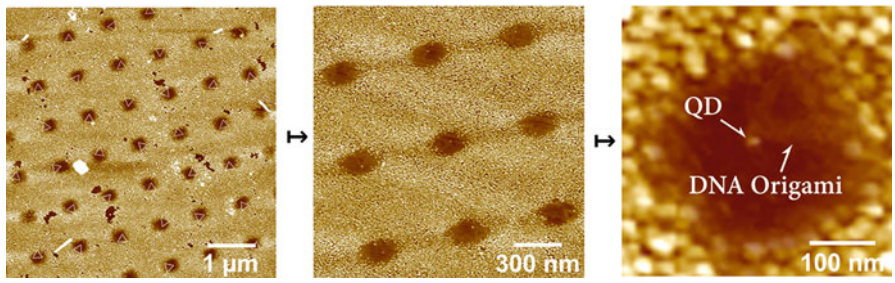

Fig. 2 AFM images of DNA origami immobilization in nanoapertures

3.4 Fluorescence Microscopy

Fluorescence microscopy is applied for further confirmation of the controlled immobilization of DNA origami. We verify the functionalized patterned coverslip based on the presence of Qdot-labeled DNA origami immobilized in the nanoapertures (*see* **Note 16**).

3.4.1 Sample Preparation

1. Keep the slide wet after the last step of surface functionalization (*see* Subheading 3.2, **step 10**). Wash with water and avoid drying out the sample), (*see* **Note 17**).
2. Place the coverslip face down on a glass microscope slide and form a liquid environment between the coverslip and the slide.
3. Seal the coverslip edge with fingernail polish (*see* **Note 18**).

3.4.2 Confocal Microscopy

An inverted confocal fluorescence microscope capable of epifluorescence microscopy is used to image the sample. Oil immersion lenses with 63× magnification are suitable for imaging the nanoarrays.

1. Find and focus on the pattern in white light.
2. Switch to the fluorescence channel (emission maxima of about 605 nm). Use live imaging to adjust the focus to reveal the fluorescent QD array (*see* **Note 19**).
3. Proceed to capture micrographs of the nanoarray (*see* Fig. 3).

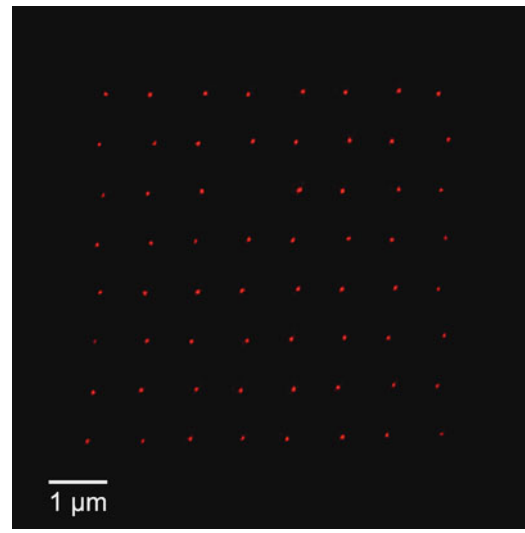

Fig. 3 Epifluorescence microscopy image of the nanopatterned Qdots-labeled DNA origami: excitation 550 nm, emission 568 nm. 8 × 8 dots array with 1 µm space between each dot

4 Notes

1. Make sure all glassware used is clean, i.e., washed with detergent, rinsed in DI water, rinsed with ethanol, and blown dry with a stream of inert gas (Ar or N_2).
2. Both glass coverslips and silicon substrates can be used in this strategy. The cleaning procedure remains the same. Using a Teflon mini-rack can help to easily transport substrates between different solutions, i.e., from piranha solution to DI water, from DI water to ethanol, etc.
3. When handling samples, especially when washing and drying with the use of tweezers, always make sure to rinse and blow dry toward the tweezers; this prevents the transfer of any contaminants from gloves and tweezers onto the samples.
4. Clean the slides immediately prior to the metal deposition; if it is allowed to sit in air, it will accumulate contaminants. It is recommended to keep and transfer slides within well plates sealed with Parafilm.
5. For glass coverslips (which are transparent, thus making it hard to judge which is the patterned side), use a diamond pen to mark the clean side of coverslips (when stored in a well-plate, the side that is face-up is the clean side). For silicon substrates, the shiny side is the clean side. These slides will be coated with the metal and used for further surface modification.
6. Place the thickness detector on a similar level as the sample substrates. This will help in accurately monitoring the metal evaporating process. It is recommended to verify this thickness via AFM analysis and to keep the metal layer thickness lower than 10 nm.
7. Annealing is essential for the metal layer, because it helps in forming a flat metal surface and reduces its roughness. Silicon slides may require a longer annealing time but typically need no more than 2 h. After annealing, the metal layer turns from a dark grey color to a light pink (on the glass coverslip).
8. The pattern size is designed based on the working condition of the FIB system. The scale can be increased either by increasing the number of nanoapertures or by importing a larger bitmap image (BMP) file. The aperture arrays can usually be visible in an optical microscope as dot arrays, or as fluorescent dots arrays under confocal microscopy once modified DNA nanostructures have been placed in the nanoapertures. AFM is the best method to characterize the structures in the nanoapertures.
9. The patterning is carried out close to the marking area. Because the nanoapertures are invisible to the eye, this will help in

finding the patterned area in the following AFM and fluorescence microscopy characterization.

10. Cut the carbon conductive tabs into small pieces (5 mm × 5 mm is suggested when using a Ø 13 mm coverslip or a 10 mm × 10 mm square silicon chip) and do not press too firmly when sticking the slides onto the stub mount. The use of the small area of tab will help in removing slides from SEM/-FIB stub mount after surface patterning without breaking the fragile coverslips. This will also help make it easier to clean the sticky residue on back of the slides. Using a thin copper conductive tape bridge between the substrate surfaces and the stub mount will help in evening out the charge on the sample surface, since the coverslip itself is not conductive. When applying FIB on the sample surfaces, we observe less charge migration or drift compared to not using a copper tape bridge.
11. It is recommended to focus on the diamond pencil scratched marking. Avoid focusing directly on the desired working area. The metal layer is very thin (less than 10 nm), so if the ion beam is applied upon the thin metal layer for too long, or too strongly during focusing, it will affect the surface integrity of the pattern. Because the patterned area will be close to the mark, focusing on the mark will bring in focus the working area as well.
12. The parameter settings of the milling program depend on the FIB system. In our FIB system, when applying milling parameters of 150 nm × 150 nm square, 5 nm depth (milled twice), we get approximately 200 nm × 200 nm apertures with 10 nm depth (which is enough to expose the glass/silicon surface and it is suitable for DNA origami placement). Milling twice ensures that the bottom of the apertures will be flat while avoiding any remnants of metal in the aperture.
13. Carefully remove the glass slide from the stub mount using tweezers and a scalpel to prevent the fragile substrate from breaking. If it is stuck too hard, heat up the slide and the stub mount to around 100 °C and peel with a scalpel. Use acetone to gently remove the remaining carbon tab on the back of slide.
14. See the used DNA sequences in Tables 1 and 2 of this chapter; slight variations of the origami assembly protocol can be read in Chapters 17 and 18 of this book.
15. First scan with a high speed (lower resolution) and a large area to locate the pattern area, then zoom in to the patterned area using 512 lines or higher resolution to reveal the detailed structure in the nanoapertures. A scan rate of 0.5–1 Hz is recommended, using 0.5 Hz can reduce scan error but with longer scanning time. Image contrast and height threshold

need to be adjusted to show the structure of the DNA origami clearly.

16. Only patterned glass coverslip samples can be used with confocal microscopy. Because silicon slides are not transparent, confocal microscopy cannot be used for further confirmation. As the same strategy is used on glass coverslip and silicon, and the confirmation of a successful array has already been achieved via AFM, once the confirmation from confocal microscopy on the coverslips is observed, we can also assume a successful immobilization on silicon substrates.
17. Streptavidin coated Qdots are attached to DNA origami via biotinylated sticky ends. Avoid drying out the substrate surface to keep the integrity of the biotin–streptavidin conjugation.
18. Fingernail polish is recommended in sealing the coverslips on the glass slides. Any other sealing glue can be used if it dries quickly and has good sealing properties.
19. Qdot® 605 Streptavidin Conjugate was used for labelling DNA origami. A maximum of 605 nm emission in the photodetector can be used to visualize the fluorescence signal. Nanoapertures can be seen under natural light channel because of the difference in transparency of the metal layer and the exposed glass surface. Once focused on the patterned area, the microscope can be switched to the fluorescence channel to see the fluorescence from the nanoarray.

Acknowledgments

D.H. is financially supported by the Chinese Scholarship Council. We further gratefully acknowledge financial support from Queen Mary University of London.

References

1. Ishijima A, Yanagida T (2001) Single molecule nanobioscience. Trends Biochem Sci 26 (7):438–444. https://doi.org/10.1016/S0968-0004(01)01860-6
2. Cordes T, Blum SA (2013) Opportunities and challenges in single-molecule and single-particle fluorescence microscopy for mechanistic studies of chemical reactions. Nat Chem 5 (12):993–999. https://doi.org/10.1038/nchem.1800
3. Moth-Poulsen K, Bjørnholm T (2010) From nanofabrication to self-fabrication – tailored chemistry for control of single molecule electronic devices. CHIMIA Int J Chem 64(6):404–408. https://doi.org/10.2533/chimia.2010.404
4. Palma M, Abramson JJ, Gorodetsky AA, Penzo E, Gonzalez RL Jr, Sheetz MP, Nuckolls C, Hone J, Wind SJ (2011) Selective biomolecular nanoarrays for parallel single-molecule investigations. J Am Chem Soc 133 (20):7656–7659. https://doi.org/10.1021/ja201031g
5. Noh H, Hung AM, Choi C, Lee JH, Kim JY, Jin S, Cha JN (2009) 50 nm DNA nanoarrays generated from uniform oligonucleotide films. ACS Nano 3(8):2376–2382. https://doi.org/10.1021/nn900559m

6. Gerdon AE, Oh SS, Hsieh K, Ke Y, Yan H, Soh HT (2009) Controlled delivery of DNA origami on patterned surfaces. Small 5 (17):1942–1946. https://doi.org/10.1002/smll.200900442
7. Schvartzman M, Palma M, Sable J, Abramson J, Hu X, Sheetz MP, Wind SJ (2011) Nanolithographic control of the spatial organization of cellular adhesion receptors at the single-molecule level. Nano Lett 11 (3):1306–1312. https://doi.org/10.1021/nl104378f
8. Kim JD, Ahn D-G, Oh J-W, Park W, Jung H (2008) Ribosome display and dip-pen nanolithography for the fabrication of protein Nanoarrays. Adv Mater 20(17):3349–3353. https://doi.org/10.1002/adma.200800027
9. Bulyk ML (2007) Protein binding microarrays for the characterization of DNA-protein interactions. Adv Biochem Eng Biotechnol 104:65–85. https://doi.org/10.1007/10_025
10. Demers LM, Ginger DS, Park SJ, Li Z, Chung SW, Mirkin CA (2002) Direct patterning of modified oligonucleotides on metals and insulators by dip-pen nanolithography. Science 296 (5574):1836–1838
11. Lalander CH, Zheng Y, Dhuey S, Cabrini S, Bach U (2010) DNA-directed self-assembly of gold nanoparticles onto nanopatterned surfaces: controlled placement of individual nanoparticles into regular arrays. ACS Nano 4 (10):6153–6161. https://doi.org/10.1021/nn101431k
12. Junkin M, Watson J, Geest J, Wong P (2009) Template-guided self-assembly of colloidal quantum dots using plasma lithography. Adv Mater 21(12):1247–1251. https://doi.org/10.1002/adma.200802122
13. Xie W, Gomes R, Aubert T, Bisschop S, Zhu Y, Hens Z, Brainis E, Van Thourhout D (2015) Nanoscale and single-dot patterning of colloidal quantum dots. Nano Lett 15 (11):7481–7487. https://doi.org/10.1021/acs.nanolett.5b03068
14. Wang CJ, Huang L, Parviz BA, Lin LY (2006) Subdiffraction photon guidance by quantum-dot cascades. Nano Lett 6(11):2549–2553
15. Abramson J, Palma M, Wind SJ, Hone J (2012) Quantum dot Nanoarrays: self-assembly with single-particle control and resolution. Adv Mater 24(16):2207–2211
16. Scheible MB, Pardatscher G, Kuzyk A, Simmel FC (2014) Single molecule characterization of DNA binding and strand displacement reactions on lithographic DNA origami microarrays. Nano Lett 14(3):1627–1633. https://doi.org/10.1021/nl500092j
17. Koirala D, Shrestha P, Emura T, Hidaka K, Mandal S, Endo M, Sugiyama H, Mao H (2014) Single-molecule mechanochemical sensing using DNA origami nanostructures. Angew Chem Int Ed 53(31):8137–8141. https://doi.org/10.1002/anie.201404043
18. Voigt NV, Torring T, Rotaru A, Jacobsen MF, Ravnsbaek JB, Subramani R, Mamdouh W, Kjems J, Mokhir A, Besenbacher F, Gothelf KV (2010) Single-molecule chemical reactions on DNA origami. Nat Nanotechnol 5 (3):200–203. https://doi.org/10.1038/nnano.2010.5
19. Sharma J, Chhabra R, Cheng A, Brownell J, Liu Y, Yan H (2009) Control of self-assembly of DNA tubules through integration of gold nanoparticles. Science 323(5910):112–116. https://doi.org/10.1126/science.1165831
20. Sharma J, Chhabra R, Liu Y, Ke Y, Yan H (2006) DNA-templated self-assembly of two-dimensional and periodical gold nanoparticle arrays. Angew Chem Int Ed Engl 45 (5):730–735. https://doi.org/10.1002/anie.200503208
21. Sharma J, Ke Y, Lin C, Chhabra R, Wang Q, Nangreave J, Liu Y, Yan H (2008) DNA-tile-directed self-assembly of quantum dots into two-dimensional nanopatterns. Angew Chem Int Ed 47(28):5157–5159. https://doi.org/10.1002/anie.200801485
22. Schreiber R, Do J, Roller EM, Zhang T, Schuller VJ, Nickels PC, Feldmann J, Liedl T (2014) Hierarchical assembly of metal nanoparticles, quantum dots and organic dyes using DNA origami scaffolds. Nat Nanotechnol 9 (1):74–78. https://doi.org/10.1038/nnano.2013.253
23. Ding B, Deng Z, Yan H, Cabrini S, Zuckermann RN, Bokor J (2010) Gold nanoparticle self-similar chain structure organized by DNA origami. J Am Chem Soc 132(10):3248–3249. https://doi.org/10.1021/ja9101198
24. Li Z, Chung SW, Nam JM, Ginger DS, Mirkin CA (2003) Living templates for the hierarchical assembly of gold nanoparticles. Angew Chem Int Ed Engl 42(20):2306–2309. https://doi.org/10.1002/anie.200351231
25. Macfarlane RJ, Lee B, Jones MR, Harris N, Schatz GC, Mirkin CA (2011) Nanoparticle superlattice engineering with DNA. Science 334(6053):204–208. https://doi.org/10.1126/science.1210493
26. Fu A, Micheel CM, Cha J, Chang H, Yang H, Alivisatos AP (2004) Discrete nanostructures

of quantum dots/au with DNA. J Am Chem Soc 126(35):10832–10833. https://doi.org/10.1021/ja046747x

27. Huang D, Freeley M, Palma M (2017) DNA-mediated patterning of single quantum dot Nanoarrays: a reusable platform for single-molecule control. Sci Rep 7:45591. https://doi.org/10.1038/srep45591
28. Hung AM, Micheel CM, Bozano LD, Osterbur LW, Wallraff GM, Cha JN (2010) Large-area spatially ordered arrays of gold nanoparticles directed by lithographically confined DNA origami. Nat Nanotechnol 5(2):121–126. https://doi.org/10.1038/Nnano.2009.450
29. Hung AM, Noh H, Cha JN (2010) Recent advances in DNA-based directed assembly on surfaces. Nanoscale 2(12):2530–2537. https://doi.org/10.1039/c0nr00430h
30. Zhang F, Nangreave J, Liu Y, Yan H (2014) Structural DNA nanotechnology: state of the art and future perspective. J Am Chem Soc 136 (32):11198–11211. https://doi.org/10.1021/ja505101a
31. Samanta A, Banerjee S, Liu Y (2015) DNA nanotechnology for nanophotonic applications. Nanoscale 7(6):2210–2220. https://doi.org/10.1039/c4nr06283c
32. Kumar A, Hwang JH, Kumar S, Nam JM (2013) Tuning and assembling metal nanostructures with DNA. Chem Commun 49 (26):2597–2609. https://doi.org/10.1039/c2cc37536b
33. Gopinath A, Rothemund PW (2014) Optimized assembly and covalent coupling of single-molecule DNA origami nanoarrays. ACS Nano 8(12):12030–12040. https://doi.org/10.1021/nn506014s

Chapter 17

Directed Protein Adsorption Through DNA Origami Masks

Saminathan Ramakrishnan, Guido Grundmeier, and Adrian Keller

Abstract

The DNA origami technique has made its way into various areas of nanotechnology, materials science, biophysics, and medicine. Among the many applications of DNA origami nanostructures, their use as masks for patterning of organic and inorganic materials by molecular lithography has received great attention. Here, we describe a protocol for the self-assembly of ordered monolayers of DNA origami nanostructures on mica surfaces and the subsequent fabrication of regular protein patterns over large surface areas via directed adsorption through the DNA origami mask. While the geometry of the pattern is determined by the shape of the DNA origami nanostructures, protein coverage inside the holes of the mask can be varied from single proteins to dense monolayers by adjusting the protein concentration and cationic strength of the adsorption buffer.

Key words DNA origami nanostructures, Self-assembly, Lithography masks, Molecular lithography, Protein patterning, Atomic force microscopy, Mica

1 Introduction

The DNA origami technique [1] enables the synthesis of molecular nanostructures with programmable shape by folding of a long, single-stranded DNA scaffold upon hybridization with a large number of short synthetic oligonucleotides, the so-called staple strands. Due to their unique sequences, each staple strand can individually be addressed and modified to carry functional entities [2]. Due to the experimental simplicity of the synthesis and the high degree of structural control provided by the technique, DNA origami nanostructures are nowadays widely used in various fields of applied and fundamental research, ranging from biophysics [3] to nanoelectronics [4].

Recently, single DNA origami shapes have also been employed as molecular lithography masks and transferred into various organic [5, 6], oxide [7–9], and metallic materials [10]. Here, we utilize the surface-assisted hierarchical assembly of two-dimensional DNA origami nanostructures into ordered monolayers for the fabrication of molecular lithography masks to direct the adsorption of proteins

Giampaolo Zuccheri (ed.), *DNA Nanotechnology: Methods and Protocols*, Methods in Molecular Biology, vol. 1811,
https://doi.org/10.1007/978-1-4939-8582-1_17, © Springer Science+Business Media, LLC, part of Springer Nature 2018

and generate regular protein patterns over large surface areas. Nanopatterning of proteins has promising applications in biosensing and tissue engineering [11]. Some of these applications require large, homogeneously patterned surface areas, which, however, are still rather challenging to fabricate with sufficient quality [12–14]. Molecular lithography masks are fabricated on freshly cleaved mica surfaces from triangular DNA origami nanostructures by surface-assisted, cation-mediated self-assembly based on the protocol of Rafat et al. [15]. DNA origami adsorption on mica surfaces is mediated by Mg^{2+} ions in the adsorption buffer, which induce a charge inversion of the mica surface. Addition of comparatively high Na^{+} concentrations, however, leads to a partial displacement of Mg^{2+} from the mica–DNA interface by Na^{+}, resulting in a reduced electrostatic attraction and an increased surface mobility of the DNA origami nanostructures. In the case of the triangular DNA origami, this increased mobility results in the formation of an ordered, densely packed DNA origami monolayer with hexagonal symmetry. The DNA origami triangles feature internal triangular cavities that act as holes in the mask. Incubation of the masked mica surface with negatively charged proteins results in the directed adsorption of the proteins onto the exposed Mg^{2+}-presenting surface areas in the holes. The protein density inside the holes depends on a variety of parameters including protein size, charge, and concentration, and ionic strength of the buffer medium. In the case of irreversible protein adsorption, the DNA origami mask may be desorbed from the mica surface after successful patterning by incubation in Mg^{2+}-free buffer containing a high concentration of Na^{+} ions, which then completely replace the Mg^{2+} ions on the mica surface.

2 Materials

Prepare all stock and working solution in ultrapure milliQ water (at least 18 MΩ cm at 25 °C). Use molecular biology grade reagents. Store the DNA origami solution at 4 °C and all other stock and working buffers at room temperature. Discard the waste solutions and materials appropriately.

2.1 DNA Origami Synthesis

1. 10× TAE/$MgCl_2$ (10× Tris–acetate–EDTA (TAE) buffer with 100 mM $MgCl_2$): dissolve 203.3 mg of $MgCl_2{\cdot}6H_2O$ in 10 mL of commercial 10× TAE buffer (*see* **Note 1**).
2. M13mp18 scaffold DNA in a suitable buffer solution at 100 nM (*see* **Note 2**).
3. A mixture of all required staple strands in water at 150 nM per staple.
4. Amicon Ultra-0.5 mL centrifugal filters with 100 kDa MWCO from Millipore (*see* **Note 3**).

2.2 Assembly of DNA Origami Monolayers

1. 10× TAE/$MgCl_2$ with 1 M NaCl: dissolve 584.4 mg of NaCl in 10 mL of 10× TAE/$MgCl_2$ buffer (*see* **Note 4**).
2. Mica substrates (grade V1–V5 as desired).
3. Waterproof marker pen.

2.3 Directed Protein Adsorption Through the DNA Origami Mask

1. 200 mM KH_2PO_4 solution: dissolve 27.218 g of KH_2PO_4 in 800 mL of water. Adjust the pH to 6.0 using orthophosphoric acid. Adjust the volume to 1 L using water.
2. 1 M $MgCl_2$ solution: dissolve 203.60 g of $MgCl_2{\cdot}6H_2O$ in 1 L of water.
3. 2 M KCl solution: dissolve 149.1 g of KCl in 1 L of water.
4. B1 buffer (20 mM KH_2PO_4, 200 mM KCl, 10 mM $MgCl_2$, pH 6.0, *see* **Note 5**): pipette 20 mL of 200 mM KH_2PO_4 (pH 6.0), 2 mL of 1 M $MgCl_2$, and 20 mL of 2 M KCl in a measuring cylinder. Adjust the final volume to 200 mL with water, mix well and store at room temperature after filtering with Corning 150 mL vacuum filter with 0.22 μm PES membranes. Add $MgCl_2{\cdot}6H_2O$ to increase the Mg^{2+} concentration to the desired value.
5. Dissolve/dilute proteins (*see* **Note 6**) for patterning at the desired concentration in B1 buffer (*see* **Note 7**).

2.4 Desorption of the DNA Origami Mask

1. 1× TAE with 200 mM NaCl: dissolve 116.88 mg of NaCl in 10 mL of commercial 1× TAE.

3 Methods

3.1 DNA Origami Synthesis

(Alternative origami assembly protocols can be perused, for example, protocols in Chapters 16 and 18 of this book.)

1. Mix 5 μL of M13mp18 scaffold solution (100 nM), 30 μL of staple solution (150 nM per staple), and 10 μL of 10× TAE/$MgCl_2$ buffer in a PCR tube. Add 55 μL of water to reach 100 μL total volume. Mix the solution using a pipette or a vortex mixer.
2. Incubate the mixture in a thermocycler using the following temperature sequence: heat to 80 °C, then decrease temperature by 0.5 °C every 12 s until 55 °C. Then decrease temperature by 0.3 °C every 48 s until 25 °C. Store the sample at 4 °C.
3. After incubation, transfer the 100 μL DNA origami solution to an Amicon filter and add 200 μL of 1× TAE/$MgCl_2$ buffer. Spin the sample in a benchtop centrifuge for 10 min at 2400 × *g*. Add 300 μL of 1× TAE buffer and repeat spinning. Remove filter and put it upside down into a fresh collection

tube to recover the remaining solution of DNA origami by spinning for 7 min at 3300 × *g*.

4. Measure the DNA origami concentration using a UV/Vis photometer and adjust concentration to 30 nM (*see* **Note 8**).
5. Store the sample at 4 °C.

3.2 Assembly of DNA Origami Monolayers

1. For a total volume of 10 μL of working solution, mix 1 μL of 1 M NaCl, 1.5 μL of DNA origami solution, and 7.5 μL of 1× TAE/$MgCl_2$ buffer, so that the final concentration of NaCl and DNA origami will be 100 mM and 4.5 nM, respectively (*see* **Note 9**).
2. Glue the mica substrate to a sample holder.
3. Cleave the mica surface 2–3 times with adhesive tape. Check that the substrate surface has been cleaved completely before continuing.
4. Draw a circle about 2 mm in diameter on the freshly cleaved mica surface using a waterproof marker pen and let the circle dry for 1 min (*see* **Note 10**).
5. Drop 3 μL of working solution inside the circle and incubate the sample for 10 min (*see* **Note 11**).
6. For atomic force microscopy (AFM) imaging of the formed DNA origami monolayer (*see* Fig. 1), gently wash the sample with water (*see* **Note 12**) and slowly dry the surface with a stream of nitrogen, argon, or ultrapure air (*see* **Note 13**).

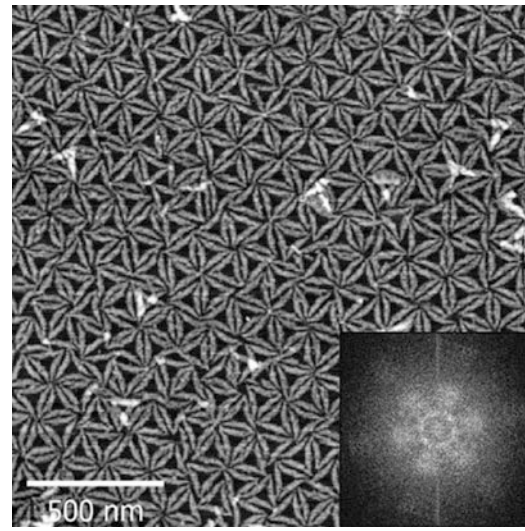

Fig. 1 AFM image of a molecular lithography mask consisting of triangular DNA origami nanostructures. The inset shows the corresponding two-dimensional fast Fourier transform, which reveals the hexagonal symmetry of the monolayer

3.3 Directed Protein Adsorption Through the DNA Origami Mask

1. For protein adsorption through the DNA origami mask, wash the formed monolayer (*see* **step 5** of Subheading 3.2, above) with 3 mL of B1 buffer instead of water and remove the excess buffer using a tissue paper.
2. Immediately drop 5 μL of the protein sample in B1 buffer onto the still wet mica surface covered with the DNA origami monolayer and incubate for 15 min (*see* **Note 14**).
3. Gently wash the sample with water (*see* **Note 12**) and slowly dry the surface with a stream of nitrogen, argon, or ultrapure air (*see* **Note 13**).

3.4 Desorption of the DNA Origami Mask

1. Incubate the mica sample after protein adsorption with 1× TAE with 200 mM NaCl (without $MgCl_2$) for 10 min (*see* **Note 15**).
2. Wash the mica surface with 5 mL of ultrapure water and slowly dry the surface with a stream of nitrogen, argon, or ultrapure air.

4 Notes

1. Because of the hygroscopic nature of $MgCl_2$, the use of $MgCl_2 \cdot 6H_2O$ is advised in order to ensure that the buffer concentrations are correct. Although this is not crucial for DNA origami synthesis and monolayer fabrication, protein adsorption may be strongly affected by small alterations in the $MgCl_2$ concentration.
2. Here, we have used the original triangular DNA origami design by Rothemund [1] based on the M13mp18 scaffold. However, protein patterning can be performed with masks based on many different DNA origami shapes [15] that may be based on different scaffolds.
3. Depending on the scaffold used, a single DNA origami nanostructures has a molecular weight in the MDa range. Therefore, filters with a MWCO of 100 kDa are used to remove excess staple strands. Filters with a lower MWCO, e.g., 30 kDa, may be used as well but might require additional spinning and washing cycles to remove all residual staples.
4. The assembly of ordered DNA origami monolayers works well with a 1:10 ratio of $MgCl_2$ to NaCl in 1× TAE buffer. 10 mM $MgCl_2$ and 100 mM NaCl are typically employed. For NaCl concentrations exceeding 150 mM, monolayer formation is delayed. For NaCl concentrations of 200 mM or higher, the Mg^{2+} will be completely replaced by Na^+, so the DNA origami monolayer will not be formed.

5. In our experiments, we have used B1 buffer because it ensures the stability of Redβ [16]. However, this buffer was also used for the proteins Sak, ferritin, and BSA [17]. Other buffer solutions may be used as well, as long as they are compatible with the protein of choice and contain a sufficient amount of Mg^{2+} that ensures the stability of the DNA origami mask. However, the required Mg^{2+} concentrations may induce aggregation of the proteins, as for instance observed in the case of ferritin [17]. In this case, different buffer solutions should be tested and the one with minimal aggregation potential selected. So far, we have performed successful patterning experiments also with 1 × TAE/$MgCl_2$ buffer, buffer AA12 (10 mM ammonium acetate, 12 mM $MgCl_2$), and buffer A (200 mM NaCl, 50 mM Tris, 10 mM $MgCl_2$).
6. Directed protein adsorption is achieved by electrostatic interactions between the protein and the Mg^{2+}-presenting negatively charged mica surface. Therefore, the protein must be negatively charged as well to bind to the Mg^{2+} bridges. This technique is thus restricted to proteins with a pI in the acidic pH range. So far, we have successfully patterned proteins with pI values ranging from 4.4 to 6.0.
7. The protein concentration required for effective patterning depends on the protein, its affinity for the mica surface, the buffer condition, and the desired protein density in the holes of the mask. Therefore, the optimal concentration has to be determined for each condition individually. As a rule, the protein density in the holes increases with protein and $MgCl_2$ concentrations (*see* Fig. 2). At the same time, proteins with a high affinity for the surface typically require lower concentrations to achieve the same pattern density.
8. In order to increase the concentration of the DNA origami stock solution, the concentration of the scaffold strand in the mixture may be increased. The current protocol uses a 30-fold excess of staples to scaffold. The ratio can also be reduced to fivefold if desired. Also, several individually assembled DNA origami samples can be filtered through one single filter, thereby increasing the concentration of the final purified sample.
9. DNA concentrations exceeding 5 nM may result in the deposition of DNA origami multilayers and should thus be avoided (*see* Fig. 3).
10. In our protocol, we have used a waterproof marker pen to draw a circle on the mica surface in which the DNA monolayer is prepared. Due to the hydrophobic nature of the waterproof ink, this circle confines the drop of sample solution within its boundaries. Without the circle, the drop would spread over the

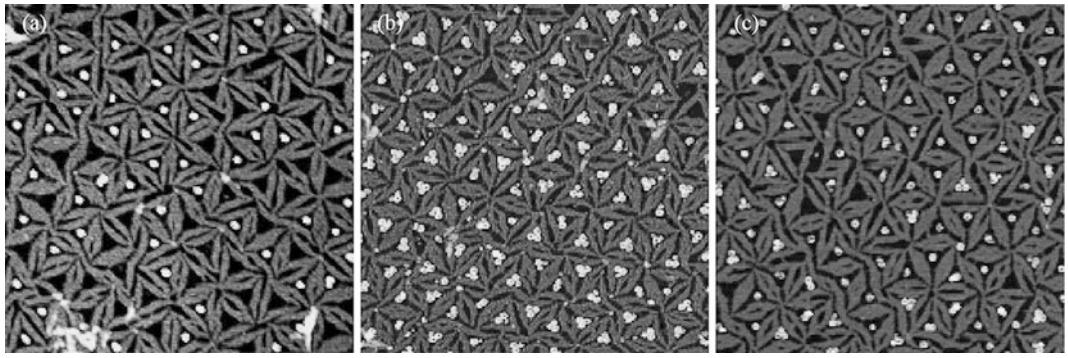

Fig. 2 AFM images of (**a**) 1 μM Redβ with 10 mM $MgCl_2$, (**b**) 3 μM Redβ with 10 mM $MgCl_2$, and (**c**) 1 μM Redβ with 30 mM $MgCl_2$ adsorbed through a DNA origami mask. The number of Redβ proteins inside the holes of the mask increases with protein and $MgCl_2$ concentrations. Images are 1.125 μm × 1.125 μm and height scales are 3 nm

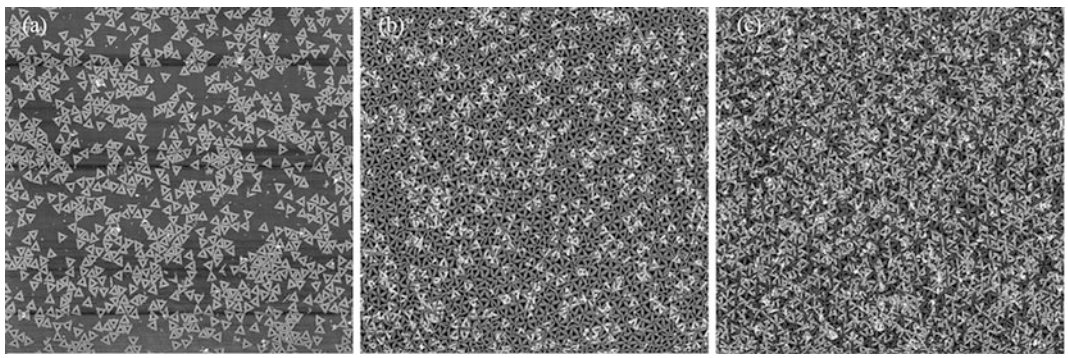

Fig. 3 AFM images of DNA origami masks after 30 s (**a**), 7.5 min (**b**), and 15 min (**c**) incubation of 30 nM DNA origami in 1× TAE/$MgCl_2$ buffer with 100 mM NaCl. The build-up of DNA origami multilayers is observed. Images are 5 μm × 5 μm and height scales are 3 nm

whole mica surface and form a very thin liquid film that dries quickly. This approach is therefore used to reduce the amount of DNA sample required for incubation. If the mask is desired to cover the whole sample surface, this circle can be omitted but then the volume of the deposited drop will have to be increased considerably.

11. As a rule, longer incubation times yield monolayers with less defects. Overnight incubation of 1 nM DNA origami was found to result in a DNA origami monolayer of very high quality. Incubation should always be performed in a closed environment such as a closed and tape-sealed small sample box in order to minimize evaporation of the sample. For long incubation times exceeding a few minutes, the humidity in the box should be increased. This can be achieved by modifying a large sample box with a smaller elevated stage. The bottom of

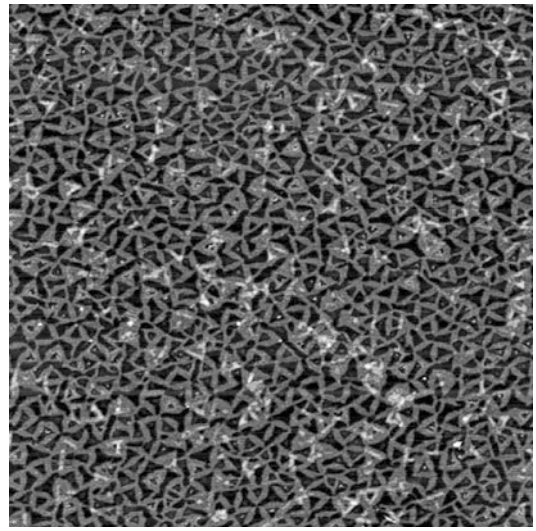

Fig. 4 AFM image of an inadequately washed DNA origami mask which shows distorted and displaced DNA origami nanostructures. The image is 3 μm × 3 μm and the height scale is 3 nm

the large box can then be covered with a small amount of water while the mica sample is placed on the stage.

12. Washing the sample is an important step to remove excess DNA and residual buffer. However, excessive or inadequate washing may distort, damage or even desorb the DNA origami by crystallization of residual buffer on the surface upon drying or washing out of stabilizing Mg^{2+} ions, respectively (*see* Fig. 4). The following washing procedures have successfully been used by us: (a) Hold the mica sample with tweezers almost vertically and gently drop water on its surface using a Pasteur pipette. Make sure that the drops are running across the surface and do not stay in one place. Typically, a few ml of water should suffice for efficient washing. (b) Hold the sample vertically with tweezers and dip it slowly into a beaker filled with water. Keep it under water for 30–60 s. Slowly remove the sample. Repeat up to three times if necessary. However, the washing protocols need to be optimized individually by each person since small variations may yield very different results.
13. Excessive blowing damages the adsorbed DNA origami. Gentle blowing at low pressure is therefore advised. In order to avoid prolonged exposure of the adsorbed DNA origami to residual water on the surface, remove excess water from the surface using a tissue paper before blow-drying.
14. During protein adsorption, it is very important not to squeeze the protein solution with force from the pipette onto surface.

Rather, the full drop of solution should be deposited at once. Otherwise, the flows of protein-containing solution along the surface generated during deposition will result in inhomogeneous and irreproducible protein coverage.

15. Desorption of the DNA origami mask requires the replacement of the Mg^{2+} bridges between the mica surface and the DNA origami by Na^{+} ions which leads to the neutralization of the surface charge. Since this replacement will also happen between the mica surface and the adsorbed protein, mask removal is only feasible for proteins that adsorb irreversibly and remain in place even in the absence of Mg^{2+} ions. Here, desorption of the DNA origami mask was demonstrated using BSA (*see* Fig. 5) which is well-known to adhere strongly and almost irreversibly to hydrophilic surfaces even at high NaCl concentrations [18]. Other proteins such as Redβ, however, may desorb together with the mask (*see* Fig. 5).

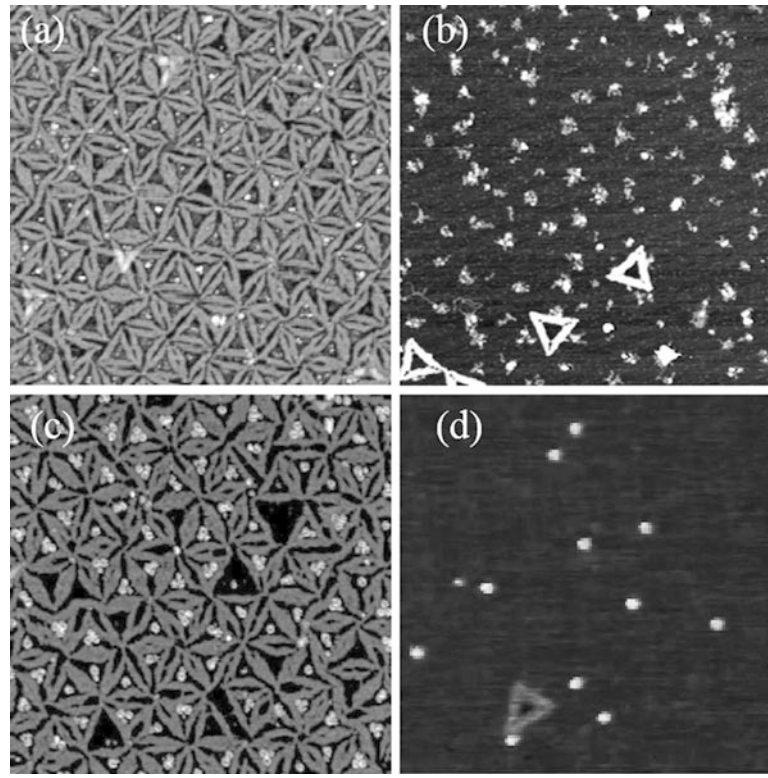

Fig. 5 AFM images of BSA (**a**, **b**) and Redβ (**c**, **d**) adsorbed through a DNA origami mask before (**a**, **c**) and after (**b**, **c**) NaCl-induced desorption of the mask. Unlike BSA, Redβ desorbs from the mica surface along with the DNA origami mask. Images are 1.125 μm × 1.125 μm and height scales are 2 nm

References

1. Rothemund PWK (2006) Folding DNA to create nanoscale shapes and patterns. Nature 440(7082):297–302. https://doi.org/10.1038/nature04586
2. Wang Z-G, Ding B (2014) Engineering DNA self-assemblies as templates for functional nanostructures. Acc Chem Res 47 (6):1654–1662. https://doi.org/10.1021/ar400305g
3. Nickels PC, Wunsch B, Holzmeister P et al (2016) Molecular force spectroscopy with a DNA origami-based nanoscopic force clamp. Science 354(6310):305–307. https://doi.org/10.1126/science.aah5974
4. Teschome B, Facsko S, Schonherr T et al (2016) Temperature-dependent charge transport through individually contacted DNA origami-based au nanowires. Langmuir 32 (40):10159–10165. https://doi.org/10.1021/acs.langmuir.6b01961
5. Surwade SP, Zhou F, Li Z et al (2016) Nanoscale patterning of self-assembled monolayers using DNA nanostructure templates. Chem Commun 52(8):1677–1680. https://doi.org/10.1039/c5cc08183a
6. Tian C, Kim H, Sun W et al (2017) DNA nanostructures-mediated molecular imprinting lithography. ACS Nano 11(1):227–238. https://doi.org/10.1021/acsnano.6b04777
7. Surwade SP, Zhao S, Liu H (2011) Molecular lithography through DNA-mediated etching and masking of SiO2. J Am Chem Soc 133 (31):11868–11871. https://doi.org/10.1021/ja2038886
8. Surwade SP, Zhou F, Wei B et al (2013) Nanoscale growth and patterning of inorganic oxides using DNA nanostructure templates. J Am Chem Soc 135(18):6778–6781. https://doi.org/10.1021/ja401785h
9. Diagne CT, Brun C, Gasparutto D et al (2016) DNA origami mask for sub-ten-Nanometer lithography. ACS Nano 10(7):6458–6463. https://doi.org/10.1021/acsnano.6b00413
10. Shen B, Linko V, Tapio K et al (2015) Custom-shaped metal nanostructures based on DNA origami silhouettes. Nanoscale 7 (26):11267–11272. https://doi.org/10.1039/c5nr02300a
11. Christman KL, Enriquez-Rios VD, Maynard HD (2006) Nanopatterning proteins and peptides. Soft Matter 2(11):928. https://doi.org/10.1039/b611000b
12. Agheli H, Malmstrom J, Larsson EM et al (2006) Large area protein nanopatterning for biological applications. Nano Lett 6 (6):1165–1171. https://doi.org/10.1021/nl060403i
13. Malmstrom J, Christensen B, Jakobsen HP et al (2010) Large area protein patterning reveals nanoscale control of focal adhesion development. Nano Lett 10(2):686–694. https://doi.org/10.1021/nl903875r
14. Singh G, Pillai S, Arpanaei A et al (2011) Highly ordered mixed protein patterns over large areas from self-assembly of binary colloids. Adv Mater 23(13):1519–1523. https://doi.org/10.1002/adma.201004657
15. Aghebat Rafat A, Pirzer T, Scheible MB et al (2014) Surface-assisted large-scale ordering of DNA origami tiles. Angew Chem Int Ed Engl 53(29):7665–7668. https://doi.org/10.1002/anie.201403965
16. Erler A, Wegmann S, Elie-Caille C et al (2009) Conformational adaptability of Redbeta during DNA annealing and implications for its structural relationship with Rad52. J Mol Biol 391 (3):586–598. https://doi.org/10.1016/j.jmb.2009.06.030
17. Ramakrishnan S, Subramaniam S, Stewart AF et al (2016) Regular nanoscale protein patterns via directed adsorption through self-assembled DNA origami masks. ACS Appl Mater Interfaces 8(45):31239–31247. https://doi.org/10.1021/acsami.6b10535
18. Jeyachandran YL, Mielczarski E, Rai B et al (2009) Quantitative and qualitative evaluation of adsorption/desorption of bovine serum albumin on hydrophilic and hydrophobic surfaces. Langmuir 25(19):11614–11620. https://doi.org/10.1021/la901453a

Chapter 18

DNA Origami Structures Interfaced to Inorganic Nanodevices

Claudia Dalmastri, Weihua Han, Stefano Vespucci, Liqian Wang, and Piero Morales

Abstract

We describe here one way to achieve hybrid DNA–inorganic nanostructures on rigid flat insulating substrates. We report methods to prepare rectangular DNA origami and incubate them onto arrays of anchoring gold nanodots either in a static solution or in a microfluidic system. We give details on the design and lithographic methods employed to pattern usable arrays of gold nanoanchors on naturally oxidized silicon wafer chips. Scanning electron and atomic force microscopy methodological details are also given for obtaining the relevant characterizations of the immobilized and ordered DNA origami.

Key words Bio-inorganic self-assembly, DNA origami, e-beam lithography, DNA breadboards

1 Introduction

The development of the DNA origami self-assembling method [1] and the consequent ability to assemble various materials at specific locations on discrete DNA based nanostructures [2–6] hold great promise for exploitation in molecular electronics, photonics, and biomedicine [7–10]. In spite of this, connecting DNA nanostructures to metallic nanostructures at specific positions is still a rarely addressed applicative issue in nanotechnology. The issue is however of high importance for use of origami structures as breadboards for molecular electronics and nanosensing arrays since the metallic nanostructures may serve as electrodes for input/output of signals. If anchoring conductive sites of suitable thickness are obtained, the DNA origami can be immobilized at a sufficient distance from the insulating substrate to plug-in hundreds of functional molecular components, even on both faces of the breadboards.

Aiming at establishing a viable fabrication technology for the self-assembly of such hybrid inorganic–organic nanodevices, we made nanometric anchoring gold dots on an oxidized silicon

Giampaolo Zuccheri (ed.), *DNA Nanotechnology: Methods and Protocols*, Methods in Molecular Biology, vol. 1811, https://doi.org/10.1007/978-1-4939-8582-1_18, © Springer Science+Business Media, LLC, part of Springer Nature 2018

wafer surface by electron-beam lithography at the corners of squares, rectangles or triangles, with inter-dot spacing matching the sites of thiol functionalized oligonucleotides within the DNA origami, close to their corners. We then incubated DNA origami of matching shapes and sizes in aqueous solution on the patterned Si surface. Given sufficient time, the origami could dock onto the anchoring points and establish two sulfur–metal covalent bonds at each corner of the DNA nanostructure, leading to stable immobilization at the designed location. Finally, docking and immobilization were characterized by scanning probe and electron microscopy.

The new hybrid technology that we are developing combines methods deriving both from solid-state microelectronics and from biochemistry. The design of the inorganic, nanopatterned substrates must be carefully adapted to the size and shape of the DNA nano-breadboards, taking into consideration the parameters that affect self-assembly of DNA origami on the conductive anchoring dots, the incubation conditions, as well as the needs of systematic characterization of a statistically relevant number of devices. Furthermore, the incubating solution should be free from contaminants and unassembled oligonucleotides, and the negative charges of both DNA and silicon dioxide substrate have to be neutralized to optimize docking on the gold nanoanchors and minimize nonselective adsorption on the substrate. (*See* also Chapters 16 and 20 of this volume for alternative methods for the arrangement of DNA origami on surfaces.)

2 Materials

For performing this protocol, a researcher needs availability and expertise in use of a number of nanotechnology and biochemistry instrumentations, including vacuum metal evaporation, e-beam lithography (we used a JEOL 9300), scanning electron microscopy (field-emission gun SEM), atomic force microscopy, a PCR thermocycler. Use of microfluidics additionally requires specific instrumentation and expertise.

2.1 DNA Origami

This method is derived from our work done on the rectangular DNA origami originally reported by Rothemund [1], a rectangular structure of approximately 75 nm × 95 nm. This structure is self-assembled by the DNA origami method from the single-strand DNA (ssDNA) of the M13 bacteriophage (the scaffold, or backbone) and 224 synthetic oligonucleotides (staples) with sequences complementary to selected tracts of the backbone. The correct DNA pairing results in a rectangular origami with the DNA chains axes perpendicular to the long side of the rectangle. Our work on the DNA origami was done in collaboration with the Aarhus University cDNA Research Group.

1. 0.1 μM M13mp18 DNA (7249 nt length) solution in ultrapure water, purchased from New England Biolabs. Store at −20 °C.
2. 100 μM stock solutions of all the staple oligonucleotides in ultrapure water (Sigma-Aldrich or other preferred supplier). Most staples are purchased as desalted oligonucleotides, while only the 8 thiol (C6 S-S)-modified oligonucleotides were purified by HPLC. The sequences of all oligonucleotides used in our experiment can be found in ref. [11].
3. Amicon Ultra 0.5 mL centrifugal filters units, 3 kDa and 100 kDa MWCO.
4. 10× TAE Mg: 400 mM Tris, 200 mM acetic acid, 10 mM EDTA, pH 8.0. Sterilized by autoclaving.
5. 20 mM TCEP (Tris(2-carboxyethyl)phosphine hydrochloride) in 1× TAE Mg.

2.2 Patterned Si Substrates

1. 10 cm diameter silicon wafers, 0.5 mm thickness, polished on one face. Crystallographic orientation is irrelevant for this application.
2. High purity chromium metal for evaporation (metal chips or foil).
3. 99.99% pure gold wire (1 mm diameter) (Engelhard Industries).
4. 495 kg/mole poly(methylmethacrylate) (PMMA) (Microchem Corp., EM Resist Ltd. or other supplier).
5. Isopropyl alcohol (microelectronics grade).
6. Acetone (microelectronics grade).
7. IPA-MIBK: 3:1 mix of Isopropyl alcohol:methyl-isobutyl ketone (microelectronics grade).
8. Microposit Stripper 1165 or similar (n-methyl pyrrolidone).

3 Methods

3.1 DNA Origami Assembly and AFM Characterization

3.1.1 Synthesis and Purification

This method is not substantially different from the original method found in ref. [1]. Alternative protocols for the assembly of origami (as performed by other groups) can be found in Chapters 16 and 17 of this book.

1. Deprotect or reduce any disulfide bonds in thiolated oligos by adding 10 M equivalents of TCEP in 1× TAE Mg buffer. Stir in an orbital shaker at room temperature for about 10 min.
2. Load each reduced oligo on one Amicon Ultra 0.5 mL centrifugal filter unit (3 kDa cut-off).

3. Add 400 μL of 1× TAE Mg on the Amicon Ultra and spin in a benchtop microcentrifuge according to the manufacturer's instructions. Repeat twice.
4. Recover the cleaned reduced oligonucleotide by inverting the filter unit and briefly spinning.
5. Prepare intermediate mix stocks containing the staple oligos at appropriate concentration ranging between 5 and 20 μM each. Mixtures can be stored at −20 °C.
6. Assemble 2 μL of 0.1 μM M13mp18 DNA (final concentration, 10 nM) with the proper volumes of staple mixtures, to gain a final concentration of 100 nM of each strand, and 2 μL of 10× TAE Mg buffer. Bring to 20 μL with ultrapure water.
7. Do a thermal annealing as follows: from 80 °C to 55 °C at 1 °C/min, from 55 °C to 45 °C at 1 °C/3 min; from 45 °C to 15 °C at 1 °C/min; incubate at 4 °C for 2 h. The entire cycle lasts about 5 h.
8. Add 200 μL of 20 μM TCEP in 1× TAE Mg to 10 μL of origami assembly mix (containing 10 nM origami). Incubate in an orbital shaker at room temperature for 1 h at 50 rpm (*see* **Note 1**).
9. To remove excess of staple strands, perform a wash with Amicon Ultra 100-kDa centrifugal filter unit following the same directions as in **steps 2–4**, above.
10. Recover the origami from the centrifugal filter unit and adjust its concentration to 5 nM.

3.1.2 Preparation of AFM Specimens for DNA Origami Characterization

Self-assembled DNA origami are mainly characterized by AFM on flat crystalline surfaces, due to the need to obtain reliable information on the thickness of the synthesized nanostructures. Mica is normally used as a substrate for the characterization since it is inexpensive, easy to cleave to obtain fresh uncontaminated surfaces, and transparent, which eases optical microscopy observation.

1. Cut a 0.5 mm thick mica foil in small squares of a few mm side using sharp scissors. Write one to several small dots on both faces of the mica squares using a permanent felt pen (*see* **Note 2**).
2. Cleave a mica square in two parts of approximately same thickness by carefully prying it apart using the tip of sharp tweezers.
3. Glue each half on the AFM microscopy support (such as a microscope glass slide or what needed in the AFM in use), leaving the unmarked, clean face exposed.
4. Lay a few 1 μL droplets of DNA origami solution (1–5 nM) in TAEMg buffer on the non marked, freshly cleaved, mica surfaces, in positions corresponding to the marks observable on

the other face. Leave 5 min to incubate in a humidity-saturated chamber.

5. Rinse the sample gently by depositing a few drops (100 μL each approx.) of ultrapure water on the specimen tilted at an angle such that the drops slowly flow away.
6. Dry slowly with a purified air stream. Now the specimen can be characterized by AFM (*see* **Note 3**).

3.2 Inorganic Substrates and Conducting Nanoanchors

3.2.1 Design of the Si Chip Substrates for DNA Origami Incubation

It is important that the DNA origami–nanodots (NDs) docking experiments are performed (a) in parallel, to compare the different relevant parameters (e.g., concentrations or anchoring geometries), and (b) over a large number of docking sites, to have statistically significant data.

One of the problems encountered in characterizing specific nanodevices, is pointing at the location of each device (or group of devices) in a large area substrate. In the assessment of a fabrication protocol, this implies the construction of a hierarchy of progressively smaller structures starting from optically observable patterns. The nanopatterned substrates should therefore be prepared according to a design that responds to all these requirements, and our best design aims at a wide versatility while also focusing on the optimization of the use of the 10 cm diameter Si wafers.

Since we attempted immobilization of rectangular and triangular origami, we planned the possibility of having different immobilization geometries (square and rectangular for the 70×95 nm^2 origami; triangular for the 120 nm sided triangular origami), and several large arrays of devices within the same chip.

Additionally, each chip can be used for origami immobilization both in a static solution and in a microfluidic system using device arrays aligned along the microflow channels. The design we describe here (*see* Fig. 1) allows to incubate different arrays of anchoring NDs with μL-sized droplets of DNA origami solution (up to six 1 μL droplets on one chip) at different concentrations both of $MgCl_2$ and of origami of different shapes, in the same experiment. When the microfluidic incubation is used, it allows for simultaneous incubation of three different solutions, each one over the nine arrays of each of the available geometries.

1. By e-beam lithography, in a 10 cm diameter wafer, pattern twenty-five (5×5) square identical chips having 8 mm side and containing groups of arrays (*see* Fig. 1a) as specified in the following.
2. Design the pattern in each square chip to contain three vertical rows of nine subgroups (27 identical subgroups per specimen, sketched and optically imaged in Fig. 1b) (*see* **Note 4**).

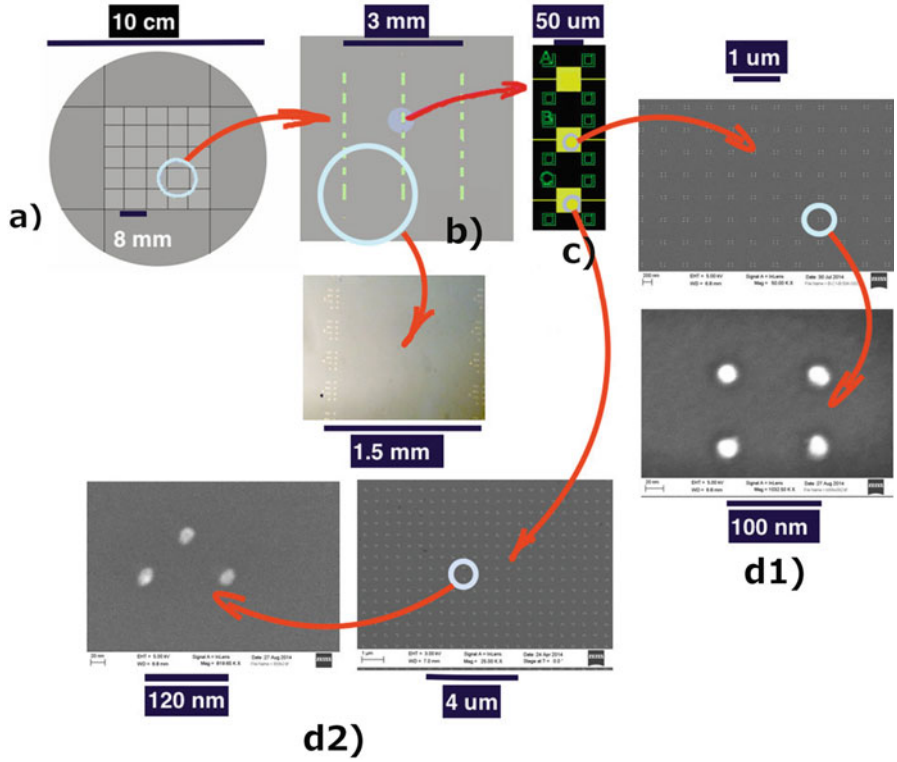

Fig. 1 (a) The organization of groups of arrays in each of the 25 chips obtained by a 10 cm diameter Si wafer; (b) three vertically aligned rows, of nine groups of square arrays, spaced 1.5 mm from each other to match the spacing of the three channels of our microfluidic incubation system; (c) each of these nine groups contains three arrays, labelled respectively Aij ($i = 1–3$, $j = 1–9$), corresponding to NDs arranged in a square geometry; Bij, corresponding to a rectangular geometry (d1), Cij with NDs arranged in a triangular geometry (d2). A and B type arrays will immobilize the rectangular origami, while C type arrays are designed to host triangular origami

3. Make each subgroup so that it contains three sub-subgroups (A, B, C) referring to different geometries of the arrangement of the anchoring NDs: at the corners of a square (80 nm side center to center; A, sketched in Fig. 1c), of a rectangle (100 nm × 80 nm; B, imaged in Fig. 1d1); and of an equilateral triangle with 120 nm side (C, imaged in Fig. 1d2).
4. Label the sub-sub groups by e-beam lithography as Aij, Bij, Cij with $i = 1...3$ and $j = 1...9$, the gold labels being large enough (30 μm side) that each specific array is promptly identified by use of a normal stereoscope and by the built-in optical microscope of the AFM used for detailed characterization. The edges of each array are within four optically observable square marks (*see* Fig. 1c).
5. Make each sub-subgroup A, B, C, as an array containing 10^4 (100 × 100) sets of anchoring NDs (devices), spaced, in our case, either 500 or 1000 nm from each other, depending on the fabricated batch (*see* Fig. 1d1, d2) (*see* **Note 5**).

3.2.2 E-Beam Lithography (EBL) Patterning of Anchoring NDs

All steps of the e-beam lithography procedure should be performed in a 100-class clean room facility, or better.

Electron beam lithography is a well-established technology to fabricate metal features in the sub- 20 nm range [13, 14], but it involves a large number of significant parameters, which can be critical in the spatial range required by this technology. These parameters must be adjusted to the available equipment and to the specific fabrication needs. Here we synthetically describe the procedure we used, which produced sufficiently resolved anchoring NDs as previously described [11, 12] (*see* Fig. 2 and **Note 6**).

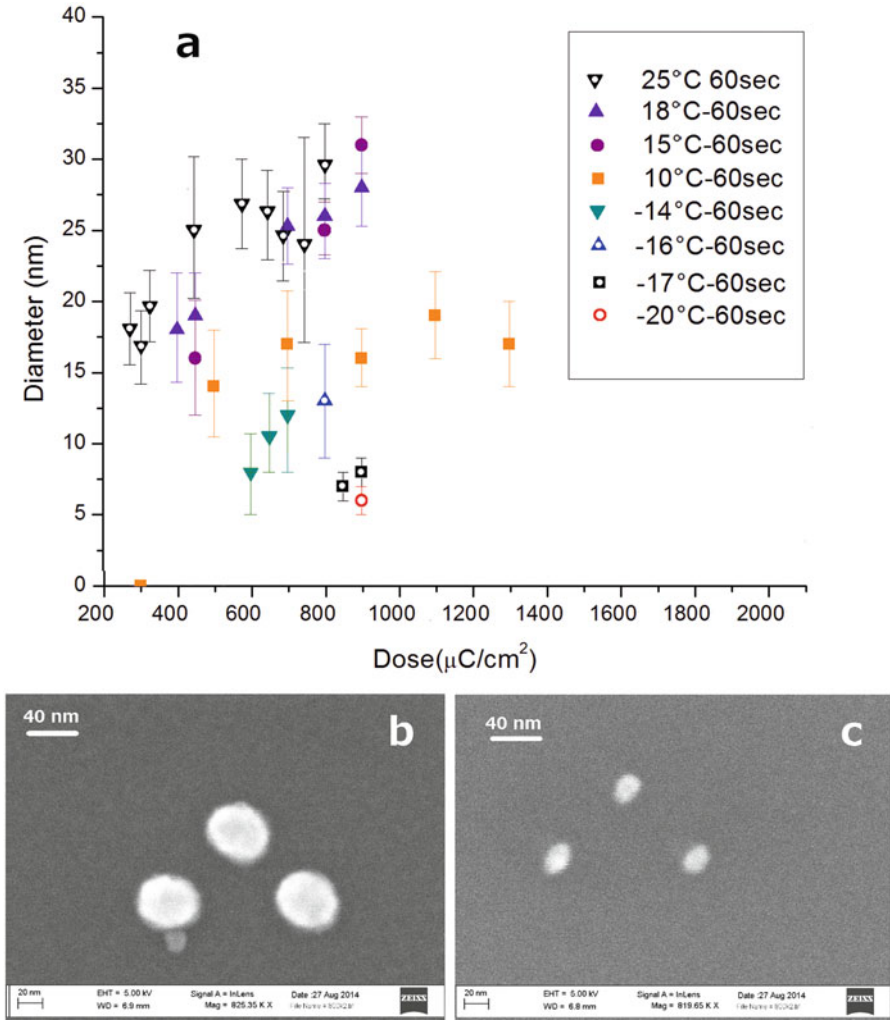

Fig. 2 The dose dependence of the dot diameter at different development temperatures is plotted in (**a**), while some examples of the dots obtained at high dose (100 μC/cm^2) for development at 25 °C and at −20 °C as imaged by SEM are reported in (**b**) and (**c**) respectively

1. Spin-coat a layer of poly(methylmethacrylate) (PMMA) of 495 kg/mole to a thickness of about 30 nm on the cleaned silicon wafer substrate (conditions necessarily vary depending on available instrumentation).
2. Bake the substrate at 180 °C for 5 min on a hot plate just prior to e-beam exposure.
3. Expose the PMMA coated Si substrate of all samples using the 100 keV beam from the cold-cathode field emission EBL machine with 2 nA filament current and nominal spot size of about 4 nm (*see* **Note 7**). *See* Subheading 3.2.1 above for the design of the EBL exposure.
4. Develop the specimens for 60 s using IPA-MIBK at the temperature that most suits the specific experiment (*see* Fig. 2).
5. Rinse with IPA and blow-dry with nitrogen (*see* **Note 8**).
6. By using a thermal evaporator in high vacuum, deposit a 1.5–2 nm thick chromium underlayer to enhance gold adhesion, and then a gold layer of a thickness ranging approximately between 2 and 10 nm. Thin layers will cause the origami to adhere to the substrate, thick ones will provide suspended origami breadboards.
7. Lift-off the resist phase by immersion of the sample in a hot bath of Microposit stripper 1165 for 1 h.
8. Wash for 2 min in an ultrasonic bath with acetone and then for 2 min with IPA.
9. Blow-dry in a stream of purified air.

3.2.3 Dicing of the Nanofabricated Chips

After patterning, the 25 square chips need to be mechanically diced out of the wafer with 10 μm precision (*see* Fig. 3 and **Note 9**) for alignment of the three rows of devices in the incubation systems.

1. Arrange the wafer for dicing by a rotary diamond blade, with the patterned surface facing down on an O-ring seal that prevents the cooling fluid to contaminate the gold ND arrays.
2. Achieve a fine control of the vertical position of the wafer with respect to the diamond rotating blade and produce a deep ditching through 200–300 μm of the 500 μm wafer thickness.
3. Obtain the 25 identical chips by breaking the ditched wafer by a slight mechanical torque with minimal production of debris.
4. Remove any present debris with a blow of purified air only from those chips where Si microscopic fragments are observable by optical microscopy inspection.
5. If necessary, perform additional cleaning of the chips by sonication for a few minutes, first in ultrapure water, then in acetone, and finally in isopropyl alcohol.

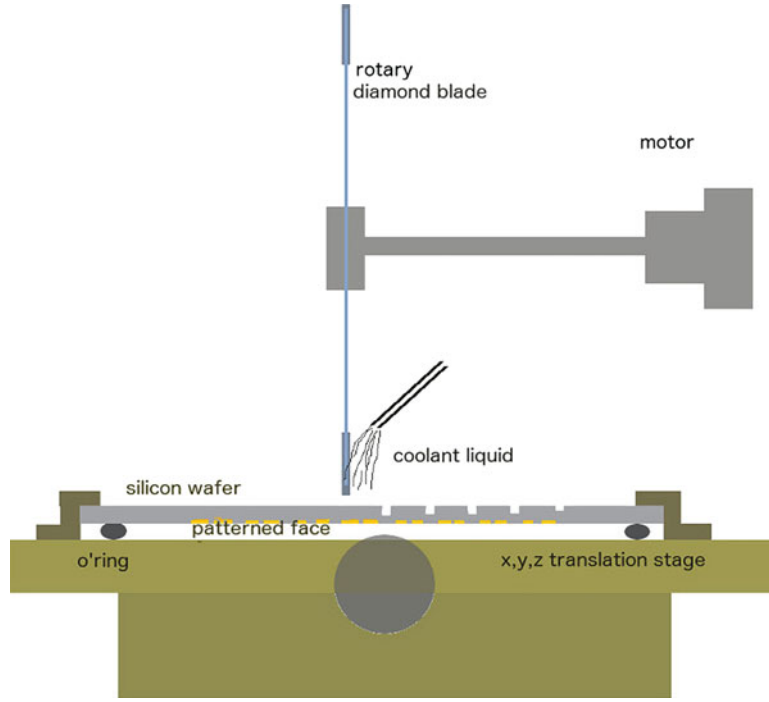

Fig. 3 The rotary diamond-blade dicing machine used to obtain the 8 mm × 8 mm chips was modified so that the polished wafer surface does not touch any other surface nor it is contaminated by the cooling liquid

3.2.4 Characterization of Patterned Silicon Chips

Gold nanopatterned substrates are characterized by field emission scanning electron microscopy (FEG-SEM) and by atomic force microscopy (AFM). The aim of characterization is determining the repeatability of the fabrication process over large distances, and controlling the anchoring NDs shapes, precision, positioning and distribution of both vertical and horizontal sizes. To this aim, the two techniques are complementary: FEG-SEM is highly precise in the determination of spacing and lateral sizes, while it supplies poor information on the 3D shape and height of NDs. On the other hand, AFM measures the NDs height with Ångström precision, while its lateral resolution is strongly affected by the unknown shape and width of the probe, beyond the nonlinear behavior of the scanning piezoelectric ceramics, and the larger influence of thermal drifts, due to longer scanning times. Therefore, since correct attachment of DNA origami on gold NDs strongly depends on their size, shape and spacing, simultaneous use of the two techniques is compulsory to obtain a complete and detailed characterization.

1. For characterization of the anchoring NDs, use FEG-SEM at acceleration voltages between 1 and 5 kV, and at a working distance of a few mm with the specimen perpendicular to the beam (*see* **Note 10**).

2. Use the AFM always in intermittent contact mode to minimize probe and sample wear (*see* **Notes 11–12**). Keep the probe oscillation amplitude to a minimum and the setpoint to 35–40% of the free oscillation amplitude. Scanning speeds are normally up to 8 μm/s for first quick imaging and 2 μm/s for the detailed characterization. Use a pixel size of about 2 nm.

3.3 Incubation of DNA Nanostructures onto Nanopatterned Chips

3.3.1 Static Immobilization of DNA Nanostructures onto Inorganic Anchoring Points

The small size of the anchoring gold dots, compared to the naked SiO_2 surface, requires long incubation times to allow the dispersed origami nanostructures in solution (at 5 nM concentration) to come in contact with the reactive gold that binds the sulphur atoms at their corners. Static incubation is made by depositing different droplets of origami solution on the 8 × 8 mm chip, covering one or more of the 27 available groups of arrays (*see* **Note 13**).

Furthermore, since both DNA and the SiO_2 surface are negatively charged, it is essential that the substrate surface charges be at least partially neutralized by adding positive Mg^{2+} ions to the solution (*see* **Note 14**).

1. Prepare a 5 nM solution of the purified, thiol-functionalized DNA origami in TAE Mg adding $MgCl_2$ at different concentrations. The total Mg^{2+} concentration should range between 75 and 100 mM (*see* **Note 14**).
2. Under stereoscopic observation, carefully lay 1 μL drops of 5 nM origami solution on selected locations of the 8 × 8 mm chips.
3. Immediately transfer to the controlled-humidity chamber (*see* also step 4 of 3.1.2 and **Note 13**) and incubate at room temperature for approximately 40 h.
4. Remove the specimen from the humid chamber, rinse it immediately in ultrapure water, and dry it in a gentle stream of purified, dry air (*see* **Note 15**).
5. Microscopy characterizations can now be performed on the central portions of the areas originally covered by the drops of origami solutions (*see* **Note 16**).

3.3.2 Microfluidic Immobilization of DNA Nanostructures onto Gold Anchoring Points

The microfluidic system we designed and realized has three channels carved in PMMA, along which a maximum of 10 μL of solution can be flowed at the desired speed. The channel section is rectangular, 120 × 60 μm^2, three sides of it carved in the PMMA block, the fourth being the nanopattened Si chip (*see* Fig. 4) that is pressed against a silicone rubber seal on the PMMA body. Channels are separated by 1.5 mm, matching the separation of the three rows of nine sets of arrays on the chip. A micrometric slide allows fine alignment of the microflow channels on the rows of nine NDs arrays.

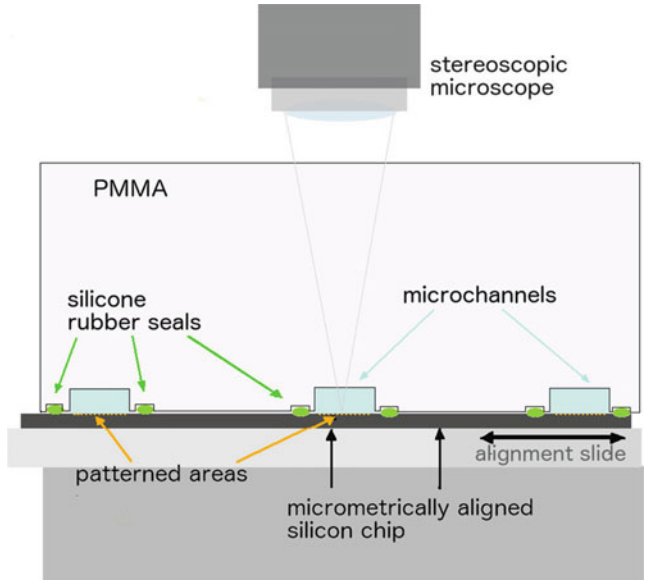

Fig. 4 Section schematics of the microfluidic system: the rectangular section microchannels are carved in a transparent PMMA block and are 6 mm long, 120 μm wide, and 60 μm deep; the patterned 8 × 8 mm silicon chip is aligned on the microchannels so that the NDs arrays are exposed to the DNA origami solution flow. A stereoscope allows such alignment looking through the transparent block. A soft silicone rubber gasket seals the gap between the Si wafer chip and the PMMA

To investigate the effect of the solution parameters, each channel incubates all types of anchoring dots geometries (square, rectangular and triangular, A, B, C) included in the nine replicas. DNA origami solutions can be loaded at different $MgCl_2$ concentration (50–150 mM) or origami concentrations (1–5 nM) in the three 10 μL reservoirs corresponding to the different channels. All three channels have the same flow speed. In each channel, we flow 10 μL of origami solution for 35 h. Since the volume of each channel is 5.76×10^{-2} μL, we attain a complete change of solution in the channel approximately every 10 min, with the solution flowing at 13.3 μm/s (*see* **Note 17**).

The detailed operative instructions for performing this procedure strongly depend on the highly diversified microfluidic apparatuses that are in use in different labs and will not be described here.

3.3.3 Microscopy Characterization of DNA Origami on NDs

Large area imaging of the immobilized DNA origami on gold anchoring NDs is first performed by FEG-SEM imaging. To avoid damage or quick evaporation of the DNA suspended across the gold NDs, a very low acceleration voltage should be used at the cost of some loss of resolution. This is also needed to minimize penetration of the primary electron beam into the bulk silicon with

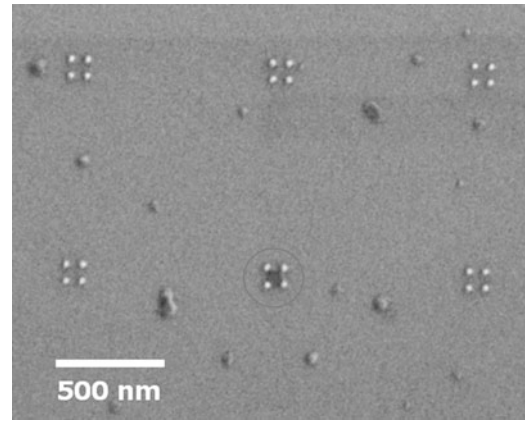

Fig. 5 FEG-SEM imaging of gold NDs immobilized origami shows both the correctly docked origami (circled) and the level of contamination of the substrate from solution residues after a 40 h incubation

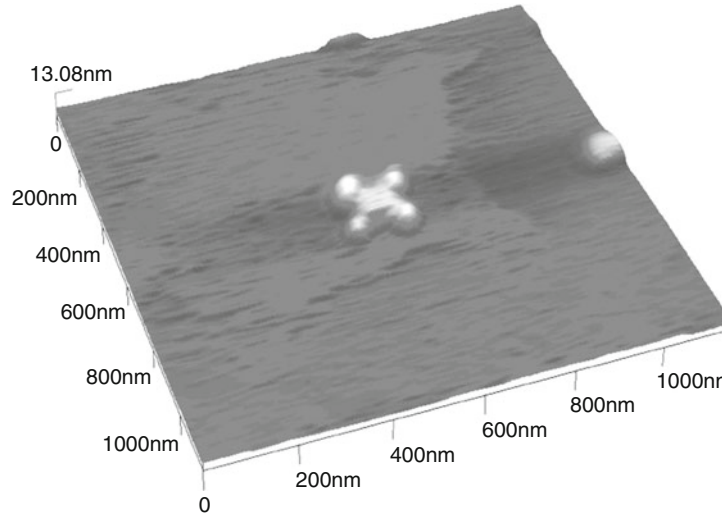

Fig. 6 AFM scan showing a single origami correctly docked across gold NDs and suspended well above the substrate surface

consequent generation of secondary electrons obscuring the weak signal from the DNA. The best compromise was found at 200–300 V, using the in-lens detector: in this way, DNA is still well observable, at magnification around 150kX, for a reasonably long time to allow for image optimization. A typical FEG-SEM image of origami suspended across gold NDs is reported in Fig. 5.

AFM imaging and characterization of the immobilized nanostructures is mostly performed in air, always in intermittent contact

mode to minimize interaction with the suspended soft origami (*see* Fig. 6). The settings and procedures are the same as discussed for NDs characterizations (*see* Subheading 3.2.4).

4 Notes

1. *Pretreatment of thiol-modified strands* is suggested to break any disulfide bonds that may have formed making those oligos unavailable for the desired assembly. TCEP treatment on the assembled origami is made in order to reduce the disulfide bonds that may have formed between the origami structures due to presence of thiolated oligos near their corners.
2. The felt pen marks on the glued face, clearly observable optically, will be used to address the AFM probe onto the origami incubated areas.
3. Accurate AFM characterization of the DNA origami is required both to check for successful assembly of the designed nanostructure and for structure comparison with origami immobilized on NDs; therefore, accurate calibration of the instruments is needed. We commonly calibrate the AFM X,Y scanner by measuring the spacing between the gold NDs arranged in a square pattern in a clean specimen, obtaining a calibration factor for both scanning directions. We then compare the corrected images with the images obtained by means of a calibrated SEM to check and adjust the calibration of the AFM. This procedure supplies reasonably accurate size measurements but, given the unknown thermal drift in non-patterned mica substrates, we estimate in any case an uncertainty of a few percent (4–5 nm) on the lateral sizes of the mica-adsorbed origami.
4. Make the spacing between the three rows of groups (1.5 mm in our case) to match the (three) channels of the microfluidic incubation system.
5. The denser packing allows easier comparison of more devices within a single AFM scan.
6. Aiming at defining the limits of precision in the immobilization of DNA nanostructures, we need to assess the smallest ND size that can be reliably achieved. Since the dose threshold, and consequently the minimum dot size, depend on the development step temperature [14], we also investigated such behavior, aiming at decreasing reliably the dot size. As shown in Fig. 2, the lower is the temperature, the higher is the dose threshold needed to open the 30 nm resist layer, but it is at the lowest temperatures that we can achieve resist apertures, and therefore dots, below 10 nm. In general, depending on the most suitable tradeoff between positioning precision and rate

of assembly of the DNA origami breadboards on the NDs, one can decide the most convenient dot size and consequently the optimal dose and development temperature. The plot in Fig. 2a, together with two examples of high dose lithography at high (Fig. 2b) and low (Fig. 2c) development temperature, can act as a rough guideline. Our best tradeoff was around 60–70 μC/cm^2 at room temperature (dot diameter around 20–25 nm, but if higher precision is needed lower temperatures are required. With these sizes, repeatability of the patterns is excellent.

7. Beyond decreasing the beam size, the high electron energy produces less forward scattering and the beam is less broadened, giving a less pronounced resist undercut; the process becomes less sensitive (lower throughput) but more precise, increasing the applicable dose range [14].
8. If residues of resist from the pattern prior to metal evaporation are still present at this stage, further cleaning can be performed by brief reactive ion etching (RIE) (for 6 s, in our system).
9. It is extremely important that the patterned surface of each chip is free from contamination or debris. Although the polished wafers from the foundry are originally extremely clean, the dicing procedure normally contaminates the surface with electrically charged Si fragments from the cut. It is therefore preferable to avoid laying the polished wafer surface on a mat for diamond tip scribing at the back, followed by breaking.
10. In our case, NDs were designed to attach origami at the corners of squares, rectangles and triangles. In the case of immobilization on the designed square geometry with 80 nm side, we commonly measure an average center-to-center distance of 81 nm between nearest neighbor dots.
11. We use standard silicon cantilevers with Si pyramidal tips having a guaranteed radius of curvature (R_c) below 10 nm. The typical probe force constants are 5 N/m and the resonance frequencies are in the range 120–170 kHz.
12. In spite of the care taken in minimizing the interaction, comparison with SEM images suggests that the tips quickly wear to R_c of approximately 15–20 nm, due to the inevitable lateral collisions experienced by the probe on the sharply rising NDs (ND height is approximately between 4 and 12 nm).
13. To avoid evaporation of the droplets, the specimen must be kept in a small temperature-controlled chamber in which a saturated humidity atmosphere is maintained. A small window at the top of the chamber (heated to avoid humidity condensation) allows stereomicroscopic observation of the droplets, to check that they do not appreciably decrease in size due to evaporation.

14. We tested the use of $MgCl_2$ at a concentration between 50 and 155 mM. We found that the optimal concentration is around 75–100 mM: at lower concentration negatively charged DNA is electrostatically repelled from the surface and no DNA structures deposit anywhere, whereas at the highest concentrations large lumps of materials bind to the surface, preferentially around the gold NDs, making AFM imaging impossible in most areas. Only in the optimized range of Mg^{2+} concentration, we could observe a large amount of DNA rectangular structures correctly immobilized across their anchoring gold NDs.
15. The rinsing procedure is necessarily gentle, being a tradeoff between the need for a clean substrate and the risk of disrupting the eight thiol bonds holding the suspended origami in place; thus, the dried specimens remain always contaminated by solution residues.
16. Microscopic inspection of the specimens shows that a lot of DNA origami and buffer salts lay in large lumps along a circle at the edge of the deposited solution droplet. Consequently, successful observation of the immobilized origami is restricted to the center of the area where the droplet had been deposited. To avoid such precipitation at the droplet edge, and the consequent depletion of the solution, a microfluidic system can be used to flow the solution continuously over the NDs arrays.
17. This speed could turn out to be too high; although in the microfluidic system the solution is no longer depleted by static precipitation at the edge of the droplets, we do not witness an appreciable difference in the immobilization rate between specimens incubated in static conditions and those incubated in the microfluidic system, as we would instead expect.

References

1. Rothemund PWK (2006) Folding DNA to create Nanoscale shapes and patterns. Nature 440:297. https://doi.org/10.1038/nature04586
2. Li H, LaBean TH, Kenan DJ (2006) Single-chain antibodies against DNA aptamers for use as adapter molecules on DNA tile arrays in nanoscale materials organization. Org Biomol Chem 4:3420. https://doi.org/10.1039/b606391h
3. Maune HT, Han S, Barish RD, Bockrath M, Goddard WA, Rothemund PWK, Winfree E (2010) Self-assembly of carbon nanotubes into two-dimensional geometries using DNA origami templates. Nat Nanotechnol 5:61. https://doi.org/10.1038/NNANO.2009.311
4. Hung AM, Micheel CM, Bozano LD, Osterbur LW, Wallraff GM, Cha JN (2010) Large-area spatially ordered arrays of gold nanoparticles directed by lithographically confined DNA origami. Nat Nanotechnol 5:121. https://doi.org/10.1038/NNANO.2009.450
5. Voigt NV, Tørring T, Rotaru A, Jacobsen MF, Ravnsbæk JB, Subramani R, Mamdouh W, Kjems J, Mokhir A, Besenbacher F, Gothelf KV (2010) Single molecule chemical reactions on DNA origami. Nat Nanotechnol 5:200. https://doi.org/10.1038/NNANO.2010.5
6. Tintoré M, Gàllego I, Manning B, Eritja R, Fàbrega C (2013) DNA origami as a DNA repair Nanosensor at the single-molecule level. Angew Chem Int Ed 52:7747. https://doi.org/10.1002/anie.201301293

7. Scheible MB, Pardatscher G, Kuzyk A, Simmel FC (2014) Single molecule characterization of DNA binding and strand displacement reactions on lithographic DNA origami microarrays. Nano Lett 14:1627. https://doi.org/10.1021/nl500092j
8. Tuukkanen S, Kuzyk A, Jussi Toppari J, Häkkinen H, Hytönen VP, Niskanen E, Rinkiö M, Törmä P (2007) Trapping of 27 bp-8 kbp DNA and immobilization of thiol-modified DNA using dielectrophoresis. Nanotechnology 18:295204. https://doi.org/10.1088/0957-4484/18/29/295204
9. Wang R, Palma M, Penzo E, Wind SH (2013) Lithographically directed assembly of one-dimensional DNA nanostructures via bivalent binding interactions. Nano Res 6:409. https://doi.org/10.1007/s12274-013-0318-6
10. Kim KN, Sarveswaran K, Mark L, Lieberman M (2010) DNA origami as self-assembling circuit boards. Unconventional Computation, Proceedings 6079:56
11. Morales P, Wang L, Krissanaprasit A, Dalmastri C, Caruso M, De Stefano M, Mosiello L, Rapone B, Rinaldi A, Vespucci S, Vinther J, Retterer S, Gothelf KV (2016) Suspending DNA Origami Between Four Gold Nanodots. Small 12(2):169–173. https://doi.org/10.1002/smll.201501782
12. Wang L, Dalmastri C, Mosiello L, Rapone B, Retterer S, Krissanaprasit A, Gothelf KV, Morales P (2015) Coupling DNA Nanobreadboards to solid state conductors. EAI, Energia Ambiente, Innovazione 3:85–94
13. Kohler M, Fritzsche W (2007) Nanotechnology: an introduction to Nanostructuring techniques. Wiley-VCH, Weinheim
14. Mohammad MA, Muhammad M, Dew SK, Stepanova M (2012) Fundamentals of electron beam exposure and development. In: Stepanova M, Dew S (eds) Nanofabrication. Springer-Verlag, Wien, pp 11–41. https://doi.org/10.1007/978-3-7091-0424-8_2

Chapter 19

Tuning Gold Nanoparticles Plasmonic Properties by DNA Nanotechnology

Valentina Masciotti, Denys Naumenko, Marco Lazzarino, and Luca Piantanida

Abstract

The engineering of the optical and plasmonic properties of metallic nanostructure is one of the key ingredients for the complete control of materials at the nanoscale. Here we show how it is possible to control the plasmonic resonance of complex architectures of gold nanoparticles using the peculiar properties of DNA Watson and Crick pairing rules. In this chapter, we will first introduce all the steps required to generate, purify, and characterize DNA nanostructures, then we will guide the reader to the main steps required to decorate them with a precise amount of gold nanoparticles and, finally, we will describe the main approach used to characterize their plasmonic response.

Key words DNA origami, Gold Nanoparticle, LSPR, Plasmon resonance, Dimers, DNA nanostructures

1 Introduction

The unique optical properties of noble metal nanoparticles are known since antiquity. The considerable progress recently achieved on the control of their chemical synthesis boosted the production of an infinite zoology of shapes, sizes, compositions, and, consequently, optical characteristics, which can be all explained in the framework of a single phenomenon known as localized surface plasmon resonance (LSPR). Plasmons are collective oscillation of conduction band electrons induced by the electromagnetic radiation at noble metal surface level [1]. In case of nanoparticles, plasmons are confined to the surface and are non–propagating. The plasmon resonance frequency of isolated nanoparticles depends on the size, on the material, and on the permittivity of the medium in which they are embedded. When, on the contrary, nanoparticles are not isolated they can mutually influence each other; when two nanoparticles are closer than 2.5 times their diameter, their plasmons interact, increase their strength, and shift

Giampaolo Zuccheri (ed.), *DNA Nanotechnology: Methods and Protocols*, Methods in Molecular Biology, vol. 1811, https://doi.org/10.1007/978-1-4939-8582-1_19, © Springer Science+Business Media, LLC, part of Springer Nature 2018

their resonance [2]. This principle has been exploited to build a plasmon ruler, which uses the resonance shift to precisely define the distance between two gold nanoparticles (AuNP) when the size and the geometry are well known [3]. Since DNA is a versatile and programmable material for self-assembly, DNA-based plasmonic nanostructures represent a perfect platform on which plasmonic-based light engineering can be created. More specifically, DNA can be used to drive the assembly of DNA functionalized AuNP: pioneers in this field were Chad Mirkin, who described the formation of macroscopic colloidal crystal lattices upon the hybridization of DNA-AuNP conjugates [4] and Paul Alivisatos who employed DNA duplex to link two gold nanoparticle with a predefined length [5]. More recent efforts with nanoscale metals functionalized with thiolated oligonucleotides led to hierarchical structures and achieved noticeable prominent plasmonic effects [6, 7]. This approach was successfully applied to the design of biosensors [8–10], Raman scattering enhancers [11–13], fluorescence emission [14], and also molecular rulers [2, 15–18]. We developed an efficient AuNP dimer formation using 20 nm AuNP and short DNA oligonucleotides [19], tuning the assembling length in steps of one single nucleotide (nt, 0.34 nm) [20]. The latter is based on the DNA-induced aggregation and disaggregation and on the fine-tuning of the complementary ssDNA self-passivation. DNA origami is a bottom-up molecular self-assembly technology which offers the possibility to design the folding of 2D/3D nanostructure in a one-pot reaction, allowing for nanoscale programmability in shape and dimension and the spatial addressability of organic molecules, biological targets, and metal nanoparticles [21]. This technique provided additional advancement in the design of self-assembled nanostructures [22–25] with particular focus on the plasmonic DNA–nanoparticle hybrid structures [26–28]. Yan's group successfully decorated a triangular shape DNA origami with self-similar sequences of AuNP showing a remarkable electromagnetic field localization [29, 30]. More recently, Na's and Liedl's groups planned a metamolecule of DNA origami to organize plasmonic nanoparticles in three dimensions and to drive the metamolecules to distinct conformational states while registering the circular dichroism response [31]. We created a planar DNA origami hatch provided with a flexible wing which was controlled, in its motion, by a DNA target recognition; then, placing two AuNP between the base and the wing, we were able to tune the LSPR response through the addition of specific targets [32]. Here we present a reproducible method to handle AuNP dimers controlling the distance between them using a DNA structure, detectable through their LSPR: first we introduce how to prepare DNA-based AuNP dimers through a controlled aggregation-disaggregation method and then how to exploit a DNA origami structure as predefined platform to precisely position

AuNP. The formation of dimers, both in the first and second case, has been investigated by UV–visible (UV-Vis) spectroscopy after agarose gel electrophoresis separation.

2 Materials

2.1 Gold Nanoparticle Functionalization and Dimerization

All solutions are prepared with ultrapure deionized water with a resistivity of 18.2 MΩ cm at 25 °C, TOC level <5 ppb (Milli Q® Reference, Merck Millipore). Ultrapure water has been used at room temperature and in non–sterile condition (unless specified otherwise).

1. *0.5 M EDTA pH 8.0 solution*: add 146.12 g of anhydrous EDTA (ethylenediaminetetraacetic acid) into 800 mL of ultrapure water in a 1 L glass bottle. Stir vigorously on a magnetic stirrer and adjust the pH to 8.0 with NaOH pellets to allow all the EDTA powder to completely dissolve. Use ultrapure water to bring the final volume to 1 L.
2. *1× TBE buffer (90 mM Tris–borate, 2 mM EDTA)*: add 10.9 g of Tris base and 5.5 g of boric acid into 800 mL of ultrapure water in a 1 L glass bottle. Add 4 mL of 0.5 M EDTA pH 8.0. Stir vigorously on a magnetic stirrer plate until complete dissolution of the solutes and then adjust the pH to 7.6 with HCl. Use ultrapure water to bring the final volume to 1 L. Filter with a 0.22 μm filter to prevent the formation of precipitates.
3. *50× TAE buffer (2 M Tris, 1 M acetic glacial acid, 50 mM EDTA)*: add 242 g of Tris base and 57.1 mL of glacial acetic acid to 800 mL of ultrapure water in a 1 L glass bottle. Add 100 mL of 0.5 M pH 8.0 EDTA solution. Stir vigorously on a magnetic stirrer plate and adjust the pH to 7.6 with HCl. Use ultrapure water to bring the final volume to 1 L.
4. *5 M NaCl solution*: dissolve 14.61 g of NaCl in 50 mL of ultrapure water and vortex until dissolved.
5. *1× TAE buffer* with *0.1 M NaCl*: mix 1 mL of 50× TAE with 1 mL of 5 M NaCl and 48 mL of ultrapure water.
6. 1 M NaH_2PO_4: dissolve 119.98 g of NaH_2PO_4 (MW = 119.98 g/mole) in ultrapure H_2O to make a final volume of 1 L.
7. 1 M Na_2HPO_4: dissolve 141.96 g of Na_2HPO_4 (MW = 141.96 g/mole) in ultrapure H_2O to make a final volume of 1 L.
8. *0.5 M SPB (sodium phosphate buffer, pH 7.0)*: mix 387 mL of 1 M Na_2HPO_4 with 113 mL of 1 M NaH_2PO_4 and bring to 1 L with ultrapure water.

9. *Agarose gel 3.6% (or 1%)*: weight 3.6 g (or 1 g) of agarose and dissolve in 100 mL of 0.5× TBE or 1× TAE buffer. Use a microwave oven to boil the solution and allow the agarose to dissolve into the buffer (*see* **Note 1**). Once the powder is well dissolved, leave the bottle at room temperature for a few seconds to allow the removal of all air bubbles. After cooling to about 50 °C (a thermostatic bath could help to maintain the temperature), add 1× GelRed™ staining solution and pour it into the gel casting tray. Let it cool down to room temperature and to a complete hardening before loading the samples.
10. *6× Loading buffer*: 60% glycerol in 1× TAE buffer (*see* **Note 2**).
11. UV-Transilluminator, ECX-F15.M (Vilber Lourmat).
12. D-Tube dialyzers devices (Merck-Millipore).
13. Syringe nylon filters with 0.22 μm cutoff.
14. Gold colloids (AuNP), diameter of 20 nm supplied in water, having trace amounts of citrate as stabilizer [33], tannic acid and potassium carbonate, extinction coefficient: 9.406×10^8 M^{-1} cm^{-1}, 1 OD at 520 nm, 7.0×10^{11} particles/mL (Ted Pella, Inc).
15. BSPP (4–4′-Bis (p-sulfonatophenyl) phenylphosphine dihydrate dipotassium salt), 97% (Sigma-Aldrich, Inc).
16. 0.5 mM BSPP and 2.5 mM BSPP solutions in ultrapure water.
17. 99.8% Methanol (J.T. Baker).
18. *0.8 M DTT reducing solution*: add 0.123 g of DTT (*1,4-Dithiothreitol*) in 1 mL of ultrapure water and vortex until dissolution [34].
19. Custom DNA oligonucleotides and their reverse complement strands composed by sequences of 11, 16, 21 nucleotides (approximate length 3.7 nm, 5.4 nm and 7.1 nm) modified at 3′ end with a thiolated group.
20. NAP-5/NAP-10 filtration columns (GE Healthcare) (*see* **Note 3**).
21. 1 mL Quartz cuvette.
22. Spectrophotometer (PerkinElmer, LAMBDA 25).
23. Amicon® Ultra 0.5 mL, cutoff 100 kDa (Merck-Millipore).
24. Centrifuge (Eppendorf 5418 or equivalent).
25. D-Tube Dialyzers devices (Merck-Millipore), size Midi (according to the gel band size).

2.2 DNA Origami Synthesis and Characterization

During DNA origami synthesis, it is recommended to work under sterile conditions. All materials (plastic tips, tubes, buffers, and ultrapure water) should be sterilized in an autoclave with a standard cycle (121 °C for 20 min at 1 atm). All solutions should be prepared with ultrapure water.

1. *10× TAEMg buffer:* dilute the 50× TAE buffer and make 125 mM $MgCl_2$.
2. 100 μM solutions of staple oligonucleotides with an average length of 32 nt (in ultrapure water) (Sigma-Aldrich) (*see* **Note 4**).
3. 250 μg/mL solution of M13mp18 (a 7249 nt long M13 *lac* phage vector) (New England BioLabs Inc.).
4. Thermocycler (BIOER).
5. Amicon® Ultra 0.5 mL, cutoff 100 kDa (Merk-Millipore).
6. Centrifuge (Eppendorf 5418 or equivalent).
7. 1% agarose gel
8. *Ladder 2-Log* (New England BioLabs Inc.): mix 1 μL of ladder 2-Log (1 μg/mL, 0.1–10 kb), 1 μL of 6× Blue Loading Dye, and 4 μL of ultrapure water.
9. UV-Transilluminator, ECX-F15.M (Vilber Lourmat).
10. Muscovite Mica grade V1 (TedPella, Inc).
11. Olympus OMCL-TR400PSA AFM probes (pyramidal tip: spring constant 0.02–0.08 N/m, resonant frequency 34–11 kHz).
12. Atomic Force Microscope (JPK Nanowizard II or equivalent).

2.3 DNA Origami–Gold Nanoparticle Functionalization

All solutions should be prepared using ultrapure water at room temperature and without sterilizing it (unless specified otherwise).

1. *DNA origami* solution (*see* Subheading 3.3).
2. ssDNA-coated gold colloids (AuNP), diameter of 20 nm (*see* Subheading 3.1).
3. 1% Agarose gel.
4. UV-Transilluminator, ECX-F15.M (Vilber Lourmat).
5. Electrophoresis cell (Peqlab Biotechnologie GmbH).
6. Electrophoretic power supply (Major Science).
7. Centrifuge (Eppendorf 5418 or equivalent).
8. Thermostatic bath (Sonorex Digitec, Bandelin).

2.4 SEM Characterization of the Gold Nanoparticles–DNA Hybrid Structures

All solutions are prepared with ultrapure deionized water at room temperature and in non–sterile condition (unless specified otherwise).

1. *Gold NPs dimers* (*see* Subheading 3.1) *and/or DNA origami decorated with AuNP* solution (*see* Subheading 3.4).
2. A 5 mm × 5 mm chip diced out of a (100) Silicon wafer with a layer of silicon oxide of 200 nm (Addison Engineering, Inc.).
3. Plasma cleaner (Diener electronic GmbH & Co. KG).
4. Scanning electron microscope SUPRA 40 (Zeiss).
5. Paper wipers (Kimberly-Clark Worldwide, Inc.).

2.5 Gel-Direct LSPR Measurement

To measure the absorbance of AuNP constructs directly from the agarose gel bands, a spatially resolved spectrometer was assembled. The setup should comprise the following items and is represented in Fig. 1.

1. Inverted optical microscope (Axiovert 200, Zeiss) operating in transmission mode.
2. 100× immersion objective (NA 1.45, α Plan-FLUAR, Zeiss).
3. XY manual or motorized micropositioning system to position the sample at the center of the gel band and Z manual positioner to focus the beam 50 μm upper the glass surface.
4. Spectrometer (Shamrock SR-750, 750 mm of optical path, Andor Technology plc.).
5. CCD camera (DVC 1412).
6. Linear CCD (TE-Cooled electron multiplied CCD Newton DU971-UVB, Andor Technology plc.).
7. Broad band illumination source covering the spectrum from 400 nm to 700 nm (halogen lamp HAL 100 illuminator, Zeiss).
8. Samples run in agarose gel (*see* **step 5** in Subheading 3.4).
9. Razor blades.
10. Glass coverslips.
11. Sample holder for coverslips.

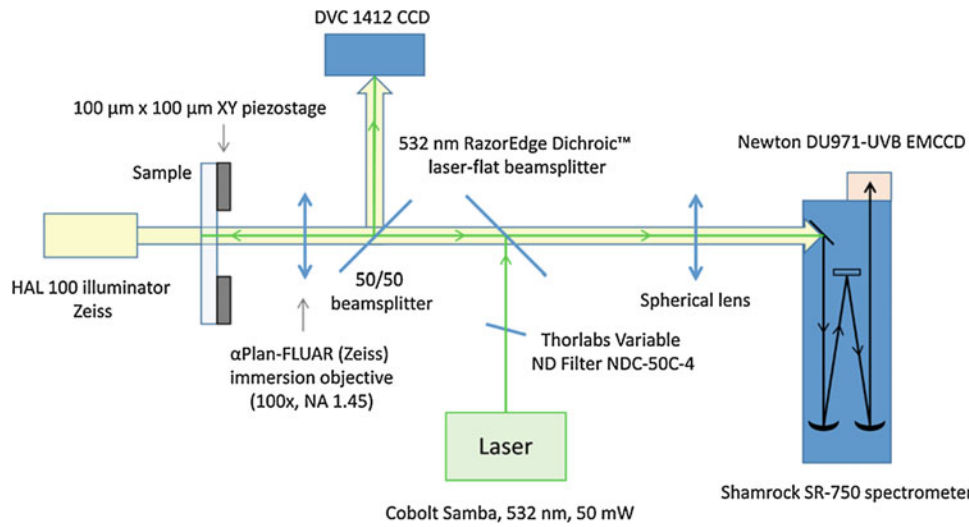

Fig. 1 A schematic drawing of the experimental setup

3 Method

3.1 Gold Nanoparticle Functionalization with DNA Oligonucleotides

Perform all procedures at room temperature, unless otherwise specified. Sterile conditions are not required.

3.1.1 Gold Nanoparticle Preparation

1. Coat gold nanoparticles (AuNP) with BSPP to prevent aggregation in highly concentrated solution [35]: add 14.4 mg of BSPP (pure) to 36 mL of gold colloid solution (from manufacturer) to reach an overall concentration of 0.5 mM and let it stabilize overnight in a continuous but gentle stirring.
2. Progressively add tiny amounts of NaCl waiting for the complete dissolution after every addition and keep stirring until the color changes from ruby red to purple/light grey. Quickly put the solution in 2 mL tubes and centrifuge at 10,000 × *g* for 10 min.
3. Remove the supernatant if transparent and resuspend the AuNP with a solution of 0.5 mM BSPP (*see* **Note 5**). Reduce the number of tubes using the smallest possible volume of 0.5 mM BSPP and unifying the obtained volumes.
4. Add 50% in volume of methanol (*see* **Note 6**) and centrifuge again (10,000 × *g*, for 10 min).
5. Repeat **steps 3** and **4** until you reduce the volume to 2 mL of solution. Use 2.5 mM BSPP for the last resuspension. Store at 4 °C (*see* **Note 7**).
6. Dilute 20 μL of the highly concentrated solution by adding 380 μL of ultrapure water (dilution 1:20). Measure the absorbance of the diluted solution in a quartz cuvette using the spectrophotometer. Determine the AuNP concentration from the maximum of the peak at 520 nm using the extinction coefficient provided by the manufacturer company (*see* **Note 8**).

3.1.2 DNA Oligonucleotide Preparation

Since the commercial DNA oligonucleotides are usually protected with a disulfide bond, the thiol group has to be activated before reacting with the nanoparticles gold surface.

1. Reduce 60 μL of 100 μM oligonucleotide solution (it is the amount to obtain 2 mL of 3 μM oligo) adding 60 μL of 0.8 M DTT, 10 μL 5 M NaCl, and 3.2 μL of 0.5 M SPB buffer (pH 7.0). Bring the volume to 160 μL with ultrapure water. Leave the solution ageing on a tube rotator for at least 2 h.
2. Dilute the highly concentrated nanoparticles solution: prepare 0.5 mL of 3 nM AuNP (according to the desired DNA molecules–NPs ratio: we use approximately 4000).

3. To allow the bond between gold surface and oligonucleotides thiol group we have to purify the DNA solution from the DTT molecules resulting in non–reducing environment.
4. Filter the DNA solution with NAP-5/NAP-10 columns (*see* **Note 9**): add 340 μL of ultrapure water to the 160 μL of reduced oligos solution (to reach 500 μL, the maximum volume accepted by NAP-5) and fill an equilibrated NAP-5 column with the sample, discarding the eluted volume. Add 1 mL of H_2O, letting the eluted volume drip directly on an equilibrated NAP-10 column. Add 1.5 mL of H_2O to the NAP-10 column, collecting the 1.5 mL of eluted solution (containing the purified DNA molecules) in a 2 mL tube.
5. Right before the AuNP addition, it is useful to take few microliters of filtered DNA solution to check the DNA concentration using a small volume spectrophotometer (like a NanoDrop-2000) (*see* **Note 10**).

3.1.3 Gold Nanoparticle Functionalization and Purification

The salt ageing process will provide the necessary ionic strength for DNA strands stability and will avoid aggregation between nanoparticles.

1. Immediately after the filtration of the reduced oligos, add the 0.5 mL of 1 nM diluted AuNP solution to the 1.5 mL oligonucleotide preparation. It is crucial to avoid the oxidation of thiol groups and the creation of disulfide bonds (most favorite than the reduced form). Leave the solution in agitation on a tube rotator overnight.
2. Add 40 μL of 0.5 M SPB to the 2 mL solution and leave it in agitation on a tube rotator overnight.
3. Add 6.7 μL of 5 M NaCl for six times over a 48 h time, to reach 0.1 M final concentration (*see* **Note 11**).
4. In order to allow the coupling of the DNA coated AuNP to external complementary DNA strands, the excess of oligonucleotides that did not react must be filtered out from the solution. Filter out the unreacted oligos in the 2 mL solution using Amicon® Ultra 0.5 mL (cutoff 100 kDa) following the manufacturer protocol (we use 14,000 × *g* for 1.5 min). Wash the 50 μL retained volume obtained with 450 μL of 1× TAE, 0.1 M NaCl three times through centrifugal steps as before. Collect the final retained volume obtained turning upside down the Amicon® Ultra filter in a clean collector tube and centrifuging it at 2000 × *g* for 3 min.
5. Resuspend the dark red precipitate in approximately 700 μL of 1× TAE, 0.1 M NaCl buffer.
6. For future uses of the functionalized NPs it is important measure the concentration of the solution using a spectrophotometer.

7. Agarose gel electrophoresis can be used to check the stability of the DNA functionalized AuNP against aggregation: add 3 μL of 6× loading buffer to approximately 17 μL of AuNP solution and load it on a 3.6% agarose gel casted in 1× TAE buffer and stained with 1× GelRed™. Run the electrophoresis for about 15 min at approximately 7 V/cm and check if the solution is still red colored during the run. Under the UV transilluminator, check if the red band corresponds to a DNA stained band to confirm the DNA-AuNP link.

3.2 Gold Nanoparticle Dimer Creation via DNA Functionalization

To create gold nanoparticle (AuNP) dimers, the solution of AuNP functionalized with DNA oligonucleotide (DNA-A) and the solution of AuNP functionalized with the complementary DNA oligonucleotide (DNA-C) are processed separately and then mixed as described above. The disaggregation method starts from a complete aggregated NPs solution and provides the dimers formation upon the addition of controlled amount of one of the two DNA complementary strands. The separation of aggregates composed by a different number of AuNP was carried out with electrophoretic analysis.

3.2.1 Creation of Gold Nanoparticle Dimers via Disaggregation

Both solutions of functionalized AuNP (DNA-A and its complementary DNA-C) must be free from all unreacted free oligonucleotides (*see* Subheading 3.1.3, above).

1. Mix two oligo-functionalized AuNP solutions in a 1:1 volume ratio (typical 100 μL each) resulting in fast aggregation of large nanoparticles clusters.
2. Add a controlled molar concentration of one of the two complementary strands. We use a fivefold excess with respect to the initial DNA concentration used in the AuNP functionalization reaction volume (*see* **Note 12**).
3. Heat the solution for 45 min at 50 °C and let cool to room temperature for at least 1 h in a tube rotator. The returning reddish color of the solution reveals an effective disaggregation of AuNP in small clusters.

3.2.2 Dimer Visualization Through Gel Electrophoresis and Collection

1. Prepare a 3.6% agarose electrophoretic gel and load 20 μL of dimers solution. Run the gel for approximately 15 min until the separation of little reddish bands becomes visible. These bands represent the AuNP aggregates with a discrete number of gold spheres. The monomers run quicker than dimers and trimers (*see* Fig. 2).
2. Cut out precisely the second band counting from the running front. This band contains the dimers population (*see* **Note 13**).
3. Place the gel band in a D-Tube Dialyzers device and extract the reddish AuNP from the band according to the manufacturer's

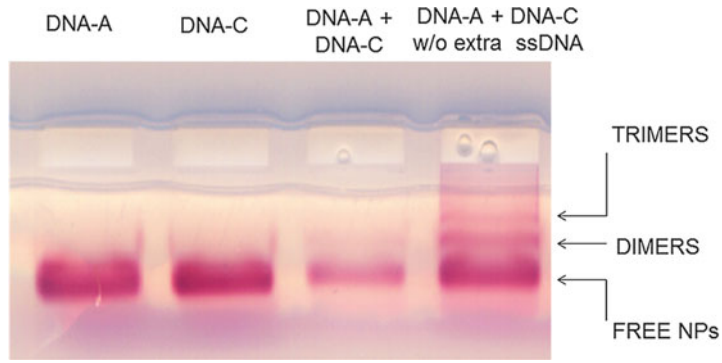

Fig. 2 Agarose gel of DNA-functionalized AuNP. DNA-A is one type of oligonucleotide-bearing AuNP; DNA-B is the AuNP bearing the oligonucleotide with a sequence complementary to those bound on DNA-A; DNA-A + DNA-C is the mix of DNA-A and DNA-B without removing the unbound oligonucleotides (the narrow band is the result of the hybridization of free complementary oligos to those bound on the AuNP); the last lane shows the result of mixing DNA-A and DNA-B after removing all unbound excess oligonucleotides

protocol. This allows the highest purity of the extracted aggregate (*see* **Note 14**).

4. Centrifuge the solution obtained for 8 min at 16,000 × *g* to concentrate the AuNP dimers in a pellet.
5. Remove the supernatant volume, until ~20 μL are left. Resuspend the pellet in the obtained volume and store at 4 °C.

3.3 DNA Origami Synthesis

3.3.1 DNA Origami Synthesis and Purification

1. Mix equal amounts of 100 μM staple oligonucleotides belonging to a structural module (i.e., core, edges, and catchers of the desired structure) to form a pool [36]. Group the about 200 oligonucleotides in three staple pools (*see* **Note 15**) such that each staple is present at the same concentration (160 nM).
2. Add together 100 μL of each of the three staple pools (160 nM), 7.15 μL of 250 μg/mL M13mp18 scaffold strand (equal to 111.6 nM), 50 μL of 10× TAEMg buffer, and 142.8 μL of ultrapure water. Vortex briefly and spin down the sample.
3. Divide the volume in five 200 μL tubes (100 μL each), load in the thermocycler and start the temperature program. The folding of DNA origami requires an initial heating to dehybridize double helices or secondary structures: 90 °C for 2 min, followed by slowly cooling down to room temperature along 5 h (*see* **Note 16**).
4. Pool the contents of the five tubes. Save 8 μL in a separate tube in order to analyze it later through electrophoresis and load all the rest in a single Amicon® Ultra 0.5 mL 100 kDa cutoff filter.

5. Centrifuge the solution using Amicon® Ultra 0.5 mL to purify the DNA origami from the excess of free DNA staple strands. Following the manufacturer's protocol centrifuge at 14,000 × *g* for 1.5 min (filtering step), then wash with 450 μL of 2× TAEMg.
6. Repeat **step 5** four times, carefully removing the filtered liquid at each filtering step.
7. Turn the filter upside down in a new Amicon® collecting tube and centrifuge at 2000 × *g* for 3 min. The final obtained volume should be ~50 μL.
8. Run a gel electrophoresis to analyze the folding quality and the concentration of the DNA origami. An example of typical loading of four gel wells:
   (a) 6 μL of 2-Log DNA Ladder solution.
   (b) 6 μL of ultrapure water + 0.3 μL of M13mp18 + 2 μL of 6× loading buffer.
   (c) 8 μL of unfiltered DNA origami sample + 10 μL of ultrapure water + 2 μL 6× loading buffer.
   (d) 8 μL of filtered DNA origami sample + 10 μL of ultrapure water + 2 μL 6× loading buffer (*see* Fig. 3).
9. Analyze the gel with a transilluminator and evaluate the band intensity using ImageJ software (as described in the ImageJ user guide) considering the intensity of the band of the unfiltered DNA origami sample with a concentration of 1.6 nM (the theoretical concentration), calculate the increased concentration after the filtration/volume reduction.

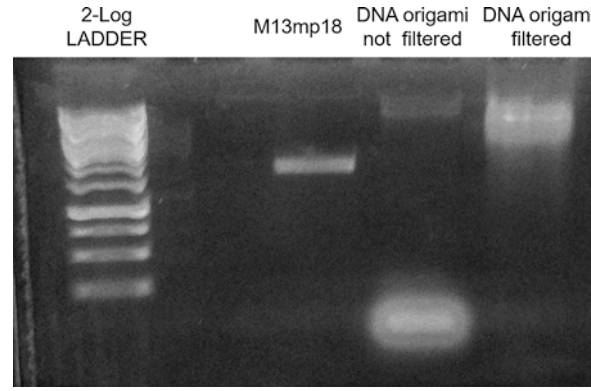

Fig. 3 Agarose gel electrophoresis of DNA origami before and after the Amicon filtration. The gel confirms the correct folding of the DNA origami and its concentration after the filtration process. The DNA origami scaffold (M13mp18), runs faster than DNA origami structure due to the lower molecular weight, is used as a control of the self-assembly. 2-Log is the molecular weight ladder

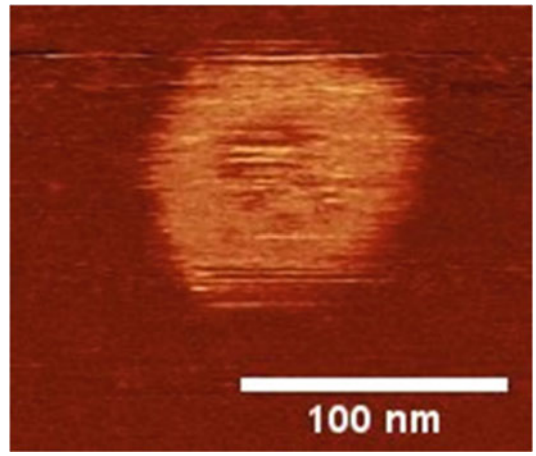

Fig. 4 A representative amplitude modulation AFM image of a hatch DNA origami structure recorded in solution

3.3.2 Atomic Force Microscope Characterization of DNA Origami Structure

1. For the AFM characterization, spread a small aliquot of the DNA origami sample on a freshly cleaved mica surface (with size and shape compatible with the AFM in use) in 2× TAEMg buffer (*see* **Note 17**).
2. Leave the sample incubating on mica for at least 5 min, preventing the solution from drying. Perform AFM imaging in liquid in amplitude modulation mode (AM AFM) (*see* **Note 18**) according to the microscope manufacturer's instructions or to the user's experience (*see* Fig. 4). We have successfully used a JPK Nanowizard II, a VEECO Multimode with Nanoscope V control or an Asylum MFP3D AFM system.

3.4 DNA Origami–Gold Nanoparticle Functionalization

1. Mix the ssDNA coated AuNP solution (*see* Subheading 3.1) with DNA origami solution (*see* Subheading 3.3) with 2:1 concentration ratio AuNP (6 nM) / DNA origami binding site (3 nM)- (*see* **Note 19**). If the AuNP solution is not sufficiently concentrated, centrifuge it at 10,000 × *g* for 3 min and pipette away the excess of volume (*see* **Note 20**).
2. Incubate the obtained mixed solution at 50 °C for 45 min in a thermostatic bath and let the sample cool down to room temperature over 16 h.
3. Run an agarose gel electrophoresis loading a sample made with 10 μL of the solution and 2 μL of 6× loading buffer in a 1% agarose. If the functionalized AuNP are attached to the DNA origami structure, the electrophoresis will show a reddish colored band also visible under UV light thanks to DNA staining (*see* Fig. 5).
4. Cut the agarose gel band with a razor blade in order to use it for the optical measurements.

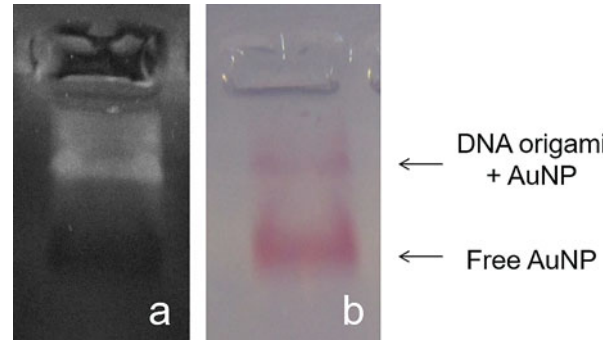

Fig. 5 UV (a) and visible light (b) image of the agarose gel electrophoretic analysis of DNA origami functionalized with AuNP

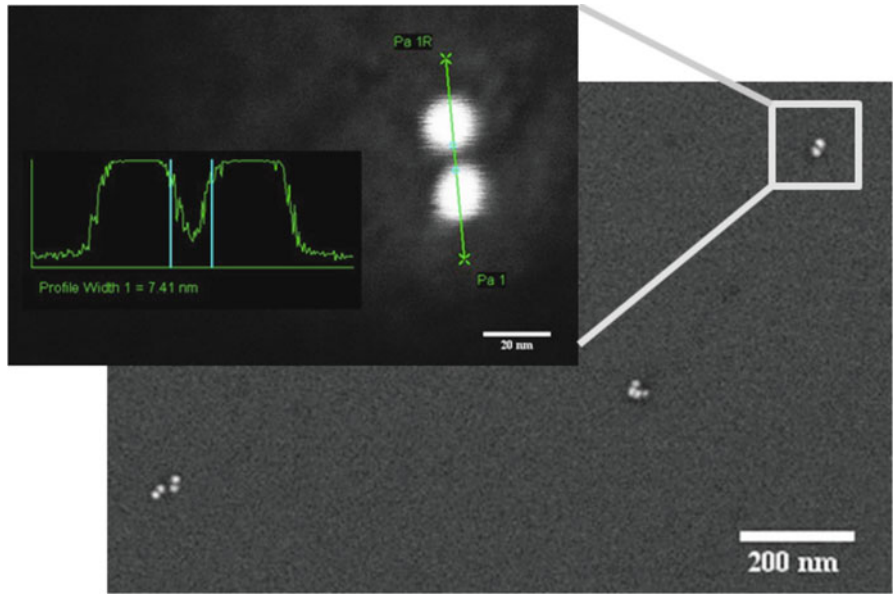

Fig. 6 SEM image of AuNP dimers directly extracted from the gel band. The inter-particle distance (insert) is in agreement with the length of the DNA oligonucleotides that coat the surface

3.5 SEM Characterization of the Gold Nanoparticles–DNA Hybrid Structures

1. Treat the silicon chip with oxygen plasma for 2 min at 80 W to make the surface more hydrophilic.
2. Drop 5 μL of purified solution of AuNP dimers (*see* Fig. 6) or a solution of DNA origami decorated with AuNP (*see* Fig. 7) and let it adsorb for 7 min.
3. Wash twice with ultrapure water to avoid salt crystals formation and let it dry leaning on blotting paper.
4. Image the sample with Scanning Electron Microscope. In our experiments SEM images were recorded with a SUPRA 40 (Zeiss) at 2 kV of acceleration voltage, a working distance between 2 and 5 mm and a filament current of 2.3 A.

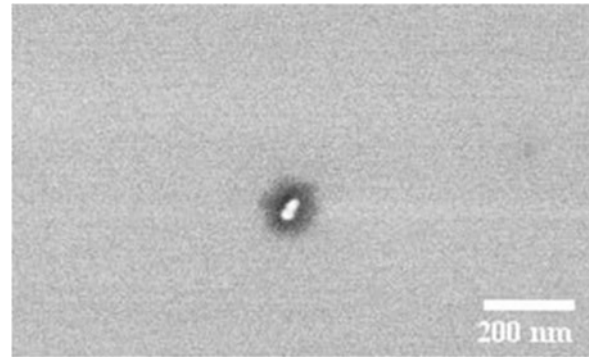

Fig. 7 Representative SEM image of DNA origami functionalized with AuNP in two sites

3.6 Gel-Direct Measurement of LSPR Absorption

The coverslip is mounted on the sample holder on the XY stage of the microscope. Before extinction measurements in the range of LSPR for AuNP (500–600 nm wavelength), the optical alignment is performed using a 532 nm laser (green lines in Fig. 1). The laser light is delivered to the inverted microscope and then focused on the coverslip surface by the 100× immersion objective. The reflected light is collected by the same objective and directed either on a monitoring CCD (DVC 1412) or into a spectrometer equipped with TE-cooled CCD. The shape of the laser spot is carefully analyzed by both CCDs and the required alignment is performed.

1. Cut out the gel in such a way to include the bands of interest but not exceed a lateral size of 10 mm by 10 mm for the slice.
2. Place the gel slice onto a clean glass coverslip maintaining the same orientation as in the gel (the gel running direction is parallel to the microscope focal plane).
3. Acquire the lamp spectrum through a gel region outside the AuNP bands. The measured spectra are necessary for the extinction calculation (*see* **Note 21**).
4. Calculate the actual extinction spectra: a basic equation used to calculate the extinction is $A + S + R + T = 1$, where A is absorption, S is scattering, $A + S = E$ is extinction, R is reflection, and T is transmission of the light. Neglecting the differences in the light reflection from the surfaces of clean gel and the one with AuNP, the extinction can be calculated as $E = 1 - T$. Thus, a final equation to calculate the extinction is: $E = (I_0 - I_i)/(I_0 - I_{bg})$ where I_i is the corresponding intensity of light passed through each band and I_0 is the intensity of light passed through the clean gel in a position without nanoparticles (and DNA origami in general). I_{bg} is the measured dark thermal noise of CCD (*see* **Note 22**). An example of extinction spectra is displayed in Fig. 8 [32].

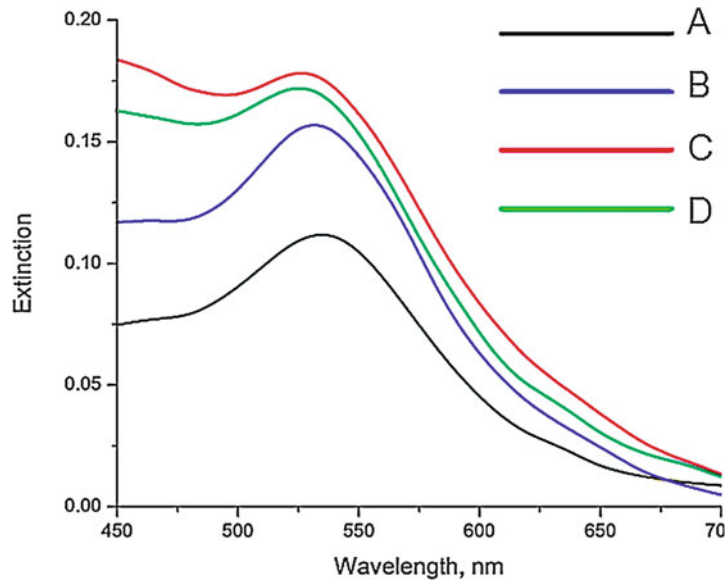

Fig. 8 The raw extinction spectra of gold nanoparticles dimers show an increasing blue shift with respect to the (A) initial peak position (B: 6.0 ± 1.0 nm, C: 5.7 ± 0.5 nm and D: 3.6 ± 0.7 nm) that correlates with the increasing interparticle distance

5. Using the XY micro positioning system, maximize the extinction signal at a fixed wavelength (for instance 550 nm). Then acquire extinction spectra at least in five different positions along each lane, check for spectra reproducibility and average them.

4 Notes

1. Do not leave the bottle unattended or sealed during the process: too vigorous boiling can force the solution out of the bottle or lead to explosion if the bottle is tightly closed.
2. Glycerol is a viscous solution and cutting the pipette tip apex can help in releasing the loaded volume.
3. Molecules larger than the largest pores in the matrix are excluded from the matrix and elute first; intermediate size molecules penetrate the matrix to various extents, depending on their size. Penetration of the matrix retards progress through the column: very small molecules elute last.
4. It is possible to mix together the oligonucleotides in three parts following their structural role (i.e., mix for central structure strands, mix for the catcher strands, and mix for strands at the edge): this allows the modification of one function (i.e.,

introduce new catchers for different targets) without re–preparing all the solutions from scratch.

5. It is helpful to use a small volume to resuspend the AuNP pellet and to transfer the same volume to another tube. In this way, it is possible to reduce the number of tubes used to concentrate the nanoparticles solution.
6. Methanol is toxic, so it must be used under a chemical hood.
7. Monitor the solution ruby red color during storage because it is an important indicator of good stability and resistance against aggregation.
8. The absorbance curve broadening could help to understand the degree of AuNP aggregation and the peak position could highlight the covering of the colloids [2].
9. NAP-5 and NAP-10 filtration columns require a vertically support with clamps to hold in place the column during the filtration and elution. The columns can be re–used for the filtration of the same sample (do not cross different DNA solutions in the same column) many times. Washing them with ultrapure water three times before and after use will elute away all the remained DTT molecules and will re–equilibrate them for a new use.
10. In this way we can calculate, a posteriori, the effective DNA molecules/AuNP ratio.
11. The solution color must remain ruby red during the process indicating no AuNP aggregation.
12. Example: initial DNA strand concentration of 3 μM means 15 μM of DNA strand addition.
13. The use of a razor blade allows to be more precise and to get rid of the unwanted AuNP aggregates.
14. Alternatively, to collect the AuNP aggregates from the gel band a downstream pocket could be cut right after the desired band and filled with running buffer. Continue the electrophoresis run at 150 V till all the dimer aggregates fall down to the pocket and then collect the volume in a vial. This method does not need any specific device but it delivers worse results in the terms of dimers aggregates purity.
15. The average length of the oligonucleotides can be modified at the project level; giving the staples larger binding domains with the scaffold helps to achieve higher binding specificity and higher binding energy which increase the melting temperature [22].
16. The length of the thermal annealing ramp is correlated with the complexity of the achievable structure (i.e., the 3D architecture require more time to reach the most stable configuration) [23].

17. Mg^{2+} cations act as bridges between the negatively charged phosphate backbone of the DNA and surface, thereby increasing the adhesion of the DNA onto the mica surface [37].
18. We recommend Olympus OMCL-TR400PSA tips with a force constant of 0.08 N/m and a resonance frequency of 34 kHz, in air.
19. Doubling the concentration of functionalized AuNP respect to DNA origami provides a good saturation of the binding sites on the DNA structure.
20. Try to remove the excess of volume only when the supernatant is transparent. As an example: to double the concentration take double of the needed volume and centrifuge AuNP solution, and after the centrifugation step just remove half the volume to obtain the right concentration.
21. Check that gel is not drying during measurement: if necessary place a wet cloth around the sample to minimize water evaporation. As a result of drying, the gel shrinks forcing AuNP closer and thus changing the absorption spectra.
22. It should be noted that the normalization of extinction spectra is often applied to analyze the LSPR peak positions, however, the normalization procedure influences on the width of LSPR peak and often complicates the analysis when a role of AuNP dimers or aggregates should be discriminated.

References

1. Ghosh SK, Pal T (2007) Interparticle coupling effect on the surface plasmon resonance of gold nanoparticles: from theory to applications. Chem Rev 107(11):4797–4862. https://doi.org/10.1021/cr0680282
2. Reinhard BM, Siu M, Agarwal H, Alivisatos AP, Liphardt J (2005) Calibration of dynamic molecular rulers based on plasmon coupling between gold nanoparticles. Nano Lett 5 (11):2246–2252. https://doi.org/10.1021/nl051592s
3. Liu GL, Yin Y, Kunchakarra S, Mukherjee B, Gerion D, Jett SD, Bear DG, Gray JW, Alivisatos AP, Lee LP, Chen FF (2006) A nanoplasmonic molecular ruler for measuring nuclease activity and DNA footprinting. Nat Nanotechnol 1(1):47–52. https://doi.org/10.1038/nnano.2006.51
4. Mirkin CA, Letsinger RL, Mucic RC, Storhoff JJ (1996) A DNA-based method for rationally assembling nanoparticles into macroscopic materials. Nature 382(6592):607–609. https://doi.org/10.1038/382607a0
5. Alivisatos AP, Johnsson KP, Peng X, Wilson TE, Loweth CJ, Bruchez MP Jr, Schultz PG (1996) Organization of 'nanocrystal molecules' using DNA. Nature 382 (6592):609–611. https://doi.org/10.1038/382609a0
6. Zheng Y, Li Y, Deng Z (2012) Silver nanoparticle-DNA bionanoconjugates bearing a discrete number of DNA ligands. Chem Commun 48(49):6160–6162. https://doi.org/10.1039/c2cc32338a
7. Yoon B, Luedtke WD, Barnett RN, Gao J, Desireddy A, Conn BE, Bigioni T, Landman U (2014) Hydrogen-bonded structure and mechanical chiral response of a silver nanoparticle superlattice. Nat Mater 13(8):807–811. https://doi.org/10.1038/nmat3923
8. Elghanian R, Storhoff JJ, Mucic RC, Letsinger RL, Mirkin CA (1997) Selective colorimetric detection of polynucleotides based on the distance-dependent optical properties of gold nanoparticles. Science 277(5329):1078–1081
9. Liu J, Lu Y (2005) Fast colorimetric sensing of adenosine and cocaine based on a general

sensor design involving aptamers and nanoparticles. Angew Chem 45(1):90–94. https://doi.org/10.1002/anie.200502589

10. Chen JI, Chen Y, Ginger DS (2010) Plasmonic nanoparticle dimers for optical sensing of DNA in complex media. J Am Chem Soc 132 (28):9600–9601. https://doi.org/10.1021/ja103240g
11. Graham D, Thompson DG, Smith WE, Faulds K (2008) Control of enhanced Raman scattering using a DNA-based assembly process of dye-coded nanoparticles. Nat Nanotechnol 3 (9):548–551. https://doi.org/10.1038/nnano.2008.189
12. Qian X, Zhou X, Nie S (2008) Surface-enhanced Raman nanoparticle beacons based on bioconjugated gold nanocrystals and long range plasmonic coupling. J Am Chem Soc 130 (45):14934–14935. https://doi.org/10.1021/ja8062502
13. Lim DK, Jeon KS, Kim HM, Nam JM, Suh YD (2010) Nanogap-engineerable Raman-active nanodumbbells for single-molecule detection. Nat Mater 9(1):60–67. https://doi.org/10.1038/nmat2596
14. Zhang J, Fu Y, Chowdhury MH, Lakowicz JR (2007) Metal-enhanced single-molecule fluorescence on silver particle monomer and dimer: coupling effect between metal particles. Nano Lett 7(7):2101–2107. https://doi.org/10.1021/nl071084d
15. Sonnichsen C, Reinhard BM, Liphardt J, Alivisatos AP (2005) A molecular ruler based on plasmon coupling of single gold and silver nanoparticles. Nat Biotechnol 23 (6):741–745. https://doi.org/10.1038/nbt1100
16. Reinhard BM, Sheikholeslami S, Mastroianni A, Alivisatos AP, Liphardt J (2007) Use of plasmon coupling to reveal the dynamics of DNA bending and cleavage by single EcoRV restriction enzymes. Proc Natl Acad Sci U S A 104(8):2667–2672. https://doi.org/10.1073/pnas.0607826104
17. Skewis LR, Reinhard BM (2008) Spermidine modulated ribonuclease activity probed by RNA plasmon rulers. Nano Lett 8 (1):214–220. https://doi.org/10.1021/nl0725042
18. Wang H, Reinhard BM (2009) Monitoring simultaneous distance and orientation changes in discrete dimers of DNA linked gold nanoparticles. J Phys Chem C Nanomater Interfaces 113(26):11215–11222. https://doi.org/10.1021/jp900874n
19. Piantanida L, Naumenko D, Lazzarino M (2014) Highly efficient gold nanoparticle dimer formation via DNA hybridization. RSC Adv 4(29):15281–15287. https://doi.org/10.1039/C3RA47478J
20. Devries GA, Brunnbauer M, Hu Y, Jackson AM, Long B, Neltner BT, Uzun O, Wunsch BH, Stellacci F (2007) Divalent metal nanoparticles. Science 315(5810):358–361. https://doi.org/10.1126/science.1133162
21. Wang ZG, Song C, Ding B (2013) Functional DNA nanostructures for photonic and biomedical applications. Small 9(13):2210–2222. https://doi.org/10.1002/smll.201300141
22. Rothemund PW (2006) Folding DNA to create nanoscale shapes and patterns. Nature 440 (7082):297–302. https://doi.org/10.1038/nature04586
23. Douglas SM, Dietz H, Liedl T, Hogberg B, Graf F, Shih WM (2009) Self-assembly of DNA into nanoscale three-dimensional shapes. Nature 459(7245):414–418. https://doi.org/10.1038/nature08016
24. Sacca B, Niemeyer CM (2011) Functionalization of DNA nanostructures with proteins. Chem Soc Rev 40(12):5910–5921. https://doi.org/10.1039/c1cs15212b
25. Torelli E, Marini M, Palmano S, Piantanida L, Polano C, Scarpellini A, Lazzarino M, Firrao G (2014) A DNA origami nanorobot controlled by nucleic acid hybridization. Small 10 (14):2918–2926. https://doi.org/10.1002/smll.201400245
26. Shen X, Zhan P, Kuzyk A, Liu Q, Asenjo-Garcia A, Zhang H, de Abajo FJ, Govorov A, Ding B, Liu N (2014) 3D plasmonic chiral colloids. Nanoscale 6(4):2077–2081. https://doi.org/10.1039/c3nr06006c
27. Shen X, Song C, Wang J, Shi D, Wang Z, Liu N, Ding B (2012) Rolling up gold nanoparticle-dressed DNA origami into three-dimensional plasmonic chiral nanostructures. J Am Chem Soc 134(1):146–149. https://doi.org/10.1021/ja209861x
28. Lan X, Chen Z, Dai G, Lu X, Ni W, Wang Q (2013) Bifacial DNA origami-directed discrete, three-dimensional, anisotropic plasmonic nanoarchitectures with tailored optical chirality. J Am Chem Soc 135(31):11441–11444. https://doi.org/10.1021/ja404354c
29. Sharma J, Chhabra R, Andersen CS, Gothelf KV, Yan H, Liu Y (2008) Toward reliable gold nanoparticle patterning on self-assembled DNA nanoscaffold. J Am Chem Soc 130 (25):7820–7821. https://doi.org/10.1021/ja802853r
30. Ding B, Deng Z, Yan H, Cabrini S, Zuckermann RN, Bokor J (2010) Gold nanoparticle self-similar chain structure organized by DNA

origami. J Am Chem Soc 132(10):3248–3249. https://doi.org/10.1021/ja9101198

31. Kuzyk A, Schreiber R, Zhang H, Govorov AO, Liedl T, Liu N (2014) Reconfigurable 3D plasmonic metamolecules. Nat Mater 13(9):862–866. https://doi.org/10.1038/nmat4031
32. Piantanida L, Naumenko D, Torelli E, Marini M, Bauer DM, Fruk L, Firrao G, Lazzarino M (2015) Plasmon resonance tuning using DNA origami actuation. Chem Commun 51(23):4789–4792. https://doi.org/10.1039/c5cc00778j
33. Brewer SH, Glomm WR, Johnson MC, Knag MK, Franzen S (2005) Probing BSA binding to citrate-coated gold nanoparticles and surfaces. Langmuir 21(20):9303–9307. https://doi.org/10.1021/la050588t
34. Bidault S, Polman A (2012) Water-based assembly and purification of Plasmon-coupled gold nanoparticle dimers and Trimers. Int J Optics 2012:5. https://doi.org/10.1155/2012/387274
35. Thompson DG, Stokes RJ, Martin RW, Lundahl PJ, Faulds K, Graham D (2008) Synthesis of unique nanostructures with novel optical properties using oligonucleotide mixed-metal nanoparticle conjugates. Small 4 (8):1054–1057. https://doi.org/10.1002/smll.200700938
36. Castro CE, Kilchherr F, Kim DN, Shiao EL, Wauer T, Wortmann P, Bathe M, Dietz H (2011) A primer to scaffolded DNA origami. Nat Methods 8(3):221–229. https://doi.org/10.1038/nmeth.1570
37. Kopielski A, Csaki A, Fritzsche W (2015) Surface mobility and ordered rearrangement of immobilized DNA origami. Langmuir 31 (44):12106–12110. https://doi.org/10.1021/acs.langmuir.5b03137

Chapter 20

DNA-Assisted Molecular Lithography

Boxuan Shen, Veikko Linko, and J. Jussi Toppari

Abstract

During the past decade, DNA origami has become a popular method to build custom two- (2D) and three-dimensional (3D) DNA nanostructures. These programmable structures could further serve as templates for accurate nanoscale patterning, and therefore they could find uses in various biotechnological applications. However, to transfer the spatial information of DNA origami to metal nanostructures has been limited to either direct nanoparticle-based patterning or chemical growth of metallic seed particles that are attached to the DNA objects. Here, we present an alternative way by combining DNA origami with conventional lithography techniques. With this DNA-assisted lithography (DALI) method, we can create plasmonic, entirely metallic nanostructures in a highly accurate and parallel manner on different substrates. We demonstrate our technique by patterning a transparent substrate with discrete bowtie-shaped nanoparticles, i.e., "nanoantennas" or "optical antennas," with a feature size of approximately 10 nm. Owing to the versatility of DNA origami, this method can be effortlessly generalized to other shapes and sizes.

Key words Nucleic acids, DNA nanotechnology, DNA origami, Self-assembly, Thin films, Metal nanostructures, Nanoparticles, Plasmonics

1 Introduction

Today, there exist various different techniques to create nucleic acid nanoarchitectures with well-controlled dimensions and features [1, 2]. During the past 10 years, the most commonly used method to build with nucleic acids has been a DNA origami [3, 4], which is based on folding a long scaffold strand into a desired shape with the help of dozens of short staple strands. Conventionally, this method allows users to design custom two- and three-dimensional shapes with dimensions of 1–100 nm with nanometer-scale feature sizes. Recently, even more sophisticated and fully automated techniques to create user-defined DNA structures have become available [5]. It is noteworthy that along the evolution of the design techniques, the structural DNA nanotechnology has taken huge steps toward the phase where the real-life applications start to emerge. In general, these DNA nanostructures can serve as modular platforms for accurate molecular-level assembling of materials. Recent examples

Giampaolo Zuccheri (ed.), *DNA Nanotechnology: Methods and Protocols*, Methods in Molecular Biology, vol. 1811,
https://doi.org/10.1007/978-1-4939-8582-1_20, © Springer Science+Business Media, LLC, part of Springer Nature 2018

of DNA-based applications include artificial ion channels [6] and enzyme cascades [7], plasmonic devices [8], drug-delivery vehicles [9] and versatile templates for nanoelectronics [10–12] and nano-optics [13].

Besides the abovementioned examples, one intriguing possibility would be to utilize the superior spatial addressability of such structures for creating (entirely) metallic designer nanoshapes for plasmonics and electronics. However, this has proven to be somewhat challenging. In fact, there are ways to realize such structures by using metal nanoparticle-based patterning and chemical growth of the attached seed particles [8, 14–20], but alas, these methods often suffer from low resolution and may yield grainy or discontinuous structures.

Here, we present a novel method to produce well-controlled metallic nanostructures by genuinely combining the bottom-up assembly of DNA nanostructures with conventional top-down lithography techniques. We use a bowtie-shaped DNA origami as an example object and transfer its spatial information to a metallic structure. The technique is based on selective silicon dioxide growth on a silicon substrate onto which the DNA origami structures have been deposited [21, 22]. As the oxide primarily grows on the bare areas of the chip, the process will yield a layer that contains discrete origami-shaped holes or the so-called "origami silhouettes." This stencil-like oxide layer can be further used as a mask in the following etching and metal deposition steps [22]. With this method, we can create precise gold nanoantennas on transparent substrates that can be used, for example, as molecular-level plasmonic sensors or in surface-enhanced Raman spectroscopy [23].

2 Materials

All solutions should be prepared using ultrapure water (e.g., MilliQ, 18.2 MΩ cm at 25 °C).

2.1 DNA Origami Preparation

2.1.1 DNA Origami Materials

1. 7249-nucleotide long viral single-stranded DNA (ssDNA), M13mp18 at 100 nM concentration (Tilibit Nanosystems).
2. A set of short staple strands at 100 μM concentration. A bowtie-shaped DNA origami, used as an example here, includes in total 205 different staple strands: 118 core strands and 87 side strands with TTTTTTTT-overhangs for preventing stacking of the origami structures. The full list of sequences can be found in ref. [23].
3. 2.5× TAE buffer with Mg: 100 mM Tris, 47.5 mM acetic acid, 2.5 mM EDTA, 31.25 mM $MgCl_2$, pH = 8.3.

2.1.2 Optional Purification of DNA Origami

1. Millipore Amicon Ultra Centrifugal Filters, 0.5 mL with 100 kDa molecular weight cutoff (MWCO).
2. 1× TAE buffer with Mg: dilute from 2.5× (*see* above, Subheading 2.1.1) using ultrapure water.

2.2 DNA-Assisted Lithography

2.2.1 Substrate Preparation

1. Sapphire wafer (University Wafers): 50.8 mm in diameter, C→M orientation, double-side-polished, 430 μm thick.
2. Dicing saw equipped with a blade for sapphire.
3. Isopropanol (IPA).
4. Acetone.
5. Ultrasonicator.
6. Cotton sticks.
7. Oxford Plasmalab 80 Plus chemical vapor depositor (CVD) equipped with silane (5% SiH_4 in 95% N_2).

2.2.2 DNA Origami Immobilization

1. Oxford Plasmalab 80 Plus reactive ion etcher (RIE) equipped with O_2.
2. DNA origami solution (20 nM) in the origami folding buffer (*see* Subheading 3.1).
3. 1× TAE buffer with 500 mM magnesium acetate (MgAc).

2.2.3 SiO_2 Mask Growth

1. Glass desiccator (1.5 L in volume).
2. Silica gel with indicator (granulate), bead size approximately 1–3 mm (Merck).
3. Environmental chamber (WEISS).
4. Tetraethyl orthosilicate (TEOS, ≥99.0%).
5. Ammonium hydroxide (NH_4OH) water solution of 25% concentration.

2.2.4 Lithography Steps

1. Oxford Plasmalab 80 Plus RIE equipped with SF_6, CHF_3 and O_2.
2. Ultra-high vacuum (UHV) e-beam evaporator equipped with Cr and Au.
3. Hydrofluoric acid (HF, 38% in H_2O).

2.3 Characterization (SEM, AFM, Gel Electrophoresis)

1. Raith eLine scanning electron microscopy system.
2. AFM (Veeco, Dimension 3100) operating in tapping mode.
3. Gel running buffer (1× TAE with 11 mM $MgCl_2$): 40 mM Tris, 19 mM acetic acid, 1 mM EDTA, 11 mM $MgCl_2$.
4. Agarose gel: prepare 2% agarose gels by dissolving 2 g of agarose in 100 mL of gel running buffer. Mix and heat the solution shortly in a microwave oven in order to dissolve agarose properly. Allow the solution to cool a bit and finally

stain with 100 μL of ethidium bromide (EthBr) solution (0.625 mg/mL). Cast immediately.

5. DNA origami samples (*see* Subheading 3.1).
6. 6× loading dye (New England Biolabs).
7. M13mp18 ssDNA (Tilibit Nanosystems).

3 Methods

3.1 DNA Origami Preparation

The chosen origami shape is a two-dimensional bowtie-shape (*see* **Note 1**) that is designed in square lattice geometry [24] using caDNAno and CanDo softwares [25]. The structure comprises of a 7249 bases long M13mp18 plasmid scaffold and 205 short oligonucleotides that fold the scaffold into the desired shape in a thermal annealing process. The structure is twist-corrected, i.e., the twist resulting from the square lattice packing [24] is relaxed by additional base skips in the design [26]. The staple design, core staple sequences, side strands, and the thermal ramp for folding have been adapted from ref. [23]. The excess staple strands can be optionally removed after annealing by a nondestructive spin-filtering procedure.

3.1.1 DNA Origami Annealing

The concentration of the scaffold strand in the total reaction volume of 100 μL is 20 nM and the concentration of magnesium is 12.5 mM (*see* **Note 1**). The staple strands are used in tenfold excess compared to the M13mp18 scaffold strand.

1. Prepare the staple strand mix (each staple at about 500 nM concentration): pipet equal amounts of each 205 staple strands (at 100 μM) and mix them together.
2. Add 40 μL of staple strand mix to 20 μL of 100 nM M13mp18 ssDNA and 40 μL of 2.5× TAE buffer (with Mg).
3. Anneal the solution from 90 to 70 °C with the increments of 0.2 °C/8 s, from 70 to 60 °C with the increments of 0.1 °C/8 s, and from 60 to 27 °C with the increments of 0.1 °C/2 min. Store the solution at 12 °C. The theoretical maximum concentration of DNA origami is 20 nM (assuming 100% yield in folding).

3.1.2 Optional Purification of DNA Origami

Most of the excess staples can be removed in a nondestructive spin-filtering process. This is not a necessary step, since the small staple strands do not interfere in the chemical vapor deposition of the silicon oxide layer (*see* Subheading 3.2.3). However, in the spin-filtering process, the buffer can be exchanged (from TAE-based buffer to a buffer of choice). Here, the purification is described using 1× TAE buffer (with Mg). For filtering, 0.5 mL Millipore Amicon Ultra Centrifugal Filters with 100 kDa MWCO are used.

1. Add 50 μL of DNA origami solution to one Amicon Ultra Centrifugal filter and dilute to 500 μL using 1× TAE buffer (with Mg).
2. Centrifuge the solution for 3 min at 14,000 × *g* and discard the filtrate .
3. Add 450 μL of TAE buffer (with Mg) to the filter and centrifuged again for 3 min using 14,000 × *g*. Discard the filtrate.
4. Repeat **step 3** above for two more times.

Gently pipet the retentate out from the filter unit. Alternatively, the filter can be turned upside down in a fresh container and spun for 2 min at 1000 × *g* in order to collect the rest of the solution from the filter. Typically, the filtration procedure yields 17–20 μL of purified origami solution.

3.2 DNA-Assisted Lithography (DALI)

In this DNA-assisted lithography (DALI) method, gold (entirely metallic) nanostructures with the shape of a bowtie antenna are fabricated on a sapphire substrate. Depending on the reactive ion etching conditions, the metallic structures can assume two different shapes: connected triangles or two separate triangles with a 5–20 nm gap between them (for more details, *see* **Note 2**). A complete protocol with all fabrication steps is shown in Fig. 1. This section contains the detailed protocols for all the steps (divided into subsections) in the same order as in Fig. 1.

3.2.1 Substrate Preparation

1. Cut the sapphire wafer first into 7 mm × 7 mm chips with a dicing saw. As a standard practice, glue the backside of the wafer to a piece of tape in order to fix the position of the wafer in the flow of cooling water while cutting.
2. Clean the chips in hot acetone and transfer them into IPA. Ultra-sonicate for 2 min. If there is still glue residue on the surface of the chip, remove it by gently rubbing the surface with a cotton stick.
3. After cleaning, dry the sapphire chips using nitrogen flow.
4. Deposit an approximately 50 nm layer of amorphous silicon (a-Si) on top of the sapphire chip by using plasma enhanced chemical vapor deposition (PECVD). The process parameters are listed in Table 1. The deposition rate is roughly 36 nm/min (*see* **Note 3**).

3.2.2 DNA Origami Immobilization

Silicon and native oxide layers are neutral in charge without any treatment. To adsorb the negatively charged DNA origami, the surface has to be treated with either O_2 plasma or piranha solution in order to make it slightly negatively charged. With the help of divalent cations, e.g., Mg^{2+}, DNA origami can be subsequently immobilized to the substrate. To increase the adsorption yield,

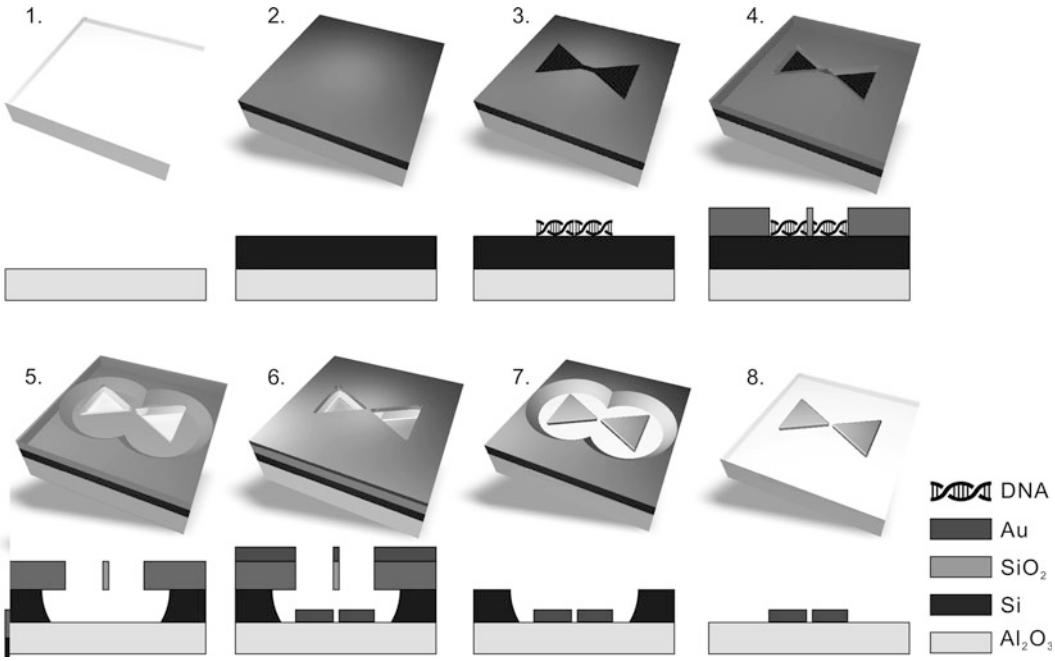

Fig. 1 Schematic 3D representations and cross section views of all the fabrication steps (adapted from Ref. [23])

Table 1
Parameters for a-Si PECVD

5% SiH_4 in 95% N_2 flow	500 sccm
Pressure	1000 mTorr
R.F. power	15 W
Temperature	250 °C
Time	1.5 min

Mg^{2+} concentrations should typically be higher than in the standard folding buffers. In this protocol, we use O_2 plasma since reactive ion etching (RIE) is essential also in the later fabrication steps.

1. Mix 8 μL of DNA origami solution (20 nM), 8 μL of 1× TAE buffer and 4 μL of 1× TAE buffer with 500 mM Mg^{2+}. This results in 20 μL of solution with the final Mg^{2+} concentration of 100 mM (*see* **Note 4**).
2. Use O_2 plasma in a RIE chamber to make the a-Si surface on the sapphire chips hydrophilic and negatively charged (*see* **Note 5**). The process parameters are listed in Table 2.

Table 2
Parameters for O_2 plasma reactive ion etching (RIE)

O_2	50 sccm
Pressure	40 mTorr
R.F. power	200 W
Temperature	30 °C
Time	20 min

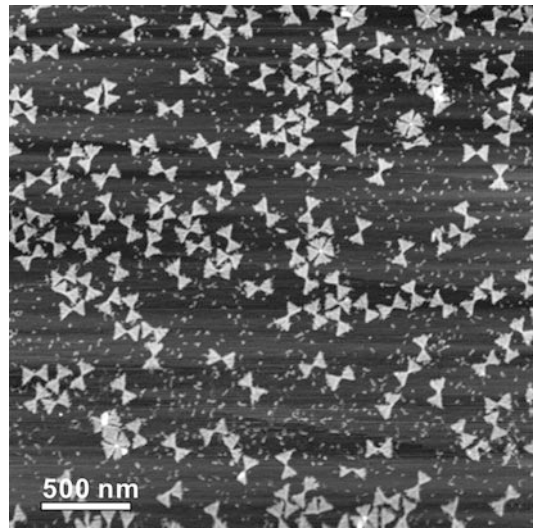

Fig. 2 AFM micrograph of bowtie DNA origami immobilized on silicon (adapted from Ref. [23])

3. Drop 10 μL of the DNA origami solution on a treated sapphire chip and incubate for 5 min in a closed chamber to prevent from drying.
4. Wash the excess DNA origami away gently by using 60 μL of ultrapure water. Repeat the wash three times (*see* **Note 6**).
5. Dry the sample with nitrogen gas flow. An AFM image of a typical sample after the DNA origami deposition is shown in Fig. 2.

3.2.3 Negative SiO_2 Mask Growth

The key step of this lithographical method is to transfer the programmable shape of the DNA origami to a negative SiO_2 mask that can be used in the later steps (conventional microfabrication). This selective SiO_2 deposition method is adapted from ref. [21].

1. Incubate 100 g of silica gel in a flat Petri dish (or similar container) in an environmental chamber at room temperature and 80% relative humidity for 20 h.

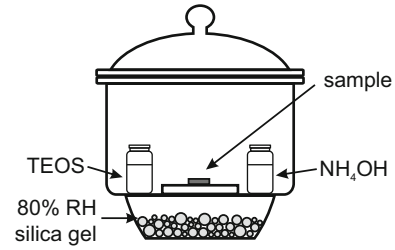

Fig. 3 Schematic illustration of the reaction chamber setup for growing SiO_2 in a room temperature CVD process (adapted from Ref. [23])

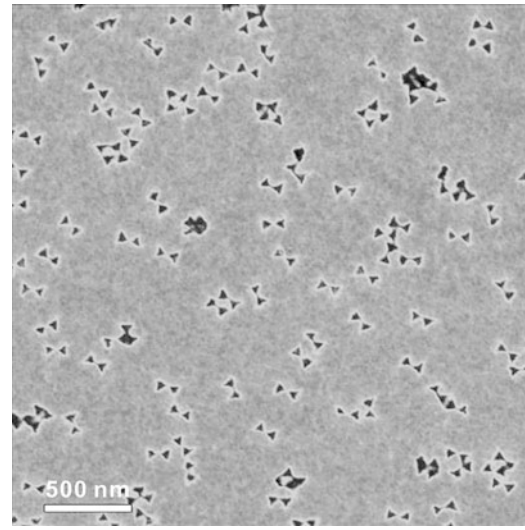

Fig. 4 AFM micrograph after the SiO_2 deposition. The SiO_2 layer contains DNA origami—shaped holes (adapted from Ref. [23])

2. Place the incubated silica gel at the bottom of a 1.5 L desiccator. On top of that, place two small vials, one containing 10 mL of TEOS and the other containing 10 mL of 25% NH_4OH, on opposite sides of the sample on a small stage (*see* **Note 7**). A schematic illustration of the desiccator setup is shown in Fig. 3.
3. Seal the desiccator and incubate for 22 h at room temperature. Take the sample out and dispose of the waste chemicals.
4. Image the grown SiO_2 layer with origami-shaped holes using AFM (*see* Fig. 4).

3.2.4 Etching of SiO_2 and Si Sacrifice Layer

The result from the previous step (Subheading 3.2.3) should be a 10–20 nm thick SiO_2 layer. However, this thickness is not usually sufficient as a mask for creating nanostructures having thicknesses more than 10 nm. Therefore, the silicon support underneath the oxide needs to be removed so that there will be enough space to deposit the metal layer. In addition, the undercut due to the

Table 3
Parameters for RIE SiO_2 etching

CHF_3	25 sccm
Ar	25 sccm
Pressure	30 mTorr
R.F. power	100 W
Temperature	25 °C
Time	18 s

Table 4
Parameters for RIE Si etching

O_2	8 sccm
SF_6	100 sccm
Pressure	90 mTorr
R.F. power	50 W
Temperature	30 °C
Time	35 s

isotropic etching of Si will also help in the lift-off process. Before the Si etching (Table 4), a short SiO_2 etching is performed (Table 3), since there is actually a very thin layer of SiO_2 on top of DNA origami.

1. Vent the RIE chamber and place the sample in the chamber.
2. Evacuate chamber to the base pressure and run a SiO_2 etching process with the parameters presented in Table 3 (*see* **Note 2**).
3. Keep the sample in the vacuum chamber and immediately run a Si etching program with parameters listed in Table 4.
4. Vent the RIE chamber and take the sample out for physical vapor deposition (PVD) of metals.

3.2.5 Physical Vapor Deposition (PVD) of Metals

Gold is an excellent material for plasmonics and a very stable metal. It will not suffer from oxidation like other more reactive metals such as silver and copper. For this reason, we will use it as an example in this recipe. Unfortunately, gold is also notorious for its poor adhesion to common substrates. To improve adhesion, either chromium (Cr) or titanium (Ti) is usually used as a stick-layer between the substrate and the deposited gold layer. In this method, we use Cr, since Ti is prone to HF etching. For the PVD of metals, we use e-beam evaporation in UHV conditions.

1. Vent the UHV chamber (or the load chamber) and load the sample (via the load chamber, if present).
2. Evacuate the chamber and bring the sample to the evaporation position.
3. Face the sample away from metal crucible and start to heat the Cr target slowly until the evaporation rate stabilizes at 0.1 nm/s.
4. Start the deposition onto the sample by turning the sample face toward the metal target in perpendicular orientation.
5. Stop the deposition by turning the sample around again when the evaporated thickness reaches 2 nm.
6. Stop the heating and wait until Cr is cooled.
7. Switch the metal target from Cr to Au without breaking the vacuum (*see* **Note 8**).
8. Heat the gold target slowly until the evaporation rate stabilizes at 0.05 nm/s.
9. Face the sample toward the gold crucible and evaporate 20 nm of gold to the sample.
10. Stop the evaporation by turning the sample around again.
11. Slowly cool down until the gold is not glowing red anymore.
12. Unload the sample by venting the chamber directly (or via the load chamber if available).

After this step the metallic film with the DNA origami-shaped openings can be seen under SEM (*see* Fig. 5).

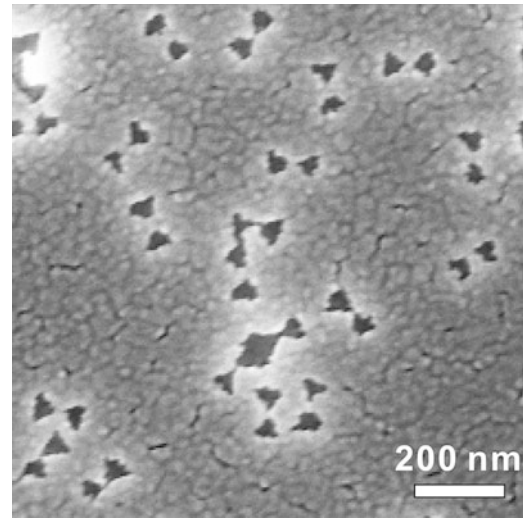

Fig. 5 SEM micrograph of a sample after the Cr and Au deposition and before HF lift-off (adapted from Ref. [23])

3.2.6 HF Lift-Off

The metallic nanostructures having the same shapes as the DNA origami templates are already formed during the previous step and they lie underneath the SiO_2 mask. To reveal the fabricated structures, the metal layer on top of SiO_2 mask needs to be removed together with the mask. This can be realized by HF etching (lift-off process). WARNING: HF is a very aggressive and poisonous acid, it can cause deep tissue damages and systemic toxicity, and therefore proper protection and training for emergency handling must be carried out in advance.

1. Pour enough 38% HF solution in an open plastic container until the sample can be fully submerged in the liquid.
2. Use plastic tweezers to dip the sample in HF and gently stir the sample to facilitate the detachment of big pieces of gold film.
3. After the gold film is fully detached, place the sample into a container filled with water.
4. Rinse the sample with water and dry with nitrogen gas.
5. Dispose the HF with care according to regulations.

3.2.7 Post Reactive Ion Etching (Post-RIE) of Si

This step is to remove the remaining a-Si layer by RIE. This can be carried out using the same Si etching program as in Table 4. Sometimes the Si layer detaches already in the HF-based lift-off process (it can be easily noticed by the change of the sample color), and in that case this post-RIE etching step is optional.

3.3 Characterizations

3.3.1 Gel Electrophoresis for DNA Origami

The gel electrophoresis can be used to verify the quality of the DNA origami folding. It is based on the comparison of the running speeds of the free scaffold strand (M13mp18 ssDNA) and the folded product.

1. Add 10 μL of the DNA origami to 2 μL of 6× loading dye.
2. Dilute M13mp18 ssDNA (at 100 nM) to 20 nM concentration with the folding buffer (1× TAE with Mg) and add 10 μL of 20 nM M13mp18 to 2 μL of 6× loading dye. Use the scaffold strand as a reference sample.
3. Load the wells with 10 μL of each sample.
4. Run the gel with a constant voltage of 90 V for 45–60 min and image under UV-light (*see* **Note 9**).

3.3.2 Atomic Force Microscopy (AFM)

The AFM can be used for characterizing the sample after the DNA origami structures have been deposited on the substrate and for verifying the successful production of the origami-shaped silhouettes. The AFM imaging is usually carried out in tapping mode with a scan size varying from 1 to 10 μm. The tip velocity ranges from 2 to 15 μm/s.

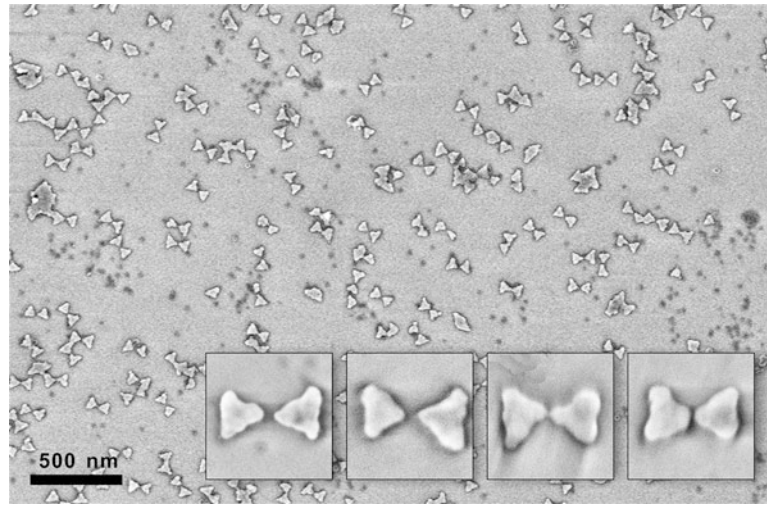

Fig. 6 SEM micrograph of gold nanosized bowtie-antennas on a sapphire substrate. Insets depict individual antennas with higher magnification. Insets are 150 nm × 150 nm in size (adapted from Ref. [23])

3.3.3 Scanning Electron Microscopy (SEM)

The sapphire substrate is an insulator and thus imaging with scanning electron microscope induces charging of the sapphire. To reduce the distortion caused by the charging effect, low acceleration voltages (5–10 kV) should be used. In addition, the scanning time should be minimized in order to reduce the current on a small area. The images were taken with a 30-μm aperture in a continuous averaging mode. Brightness and contrast levels have to be adjusted frequently to compensate the charging effect. A typical SEM image of the final product is shown in Fig. 6. As it can be seen in Fig. 6, with this presented method it is possible to produce precise gold nanoantennas on a sapphire substrate with a high yield and sub-10-nm resolution.

4 Notes

1. In this protocol, a 2D bowtie-shaped DNA origami is used. However, the method could be generalized for other shapes and 3D origami structures. Usually 3D structures should be folded using a longer thermal ramp (e.g., annealing from 65 to 40 °C with the increments of 1 °C per 3 h). In addition, 3D structures need more magnesium (~20 mM) than the 2D structures (12.5 mM) for successful folding.
2. The RIE etching time of SiO_2 is the key step for creating the gap between two triangles in a metallic bowtie antenna. This is due to the SiO_2 growth orientation. The abovementioned SiO_2 growth by CVD happens primarily perpendicular to the

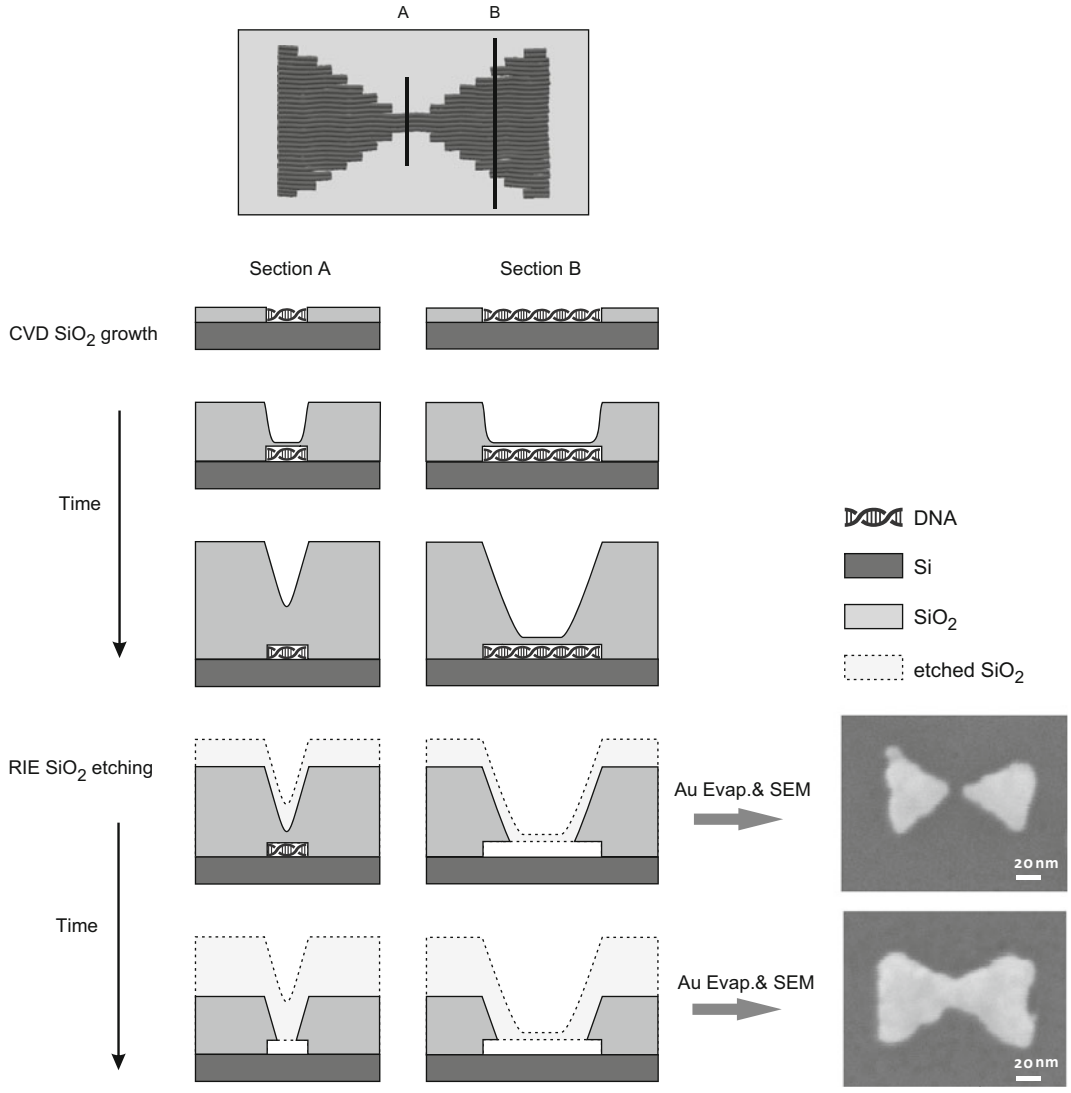

Fig. 7 Illustrations demonstrate how bowtie antennas with or without gap can be fabricated by tuning the CVD growth and RIE etching times. Origami structure has only four helices in parallel at the Section A, and therefore, as the oxide deposition time increases, the oxide walls around the narrow bridge may eventually merge together and result in thickness differences of the oxide layer (compare to section B) (adapted from Ref. [23])

surface, but SiO_2 can also grow slowly on the SiO_2 walls that have already been formed. This makes the cross-sectional profile of the SiO_2 layer to look like a trapezoid shown in Fig. 7. If the layer is let to grow long enough, the oxide walls will eventually merge on top of the origami. At the narrowest part of the DNA origami, the oxide walls will merge sooner than the walls at the wide areas, and thus, produce a thicker oxide layer on top of the origami. If one can etch only through the thin

SiO_2 on top of the wide origami areas but not through the narrow bridge, a silhouette with a gap will be formed. Thus, eventually the final product (metallic shape after the evaporation) will also have a gap. It is noteworthy that the exact RIE etching time has to be optimized for specific instruments and CVD conditions. If the resulting metal nanoparticles look like circular or rectangular disks, it indicates that the etching time is too long. On the contrary, if nanoparticles are not formed or if only some parts of the nanoparticles are seen, it is a sign of too short etching.

3. The deposition rate may vary depending on the used instruments. The 50 nm thickness is chosen here to accommodate 20 nm of metal. As a rule of thumb, the Si layer should be at least twice as thick as the deposited metal layer in order to achieve a clean lift-off procedure. On the other hand, the isotropic etching of Si should also be taken into consideration. Etching through a thicker Si layer makes the undercut effect more prominent. Therefore, if the deposited DNA origami structures are initially very close to each other, the undercut chambers may get connected and the silicon oxide might collapse. However, anisotropic RIE etching (Deep Reactive Ion Etching, DRIE) [27] could be used to tolerate thicker Si layers.
4. It has been observed that for some 2D DNA origami designs (for example Rothemund rectangles [3]), the immobilization onto a SiO_2 surface with 100 mM Mg^{2+} may yield partially folded structures (the structures tend to "roll up"). To decrease the folding, less concentrated Mg^{2+} buffer should be used (as low as 30 mM has been tested). However, low Mg^{2+} will result in sparser deposition due to weaker adsorption forces.
5. Piranha solution can also make the Si surface hydrophilic and negatively charged. Usually 1–2 min RIE O_2 plasma treatment is already sufficient to make the surface negatively charged. However, the high power RIE O_2 plasma can additionally bombard the surface and flatten the rough CVD-grown Si surface. This may improve the fabrication resolution.
6. Because the adsorption of DNA origami to SiO_2 is rather weak, the washing technique can greatly affect the surface density of the origami deposition. One should carefully optimize the washing step: washing should not be too harsh since it could disturb the origami adsorption, but on the other hand, the cleaning should be carried out properly in order to remove all the salt residues. Alternatively, one may consider using a spray-coating technique for depositing DNA origami structures at large scales [28].
7. Usually, room temperature CVD process is transport-limited, meaning that the transport speed of a gas phase reactant will

dominate the growth rate. Therefore, the concentration of TEOS and the positioning of the chip in the chamber have a significant influence on the growth thickness of the SiO_2. Generally, the fresher the TEOS solution, the higher is the growth rate. In addition, the sample chip should be placed close to the TEOS vial, since there is also a concentration gradient in the chamber. Any small change of the CVD conditions may cause different final thicknesses of the grown SiO_2 layer, and therefore, the SiO_2 RIE etching time should be adjusted accordingly.

8. Deposited Cr should not get oxidized before Au is evaporated in order to avoid loss of adhesion.
9. The quality of folding and optional purification is sufficient if the origami band appears to be narrow and intense (and if the origami run with a different speed than the M13mp18 reference). If the purification step is performed, the staple strands should disappear from the gel image. In these conditions, bowtie origami runs slower than the scaffold strand. However, the running speed of an origami object is strongly dependent on its shape and size. (For example, compact 3D DNA origami runs usually faster than the scaffold strand.)

Acknowledgments

Financial support from the Academy of Finland (projects 286845, 130900, 218182, 263526, 289947, 135193), Jane and Aatos Erkko Foundation, Sigrid Jusélius Foundation, Vilho, Yrjö and Kalle Väisälä Foundation and Finnish Cultural Foundation is gratefully acknowledged. This work was carried out under the Academy of Finland Centers of Excellence Programme (2014–2019).

References

1. Jones MR, Seeman NC, Mirkin CA (2015) Programmable materials and the nature of the DNA bond. Science 347:1260901. https://doi.org/10.1126/science.1260901
2. Nummelin S, Kommeri J, Kostiainen MA, Linko V (2018) Evolution of structural DNA nanotechnology. Adv Mater 30:1703721. https://doi.org/10.1002/adma.201703721
3. Rothemund PWK (2006) Folding DNA to create nanoscale shapes and patterns. Nature 440:297–302. https://doi.org/10.1038/nature04586
4. Douglas SM, Dietz H, Liedl T, Högberg B, Graf F, Shih WM (2009) Self-assembly of DNA into nanoscale three-dimensional shapes. Nature 459:414–418. https://doi.org/10.1038/nature08016
5. Linko V, Kostiainen MA (2016) Automated design of DNA origami. Nat Biotechnol 34:826–827. https://doi.org/10.1038/nbt.3647
6. Langecker M, Arnaut V, Martin TG, List J, Renner S, Mayer M, Dietz H, Simmel FC (2012) Synthetic lipid membrane channels formed by designed DNA nanostructures. Science 338:932–936. https://doi.org/10.1126/science.1225624
7. Linko V, Nummelin S, Aarnos L, Tapio K, Toppari JJ, Kostiainen MA (2016) DNA-based enzyme reactors and systems. Nanomaterials 6:139. https://doi.org/10.3390/nano6080139
8. Kuzyk A, Schreiber R, Fan Z, Pardatscher G, Roller E-M, Högele A, Simmel FC, Govorov

AO, Liedl T (2012) DNA-based self-assembly of chiral plasmonic nanostructures with tailored optical response. Nature 483:311–314. https://doi.org/10.1038/nature10889

9. Linko V, Ora A, Kostiainen MA (2015) DNA nanostructures as smart drug-delivery vehicles and molecular devices. Trends Biotechnol 33:586–594. https://doi.org/10.1016/j.tibtech.2015.08.001
10. Maune HT, Han S, Barish RD, Bockrath M, Goddard WA III, Rothemund PWK, Winfree E (2010) Self-assembly of carbon nanotubes into two-dimensional geometries using DNA origami templates. Nat Nanotechnol 5:61–66. https://doi.org/10.1038/nnano.2009.311
11. Shen B, Linko V, Dietz H, Toppari JJ (2015) Dielectrophoretic trapping of multilayer DNA origami nanostructures and DNA origami-induced local destruction of silicon dioxide. Electrophoresis 36:255–262. https://doi.org/10.1002/elps.201400323
12. Tapio K, Leppiniemi J, Shen B, Hytönen VP, Fritzsche W, Toppari JJ (2016) Toward single electron nanoelectronics using self-assembled DNA structure. Nano Lett 16:6780–6786. https://doi.org/10.1021/acs.nanolett.6b02378
13. Gopinath A, Miyazono E, Faraon A, Rothemund PWK (2016) Engineering and mapping nanocavity emission via precision placement of DNA origami. Nature 535:401–405. https://doi.org/10.1038/nature18287
14. Ding B, Deng Z, Yan H, Cabrini S, Zuckermann RN, Bokor J (2010) Gold nanoparticle self-similar chain structure organized by DNA origami. J Am Chem Soc 132:3248–3249. https://doi.org/10.1021/ja9101198
15. Tan SJ, Campolongo MJ, Luo D, Cheng W (2011) Building plasmonic nanostructures with DNA. Nat Nanotechnol 6:268–276. https://doi.org/10.1038/nnano.2011.49
16. Helmi S, Ziegler C, Kauert DJ, Seidel R (2014) Shape-controlled synthesis of gold nanostructures using DNA origami molds. Nano Lett 14:6693–6698. https://doi.org/10.1021/nl503441v
17. Sun W, Boulais E, Hakobyan Y, Wang WL, Guan A, Bathe M, Yin P (2014) Casting inorganic structures with DNA molds. Science 346:1258361. https://doi.org/10.1126/science.1258361
18. Pilo-Pais M, Goldberg S, Samano E, LaBean TH, Finkelstein G (2011) Connecting the nanodots: programmable nanofabrication of fused metal shapes on DNA templates. Nano Lett 11:3489–3492. https://doi.org/10.1021/nl202066c
19. Schreiber R, Kempter S, Holler S, Schüller V, Schiffels D, Simmel SS, Nickels PC, Liedl T (2011) DNA origami-templated growth of arbitrarily shaped metal nanoparticles. Small 7:1795–1799. https://doi.org/10.1002/smll.201100465
20. Shen B, Tapio K, Linko V, Kostiainen MA, Toppari JJ (2016) Metallic nanostructures based on DNA nanoshapes. Nanomaterials 6:146. https://doi.org/10.3390/nano6080146
21. Surwade SP, Zhou F, Wei B, Sun W, Powell A, O'Donnell C, Yin P, Liu H (2013) Nanoscale growth and patterning of inorganic oxides using DNA nanostructure templates. J Am Chem Soc 135:6778–6781. https://doi.org/10.1021/ja401785h
22. Shen B, Linko V, Tapio K, Kostiainen MA, Toppari JJ (2015) Custom-shaped metal nanostructures based on DNA origami silhouettes. Nanoscale 7:11267–11272. https://doi.org/10.1039/c5nr02300a
23. Shen B, Linko V, Tapio K, Pikker S, Lemma T, Gopinath A, Gothelf KV, Kostiainen MA, Toppari JJ (2018) Plasmonic nanostructures through DNA-assisted lithography. Sci Adv 4:eaap8978. https://doi.org/10.1126/sciadv.aap8978
24. Ke Y, Douglas SM, Liu M, Sharma J, Cheng A, Leung A, Liu Y, Shih WM, Yan H (2009) Multilayer DNA origami packed on a square lattice. J Am Chem Soc 131:15903–15908. https://doi.org/10.1021/ja906381y
25. Castro CE, Kilchherr F, Kim D-N, Shiao EL, Wauer T, Wortmann P, Bathe M, Dietz H (2011) A primer to scaffolded DNA origami. Nat Methods 8:221–229. https://doi.org/10.1038/nmeth.1570
26. Dietz H, Douglas SM, Shih WM (2009) Folding DNA into twisted and curved nanoscale shapes. Science 325:725–730. https://doi.org/10.1126/science.1174251
27. Marty F, Rousseau L, Saadany B, Mercier B, Français O, Mita Y, Bourouina T (2005) Advanced etching of silicon based on deep reactive ion etching for silicon high aspect ratio microstructures and three-dimensional micro- and nanostructures. Microelectron J 36:673–677. https://doi.org/10.1016/j.mejo.2005.04.039
28. Linko V, Shen B, Tapio K, Toppari JJ, Kostiainen MA, Tuukkanen S (2015) One-step large-scale deposition of salt-free DNA origami nanostructures. Sci Rep 5:15634. https://doi.org/10.1038/srep15634

Chapter 21

Constructing Free Energy Landscapes of Nucleic Acid Hairpin Unfolding

Micah J. McCauley, Ioulia Rouzina, and Mark C. Williams

Abstract

Single nucleic acid molecules form hairpins that may stabilize secondary and tertiary structures as well as perform enzymatic and other chemical functions. Considerable progress has been made in the effort to understand the contributions of various factors to the stability of a given hairpin sequence. For a given sequence, it is possible to compute both the most likely structural arrangements and their associated free energies over a range of experimental conditions. However, there are many observed hairpin irregularities for which the energies and function are not well understood. Here we examine the irregular RNA Transactivation Response (TAR) hairpin from the HIV-1 genome. Using single molecule optical tweezers, the hairpin is force unfolded, revealing the overall unfolding free energy and the character of the transition state. These measurements allow the construction of a simple energy landscape from unfolding measurements, which can be directly compared to a theoretical landscape. This method is easily adapted to other structures, including the effects of noncanonical bases and even ligand binding.

Key words Free energy landscape, Transition state, Optical tweezers, Mfold, RNA/DNA hairpin, Force spectroscopy

1 Introduction

Nucleic acids form hairpins and other secondary and tertiary structures that are found in a variety of settings. These structures serve not only to enhance the stability of a duplex element but may participate in chemical activity as well [1, 2]. An example is the 59-base RNA hairpin known as the transactivation-response element (TAR). A part of the HIV-1 viral genome, TAR forms a stable hairpin that binds with a protein known as the transactivator of transcription (TAT), facilitating faithful translation [3, 4]. A key question surrounding this hairpin asks how such a relatively long, stable hairpin may be unfolded during the subsequent step of reverse transcription. Determining the energy landscape of this hairpin is essential to answer this question.

Giampaolo Zuccheri (ed.), *DNA Nanotechnology: Methods and Protocols*, Methods in Molecular Biology, vol. 1811,
https://doi.org/10.1007/978-1-4939-8582-1_21, © Springer Science+Business Media, LLC, part of Springer Nature 2018

In this work, we describe experiments that allow the construction of a simple energy landscape from measurements of hairpin unfolding. This work combines several recently developed techniques in nonequilibrium energy estimation and landscape modeling into a single protocol that allows both the unfolded and the transition states to be determined [5–8]. These states may be assembled to create a simple picture of the unfolding energy landscape. Comparisons may be made with a theoretical landscape generated by the base pair energy given by the mfold server [8–10]. Comparing the parameter values derived from experiment, including the equilibrium opening length and energy, as well as kinetic unfolding rate, to their theoretical values is typically done to establish the self-consistency of the measurements. The additional information provided by the transition state parameters allows greater insight into the unfolding stability and pathway.

This technique may then be used to deduce the effects due to noncanonical base pairing and irregular structure elements, including bubbles and mismatches that are not parametrized by mfold or other nucleic acid databases. These elements can be experimentally introduced into hairpins one at a time, and their effects on all fitted parameter values quantified using this approach. This also includes the stability of novel elements of nucleic acid secondary or tertiary structures (base triplexes, methylated or other modified bases, pseudo-loops, etc.) [11]. Furthermore, the effects of these noncanonical structural elements on overall hairpin stability can be directly studied very close to physiological conditions. This contrasts with the very high temperatures required to probe RNA hairpin stability by thermal melting [12]. Finally, the effect of ligands or proteins binding specifically to structural nucleic acid elements can be experimentally characterized by contrasting the landscapes for ligand-bound and unbound hairpins [7].

2 Materials

The preparation of hairpins with long handles and labels has been described previously [7], and related methods can be found in the previous edition of this book [13, 14]. Furthermore, the dual beam optical tweezers have been described at length elsewhere [15, 16]. The following section will only briefly outline the essential parts of these techniques necessary to perform the method of simple landscape measurement and construction, and stress the comparison with the theoretical energy landscape using the energies of mfold.

2.1 Labeled Hairpins and Handles

1. The TAR hairpin is prepared with additional flanking sequences by in vitro transcription of a DNA template using T7 RNA polymerase then purified by denaturing 10% polyacrylamide electrophoresis gel [7].

2. Hairpins are then ligated to long DNA handles, prepared from pBR322 plasmids, which have been labeled with biotin, and digoxigenin and incorporating custom oligomers (*see* **Note 1**). The final construct is illustrated in Fig. 1 [7].
3. A control may also be created that does not incorporate the hairpin. This is useful to check the elasticity of the construct (instrument and the handles) and to verify the activity of the labels.

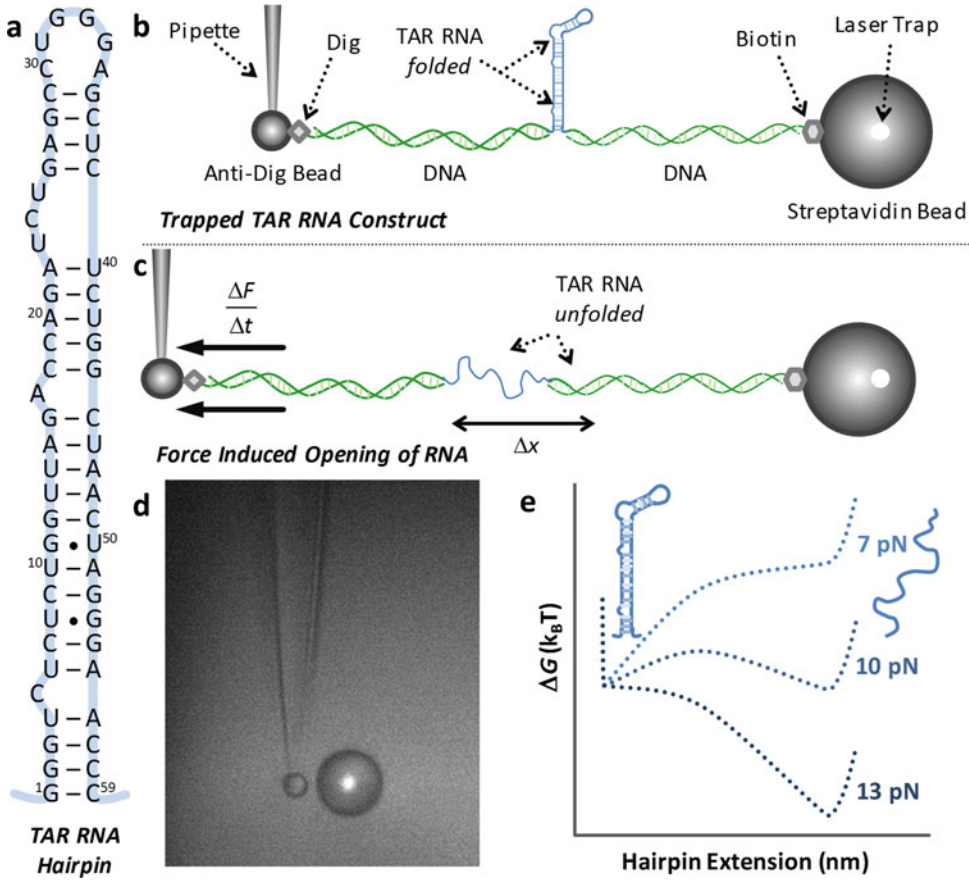

Fig. 1 Probing energy landscapes with force ramp optical tweezers. (a) Sequence and optimal folded structure of the TAR RNA hairpin from HIV-1. Fifty-nine bases form an irregular hairpin of 24 pairs, punctuated by several bubbles, and incorporating two noncanonical ('wobble') pairs. (b) Optical tweezers schematic shows a single TAR RNA hairpin (blue) flanked by long DNA handles (green), and tethered between two polystyrene beads of opposing chemistry to the labeled handles. A dual beam optical trap holds the 5.0 μm diameter streptavidin-coated bead while the 2.1 μm diameter anti-digoxigenin coated bead is fixed onto a micropipette. (c) A force-ramp experiment increases the force at a given rate (r) until the hairpin unfolds. (d) CCD image of a tethered bead and folded hairpin. (e) Decrease of the unfolded state free energy relative to the folded state in the presence of increasing forces

2.2 Mfold

1. The RNA or DNA sequence should be readied, and may be simply input at the website [17];

   http://unafold.rna.albany.edu/?q=mfold.

   Conditions should match experiment as closely as possible. When folding RNA, the temperature is assumed fixed at 37°C (*see* **Note 2**) while the salt is also fixed at 1 M Na^+ (no divalent ions are assumed to be present) (*see* **Note 3**). For DNA, temperature and ionic concentration may be varied.
2. The relevant output includes the folded structure as shown in Fig. 1 for TAR (*see* **Note 4**). Additionally, the free energy of this folded structure will be given (ΔG_o). Furthermore, the energy of each base pair will be provided; $G_i(n_i, F = 0)$, such that $\Sigma_i\ G_i(n_i, 0) = \Delta G_o$ recovering the total free energy (*see* **Note 5**).

2.3 Optical Tweezers

1. A dual beam optical tweezers was constructed and refined to be capable of sub-nanometer positioning and subpicoNewton force measurement [15]. Briefly, during an experiment, counterpropagating lasers (*Lumics*) are brought to the same focus with a pair of water immersion high NA objectives (*Nikon*), forming the trap.
2. A custom flow cell, incorporating a micropipette tip (*WPI*) and flow tubing (*Warner Instruments*) is fixed onto a piezoelectric stage (*nPoint*), and placed between the objectives so that the optical trap lies inside the flow cell.
3. Experimental buffer: 10 mM HEPES, pH 7.5, 100 mM NaCl.
4. A polystyrene bead, 2 μm in diameter and coated in anti-digoxigenin (*Spherotech*), is fixed by suction onto the micropipette tip while a 5 μm diameter bead coated in streptavidin (*Bangs Labs*) may be held in the trap. A single construct (RNA hairpin and DNA handles) may be caught and tethered between these two beads.
5. During a force-ramp experiment, the nucleic acid construct is initially held at low tension. The extension is progressively increased, and the force measured. Increasing tension gradually tilts the energy landscape to favor the unfolded force (Fig. 1). The rate of force increase is measured (r) and corresponds to a loading rate (*see* **Note 6**).

3 Methods

During a cycle of nucleic acid extension and release (Fig. 2), an unfolding event is observed as a sudden increase in the observed extension as the applied force is increased. The force responses of the folded and unfolded construct are each characterized by elastic polymer models (*see* **Note 7**). The unfolding force (F_{op}) and the

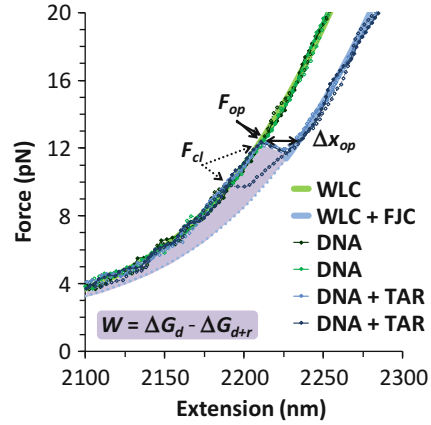

Fig. 2 Cycles of extension and release during force induced unfolding of the TAR hairpin. Measured forces for progressively increasing extensions for DNA (green) and DNA handles including a single TAR RNA hairpin (blue). In both cases, extension (solid symbols and lines) and release (open symbols and dotted lines) are fully reversible, and two sequential cycles on the same contracts are shown for each case. When the TAR hairpin is present, a sudden event is evident upon extension, corresponding to the full unfolding of the hairpin, which folds upon release. Unfolding may be characterized by an increase in length (Δx_{op}) at the critical force (F_{op}). The work of unfolding (W_{op}) corresponds to the shaded area indicating the work required to extend the DNA handles and folded hairpin minus the work required to extend the handles and a fully *unfolded* RNA hairpin ($\Delta W_d - \Delta W_{d+r}$). Folding is also characterized by a critical force (F_{cl}) and a work of folding W_{cl}, not shown). Thick lines denote models of elasticity for the worm-like chain (WLC) and linear combinations of the WLC and the freely jointed chain (FJC), which characterize double stranded DNA and single stranded RNA, as described in the text

length increase (Δx_{op}) may be identified (*see* **Note 8**), as well as the corresponding force for hairpin refolding (F_{cl}). For good statistics, these parameters should be measured over $N > 200$ cycles. For what follows, we apply the method to an $N = 260$ data set, spread over three distinct loading rates (r = 30 pN/s, 10 pN/s and 0.8 pN/s).

3.1 Determining Unfolding Lengths

1. All $N = 260$ measured unfolding lengths (Δx_{op}) are plotted in Fig. 3, across the three loading rates. The average length will change somewhat with the force dependent elasticity of unfolded RNA. Measured widths of these distributions reflect some instrumental noise and fluctuations in hairpin structure and stability.
2. Convert the measured widths to the number of bases unfolded, using the appropriate polymer model (*see* **Notes 7** and **9**). The mean number of released bases should be the nearly the same within the standard error (*see* Table 1).

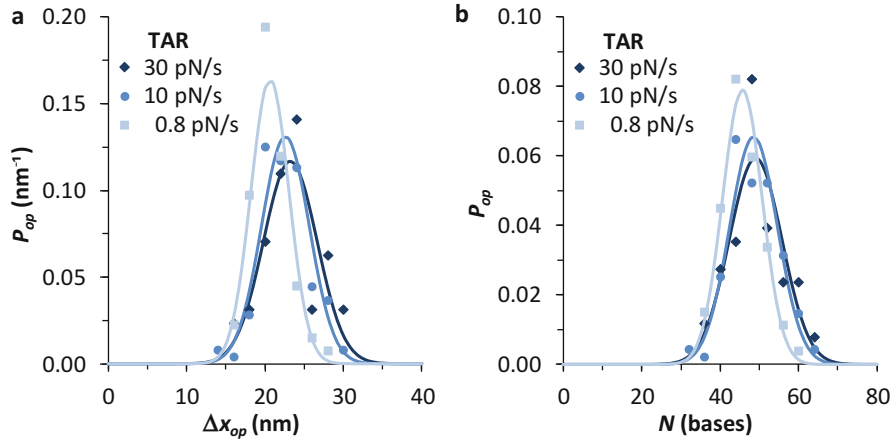

Fig. 3 Measured hairpin lengths and bases released during unfolding. (**a**) Probability distributions ($n = 250$) for the measured lengths during unfolding (Δx_{op}), for several loading rates ($r = 30$ pN/s, diamonds; 10 pN/s, circles; 0.8 pN/s—squares). (**b**) Once corrected for force-dependent polymer elasticity, the mean number of unfolded bases becomes independent of loading rates ($r = 30$ pN/s, diamonds; 10 pN/s, circles; 0.8 pN/s, squares) within uncertainty. Averaging over all three rates gives an opening length of $N = 47.8 \pm 1.3$ bases, out of the 59-base hairpin

Table 1
Characterizing the unfolded state of the TAR hairpin

ν (pN/s)	Δx_{op} (bases)	ΔG_o (k_BT) Integrated	ΔG_o (k_BT) Crooks	ΔG_o (k_BT) Bennett	ΔG_o (k_BT) Jarzynski
30 pN/s	49.1	–	45.0	46.0	44.4 ± 0.6
10 pN/s	48.6	–	43.0	45.5	–
0.8 pN/s	45.7	43.5 ± 0.5	42.0	41.5	–
Average	47.8 ± 1.3		43.3 ± 0.9	44.2 ± 1.6	
Mfold	47 ± 1		43.3 ± 0.9		

Measured opening length (Δx_{op}) and unfolding energy (ΔG_o) of the hairpin at 22 °C and 100 mM Na^+, compared to theoretical predictions. The unfolding length was found and is shown in Fig. 3. Free energies of unfolding were found using various techniques. The integrated energy is the energy measured according to Fig. 2, at the slowest, quasi-equilibrium loading rate. Nonequilibrium techniques include the methods of Crooks (Eq. 2) and Bennett (Eqs. 3 and 4) as shown in Fig. 4. Jarzynski's equality (Eq. 5) was applied to the highest loading rate (Eq. 1), where it returned the clearest result. Values of Δx_{op} and ΔG_o deduced from Mfold exclude the frayed lower stem as shown in Fig. 6. Uncertainties represent SEM for $N = 260$.

3.2 Free Energies of Unfolding

1. The work performed by the instrument during unfolding (W), includes contributions from the direct energy of base pair disruption as well as entropic changes due to the elasticity of both the double stranded DNA handles and the single stranded RNA hairpin [18]. The shaded area of Fig. 2 subtracts the work required to extend the fully unfolded construct (the handles

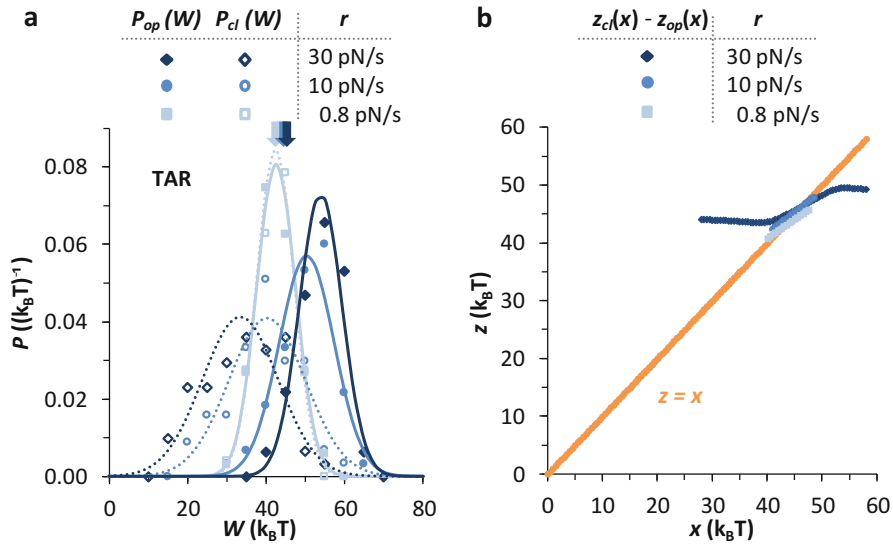

Fig. 4 Determining the equilibrium free energy of unfolding. (**a**) Observed probability distributions ($n = 250$) of unfolding and folding work, $P(W_{op})$ (solid symbols) and $P(W_{cl})$ (open symbols), at varying pulling rates ($r = 30$ pN/s, diamonds; 10 pN/s, circles; 0.8 pN/s, squares). Lines are best fit Gaussians to guide the eye ($P(W_{op})$, solid; $P(W_{cl})$, dotted), and the crossing points, $P(W_{op}) = P(W_{cl})$, are approximate locations of the equilibrium free energy, $W = \Delta G_o$ (highlighted by the arrows). Averaging over all three rates gives $\Delta G_o = 43.3 \pm 0.9\ k_BT$. At the slowest pulling rate of 0.8 pN/s, $P(W_{op}) = P(W_{cl})$ everywhere and opening and closing are in equilibrium, and here $\Delta G_o = 43.5 \pm 0.5\ k_BT$. (**b**) Calculating the equilibrium free energy over all pulling rates using the method of Bennett, according to Eq. 3. The crossing point of $z_{cl}(x) - z_{op}(x)$ and x, averaged over all rates, gives $\Delta G_o = 44.2 \pm 1.6\ k_BT$. All individual and averaged values are summarized in Table 1

and single stranded RNA, ΔG_{d+r}) from a fully folded construct (stretching the handles only, ΔG_d) over the same range of extensions (*see* **Note 10**). This area, $W = \Delta G_d - \Delta G_{d+r}$ is calculated numerically (*see* **Note 11**). The work returned during folding is calculated similarly. Distributions of the probability of observing a given measured work for unfolding ($P_{op}(W)$) and folding ($P_{cl}(W)$) are arranged in Fig. 4 (*see* **Note 12**).

2. For the case where $P_{op}(W) = P_{cl}(W)$ (for the rate 0.8 pN/s in Fig. 4), the rate of opening and closing at the opening force is in quasi-equilibrium. Here the average measured value of W represents the free energy of unfolding the hairpin (ΔG_o). *See* Table 1.
3. At faster pulling rates, $P_{op}(W) \neq P_{cl}(W)$ (except at a single crossing point, see below), and the measured work will not represent the equilibrium free energy of unfolding. Calculating the weighted average of the measured *nonequilibrium* work returns the *equilibrium* free energy of the hairpin, according to [19];

$$\Delta G_o = -k_B T \ln \left\langle \exp\left(-\frac{W}{k_B T}\right) \right\rangle \tag{1}$$

This value is shown in Table 1 for the fastest loading rate of 30 pN/s (*see* **Note 13**).

4. Alternatively, at nonequilibrium loading rates, $P_{\text{op}}(W) = P_{\text{cl}}(W)$ at a single crossing point (assuming the distributions overlap at all). In general, the opening and closing probability distributions are related [6];

$$\frac{P_{\text{op}}(W)}{P_{\text{cl}}(W)} = e^{(W-\Delta G_o)/k_B T} \tag{2}$$

At the crossing point (shown by the arrows in Fig. 4), $W = \Delta G_{\text{o}}$, and the free energy may be extracted (*see* **Note 14**). *See* Table 1 for results across all three loading rates, and the averaged values.

5. The most general technique of energy estimation may be used at any loading rate and does not require the distributions to cross. The technique is to plot the following, referred to as Bennett's equation [20–22];

$$z_{\text{cl}}(x) - z_{\text{op}}(x) = \frac{\Delta G_o}{k_B T} \tag{3}$$

The opening and closing functions $z_{\text{cl}}(x)$ and $z_{\text{op}}(x)$ are averages over all the values of the measured work (W), weighted by the (arbitrary) probability function (f_{x}), as a function of an independent variable (x):

$$\begin{aligned} z_{\text{op}}(x) &= \ln \left\langle f_x(W) \exp\left(-\frac{W}{k_B T}\right) \right\rangle_{\text{op}}, \quad z_{\text{cl}}(x) \\ &= \ln \left\langle f_x(W) \right\rangle_{\text{cl}}, \quad f_x(W) = \frac{\exp\left(\frac{x}{2k_B T}\right)}{1 + \exp\left(\frac{x-W}{k_B T}\right)} \end{aligned} \tag{4}$$

The intersection of $z_{\text{cl}}(x) - z_{\text{op}}(x)$ with the line $z = x$ gives the equilibrium free energy ΔG_{o}, which is shown for each loading rate in Fig. 4 and averaged in Table 1 (*see* **Note 15**).

3.3 Quantifying the Transition State Barrier

1. Probability density distributions of the measured hairpin opening force (F_{op}) for all loading rates are shown in Fig. 5. Distributions are characterized by a single clear peak, which is generally not Gaussian in shape. Distributions of the measured closing force (F_{cl}) may also be fit (*see* **Note 16**), though hairpin closing is often not a two-state process (as is the case here, *see* **Note 17**) [23, 24].

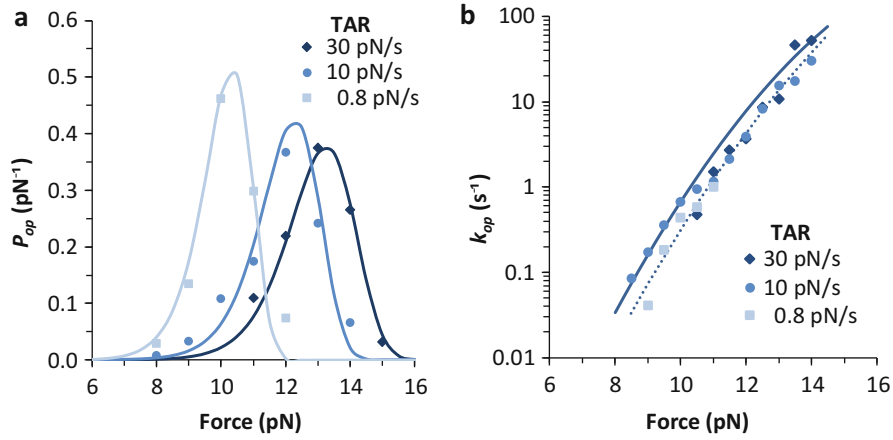

Fig. 5 Measuring the unfolding force at various pulling rates. (**a**) Measured distributions ($n = 250$) for the probability of unfolding ($P_{op}(F)$, for $r = 30$ pN/s, diamonds; 10 pN/s, circles; 0.8 pN/s, squares). Fits to the model of Dudko (Eqs. 5 and 6) are preformed simultaneously to all rates for the shape factors of $\nu = ½$ (solid lines) and $\nu = ⅔$ (dotted lines) then averaged to obtain the final values including uncertainty of $\Delta x^{\dagger}_{op} = 9.9 \pm 1.1$ nm, $\Delta G^{\dagger}_{op} = 27.0 \pm 2.2\ k_B T$ and $k^{o}_{op} = (8 \pm 5) \times 10^{-9}\ s^{-1}$ withχ\upsilon$^2 \sim 1$. (**b**) Force dependent opening rates ($k_{op}(F)$, for $r = 30$ pN/s, diamonds; 10 pN/s, circles; 0.8 pN/s, squares), calculated from the probability distributions of (**a**) using Eqs. 7 and 8. Fits from (**a**) to Eqs. 5 and 6 are plotted as the solid line, while a fit to $k_{op}(F)$ using Eq. 5 directly is plotted as the dotted line. All fitted values and uncertainties are shown in Table 2

2. The opening force distributions may be fit to a dynamic force spectroscopy model that describes the rate of hairpin opening (k_{op}) and the probability of opening (P_{op}) as a function of the applied force (F), assuming a single transition state [5, 25];

$$k_{op}(F) = k^{o}_{op}\left(1 - \frac{x^{\dagger}_{op}F}{\Delta G^{\dagger}_{op}}\nu\right)^{1/\nu - 1} \exp\left\{\frac{\Delta G^{\dagger}_{op}}{k_B T}\left[1 - \left(1 - \frac{x^{\dagger}_{op}F}{\Delta G^{\dagger}_{op}}\nu\right)^{1/\nu}\right]\right\} \tag{5}$$

$$P_{op}(F) = \frac{k_{op}(F)}{r}\exp\left\{\frac{k^{o}_{op}}{x^{\dagger}_{op}r} - \frac{k_{op}(F)}{x^{\dagger}_{op}r}\left(1 - \frac{x^{\dagger}_{op}F}{\Delta G^{\dagger}_{op}}\nu\right)^{1 - 1/\nu}\right\} \tag{6}$$

Fits return the distance to the transition state $\left(x^{\dagger}_{op}\right)$, barrier height $\left(\Delta G^{\dagger}_{op}\right)$, and natural (force-free) rate of unfolding $\left(k^{o}_{op}\right)$ (*see* **Note 18**). The shape factor (ν) may also be determined by the fit, though it is more common to fix the value (*see* **Note 19**). Fits to these equations tend to be unstable (*see* **Note 20**) and uncertainties in the fitted parameters (especially k^{o}_{op}) may be high.

Table 2
Characterizing the transition state of the TAR hairpin

Source	$x_{op}^{\dagger}$ (nm)	$\Delta G_{op}^{\dagger}$ (k_BT)	k_{op}^{o} (s^{-1})
$k_{op}(F)$	10.2 ± 0.3	30.7 ± 1.0	$(0.11 \pm 0.03) \times 10^{-8}$
$P_{op}(F), F_{op}^{max}$ P_{op}^{max}	10.0 ± 0.5	22 ± 5	–
$P_{op}(F), \nu = 1/2$	11.0 ± 0.2	29.1 ± 0.7	$(0.12 \pm 0.03) \times 10^{-8}$
$P_{op}(F), \nu = 2/3$	8.7 ± 0.2	24.9 ± 0.7	$(1.4 \pm 0.4) \times 10^{-8}$
$P_{op}(F)$, average	9.9 ± 1.1	27.0 ± 2.2	$(0.8 \pm 0.5) \times 10^{-8}$
Mfold	11.3 ± 0.9	30.7 ± 2.0	–

Measured distances to the transition state $\left(x_{op}^{\dagger}\right)$, barrier height $\left(\Delta G_{op}^{\dagger}\right)$ and natural (force-free) rate of unfolding $\left(k_{op}^{o}\right)$ of the hairpin at 22°C and 100 mM Na^+, compared to theoretical predictions. Each approach (source) fits all loading rates simultaneously. Fits to the force dependent opening rate of Eq. 5 are shown in Fig. 4, and fits to Eq. 13 utilize the peak forces of the distributions of Fig. 4. Global fits to the full distributions of unfolding according to the theory of Dudko (Eqs. 5 and 6) were performed with two limiting shape factors of ($\nu = 1/2$ and $2/3$), then averaged to obtain the final values as shown. Theoretical values determined from Mfold were found as shown in Fig. 6. Uncertainties represent SEM for $N = 260$.

3. To complement these results and to judge their reliability, Eq. 5 may be fit to the force-dependent opening rates. It is first necessary to find the survival probability $S_{op}(F)$ from the distributions of opening forces [7];

$$S_{op}(F) = 1 - \int_{F_{min}}^{F} P_{op}(F')dF' \tag{7}$$

From these distributions, the measured experimental values of the opening rate $k_{op}(F)$ may be determined at each force (F) for each loading rate (r) (*see* **Note 21**);

$$k_{op}(F) = r \cdot \frac{P_{op}(F)}{S_{op}(F)} \tag{8}$$

The values of $k_{op}(F)$, shown in Fig. 5, are approximately independent of r. The direct fit to Eq. 5 is also shown and the results are summarized in Table 2 (*see* **Note 22**).

3.4 Comparing Theory to Experiment

1. The energies per base pair provided by mfold may be arranged to create the energy landscape. As in Fig. 6 for TAR RNA, and starting at the base of the hairpin, the values of $G_i(n_i, F = 0)$ may be progressively summed over each base pair, n_i, to represent the cumulative energy required to unfold the hairpin. Finally, $\Sigma_i\ G_i(n_i, 0) = \Delta G_o$ at the apical loop (*see* **Note 23**).
2. To model the effect of applied force, remove the energy of stretching $-F\Delta x_i \cdot n_i$ from the landscape, to give $G_i(n_i, F)$

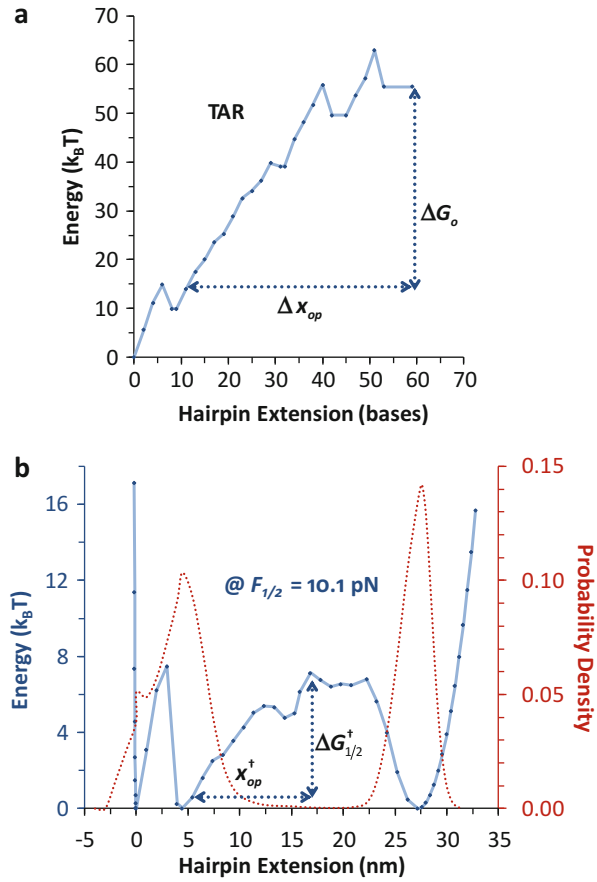

Fig. 6 Theoretical energy landscapes for the TAR RNA sequence. (**a**) Individual base energies are integrated starting from the lowest part of the hairpin stem using pairing/stacking energies from mfold. The end is the theoretical total hairpin energy of $\Delta G_0 = 55.5\ k_BT$, calculated at standard experimental conditions of 37 °C and 1.0 M NaCl. Removing the frayed end of the stem as described in the text gives a theoretical free energy of $\Delta G_0 = 41.5 \pm 1.5\ k_BT$ to unfold $N = 47 \pm 1$ bases (**b**) The free energy landscape of (**a**) with the work of stretching removed ($\Delta G_0 - F\Delta x$) (solid line) until the probability of observing the unfolded state reaches 0.5 (the normalized probability density is represented by the dotted line). At this force, $F_{1/2}$, a transition state barrier may be identified: $x^{\dagger}_{op} = 11.3 \pm 0.9$ nm and $\Delta G^{\dagger}_{op} = 30.7 \pm 2.0\ k_BT$. These values are shown on Tables 1 and 2 and compared to experimental values

(*see* **Note 24**). Furthermore, the probability density reflecting the occupancy of a given fraction of unfolded RNA may be calculated ($p \sim e^{-Gi(ni,\ F)}$) [8, 10]. At a critical force, the occupancy will be equally split between the folded and unfolded state, and at this force ($F_{½}$), the energy of the folded and unfolded state should be roughly equal (*see* **Note 25**).

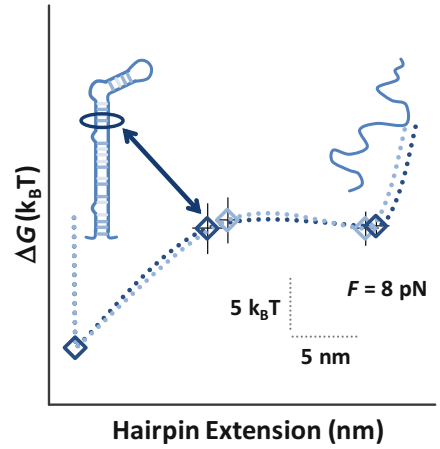

Fig. 7 Comparing theory and experiment for the unfolded and transition states for TAR. Smoothed energy landscapes, quantified by a folded, unfolded and transition state. Theoretical (cyan) and experimental (blue) values are taken from Tables 1 and 2, including uncertainty. Values for the transition and the unfolded state agree well within uncertainty

3. The force-affected landscape $G_i(x_i, F_{1/2})$ may be drawn (*see* **Note 26**) and a transition state may be identified, allowing the distance to the transition state $\left(x_{op}^{\dagger}\right)$, barrier height $\left(\Delta G_{op}^{\dagger}\right)$ to be estimated (*see* **Note 27**). In turn, the opening length (Δx_{op}) and free energy of unfolding (ΔG_o) may be found (*see* **Note 28**).
4. The values of the location and height of the transition state are plotted in Fig. 7 (*see* **Note 29**). Both theory and experiment show that the interrupted structure of TAR not only reduces the energy of the folded state relative to a fully matched hairpin, but shifts the location of the transition state.
5. It is possible that a specific location cannot be modeled by mfold or there are strong deviations between theory and experiment due to the presence of a noncanonical nucleic acid element or a stabilizing/destabilizing binding ligand at that site. The theoretical landscape may be modified at that location, until the landscapes match within experimental uncertainty [7]. Thus, the effect of these noncanonical elements may be deduced.

4 Notes

1. A 3400-base pair biotin-handle was prepared by PCR amplification of plasmid pBR322 using custom 5′-biotinylated primers followed by EcoR1 digestion. A 3100-base pair

digoxigenin handle was prepared by PCR amplification of plasmid pBR322 using custom 5′-DIG-labeled primers followed by BspE1 digestion. Each handle should be purified on a 0.8% agarose gel.

2. An older version of the folding server (version 2.3) does allow temperature to be varied.
3. In the case of TAR RNA presented here, the experimental conditions of 22 °C and 100 mM Na^+ do not match the mfold conditions of 37 °C and 1 M Na^+. However, the loss in hairpin stability by increasing temperature is nearly equally offset by the increase in stability driven by the increase in ionic concentration [26].
4. This work assumes that only one folded structure will exist or that one structure will be significantly more favorable over others (based on the free energy). Hairpins with multiple folded structures or folding intermediates can be analyzed, but are not the subject of this protocol [27].
5. The total energy for TAR includes the destabilizing effects due the presence of mismatches and bubbles. However, there is greater error in the energy contributions of noncanonical structural elements versus full matched sequences.
6. The rigidity of the overall experimental construct ($\kappa = \mathrm{d}F/\mathrm{d}L$) may be broken down into three components; the rigidity of the closed hairpin (κ_{NA}) the rigidity of the dsDNA linker (κ_{dsDNA}) and the rigidity of the optical trap (κ_{OT});

$$\frac{1}{\kappa} = \frac{1}{\kappa_{\mathrm{NA}}} + \frac{1}{\kappa_{\mathrm{OT}}} + \frac{1}{\kappa_{\mathrm{dsDNA}}} \tag{9}$$

While the hairpin rigidity is large, the rigidity of the DNA handles must be found [28];

$$\frac{1}{\kappa_{\mathrm{dsDNA}}} = \frac{L}{dF_{\mathrm{WLC}}/d(x/L)} = \frac{2L\beta l_p\left(1+F\beta l_p\right)}{3+5F\beta l_p+8\left(F\beta l_p\right)^{5/2}} \approx \frac{L}{4F\left(F\beta l_p\right)^{1/2}} \tag{10}$$

The last expression applies at higher forces ($F > 0.1$ pN). At $F = 15$ pN, $\kappa_{\mathrm{dsDNA}} = 0.3$ pN/nm [7]. The instrument used in this work has a stiffness of $\kappa_{\mathrm{OT}} = 0.08$ pN/nm. The force-independent stiffness of the trap dominates the pulling rate, though the pulling rates were also checked against the values reported in each experiment. Furthermore, this stiffness was used to correct the measured extension. In an experiment where κ_{dsDNA} dominates, calculating the extensions and the pulling rate becomes more difficult.

7. The elasticity of double stranded DNA is described by the worm-like chain model of continuous elasticity that reveals the length $b(F)$ [15, 29];

$$b(F) = B_{\mathrm{ds}}\left[1 - \frac{1}{2}\left(\frac{k_B T}{P_{\mathrm{ds}} F}\right)^{1/2} + \frac{F}{S_{\mathrm{ds}}}\right] \tag{11}$$

DNA is characterized by a contour length ($B_{\mathrm{ds}} = 0.340 \pm 0.001$ nm/bp), a persistence length ($P_{\mathrm{ds}} = 30 \pm 4$ nm) as expected for the short DNA constructs used here [30–32] and elastic modulus ($S_{\mathrm{ds}} = 1200 \pm 200$ pN), which compare well with previous known values. The single stranded RNA of unfolded TAR is modeled by the freely jointed chain [15, 29];

$$b(F) = B_{\mathrm{ss}}\left[\coth\left(\frac{2P_{\mathrm{ss}}F}{k_B T}\right)^{1/2} - \frac{1}{2}\frac{k_B T}{P_{\mathrm{ss}} F}\right] \cdot \left[1 + \frac{F}{S_{\mathrm{ss}}}\right] \tag{12}$$

Single stranded RNA is described by an overall contour length ($B_{\mathrm{ss}} = 0.570 \pm 0.001$ nm/bp), persistence length ($P_{\mathrm{ss}} = 0.8 \pm 0.2$ nm) and an elastic modulus ($S_{\mathrm{ss}} = 800 \pm 200$ pN).

8. If the distributions of measured bases released show more than one peak or if the average number varies across the loading rates, this may be taken as evidence that opening (or closing) involves more than two states.
9. The measured opening length in nm is the difference between the unfolded length and the width of the folded RNA stem (usually considered to be ~2 nm) [8]. So, this length should be added to the measured length to recover the number of bases released.
10. An alternative method of work estimation determines the total work between the start and end of hairpin unfolding, from $(F_{\mathrm{op}}(x), x)$ to $(F_{\mathrm{op}}(x), x + \Delta x_{\mathrm{op}})$. This represents the work required to open the hairpin and to stretch the single stranded RNA to F_{op} (and this must be removed to recover the work of hairpin opening) [21, 33]. The precise choice of endpoints is arbitrary, if polymer elasticity is properly considered.
11. Though the data may be integrated directly, this may be unacceptably prone to error. Eqs. 11 and 12 may be integrated up to F_{op}, with a correction for the instrument stiffness shown in Fig. 2.
12. The data is fitted to a Gaussian to guide the eye, though the distribution of the data may not be strictly Gaussian. The error introduced by this assumption is within the reported uncertainty of these results.

13. This method, though potentially very accurate, suffers from the exponential weighting of the measured work. Measurement outliers have a significant effect on the average, and this effect is one-sided as noisy data leads to low estimates of the free energy. In optical tweezers experiments as these, the relative noise becomes larger at low force. The result reported here is only for the highest loading rate where the measured forces are high.
14. In the case where the distributions fully overlap, the crossing point may be taken to be the peak.
15. All the free energy estimates in Table 1 are the same within uncertainty, though the applicability of each method may be limited in various circumstances. The method of Bennett (Eqs. 3 and 4) is the most robust.
16. Fits to the closing state should complement results from fits to the opening state within uncertainty. For the transition state, $\Delta x_{\mathrm{op}} = x^{\dagger}_{\mathrm{op}} + x^{\dagger}_{\mathrm{cl}}$ and $\Delta G_o = \Delta G^{\dagger}_{\mathrm{op}} - \Delta G^{\dagger}_{\mathrm{cl}}$.
17. Folding pathways may involve multiple intermediates, including nonsequential (parallel) paths and even misfolded configurations of local energy minima.
18. Several algorithms exist that produce best fits to the data. A robust nonlinear algorithm by Marquardt–Levenberg returns a minimized value of chi-squared to facilitate parameter estimation [34].
19. Equations 5 and 6 are exact solutions to Kramers theory for two cases of specific potential energy surfaces; $\nu = ½$ (a cusp barrier) and $\nu = ⅔$ (a linear and cubic barrier) [28]. These were the cases that could be solved analytically. To get a sense of the dependence of the fitted parameters on these assumptions, fits are performed for each case, then averaged, as done in Fig. 5 and Table 2 [18].
20. Fitting to Eqs. 5 and 6 is particularly difficult as several local minima may exist that correspond to unreasonable physical results. A robust array of starting values may not lead to a single solution and some help may necessary to pick the best starting values. The following equation relates the peak values of $P_{\mathrm{op}}(F)$: $F^{\max}_{\mathrm{op}}$ and $P^{\max}_{\mathrm{op}}$ to the transition state parameters $x^{\dagger}_{\mathrm{op}}$ and $\Delta G^{\dagger}_{\mathrm{op}}$;

$$\frac{\Delta G^{\dagger}_{\mathrm{op}}}{k_B T} = \frac{F^{\max}_{\mathrm{op}} x^{\dagger}_{\mathrm{op}}}{k_B T}\left[\frac{x^{\dagger}_{\mathrm{op}}}{x^{\dagger}_{\mathrm{op}} - P^{\max}_{\mathrm{op}} k_B T \cdot e}(1-\nu)\right] \tag{13}$$

Reading the values of $F^{\max}_{\mathrm{op}}$ and $P^{\max}_{\mathrm{op}}$ from Fig. 5 produces reasonable pairs of $x^{\dagger}_{\mathrm{op}}$ and $\Delta G^{\dagger}_{\mathrm{op}}$, shown in Table 2, which serve as initial guesses for the fits. The robustness of these fits must

still be checked by varying the starting guesses and also by plotting the local minima versus each fitted parameter.

21. Similar expressions apply to the closing probability $P_{cl}(F)$, though consistent results for $k_{cl}(F)$ could not be obtained (the values at each force are not independent of r).
22. The values in Table 2 agree well within uncertainty, suggesting these methods are robust. However, the errors are highest for the natural rate of unfolding.
23. Energies and lengths for nonpaired bases (including those at the apical loop) must be counted individually as well.
24. Here Δx_i is the length between successive base pairs and loops, labeled as n_i. The effect of applied tension on the energy landscape is shown in Fig. 1.
25. Also, it is approximately true that $\Delta G_o = F_{1/2} \cdot \Delta x$.
26. The data was smoothed and potentials were added at either end. The unfolded hairpin includes an elasticity required to stretch single stranded RNA $\sim kx^2$ while the folded hairpin has a repulsive Morse potential $\sim D(1 - e^{-ax})^2$ [8].
27. The lowest part of the hairpin is typically observed to fray open by a few base pairs. In the case of TAR RNA shown here, the landscape and occupancy indicate that at $F_{1/2}$ the folded state does not correspond to a hairpin with all the base pairs intact. Rather, the lowest four pairs up to the C bulge (in Fig. 1) are frayed open (presumably at a low force and this fraying is not detected). So, the theoretical values for the unfolded and transition states are measured from this mostly folded state, and these values are compared to experiment in Tables 1 and 2.
28. The value of the unfolding length at $F_{1/2}$ is $\Delta x_{op} = 21.8 \pm 0.5$ nm. The mean value of the unfolding length from Fig. 3 is $\Delta x_{op} = 22.0 \pm 1.0$ nm, though this is averaged across a range of unfolding forces. The number of unfolded bases is force independent, and a better measure of the opening length.
29. A smooth landscape has been assumed for clarity. Furthermore, the theoretical and experimental landscapes are shown for an external force of $F = 8$ pN, where the transition state is more clearly defined.

Acknowledgments

This work was supported by grants NIH GM072462 and NSF MCB-1243883 to M.C.W.

References

1. Cech TR, Zaug AJ, Grabowski PJ (1981) In vitro splicing of the ribosomal RNA precursor of Tetrahymena: involvement of a guanosine nucleotide in the excision of the intervening sequence. Cell 27(3 Pt 2):487–496
2. Kruger K, Grabowski PJ, Zaug AJ, Sands J, Gottschling DE, Cech TR (1982) Self-splicing RNA: autoexcision and autocyclization of the ribosomal RNA intervening sequence of Tetrahymena. Cell 31(1):147–157
3. Levin JG, Guo J, Rouzina I, Musier-Forsyth K (2005) Nucleic acid chaperone activity of HIV-1 nucleocapsid protein: critical role in reverse transcription and molecular mechanism. Prog Nucleic Acid Res Mol Biol 80:217–286. https://doi.org/10.1016/S0079-6603(05)80006-6
4. Berkhout B, Jeang KT (1992) Functional roles for the TATA promoter and enhancers in basal and tat-induced expression of the human immunodeficiency virus type 1 long terminal repeat. J Virol 66(1):139–149
5. Dudko OK, Mathe J, Szabo A, Meller A, Hummer G (2007) Extracting kinetics from single-molecule force spectroscopy: nanopore unzipping of DNA hairpins. Biophys J 92 (12):4188–4195. https://doi.org/10.1529/biophysj.106.102855
6. Crooks GE (1999) Entropy production fluctuation theorem and the nonequilibrium work relation for free energy differences. Phys Rev E 60(3):2721–2726
7. McCauley MJ, Rouzina I, Manthei KA, Gorelick RJ, Musier-Forsyth K, Williams MC (2015) Targeted binding of nucleocapsid protein transforms the folding landscape of HIV-1 TAR RNA. Proc Natl Acad Sci U S A 112 (44):13555–13560. https://doi.org/10.1073/pnas.1510100112
8. Woodside MT, Behnke-Parks WM, Larizadeh K, Travers K, Herschlag D, Block SM (2006) Nanomechanical measurements of the sequence-dependent folding landscapes of single nucleic acid hairpins. Proc Natl Acad Sci U S A 103(16):6190–6195. https://doi.org/10.1073/pnas.0511048103
9. Zuker M (2003) Mfold web server for nucleic acid folding and hybridization prediction. Nucleic Acids Res 31(13):3406–3415. https://doi.org/10.1093/nar/gkg595
10. Woodside MT, Anthony PC, Behnke-Parks WM, Larizadeh K, Herschlag D, Block SM (2006) Direct measurement of the full, sequence-dependent folding landscape of a nucleic acid. Science (New York, NY) 314 (5801):1001–1004. https://doi.org/10.1126/science.1133601
11. Shokri L, McCauley MJ, Rouzina I, Williams MC (2008) DNA overstretching in the presence of glyoxal: structural evidence of force-induced DNA melting. Biophys J 95 (3):1248–1255. https://doi.org/10.1529/biophysj.108.132688
12. Einert Thomas R, Netz Roland R (2011) Theory for RNA folding, stretching, and melting including loops and salt. Biophys J 100 (11):2745–2753. https://doi.org/10.1016/j.bpj.2011.04.038
13. Cecconi C, Shank EA, Marqusee S, Bustamante C (2011) DNA molecular handles for single-molecule protein-folding studies by optical tweezers. Methods Mol Biol 749:255–271. https://doi.org/10.1007/978-1-61779-142-0_18
14. McCauley MJ, Williams MC (2011) Measuring DNA-protein binding affinity on a single molecule using optical tweezers. Methods Mol Biol 749:305–315. https://doi.org/10.1007/978-1-61779-142-0_21
15. Chaurasiya KR, Paramanathan T, McCauley MJ, Williams MC (2010) Biophysical characterization of DNA binding from single molecule force measurements. Phys Life Rev 7 (3):299–341. https://doi.org/10.1016/j.plrev.2010.06.001
16. McCauley MJ, Williams MC (2009) Optical tweezers experiments resolve distinct modes of DNA-protein binding. Biopolymers 91 (4):265–282. https://doi.org/10.1002/bip.21123
17. Zuker M, Markham N (2017) The mfold Web Server. The RNA Institute, College of Arts and Sciences, State University of New York at Albany, Albany. http://unafold.rna.albany.edu/?q=mfold. Accessed June 2017
18. Greenleaf WJ, Frieda KL, Foster DAN, Woodside MT, Block SM (2008) Direct observation of hierarchical folding in single Riboswitch aptamers. Science (New York, NY) 319 (5863):630–633. https://doi.org/10.1126/science.1151298
19. Jarzynski C (1997) Nonequilibrium equality for free energy differences. Phys Rev Lett 78 (14):2690–2693. https://doi.org/10.1103/PhysRevLett.78.2690
20. Bennett CH (1976) Efficient estimation of free energy differences from Monte Carlo data. J Comput Phys 22(2):245–268. https://doi.org/10.1016/0021-9991(76)90078-4

21. Collin D, Ritort F, Jarzynski C, Smith SB, Tinoco I, Bustamante C (2005) Verification of the crooks fluctuation theorem and recovery of RNA folding free energies. Nature 437 (8):231–234. https://doi.org/10.1038/nature04061
22. Crooks GE (2000) Path-ensemble averages in systems driven far from equilibrium. Phys Rev E 61(3):2361–2366. https://doi.org/10.1103/PhysRevE.61.2361
23. Li PT, Collin D, Smith SB, Bustamante C, Tinoco I Jr (2006) Probing the mechanical folding kinetics of TAR RNA by hopping, force-jump, and force-ramp methods. Biophys J 90(1):250–260. https://doi.org/10.1529/biophysj.105.068049
24. Zhang Y, Dudko OK (2013) A transformation for the mechanical fingerprints of complex biomolecular interactions. Proc Natl Acad Sci 110 (41):16432–16437. https://doi.org/10.1073/pnas.1309101110
25. Dudko OK, Hummer G, Szabo A (2006) Intrinsic rates and activation free energies from single-molecule pulling experiments. Phys Rev Lett 96(10):108101. https://doi.org/10.1103/PhysRevLett.96.108101
26. Vieregg J, Cheng W, Bustamante C, Tinoco I Jr (2007) Measurement of the effect of monovalent cations on RNA hairpin stability. J Am Chem Soc 129(48):14966–14973. https://doi.org/10.1021/ja074809o
27. Pierse CA, Dudko OK (2017) Distinguishing signatures of multipathway conformational transitions. Phys Rev Lett 118(8):088101. https://doi.org/10.1103/PhysRevLett.118.088101
28. Dudko OK, Hummer G, Szabo A (2008) Theory, analysis, and interpretation of single-molecule force spectroscopy experiments. Proc Natl Acad Sci U S A 105 (41):15755–15760. https://doi.org/10.1073/pnas.0806085105
29. Smith S, Finzi L, Bustamante C (1992) Direct mechanical measurements of the elasticity of single DNA molecules by using magnetic beads. Science (New York, NY) 258 (5085):1122–1126. https://doi.org/10.1126/science.1439819
30. Onoa B, Dumont S, Liphardt J, Smith SB, Tinoco I Jr, Bustamante C (2003) Identifying kinetic barriers to mechanical unfolding of the T. thermophila ribozyme. Science (New York, NY) 299(5614):1892–1895. https://doi.org/10.1126/science.1081338
31. Seol Y, Li J, Nelson PC, Perkins TT, Betterton MD (2007) Elasticity of short DNA molecules: theory and experiment for contour lengths of 0.6-7 microm. Biophys J 93(12):4360–4373. https://doi.org/10.1529/biophysj.107.112995
32. Peters JP, Mogil LS, McCauley MJ, Williams MC, Maher LJ 3rd (2014) Mechanical properties of base-modified DNA are not strictly determined by base stacking or electrostatic interactions. Biophys J 107(2):448–459. https://doi.org/10.1016/j.bpj.2014.04.066
33. Tinoco I Jr, Li PT, Bustamante C (2006) Determination of thermodynamics and kinetics of RNA reactions by force. Q Rev Biophys 39 (4):325–360. https://doi.org/10.1017/S0033583506004446
34. Press WH, Teukolsky SA, Vetterling WT, Flannery BP (2002) Numerical Recipies in C: the art of scientific computing. Cambridge University Press, Cambridge

Erratum to: Selection of Structure-Switching DNA Aptamers Binding Soluble Small Molecules and SPR Validation of Enrichment

Enrico Tenaglia, Fabio M. Spiga, and Carlotta Guiducci

Erratum to:
Chapter 13 in: Giampaolo Zuccheri (ed.),
***DNA Nanotechnology: Methods and Protocols*,**
Methods in Molecular Biology, vol. 1811,
https://doi.org/10.1007/978-1-4939-8582-1_13

The original version of the book was published without the co-author "Fabio M. Spiga" in Chapter 13. The missing author name and affiliation has now been updated as given below:

Fabio M. Spiga
Institute of Bioengineering, Ecole Polytechnique Fédérale De Lausanne (EPFL), Lausanne, Vaud, Switzerland

The updated online version of this chapter can be found at
https://doi.org/10.1007/978-1-4939-8582-1_13

Giampaolo Zuccheri (ed.), *DNA Nanotechnology: Methods and Protocols*, Methods in Molecular Biology, vol. 1811,
https://doi.org/10.1007/978-1-4939-8582-1_22, © Springer Science+Business Media, LLC, part of Springer Nature 2018

INDEX

A

Agarose gel electrophoresis 15, 16, 18, 281, 287, 289, 291
Aminopropyl triethoxysilane (APTES) 68, 70, 74, 141, 145, 147, 165, 167
Aptamers 89, 183–196
Atomic force microscopy (AFM) 12, 14, 16, 18–20, 110, 117, 118, 125, 126, 154, 167, 168, 232, 234, 245, 247, 249, 256, 259–261, 264–268, 271, 272, 274, 277, 283, 289, 290, 305, 306, 309
Atomic force microscopy (AFM) sample preparation 16

B

λ Bacteriophage DNA 201
Beta-2-microglobulin (β2m) 152–154, 158–160
Biosensors 103, 115–134, 173, 195, 280

C

caDNAno 210, 211, 213, 214, 302
Cationic PNA 50

D

Dielectrophoresis 202, 203
Dissipation monitoring 101–114
DNA crystals 4, 101–113, 260, 280, 291
DNA-directed immobilization (DDI) 151–161
DNA immobilization 101, 103, 104, 109, 110, 113, 151–161, 184, 207, 232, 243, 245, 246, 264, 272, 274, 301, 312
DNA lattice 5, 211, 280
DNA methylation 173, 174, 178–180
DNA methyltransferase 174, 179, 180
DNA Nanoswitch 79–97
DNA nanotechnology ..... v, 1–8, 80, 81, 86, 90, 115, 116, 279–295, 299
DNA origami ..... v, 6, 8, 11, 209–228, 232, 242, 243, 245, 246, 248, 249, 253–261, 263–277, 280, 282, 283, 288–292, 295, 299–304, 306–310, 312
DNA purification 14–19, 21, 45, 143, 144, 177, 188, 193, 288, 289, 301, 302
DNA sequence design 87, 117, 119–121, 131, 132
DNA tweezers 266

E

Electrochemical detection 117, 119, 128–131
Electron-beam lithography 264, 267, 268
Energy landscapes 315–330
λ-Exonuclease 186, 188, 193
Exonuclease– DNA polymerase 13, 19, 26, 28, 29, 31
Exonuclease– Klenow polymerase 26, 28, 29, 31

F

Fluorescence microscopy 232, 234, 242, 246, 248
  confocal 234, 246
Focused ion beam (FIB) 232, 241–243, 247, 248
Four-way junctions 3

G

G-based nanostructures 25
Gold nanodots 263
Gold-nanoparticle-DNA hybrid 279–295
Gold nanoparticles 24, 164–168, 170, 279–295
G-quadruplex 24

H

Hairpin unfolding 315–330
Heavy metal ions 138
HeLa cells 68, 71, 73
Holliday junctions 2, 11, 209, 215, 216
Homopolymeric DNA 23, 24, 45
Hoogsteen hydrogen bonds 24, 80
HPLC Purification 27, 29, 30, 32–34, 36–39, 41–44, 58, 109
Hybridization chain reaction (HCR) 86, 115–134

L

Localized surface plasmonic resonance (LSPR) 163–170, 279, 280, 284, 292, 293, 295
  characterization 164, 279

Giampaolo Zuccheri (ed.), *DNA Nanotechnology: Methods and Protocols*, Methods in Molecular Biology, vol. 1811, https://doi.org/10.1007/978-1-4939-8582-1, © Springer Science+Business Media, LLC, part of Springer Nature 2018

M

Magnetic microbeads 187, 188, 190
Mercaptohexanol 105, 187, 193
Metal nanoclusters 173
Mesoporous silica nanoparticles 67–70, 72–75
Microarray 137, 138, 151
Microchannels 138, 139, 141, 143–145, 273
Microelectrodes 97, 199, 200, 207
Microfluidics 138, 164, 166, 264, 267, 268, 272–274, 277
MicroRNAs (miRs) 49, 58, 117, 119, 131
Molecular dynamics (MD) 210–218, 220, 221, 223, 224, 226, 228
Molecular lithography masks 253, 256, 299–313

N

NAMD 210, 211, 215–220, 222, 223
Nanoantennas 300, 310
Nanoarray 151, 242, 246, 249
Nanografting 151–161
Nanolithography ..... v, 151, 158
Nanopatterning 231–233, 241–243, 245, 246, 254, 264, 267, 271–273, 275
Nanostructured biosensor 138
Nanowires 23–46
Nucleic acids hairpins 315–330

O

Oligo-ethylene glycol alkylthiol self assembled monolayers 154
Oligonucleotide purification 30, 33, 35, 38–40, 42, 43, 45
Optical tweezers 316–318, 329

P

PCR 11, 14, 17, 36, 118, 124, 143, 183–191, 193, 194, 243, 255, 264, 325
Peptide nanoarrays 151, 153, 158–160
pH-dependent nanoswitch 82, 86, 90
pH-dependent triplex DNA 80, 86, 88–90
PNA 49–62
  delivery to cells 50, 58, 66
  purification 52, 57–59
  synthesis 50, 52, 53, 55, 57, 60
Polyacrylamide gel electrophoresis 187, 316
Protein adsorption 253–261

Q

Q factor of oscillation 102
Quantum dots (QDs) 232, 243, 246
Quartz-crystal microbalance 101–113

R

Reactive ion etching (RIE) 276, 301, 303–305, 307, 309–313

S

Scanning electron microscopy (SEM) 74, 232, 233, 248, 264, 269, 271, 273, 274, 276, 283, 291, 292, 301, 308, 310, 320, 324
Self-assembled monolayers 109, 113, 153–155, 158, 163–170, 242, 253–259
Silanization 165–167
Silver nanoclusters 173–180
Small interference RNA (siRNA) 65, 67, 71
Stopped-flow measurements 92, 93
Strand displacement 86, 87, 103, 104, 113, 116
Surface acoustic wave resonator 202
Surface immobilization 101–113, 184
Surface plasmon resonance (SPR) 180, 183–196
Systematic evolution of ligands by exponential enrichment (SELEX) 183–185, 187–195

T

Triple helix 80, 82
Triplex DNA 42, 80, 81, 86, 89, 90

U

Ultra-flat gold 126, 153, 154, 158
Unfolding energy 316, 320
Unfolding force 318, 323, 330
Unfolding measurements 315
Universal pH buffer 82, 84, 90–93, 96, 97

V

VMD 211, 215, 217, 218, 224–227

Z

Zeolite-L 67–70, 74